HOLLOW-CORE FLOOR SLAB PERFORMANCE FOLLOWING A SEVERE EARTHQUAKE

A thesis
submitted in partial fulfilment
of the requirements for the Degree
of
Doctor of Philosophy
at the
University of Canterbury
by
Jeffrey Matthews

University of Canterbury
Christchurch, New Zealand

2004

Table of Contents:

This Page is Blank

List of Figures:

This Page is Blank

List of Tables:

This Page is Blank

Abstract:

Hollow-core floor slabs are the dominant flooring systems used in New Zealand since the 1980's. This study experimentally investigates the seismic performance of precast hollow-core floors including three-dimensional effects of an entire floor system within a two-way moment resisting frame. In order to experimentally assess the seismic performance of a large super-assemblage a new type of self-equilibrating loading frame was designed and built. A full-scale super-assemblage based on a multi-storey prototype was constructed and tested under quasi-static cyclic loading. The capacity designed precast concrete frame performed very well but the performance of the floor itself was quite poor. Incipient failure of the precast floor occurred at an interstorey drift of 1.9 percent, while complete collapse of the floor occurred at a drift of 2.5 percent. A rainflow counting method is developed to enable the amount of beam elongation to be predicted during an earthquake. This is particularly important in determining the required seating length for the precast hollow-core flooring units. Based on the results of this investigation new connection (seating) details are proposed for attaching the hollow-core units to the supporting beams to try to improve the performance of the hollow-core units.

This Page is Blank

Acknowledgements:

The research presented in this thesis was conducted at the Department of Civil Engineering at the University of Canterbury under the supervision of Professor Des Bull and Professor John Mander. I wish to sincerely thank both Des and John for their ongoing support throughout this project both as supervisors and as colleagues.

This project would not have been possible without the financial support provided by: University of Canterbury; Earthquake Commission; Cement and Concrete Association of New Zealand; Building Research Authority of New Zealand; Technology New Zealand; Firth Industries Ltd; Stresscrete; Stahlton Prestressed Flooring; Precast Components; Pacific Steel; Holmes Consulting Group and Construction Techniques Ltd. These contributions are greatly acknowledged.

A special thanks needs to go to all the Civil Engineering technicians who have helped on this project. In particular, to Russell McConchie for his guidance, Richard Newton for designing the electronic software to control the super-assemblage (and for being Richard!!), Ray Allen for the endless hours he spent welding my loading frame and Melody Callahan for solving all my printing, website and conference presentation issues. Further acknowledgement is due to Associate Professor Richard Fenwick for his help and guidance and Len McSaveney from Golden Bay Cement.

Thanks for all the postgrads and students I've been involved with during my studies. In particular I would like to mention the following colleagues who have played a special part: Chris Allington, Rob Presland, Mark Ellis, Tony Parkes, Renee Lindsay, Rolando Castillo, David Lau as well as Al, Jason, Andrew, Dave, Dean, and Iwan.

Also thanks to some of my friends outside of University: Ben and Sarah Lamb; Scott Harvey; Dave Manley and Melanie Allington who have given me great support.

Finally, a special thanks to Mum, Dad, Grant, Ray and Julie for their love and support during my studies, without this, my project would have been a lot more difficult.

This Page is Blank

Chapter 1

Introduction

1.1 Background

Since the 1980's, the use of precast concrete construction has become commonplace in New Zealand. This is mainly due to improved economics due to the speed of erection and increased precision obtained from having the components constructed off site. Some areas of concern have been raised by the New Zealand construction industry as to the performance of precast buildings during earthquakes. In the 1994 Northridge earthquake (Norton et al, 1994), some serious deficiencies were exposed. The investigation proposed here responds to the call made by the New Zealand study groups responsible for writing the *Guidelines for the use of Structural Precast Concrete in Buildings* (Centre for Advanced Engineering, 1999).

A major concern has been the attachment of precast hollow-core units to the lateral force resisting system. If the connection between the hollow-core unit and the perimeter beam were to fail, due to the hollow-core unit losing its seating support, sections of the floor could collapse, possibly leading to a partial (or full) collapse of the building. In New Zealand, the designer uses a "capacity design" approach to prevent the collapse of the building from happening in an earthquake. However, the performance of these floor-to-frame connection details is not greatly known. Researchers such as Mejia-McMaster and Park (1994), Herlihy and Park (2000) and Oliver (1998) have undertaken investigation of single isolated connections to observe the phenomena of loss of support and to make recommendations to minimise the effects caused by it. This study seeks to investigate the overall performance of a

portion of a building, but with a particular emphasis on a single floor including the three-dimensional effects.

The research programme involves the examination of the performance of a full-scale super-assembly, which is representative of a typical precast concrete building under severe earthquake conditions.

1.2 Earthquake Observations

Northridge, January 17 1994

Following the January 1994 Northridge earthquake, the New Zealand Earthquake Society sent a reconnaissance team to Northridge to learn from the observed failures. The published report (Norton et al 1994) summarised the findings and observations from the reconnaissance trip. One particular case study was on the poor performance of the Meadows Apartments. Within this group of structures, there was a collapse of a portion of the car-parking building. This failure appeared to be due to the hollow-core unit losing its seat and collapsing. From the photographs in Figure 1-1 it is possible to see that there were several ways a hollow-core floor could fail. The first, being the hollow-core unit loses its seat and collapsing as a complete unit (Figure 1-1(a)). The second is the hollow-core unit separating from it topping slab (referred to as delamination) and collapsing, leaving the topping slab intact (Figure 1-1(b)). The third is the splitting of the hollow-core units webs leaving the topping slab and the top half of the hollow-core unit intact while the bottom of the unit collapses (Figure 1-1(c)).

It was these failures that raised concern about the possible poor performance of the connection between the hollow-core floor unit and the supporting beams, as the construction methods used in New Zealand are not dissimilar to that used in California.

(a) Collapse of a complete section of floor

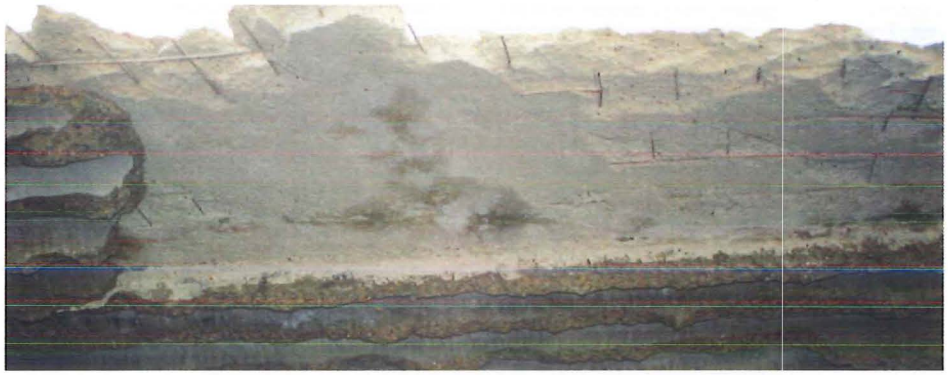

(b) A section of cast insitu topping remains while the hollow-core unit has delaminated and collapsed

(c) A section of the hollow-core units webs have split. The bottom section has collapsed while the top section remains attached to the topping

Figure 1-1 Failure of the Meadows Apartment car park, Northridge 1994 (Norton et al, 1994)

The Meadows car park was not the only structure to fail during the Northridge earthquake. The above mentioned report along with many others (such as Holmes and Somers (1995) and Iverson and Hawkins (1994)) shows extensive damage and collapse of other precast flooring structures, in particular parking structures with precast double tees. The types of failures seen were similar to what was seen in the hollow-core case study and all revolved around seating issues or loss of support that lead to the failure. Once the seat had been damaged or lost it usually lead to some form of failure. Two additional examples are shown in Figure 1-2.

(a) Partial collapse of the Northridge Fashion Centre parking garage

(b) Complete collapse of the Kaiser West Los Angeles Parking garage (only the stairwell remains)

Figure 1-2 Parking structure failures following the Northridge earthquake (Holmes and Somers, 1995)

Armenia, December 7, 1988

The Armenian earthquake had mass devastation with hundreds of buildings completely collapsed or extensively damaged. A reconnaissance report (Wyllie and Filson, 1989) showed that a large proportion of these structures were buildings that had precast hollow-core floors, the exterior frame or structural walls varied on all the structures. A large number of the problems with these structures were the connection of the hollow-core unit to the lateral force resisting system (LFRS). Little or no detailing was used to attach the hollow-core units to the LFRS. Whereas in Northridge it was thought that adequate detailing practice was generally employed. This lack of detailing lead to the large number of building collapses. The typical connection detail used in Armenia to connect the hollow-core unit to the LFRS was to simply lay the hollow-core units between the LFRS without positive metal anchors to the LFRS and without interconnections between the hollow-core planks. The lack of a cast insitu topping slab therefore made it difficult to increase the structural capacity of the system. Figure 1-3 shows photographs of some of the devastation that took place.

1.3 Scope of work

In this research, a super-assemblage portion of a typical precast concrete building will be built and tested to investigate the likely building performance during a severe earthquake. The investigation will focus the effect that both the hollow-core floor slab has on the moment resisting frame and the moment resisting frame has on the hollow-core floor units. Not all the issues mentioned are strictly only applicable to hollow-core floors. Some of the problems are more generic, applying to a range of precast flooring types. Hollow-core floor slabs are being investigated in this research because it has been the predominant flooring system used in New Zealand since the 1980's.

(a) Collapse of a masonry structure incorporating hollow-core floor slabs

(b) Collapse of a 5 storey precast frame structure incorporating hollow-core floor slabs

Figure 1-3 Failures observed following the Armenia earthquake (Wyllie and Filson, 1989)

Other issues to be examined will be:

- Whether the current assumption that the compression struts within the floor diaphragm can be transferred to the corner nodes or whether an alternative location needs to be studied (strut and tie detailing).
- The effect beam elongation has on both the frame and the hollow-core units.
- To determine the amount of negative moment strength enhancement the floor diaphragm provides to the perimeter frame.

- To determine the level of damage at varying drift levels during the testing programme.
- To determine the likely performance of the most common detail used in connection of the hollow-core unit to the perimeter beam, used in New Zealand since the 1980's.

1.4 Origin of the test specimen

This experimental programme focuses on a lower storey in a multi-level precast concrete frame building, typically the second through fourth storeys. The first storey is not being studied due to the effects that the non-hinging foundation beams has on the first storey performance.

Since an earthquake can cause a structure to move in any direction the corner of the building is being examined. Several areas of interest have been raised about the likely performance of the corner of the structure, particularly in reference to the seating of the hollow-core floor units on supporting beams.

A drawing showing the origin of the super assemblage is shown in Figure 1-4.

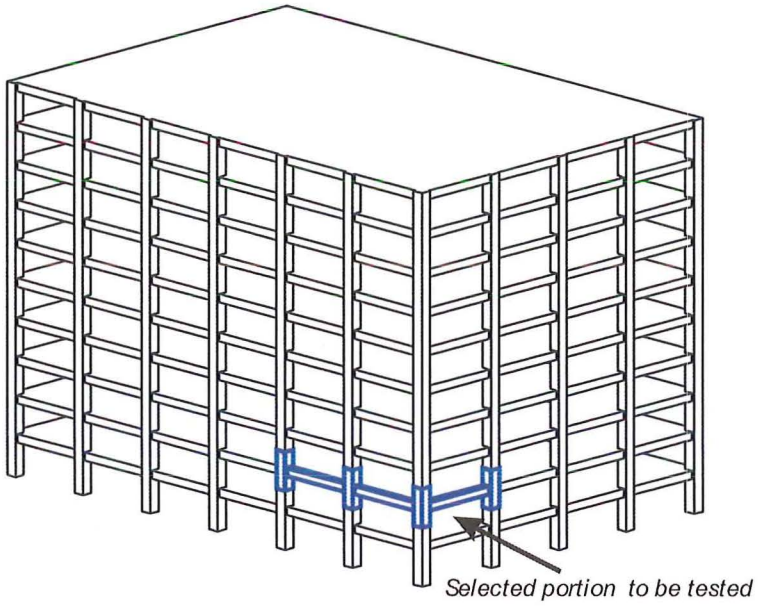

Figure 1-4 Origin of the super assemblage to be testing.

1.5 Details of the super-assemblage

1.5.1 Test specimen dimensions

The super-assembly is a two-bay by one-bay moment resisting frame structure incorporating pretensioned precast hollow-core floor units. The floor units are orientated so that they run parallel with the two-bay edge of the structure. The hollow-core units are seated on the two end beams and span past the central column.

The dimensions for this super assemblage have been based on the typical dimensions used in construction around New Zealand. The column centreline spacing is 6.1m, the columns are 750mm square while the perimeter beams are 750mm deep and vary between 450mm and 400mm wide. The width of the beam depends on whether the hollow-core is seated on the beam or not. The back tie beam was 400mm wide and 250mm deep. The buildings interstorey column height is 3.5m. These dimensions are summarised in Figure 1-5.

The moment resisting frame itself has three perimeter beams and one tie beam. The perimeter beams are located on the West, South and East sides while the tie beam is placed on the North side of the super-assemblage. The reason for a shallow tie beam was because in a real structure there is not usually a beam present at that location, usually there would be more floor units. The tie beam was required to represent the remainder of the floor and to provide a tie member to ensure the northern columns displaced in the desired manner.

Refer to Appendix B for the design of the super-assemblage.

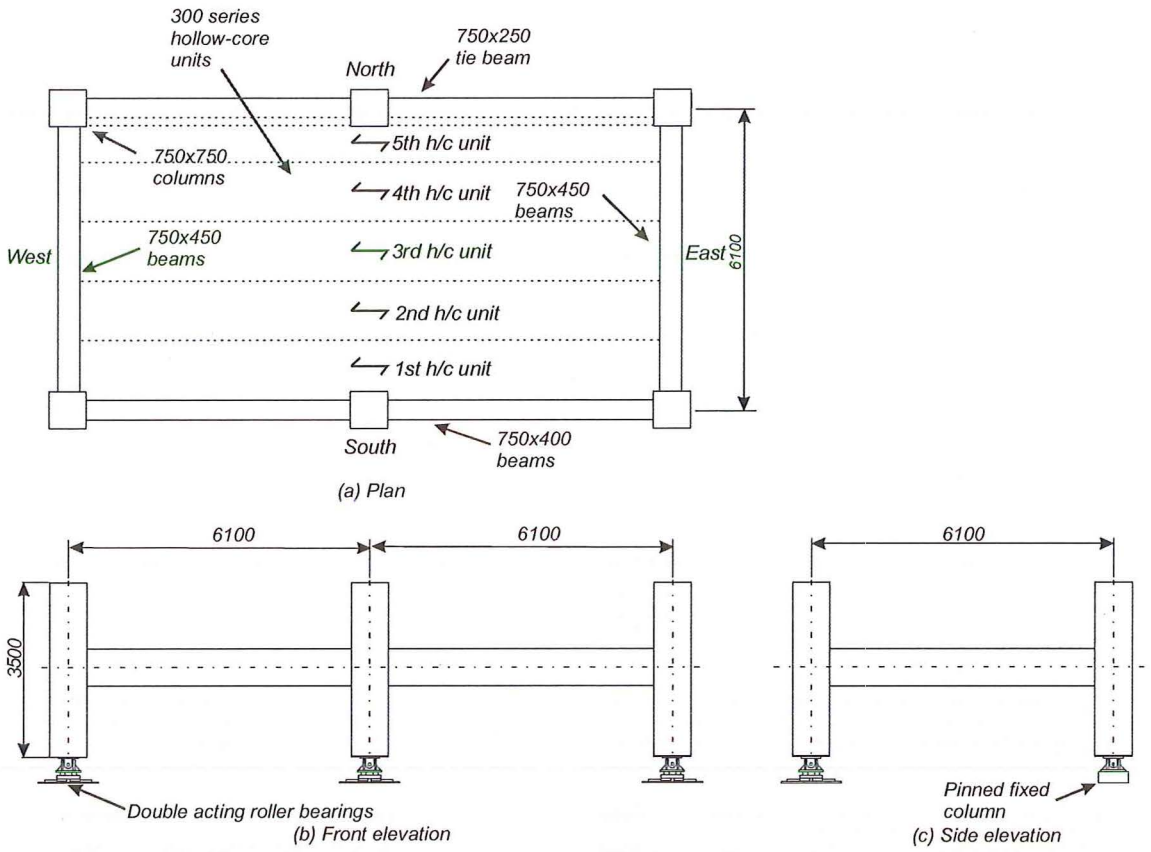

Figure 1-5 A plan and elevation of the super assemblage.

1.5.2 Construction of the super-assemblage

The super-assemblage was constructed as if it would be on a construction site. The top and bottom units of the column were precast, as was the full beam column joint with half beams attached. The mid-span lap splices within the beams, the top half of the precast beams and the cast insitu concrete topping were all poured together to tie the specimen together. This type of construction followed the procedure outlined in the *Guidelines for the Use of Structural Precast Concrete in Buildings* (Centre for Advanced Engineering, 1999).

1.5.3 Precast Prestressed Hollow-core Flooring

Hollow-core floor units are prestressed precast concrete elements extruded using an extrusion machine and "zero slump" concrete. The units themselves are cast on a long bed (up to 100 metres) in one continuous pour and then cut to length once the units have cured. Before the units are extruded a series of prestressing strands are tensioned along the casting bed and then the extruder moves along the bed forming the units (refer to Figure 1-6).

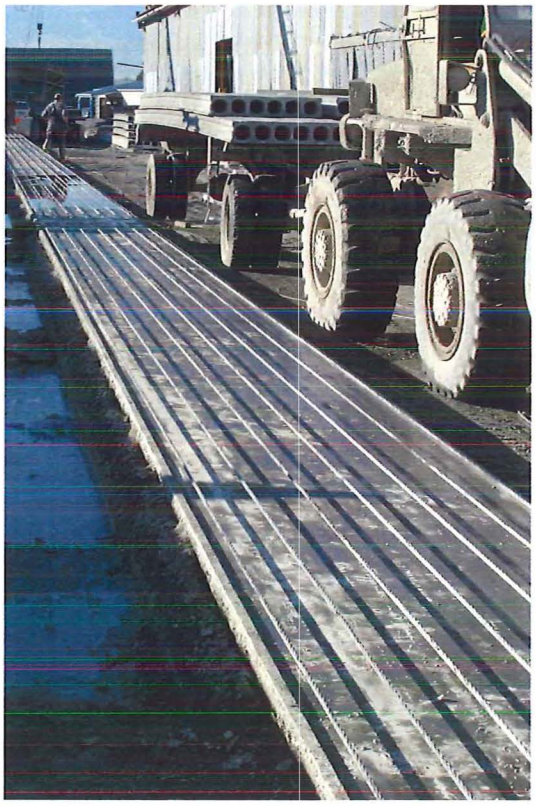

(a) Prestressing strands in place for the units are extruded

(b) Hollow-core unit being extruded

Figure 1-6 Extrusion of a hollow-core floor unit

Hollow-core units are available in various depths. The most common being 200, 300 and 400 mm deep. The units are usually denoted by their depth, i.e. a 300mm deep hollow-core unit is referred to as a 300 series unit. A typical cross section is shown in Figure 1-7 and section properties are given in Table 1-1.

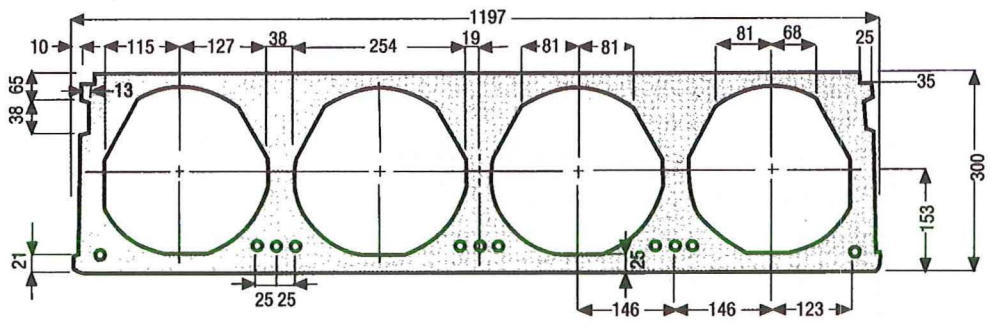

Figure 1-7 A typical cross section for a 300 series unit

Table 1-1 The section properties for a 300 series hollow-core unit

Unit	Area (m^2)	Yb (mm)	I (m^4)	Self weight (kPa)
300 Dycore/Partek	0.1606	153	2.04×10^{-3}	3.20

1.5.4 The connection detail tested

The connection detail to be tested was considered to be the most common connection used in New Zealand since the 1980's. The connection between the hollow-core unit and its supporting beam consisted of seating a hollow-core unit on the cover concrete of the supporting beam. The hollow-core unit is bedded on a mortar/grout pad to create a level seat. The reinforcement detail used to provide continuity across the connection was hooked starter bars spaced at 300mm centres. The starter bars were lapped with cold-drawn wire (non-ductile) reinforcing mesh within the cast insitu concrete topping slab. Figure 1-8 shows the connection detail used.

Although the nominal seat length was 50mm, the actual seat lengths used were 20mm and 40mm at the East and West ends respectively. The reason why the seat length was smaller than nominally specified was because the precast units arrived short in length, as is commonly found to be on site.

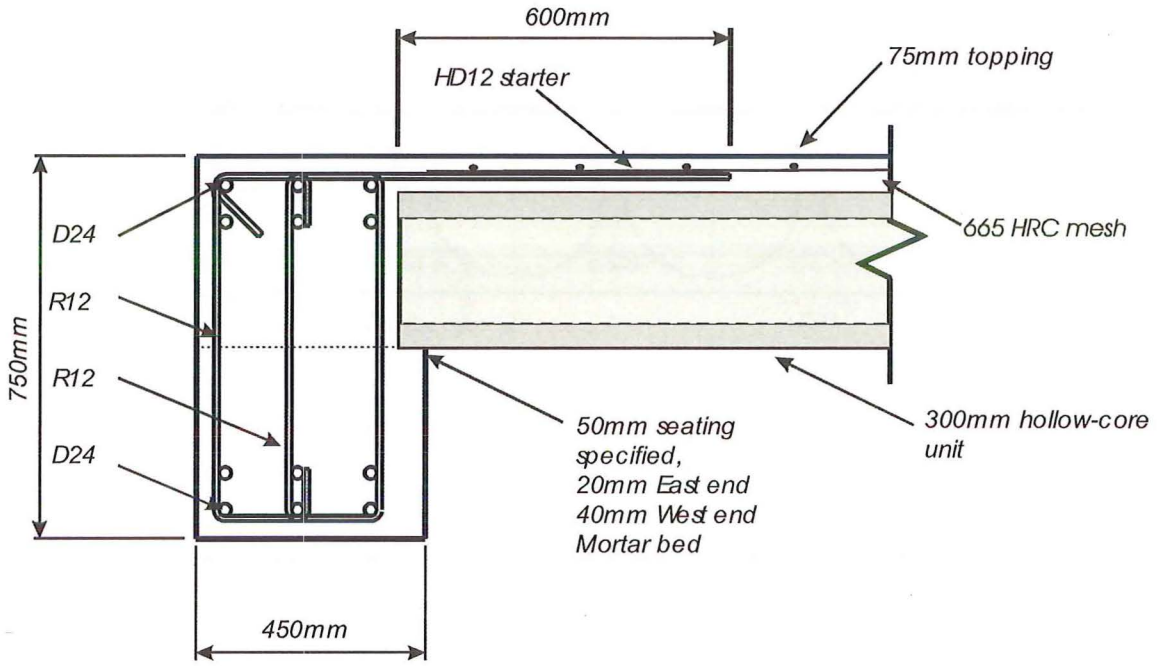

Figure 1-8 The connection detail used to connect the hollow-core units to its supporting beam.

1.6 What then is particularly new in this thesis?

Numerous two-dimensional studies (Mejia-McMaster and Park (1994), Herlihy and Park (2000) and Oliver (1998)) of the connection between a hollow-core floor unit and its supporting beam within a moment resisting frame have been studied. However none of these tests have investigated either the three-dimensional behaviour of this connection of the hollow-core unit to its supporting beam. This research programme designed and built a full-scale three-dimensional super-assemblage to test the affect that some realistic seismic displacements had on a precast concrete moment resisting frame structure incorporating hollow-core floor slabs.

In order to load and displace the super-assemblage a self-equilibrating loading frame was developed as the Department of Civil Engineering Structures laboratory did not have a structural wall that could be used as a reaction frame. The self-equilibrating loading frame was developed so that not only could the super-

assemblage be loaded in two principal directions but it could also be used to test other types of structures provided the new structure had the same general dimensions.

As the super-assemblage was testing an existing type of construction, a new loading history was developed to mimic the displacements that this type of structure would experience during a real earthquake event. This is described in Chapter 2.

A new macro-modelling theory for predicting the amount of beam elongation expected in a moment resisting frame is developed and verified against this current research programme as well as the results from other previous researchers studies. The prediction of beam elongation is particularly important when designing the seat length for precast floor units.

Guidelines for estimating the amount that the floor slab contributes to the lateral strength of the super-assemblage has been developed based on rigid body kinematics. Two types of mechanisms are examined, one for an exterior plastic hinge and another for an interior plastic hinge. The interior plastic hinge mechanism should be used when a prestressed precast unit spans past an intermediate column. For prestressed precast units that are seated on a beam then an exterior hinge mechanism should be used.

When detailing the floor diaphragm for a strut and tie solution a modification is made to the locations of where the struts, that form within a floor diaphragm, should be transferred to the perimeter moment resisting frame. The need for the change is due to the deformation modes that occurred in the super-assemblage during the experimental programme.

Brief comments are made on possible retrofit details that can be used to enhance the performance of the current New Zealand building stock (in an earthquake) that might have potential loss of seating issues. Comments have been

made on some new connection details that should be used for all new construction in New Zealand that incorporate hollow-core floor units.

The key indicator in determining the performance of the hollow-core unit connection detail is the relative rotation between the hollow-core unit and the supporting beam. Within this document this relative rotation has been defined as interstorey drift as the building investigated was considered to be a generic New Zealand moment resisting concrete frame building in which the interstorey drift closely relates to the relative rotation. In terms of predicting the amount of reinforcement slab activated as flange steel within a structure, the relative rotation between the hollow-core unit and the supporting beam should be used. As torsion of the beams supporting the hollow-core units reduces this relative rotation, it is considered conservative to assume that the relative rotation and interstorey drift are one and the same. A designer is reminded that if a true assessment of risk or damage to the floor system is required then the designer should focus on the relative rotation between the hollow-core unit and the supporting beam as it is less conservative that using the interstorey drift as the indicator.

There are so many things

that you really should know.

And that's why I'm bothering

telling you so

Seuss (1982)

1.7 References

Centre for Advanced Engineering, 1999, *Guidelines for the Use of Structural Precast Concrete in Buildings*, Centre for Advanced Engineering, University of Canterbury, Christchurch, New Zealand, 141 pp

Herlihy M.D and Park R, 2000, *Precast Concrete Floor Support and Diaphragm Action*, Research Report 2000-13, Department of Civil Engineering, University of Canterbury, Christchurch, New Zealand.

Holmes W.T and Somers P, 1995, *Northridge Earthquake of January 17, 1994, Reconnaissance Report Vol 2*, Earthquake Spectra, Vol 11

Iverson J.K and Hawkins N.M, 1994, *Performance of Precast/ Prestressed Concrete Building Structures During Northridge Earthquake*, PCI Journal, March-April, Vol 39, No. 2, pp38-55

Mejia-McMaster J.C and Park R., 1994, *Tests on Special Reinforcement for the End Support of Hollow-Core Slabs*, PCI Journal, September-October, Vol 39, No. 5, pp. 90-105.

Norton, J.A, King, A.B, Bull, D.K, Chapman, H.E, McVerry, G.H, Larkin, T.J, Spring, K.C, 1994, *Northridge Earthquake Reconnaissance Report*, Bulletin of the New Zealand National Society for Earthquake Engineering, December, Vol. 27, No.4.

Oliver S. J, 1998, *The Performance of Concrete Topped Precast Hollow-core Flooring Systems Reinforced With and Without Dramix Steel Fibres Under Simulated Seismic Loading*, Master of Engineering Thesis, Department of

Civil Engineering, University of Canterbury, Christchurch, New Zealand, 176pp.

Seuss Geisel, T, 1982, *Oh Say Can You Say*, The New Press, New York

Wyllie L.A and Filson J.R, 1989, *Armenia Earthquake Reconnaissance Report*, Earthquake Spectra, August

Chapter 2

Estimating Seismic Demands for loading structural components in laboratory experiments

2.1 Introduction

When the dependable cyclic capacity of a structural element (or super-assembly) is to be determined from a laboratory experiment there are three areas of particular interest: the displacement amplitude demand; the cyclic loading demand; and how the needs of the two above mentioned demands are met.

The displacement amplitude demand of an experiment should match the drift/displacements expected of a real structure during an earthquake. The location of the structure to the earthquake rupture, local site conditions, its height and natural period will affect the type of shaking experienced. For a near field earthquake a large pulse can be expected whereas for a far field earthquake several smaller drift amplitudes are expected. The magnitude of the shaking of the earthquake experienced will also determine the return period, i.e. is the earthquake considered a relatively frequent or a rare event?

The cyclic loading demand imposed onto a structure is the number of reversing cycles the structure is exposed to at various drift amplitudes during an earthquake. Therefore, the number of cycles imposed on a laboratory experiment is critical in determining the likely performance of a structural element or structure during an earthquake when the experiment is conducted to assess seismic capacity. If too many large cycle amplitudes are imposed then the applied demand will be too harsh and

considered unrealistic, while on the contrary if the number of loading cycles is insufficient then the structure will perform better than it would in a real earthquake event.

Historically, the dependable cyclic capacity of structural elements has been determined in laboratory experiments, such as those undertaken at the University of Canterbury and elsewhere, using a quasi-static ductility-based cyclic loading protocol. The merits of this form of testing, amongst others, has been summarised by Park (1989).

Implicit in this form of testing is the general assumption that the ductility-based loading protocol is sufficient because it is conservative and permits a dependable performance to be obtained. This is in keeping with code-implicit conservative load (or displacement) and resistance factor concepts that comply with $\phi \hat{C} \geq \gamma \hat{D}$ (Cornell et al 2002) where ϕ = drift capacity reduction factor; $\hat{C}$ = median drift capacity; γ = demand amplification factor; and $\hat{D}$ = median drift demand under a prescribed ground motion intensity. When designing new structures, it is appropriate that the foregoing inequality hold.

For existing structural systems, however, it is contended that it is important to assess performance expectations in keeping with probable demands. Therefore, this research questions whether the customary quasi-static ductility-based loading protocols that have historically been adopted are appropriate for the testing of existing construction. A methodology is proposed for defining a displacement history that is more in keeping with probable demands.

If the customary ductility-based loading protocol was to be used in the performance assessment of an experiment, a comparison can be made with results

obtained using the benchmark loading history for contemporary detailing. However, if the specimen being tested performs poorly (under the quasi-static ductility-based loading protocol) then there is the possibility of criticism that the poor performance was due to the unrealistically harsh loading pattern used. This is of particular importance when investigating the likely performance of an existing structure (or structural system). Moreover, the level of ground shaking necessary to cause various intermediate states of damage, may not be easily inferred.

This chapter firstly reviews the literature on probabilistic assessment of drift and cyclic demand. Then a review of the various loading methods available along with discussion on their respective advantages and disadvantages is made. An assessment of the drift amplitude demand using a time history study is undertaken and then verified in terms of the cyclic demand. Finally, brief comment is made on the likely displacement pattern required to experimentally test full-scale portions of structural systems.

2.2 Probabilistic Assessment of Drift Demand

Cornell et al (2002) stated that given a spectral acceleration (S_a) it was possible to predict a drift demand. This is given by

$$D' = a(S_a)^b \qquad \textbf{(2-1)}$$

in which D' = drift demand; a = coefficient determined by non-linear time history analyses and b = 1 for moment frames as found by Luco and Cornell (2000). The assumption of b = 1 is consistent with the well-known equal displacement rule that suggests for moderate period structures (without major strength degradation) the inelastic displacement demands are similar to the demands imposed on a linear

structure as shown in Figure 2-1.

Martínez (2002) shows in Figure 2-2 the variability of results from some 20 earthquake ground motions scaled such that they each have a spectral acceleration of $S_a(T=1sec)=1g$. This variability explains the distribution curves shown in Figure 2-1 showing the spread of results away from the median values expressed by Equation (2-1).

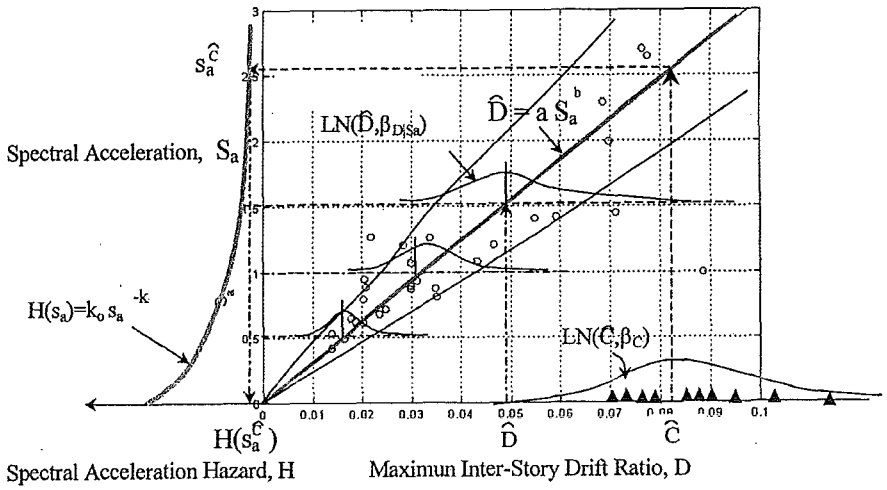

Figure 2-1 Graph showing the linear variation of drift demand verse spectral acceleration (Cornell et al, 2002)

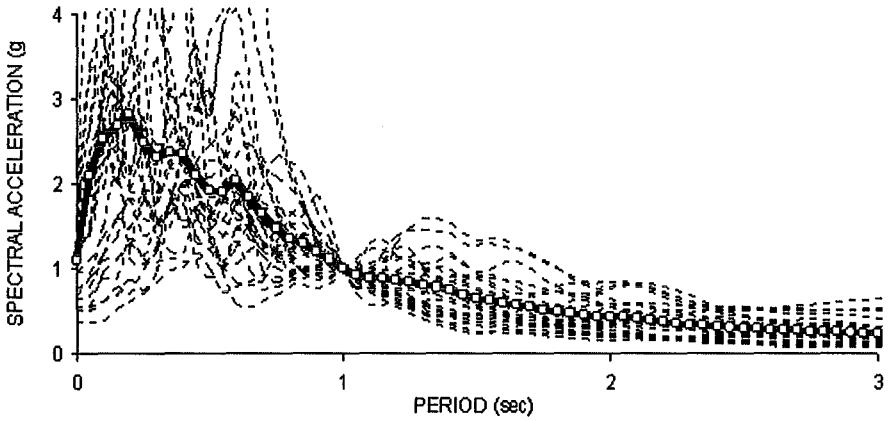

Figure 2-2 An example of the variation in spectral acceleration for various periods (Martínez, 2002)

Cornell et al (2000) suggests that due to this variability, a 90 percent confidence interval be adopted, rather than the median value, when determining a realistic drift demand. This ensures that there is only a ten percent chance that a design demand

drift will not be exceeded during an earthquake.

Luco and Connell (2000) undertook a study on steel moment resisting frame structures. Their results showed an increase between the median result and the 1-sigma value (84th percentile value off a log-normal plot) was approximately 2.0 as shown in Figure 2-3.

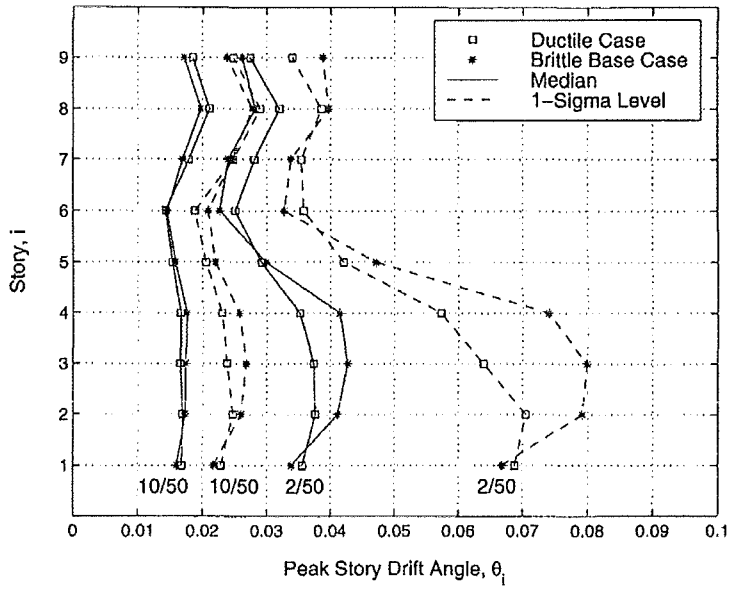

Figure 2-3 Storey height versus peak interstorey drift obtained from Luco and Cornell (2000)

Lee and Foutch (2002) also compared the difference between the median response and both the 84th percentile and 95th percentile values. Their results showed a multiplier between 1.5-2 for the 84th percentile results and a multiplied over greater than 2.0 for the 95th percentile values.

Lupoi et al (2002) used the reliability-based approach for the seismic design and assessment of steel structures developed by Cornell et al (2002) on reinforced concrete structures. Their paper was one of the first attempts to apply this method of assessment to reinforced concrete structures.

2.3 Cyclic Demand

Traditionally, the benchmark for an adequate level of performance of a structure, as stated by the old New Zealand Loadings Code (NZS4203:1984), was that a structure should withstand four cycles of loading to a ductility of four without the strength of the component reducing by 20%. This statement (in terms of the number of cycles) was based on the North-South component of 1940 El Centro earthquake record, as at that time El Centro was one of the few earthquake records available.

To represent this in an experiment a uniform-amplitude deformation history consisting of a certain number of cycles that cause the same damage to the structure as a non-uniform deformation history is required to be determined.

Chang and Mander (1994), Mander and Dutta (1996) and Dutta and Mander (2001) used cycle counting techniques to attempt to equate the damage produced in an earthquake record with the damage produced in cyclic load experiments. The researchers used the concept of an effective constant cyclic amplitude that can be referenced to the design spectral displacement produced for an elastic model of the structure. This approach can be incorporated directly if the experimental programme involves constant amplitude tests; a Miner's approach is required for variable amplitude experiments. These concepts are described below.

Chang and Mander (1994) stated that for an elastic structure the equivalent number of cycles at a spectral displacement could be determined in one of two ways. The method that is used depends on whether the applied cycles are constant or varying in amplitude. For constant amplitude cycles the strain amplitude (ε_a) in the time history is defined by

$$\varepsilon_a = c\left(N_f\right)^b \qquad \textbf{(2-2)}$$

in which N_f = number of cycles to failure at that amplitude, b and c = fatigue coefficients obtained from regression analysis of a number of constant strain amplitude tests.

In the case of variable amplitude tests, two questions are often asked: (i) how is the damage accumulated; and (ii) how to count the various cycles. It is common practice to assume that the damage is accumulated linearly (Miner's rule), therefore, the number of various amplitude cycles, to produce the same level of damage, can be converted into an equivalent constant strain test by equating the damage so that for n cycles (where $n<N_f$), the total damage fraction (D) is

$$D = \sum_i \frac{1}{N_{fi}} = \frac{N_c}{N_{feff}} = \frac{n}{N_{feff}} \qquad \textbf{(2-3)}$$

in which N_{fi} = number of cycles at a given strain amplitude; N_c = equivalent number of a predefined strain amplitude ε_{aeff} (where ε_{aeff} = effective amplitude similar to a root-mean-square (RMS) value of the strain history that inflicts fatigue damage); and N_{feff} number of cycles to failure at the same amplitude.

When examining the results for the 1940 El Centro earthquake it can be seen that the results Chang and Mander (1994) show four cycles of ductility four similar to that assumed by NZS4203:1984. For a one second period structure the El Centro earthquake experiences approximately four cycles of significant displacement (Figure 2-4(a)). In Figure 2-4(a) N_c = number of equivalent elastic cycles as a RMS value. The various lines on the graph refer to different asymmetric values of the displacement history. The results show that the number of cycles is almost independent of the asymmetry of the displacement history. For a 1 second period structure the number of cycles is approximately four.

Mander and Dutta (1996) and Dutta and Mander (2001) coupled with the work

of Chang and Mander (1994) investigated the effective (RMS) number of inelastic cycles of loading. Their results found that an effective inelastic cycle was equal to 70% of the maximum expected displacement. The number of cycles (N_c) at the effective (RMS) amplitude can be estimated by

$$N_c = 7T^{-1/3}; \quad 4 \le N_c \le 20 \tag{2-4}$$

in which T = natural period of the structure. These results are best illustrated as a design envelope as shown in Figure 2-4(b). This envelope was determined using the outer limit values for the number of cycles. Note that $2N_c$ = the number of reversals to failure.

Malhotra (2002) discusses a method to determine the number of significant displacement cycles that can be expected during an earthquake, as the amplitude of the load as defined by the seismic response spectra is not sufficient to evaluate the seismic resistance of the structure. The reason for this is because as the number of load cycles increase the strength, stiffness and energy dissipation generally reduce.

The method of Malhotra (2002) is similar to that proposed Chang and Mander (1994), Mander and Dutta (1996) and Dutta and Mander (2001) above in that it creates a uniform-amplitude deformation history consisting of a certain number of cycles that cause the same damage to the structure as a non-uniform deformation history. Malhotra proposed that the number of equivalent uniform-amplitude deformations (N_{cy}) is determined by

$$N_{cy} = \frac{1}{2}\sum_{i=1}^{2n}\left(\frac{u_i}{u_{\max}}\right)^c \tag{2-5}$$

in which n = the number of half cycles in the time history; u_i = the deformation amplitude for the i^{th} half cycle, u_{max} = the deformation caused by a full cycle of the

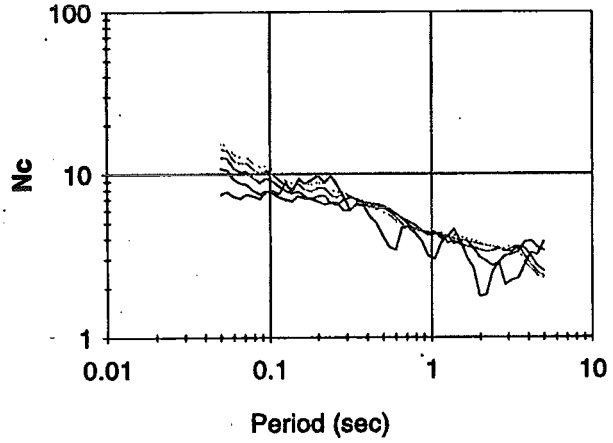

(a) Elastic equivalent number of cycles (Chang and Mander, 1994)

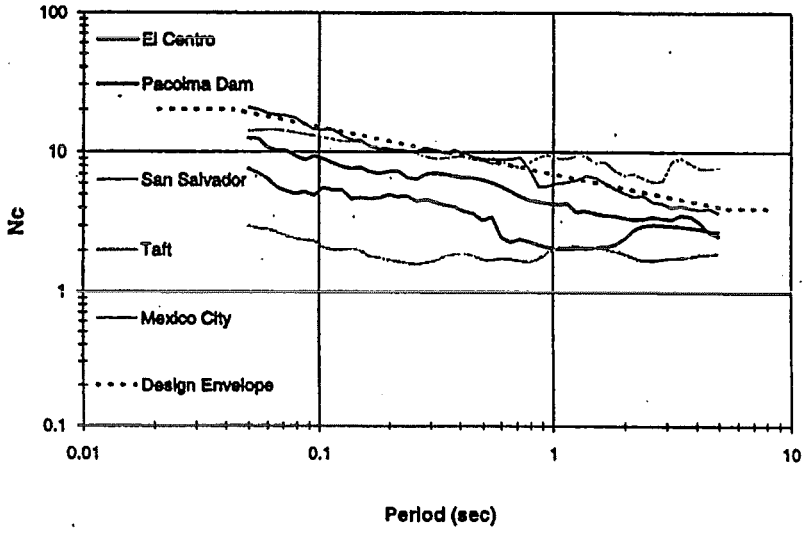

(b) Effective number of inelastic cycles (Dutta and Mander, 2001)

CYCLIC-DEMAND SPECTRUM

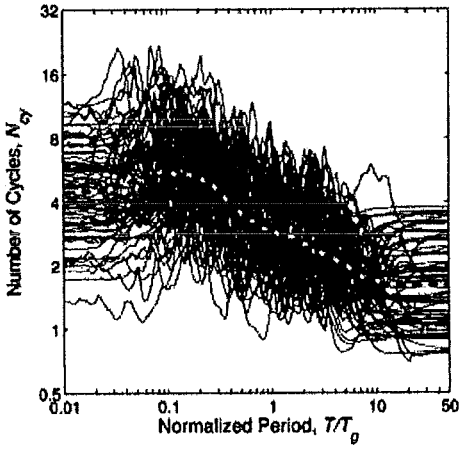

(c) An example of the equivalent number of cycles determined by Malhotra (2002)

Figure 2-4 Summary showing the determination of the cyclic demand by various researchers

largest amplitude; and c = is a structural damage parameter found from experiment (typically equal to 2).

Malhotra states that Equation (2-5) depends on the damage exponent, c, and the shape of the deformation history. The amplitude of the deformation history does not affect Equation (2-5), however, the number of cycles of the deformation history does depend on the effective period and damping of the structure, and the shape of the displacement, velocity and acceleration histories.

An example showing the variability of the results for varying periods is shown in Figure 2-4(c). For the graph the natural period of the structure (T) has been normalised by the ground motion central period, T_g. The central period ground motion is defined as

$$T_g = 2\pi\sqrt{\frac{PGD}{PGA}} \tag{2-6}$$

in which PGD = peak ground displacement; and PGA = peak ground acceleration.

If $T<T_g$ then the structure is considered stiff and if $T>T_g$ then the structure is considered flexible. Figure 2-4(c) shows the results of 71 ground motions with 10% critical damping and c = 2. The dashed line is the average for the 71 motions. The basic trend of these results is similar to that of Chang and Mander (1994), Mander and Dutta (1996) and Dutta and Mander (2001) in that as the natural period of the structure increases the number of cycles reduces due to the structures increased flexibility.

2.4 A Review of Types of Experimental Loading Histories

2.4.1 Quasi-Static Ductility-Based Reversed Cyclic Loading

The quasi-static ductility-based reversed cyclic loading method will herein be referred to as ductility-based loading. This loading method has been summarised by Park (1989).

Most experimental programmes undertaken are loaded by hydraulic actuators in which the strain rate and displacement of a real earthquake is not attempted. Instead the structure is displaced to some predetermined levels of ductility (μ) such as μ=±2, ±4, ±6 and ±8. Due to the slow level of loading, experiments typically take several days to complete. The advantage of this type of loading is that the testing procedure is simple and does not require high-powered computers to control the system. Ductility-based loading gives a conservative underestimation of the structures strength due to the low applied strain rate.

The ductility-based loading protocol has been used to test various sub-assemblages at the University of Canterbury and elsewhere since the 1960's. The loading history consists of loading the specimen to three-quarters of its nominal lateral strength ($\Delta_{0.75}$). Once this is determined then linear interpolation is used to determine a reference or experimental "yield" displacement (Δ_y)

$$\Delta_y = \frac{4}{3}\Delta_{0.75} \qquad \textbf{(2-7)}$$

Once the experimental "yield" displacement is found the target lateral displacement of the sub-assembly associated with the intended displacement ductility can be determined by using the reference yield displacement. The component displacement ductility (μ_Δ) is calculated by

$$\mu_{\Delta} = \frac{\Delta}{\Delta_y} \qquad (2\text{-}8)$$

in which Δ = the displacement; and Δ_y = the experimentally defined or "reference" yield displacement.

The loading sequence itself consists of two completely reversing load cycles at each ductility level of ±2, ±4, ±6 and ±8. This typical loading protocol is shown in Figure 2-5(a). The principal advantages of this method are: (i) element ductility is not structure dependent; (ii) the protocol permits incremental damage to be observed; (iii) the test protocol does not require sophisticated high speed test equipment; and (iv) a conservative (dependable) displacement ductility capacity is obtained.

By contrast, the principal disadvantages of this test method are: (i) excessive demands from lower amplitude cycles may be imposed on components when compared to more realistic cyclic demands; (ii) initial small amplitude loading cycles may impede large load cycle performance; and (iii) the definition of the ultimate member strength may not be clearly defined for the system, therefore it is neither possible to define $\Delta_{0.75}$ (in Equation (2-7)) nor Δ_y, and hence μ_{Δ} is either ill-defined or undefined.

Regarding the latter disadvantage, it has been a more recent custom to abandon the historical ductility-based protocol in favour of a "drift" based protocol. In this method two reversed cycles (sometimes three) of sinusoidal loading are performed at interstorey drift (θ) amplitudes of θ = ±0.5%, ±1.0%, ±2.0%, ±3.0% ... until failure occurs.

2.4.2 Pseudo-dynamic test method

The pseudo-dynamic test method was first proposed by Takanashi et al (1974). The

test procedure is a type of closed loop control where on-line control (of the actuators) and experimental measurements to simulate the dynamic response of a structure are connected via computational modelling of the remainder of the structure.

This test method is summarised by Pampanin et al (2000). By using the initial values of the mass, stiffness and damping matrices the equations of motion for a multi-degree of freedom (MDOF) system is subjected to a dynamic load vector, f(t). A flexibility test is used to calculate the initial stiffness matrix while the damping matrix is analytically modelled. Thus, the resultant displacement vector is applied to the structure and the actuator restoring forces, r(t), are calculated and then fed back into the equations of motion so that the target displacement vector at the next step can be calculated. Figure 2-5(b) shows a schematic of the pseudo-dynamic test procedure.

The advantages of this test method are: (i) the loading follows a specific earthquake closely; and (ii) the likely response of the real structure for the given earthquake is obtained directly.

The disadvantages of this test method are: (i) this type of loading is both structure and earthquake specific; (ii) since one can not be certain that the correct earthquake was chosen, strictly several repetitions of the experiment should be conducted—however, this can rarely be afforded especially for large experiments; and (iii) potential drift problems due to instability problems may occur.

2.4.3 Quasi-Earthquake Displacement (QED) Experimentation

This method of experimental control proposed by Dutta et al (1999) is an closed-loop control method (as explained below) in which the vertical loading and P-Δ effects can be studied. Ahead of the experiment, the seismic displacements and forces are predicted for numerous ground motions by using a non-linear time history

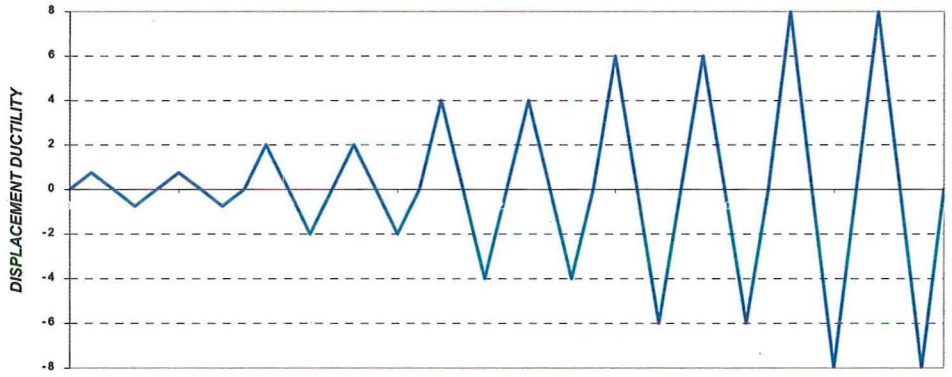

(a) Historical ductility-based loading protocol

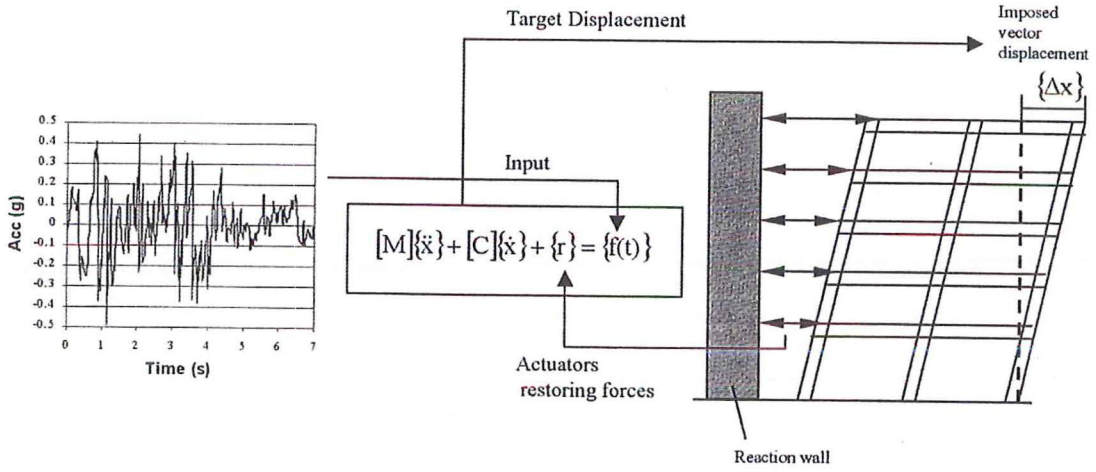

(b) A schematic of the pseudo-dynamic procedure (Pampanin et al, 2000)

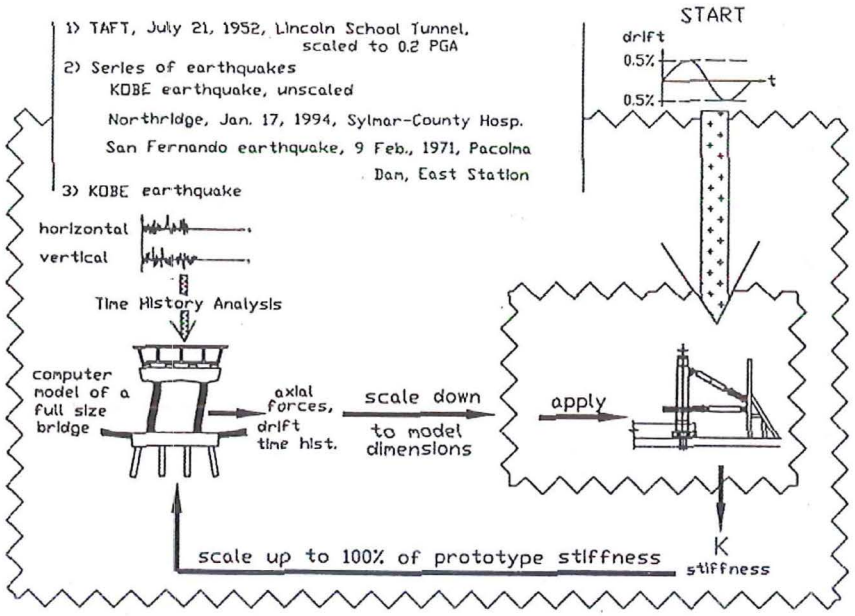

(c) Computational model and the algorithm used in the QED experimentation (Dutta et al, 1999)

Figure 2-5 Comparison of the various loading histories

computational simulation. Then, critical portions of the earthquake motions (of different shaking intensities) are selected and joined together to form an experimental test protocol. This method of loading allows both a full sized and scaled prototype to be modelled by any reasonable inelastic analysis program and to be subjected to a dynamic input. Once the magnitude of the forces and displacements are obtained from the analysis programme the results can then be scaled appropriately and used in the experimental investigation on the model structure. A schematic of the QED procedure is shown in Figure 2-5(c).

Although in principle, this is similar to the above mentioned pseudo-dynamic test method, the principal advantage of the QED approach is it uses a simple open-loop controller that avoids all the attendant problems of closed-loop control. Although the QED method still tends to be structure specific, which is a disadvantage, it has the scope for being generalised for a class of structural systems. The research presented herein seeks to extend the QED approach to a general class of structural system where the bounds on performance demands are set probabilistically.

2.5 Assessment of Drift Demand

As explained earlier in this chapter, the magnitude of the imposed displacement cycles and the number of cycles are the major variables required in determining a realistic loading history. To assess the expected demand for a reinforced concrete structure a time history study was required. This study investigates a number of variables in order to determine the principal structure dependent parameters—that is drift amplitude and cyclic demand. Some additional questions that might arise include: (i) What effect does various height structures have in terms of localised interstorey drift demands? (ii) What affect does a near-field earthquake versus far-field earthquake have on the

localised interstorey drift demands? and (iii) What effect do earthquake records that are scaled by different means have on the localised interstorey drift demands?

2.5.1 Prototype Buildings

The dimensions of the "prototype buildings" investigated herein were based on the dimensions a representative sample of buildings idealised from professional practice as constructed principally in New Zealand from the 1980's through 1990's. Four different height buildings were studied, namely 3, 6, 9 and 12 stories as shown in Figure 2-6. For the purposes of the study, the buildings were assumed square and torsionally stable.

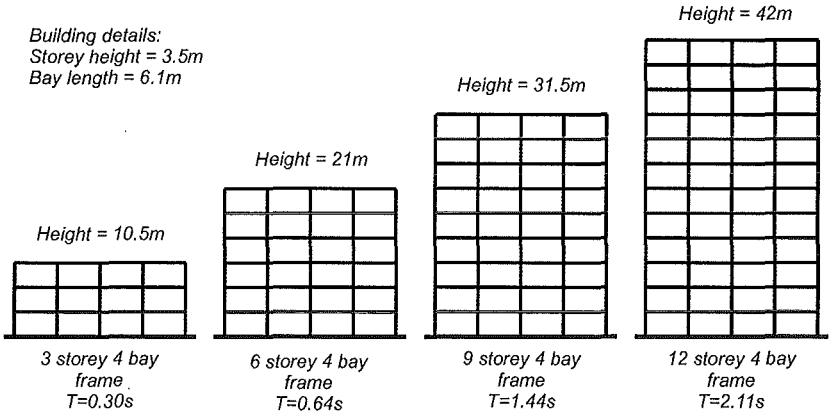

Figure 2-6 Design test buildings

Each building had the following dimensions: Storey height = 3.5m; Bay length = 6.1m; Number of bays = 4; Column dimensions = 750mm×750mm; Beam dimensions = 750mm×400mm; Basic live load = 2.5kPa; Superimposed dead load = 0.75kPa; hollow-core unit used = 300mm deep; and concrete topping slab thickness = 75mm.

The "prototype buildings" were designed as a typical New Zealand precast concrete structure in accordance with the New Zealand Concrete Structures Standard (NZS3101:1995). The member sizes were based on typical dimensions used during the 1980's and 1990's and were associated with a maximum allowable interstorey

drift of two percent. The resulting perimeter beam reinforcement ratios were typically in the order of 0.01 (one percent). Capacity design for the reinforcement details of the frame members was used throughout.

2.5.2 Earthquake records studied

In order to simulate the likely seismic performance of the test buildings, a suite of earthquake records was chosen for the time history analysis. These records included both near and far field effects, since earthquakes of both of these natures are expected within highly active seismic regions, including New Zealand. Listed in Table 2-1 are the various earthquakes along with their peak ground acceleration (PGA), spectral acceleration at the one-second period (F_vS_1), and location of the earthquake and whether it is a near or far field event.

The suite of earthquake records used could be classified into three classes of earthquake. The first are unmodified records, i.e. a true earthquake record such as El Centro 1940 (EL40NSC). The second type of record is one that has been scaled to represent the response spectra for a New Zealand event, such as 4203OLY1. The third type of record is one that has had its record scaled so that the one second fundamental period has an acceleration of 1*g* (an example of this type is SEC1 where $F_vS_1=1g$).

All the records labelled 4203XXX are records that have been scaled to match the design spectra for the New Zealand Loading Standard (NZS4203:1992). All the records have a zone factor of one (Z=1), a structural risk factor of one (R=1) and are based on an intermediate soil condition. Scaling of the records was carried out the following way. Once the response spectra for the given site are obtained (as determined from NZS 4203:1992), the existing earthquake record then has its spectral acceleration adjusted to match that of the design spectra. All the points above the

design response spectra are reduced while the points below the spectra are increased. Once the spectral acceleration is adjusted, it is then possible to generate new spectral acceleration, velocity and displacement graphs. The computer programme called *NZ4203* developed by Carr (2002) scales all the records to the New Zealand design response spectrum as defined by the loadings code, NZS4203:1992. The method by which these records are scaled is based on the *Response Spectrum Compatible Accelerogram* method by Clough & Penzien (1993).

Certain records were scaled such that $F_vS_1=1g$, this is in keeping with emerging United States (US) code practice where design spectra are expressed in terms of spectral ordinates at 0.3 and 1.0 second periods. The one second period was chosen here, as it is the representative period of tall building structures. For such periods the variability between the design spectrum and the records at periods other than one second (i.e. between 0.5 and 2.0 seconds) gives better agreement than using PGA as the principal parameter describing the design spectra.

By having the record scaled for a fundamental period of one second, it ensures that the amount of scatter is limited for structures whose natural period is close to one second. This can be seen in Figure 2-2 where Martínez (2002) has shown a suite of earthquake records that have been scaled to $F_vS_1=1g$. The fundamental periods for the buildings analysed was computed to be 0.30, 0.64, 1.44 and 2.11 seconds for the 3, 6, 9 and 12 storey building frames, respectively as shown in Figure 2-6.

2.5.3 Analysis results

When examining the results from the time history analyses it is possible to look at either the general building performance or the localised floor behaviour. The general building performance focuses on the roof displacement versus time. This gives a

general overview of the buildings performance but does not give the maximum interstorey drift. The building drift (D_b) is defined as

Table 2-1 The suite of earthquakes used for the time history studies.

Record Number	Record Name	Location	Near or far field	PGA (*g*)	F_vS_1
1	EL40NSC	El Centro USA 1940	Far	0.35	0.52
2	TAFTNW	Kern County USA 1952	Far	0.16	0.13
3	SYFF943	Sylmar Northridge USA 1994	Near	0.84	1.05
4	SYLM949	Sylmar Northridge USA 1994	Near	0.8	0.93
5	KOBE95NS	Kobe Japan 1995	Near	0.84	1.23
6	KOBE95EW	Kobe Japan 1995	Near	0.64	1.53
7	4203EC1	El Centro USA 1940	Far	0.338	0.42*
8	4203EC2	El Centro USA 1940	Far	0.362	0.51*
9	4203OLY1	Olympia Puget Sound USA	Far	0.433	0.49*
10	4203OLY2	Olympia Puget Sound USA	Far	0.414	0.5*
11	4203TFT1	Kern County USA 1952	Far	0.433	0.49*
12	4203TFT2	Kern County USA 1952	Far	0.364	0.5*
13	SEC1	El Centro USA 1940	Far	0.683	1.0
14	SSF1	San Fernando USA 1971	Far	0.959	1.0
15	SSF5	San Fernando USA 1971	Far	1.344	1.0
16	SIV1	Imperial Valley USA 1999	Far	1.729	0.83
17	SKB1	Kobe Japan 1995	Near	0.55	0.38
18	SKB2	Kobe Japan 1995	Near	0.517	0.54
19	SNOR1	Northridge USA 1994	Near	0.552	0.78
20	SNOR2	Northridge USA 1994	Near	0.777	0.57

* These records have been scaled to match the design spectrum for NZS4203:1992

$$D_b = \frac{\Delta_{\max}}{H_t} \quad \textbf{(2-9)}$$

in which Δ_{max} = the maximum roof displacement; and H_t = the height of the structure.

However, it is considered to be more important to ascertain the maximum interstorey drift, as this is the principal indicator of structural damage. The storey drift (D) is calculated by

$$D = \frac{\Delta_S}{h_S} \quad \textbf{(2-10)}$$

in which Δ_S = the maximum storey displacement (found by subtracting the displacement between the centre of the storey height above and below the particular floor in question); and h_S = the interstorey height (3.5m for all the structures analysed in this study).

Figure 2-7 shows the difference in results between the overall structural drift and the interstorey drift at the first storey. In general, a trend is evident that demonstrates the local drift is in the order of 100 percent greater than the overall structural drift. This is attributed to a combination of factors including higher mode effects and high shears causing greater deformations in the lower stories.

By examining all the time history results (these can be found in Appendix A), it became clear that there was no common trend between all the various results that aided in the development of the new loading sequence. One issue that was evident was that the number of load cycles applied by the ductility based loading method was significantly more than any of the results from these studies showed. Another issue from the analyses was that there was a noticeable difference between a near and far field event. The near field event usually had one large pulse with several smaller pulses while the far field event had a large number of medium sized pulses. An

example of both of these records is shown in Figure 2-8.

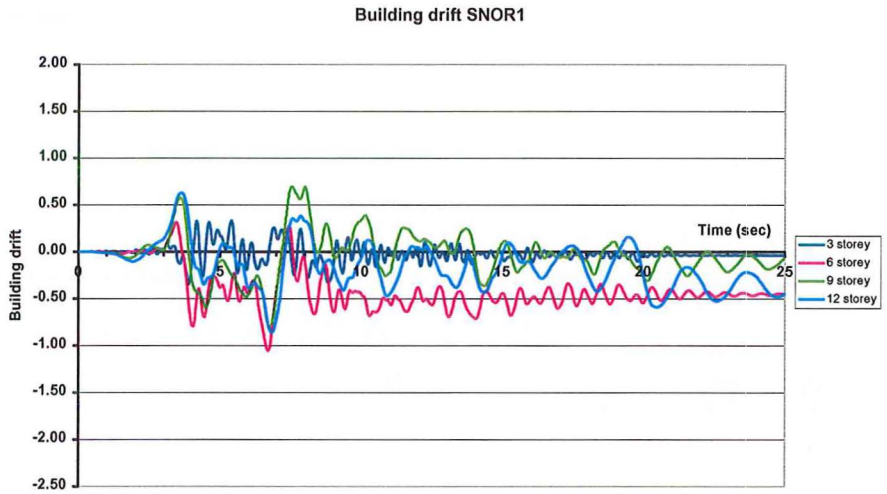

(a) Overall building performance

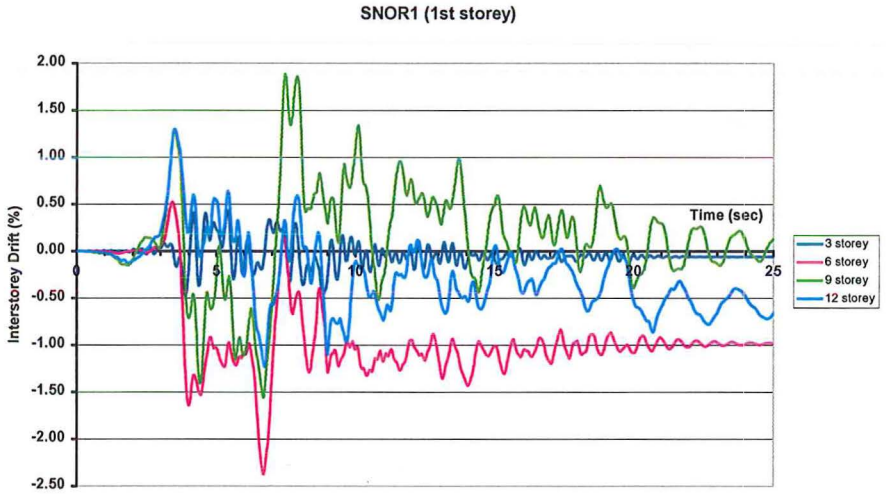

(b) Localised storey performance; in this case for the first storey

Figure 2-7 Comparison between the overall building performance and a localised storey performance.

Most of the results, particularly the near field motions, showed that the structures displaced predominately asymmetrically. Almost all the displacement histories resulted in a residual drift at the end of the record, while the maximum interstorey drifts were larger in one direction compared to the opposite direction. Both of these trends can be seen in Figure 2-8 for the near field response.

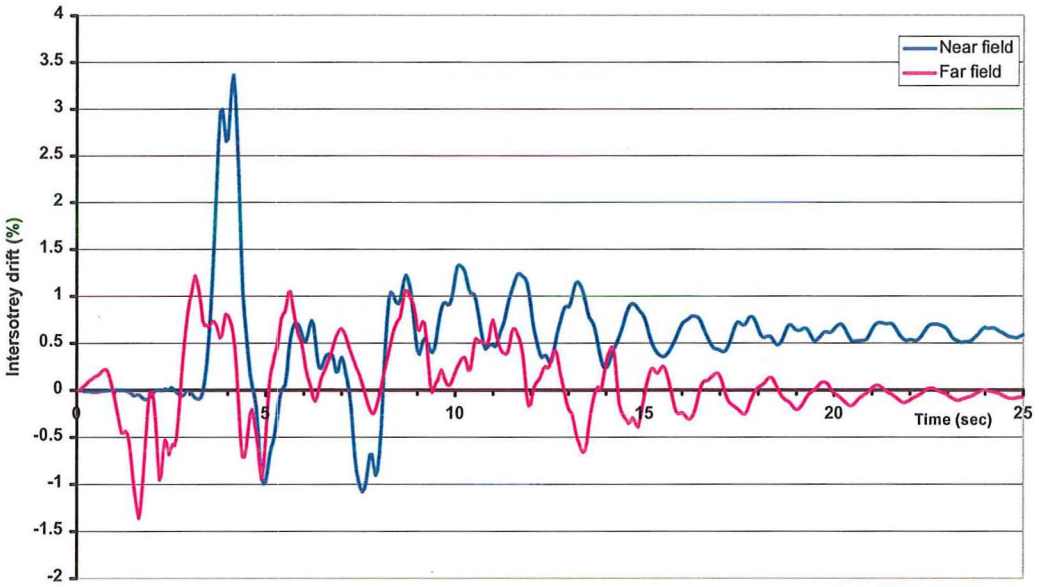

Figure 2-8 Typical results from a near field and far field earthquake (both of these graphs represent the first floor in a nine storey structure)

2.6 Drift demand

Following the time history analyses it became clear that no common trend, in terms of the magnitude of the interstorey drift, could be obtained from the results. Therefore verification was required to ensure that the load/displacement cycles applied were not overly demanding. Firstly, to do this the results needed to be normalised so that all the various forms of earthquake motions had a common variable. The results were normalised by plotting the maximum interstorey drift for each structure height and earthquake versus the F_vS_1 value (the spectral acceleration at 1 second). This value of 1 second was used as a number of the earthquake records had been scaled to experience 1*g* of acceleration for a 1 second period structure. The interstorey drift versus F_vS_1 plots are shown in Figure 2-9. Once plotted it was possible to determine the median values for the spread of results (line of best fit). It should be noted that for the three-storey structure the interstorey drift was plotted against PGA rather than F_vS_1. This was because for low period structures (0.3 seconds in the case of the three

storey structure) the amount of variability in the spectral acceleration is large (Martínez, 2002) as can be seen in Figure 2-2, therefore more meaningful results were obtained if the three storey structures results were plotted against PGA.

The variability of the data presented in Figure 2-9 can be better understood by plotting the results in an alternative form. By assuming b=1 in Equation (2-1) and then rearranging gives

$$a = \frac{D'}{S_a} \qquad \textbf{(2-11)}$$

in which a = drift index parameter.

If the data is ranked from smallest to largest and then plotted in the form of a cumulative distribution the median value (50^{th} percentile) can be found. These results are plotted as data points in Figure 2-10. Also plotted in Figure 2-10 in a continuous curve that is a best fit to a lognormal probability distribution. Only two parameters are needed to describe this distribution, the median (50^{th} percentile), ã, and the lognormal coefficient of variation, β (sometimes called the dispersion factor). From these plots it is evident that the results conform quite well to a cumulative lognormal probability distribution.

The results show values of β =0.60, 0.45, 0.40 and 0.45 for the respective 3, 6, 9 and 12 storey buildings considered. These values of β agree well with the results of Lupoi et al (2002) whose β values ranged between 0.44 and 0.58. From the results, it is evident that to ensure a 90^{th} percentile confidence interval, the observed drifts should be amplified by a factor of least 1.9 above their expected (median) values. It is therefore contended that for dependable seismic performance any experimental assessment of seismic capacity should have a factor of some two times the expected value of the drift demand.

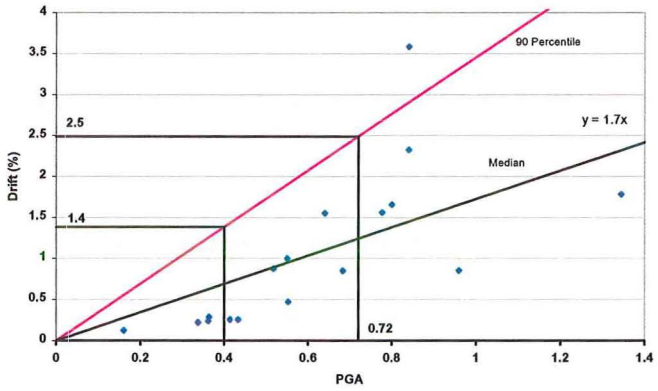

(a) Drift vs PGA for the 3 storey structure

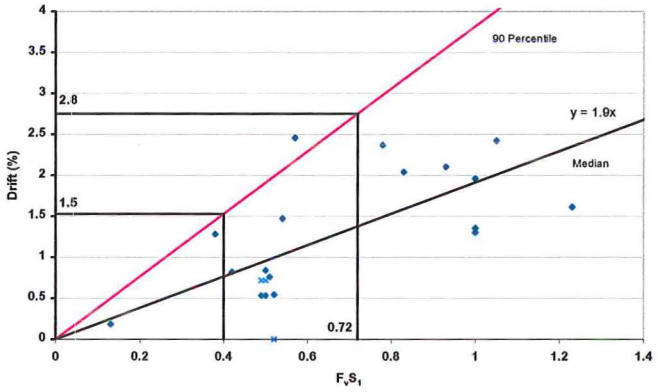

(b) Drift vs F_vS_1 for the 6 storey structure

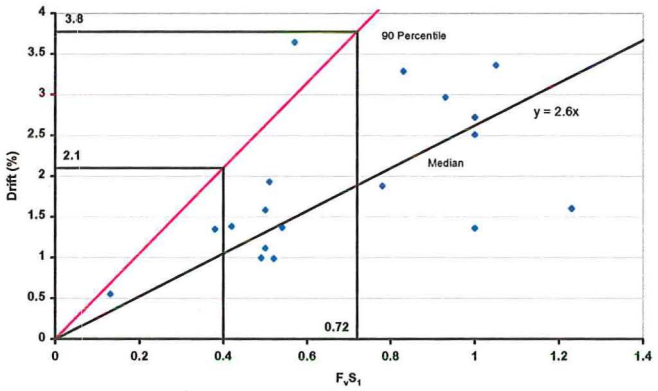

(c) Drift vs F_vS_1 for the 9 storey structure

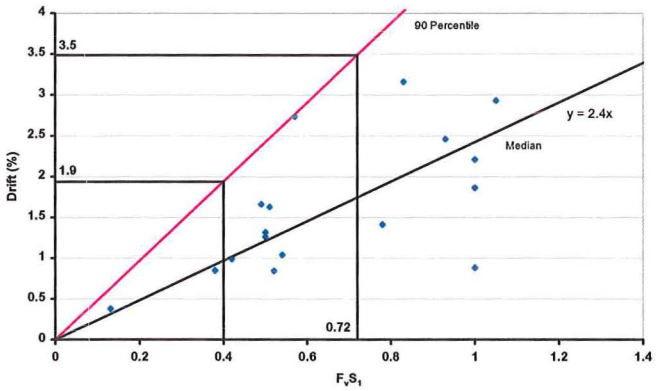

(d) Drift vs F_vS_1 for the 12 storey structure

Figure 2-9 Interstorey drift amplitude versus F_vS_1 (and PGA) plots

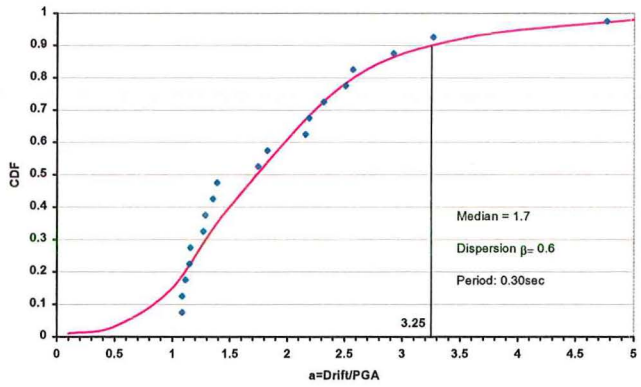

(a) CDF for 3 storey structure

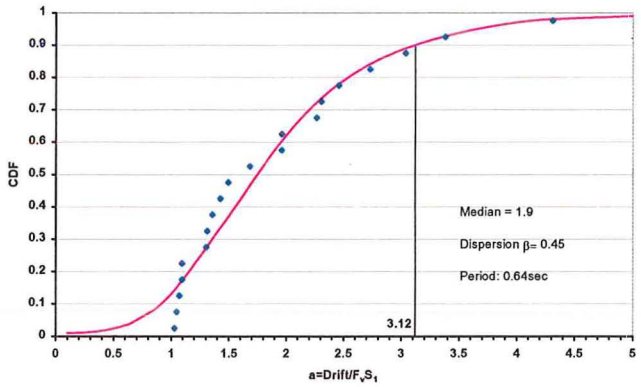

(b) CDF for 6 storey structure

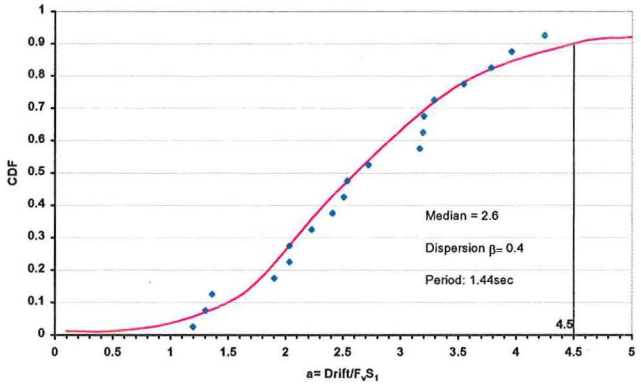

(c) CDF for 9 storey structure

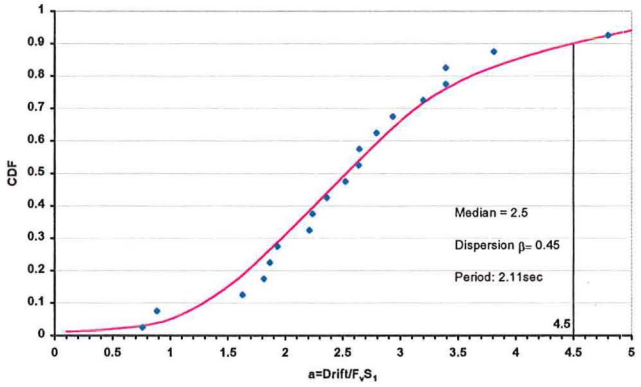

(d) CDF for 12 storey structure

Figure 2-10 Cumulative distribution function plots for all the structures.

By combining all the results into one single plot, Figure 2-11(a), it can be seen that the results are not particularly structure dependent as there is an even distribution of results for each structure. When these results are combined to produce a composite cumulative distribution with a median, $\tilde{a}$=2.0 and β=0.52. Interestingly, the value for β falls in midrange of the aforementioned findings of Lupoi et al (2002), presumably for a completely different suite of earthquake ground motions. Figure 2-11(b) shows that a 90th percentile value of 1.95 (times the median value) is obtained. These results justify the use of a 2.0 multiplier when assigning dependable (confidence) limits.

Although the median line is plotted on the interstorey drift versus F_vS_1 (or PGA) plot a more meaningful line is the 90th percentile value. This gives a dependable upper limit to the interstorey drift for a given F_vS_1 (or PGA) in which there is a probability of exceedance equal to 10%.

Once the 90th percentile lines have been generated on the various plots (Figure 2-9) it was possible to determine the expected interstorey drifts for the different height structures for both a 10% in 50 years, "Design Basis Earthquake (DBE)" and a 2% in 50 years, "Maximum Considered Earthquake (MCE)". The DBE is based on a peak ground acceleration of 0.4g whereas the MCE is equal to 0.72g (1.8×DBE). The multiplier of 1.8 used to convert a DBE to a MCE is determined from the relationship between the structural risk factor and the earthquake return period as set out in NZS4203:1992. These results are summarised in Table 2-2.

From Figure 2-9 it can be seen that the 9 and 12 storey buildings had the largest response from the ground shaking. Therefore, it is proposed that the drift index parameter, a, (from Equation (2-11)) should be taken as 2.5 and the DBE and MCE values are calculated as

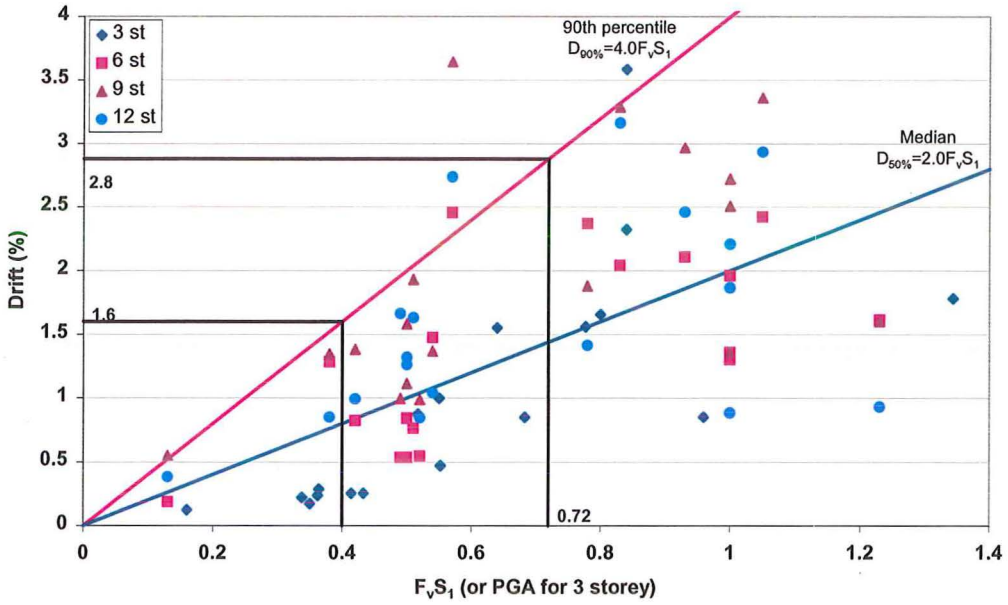

(a) An interstorey drift versus F_vS_1 (and PGA) plot for all the structures

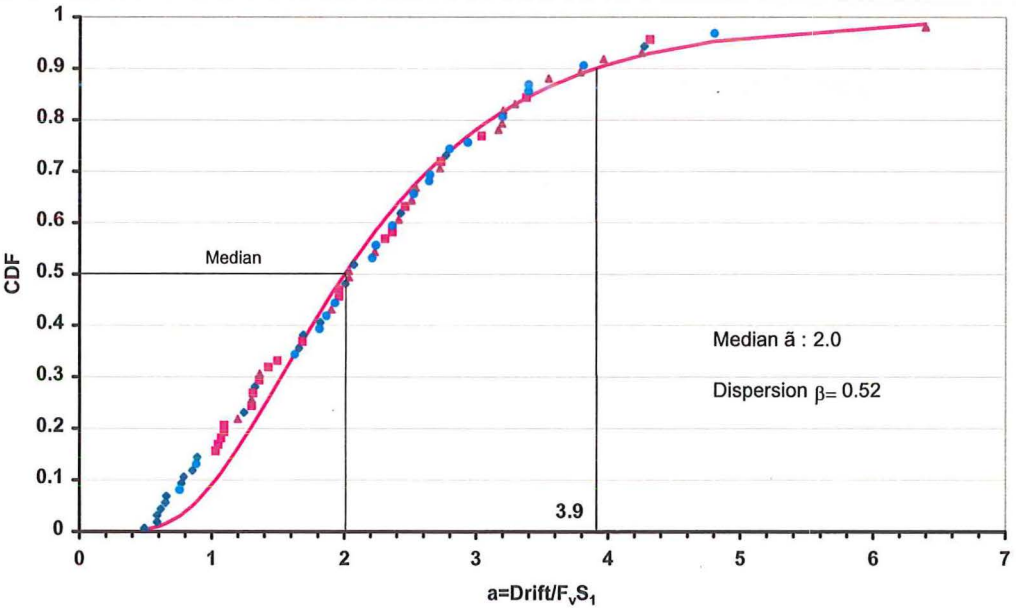

(b) A cumulative distribution function plot for all the structures

Figure 2-11 Combined results for the four different building heights examined

$$DBE \Rightarrow \widetilde{D} = 2.5 \times 0.4 = 1.0\% \quad \textbf{(2-12)}$$

$$DBE \Rightarrow D_{90\%} = 2\,\widetilde{D} = 2 \times 1.0 = 2.0\% \quad \textbf{(2-13)}$$

$$MCE \Rightarrow D_{90\%} = 1.8 \times D_{90\%,DBE} = 1.8 \times 2.0 = 3.6\% \quad \textbf{(2-14)}$$

These values for the DBE and MCE have been added to Table 2-2 as the adopted nominal outcomes.

Table 2-2 The 90th percentile interstorey drifts that correspond to a Design Basis Earthquake (DBE=10% in 50 years) and Maximum Considered Earthquake (MCE=2% in 50 years) for the various height structures

Number of Stories	DBE Drift	MCE Drift
3	1.4%	2.5%
6	1.5%	2.8%
9	2.1%	3.8%
12	1.9%	3.5%
Adopted Nominal Outcome	2.0%	3.5%

2.7 Cycle Verification

Following the determination of the expected drift demand, the number of effective cycles of displacement at the maximum drift amplitude (N_{eff}) as explained by Mander and Dutta (1996) can now be determined by

$$\frac{N_{eff}}{N_c} = \left(\frac{x_{eff}}{x_{\max}}\right)^2 = 0.7^2 \approx 0.5 \qquad \textbf{(2-15)}$$

in which x_{eff} = effective (RMS) displacement; and x_{max} = maximum displacement amplitude. 0.7 was obtained from the study undertaken by Mander and Dutta (1996).

By substituting the result from Equation (2-15) into Equation (2-4) N_{eff} becomes

$$N_{eff} = 3.5T^{-1/3} \; ; 2 \le N_{eff} \le 10 \qquad \textbf{(2-16)}$$

For the structures analysed the effective (RMS) number of cycles equates to 5.2, 4.1, 3.1 and 2.7 for the 3, 6, 9 and 12 storey structures, respectively. When

examining the time history results in Figure 2-12 and Appendix A these trends can be observed.

From Section 2.6, a value of 2.0% was obtained for a Design Basis Earthquake. Knowing the maximum DBE drift, a new loading history can be proposed (refer to Chapter 4 for the details on the proposed loading history) and then checked using Equation (2-17), a modified Equation (2-15), to ensure that the $\sum N_{eff}$ lies within the limits for the maximum and minimum number of equivalent cycles. The individual drift maxima to be used in the proposed loading history along with $\sum N_{eff}$ are shown in Table 2-3.

$$N_{eff} = N_c \left(\frac{D}{x_{\max}} \right)^2 \qquad \textbf{(2-17)}$$

in which D = drift amplitude imposed during the loading cycle; and $x_{max} = 2.0\%$

As reported earlier for the 3, 6, 9 and 12 structures analysed the effective (RMS) number of cycles equates to 5.2, 4.1, 3.1 and 2.7, respectively. The $\sum N_{eff}$ results in Table 2-3 at the end of the loading history agree well with these values.

Table 2-3 Equivalent number determined using a low cycle fatigue basis

Drift Amplitude, D	$N_{eff} = N_c \left(\frac{D}{2.0} \right)^2$	$\sum N_{eff}$
0	0	0
0.5	0.03	0.03
-0.5	0.03	0.06
1.0	0.06	0.12
-1.0	0.06	0.18
2.5	0.78	0.96
-2.0	0.50	1.46
3.5	1.53	2.99
-3.5	1.53	4.52

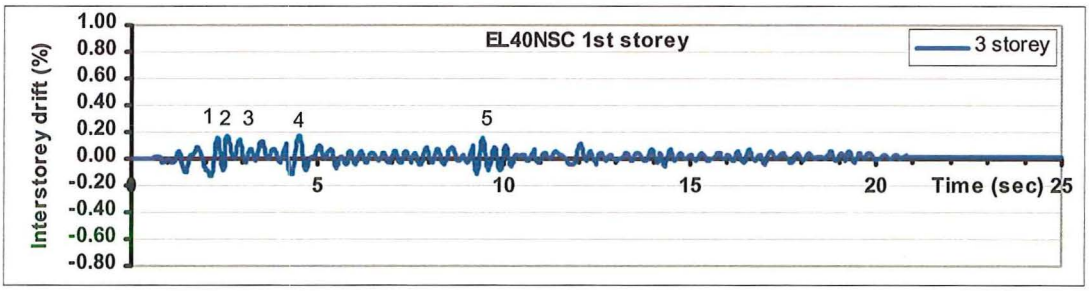

(a) 3 storey building response showing 5 peak cycles

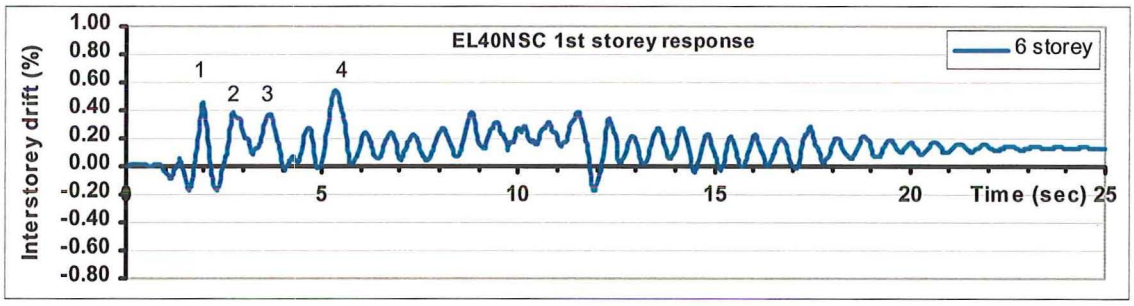

(b) 6 storey building response showing 4 peak cycles

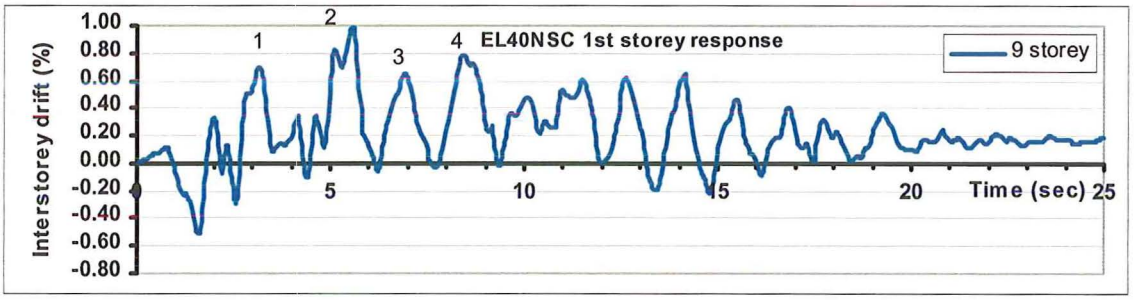

(c) 9 storey building response showing 4 peak cycles

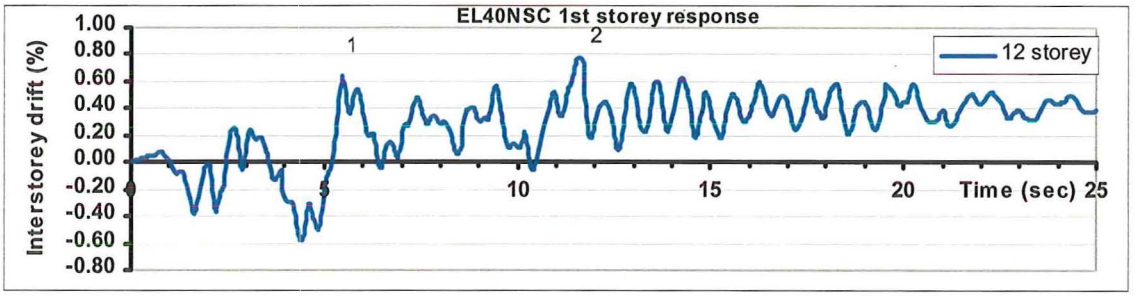

(d) 12 storey building response showing 2 peak cycles

Figure 2-12 Interstorey drift versus time plot for the four prototype buildings showing first storey response for the 1940 El Centro earthquake.

2.8 Concluding Remarks

Existing methods of assessing dependable capacity of structural elements, such as the ductility-based loading protocol, should not be used in the seismic assessment of existing structures—particularly those with critical structural weaknesses. This is because it is important to relate damage states back to expected seismic demands necessary to cause these states of damage.

This study has shown that there are two important facets of seismic assessment of existing structural systems: (i) the seismic displacement (or interstorey drift) demand for which there is a 90 percent confidence this will not be exceeded; and (ii) the effective number of cycles of loading at the maximum displacement.

It is shown herein, that although structures may have been designed for a 2.0% interstorey drift limit due to material property characteristics and in-built over-strength, on average the seismic demand for a Design Basis Earthquake (10% in 50 years) will be in the order of only 1.0% drift. However, there is a wide range of possible results and to be 90 percent confident that all possibilities are captured, then the demand drift is 2.0%.

There is an international trend of best practice that is emerging toward using the 2% in 50 years (approximately 2500 year return period) as the maximum considered earthquake (MCE). For a 90% confidence of assessing the demand for such an event the interstorey drift is 3.6%.

The results of the research undertaken by Luco and Cornell (2000) and Lee and Foutch (2002) are in keeping with the current observations where a multiplier of 2.0 was used to determine the 90^{th} percentile values from the median values.

Using cycle counting methods it is possible to ensure that any displacement

history proposed for structural testing of components with critical weaknesses is reflective of the performance from a range of earthquake demands including near and far-field effects.

2.9 References

Carr A.J, 2002, *NZ4203 program*, Computer program library, Department of Civil Engineering, University of Canterbury

Chang G.A and Mander J.B, 1994, *Seismic Energy Based Fatigue Damage Analysis of Bridge Column: Part II-Evaluation of Seismic Demand*, Technical Report NCEER-94-0013, National Center for Earthquake Engineering research, State University of New York at Buffalo

Clough R.W and Penzien J, 1993, *Dynamics of Structures, second edition*, McGraw-Hill

Cornell C.A, Jalayer F, Hamburger R.O and Foutch D.A, 2002, *Probabilistic Basis for 2000 SAC Federal Emergency Management Agency Steel Moment Frame Guidelines*, ASCE Journal of Structural Engineering, April, pp 526-533

Dutta A and Mander J.B, 2001, *Energy Based Methodology for Ductile Design of Concrete Columns*, ASCE, Journal of Structural Engineering, December, pp 1374-1381

Dutta A, Mander J.B and Kokorina T, 1999, *Retrofit for Control and Reparability of Damage*, Earthquake Spectra Vol 15, No. 4, November

Lee K and Foutch D.A, 2002, *Seismic Performance Evaluation of Pre-Northridge Steel Frame Buildings with Brittle Connections*, ASCE Journal of Structural Engineering, April, pp 546-555

Luco N and Cornell C.A, 2000, *Effects of Connection Fractures on SMRF Seismic*

Drift Demands, ASCE Journal of Structural Engineering, January, pp 127-136

Lupoi G, Lupoi A and Pinto P.E, 2002, *Seismic Risk Assessment of RC Structures with the "2000 SAC/FEMA" Method*, Journal of Earthquake Engineering, Vol. 6, No 4, pp 499-512

Malhotra P.K, 2002, *Cyclic-demand spectrum*, Earthquake Engineering and Structural Dynamics, Vol 31, pp 1441-1457

Mander J.B and Dutta A, 1996, *A Practical Energy-Based Method Design Methodology for Performance Based Seismic Engineering*, Proceedings for the 65th Annual SEAOC Convention, Maui Hawaii, pp 319-338

Martínez M.E, 2002, *Performance-Based Seismic Design and Probabilistic Assessment of Reinforced Concrete Moment Resisting Frame Structures*, Master of Engineering Thesis, Department of Civil Engineering, University of Canterbury, Christchurch, New Zealand

NZS3101:1995, *Concrete Structures Standard-The Design of Concrete Structures*, Standards New Zealand, Wellington New Zealand

NZS4203:1984, *Code of Practice for General Structural Loading for Buildings*, Standards New Zealand, Wellington, New Zealand

NZS4203:1992, *Code of Practice for General Structural Loading for Buildings*, Standards New Zealand, Wellington, New Zealand

Pampanin, S., Priestley, M.J.N, Sritharan, S., 2000, *Precast Seismic Structural Systems: PRESSS Phase 3. The Five Story Precast Test Building. Vol 3-4. Frame Direction Response,* SSRP Report 2000/08, University of California, San Diego.

Park R., 1989, *Evaluation of ductility of structures and structural assemblages from*

laboratory testing, Bulletin of the New Zealand National Society for Earthquake Engineering, Vol. 22, No. 3, Sept, pp 155-166.

Takanashi K et al, 1975, *Nonlinear Earthquake Response Analysis of Structures by a Computer-Actuator On-Line System*, Bulletin of Earthquake Resistant Structure Research Center, Institute of Industrial Science, University of Tokyo, No. 8

Chapter 3

Design and Construction of a Self-Equilibrating Lateral Loading Apparatus for Conducting Full Scale Experiments on Structural Super-Assemblies.

3.1 Introduction

Structural experiments have historically focused on testing one-dimensional (1D) or two-dimensional (2D) sub-assemblages of beams and columns. Less effort has been placed on investigating full three dimensional (3D) performance due to the high cost, large time commitment and significant laboratory space demands. Consequently, most laboratory infrastructure has been geared to test specimens less than 4 metres in height without the need for elaborate strong-wall and strong-floor systems.

Testing a full-scale 3D indeterminate structural system automatically captures second order effects that are usually not possible to account for during a two dimensional test. However, to capture these effects, it is important that the boundary conditions be carefully modelled in the experimental process. This chapter discusses certain difficulties in the abstraction of a structural model from a prototype precast concrete building system and the development of experimental apparatus that permits large lateral forces to be applied without the need of a strong-floor or strong-wall system. Of particular concern when testing concrete structures is to freely permit beam elongation (due to both elastic and inelastic behaviour of a reinforced concrete beams under bending) to occur. To achieve this it is necessary to avoid the restraint that has been reported in the past in some experimental set ups.

This chapter first describes previous experimental work and critically reviews the shortcomings in the experimental process. It then goes on to describe the development of the experimental infrastructure for the lateral loading of a two-bay by one-bay precast concrete super-assemblage.

3.2 Findings From Previous Work

Zerbe and Durrani (1989, 1990) undertook two series of experiments investigating the performance of an indeterminate structure with and without a floor slab. Their test specimens consisted of a one storey-two bay frame of reduced scale as shown in Figure 3-1 (overall dimensions of the test specimen: 1.2 m tall by 2.1 m long). Due to the test set up, any beam elongation that tried to form was restrained since the column bases were fixed and the tops of the columns were attached to a rigid header beam. The restraint of the beam elongation lead to an artificially high lateral load resistance of the frame as the beams had large compression forces induced within them. This restraint cannot be expected to form in a real moment resisting frame anywhere to the same extent as it occurred in this experiment. The exception is that of the first floor beams as the foundation beams provide some restraint to the elongation of the first floor beams via the columns of the first storey (Fenwick et al 1995). This restraint of the beam elongation meant that Zerbe and Durrani underestimated the amount of beam elongation expected.

Fenwick and Megget (1993) undertook a series of experiments to investigate the difference between uni-directional and reversing plastic hinges. The test comprised of articulating a beam attached to a rigid end block. From the results two equations were fitted to the experimental results for predicting beam elongation. Typically the beam elongation that formed ranged between 2-5% of the beam depth.

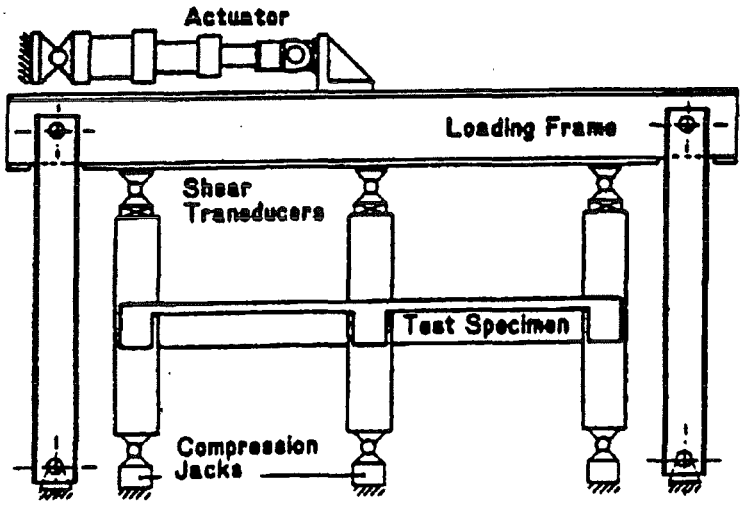

Figure 3-1 The experimental set up of Zerbe and Durrani (1989, 1990)

Restrepo et al (1993) undertook a series of experiments to investigate the performance of varying mid-span lap splices in precast concrete beams. The test comprised of laterally displacing a determinate precast concrete H frame (without a floor slab). As a result of the reversing cyclic loading the H frames grew in length. Restrepo et al (1993) then developed upper and lower bound equations for predicting beam elongation by fitting an equation to the experimental results.

Fenwick et al (1995) undertook some experimental research that consisted of the testing of a 1/3 scale, three-bay moment resisting frame. Two tests were untaken, one focusing on the frame without a slab, the other with a slab. The experimental set up is shown in Figure 3-2(a).

By having the bases of the columns fixed meant that beam elongation would be restrained (this is appropriate for the first floor of a structure as the foundation beam does not hinge). The final displaced shape (Figure 3-2(b)) of the structure was one that was not expected to occur in reality; the authors acknowledged this. Nevertheless these results were more realistic than those seen by Zerbe and Durrani.

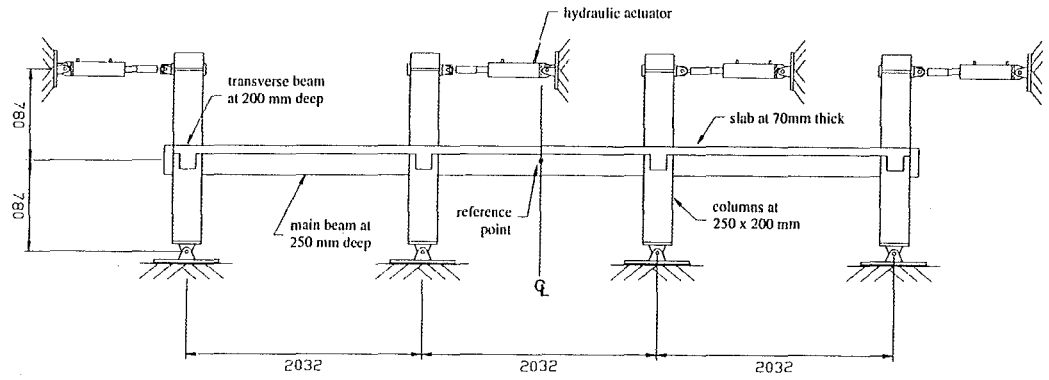

(a) Experimental set up

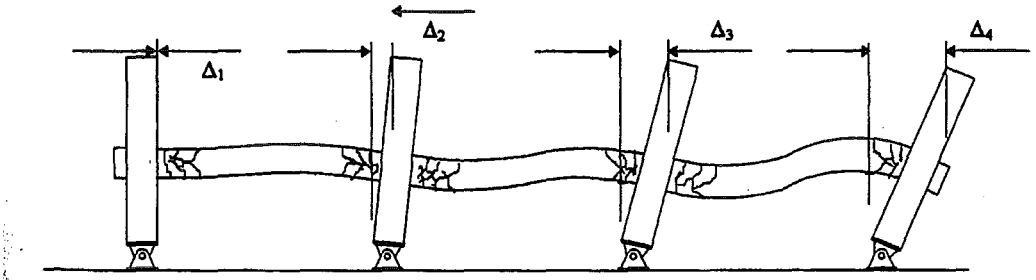

(b) Displaced shape of the test specimen at the completion of the experimental programme

Figure 3-2 Fenwick et al (1995) experimental set up and displaced shape.

The results of Fenwick et al (1995) have shown that the effect of the slab greatly increased both the initial stiffness and the overall strength of the system. The amount of elongation that occurred was similar to the expected amount of 2-5% of the beam depth (stated as the expected amount of beam elongation by both Fenwick and Megget (1993) and Restrepo et al (1993)). The slab did not appear to restrain the beams from elongating. This was due to the majority of the slab reinforcement fracturing during the test. This fracturing was predominately due to two effects: (i) the size affect (the bond of the reinforcing was extremely good due to its small bar size, larger bars would require larger bond stresses and a redistribution of strain, relieving the localised concentrations that lead to the fracturing of the reinforcement); and (ii) since the exact type of bar was not possible the bars used needed to be heat treated. Consequently, although the bars had an appropriate yield stress, the ultimate tensile

strain was poor, hence tensile fracture occurred much earlier than would normally be expected.

Fenwick et al (1996) continued on from the previous work of Fenwick et al (1995). Again, a 1/3 scale model building was constructed, but this time it was three bays and two storeys tall without a floor slab. Figure 3-3 shows the experimental set up for the testing programme. The experimental results tended to show that the first floor beams generated large compression forces while the second floor beams went into tension. The compression forces in the first floor beams were due to the rigid, non-hinging, foundation beam restraining the growth (elongation) of some of the beams of the first floor.

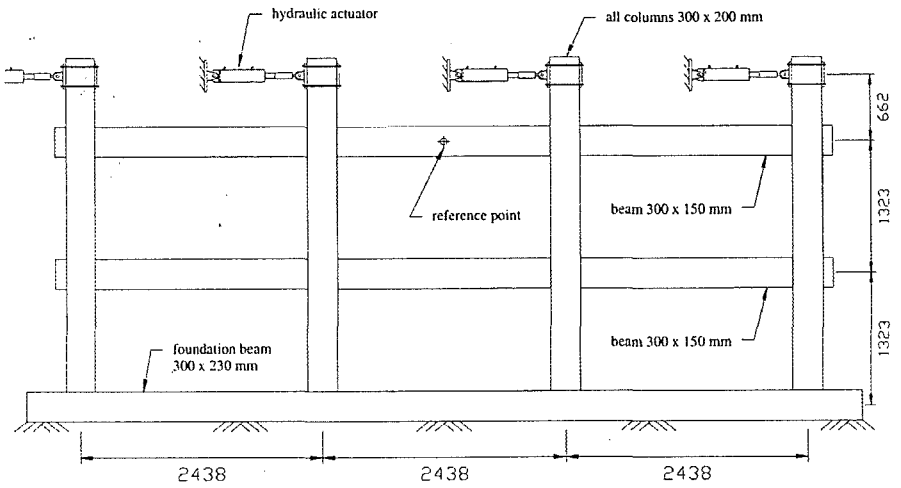

Figure 3-3 Experimental set up for Fenwick et al (1996)

Due to the loading procedure used, the overall beam elongation was restrained as the imposed displacements on the structure at various displacement ductility levels was determined from the yield displacement of the frame and it appeared that the researchers did not make any allowance for beam growth that was likely to have occurred during the experimental programme.

Lau (2001) tested three structures consisting of four bays. Two of the tests were undertaken without a floor slab and one that contained precast prestressed units. This research has shown that the floor slab restrained the beam elongation. This restraint increased the beams flexural capacity due to the axial compression forces generated within the beams. A typical set up for the experiment is shown in Figure 3-4(a). The frame was 1/3 scale with a precast prestressed rib and infill flooring system.

The manner in which this test specimen was displaced was a lot more realistic than compared to some of the earlier work described above. Figure 3-4(a) shows that the bases of the columns are not fixed to the structural floor but have hydraulic actuators attached to allow for adjustment. The experimental programme displaced the structure in such a way that all the columns were at the same inclination while ensuring that the sum of the applied shear forces at the top and the bottom of the columns across the bent were equal. This is a much closer representation of what is required to load the test specimen correctly but this still has some drawbacks. The main drawback is that although the sum of the column shears across the bent equates to zero the individual beams still have relatively large axial forces induced. Figure 3-4(b and c) gives a snapshot of lateral forces that lead to the resulting beam compressions; the compression forces indicated that the beams were restrained against some of the elongation that may occur.

The previous investigations summarised above have shown the importance of beam elongation in seismic resistant structural frames. This phenomenon is of particular importance in the assessment of precast concrete frames and floor systems as the floors can potentially be unseated under large frame side sways. Consequently, when undertaking physical experiments it is essential that the beam elongation

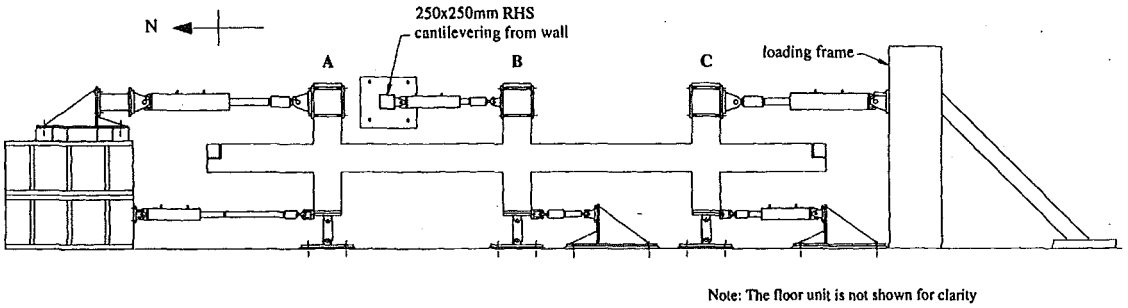

(a) Experimental set up

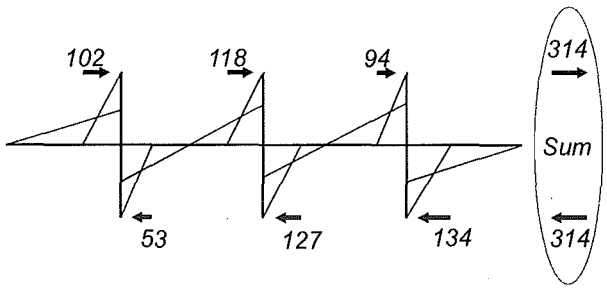

(b) Snapshot of applied loading

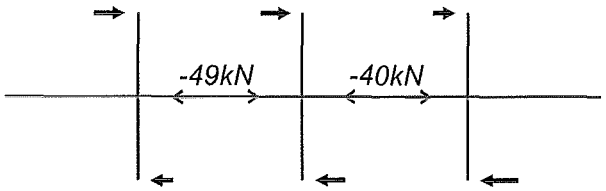

(c) Axial compressions generated within the beam

Figure 3-4 Experimental set up used by Lau (2001)

behaviour be permitted to develop in a way as close as possible to that of a real structure. That is, the lateral loading system should neither exaggerate nor restrain beam elongation.

During an earthquake the columns of a multi-storey building should remain reasonably parallel; the exception being the columns of the first storey. This is based on the assumption that the beams of the floors above and below the beams of the floor of interest will also elongate the same amount. Generally, this assumption will hold with the exception of the ground floor and perhaps the roof (occasionally the roof has beams that are designed not to hinge).

In what follows is a description of the experimental apparatus that was devised to test a full-size super-assemblage portion of a multi-storey precast concrete building. The primary focus has been to ensure that the above mentioned shortcomings regarding beam elongation and its associated secondary effects of axial compression forces in the beam members are overcome.

3.3 Loading Development to Accommodate Beam Elongation

To correctly reproduce the loading conditions on a multi-bay test assemblage the following three criteria need to be satisfied: (i) the correct displaced shape is imposed; (ii) the correct bending moments are applied to the beams; and (iii) beam elongation is neither restrained nor exaggerated. Regarding the latter, Figure 3-5 presents the elongation requirements for beams. Figure 3-5(a) and (b) show the cases where a net tension or compression exists respectively, resulting in the promotion and restraint of beam elongation. Such restraint forces must be eliminated such that $V_{top} = V_{bot}$, as shown in Figure 3-5(c). This then permits the beam to elongate without interference from the experimental rig. This is particularly important when plastic deformations exist within the beams, as shown in Figure 3-5(d).

Figure 3-6 presents the reasoning behind a sub-structure necessary to form a storey super-assemblage for an experimental investigation. If using capacity design and a strong column-weak beam philosophy is assumed, this exercise is relatively simple, as the column design (size of columns and reinforcement ratios) will be dictated by the floor and beam over-strength flexural capacities.

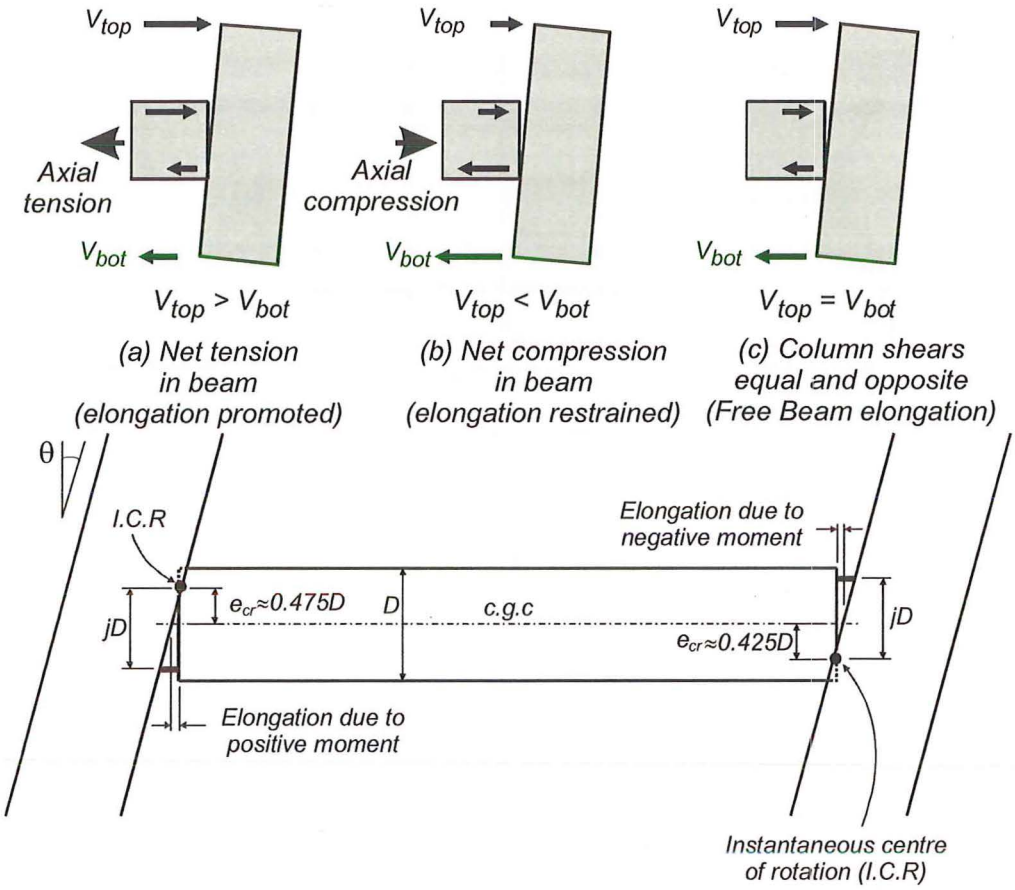

(d) The kinematics of elongation for an entire beam

Figure 3-5 Elongation of concrete beams based on rigid body rotations

The test rig developed for this large scale experiment is a complex set up as it is required to apply realistic forces to the structure so that the specimen deforms in the correct manner. Care has to be taken to ensure that any beam elongation that develops during the course of the experiment is neither exaggerated nor restrained by the lateral loading apparatus.

The fundamental component ensuring that beam elongation is neither exaggerated nor restrained is the applied column shear forces. The column shear forces induced in a building during an earthquake (for analysis purposes) are idealised as a series of vectors up the building height. This is illustrated by developing a typical shear force diagram for a building as given in Figure 3-6(a). The horizontal steps in the shear force diagram are due to the floor inertia forces and any forces resulting from the interaction of the lateral force resisting structures around the building

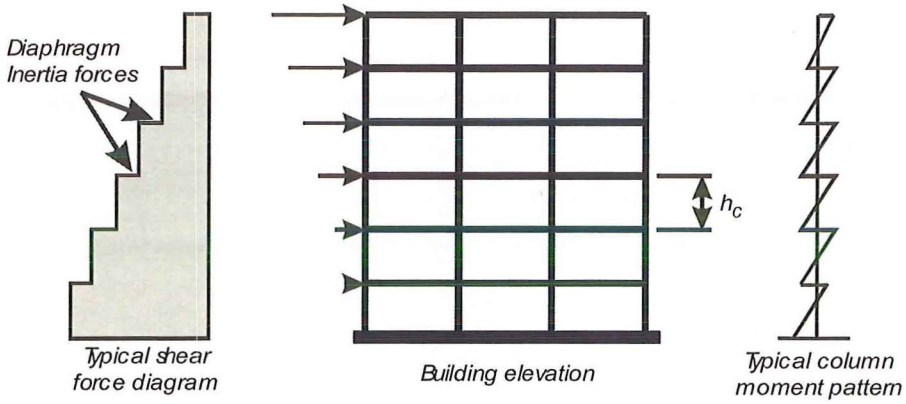

(a) Typical building shear force diagram

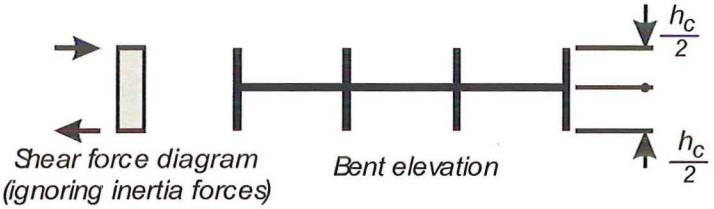

(b) Shear force diagram if the floor inertia forces are ignored.

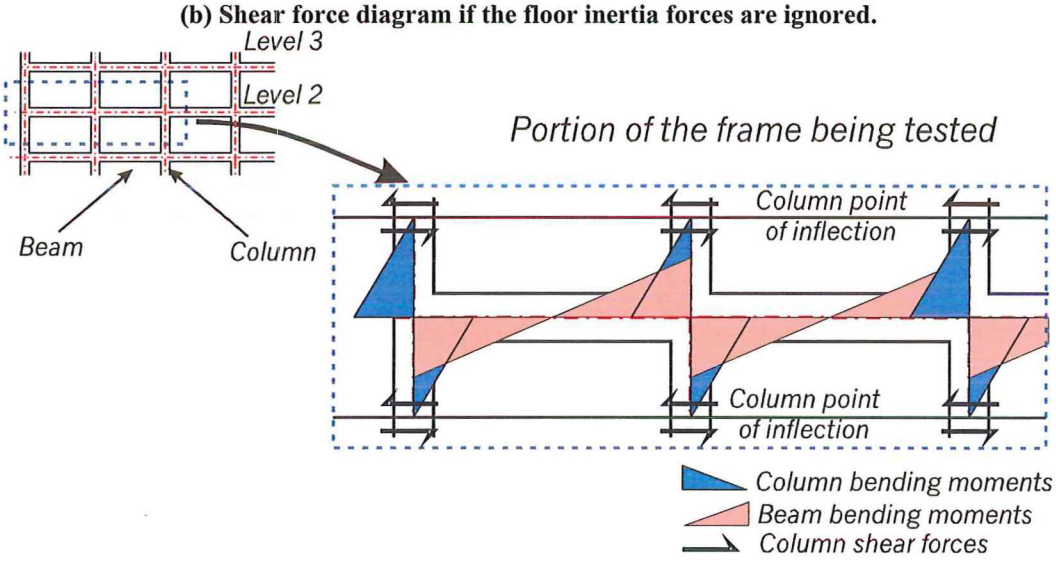

(c) Targeted bending moment diagram for the super-assembly (Note: Gravity is ignored)

Figure 3-6 Applying realistic forces

(transfer forces) from each floor level. If inertia forces and transfer forces are ignored (as the floor diaphragm itself is not loaded), then the interstorey shear force is constant—as shown in Figure 3-6(b). Since this experimental programme is a quasi-static test, rather than an experiment in real-time, then the assumption of zero floor inertia and transfer forces is valid as the test is undertaken slowly so no inertia forces within the floor diaphragm are induced due to the speed of loading. Therefore the

targeted bending moment diagram and applied loading of the super-assemblage is based on Figure 3-6(c).

The key issue, as explained earlier, for allowing beam elongation to form without interference is to keep the external applied shear forces to each column equal and opposite. As explained above, this seems to be an area that other researchers have not dealt with. If there is an out of balance force between the top and bottom applied shear forces to the column then the elongation of the beam may be either restrained or exaggerated, this principle was shown in Figure 3-5. Since the applied shear forces are equal and opposite means no compression or tension fields form within the beams as a result of the external loading.

3.4 Self-equilibrating loading frame

The overall set up for the loading frame is shown in Figure 3-7. The principles of the self-equilibrating loading frame are given in Figure 3-8. Through the principle of equal lateral forces being applied to the top and bottom of each respective column, it was possible to design the main loading frame. As a reaction strong-wall/strong floor testing system was not available, a self-equilibrating load frame was constructed for application of the lateral forces to the super-assembly. By having a diagonal load frame attached to the super-assembly, and not to the strong-floor, ensured the system was self-equilibrating. Refer to Figure 3-8(a) for the location of the applied loading.

The loading frame was designed to apply lateral forces to the top and bottom of the columns. To do this the load frame was designed to pass around the outside of the beam. The load frame had to pass around the outside of the beam so that it did not interfere with the beam itself or the connection between the beam and the floor slab. The loading frame system consisted of a double set of scissor frames as shown in

Figure 3-8(b). One scissor frame mechanism is shown in Figure 3-8(c) and works in the following way. The force applied by the hydraulic actuator is transferred through the frame legs to the pins where the frame is attached to the super-assembly.

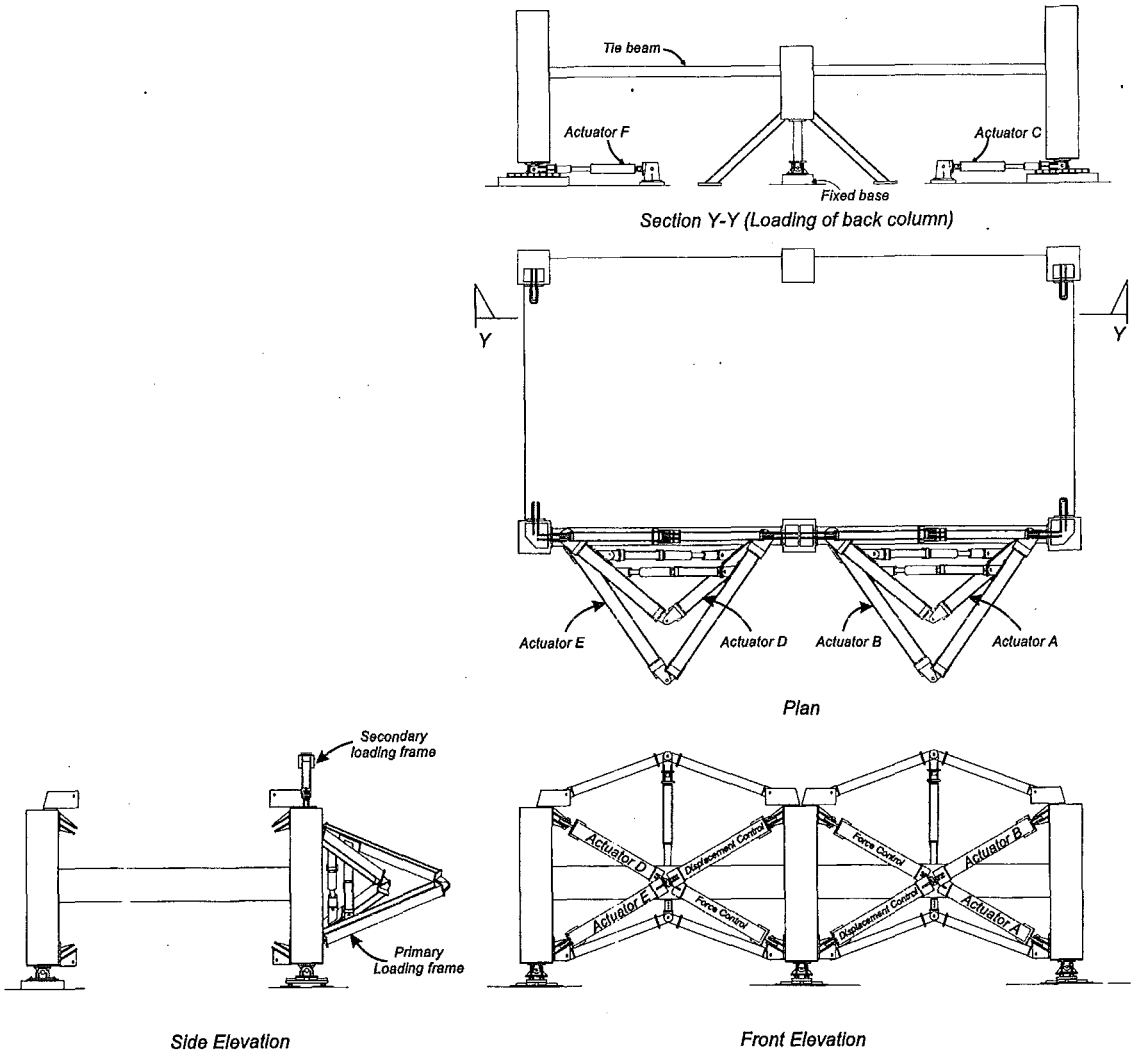

Figure 3-7 Longitudinal loading (Phase I and III)

Two sets of load frames are required to be attached to the test specimen. In order to displace the specimen one set of frames are extended (B and E), while the other set are retracted (A and D) (Refer to Figure 3-8 to see the location of the loading frames). The load from the individual scissor frame applies both a shear force and axial force to the super-assembly.

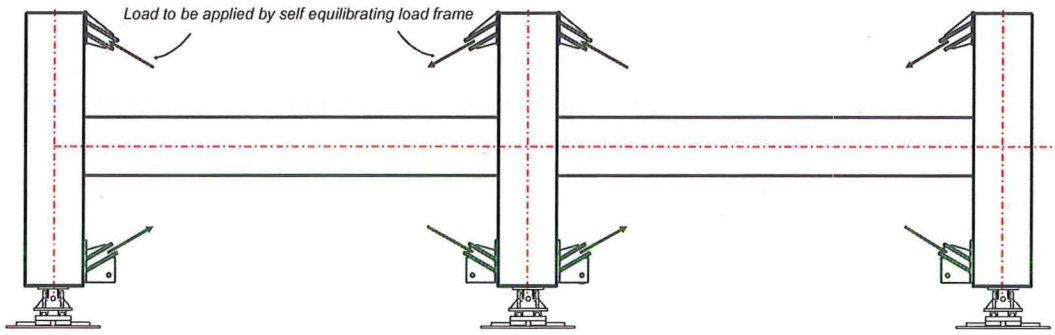

(a) Loading points to ensure the system is self-equilibrating

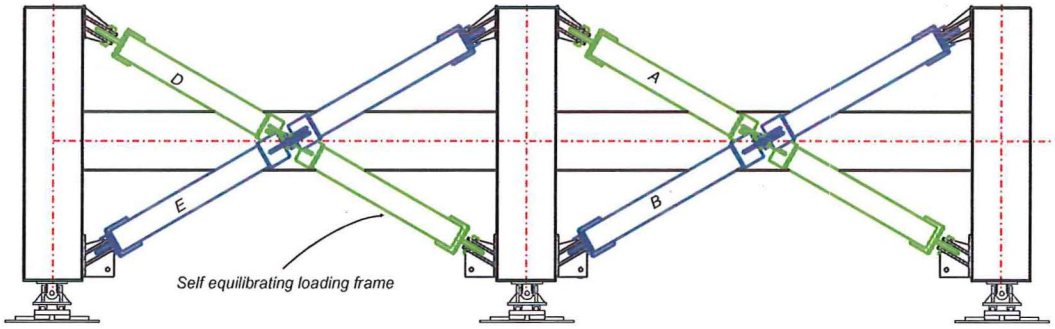

(b) Self-equilibrating loading frame in position

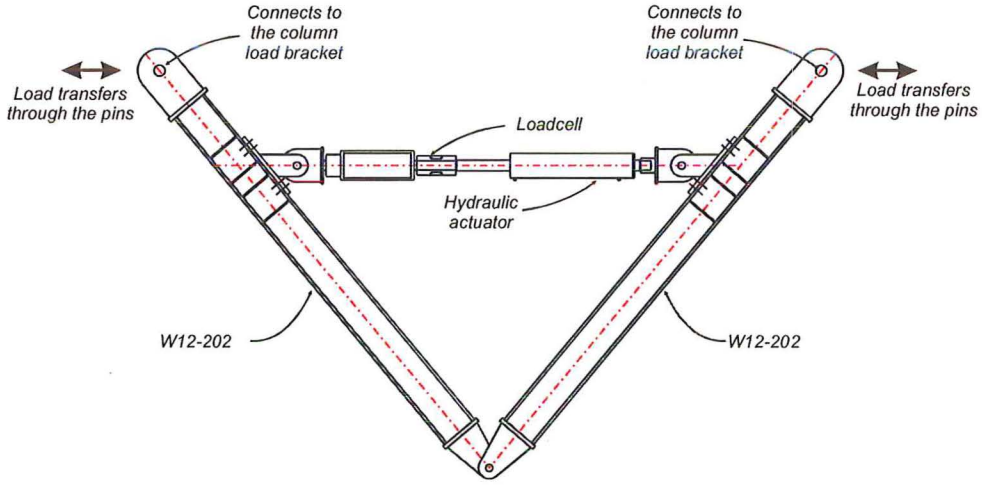

(c) Section of one pair of self-equilibrating loading frames (scissor frame)

Figure 3-8 Details on the self-equilibrating loading frame

One of the benefits of the self-equilibrating loading frame is that the axial forces within the system cancel (the exception to this is when the strength of a plastic hinge zone degrades). The forces cancel in the following way: the induced column axial forces that are generated by the truss action (Figure 3-9) are equal and opposite to the axial forces generated by the moment frame action (Figure 3-9). The truss

action is referred to as the actions generated from the localised scissor load frames while the moment frame actions are generated from the global horizontally applied lateral forces.

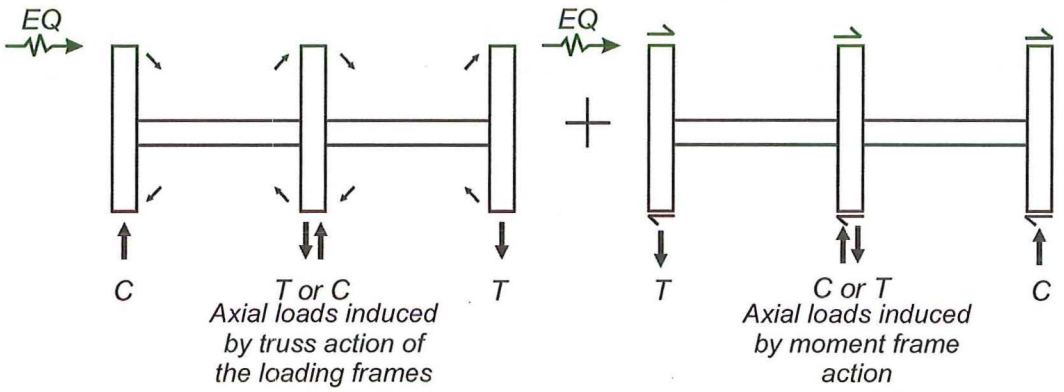

Figure 3-9 Explanation of how axial forces in the frame cancel

The initial structural system to be tested within this self-equilibrating loading apparatus was a precast concrete building with pretensioned, precast concrete hollow-core floor slabs that have a cast in place concrete topping. The load frame was designed so that it could be unbolted from the test specimen and then reattached to a new test specimen. This means that provided the bay width and column height dimensions of the test specimens remain the same, numerous types of both concrete and steel structures can be tested.

For a more detailed breakdown into the actual design of the load frame see Appendix B.

3.5 Secondary loading frame

It was deemed necessary to also provide a secondary loading frame (SLF) to ensure that the test specimen maintains the intended displaced shape during testing (i.e. the columns remain parallel). Due to the composition of the main load frame it would be possible for just the outer columns to be articulated while the inner column remains

vertical (Figure 3-10). This does not happen in a real structure, neither should it occur in test apparatus.

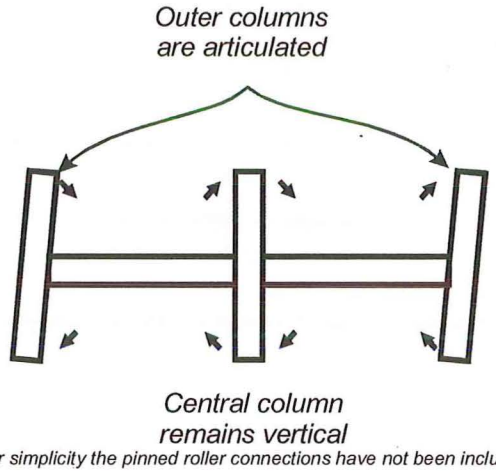

Figure 3-10 Possible displaced shape of the test specimen without the SLF

The SLF, shown in Figure 3-11, resembles an arrow shape. The SLF ensures that the three columns on the front of the specimen remain parallel at all times. The assumption that all the columns remain parallel is based on that the beams in the floors above and below the floor of interest experience the same elongation as the beams in the floor being tested. This is a realistic assumption for the second to (n-1) stories, where n = total number of stories. The first floor beams perform differently as the foundation beams below do not typically hinge and therefore do not experience significant beam elongation. If the beams supporting the roof do not hinge, as is sometimes a chosen option in design, then these beams will not elongate to the same extent as the hinging beams below. The way in which the SLF works can be understood by examining Figure 3-12. If the right hand column tries to incline more than the other columns the SLF resists this by the top of the frame resisting a tension force, T, while the bottom member sustains a compression force, C, which is of equal magnitude to T. This will then pull across the top of the other columns and push away the bottom of the columns. If the reverse was happening then the top of the SLF would be in compression while the bottom is in tension.

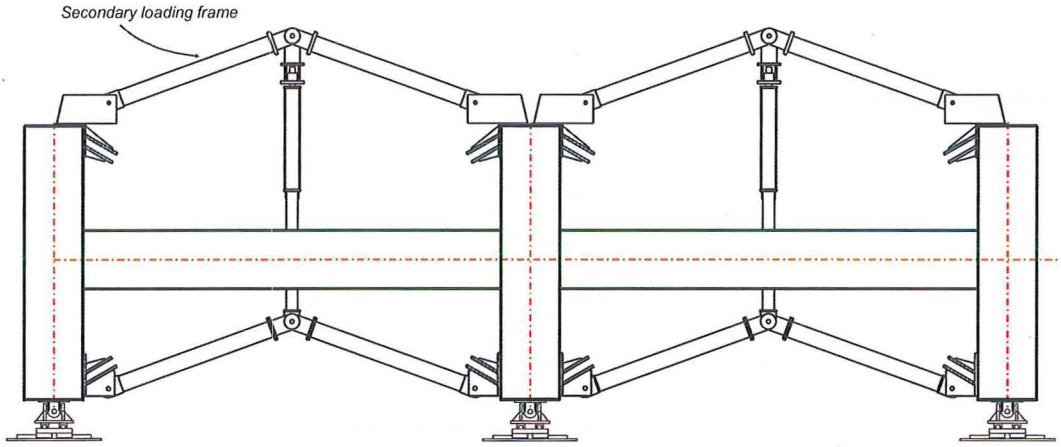

Figure 3-11 Secondary loading frame in position

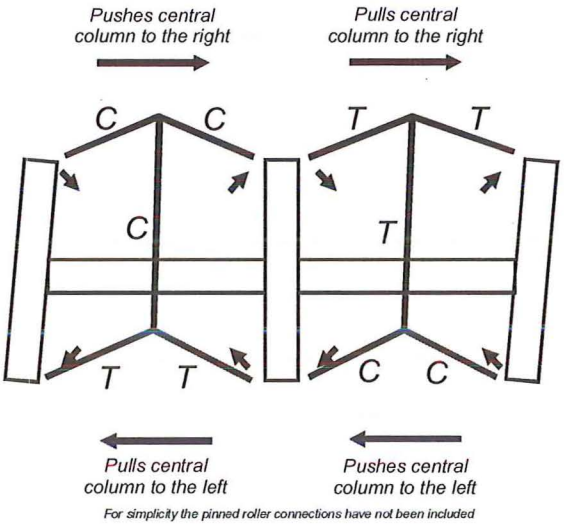

Figure 3-12 How the SLF works

The SLF also allows the beam elongation to occur. The only change to the SLF is that its initial angle of 20^0 reduces as the columns move apart. Figure 3-13 shows the change in the set up of the SLF before and after beam elongation occurs.

As explained earlier, the applied lateral force to the top and bottom of the column must be equal and opposite, this is achieved in the SLF as the top and bottom SLF arms attached to each column are parallel and one is in tension while the other is in compression.

When one of the bays within a bent degrades in strength during the experimental programme the SLF helps to redistribute the forces from the degrading bay into the adjacent stronger bay. The set up will even permit the complete

degradation of all the hinges in a beam to pin connects. The SLF then continues to provide displacement compatibility of the truss like structure—that is the columns are maintained in a parallel orientation at all times.

For more details regarding the design of the SLF see Appendix B.

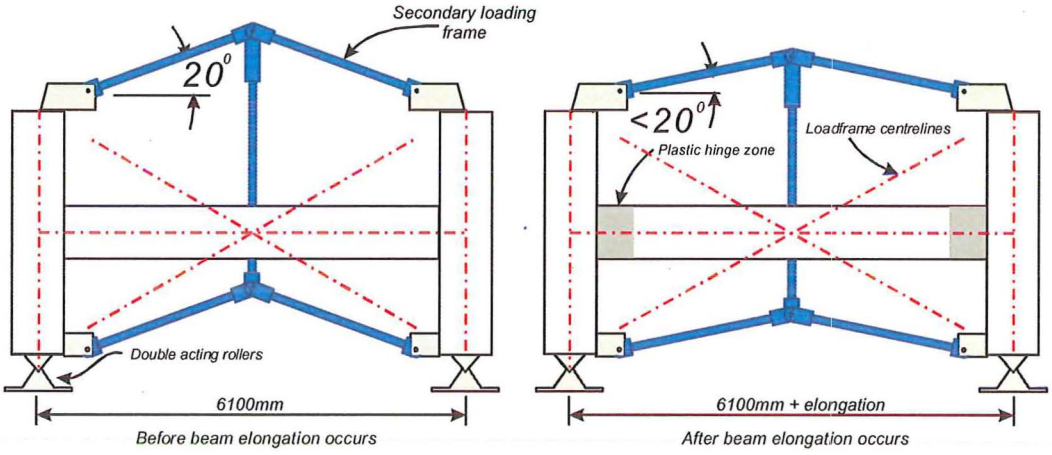

For simplicity, only the secondary frame components have been shown

Figure 3-13 SLF before and after beam elongation occurs

3.6 Back Column Loading

By using the self-equilibrating loading frame and the SLF ensures that the front frame of the super-assembly displaces as expected. Due to space and budget limitations it was not possible to attach another set of frames to the back of the specimen as seen on the front (Figure 3-14). Since the back beam was only a slender tie beam (refer to Section 1.5), a single hydraulic actuator was required to load and displace each column. The displacement of these actuators was altered to ensure the inclination of the back columns matched those of the front to ensure that no undue torsion was applied to the two transverse beams.

A rigid central column is required to tie the super-assembly to the structural floor. This component is needed because the two hydraulic actuators are not self-equilibrating, see Figure 3-7 for further explanation.

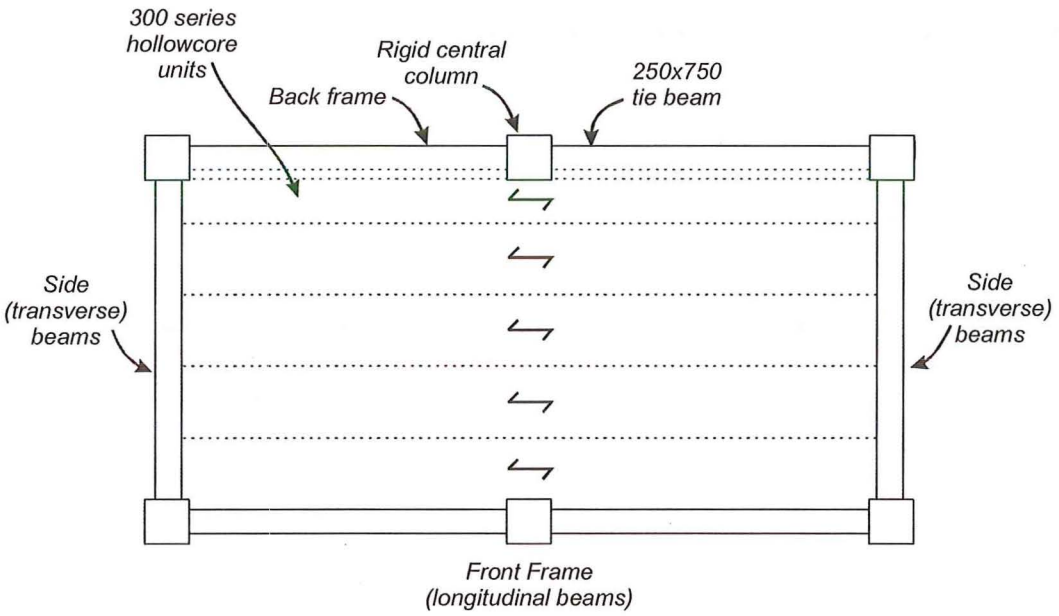

Figure 3-14 Plan of the super-assembly

3.7 Transverse loading

Since earthquake motions are not in one principal direction, the entire loading system was developed so that during the experimental programme the load frame could be detached from their initial position on the longitudinal beams and reattached onto the transverse beams. Since the longitudinal and transverse beams had the same bay length it was possible to shift the self-equilibrating loading frame from one bay to another as seen in Figure 3-15(a).

To load the central column in the transverse direction an additional load frame was required. The same principle was used to determine the manner in which the column was to be loaded, i.e. ensuring that the applied shear force to the top and bottom of the column was equal and opposite. The position of the hydraulic actuators and reaction frame is shown in Figure 3-15(b). This had to be fixed to the strong floor rather than be self-equilibrating so that it did not interfere with the floor diaphragm.

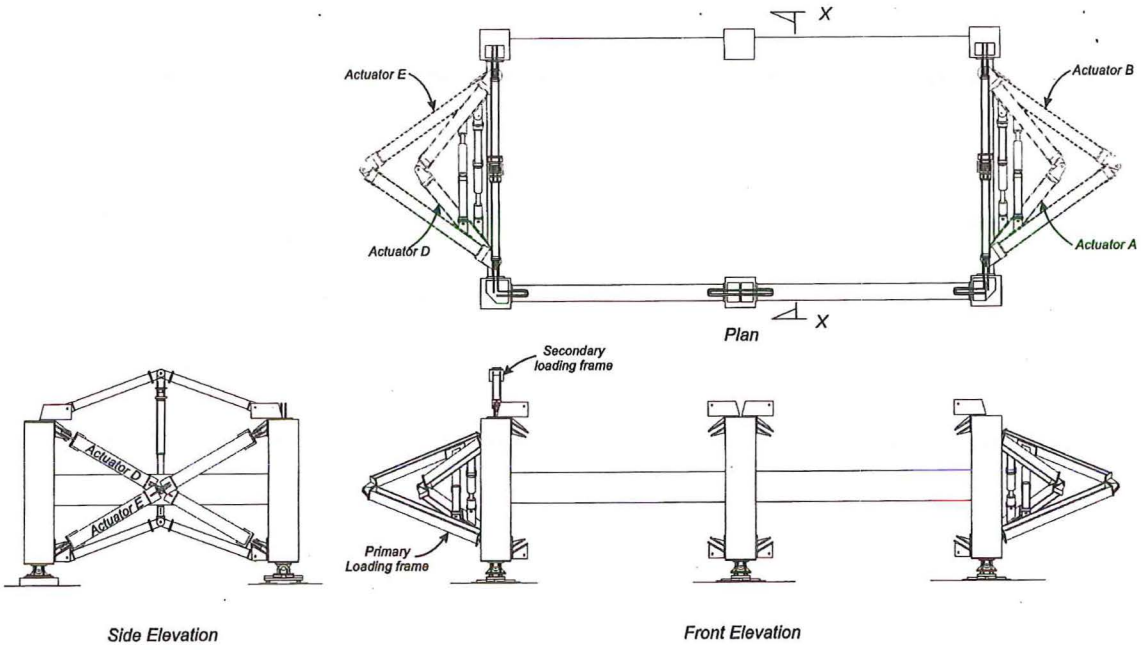

(a) Transverse loading (Phase II)

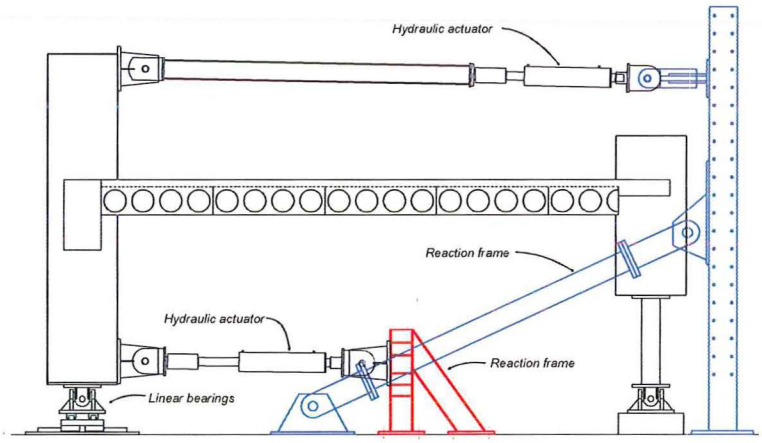

(b) Section X-X (Attachment of the hydraulic actuators to load the central column)

Figure 3-15 Plan and elevation of the erected loading frames

3.8 Electronic valve controller design

In order to control the six hydraulic actuators that load the test specimen a valve controller programme was developed in the LabVIEW software (National Instruments, 1999). A series of flow charts that explain the process of valve control for the servo-controlled actuators are described in this section.

The design of the flow charts was based on a figure showing the various stages of beam elongation (Matthews et al, 2001). As mentioned earlier, a key component was to ensure the columns had equal and opposite shear forces applied to them.

In order for the controller to be able to equalise the force in the actuators, the control algorithm consisted of three major steps (a displacement increment, a force balance increment and a column inclination adjustment increment). Firstly, the displacement controlled actuators A and D (refer to Figure 3-7 for actuator locations) were extended by a small increment. This extension causes the following load state to be applied on the column (Figure 3-16(a)). As the compressive force in actuators A or D increases the column is slowly pushed off the beam as the centre of rotation is about the fixed actuator B or E. For equilibrium, a small tension force is generated in the beam (this axial force generated is referred to as the *column face error (CFE)*). The second step is to retract the force controlled actuators B and E until the horizontal force at the top equals the horizontal force at the bottom. Now the point of rotation changes from the bottom of the column to the top. The tension force in B and E increases until it matches the compressive force in A and D. Now the *column face error* (axial force in the beam generated from the external loading) is zero. Lastly, the displacements of the back actuators (C and F) are adjusted so that the back columns inclination is the same as the central front column.

One key in ensuring that the beam elongation is neither exaggerated nor restrained is to ensure each displacement increment is small. The reason for this is so that the axial force in the beam (*column face error*) is always kept to a minimum. If the displacement increment is large then the axial force generated within the beam from the external applied loading will cause the beam elongation to be exaggerated.

Each of the displacement controlled increments causes the column to be pulled off the beam whereas the force controlled increment which reduces this prying action.

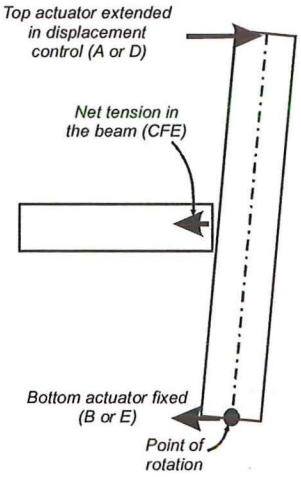

(a) Step 1-Displacement actuator extended

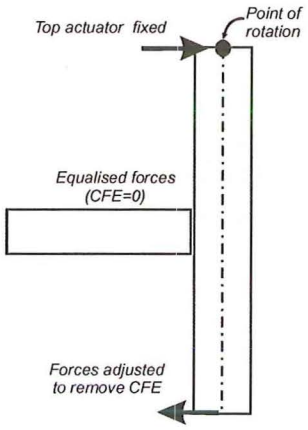

(b) Step 2-Force actuator retracted to remove CFE

Figure 3-16 Load states

To unload the specimen the reverse loading occurs. Displacement controlled actuators A and D are retracted, then the force controlled actuators B and E are then extended until the *column face error* is zero. The back actuators are then adjusted so that all columns are similarly inclined.

The program was written as a semi-automatic experimental driver that requires the user to activate each major displacement increment. This minimal required human intervention ensures the program does not wander out of control. Figure 3-17 shows this initial step with the *"Black Box"* being the automated process. The automated process undertaken by the valve controller is also shown in Figure 3-17.

While the automated process is being carried out, several checks are undertaken to ensure the system operates correctly. If any of these checks fail then an error message appears and the valve controller stops. The checks that the controller monitors during its automated stage are:

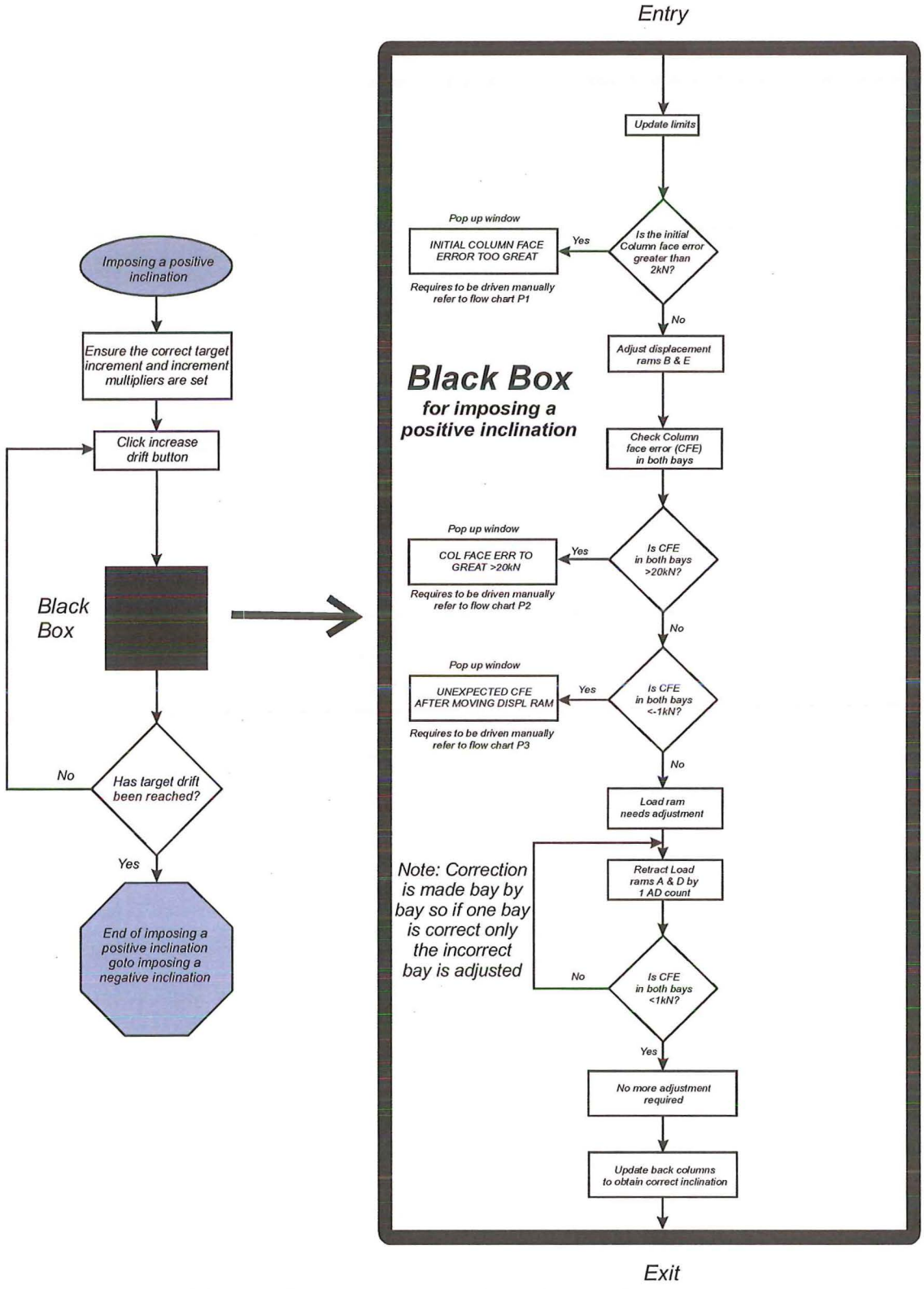

Figure 3-17 The flow charts for imposing a positive drift.

- Check 1: Column Face Error < 2kN

  This check is in place to ensure that beam elongation is not exaggerated, because when the displacement increment of the process is applied the *column face error* will increase. If there were already some significant tension in the beam then when the displacement controlled actuators is extended the beam elongation could potentially be exaggerated.

- Check 2: *Column Face Error* < 20kN

  This check is made before the force controller actuator is moved. Again this is to ensure that any beam elongation is not exaggerated.

- Check 3: Unexpected *Column Face Error* after moving a displacement controlled actuator

Each time the displacement ram is extended the *column face error* should go into tension (or less compression, depending on the direction of travel). If it does not occur then there is potentially a problem with the system that will require operator intervention.

When any significant errors occur, the operator is required to manually drive the system to a point of stability where the auto-driver can take over. Additional sets of flow charts were provided to allow the operator to correct the errors (see Appendix B).

Slight modifications to the controller were made to allow for controlling the super-assembly in the transverse direction. The basic principles for controlling the actuators were the same as for the longitudinal loading.

All the additional flow charts are attached in Appendix B.

3.9 Super-assembly details

The initial specimen to be tested in the self-equilibrating load frame was a precast concrete moment resisting frame building with a hollow-core floor slab floor. The origin of the super-assembly is from a lower storey in a multi-level precast concrete frame building (Figure 3-18), typically the second through fourth storeys. The first storey is not being studied due to the effects that the foundation beams has on the first storey performance.

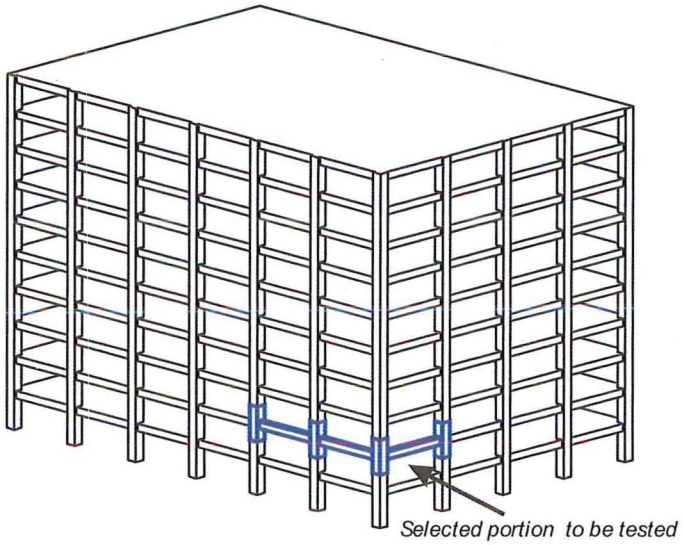

Figure 3-18 Origin of the building prototype

The specimen consisted of a two-bay by one-bay specimen that had a bay width of 6.1m. The columns were 750mm square and the perimeter beams were 750mm deep and either 450 or 400mm wide (the width depended on whether the hollow-core unit was seated on the beam or not). The hollow-core units used in the floor slab were 300mm deep (designated as "300 series"). A 75mm cast insitu concrete topping slab reinforced with cold-drawn wire (665 mesh) was used to tie the floor slab together. The detail used to connect the hollow-core unit to the supporting beam was the most common connection detail used in New Zealand since the mid 1980's. Figure 3-19 summaries the details of the super-assembly.

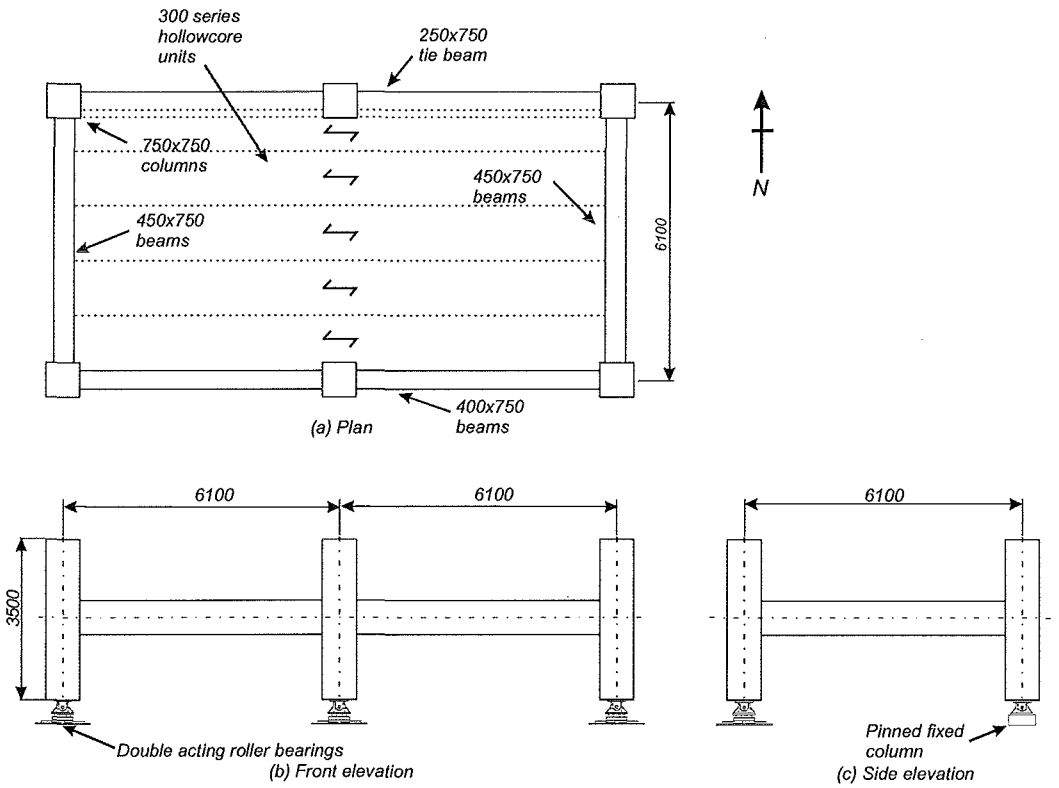

Figure 3-19 Dimensions and layout of the super-assembly

3.9.1 Reinforcement details

All the concrete components were designed in accordance to the New Zealand Concrete Structures Standard (NZS3101:1995).

Perimeter beams

When designing the perimeter moment resisting frame a contribution from the floor slab is required to be added to the frame capacity. It became clear that the amount of floor slab activation was difficult to determine so therefore several scenarios were considered (refer to Appendix B). The scenario that produced the greatest strength was then used to design the beam and the subsequent components.

The beams longitudinal reinforcement ratio was ρ_l=0.009 consisting of 6-D24 bars top and bottom. Grade 300 (f_y=300MPa) reinforcement was used for all the longitudinal and transverse reinforcement, as it was the most common grade of steel used during the 1980's.

The beams were cast as precast half-beams so that the top half of the beam plus the mid span lap splice was poured at the same time as the cast insitu diaphragm topping. This type of connection is referred to as a System 2 arrangement as defined by the *Guidelines for the Use of Structural Precast Concrete in Buildings* (Centre for Advanced Engineering, 1999).

Refer to Figure 3-20(a) for a typical beam reinforcement detail or to Appendix C for the full reinforcement details.

Columns

A capacity design approach was used to design the columns. The overstrength moments and shears acting in the beam plastic hinge zones were used to determine the design actions for the columns. As explained in the beam design the amount of enhancement from the floor diaphragm to the beams flexural strength was unknown. To enforce a strong column weak beam mechanism formed it was crucial to provide the central column extra strength protection to ensure the column did not hinge during testing. To achieve this, the central column had a relatively high percentage of longitudinal reinforcing consisting of 24-HD24 bars (ρ_t=0.022). Since the columns have 12 drossbach ducts per column, this particular column needed two bars per duct. Though this is not common practice it was considered acceptable for this test unit, as the columns performance was not a focal point. The only column performance criterion that this research required was for the columns not to form plastic hinges. The remainder of the columns had 1-HD28 bar per drossbach duct (ρ_t=0.013).

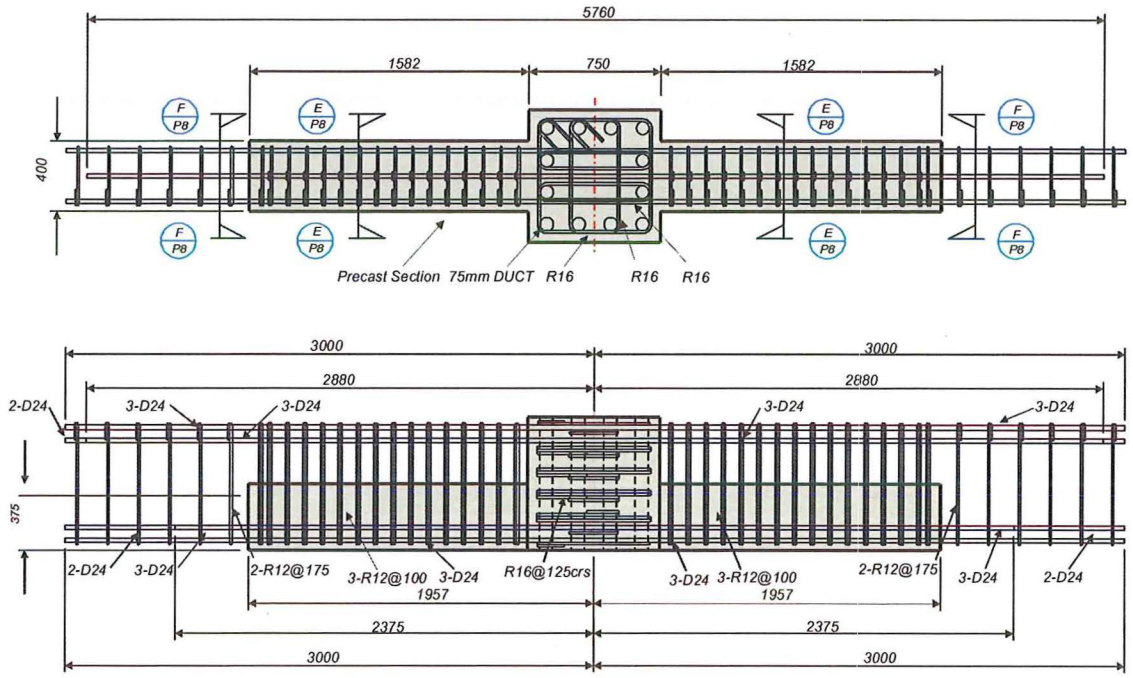

(a) Precast beam reinforcement details

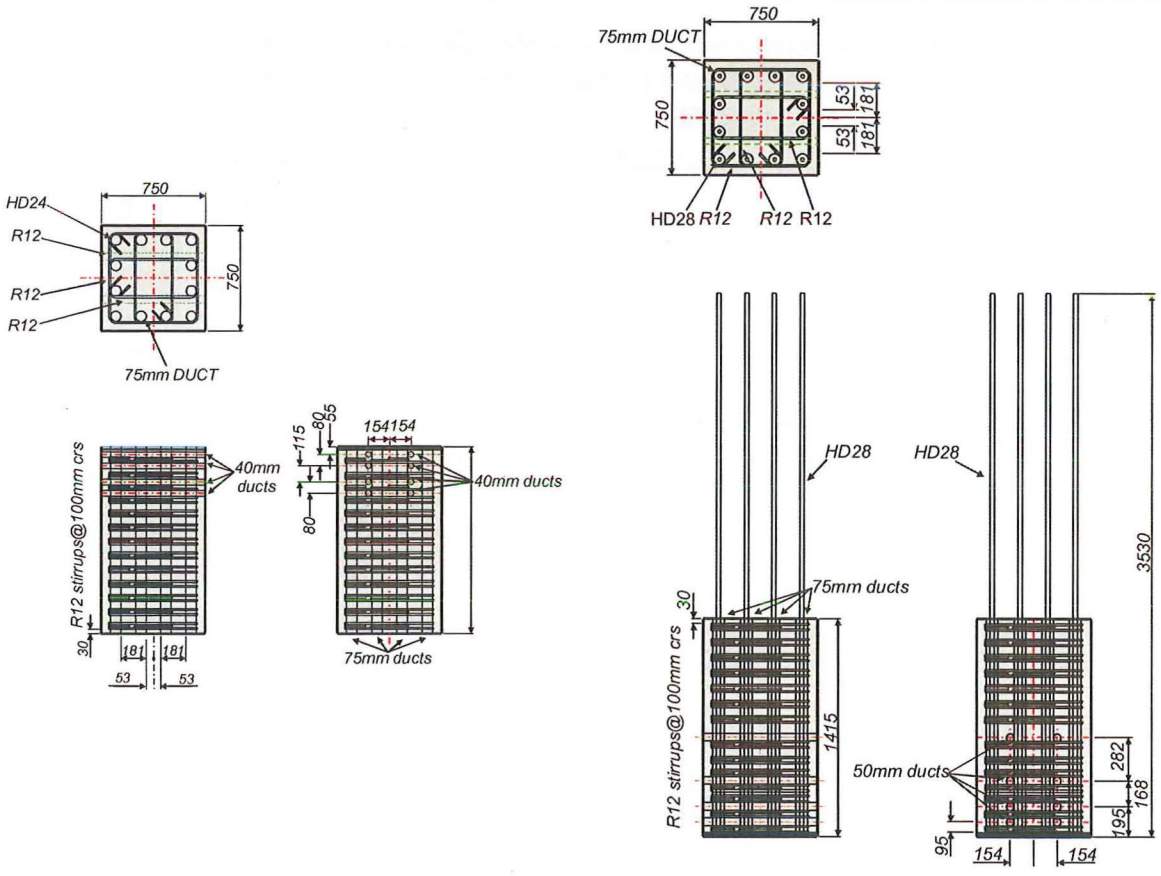

(b) Precast column reinforcement details

Figure 3-20 Typical beam and column reinforcement details

The longitudinal reinforcement at both the top and bottom of the columns was welded onto the column end plates. This ensured the endplates were not pulled off during testing due to the load being transferred from the load frame connection brackets to the columns.

Refer to Figure 3-20(b) for a typical column reinforcement detail or to Appendix C for the full reinforcement details.

Figure 3-21 shows the completed super-assembly. The white sections of concrete within the beams and the floor topping were cast insitu. The darker (shaded) coloured portions of the beams together with all the columns were precast.

Figure 3-21 An elevation showing the site cast concrete (White sections of the beams and topping)

3.9.2 The connection detail tested

The connection detail tested was considered to be the most common connection used in New Zealand over the last two decades. The connection between the hollow-core unit and its supporting beam consisted of seating a hollow-core unit on a mortar bed. The reinforcement detail was hooked starter bars (deformed 12mm, f_y=430MPa) spaced at 300mm centres (HD12@300) and being lapped with a non-ductile

reinforcing mesh within the cast insitu concrete topping. Figure 3-22 shows the connection detail used.

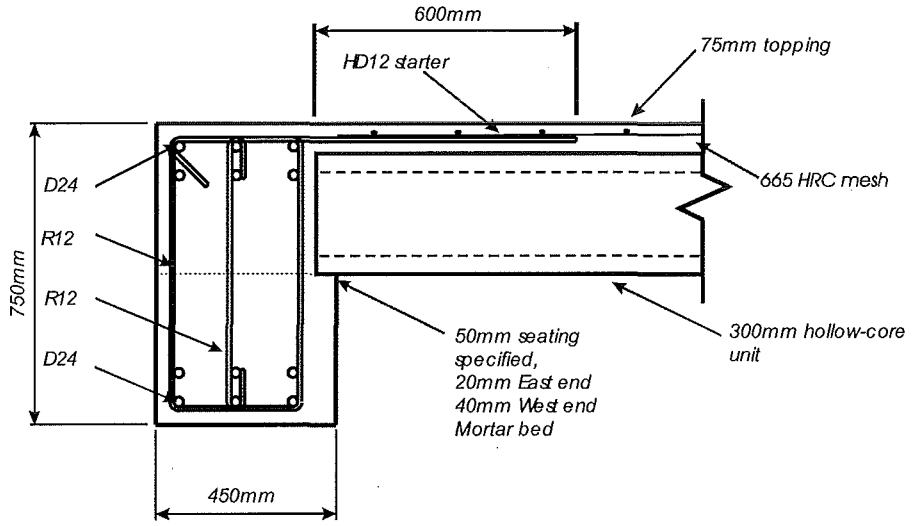

Figure 3-22 The connection detail used to connect the hollow-core units to its supporting beam.

Although the nominal seat length was 50mm, the actual seat lengths used was 20mm and 40mm at the east and west ends respectively. The reason the seat length was smaller than nominally specified was because the precast units arrived from the manufacturer short in length; this is also a common occurrence in the field, and therefore was considered a realistic condition to test.

3.10 Instrumentation

Due to the size of the specimen being tested, a sophisticated monitoring system was required to record all the test data. The data capture system used has been developed and refined at the University of Canterbury over the last few years. The following system was used to monitor and record all the forces, displacements and strains.

A central computer read, recorded and saved all the data. From the central computer there were a series of transducer boxes. Each transducer box had one of the following connected into them: temperature gauges; inclinometers; strain gauges; linear potentiometers; and loadcells.

3.10.1 Measurement of Forces

A series of six loadcells were used to monitor the force been applied to the test specimen by the hydraulic actuators. The purpose built loadcells are hollow cylinders machined from high strength steel containing strain gauges to measure the applied load.

The ten legs of the secondary loading frame were also strain gauged to act as loadcells. This allowed the redistribution of load through the system to be tracked. Since these members were long and undergo some bending when loaded in compression, the legs were required to be calibrated in both tension and compression.

The universal joints were also strain gauged to act as a loadcell. These were strain gauged for the same reason as the secondary loading frame.

3.10.2 Measurement of Displacements and Deformations

The displacements measured during the test programme were measured using inclinometers, linear potentiometers and rotary potentiometers. The following displacements were measured: inclination of the columns; relative movement between the hollow-core units and the perimeter beams; the fixed end rotations of the plastic hinge regions; beam elongation of the perimeter beams; strain in the starter bars; the overall displacement of the corner columns; shear deformation of the beams in the plastic hinge region; and general distortion of the beam column joint zones.

The inclination of the columns was defined the lateral displacement expressed as the percentage of the relative change in position of the centre of the support pins at the top and bottom of the columns, divided by the vertical distance between the centre of the pins. The change in lateral displacement was measured by rotary potentiometers mounted at the top and bottom of the columns (Figure 3-24(c)). Since the testing

programme was displacement controlled, the columns inclinometer was used to monitor the interstorey drift of the test specimen and hence control the testing. Rieker inclinometers were used as a back up to the rotary potentiometers to measure the average slope of the columns.

Linear potentiometers (Sakae) were used to measure any large displacements. The size of potentiometer used depended on their location on the test specimen and the displacement likely to occur. Figure 3-23 and 3-24 show the location of all the linear potentiometers.

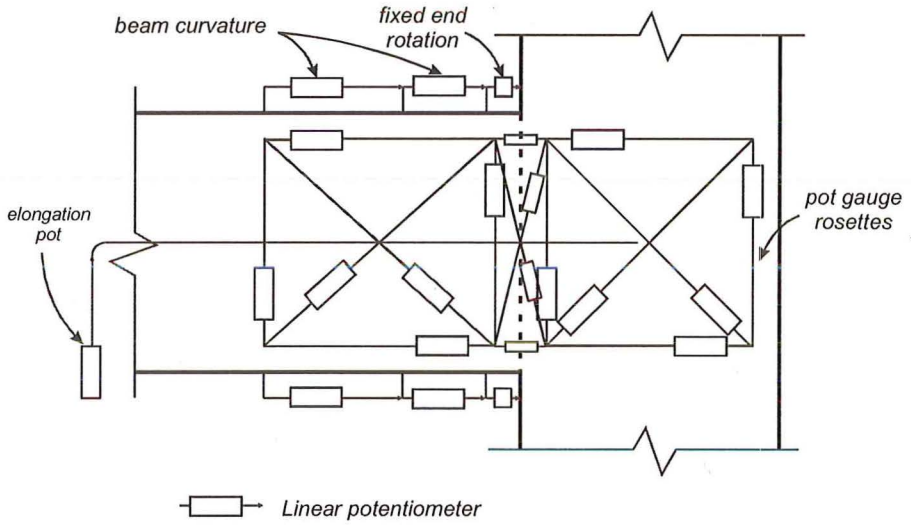

Figure 3-23 Location of linear potentiometers on the test specimen.

Twelve 30mm potentiometers were placed on the beams to measure the fixed end rotations of the columns. These were attached to the top and bottom of all the beams at the column faces. Then two more series of pots will be attached in the plastic hinge region to monitor the beams curvature. The shear deformation of both the beam column joint and beams were monitored by a series of potentiometer rosettes. The rosettes use a combination of 30 and 50mm potentiometers depending on their position within the beam and the expected deformation to occur. Figure 3-23 shows the position of the rosettes.

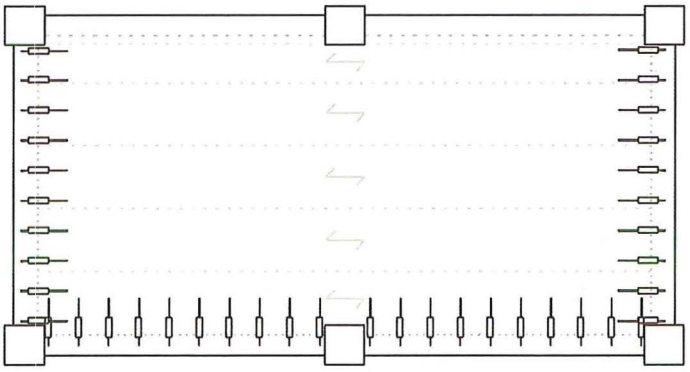

(a) Diaphragm instrumentation (on top of floor)

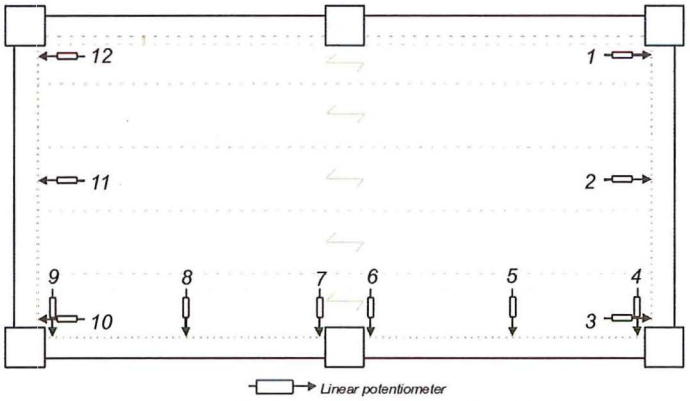

(b) Diaphragm instrumentation (under the floor)

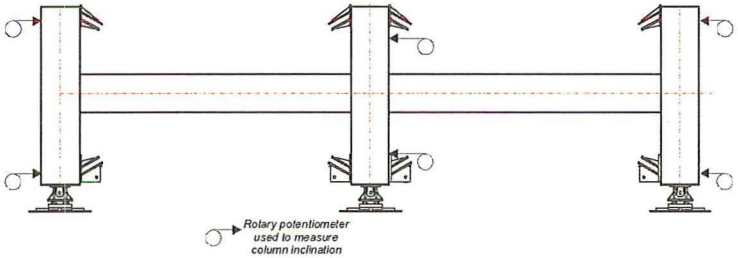

(c) Position of rotary potentiometers to measure column inclination

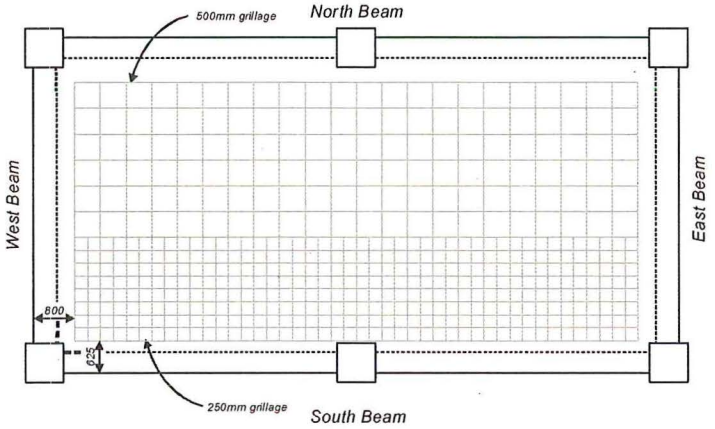

(d) Set out of the demec points across the floor diaphragm

Figure 3-24 Instrumentation details for the super-assembly

Five 200mm potentiometers were used to measure the total elongation of each plastic hinge in the beams. The elongation of each plastic hinge was measured in the following way. A wire was attached to a stub placed in the middle of each beam column joint and then run through a pulley at the mid span of the beam and connected to a linear potentiometer. This set up is shown in Figure 3-23.

A series of potentiometers were used to measure the strain induced into the starter bars by the continuity crack that formed between the supporting beam and the end of the hollow-core units (Figure 3-24(a)). The elongation of the starters also allowed a prediction to be made on the deformation mode of the transverse beam.

Twelve 50mm and 100mm potentiometers were attached to the hollow-core units along the edge of the beams to measure the relative displacement between the hollow-core units and the perimeter frame. These gauges helped to determine the deformation of the hollow-core unit relative to the perimeter beam (Figure 3-24(b)).

3.10.3 Measurement of Diaphragm strains

A grillage of "Demec" points was set out over the floor diaphragm (Figure 3-24(d)). By comparing the various Demec readings, it is possible to determine the longitudinal and transverse growth through the floor. Due to the large number of demec points to be read, it was not practical to measure the gauges at every load increment so therefore mainly the peak cycles were read.

A "Demec" (demountable mechanical) gauge is a hand-held instrument used for monitoring displacement. Two "Demec" points are bonded to the concrete so that the gauge can be placed on the two points to make a reading. The readings obtained are compared with the initial reading in order to get the change in displacement and hence the average strain.

Since a large number of Demec points were to be read, two electronic Demec gauges were developed, one with a 500mm gauge length and the other with a 250mm gauge length. The gauge used a linear potentiometer to measure the change in displacement so that the displacement could then be stored electronically. The mechanism from a standard analogue gauge was attached onto the electronic gauge. The gauge was temperature compensated because the gauge can potentially heat up while being used. The display on the gauge gave all vital information that the user required. The information displayed was: Demec number; previous measurement; previous temperature; current measurement and current temperature. Appendix B gives details of the gauges developed.

3.11 Concluding Remarks

The emphasis of the development of the experimental infrastructure, described herein, is to enable investigation to be undertaken on full-scale super-assemblies in order to properly capture 3-D behavioural effects under seismic loading. Based on previous research investigations, it is evident that beam elongation has only recently been considered as an important phenomenon in indeterminate structural assemblies. Previously all work was undertaken on determinate sub-assemblies. The simplification of test specimens from indeterminate full-scale specimens has resulted in some of this previous work giving misleading outcomes as some of the constraints or displaced shapes imposed are inadmissible in a real structure. The positive and negative aspects of previous work have formed the basis for the determination of the loading components of this experimental programme.

The floor slab is important in determining the amount of beam elongation that forms in a system. The floor slab is expected to provide some form of restraint and

potentially increase the lateral load capacity of the system. The amount of restraint depends on the floor-to-beam connection detail and the type of flooring system being used.

The key variable in designing a loading frame that neither exaggerates nor restrains beam elongation is to apply equal and opposite shear forces within each bay of a bent. This assumption is acceptable since there is no inertia loading during quasi-static testing.

Due to the limitations of the structures laboratory, at the University of Canterbury, considerable investment has been made in the experimental infrastructure by developing a self-equilibrating loading apparatus. Consequently, a large structural wall is not required to laterally load the super-assembly. This was achieved by developing a new type of loading apparatus that uses a pair of scissor load frames to apply the lateral forces to the columns of a structural super-assembly. A secondary loading frame is used to ensure that the columns deform together in the predominant mode expected in a major earthquake. To achieve this the following criteria were considered as important: (i) Beam elongation would be allowed to form without interference from the test rig; (ii) The columns remained parallel at all times; and (iii) The correct deformed shape of the test specimen occurred.

To ensure displacement compatibility, the back columns of the super-assembly had hydraulic actuators attached to ensure that all the columns had the same inclination that ensured that no experiment derived torsion was applied to the transverse beams.

By developing a series of flow charts on how the super-assembly should be loaded, it has been possible to develop a semi-automated hydraulic valve controller. This permits the complicated loading regime to be controlled with relative ease. The

valve controller undertook the simple tasks while all the decision making was made by the operator.

The self-equilibrating loading frame has been designed to apply a maximum actuator force of ±1000kN that equates to a column shear force of 640kN. The secondary loading frame maximum design actions were ±500kN and ±340kN in the diagonal and vertical legs, respectively.

3.12 References

Centre for Advanced Engineering, 1999, *Guidelines for the Use of Structural Precast Concrete in Buildings*, Centre for Advanced Engineering, University of Canterbury, Christchurch

Fenwick R.C and Megget L.M, 1993, *Elongation and load deflection characteristics of reinforced concrete members containing plastic hinges*, Bulletin of NZNSEE, Vol 26, No. 1, March, pp 28-41

Fenwick R.C, Davidson B.J and McBride A, 1995, *The influence of slabs on elongation in ductile seismic resistant concrete frames*, Proceedings for NZNSEE technical conference, Rotorua, March, pp 36-43

Fenwick R.C, Ingham J.M and Wuu P.J.Y, 1996, *The performance of ductile R/C frames under seismic loading*, Proceedings for NZNSEE technical conference, New Plymouth, March, pp 20-26

Lau D, B, N, 2001, *The Influence of Precast-Prestressed Flooring on the Seismic Performance of Reinforced Concrete Perimeter Frame Buildings*, Department of Civil and Resource Engineering, University of Auckland, Report No. 604

Matthews J.G, Bull D.K and Mander J.B, 2001, *Investigating the Loadpaths of Floor Diaphragm Forces During Severe Damaging Earthquakes*, Proceedings for New Zealand Concrete Society Conference, Taupo

National Instruments, 1999, *LabVIEW version 5.1*, National Instruments Corporation, Texas, U.S.A

Restrepo J.I, Park R and Buchanan A, 1993, *Seismic Behaviour of Connections between Precast Concrete Elements*, Research Report 93-3, Department of Civil Engineering, University of Canterbury, Christchurch, New Zealand

NZS3101:1995, *Concrete Structures Standard*, Standards New Zealand, Wellington New Zealand

Zerbe H.E and Durrani A.J, 1989, *Seismic Response of Connections in Two-Bay R/C Frame Subassemblies*, Journal of Structural Engineering, Vol 115, No. 11, November, pp 2829-2844

Zerbe H.E and Durrani A.J, 1990, *Seismic Response of Connections in Two-Bay Reinforced Concrete Frame Subassemblies with a Floor Slab*, ACI Structural Journal, Vol 87, July-August, pp 406-415

This Page is Blank

Chapter 4

Experimental Results

4.1 Introduction:

Concern has been raised about the expected performance of many of New Zealand's recently (since the 1980's) and presently constructed precast concrete buildings during a severe earthquake. One particular concern is the detailing used to attach the precast hollow-core floor units to the perimeter frame. It is hypothesized that if a large earthquake were to hit a major urban region of New Zealand, precast concrete floors in buildings would not perform as well as their cast-insitu counterparts—collapse of precast floors may be expected due to seating and articulation problems.

The super-assemblage experiment in this research represents a corner section from a lower storey in a typical precast concrete building. The specimen consists of 750mm deep beams with a bay length of 6.1m. The overall dimensions are approximately 12m long by 6m wide. The precast floor units being tested are hollow-core units that are 300mm deep (designated as "300 series"). The units are topped with a 75mm cast insitu topping that includes reinforcing mesh. The hollow-core units span past the central column and are seated on the two end beams with an actual ledge (seat) length of 20mm on the East beam and 40mm on the West beam. These provided ledges (seats) were considered to be representative of the range of seat widths adopted in the field over the past two decades. Figure 4-1 shows the super-assemblage dimensions.

The lateral loading applied to the top and bottom of the column of the super-assemblage was through a set of purpose built loading frames as shown in Figure 4-2. The super-assemblage specimen was loaded in this manner for both the longitudinal

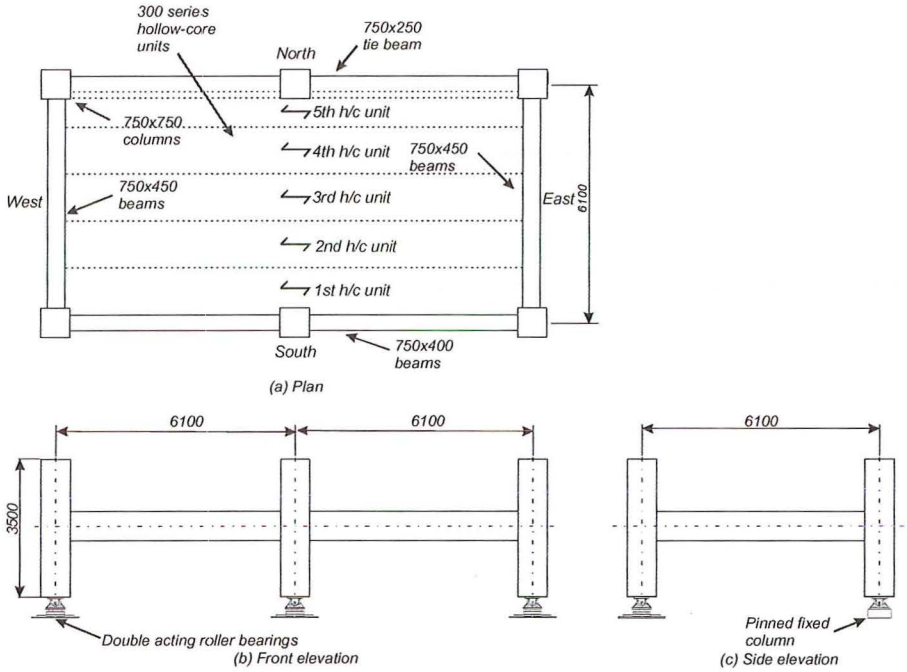

Figure 4-1 Plan and elevation of the super-assemblage tested.

(a) Longitudinal Loading **Transverse Loading**

Figure 4-2 Loading frame set up

and transverse directions. The two main loading frames are the diagonal scissor frames while a set of secondary loading frames (that resemble an arrow shape) enforces the displacement compatibility of the adjoining stories by ensuring the front columns remain parallel.

This chapter contains a general description of the visual observations as well as significant events that occurred during the experimental programme. The global hysteretic response of the super-assemblage throughout each of the experimental

loading phases is then presented and discussed. The decomposition of the lateral displacement is also presented and discussed. A visual assessment of the damage to the super-assemblage was undertaken in which the damage was assessed by both a colour coded format and a damage state format. A comparison between the two methods was made. Finally, the visual assessment was quantified using fragility theory to explain the implications of the observed damage in terms of New Zealand buildings.

4.2 Applied Displacement Pattern

Three different lateral displacement histories were applied to the super-assemblage. Each of the three histories corresponds to the three different loading phases. These histories are shown in Figure 4-3. The background to the determination of these displacement histories is explained in Chapter 2.

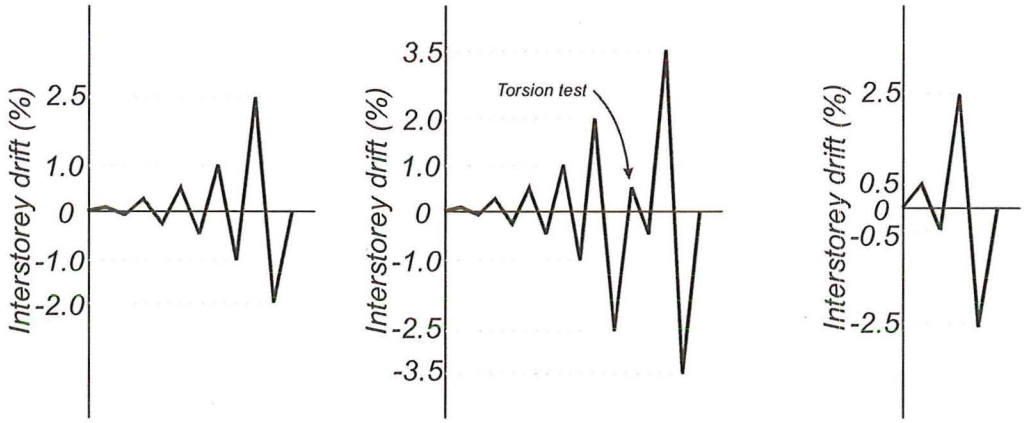

(a) Phase I-Longitudinal loading **(b) Phase II-Transverse loading** **(c) Phase III-Longitudinal loading**

Figure 4-3 Displacement histories applied to the super-assemblage

4.3 Visual Observations

The key indicator in determining the performance of the hollow-core unit connection detail is the relative rotation between the hollow-core unit and the supporting beam (Figure 4-4). Within this document this relative rotation has been

defined as interstorey drift as the building investigated was considered to be a generic New Zealand moment resisting concrete frame building in which the interstorey drift closely relates to the relative rotation. In terms of predicting the amount of reinforcement slab activated as flange steel within a structure, the relative rotation between the hollow-core unit and the supporting beam should be used. As torsion of the beams supporting the hollowcore units reduces this relative rotation, it is considered conservative to assume that the relative rotation and interstorey drift are one and the same. A designer is reminded that if a true assessment of risk or damage to the floor system is required then the designer should focus on the relative rotation between the hollow-core unit and the supporting beam as it is less conservative that using the interstorey drift as the indicator.

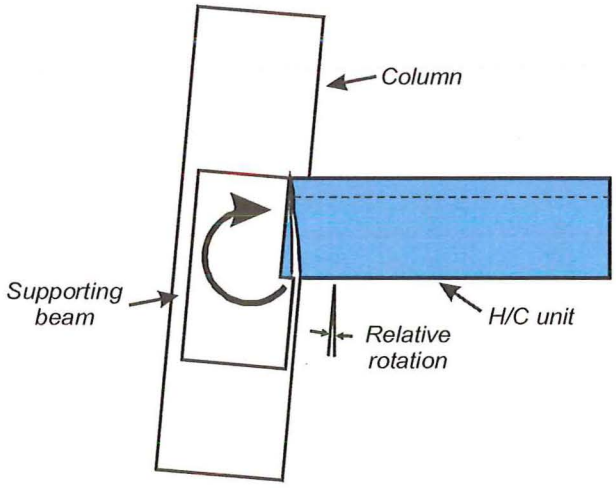

Figure 4-4 A sketch showing what is implied by relative rotation between the hollow-core unit and the supporting beam.

4.3.1 Phase I: Longitudinal Deformation

Throughout this chapter reference will be made to particular hollow-core units (i.e. 1st, 2nd, 3rd, 4th or 5th) within the super-assemblage or to the perimeter beams (i.e. North, South, East and West), refer to Figure 4-1 for their location.

The Phase I displacement sequence consists of completely reversing displacement cycles of ±0.1%, ±0.25%, ±0.5% and ±1.0% plus to half cycles to 2.5% and –2.0% (Figure 4-3(a)).

As testing progressed the seating detail used to attach the hollow-core floor units to the supporting beams (20mm or 40mm on a mortar bed) saw the end of the hollow-core (adjacent to the seat support) start to crack and show signs of distress from an early stage. The first sign of damage to the hollow-core units (primarily the first unit next to the longitudinal frame) occurred at an interstorey drift of 0.32% (Figure 4-5). At a lateral drift of 0.5% the crack widened, and the perception of this level of damage would be sufficient to cause economic loss to the building through possible restriction of occupancy while engineering assessments and attempted repairs were undertaken. As well as seating damage, a longitudinal crack formed in the soffit of the first hollow-core unit, parallel to the southern beam (Figure 4-6). This crack formed in the bottom of the hollow-core unit at the stress concentration created by removing a section of the hollow-core unit around the central column that allowed the hollow-core unit to rest against the side of the main perimeter beam. A longitudinal

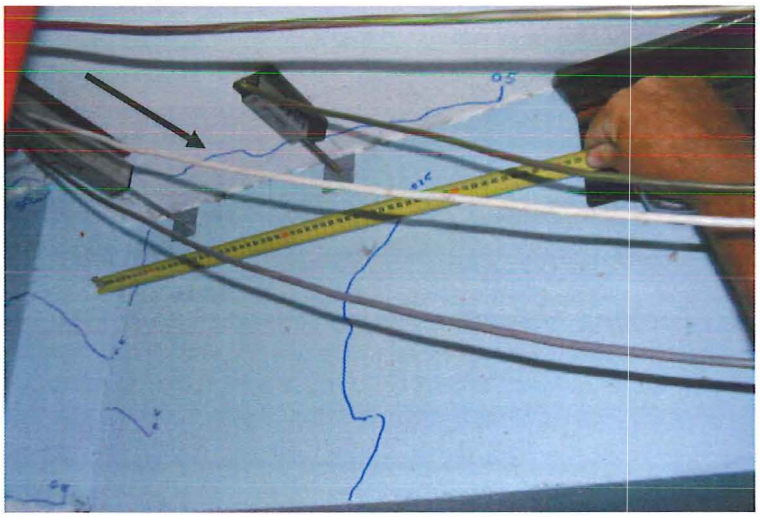

Figure 4-5. First end crack (denoted by arrow) that formed in the first hollow-core unit at a drift of 0.32% (West Beam, SW corner)

crack formed in the topping between the first and second hollow-core units and cracks, associated with the principal tensile stresses of the internal flow of forces, could be seen around the central column (Figure 4-7) at 0.5% drift. Figure 4-9(b) shows the crack patterns at the end of the ±0.5% loading cycles.

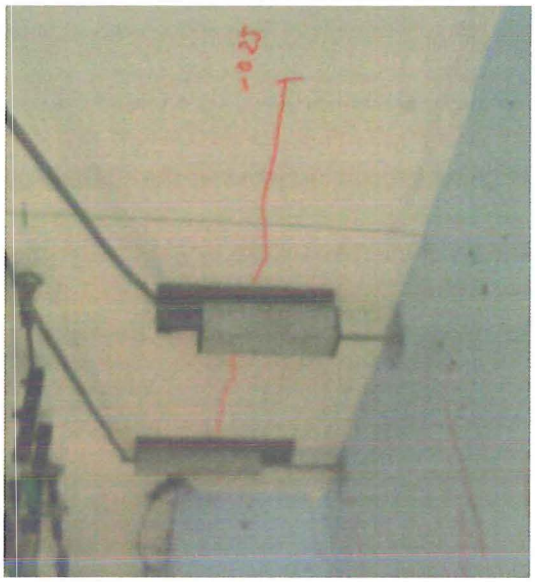

Figure 4-6. Initial hollow-core crack that formed in the soffit of the first unit.

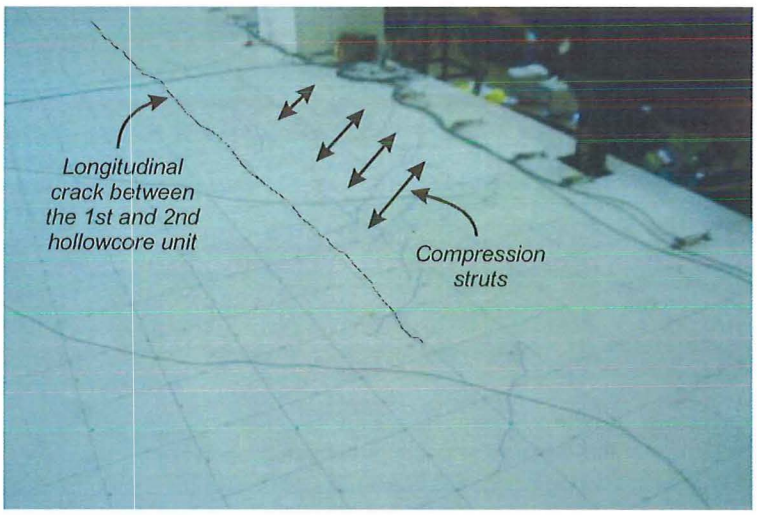

Figure 4-7 Damage around the central column at 0.5% drift

Overall the specimen behaved well up to interstorey drifts of ±1.0%. The discontinuity cracks in the topping at both ends of the super-assemblage had formed (a discontinuity crack is the crack that forms in the topping at the ends of the hollow-core unit as the beam rotates relative to the floor slab, as shown in Figure 4-8).

Delamination of the topping slab from the precast units started to occur adjacent to the columns (Figure 4-10(a)). At this time, the longitudinal crack in the soffit of the first hollow-core unit had extended the full length of the super-assemblage. Figure 4-9(c) shows the crack patterns at the end of the ±1.0% loading cycles.

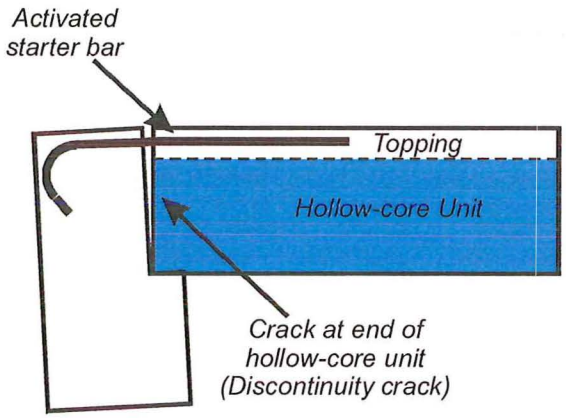

Figure 4-8 Discontinuity crack that formed between the end of the hollow-core unit and the perimeter beam

Significant cracking within the topping slab developed, as the drift increased, leading to a tear forming within the topping between the first and second hollow-core unit at a drift of 1.93% (Figure 4-11). This tear was due to the floor diaphragm suppressing the growth of the beam due to beam elongation (described in more detail in Section 7.3). Eventually the restraint of the beam elongation caused a set of internal forces (tension and compression) within the floor diaphragm that was sufficient to tear the floor diaphragm resulting in the central column translating outwards, away from the floor, and taking the first hollow-core unit with it. The tear caused the cold-drawn wire reinforcing mesh in the topping slab between the first and second hollow-core units to fracture. At 2.5% drift the tear was 9m long and its width varied between zero at the ends of the crack to 20mm at its maximum, the vertical offset between the two floor units varied between 6-10mm.

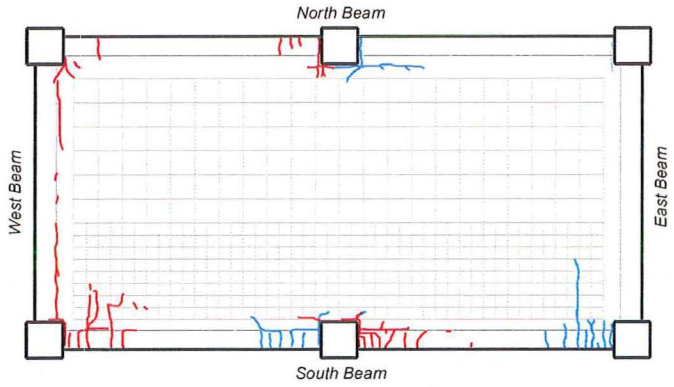

(a) Topping cracks after the ±0.25% drift cycle

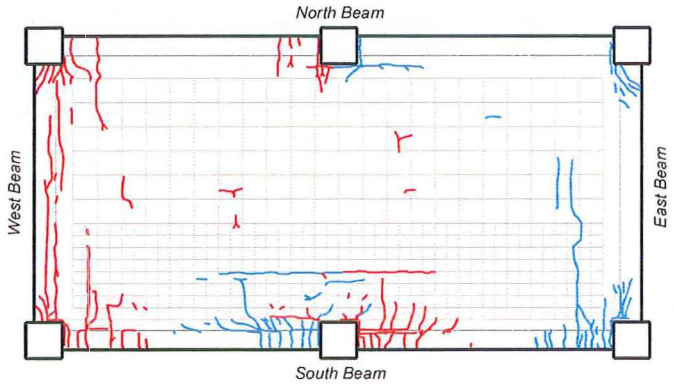

(b) Topping cracks after the ±0.5% drift cycle

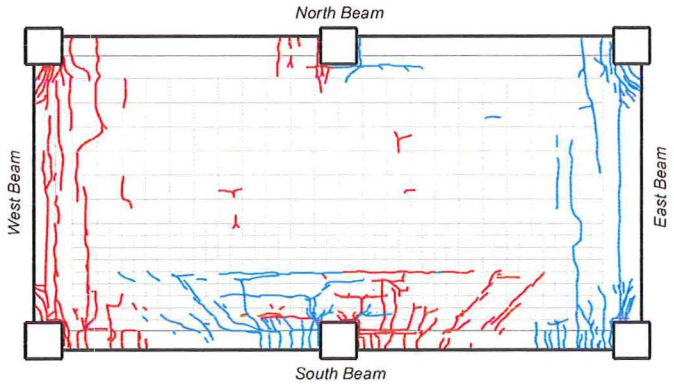

(c) Topping cracks after the ±1.0% drift cycle

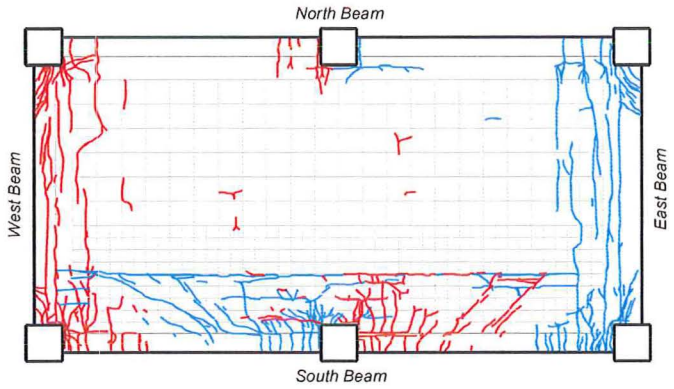

(d) Topping cracks after the +2.5% and –2.0% drift cycles

Figure 4-9 Mapping of the topping cracks during the first phase of loading. Blue cracks are due to a positive inclination while the red cracks are due to a negative inclination

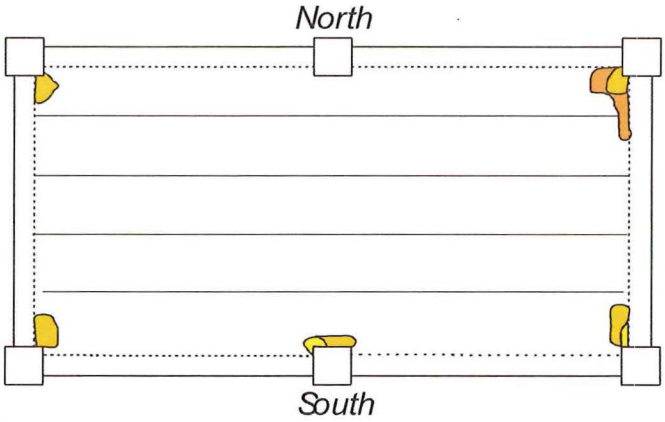

(a) Delamination after the completion of the +/-1.0% loading cycles

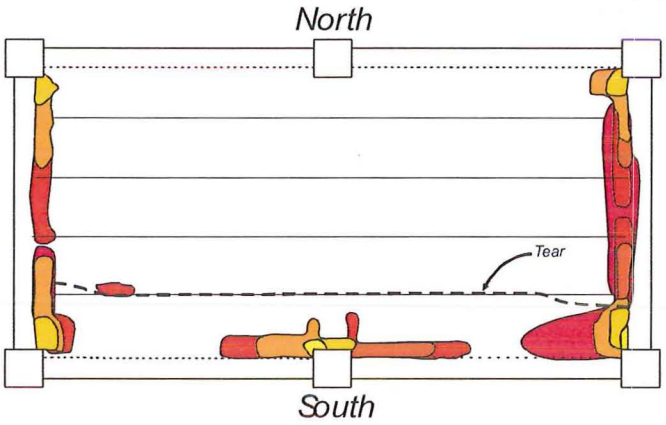

(b) Delamination at the end of Phase I

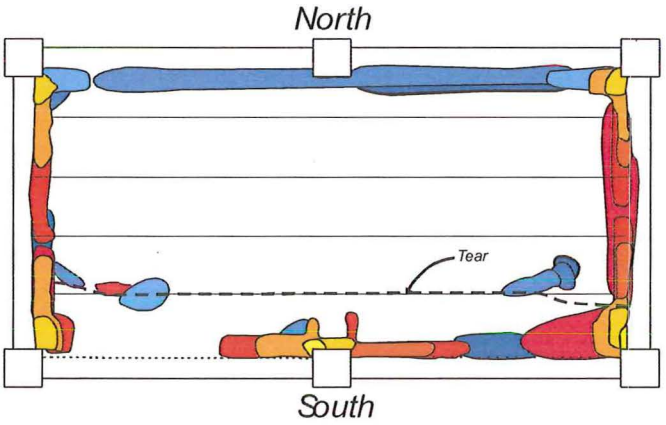

(c) Delamination map after completion of the +2.0% and -2.5% drift cycles

Figure 4-10 Mapping of the delamination of the topping from the hollow-core unit during the experimental programme

At the completion of the –2.0% cycle, the entire seating for the hollow-core units (at both ends) were damaged (Figure 4-12), with several of the units dropping 10mm. There was also significant splitting of the webs within the first hollow-core unit. The split webs started at the West end of the super-assemblage and extended 3m into the

floor slab (Figure 4-13(a)). It should be emphasised that the experimental procedure may be considered to be unconservative as it neglected the higher mode vibrational forces including vertical inertia/ loading effects. If any live load or vertical accelerations had been concurrently applied to the building it would be questionable as to whether the floor would be able to survive. At the completion of the –2.0% drift cycle the central column had displaced by 25mm transverse to the direction of loading (out from the building). This translation had caused the first floor unit to rise 12mm relative to the rest of the floor at the location of the tear. The extent of the crack propagation is shown in Figure 4-14. The translation of the central column was not only due to the elongation of the main perimeter beam (South beam) but the newly formed inverted L shaped beam (beam plus the adjacent floor acting as a flange)

Figure 4-11. Longitudinal tear that formed within the floor diaphragm at 1.93% drift (Plan view)

Figure 4-12. The entire East beam seat of the hollow-core unit has been lost

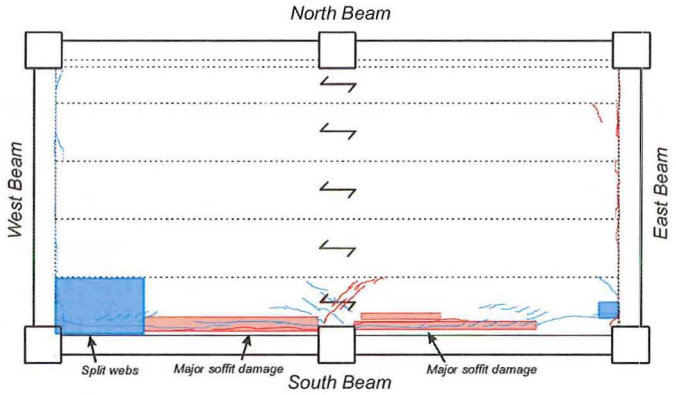

(a) Damage to the hollow-core unit at the end of Phase I

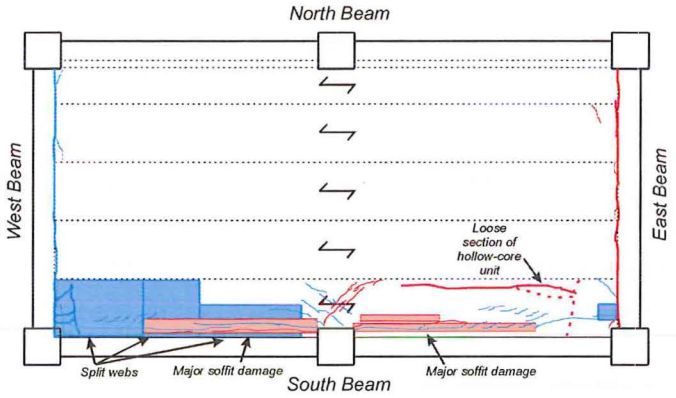

(b) Hollow-core unit damage after the +2.0% and –2.5% displacement cycle during Phase II

Figure 4-13 Damage to the underside of the hollow-core unit during the experimental programme.

contributed to some of this displacement as it tried to bend about sloping principle axes. If this column was in a real structure and the tear had formed over several floors then there is a possibility that the column could fail through buckling since the columns effective length has greatly increased.

The delamination of the floor topping at the end of Phase I of the experiment was concentrated to the two ends of the super-assemblage plus a zone around the central column, as shown in Figure 4-10(b). Figure 4-9(d) shows the crack patterns within the floor slab at the end of Phase I.

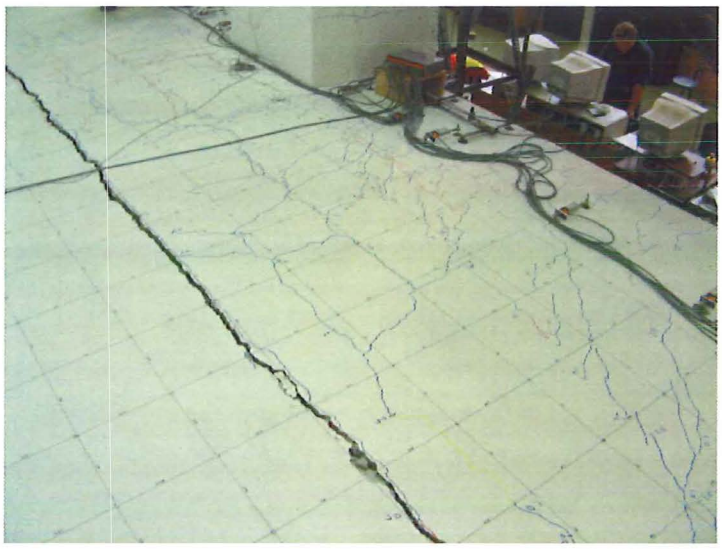

(a) Close up showing the width of tear within the floor diaphragm

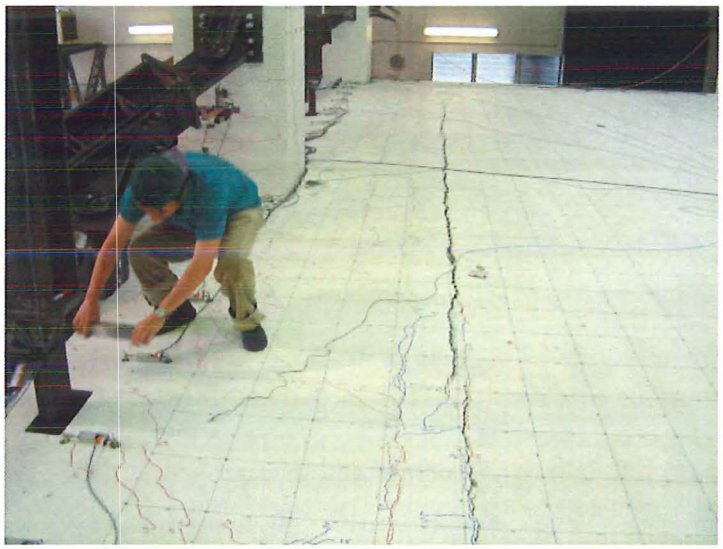

(b) Extent of cracking within the floor

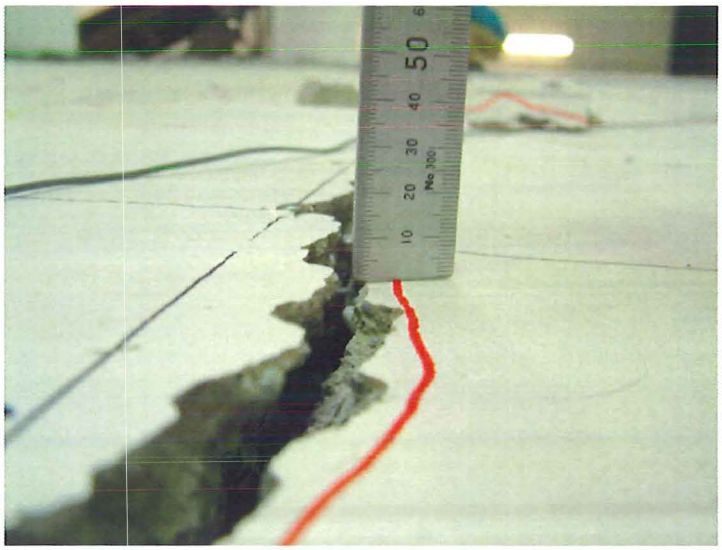

(c) The offset between the two hollow-core units

Figure 4-14. Photos of the diaphragm at the end of Phase I

4.3.2 Phase II: Transverse (Short direction) Deformation.

The Phase II displacement sequence was very similar to Phase I except for two changes. The first being, the cycles to +2.5% and –2.0% were reversed so that the loading was +2.0% and –2.5%. This was changed since the orientation of loading was in the reverse order to the previous Phase I loading. The second change was to add an additional complete cycle of ±3.5%. This cycle was added as it represented a maximum considered earthquake event. This maximum considered displacement cycle was undertaken because the super-assemblage was only going to be loaded in the transverse direction once during the experimental programme and it was thought critical to test the super assembly to these drifts to ensure avoidance of collapse could be achieved.

Therefore, the Phase II displacement sequence consists of completely reversing displacement cycles of ±0.1%, ±0.25%, ±0.5% and ±1.0% plus to half cycles to 2.0% and –2.5% then an additional cycle to ±3.5% (Figure 4-3(b)).

The major tear that formed within the floor diaphragm changed the expected performance of the super-assemblage during the transverse loading. The expected performance, by design, of the diaphragm was for the perimeter beam to rotate relative to the floor units (Figure 4-15(a)) when a negative inclination (the top of the column is displaced in a southern direction while the base of the column displaces in a northern direction) was applied. Due to the pre-existence of the longitudinal tear arising from Phase I, this was not the case. The first hollow-core unit actually lifted as the beam rotated, Figure 4-15(b). When a positive inclination (the top of the column is displaced in a northern direction while the base of the column displaces in a southern direction) was applied, the beam was expected to rotate relative to the hollow-core unit, Figure 4-15(c). Since the side of the first hollow-core was adequately bonded to

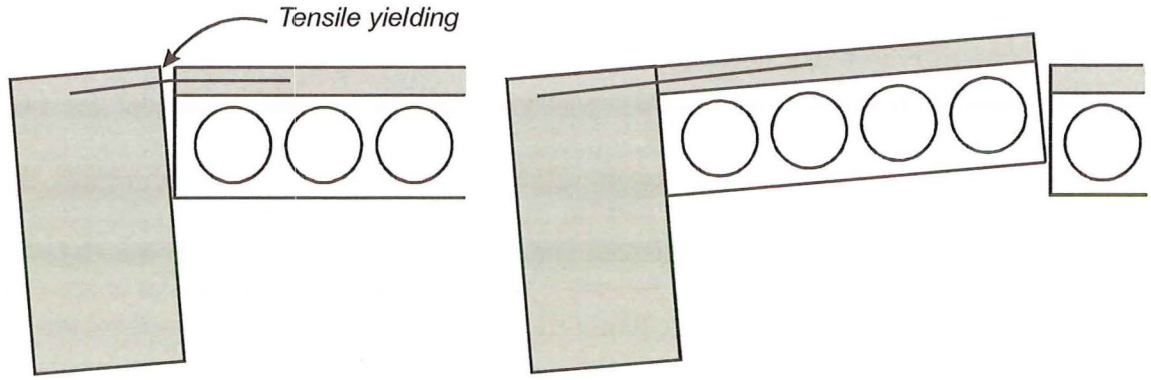

(a) Expected negative moment behaviour (by design)

(b) Observed behaviour

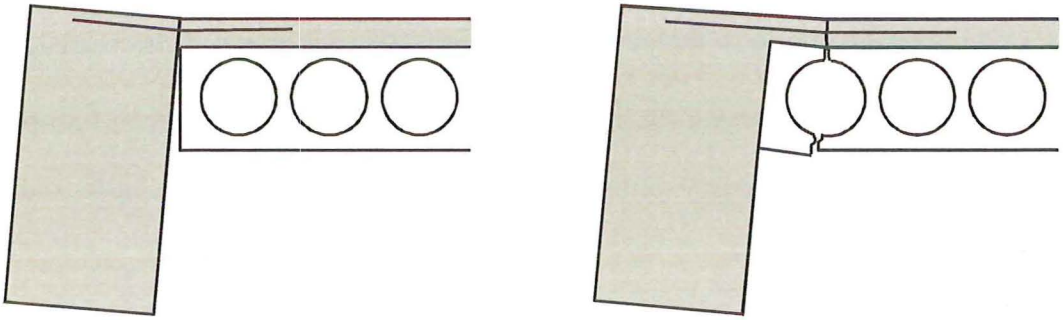

(c) Expected positive moment behaviour (by design)

(d) Observed behaviour

Figure 4-15. Expected and actual rotation of the first unit and perimeter during the transverse loading (Phase II).

the southern beam and the soffit was already cracked, the crack within the soffit of the first hollow-core unit opened further as the inclination increased (Figure 4-15(d)). The manner in which the super-assemblage displaces meant that the condition of the first hollow-core unit degraded as the transverse loading proceeded. The condition of the hollow-core units on the East beam seat deteriorated during the –1.0% drift displacement cycle. More of the mesh within the topping fractured as the diaphragm tear extended. The first sizeable piece of concrete fell out of the hollow-core unit at approximately 2.0% drift, as shown in Figure 4-16(a). Once the piece of concrete had fallen out it was possible to view, by the use of a camera, the extent of the damage within the first hollow-core unit adjacent to the perimeter beam. Extensive damage could be seen to have occurred as shown in Figure 4-16(b) and (c). The width of web

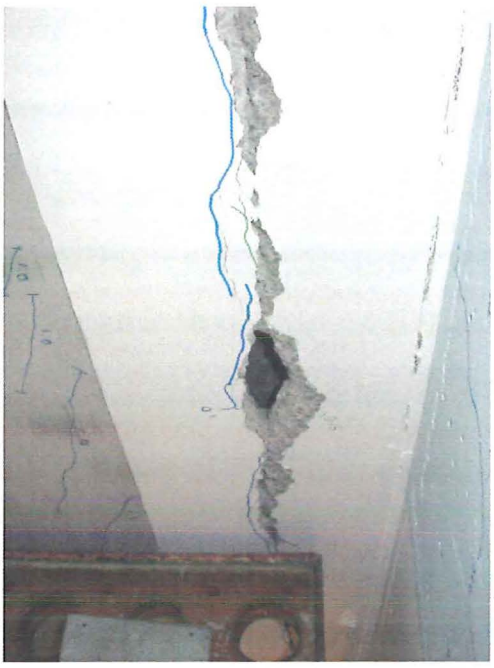

(a) Section of the hollow-core unit that fell out allowing a camera inside

(b) Looking East. Large cracks are seen in the web and the soffit of the unit

(c) Looking West. Several cracks can be seen around the dam.

Figure 4-16. Web splitting within the first hollow-core unit.

crack within the hollow-core unit was approximately 25mm. At this stage, the split webs within the first hollow-core unit had propagated halfway along the length of the unit (approximately 6m), Figure 4-13(b). Over a number of cycles, one small triangular shaped piece of concrete was holding the first floor unit up at the West end of the first hollow-core unit (Figure 4-17) as one of the prestressing strands within the hollow-core unit was still bonded into this piece of concrete. This small section of concrete could not be relied upon to hold for each and every unit during a major earthquake. Significant zones of delamination of the topping were now present within the floor diaphragm as shown in Figure 4-10(c).

Figure 4-17. Section of concrete holding up the hollow-core unit.

At –2.45% drift (on the way to –3.5%) the webs in the fifth hollow-core unit split (Figure 4-18). The length over which the webs had split was approximately two thirds of the super-assemblage (8m). The splitting of the webs was due to the horizontal shearing force applied to the hollow-core unit as it bore against the northern central column.

At the completion of Phase II, the West end of the first hollow-core unit had dropped by some 60mm. The extent of the damage can be seen in Figure 4-19. Figure

4-19(b) shows the exposed tendons after a large section of the hollow-core unit fell out.

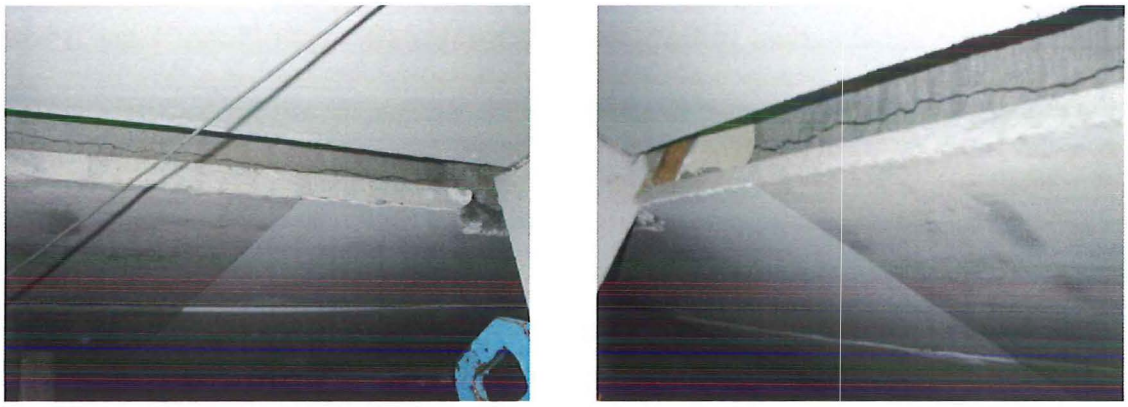

(a) The East side of the back central column **(b) West side of the back central column**

Figure 4-18. The northern (5th) hollow-core units splitting of webs.

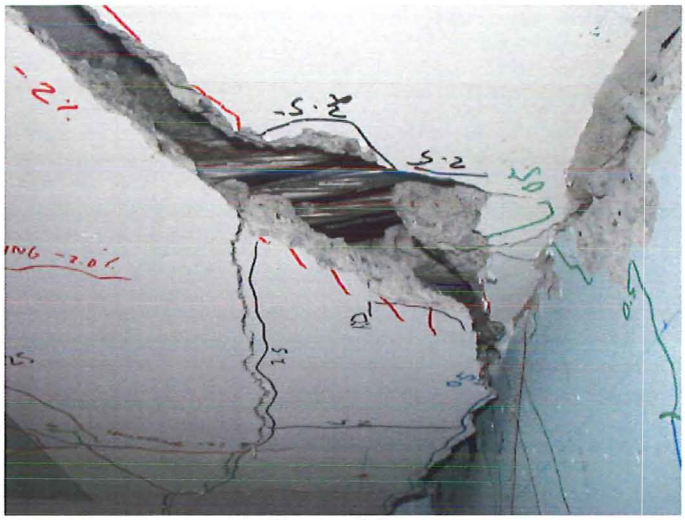

(a) West end damage

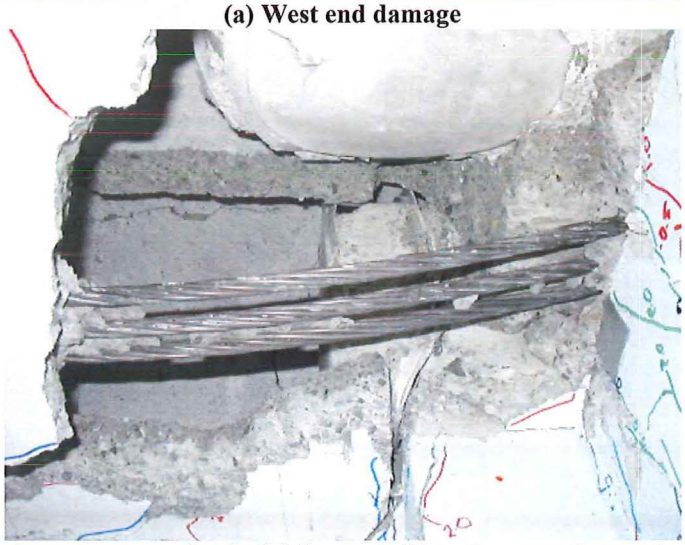

(b) Close up after a large section had fallen out. Note the curved strands are no longer supporting the hollow-core unit.

Figure 4-19. Damaged section of the first hollow-core unit at the West end.

4.3.3 Phase III: Final Longitudinal Deformation

This displacement sequence started with a cycle to ±0.5% to allow a comparison between the initial system stiffness and the stiffness after both Phases I and II were completed. The next cycle was up to ±2.5% so that a comparison between the strengths (applied base shear) in the last cycle in Phase I and the first post yield cycle of Phase III could be made.

The final displacement sequence consists of load cycles to ±0.5% and ±2.5% (Figure 4-3(c)).

During the low cycles of displacement for Phase III another relatively large section of the first hollow-core unit fell out at the West end. Upon inspecting the damage it could be clearly seen that all, but one, of the prestressing strands had been pulled out of the end of the fractured section of hollow-core that remained bonded to the West beam. The pull-out was 20mm (Figure 4-20(a) and (b)). Extensive damage could be seen when looking down the cores of this hollow-core unit (Figure 4-20(c)). A new longitudinal crack formed in the bottom of the East ends third hollow-core unit.

Eventually there was sufficient damage within the first hollow-core unit to allow the entire bottom section to drop to the floor of the laboratory as shown in Figure 4-21. This failure occurred at an interstorey drift of 2.5%. Figure 4-21(d) and (e) look very similar to some of the photos taken at the Meadows Apartment failure following the 1994 Northridge earthquake (Norton et al, 1994).

Upon further loading, to the –2.5% drift amplitude, the remainder of the floor dropped significantly, in some places up to 90mm. Figure 4-22 shows the damage within the floor just prior to the load test. Figure 4-22(a) shows the floor being pushed down by the combination of the end beam rotating and the reinforced topping while

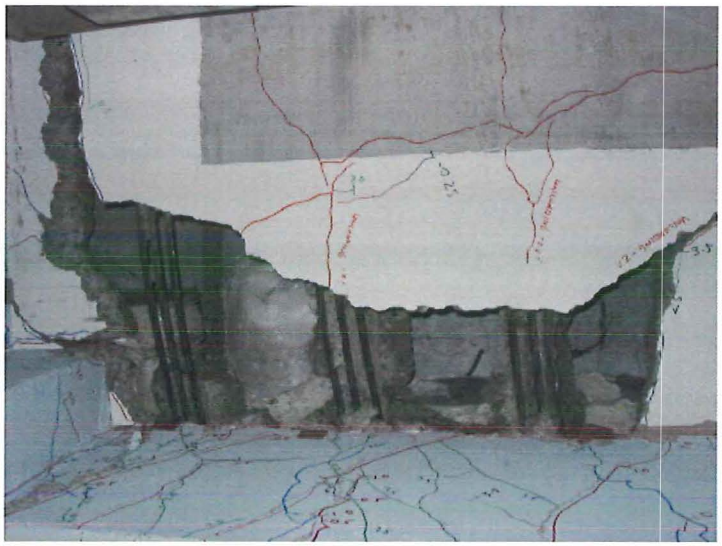

(a) Looking up at the West end of the first hollow-core unit

(b) Strand pull out

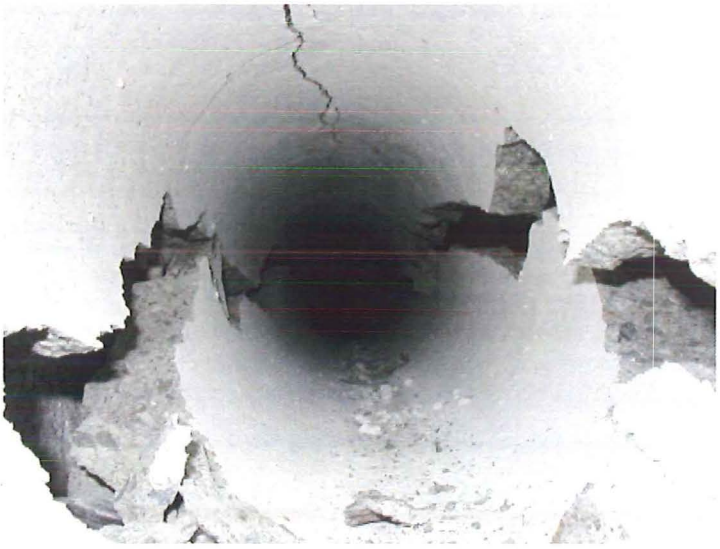

(c) Internal damage to the hollow-core unit

Figure 4-20. Damage at -0.5% drift (Phase III)

(a) The failed unit resting on the catch frame. Highlighted is the piece of concrete that was holding up the unit

(b) The first hollow-core unit just before the prop (far end) was removed.

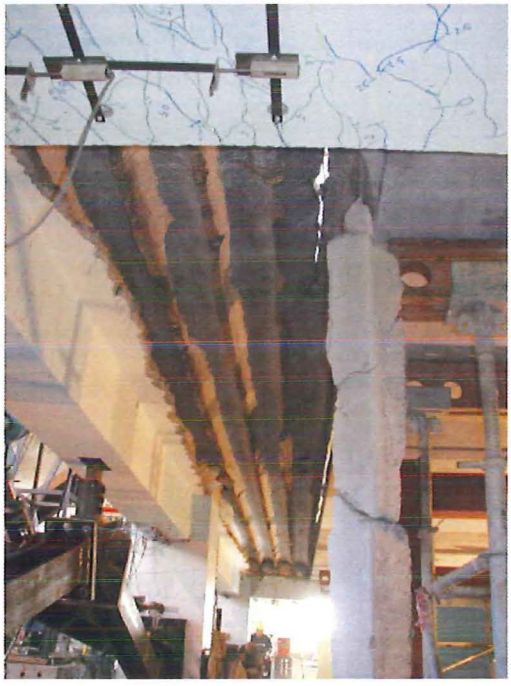

(c) After the prop was removed. The top of the unit remains in place, the soffit of the unit has fallen away.

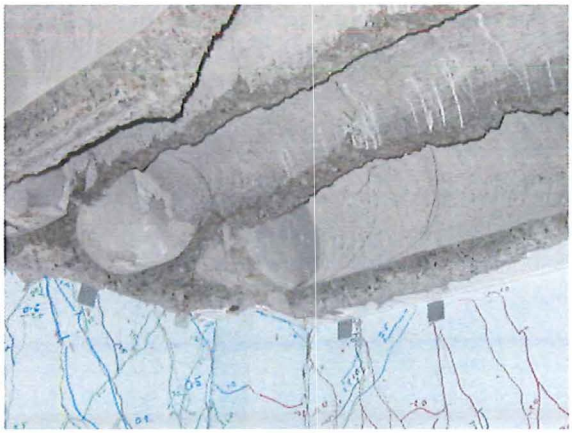

(d) Looking East. Note the end of the hollow-core units are still attached to the beam

(e) Looking West

Figure 4-21. Failure of the first hollow-core unit.

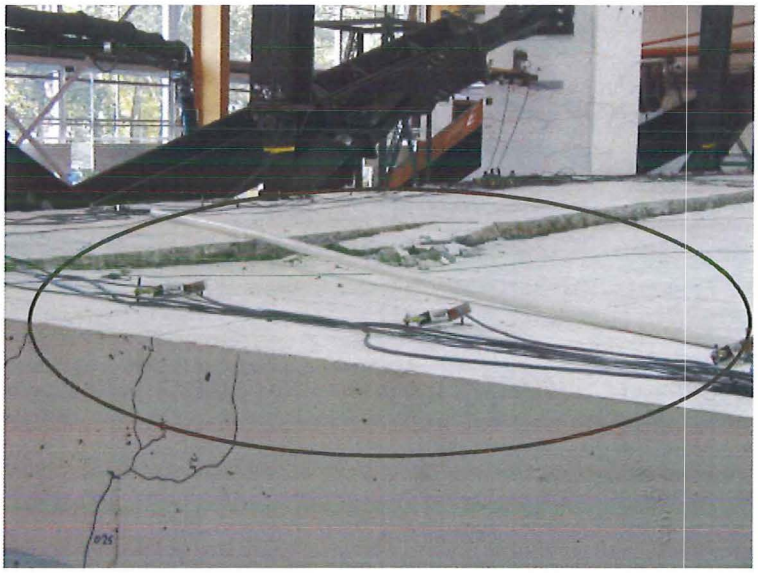

(a) Note the floor has been pushed down by the combination of the end beam rotating and the reinforced topping.

(b) Close up of the second hollow-core unit at the East end (this unit has dropped from 90mm)

Figure 4-22 Photographs of the remaining floor prior to the load test

Figure 4-22(b) shows the extent of the damage to the connection of the second hollow-core unit at its East end. A load test was carried out to see whether the floor could carry its design load. The floor failed as one complete unit when the design live load was applied. Again, the photos of this failure (Figure 4-23) were very similar to that seen in Northridge. Figure 4-23 shows the failed floor from various angles.

A more detailed breakdown of the observed results is included in Appendix D.

4.4 Significant Events

At all the maximum drift amplitudes, during the experimental programme, a series of photographs were taken. These photos include the damage to the particular plastic hinge zones, significant damage to the hollow-core units or a general overview of the test specimen. This detailed photo history is in Appendix E.

Table 4-1 presents the important stages observed during the experimental programme.

(a) Failure of the floor after the load test. Units 2, 3 and 4 failed as one.

(b) Looking up at the floor

(c) The starters and the end of the hollow-core units remain attached to the East beam.

Figure 4-23. Photos of the floor slab following the load test.

Table 4-1 Important stages during the test

Phase I

+0.25% drift	▪ First crack in hollow-core soffit
+0.32% drift	▪ First crack in hollow-core seat
+1.0% drift	▪ Soffit crack spans entire length of super-assemblage ▪ 3-4mm wide crack in hollow-core unit seat at West end (first unit) ▪ First signs of topping delamination from the precast units ▪ Longitudinal crack forms between 1st and 2nd hollow-core units (within topping)
-1.0% drift	▪ Beam spalling at East beam ▪ 2-3mm wide crack in hollow-core unit at East seat
+1.93% drift	▪ Mesh fractures across diaphragm tear (crack width approx 2mm)
+1.98% drift	▪ Continuous sound of reinforcing mesh fracturing ▪ Crack 9m long (3-4mm wide)
+2.5% drift	▪ Diaphragm crack 20mm wide, vertical offset 6-10mm ▪ Discontinuity crack 12mm wide (East end) ▪ Entire West hollow-core seat lost ▪ Significant web splitting in first unit (3m long, starting from West end), small zone around central column ▪ 1st hollow-core unit has dropped 5mm
-1% drift (on to –2%)	▪ More mesh fractures ▪ Split web splitting at East end
End of Phase I	▪ 1st hollow-core unit dropped 10-12mm, all others approximately 5mm ▪ Entire East hollow-core seat lost

Phase II

±0.5% drift	▪ Displaced shape determined by Phase I damage
-1.0% drift	▪ Diaphragm tear extends towards both transverse beams ▪ Became clear that West end of hollow-core unit is being held up by small section of concrete
+2.0% drift	▪ Camera able to be placed inside hollow-core unit to see extent of damage ▪ Web splitting had propagated at least 4m, web crack is 15-25mm wide
-2.5% drift	▪ Significant lifting of hollow-core unit (27-33mm) ▪ Diaphragm tear propagates towards each end, crack changes trajectory ▪ Increase of delamination occurs
±0.5% torsion test undertaken	▪ Performance is governed by pre-existing damage from previous testing
+3.0% drift	▪ Section of West end of hollow-core unit fails ▪ Length of split webs is now 6m ▪ Hollow-core strands have pulled out of beam and are loose
-2.45% drift	▪ Webs in 5th hollow-core unit split. Length of crack is approx. 8m
-3.5% drift	▪ 1st hollow-core unit dropped 55-60mm at West end ▪ Diaphragm tear has propagated the entire length of super assembly

Phase III

+0.5% drift	▪ 9mm difference in height between 1st and 2nd hollow-core unit at the East end
-0.48% drift	▪ Another large section of concrete fell out of the West end of the hollow-core unit ▪ Prestressing strands had pulled out 20mm ▪ 500mm long longitudinal crack forms in the third hollow-core unit (East end)
+1.59% drift	▪ East ends hollow-core units have complete flexure/ shear failure in all units (most probably occurred somewhat earlier)
+1.88% drift	▪ Visual lifting of topping occurs around central column
+2.5% drift	▪ 1st hollow-core unit fails, entire bottom half of unit collapses ▪ Top half of hollow-core unit remain attached to topping
-2.5% drift	▪ Reinforced topping are seen to push down the floor ▪ East end of hollow-core units have dropped 30-90mm ▪ Remainder of floor fails when load tested

4.5 Hysteretic Response

4.5.1 Global hysteretic performance

Phase I

Figure 4-24(a) presents the overall observed hysteretic response for the super-assemblage specimen for Phases I and III. It should be noted that there was a marked drop in strength at 1.9% drift resulting from a longitudinal tear that formed in the topping slab between the first and second hollow-core units. Apart from this strength loss, the hysteresis loops show stable performance with no pinching evident that can arise from flexure-shear cracking. The maximum base shear imposed during a positive inclination (the top of the column is displaced in a eastern direction while the base of the column displaces in a western direction) cycle was 1357kN that occurred just prior to the tearing of the floor diaphragm. Once the tear formed, the load dropped some 5 percent to 1284kN and the super-assembly gained no additional strength when loaded in the positive direction. The reason for no additional strength gain is that the width of slab acting as a tension flange was limited to the first hollow-core unit as this was the width of slab still attached to the perimeter beam. The maximum applied base shear imposed during the negative inclination (the top of the column is displaced in a western direction while the base of the column displaces in a eastern direction) cycle was 1213kN and this occurred at –2.0%.

Phase II

Figure 4-24(b) presents the overall observed hysteretic response for the East and West bays of the super-assemblage. The shape of the hysteresis loop for the second phase of loading did not appear to be affected by Phase I, the super-assembly continued to

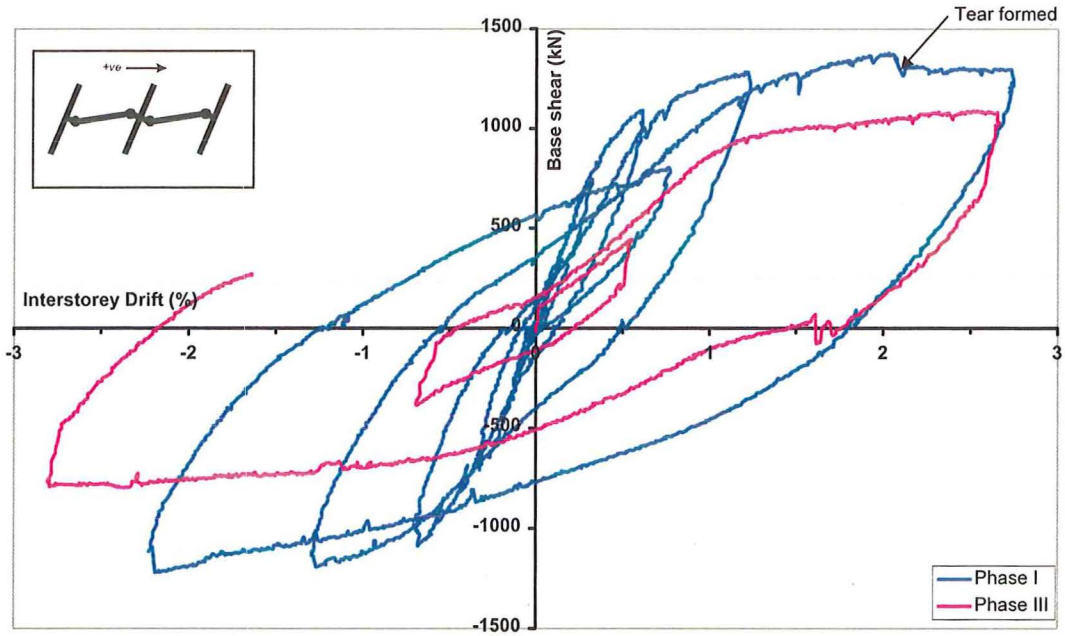

(a) Combined hysteresis loops for Phase I and III

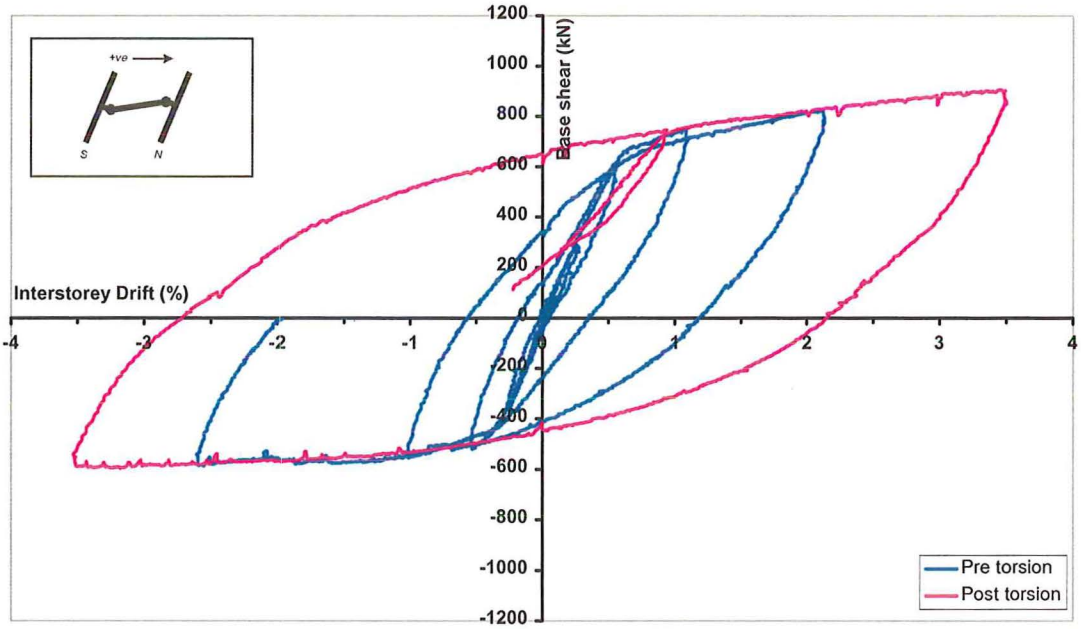

(b) Hysteresis loop for Phase II

Figure 4-24 Hysteretic performance of the super-assemblage throughout the three phases of the experiment.

gain strength with each load cycle as shown in Figure 4-24(b). The diaphragm tear did affect the amount of strength enhancement the floor diaphragm provided to the lateral strength of the super-assemblage. When a negative drift was imposed, (i.e. the South plastic hinges experience a negative moment) the diaphragm enhancement was limited because the diaphragm tear meant that the first hollow-core unit was being lifted rather than allowing the starter bars to be activated (and yield). This can be seen in Figure 4-24(b) because the applied base shear for a positive inclination is approximately 300kN greater than a negative inclination even though both directions have a symmetrical reinforcement layout. Figure 4-24(b) also shows that the small torsion test (refer to Appendix F) carried out between the –2.5% half cycle of the 3.5% half cycle did not affect the lateral strength of the super-assembly.

The maximum applied base shear was 897kN and 586kN for a positive and negative inclination, respectively. When the Phase II base shears are compared with Phase I the values were considerably less. This difference is due to two major reasons, firstly, the hollow-core units span perpendicular to the Phase II loading direction, hence the hollow-core units contribution to the lateral strength was negligible as the prestressing strands were not activated, and secondly, the diaphragm tear affected the starter bar activation during the negative inclination cycle.

If the tear had not formed, the positive and negative base shear should be more closely matched as the super-assemblage had symmetric reinforcement details in the East and West beams for both directions of loading during Phase II.

Phase III

Figure 4-24(a) shows the hysteretic response for the third phase of loading. There was still no pinching of the loop and the failure of the floor did not appear to have a major affect on the shape of the hysteresis loops of the super-assemblages. The lateral load

capacity may have been affected. Comparing the Phase III hysteresis loop with the initial Phase I response it is possible to see that the transverse loading did not affect the strength of the frame; the two curves match each other well. The Phase III applied base shear was slightly less than that applied during Phase I, this could be attributed to two features: the degradation of the first hollow-core unit and the connection of this unit to the perimeter frame and general degradation of the perimeter frame.

Refer to section 5.9 to determine the factors that contribute to the lateral strength of the super-assembly.

4.6 Decomposition of Lateral Displacements

Figure 4-25 presents the components of lateral displacement at each peak load cycle for the phases of the experiment. These components were calculated using the procedure described in Lin (1999). The results are presented as a proportion of the lateral applied displacement.

A combination of fixed end (plastic) rotation and beam flexure was the main source of lateral deformation during the loading cycles. The column deformation was not monitored during the experiment as the columns were expected to remain elastic, this assumption was correct as the columns sustained minimal cracking during the experimental programme. Typical values for the contribution from the elastic deformation of the columns can be expected to range up to 20% of the total contribution for drifts below yield (observations made from the results of Restrepo et al, 1993). Once the beam plastic hinges form, the majority of the deformation is then due to the plastic rotation within the plastic hinge zones so therefore the column contribution is minimal.

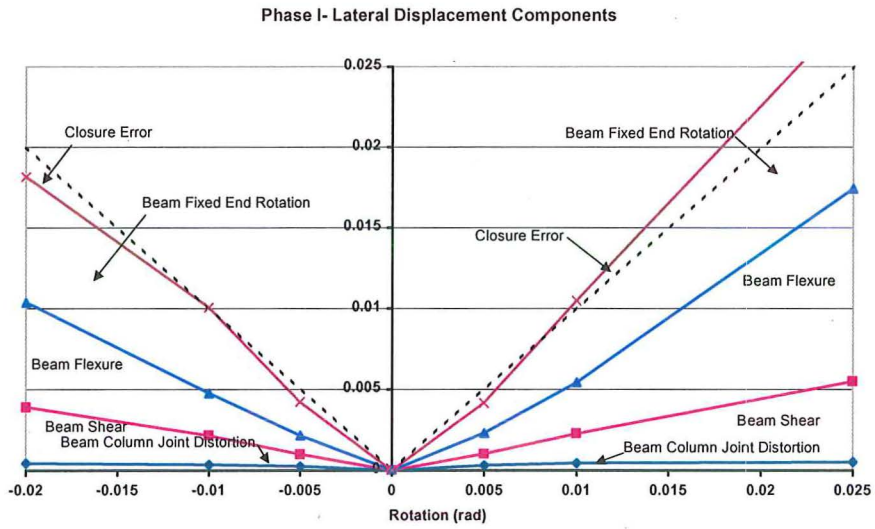

(a) Components of lateral displacement for Phase I load cycles

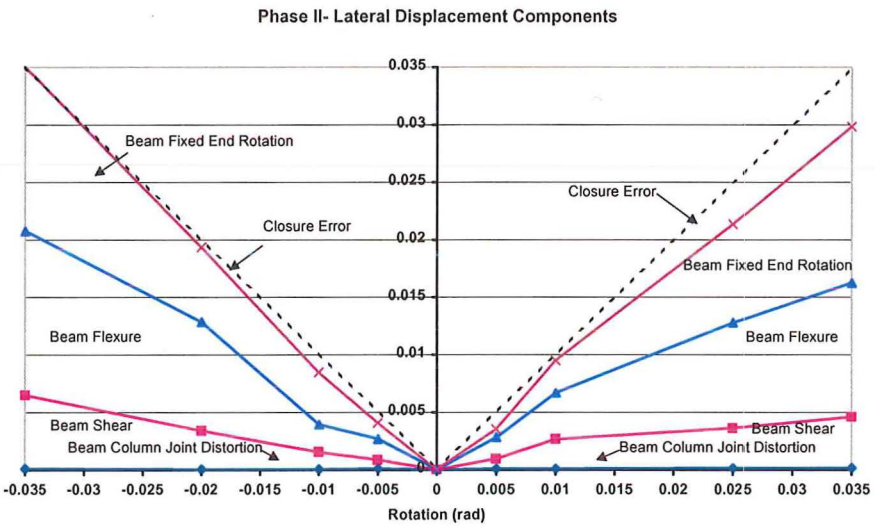

(b) Components of lateral displacement for Phase II load cycles

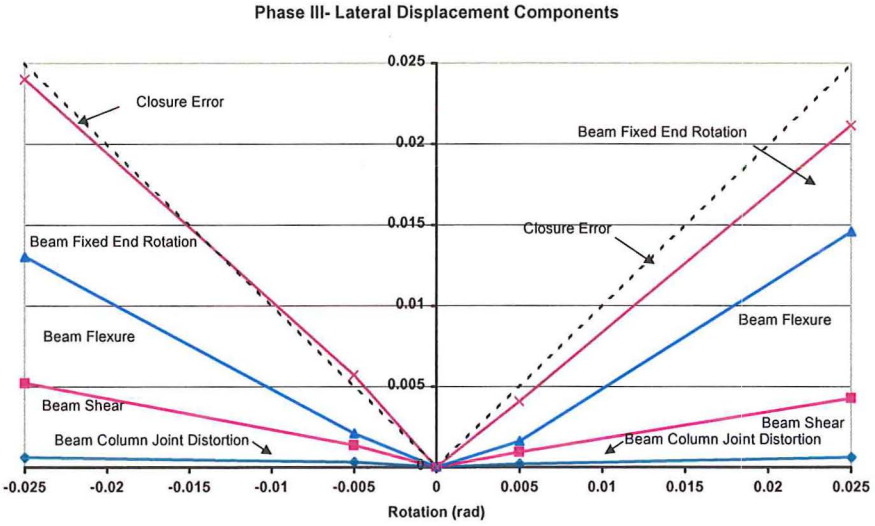

(c) Components of lateral displacement for Phase III load cycles

Figure 4-25 The components that contribute to the lateral displacement of the super-assemblage

For Phase I, Figure 4-25(a) shows that the beam column joint contribution was very low. This was observed during the test by the minimal cracking that appeared within the beam column joint. The closure error varies throughout Phase I. At low drifts the error is due to some of the deformation occurring outside the instrumented plastic hinge zones while at larger drifts the error was due to instrumentation errors.

For Phase II, Figure 4-25(b) illustrates the components of lateral displacement at each peak during the loading cycles. The results are presented as a proportion of the lateral applied displacement. As like Phase I, the fixed end rotation and beam flexure components dominated the interstorey displacement. The relatively large closure error during the positive cycles was due to instrumentation error. One potentiometer ran out of travel while another potentiometer failed.

At low drifts the fixed end rotation component was relatively low. This is because the small load cycles displacement was governed by the torsion cracks that had formed in the transverse beam during the Phase I loading. As the drifts increased the new cracks patterns that formed during Phase II governed the performance and the magnitude of all the components contributing to the lateral displacement were as expected.

Figure 4-25(c) illustrates the components of lateral displacement at each peak load cycle for Phase III. Two main factors contributed to the lateral displacement for Phase III. During the positive drift cycles, beam flexure dominated where as fixed end rotation dominated during the negative drift cycles.

4.7 Classification of Building Damage

It is becoming increasingly popular to quantify (or define) the various levels of damage to structures after an earthquake with either a colour-coded or numerical format. For the colour-coded format, the level of damage to a building has been

assessed the building is then marked (tagged) with a certain colour card from green to red. The different coloured ratings available are summarised in Table 4-2. Such a system is currently being promoted by the New Zealand Society for Earthquake Engineering. By quantifying the level of damage that a building has experienced gives guidance as to whether the building can be entered following the earthquake. If an earthquake were to occur in New Zealand then the classification of damaged buildings would be made by experienced and trained (in post-earthquake assessment) structural engineers such as the Structural Engineering division of New Zealand Urban Search and Rescue (www.usar.govt.nz).

The other form of classification is to classify the damage to the buildings by a number between one and five that also refers to the level of damage (Table 4-3).

By comparing Table 4-2 and 4-3 above it can be seen that both forms of classification are similar. Table 4-4 shows the comparison between the two types of classification.

Following the completion of the experimental testing programme it was possible to classify the super-assemblage according to the two classification methods; the results are summarised in the tables below. It should be noted that since the classification of performance between the reinforced concrete moment resisting frame and the hollow-core floor slab was so different, the two components were classified separately.

In Table 4-5 and 4-6, the marked difference in performance between the reinforced concrete moment resisting frame and the hollow-core floor slabs is evident. If the global classification of the structure were required, then the floor performance values would be stated, as these are critical to the overall structure.

Table 4-2 Colour coding for Buildings following an earthquake.

Tag Colour	Description of level of damage
Green	No damage, building occupiable
Yellow	Moderate levels of damage. Building can be entered to remove belongings
Orange	Heavy damage. Building can be entered for brief periods to remove *essential important* items only
Red	Near Collapse. Building *cannot* be entered

Table 4-3 Definition of the damage states used to classify the level of damage to a structure following an earthquake (Mander, 2003)

Damage State	Description of Damage	Post-earthquake Utility of Structure
1	None (pre-yield)	Normal
2	Minor/Slight	Slight Damage
3	Moderate	Repairable damage
4	Major/Extensive	Irreparable damage
5	Complete collapse	Irreparable damage

Table 4-4 Comparison between the colour coded and numerical damage states

Tag Colour	Corresponding Damage State
Green	1-2
Yellow	2-3
Orange	3-4
Red	4-5

Table 4-5 Colour coding classification for the super-assemblage

Tag Colour	Floor (interstorey drift)	F_vS_1 or PGA for Floor (g)	Structural Frame (interstorey drift)	F_vS_1 or PGA for Frame (g)
Green	0.1%	0.05	2%	1.0
Yellow	0.3%	0.15	2.5%	1.25
Orange	1.0%	0.5	3.5%	1.75
Red	1.9%	0.95	-	

Table 4-6 Damage state classification for the super-assemblage

Damage State	Floor (interstorey drift)	F_vS_1 or PGA for Floor (g)	Structural Frame (interstorey drift)	F_vS_1 or PGA for Frame (g)
2	0.3%	0.15	1.0%	0.5
3	0.35%	0.175	2.5%*	1.25
4	1.9%	0.95	3.5%+	1.75
5	2.5%	1.25	-	

* based on the longitudinal beams that were later repaired

+ based on the longitudinal beams that were later rebuilt

4.8 Fragility Implication of Drift Damage

In Chapter 2 a study was conducted to investigate the expected interstorey displacement (drift) demand on this class of precast concrete structure. For sake of completeness the overall result is presented in Figure 4-26. In terms of the expected (median) drift the basic finding was as follows

$$\tilde{D}_D = 2.0F_vS_1 \quad \text{(4-1)}$$

or

$$\widetilde{D}_D = 2.0PGA \tag{4-2}$$

in which $\widetilde{D}_D$ = the median (50th percentile) drift demand as a percentage of the storey height; F_vS_1 = one second spectral acceleration for tall structures (above four stories); and PGA = peak ground acceleration for low rise structures (up to four stories).

It was also demonstrated that the distribution of drift outcomes was lognormal with a lognormal coefficient of variation of β_D = 0.52 (note the subscript D stands for demand).

By inverting Equations (4-1) and (4-2), the expected (median or 50th percentile) ground motion demand needed to achieve a given median drift capacity can be found such that

$$\widetilde{F}_v S_1 = 0.5\widetilde{D}_c \tag{4-3}$$

or

$$\widetilde{PGA} = 0.5\widetilde{D}_c \tag{4-4}$$

where $\widetilde{D}_c$ = expected drift capacity of the structure.

Now the parameter $\widetilde{D}_c$ is not precisely known, but assuming that the full-scale experiment provides a reliable indicator of the expected capacity, and assuming this capacity has a coefficient of variation of β_C=0.2 (this is in keeping with the findings from Dutta (1999)), Kennedy et al (1980) has shown that the composite value of the lognormal distribution is found by

$$\beta_{C/D} = \sqrt{\beta_C^2 + \beta_D^2 + \beta_U^2} \tag{4-5}$$

in which β_C and β_D are as defined above, and β_U is a lognormal dispersion parameter for modelling uncertainty. The latter parameter has been taken as β_U=0.2. Thus applying Equation (4-5) gives $\beta_{C/D}$=0.60. This value is in keeping with results

inferred from observed damage to bridge structures in the 1994 Northridge earthquake (Mander and Basöz, 1999).

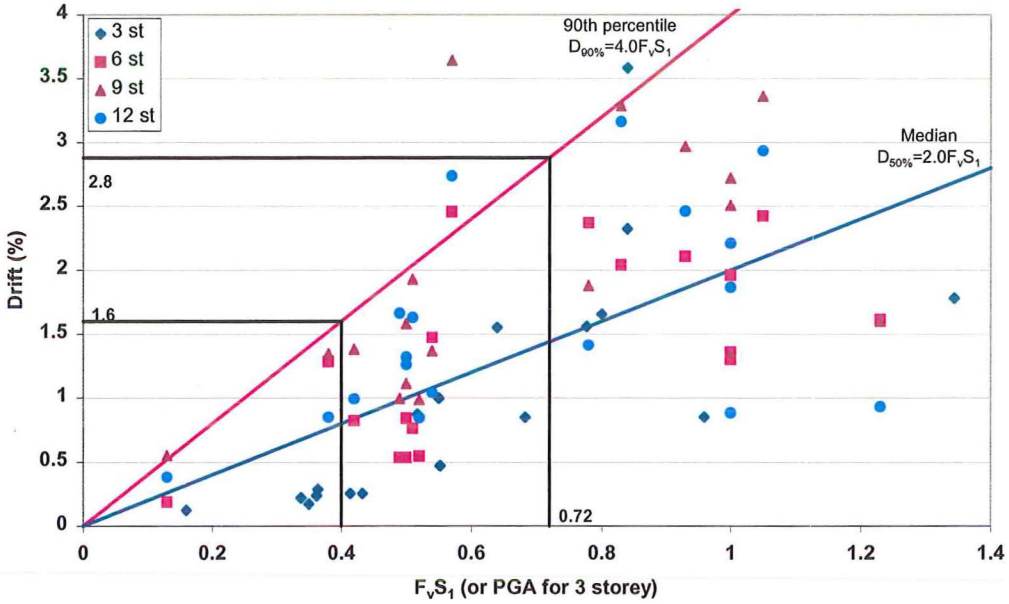

(a) An interstorey drift versus F_vS_1 (and PGA) plot for all the structures

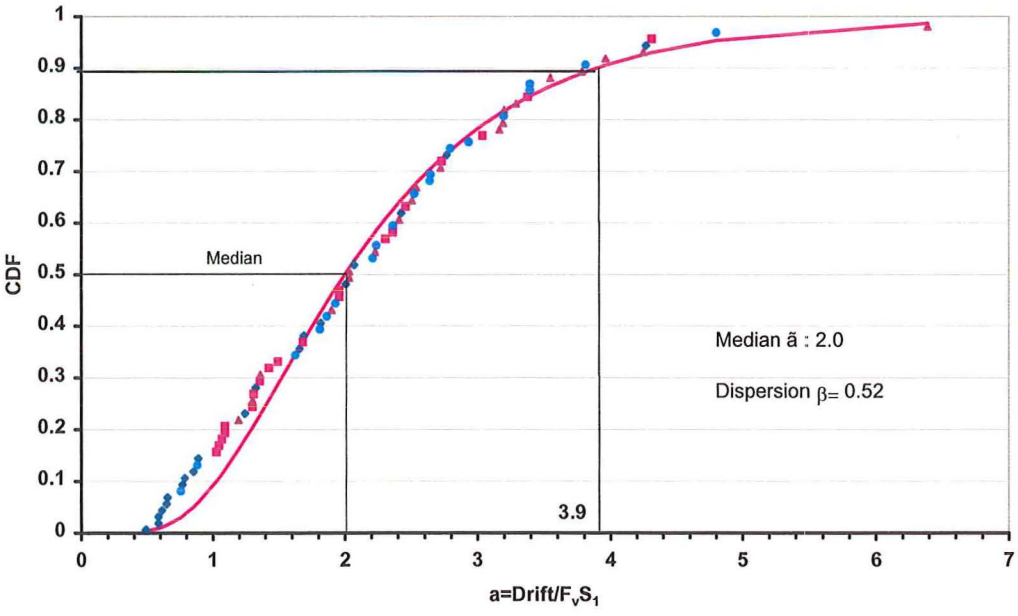

(b) A cumulative distribution function plot for all the structures

Figure 4-26 Combined results for the four different building heights examined

By using a lognormal cumulative distribution that can be described by a unit lognormal variate ξ_β (where the median = 1 and lognormal coefficient of variation β=0.6), the distribution of ground motion demands necessary to produce a given damage state outcome can be found by

$$F_v S_1 = 0.5\tilde{D}_c(DS)\xi_\beta \quad \textbf{(4-6)}$$

$$PGA = 0.5\tilde{D}_c(DS)\xi_\beta \quad \textbf{(4-7)}$$

where $\tilde{D}(DS)$ = expected value (in this case the experimentally observed drift) for a given damage state (*DS*).

From Table 4-5 and 4-6, fragility curves for precast concrete buildings constructed in New Zealand during 1980's-90's can be determined.

Figure 4-27 shows the fragility curves for the rating of the floor and frame performance in terms of the colour-coding format. Figure 4-27(a) shows that for an earthquake with a probability of occurrence of 2% in 50 years, the Maximum Considered Earthquake (MCE), F_vS_1=0.72g for Wellington, if the structures performance was classified in terms of the floor performance that 72% of structures would be expected to be red tagged (Strictly *no entry*) or have collapsed. The remaining 28% of structures would be expected to sustain a level of damage that will allow building occupants to enter into the building for *brief periods to remove essential items only*. Even under a 10% in 50 years, Design Basis Earthquake (DBE), F_vS_1=0.4g for Wellington, 35% of structures would be red tagged or have collapsed, 60% orange tagged and 5% yellow tagged. It is very probable that building owners will be surprised and concerned over the performance determined here.

Figure 4-27(b) shows that for a MCE if the structures performance is classified in terms of the frame performance (rather than the hollow-core floor) that 70% of structures might be expected to sustain minimal damage and will be able to have

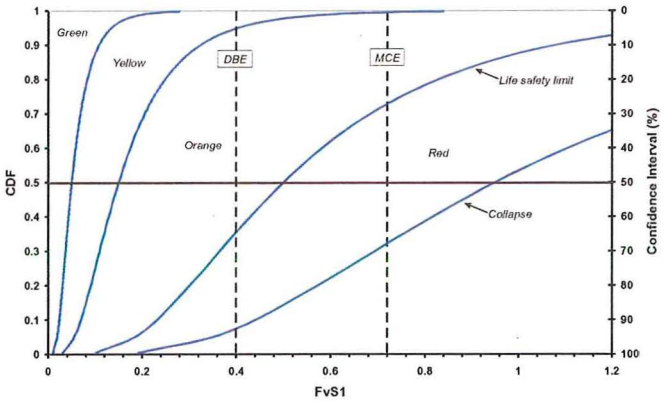

(a) Fragility curve for the floor performance when rated according to colour coding

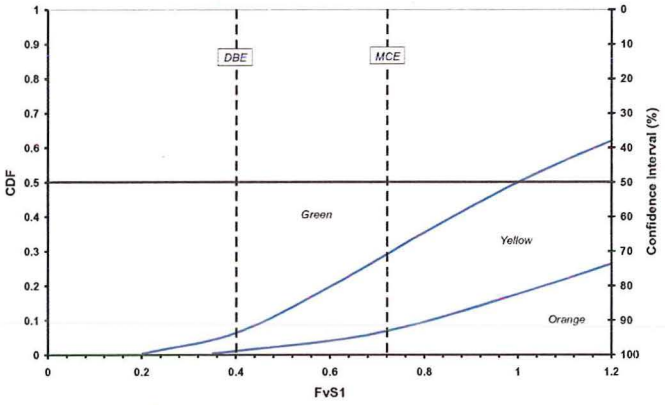

(b) Fragility curve for the frame performance when rated according to colour coding

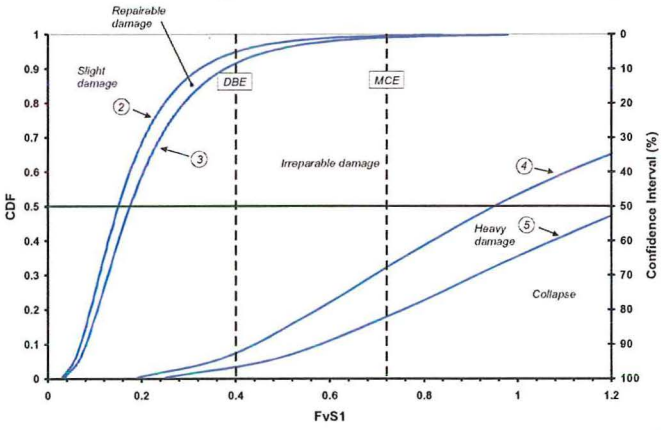

(c) Fragility curve for the floor performance when rated according to damage states

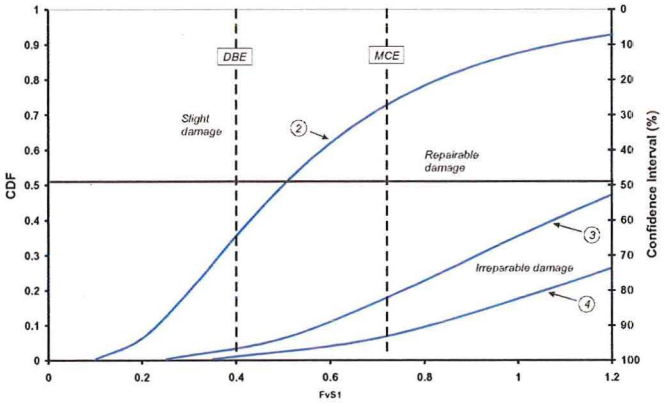

(d) Fragility curve for the frame performance when rated according to damage states

Figure 4-27 Fragility curves using both a colour-coded and numbered format for quantifying building damage

immediate occupancy (green tagged) after the earthquake, as there was little or no damage. 22% of buildings would be yellow tagged and 8% would be orange tagged. This finding is in keeping with the expectations of ductile structures designed and detailed in accordance with the principles of capacity design.

Figure 4-27 shows the fragility curves for the rating of the floor and frame performance in terms of different damage states. Figure 4-27(c) shows that for a MCE if the structures performance is classified in terms of the floor performance that 2% of structures would be expected to sustain slight or repairable damage. The remaining 98% of structures would be expected to be demolished as a result of irreparable damage or collapse, of these some 32% of floors would be expected to partially or entirely collapse leading to loss of life. Under a DBE, 92% of structures would sustain excessive damage, with some 8% potentially leading to loss of life. Ironically, some engineers may consider this to be a satisfactory outcome as there is more than 90 percent confidence that loss of life will not occur. However, given that the vast majority of the buildings would be unsafe and need demolishing, this is unsatisfactory, let alone considering that nearly 10% of structures could collapse, leading to loss of life.

Figure 4-27(d) shows that for a MCE if the structures performance is classified in terms of the frame performance (rather than the floor) that 93% of structures might be expected to sustain damage that is either slight or repairable and 7% will require demolition.

4.9 Concluding Remarks

This chapter has discussed the observations that occurred during the testing of the super-assemblage. Initial damage to the hollow-core units occurred early in the programme and the mode of failure was different to that assumed by design. The

assumed performance was for the hollow-core unit to slide off its seat as the building grew in length due to beam elongation. Eventually the damage within the system became so great that the first hollow-core unit failed, shortly afterwards, following a load test, the remainder of the floor failed.

One major point to note is that even though the floor failed, the perimeter frames beams, columns, and beam column joints remained relatively undamaged. Clearly, significant extra attention is required to be paid to the hollow-core seating details to ensure that this class of precast floor system performs at a level that is not inferior to that of the structural frame.

Once the tear formed within the floor diaphragm the amount of strength enhancement from the floor slab to the lateral strength of the super-assemblage was limited.

One important point that should be taken from these test results is even though the hysteresis loops appear to be well formed and dissipated a reasonable amount of energy these can lead to misleading results. Apart from the small drop in load when the diaphragm tore there was no evidence to indicate the overall poor performance of the system as a whole and particularly the very poor performance of the precast floor. Assessment of the frame performance alone is inadequate to determine the damage state, and hence life safety exposure, of a building. The state of suspended floors is an integral part in the overall structural assessment of such buildings.

By using fragility curves it is possible to determine the implications that the drift damage has on New Zealand constructed buildings. This study has shown that the number of buildings that would require demolition following a maximum considered earthquake (MCE) for Wellington would be low if the rating reported was that for the frame performance and well in keeping with the expectations of capacity

design. The frame performance is also a good guide for the rating for cast insitu reinforced concrete construction. If the floor performance was reported (as should be the case for precast hollow-core construction) a 2% in 50 years (MCE) event in Wellington would see almost total devastation of precast buildings that have either partially or fully collapsed. Large loss of life could also be expected. Under a 10% in 50 year (DBE) event, the situation is also not good, some 90% of buildings might be expected to be demolished including 8% that could potentially cause loss of life.

Whether the building damage is rated by the colour-coding format or by damage states the same conclusions can be drawn.

4.10 References

Dutta A, 1999, *On Energy-Based Seismic Analysis and Design of Highway Bridges*, Ph.D Dissertation, science and Engineering Library, State university of New York at Buffalo, Buffalo, NY

Kennedy R.P, Cornell, C.A, Campbell R.D, Kaplan, S and Perla H.F, 1980, *Probabilistic Seismic Safety Study of an Existing Nuclear Power Plant*, Nuclear Engineering and Design No. 59, pp 315-338

Lin C.M, 1999, *Seismic Behaviour and Design of Reinforced Concrete Interior Beam Column Joints*, PhD thesis, Department of Civil Engineering, University of Canterbury, Christchurch

Mander J.B, 2003, *Beyond Ductility: The Quest Goes On*, Symposium to Celebrate the Lifetime Contributions of Professors Emeriti Tom Paulay and Bob Park, July, Christchurch, New Zealand, pp 75-86

Mander J.B and Basöz N, 1999, *Seismic fragility curve theory for highway bridges in transportation lifeline loss estimation* in Optimising Post-Earthquake Lifeline System Reliability, TCLEE Monograph No. 16 Eds Elliot and McDonough

Chapter 5

Forensic Analysis

5.1 Introduction:

Concern has been raised regarding the likely performance of some of New Zealand's precast concrete buildings during an earthquake, in particular those constructed with hollow-core floor slabs. The failure of the Meadow Apartments during the Northridge earthquake on the 17th January 1994 has provided more information regarding the possible poor performance of this flooring system if the connection with the supporting beam is not properly detailed. A large experimental programme has been undertaken at the University of Canterbury to test the likely performance of a typical New Zealand precast concrete building during an earthquake.

The super-assembly experiment in this research represented a corner section from a lower storey of a typical precast concrete building. The specimen consisted of 750mm deep beams with a bay length of 6.1m. The overall dimensions were approximately 12m long by 6m wide. The precast floor units tested were 300mm deep hollow-core units (designated "300 series"). The units were topped with a 75mm cast insitu concrete topping slab that included cold-drawn wire reinforcing mesh. Spanning 11.8m; the hollow-core units by passed the central perimeter column that was on a 6.1m grid pattern. The hollow-core units were seated on two end beams with an actual seat (ledge) length of 20mm on the East beam and 40mm on the West beam. These provided seats were considered to be representative of the range of seat-widths adopted in the field over the past two decades (1980's and 1990's). Figure 5-1 shows the super-assembly dimensions.

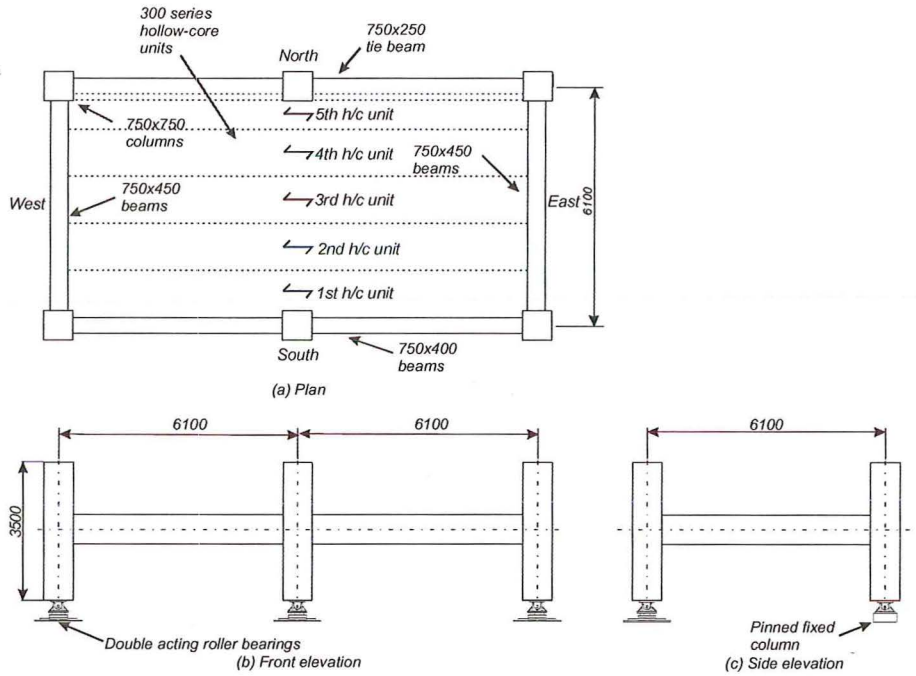

Figure 5-1 Plan and elevation of the super-assembly tested.

The lateral loading applied to the top and bottom of the column of the super-assembly was through a set of purpose built loading frames as shown in Figure 5-2. The super-assembly specimen was loaded in this manner for both the longitudinal and transverse directions. The two main loading frames are the diagonal scissor frames while a set of secondary loading frames (that resemble an arrow shape) enforces the displacement compatibility of the adjoining stories by ensuring the front columns remain parallel.

(a) Longitudinal Loading **Transverse Loading**

Figure 5-2 Loading frame set up

Being able to predict the lateral strength of a structure is particularly important for buildings designed to behave by the preferred beam side sway mechanism in which plastic hinges form at each end of the beams. As each plastic hinge forms, part of the floor diaphragm contributes to the beams hinge strength. If the amount of slab interaction is underestimated then the preferred beam-side sway mechanism may not occur. If an undesirable strong beam-weak column mechanism occurs it could prematurely lead to a partial or full collapse of a structure during a major earthquake.

This chapter presents an analysis of the following failure mechanisms observed during the experimental programme: (i) initial failure of the precast units; (ii) tearing of the floor diaphragm; (iii) bowstring effect; (iv) partial collapse of the first hollow-core unit; and (v) complete collapse of the precast units and topping. This chapter then discusses the recommendations made by design codes (NZS3101:1995 and ACI 318-02) for determining the width of floor slab contributing to the lateral strength of a structure. A theoretical prediction for the width of activated floor slab for varying interstorey drifts is then proposed. The theory is verified against the results from the current investigation in terms of global and localised strengths. Design recommendations are proposed for structures incorporating hollow-core floor slabs. Finally, comment is made on the stiffness of the super-assembly.

The key indicator in determining the performance of the hollow-core unit connection detail is the relative rotation between the hollow-core unit and the supporting beam. Within this document this relative rotation has been defined as interstorey drift as the building investigated was considered to be a generic New Zealand moment resisting concrete frame building in which the interstorey drift closely relates to the relative rotation. In terms of predicting the amount of slab activation within a structure the relative rotation between the hollow-core unit and the

supporting beam should be used. As torsion affects this relative rotation it is considered conservative to assume that the relative rotation and interstorey drift are equal. A designer is reminded that if a true assessment of risk or damage is required then the designer should focus on the relative rotation between the hollow-core unit and the supporting beam as it is less conservative that interstorey drift.

5.2 Initial cracking of the precast units under positive moment

As explained in Chapter 4 the initial failure of the hollow-core units was the unit fracturing near its end, adjacent to the seat support, as shown in Figure 5-3. This crack was observed at a drift of 0.32% and was approximately 0.5mm wide. Assuming, at the ends of the precast concrete units the tendons become debonded so the section behaves as an un-reinforced section, it is possible to show from a simple cracked section analysis that the expected crack width should be 0.74mm. This compares well with the experimental observation of 0.5mm. Full analysis details are given in Appendix F.

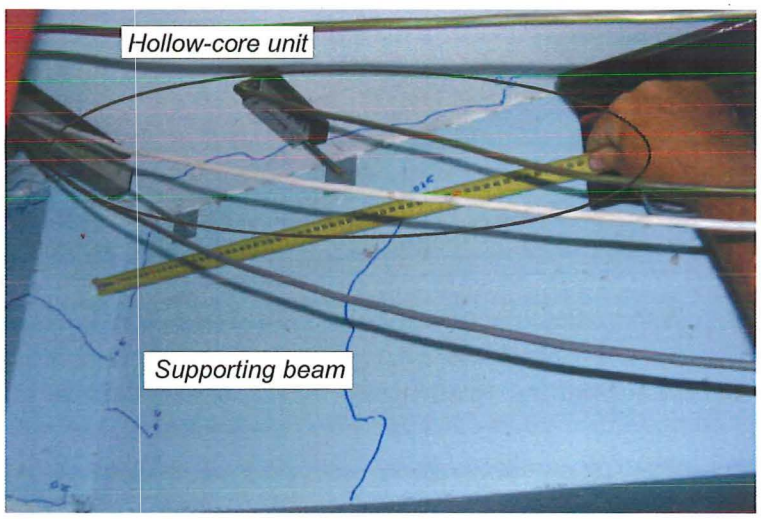

Figure 5-3 Fracturing of the end of the hollow-core unit (West Beam)

5.3 Tearing of the floor diaphragm

During the first phase of loading, a tear within the floor diaphragm occurred between the first and second hollow-core units (Figure 5-4(a)). By examining the cross section through the floor slab (Figure 5-4(b)) it can be seen that the first zone of weakness within the diaphragm, from the South beam, is the interface between the first and second hollow-core units. The connection between the South beam and the first hollow-core unit is locally strengthened by the starter bars present connecting the topping slab to the perimeter beam, plus the edge of the first hollow-core unit is well bonded to the cast insitu concrete along the top half of the South perimeter beam. At the location where the diaphragm tore, only a 75mm topping slab reinforced with cold-drawn wire mesh connects the two hollow-core units together.

The calculation as to why the floor slab tore at 1.93% is complex. The tension force generated with the floor slab is transferred into the perimeter beam by the form of a truss (Figure 5-5). These internal forces within the floor diaphragm are resisted by bending and shear as the floor tries to displace as a deep beam (Fenwick et al, 1999). In order to calculate the entire mechanism a finite element analysis is required to model the interaction of the hollow-core unit, topping slab and the beam deformation. Further work is required on this topic, as it is not greatly understood.

5.4 Bowstring effect

When a reinforced concrete frame elongates due to plastic hinges forming within the beams, the floor slab provides restraint to the beam growth, leading to an increase in the capacity of the frame. This restraint causes the floor slab to act in tension while the beam goes into compression. This phenomena is referred to as the "bowstring effect" and has been explained by Fenwick et al (1999) and can be seen in Figure 5-6.

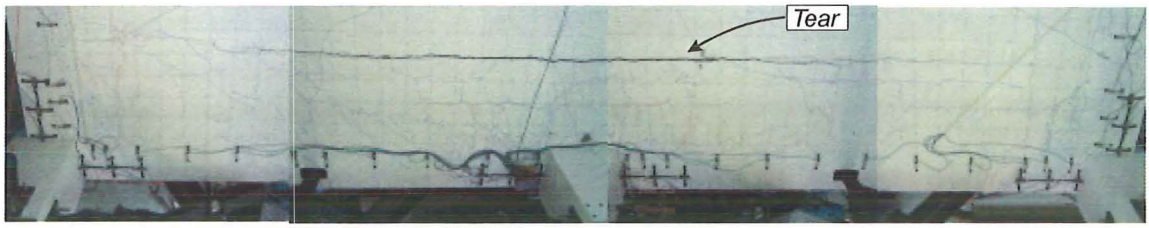

(a) Plan view showing the failure of the floor diaphragm

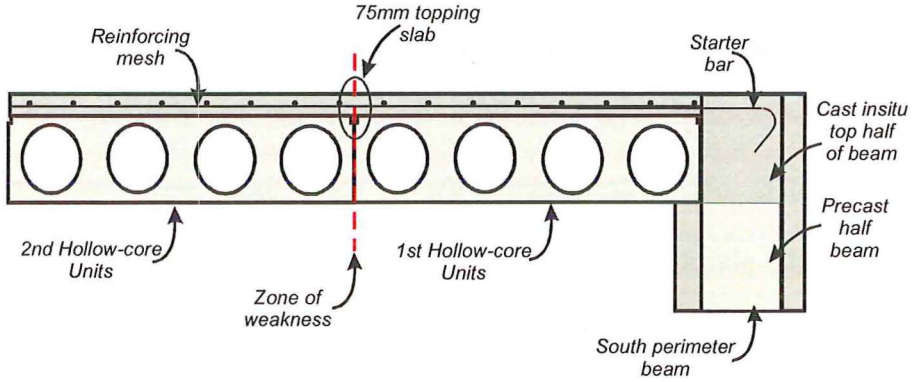

(b) Section through the floor diaphragm

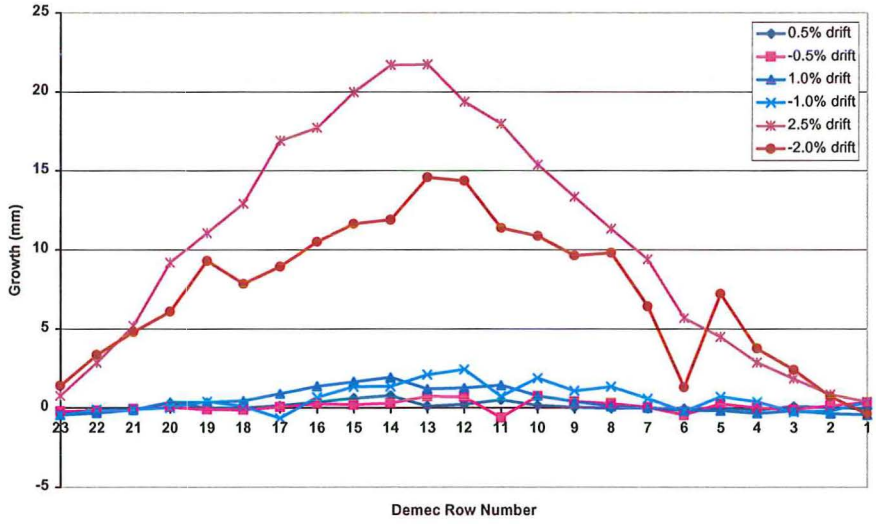

(c) Transverse growth of the floor diaphragm during the longitudinal loading before and after the diaphragm tear formed.

Figure 5-4 Details relating to the tear within the floor diaphragm.

It is called the "bowstring effect" because the beam in compression acts like a bow and the floor slab in tension acts like the string within a bow.

During the current testing programme a slightly different event occurred. When the floor diaphragm tore the width of floor slab that was in tension reduced to the width of one hollow-core unit (the unit that was still attached to the perimeter

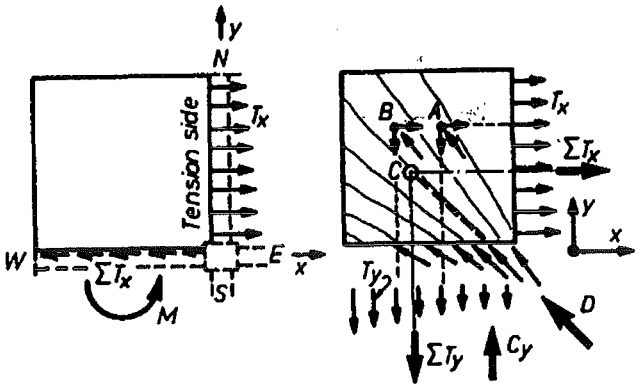

(a) Equilibrium criteria for membrane forces acting as a tension flange (Paulay and Priestley, 1992)

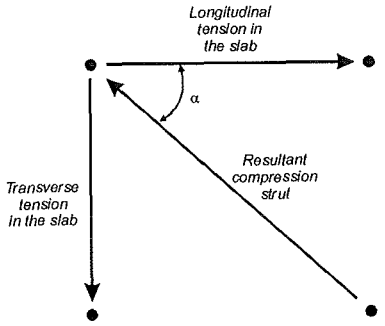

(b) A simple sketch showing the truss mechanism that formed within the floor diaphragm

Figure 5-5 Truss analogy used to determine the diaphragm contribution

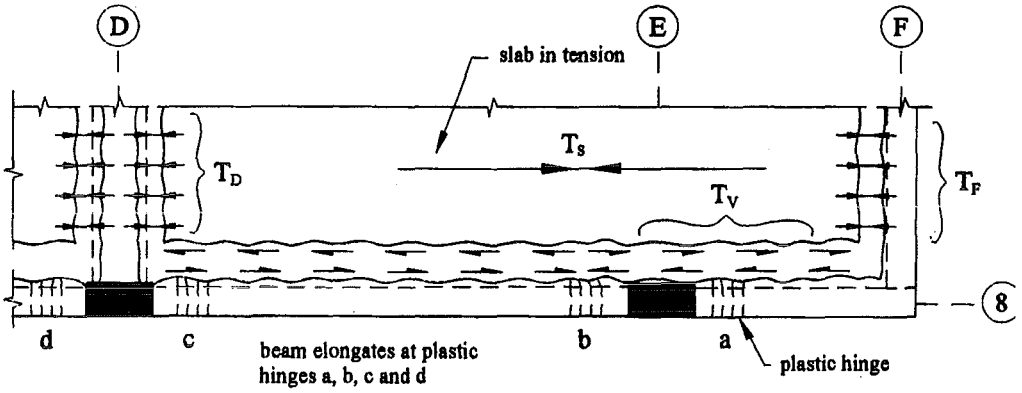

(a) A plan showing the bowstring effect within a floor slab (Fenwick et al, 1999)

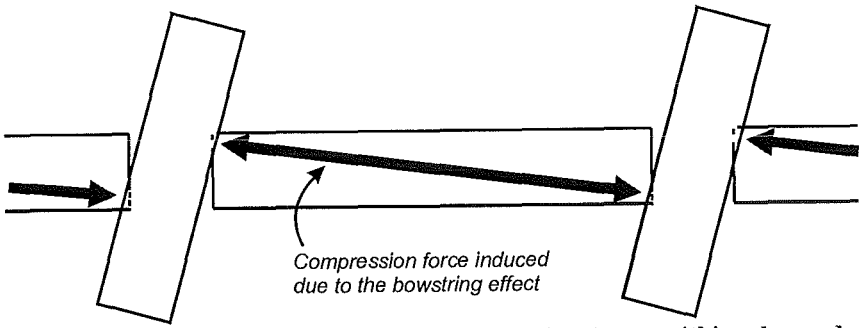

(b) Elevation of a frame showing the induced compression forces within a beam due to the bowstring effect.

Figure 5-6 A plan and elevation showing how the bowstring effect forms within a beam and floor slab

beam). The tear then enabled the central column to freely translate in a direction transverse to the direction of loading (out of the building, Figure 5-4c), as the column

was not tied into the remainder of the floor slab. The amount that the column translated can be calculated based on a force couple and a calculated moment of inertia. From calculation (see Appendix F), the column displaced 3.1mm laterally out of the building. This calculated deflection agrees well with the observed displacement of approximately 2mm at the initiation of the tear (1.93%).

5.5 Partial collapse of the first hollow-core unit

During the final phase of loading (Phase III), the first hollow-core unit (adjacent to the southern perimeter beam) partially collapsed. The failure that occurred was that the bottom of the hollow-core unit collapsed while the top half of the hollow-core unit remained attached to the cast insitu topping. This can be seen in Figure 5-7.

The failure of this hollow-core unit was due to several variables. The initial damage occurred when the end the hollow-core unit fractured (Section 5.2). Once this initial crack, had formed the additional loading caused the crack at the end of the hollow-core unit to propagate along the member. Most of the propagation was due to the displacement incompatibility between the first hollow-core unit and the perimeter frame. Since the first hollow-core unit was rigidly connected to the perimeter beam, by starters bars and the cast insitu concrete bonding the hollow-core unit to the perimeter beam, the hollow-core unit was forced to displace to the same shape as the perimeter beam (i.e. double curvature). The displacement incompatibility between the hollow-core unit and the perimeter beam can be seen in Figure 5-8. A hollow-core unit is designed as a one-way floor slab so the imposed double curvature overloaded the webs of the hollow-core unit causing the initial crack at the end of the unit to propagate along the member.

Displacement incompatibility has also been noted to occur by Lau (2001).

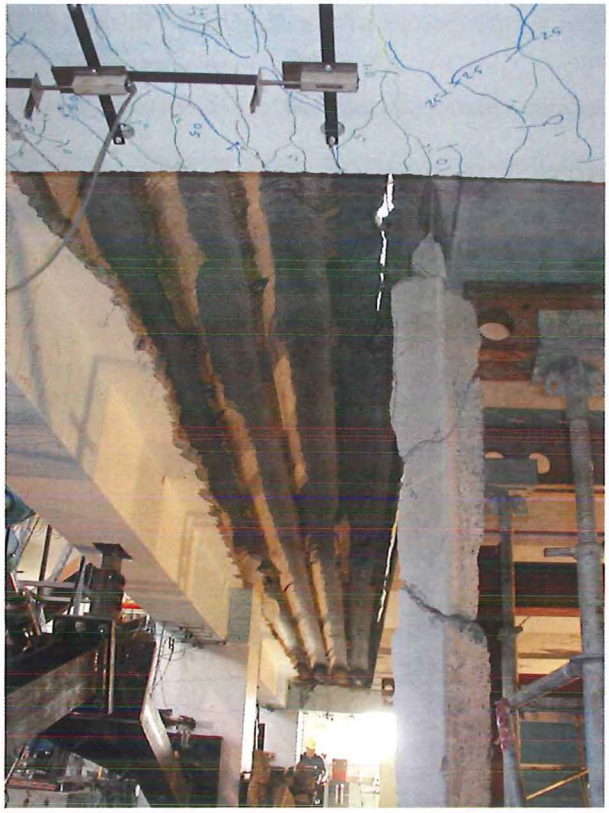

Figure 5-7 Failure of the first hollow-core unit

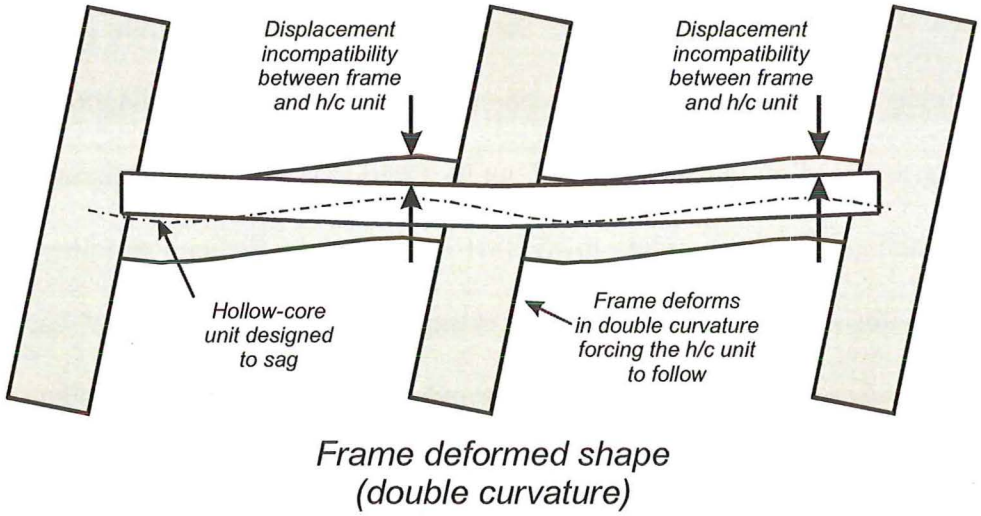

Figure 5-8 Displacement incompatibility of the perimeter beam to the first hollow-core unit

5.6 Complete collapse of the precast units and topping

The complete collapse of the remainder of the floor occurred following a gravity load test that was undertaken to check the load carrying capacity of the remaining floor.

Quantifying the actual failure of the remaining floor (Units 2, 3 and 4) was not possible during this experimental programme. Three variables were considered to be preventing the floor slab from collapsing once the end of the hollow-core units had fractured. These variables were: bond between the topping slab and the hollow-core unit; aggregate interlock across the fractured surface at the end of the hollow-core unit; and dowel action caused by the end of the prestressing strands resting on the beam seat. The contribution from each of the variables cannot be easily determined. The contribution of each variable cannot be relied upon to be present each and every time an earthquake occurred.

This is an area where considerable further research is required.

5.7 Slab widths in moment frames: The state-of-the-practice

The New Zealand Concrete Structures Standard (NZS 3101:1995) gives guidance on determining the amount of strength enhancement from the floor diaphragm. This prediction is based on the work carried out by Cheung et al (1991). Determining the width of activated slab according to NZS3101:1995 can be difficult to follow. There is often confusion as to whether the prestressing strands within the hollow-core units should be included (often the prestressing stands are assumed not to contribute to the strength enhancement). The width of floor slab assumed to be effectively anchored and hence contributing as additional tension reinforcement (according to NZS3101:1995) is not always clear. The width assumed to contribute to the negative moment capacity is the lesser of four different values as shown in Figure 5-9(a). For the reinforcement to be classed as effectively anchored it must be fully developed (i.e. the reinforcement must be sufficiently bonded so that it can develop its full strength)

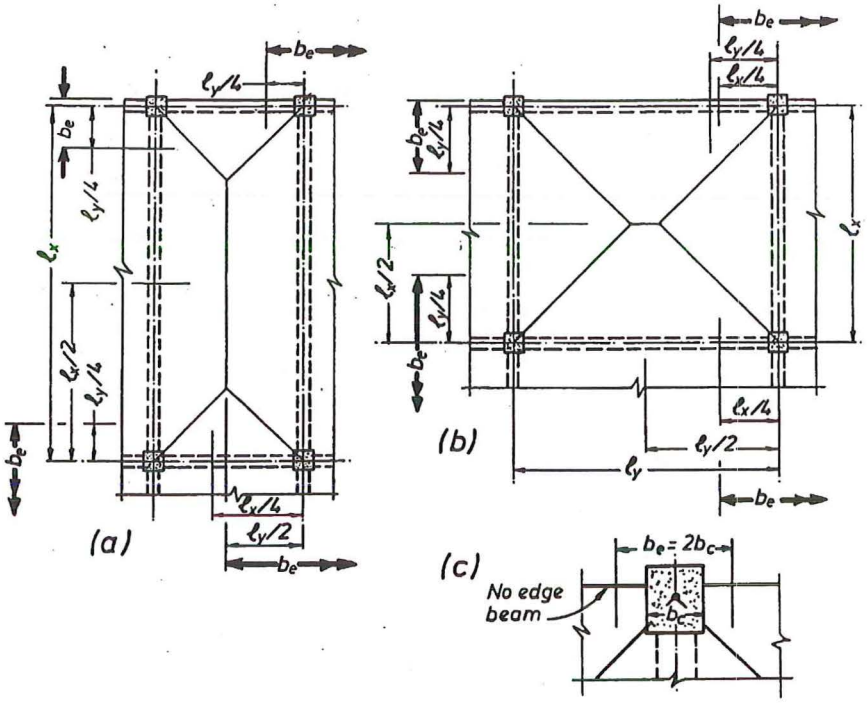

(a) Effective flanges widths as defined by Cheung et al (1991)

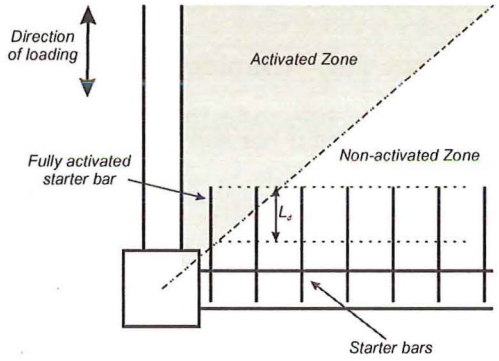

(b) Determination of the discontinuity reinforcement for Phase I

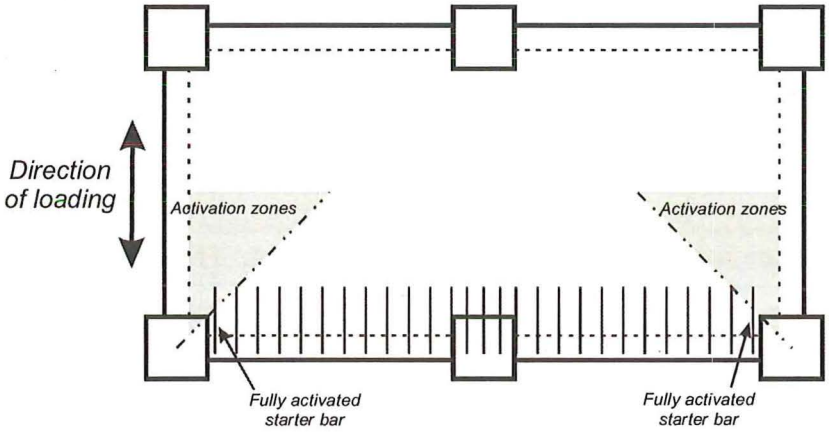

(c) Determination of the continuity reinforcement for Phase II

Figure 5-9 NZS3101:1995 and Cheung et al (1991) prediction for determining the slab activation contributing to the negative moment capacity of a plastic hinge.

when it crosses a 45-degree line drawn from the zone of interest (Figure 5-9(b) and (c) show the 45-degree activation line for the super-assembly).

The American Concrete Code, ACI 318-02, states that the effective flange width that contributes as additional tension reinforcement to the perimeter beam shall be taken as the lesser of one-twelfth the span of the beam, six times the slab thickness, and one-half the clear distance to the next web. ACI 318-02 is also unclear as to whether the prestressing strands contribute. Does the slab thickness refer to the topping slab and the hollow-core unit or only the topping slab?

5.8 Proposed theory for predicting slab activation

The method proposed to determine the moment capacity for the various connections is based on rigid body kinematics. Any reinforcement that crosses a cut made through interface between the column and beam (as shown by Section A-A and B-B in Figure 5-10) is assumed to contribute to the lateral strength of the super-assembly. The tension reinforcement within the floor slab purely acts at additional tension reinforcement. This method does not follow the 45-degree line of activation determined by Cheung et al (1991).

When determining the moment capacity of a T or L beam, the tension reinforcement within the flange is multiplied by the leverarm between the centroids of the compression force and the tension reinforcement. This principle was used to determine the moments within the super-assembly and is shown in Figure 5-10. Figure 5-10 and Table 5-1 show how the beam plastic hinge moments for the various plastic hinges were generated. T = the tension force at the plastic hinge and jD = the internal leverarm between the tension force and the centre of the compression force.

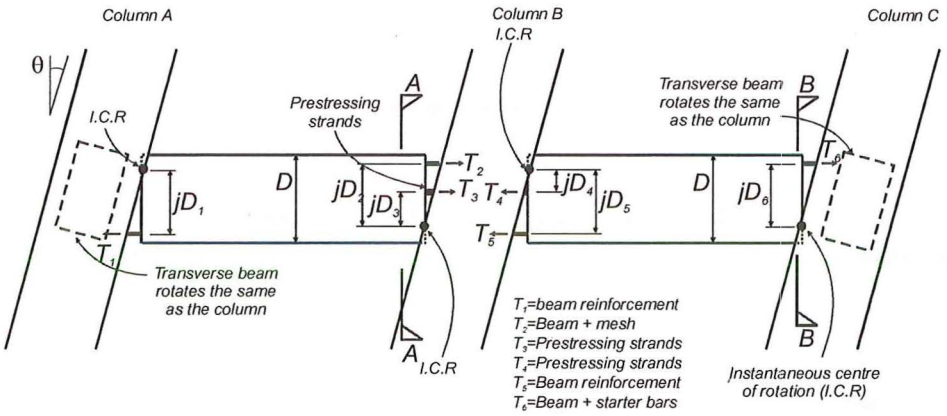

(a) A sketch showing how rigid body kinematics determine the displaced shape and in turn are used to generate the moment capacities for the various plastic hinges.

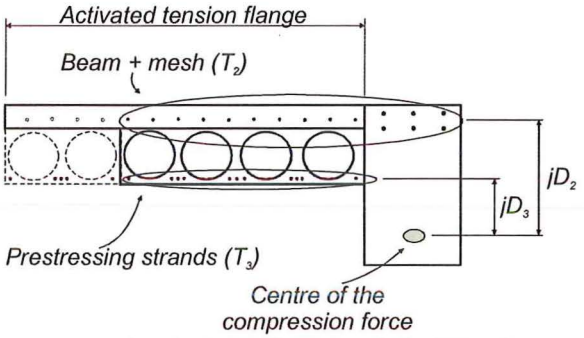

(b) Section A-A at all stages of plastification

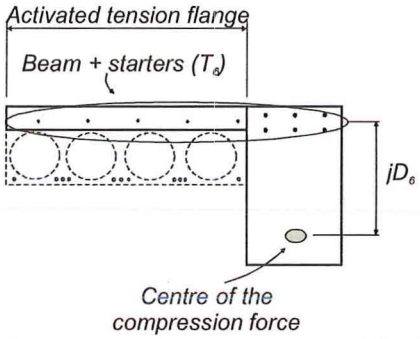

(c) Section B-B at the onset of plastification (yield)

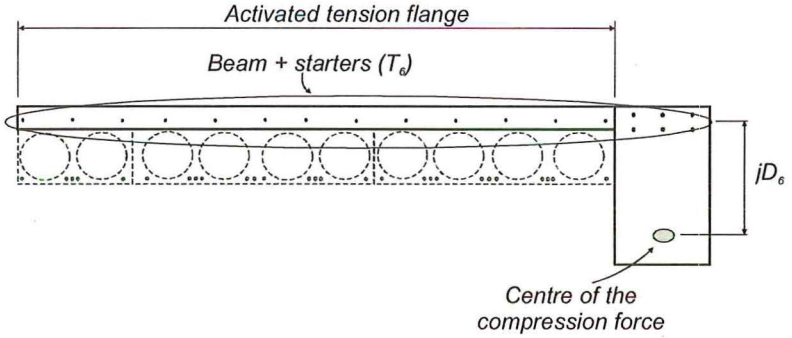

(d) Section B-B at full plastification

Figure 5-10 The use of rigid body kinematics to explain how the additional tension reinforcememnt contributes to the lateral strength of the super-assembly at different stages of progressive plastification

Table 5-1 A table summarising the calculations for the beam plastic hinge bending moments as obtained from Figure 5-10.

Plastic hinge location	Tension Force(s)	Leverarm(s)	Total Plastic Hinge Moment
Column A	T_1	jD_1	T_1jD_1
Column B-Left	T_2, T_3	jD_2, jD_3	$T_2jD_2+T_3jD_3$
Column B-Right	T_4, T_5	jD_4, jD_5	$T_4jD_4+T_5jD_5$
Column C	T_6	jD_6	T_6jD_6

Before the additional lateral strength can be determined the width of activated slab needs to be determined. This width of activation will be different for an exterior and interior plastic hinge.

When examining an exterior plastic hinge it is possible to determine that the 45-degree line of activation does not work for precast concrete. If a capacity of the connection versus length of the member plot is generated (Figure 5-11) it can be seen that the location where a potential crack will form (and hence yielding of the reinforcement occurs) is at the interface between the supporting beam and the hollow-core unit as this is the location of the lowest capacity. Hence, only the activated starter bars contribute to the additional strength (on top of the beam longitudinal reinforcement) for an external plastic hinge.

This proposed theory is used to predict the width of slab participation contributing to the lateral strength of a structure that incorporates hollow-core floor units.

Before a width of activated slab can be proposed, the amount of progressive activation of the slab reinforcement needs to be understood. For an exterior plastic hinge the rate at which the continuity reinforcement yields due to increasing lateral

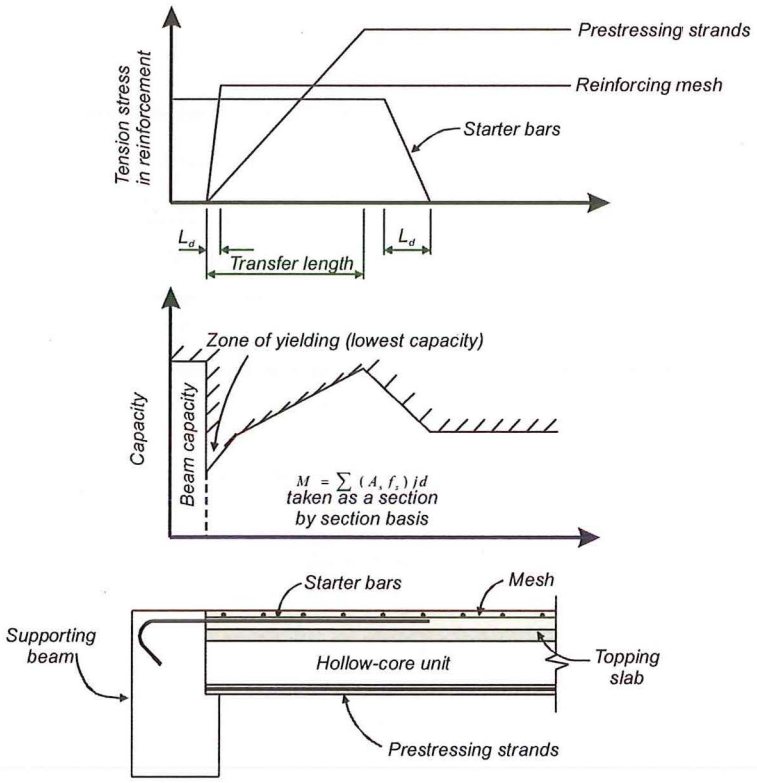

Figure 5-11 Moment capacity of the hollow-core to supporting connection

displacement is affected by the torsional stiffness of the transverse beam (Velez and French, 1989). If a beam is torsionally stiff then the lag in rotation between the end of the beam (near the column) and the centre of the beam is small, whereas, if the beam is torsionally weak then the difference between the end and the centre of the beam is large. The affect of torsion is illustrated in Figure 5-12. The width of activation should be defined in terms of a certain width of slab for various lateral displacements. Two points are selected to define this: The width of activation at the onset of yielding and the width of activation at full plasticity. The progressive activation of the tension reinforcement acting in tension has been described or implied by Cheung et al (1991), Velez and French (1989) and Lau et al (2001).

To define the activation width of the floor slab versus lateral displacement (or interstorey drift) the crack patterns observed (Figure 5-13) in the experimental programme were examined. At the onset of plastification (yield) the width of flange to

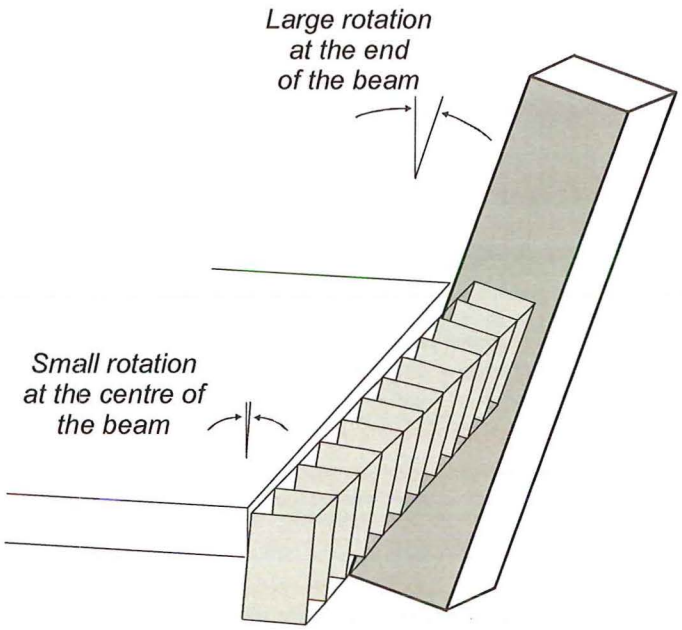

Figure 5-12 The torsional stiffness of a beam greatly affects the rate in which the starter bars (continuity reinforcement) activate as the column interstorey drift increases

be adopted should be the width of one hollow-core unit (1.2m) as evident in Figure 5-13(b). This is the width that the cracks within the exterior plastic hinge encroach into the floor slab. The second point that needs to be defined is the onset of full plasticity. As the dimensions of the building tested was considered to be typical dimensions for beam length, width, depth and hence torsional stiffness (for New Zealand construction) it can be concluded that full plastification occurred with a width of flange equating to 3.05m (for the experiment, this width equated to one-half the overall bay dimension). The interstorey drift at which full plasticity occurred is defined as 2.0%. This activated slab width versus interstorey drift plot is shown in Figure 5-14 as a tripartite curve.

For an interior plastic hinge the width of activation versus interstorey drift also needs to be defined. As there is no transverse beam present, the theory for the external plastic hinge cannot be used. Examining a cross section of the connection detail being tested (Figure 5-15) it is evident that the first hollow-core unit is extremely well connected to the perimeter beam. This connection is due to the continuity reinforcement (starter bars) protruding of the perimeter beam and into the topping slab

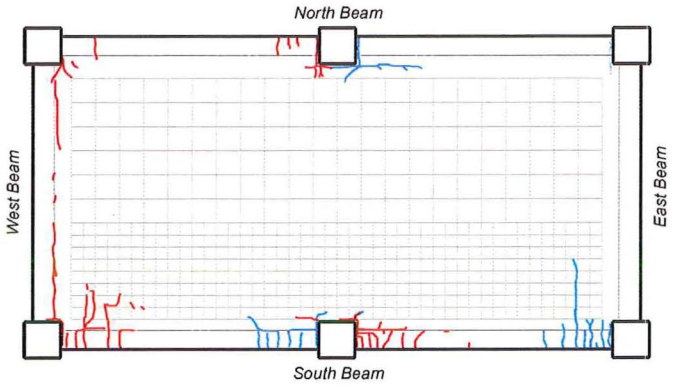

(a) Topping cracks after the ±0.25% drift cycle

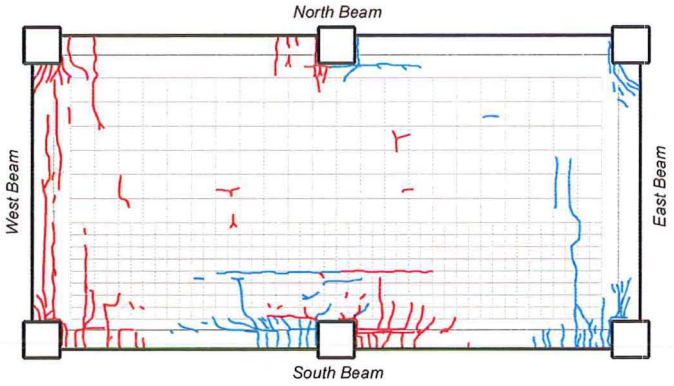

(b) Topping cracks after the ±0.5% drift cycle

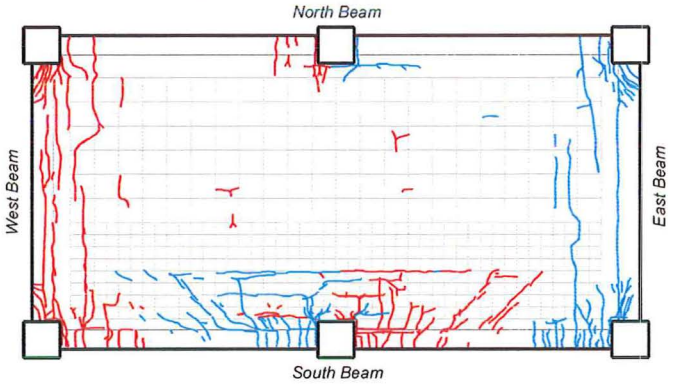

(c) Topping cracks after the ±1.0% drift cycle

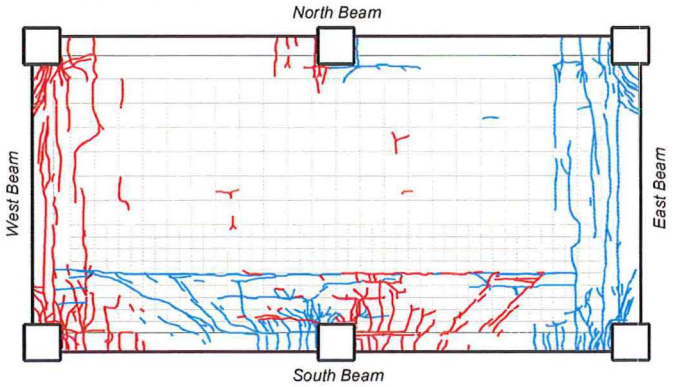

(d) Topping cracks after the +2.5% and –2.0% drift cycles

Figure 5-13 Mapping of the topping cracks during the first phase of loading. Blue cracks are due to a positive inclination while the red cracks are due to a negative inclination

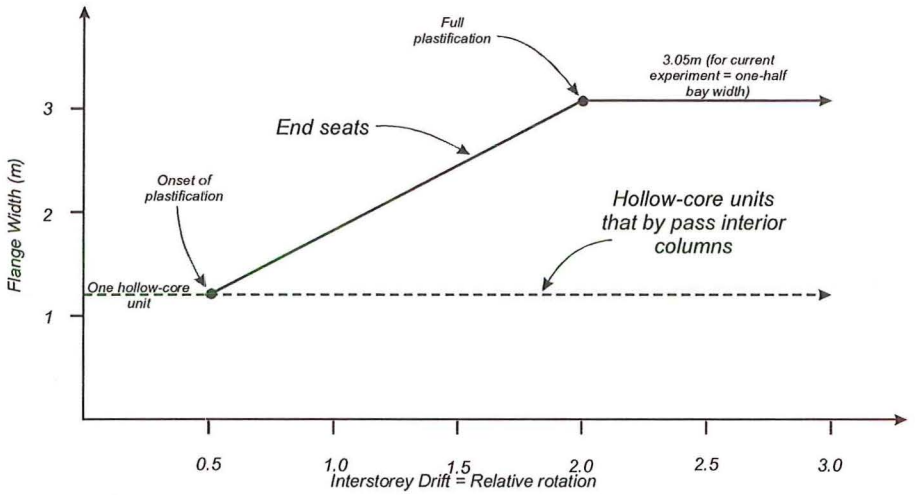

Figure 5-14 Proposed floor slab activation with increasing interstorey drift.

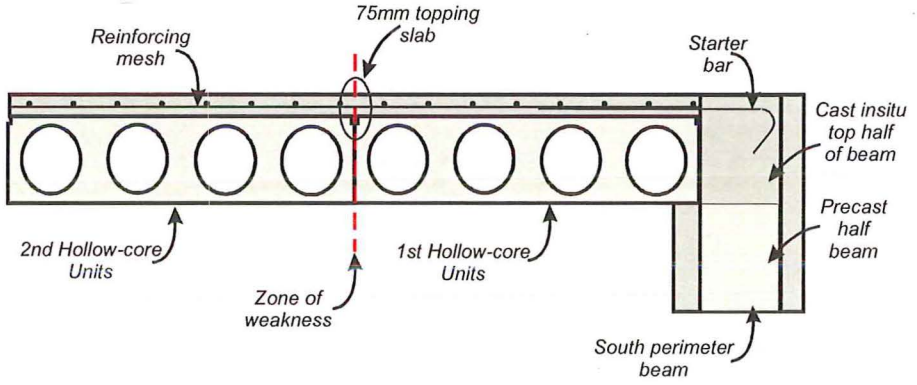

Figure 5-15 Cross section of the connection detail used at the central column

plus the chemical bond between the edge of the hollow-core unit and the cast in place concrete required to pour the top half of the beam. Therefore, at the onset of plastification (yield) the width of activated floor slab should be taken as only one hollow-core unit (1.2m). To determine when full plasticity occurs, examine again Figure 5-15. It is proposed that for full plastification the width of activated floor is also taken as one hollow-core unit (1.2m) because the only mechanism possible to transfer any additional slab activation from further out within the floor diaphragm, to the perimeter beam, the additional force has to be transferred across a highly cracked 75mm thick section of the topping slab that is reinforced with cold-drawn wire reinforcing mesh between the first and second hollow-core unit. Figure 5-14 shows the linear approximation for the slab activation for an interior plastic hinge.

5.9 Verification of what contributes to the strength of the super-assembly

By computing both a yield and ultimate base shear force (from theory utilising actual material properties measured at the time of testing) it is possible to compare the expected lateral strengths against the observed strengths. Refer to Appendix F for the calculations used to determine the lateral strengths and bending moments for this experimental programme.

Longitudinal Loading (Phases I & III):

Figure 5-16(a) shows satisfactory agreement between the observed base shear for the front perimeter (South) frame and the proposed theory when plotted against interstorey drift.

It is common practice to ignore the contribution the prestressing strands within (the prestressed units) make to the lateral strength when determining the flexural strength of the beams in accordance using NZS3101:1995 when prestressed units pass an interior column. NZS3101:1995 and ACI318-02 standards underestimate the contribution that the slab reinforcement makes to the negative moment strength of a plastic hinge (Figure 5-16). The recommendations of both these standards result in a significant underestimate in the lateral strength of the frame. This underestimation could cause a less desirable mechanism forming within the structure rather than the preferred strong column-weak beam mechanism.

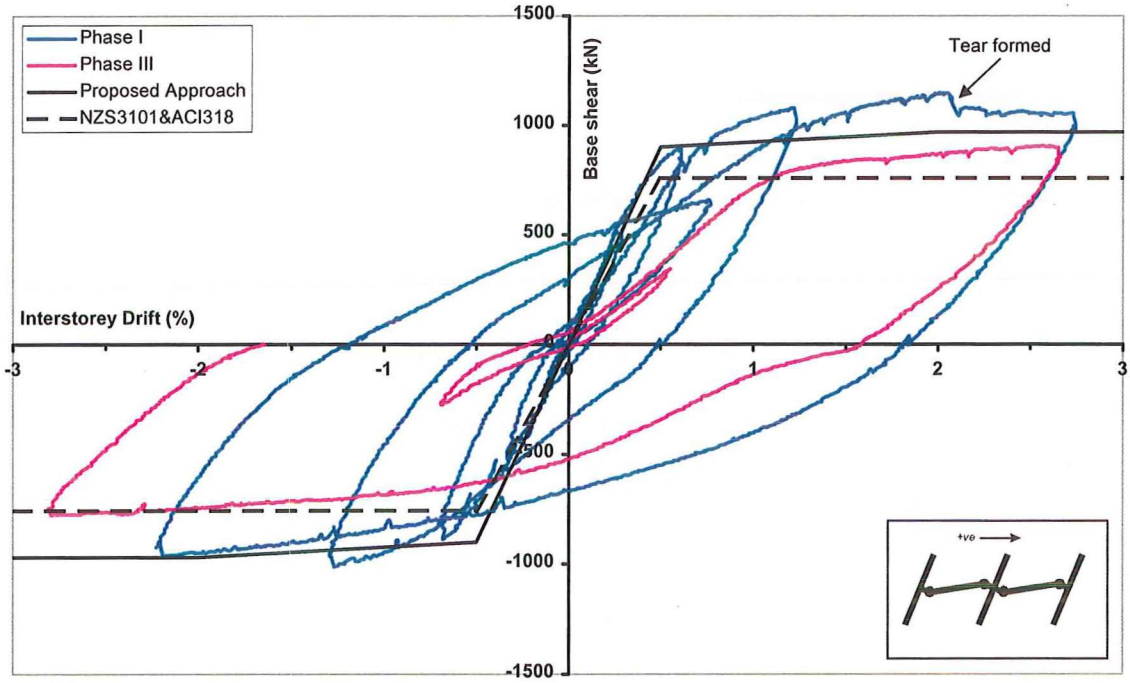

(a) Combined hysteresis loops for Phase I and III for the front (South) perimeter frame

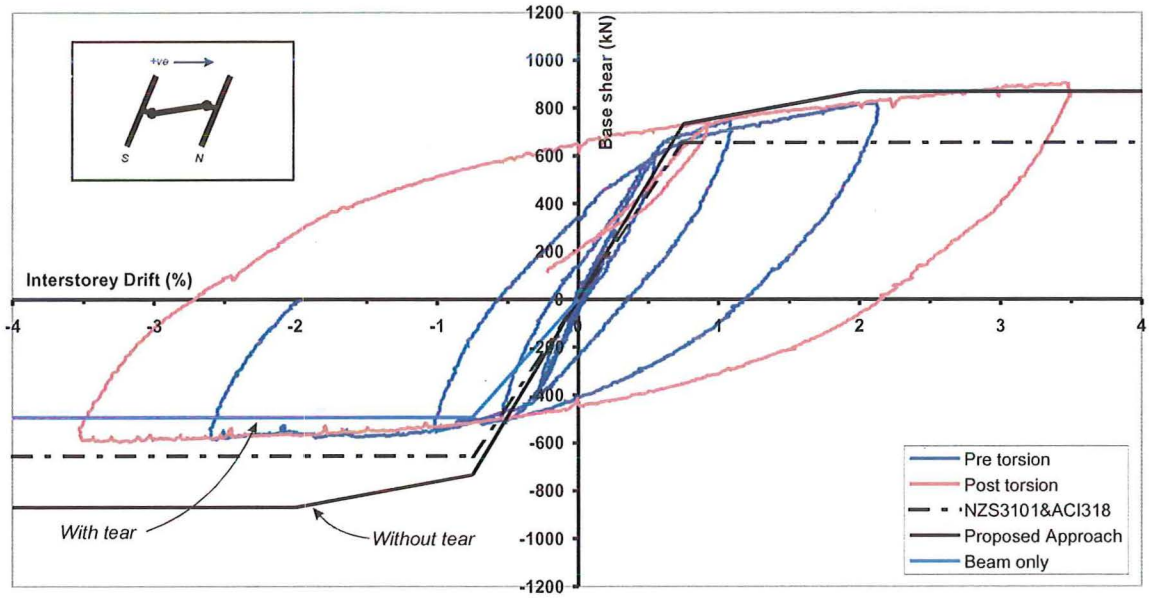

(b) Hysteresis loop for Phase II

Figure 5-16 Hysteretic performance of the super-assembly throughout the three phases of the experiment.

Transverse Loading (Phase II):

Figure 5-16(b) shows that the observed strength compared with the theoretical prediction for Phase II. The theory curve in Figure 5-16(b) was plotted using the

theory proposed for the width of slab activation at yield and full plasticity for Phase I. For a positive inclination (the top of the column is displaced in a northern direction while the base of the column displaces in a southern direction) the theory agrees well. For a negative inclination (the top of the column is displaced in a southern direction while the base of the column displaces in a northern direction) the theory overestimated the observed results. This overestimation was due to the tear that formed during Phase I. When loaded in a negative inclination the first hollow-core unit and topping slab lifted rather than allowing the starter bars to activate (and yield) (Figure 5-17).

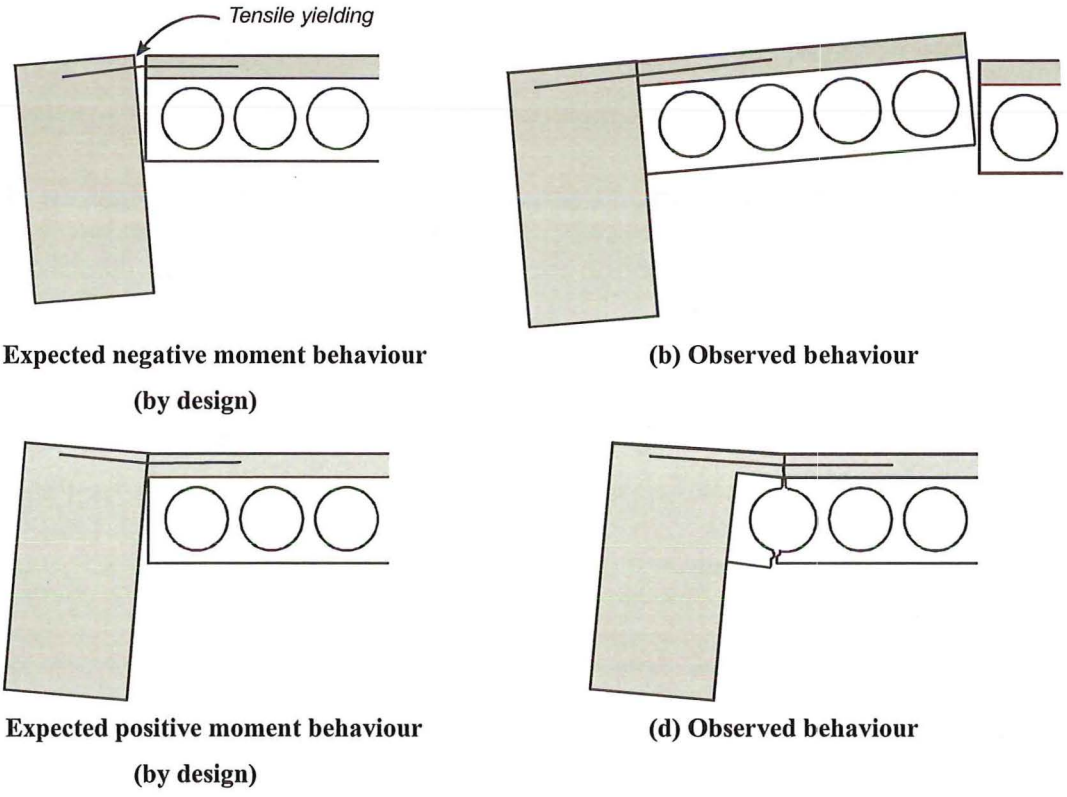

(a) Expected negative moment behaviour (by design)

(b) Observed behaviour

(c) Expected positive moment behaviour (by design)

(d) Observed behaviour

Figure 5-17. Expected and actual rotation of the first unit and perimeter during the transverse loading (Phase II).

Both NZS3101:1995 and ACI318-02 underestimate the observed capacity even though the observed lateral strength was greatly reduced due to the diaphragm tear.

5.9.1 Why does NZS3101:1995 and ACI318-02 differ from the observed capacities?

The New Zealand Concrete Structures Standard (NZS 3101:1995) gives guidance on determining the amount of strength enhancement from the floor diaphragm. The width of floor slab assumed to be effectively anchored and hence contributing (according to NZS3101:1995) is not always clear. The width assumed to contribute to the negative moment capacity is the lesser of four different values as shown in Figure 5-9(a). For the super-assembly tested the width of floor slab assumed to be contributing was 1.53m (one quarter the span of the beam). For Phase I and II, the diaphragm contribution was made up of the starters and cold-drawn wire reinforcing mesh.

ACI 318-02 states that the effective flange width shall be taken as the lesser of one-twelfth the span of the beam, six times the slab thickness, and one-half the clear distance to the next web. One-twelfth the span of the beam governs in this case and equates to 510mm. ACI 318-02 was also unclear as to whether the prestressing strands contribute. For Phase I, the diaphragm contribution was made up of the starters, cold-drawn wire reinforcing mesh and hollow-core units while for Phase II only the starter bars contribute.

When the maximum lateral strength observed during the experimental programme is compared with the calculated strengths of NZS3101:1995 and ACI 318-02 it is evident why both the standards underestimate the capacity. An example is the contribution that the starter bars make to an exterior hinge. During the experimental programme ten starter bars were activated, while NZS3101:1995 predicted one starter bar and ten cross wire of reinforcing mesh and ACI318-02 predicted two starter bars.

5.9.2 Localised strengths

The contribution that the floor diaphragm makes to the lateral strength of the super-assembly can be broken down into the individual beam plastic hinge response, rather than showing the overall base shear versus interstorey drift hysteresis plot. For each plastic hinge, a moment versus rotation graph was produced. In addition, the proposed theoretical slab activation, the actual progressive activation (obtained from the experimental data, Figure 5-18(a)) will be compared to the observed moment rotation graphs. The actual progressive activation was determined by plotting the recorded the transverse beams starter bar strains for varying interstorey drifts (Figure 5-18(b)). From Figure 5-18(b) it is possible to compare the width of slab activation with the proposed theory (Figure 5-18(c)). It can be seen that the proposed theory agrees well with the measured activation during the experimental programme.

As the beam capacity is determined as a column face moment and the beam moments generated from the base shear are calculated as centreline moments, the base shear moments were scaled to form column face moments.

Phase I:

Figure 5-19 shows that the observed capacity of the two outer columns agree reasonably well with both the proposed simplified pushover capacity and the actual capacity inferred by calculation based on the progressive activation of the starter bars. For a positive moment, the capacity is taken as the moment generated by beams longitudinal reinforcement (ignoring any slab contribution) because the slab is in compression. For a negative moment, the capacity is made up of the beams longitudinal reinforcement plus the starter bars located within the width of activated floor slab in the end transverse beam. The maximum observed width of slab activation was 3.05m. This additional reinforcement has a similar leverarm to that of the tension

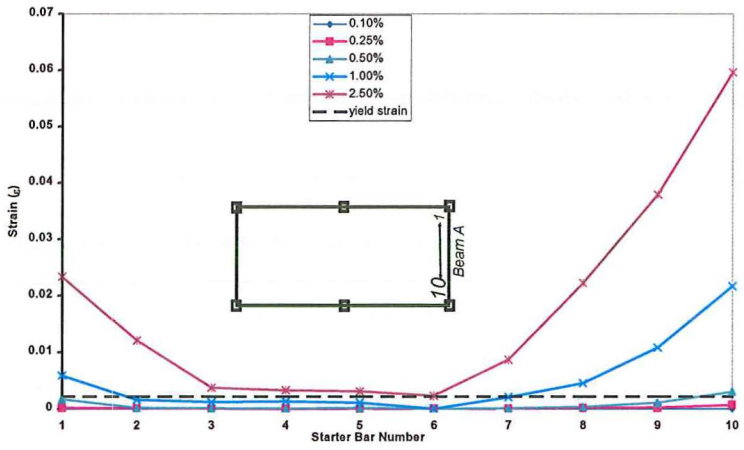

(a) A plot showing the increase in the width of the activated floor slab as determined by using starter bar strain

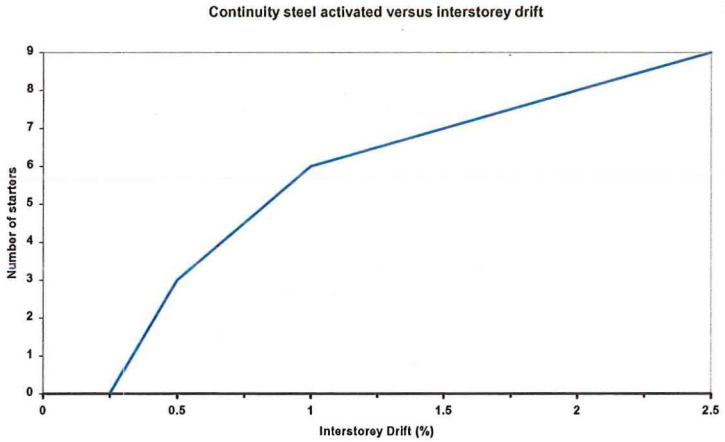

(b) Number of starter bars contributing as a tension flange for increasing levels of interstorey drift

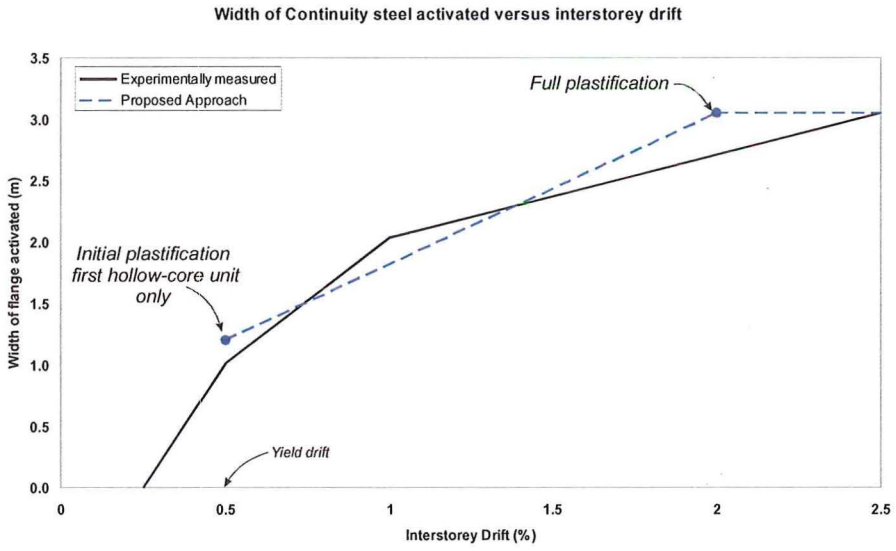

(c) A comparison between the observed starter bar activation and the predicted activation

Figure 5-18 Comparison between the proposed theory and recorded activation

reinforcement within the beam as shown in Figure 5-10. By using Figure 5-14 the moment capacity for varying interstorey drifts can be determined.

For a positive moment the observed beam capacity is greater than the nominal moment. This difference is due to the positive plastic hinge possible forming slightly off the column face. Also, at larger inclinations strain hardening of the longitudinal reinforcement will start to contribute to the lateral strength.

Figure 5-19(c) shows the sum of the column moments for the central column. This graph shows that the theoretical capacity of the system is slightly underestimated for a positive rotation (the top of the column is displaced in an eastern direction while the base of the column displaces in a western direction) before the diaphragm tore. This underestimation was due to a section of the floor slab outside the first hollow-core unit was providing some additional capacity to the lateral strength of the system. Once the tear occurred the capacity matched well. Good agreement was observed between the theory and experimental results for a negative inclination (the top of the column is displaced in a western direction while the base of the column displaces in an eastern direction).

If the individual plastic hinges each side of the central column are examined (Figure 5-19(d) and (e)), the results show good agreement with the theory. Figure 5-19(d) shows a discrepancy for both a positive and negative inclination. The reason for the underestimation of the positive inclination is explained above whereas for a negative inclination the reason is explained in Section 5.9.3.

Phase II:

Figure 5-20(a) shows the components contributing to the strength of the plastic hinge adjacent to the NE column in the East beam. When a positive moment is applied to the system, the only contributor to the capacity is the beams longitudinal

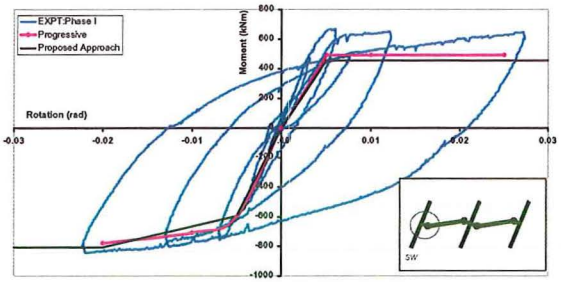

(a) SW columns moment versus rotation

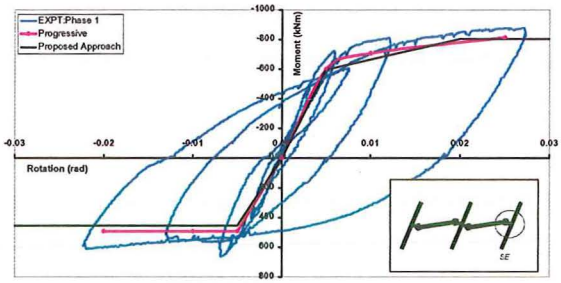

(b) SE columns moment versus rotation

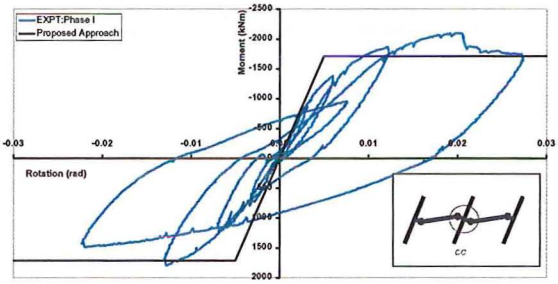

(c) Central Columns moment versus interstorey drift

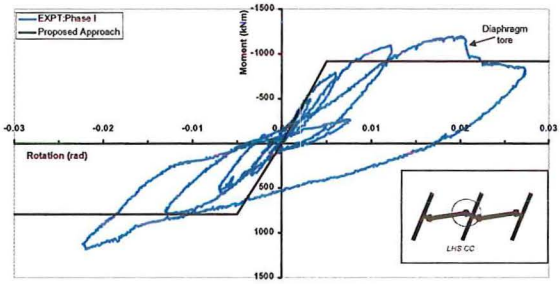

(d) Left hand side central column moments versus rotation

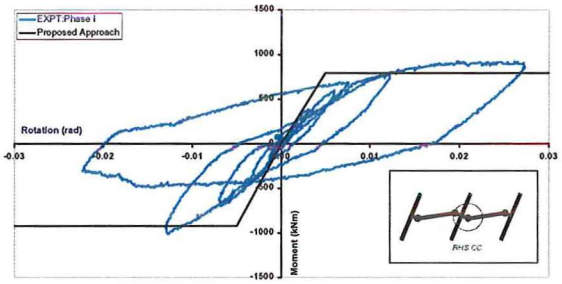

(e) Right hand side central column moments versus rotation

Figure 5-19 Individual moment versus rotation diagrams for Phase I

reinforcement. When determining the nominal moment for a negative moment the width of floor slab activated was based on the theoretical width determined for Phase I (Figure 5-14). Therefore, the negative moment capacity was the beam longitudinal reinforcement plus the number of activated starter bars in the transverse beam for varying inclination. Good agreement was observed for both the progressive activation and proposed theory during Phase II.

The SE column in East beam, Figure 5-20(b) shows less strength for a negative moment than the NE column even though both connections had symmetrical

reinforcement. The reason for the difference was due to the affect that the diaphragm tear had on the system. The tear did not allow the starters to fully contribute to the beam capacity, the first hollow-core unit was lifted rather than allowing the starter bars to be activated (and yield) as shown in Figure 5-17. The positive moments were similar to the NE column, as the diaphragm is not in tension.

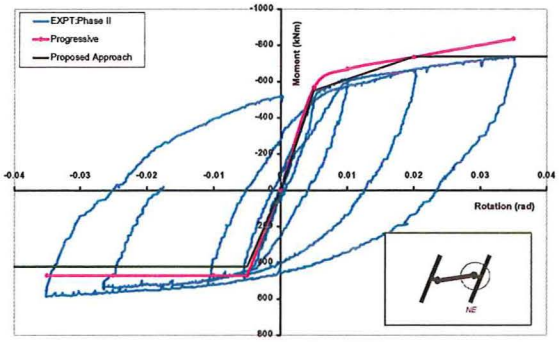

(a) NE columns moment versus rotation

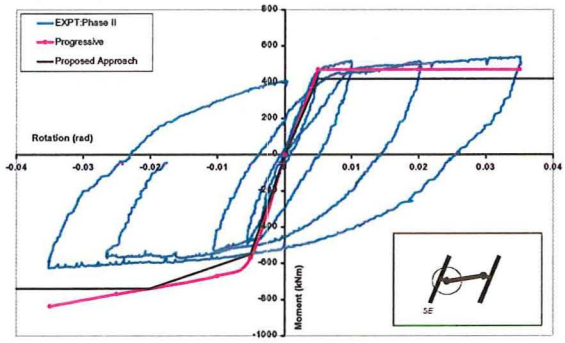

(b) SE columns moment versus rotation

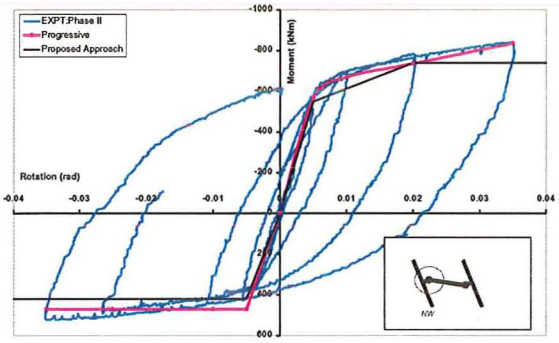

(c) NW columns moment versus rotation

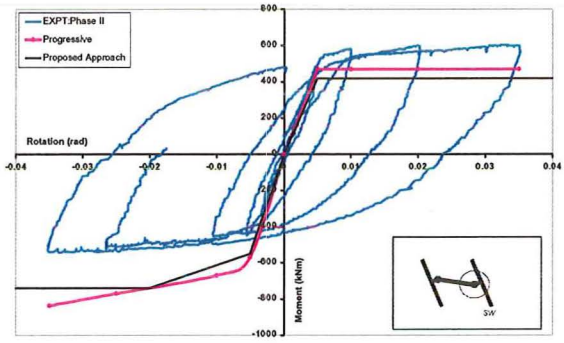

(d) SW columns moment versus rotation

Figure 5-20 Components contributing to the East and West beams capacity for Phase II

The performances of the NW and SW plastic hinges in the West beam (Figure 5-20(c) and (d)) were very similar to the corresponding NE and SE plastic hinges in the East beam. Again, the diaphragm tear influenced the performance.

Refer to Appendix F for the calculations used to determine the lateral strengths and bending moments for this experimental programme and the Phase III moment rotation plots.

5.9.3 Shortcomings

When the super-assembly was loaded, the magnitude of the columns axial loads were not measured in a consistent way to correctly infer the magnitude of the beams shear forces (during Phase I and III) as the system was indeterminate. The magnitude of the axial loads was required to determine the magnitude of the beam moments on either side of the central column. As the experimental set-up was designed to be self-equilibrating the axial loads cancel when the system is in equilibrium (refer to Chapter 3 for explanation). Once moment redistribution occurs, or a plastic hinge degrades in strength, the magnitude of the axial loads becomes important in determining the beam shear forces. During Phase I, the axial loads effectively cancelled so it was possible to determine the central column beam moments accurately. During Phase II the axial loads were not required as the super-assembly is determinate. In particular, it was during Phase III that the unknown axial loads lead to the inaccuracy of interpolating the column face moments and the beam shear forces.

5.10 Stiffness of the super-assembly

Figure 5-21 shows a comparison of the initial stiffness's of the super-assembly during the three phases of loading. Figure 5-21(a) shows the hysteresis loop used to determine the super-assemblies initial stiffness. This stiffness was calculated as 86.6 MN/m. The initial stiffness for Phase II was 34.0 MN/m (Figure 5-21(b)). This is approximately 40% of the Phase I stiffness. The difference in stiffness between the two phases is due to the initial torsion cracks that formed in the transverse beam during the Phase I loading that reduced the beams stiffness when loaded in Phase II. Also, the hollow-core units spanned perpendicular to this loading direction and hence did not contribute to the performance of the beams. Figure 5-21(c) shows the initial

stiffness for the third phase of loading. The stiffness was 29.5 MN/m, which was approximately 34% of the initial system's stiffness. The comparison in stiffness between the two phases of loading can be seen in Figure 5-21. The difference between the two stiffness's is due to the affect of the previous displacement cycles on the system.

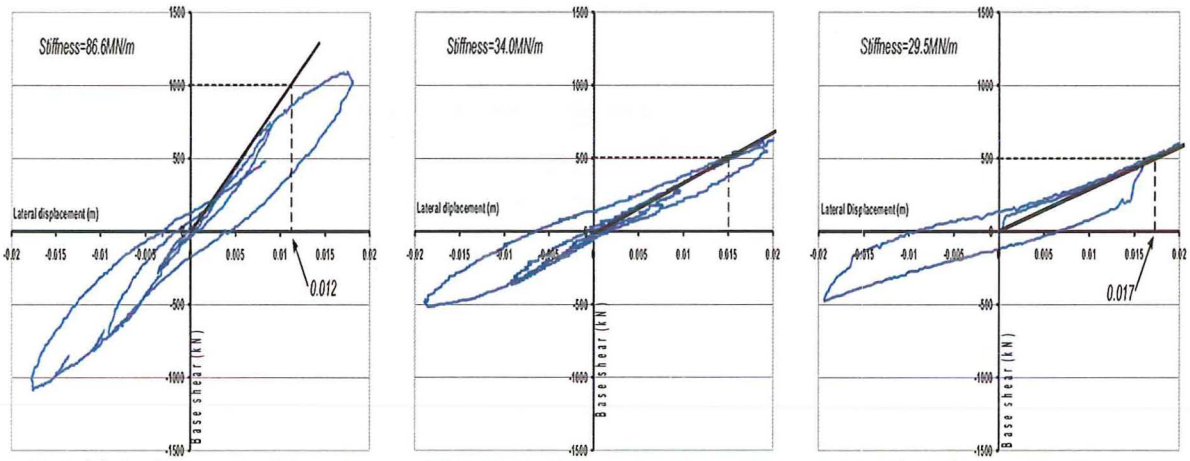

(a) Initial stiffness for Phase I loading **(b) Initial stiffness for Phase II loading** **(c) Initial stiffness for Phase III loading**

Figure 5-21 Super-assembly specimen stiffness for the three phases of loading.

5.11 Design Recommendations

From the foregoing, it is evident that NZS3101:1995 and ACI318-02 significantly underestimate the amount that the floor slab contributes to the negative moment capacity of the perimeter frame. When determining the expected amount of activation of slab reinforcement as additional tension reinforcement, the type and location of the plastic hinge plays a significant role. For exterior plastic hinges that form at the column face, the amount of slab activation for a negative moment should be determined by the area of reinforcement that crosses the continuity crack that would form at the interface between the end of the precast unit and the supporting beam (Figure 5-22). The width of activated slab that contributes to each plastic hinge varies with interstorey drift and reached a maximum equal to 3.1m. This additional tension

force is then multiplied by the leverarm between the centre of the compression force and the centre of the tension reinforcement (refer to Figure 5-10). Figure 5-14 can be used to determine the amount of slab participation at varying levels of interstorey drift. For a positive moment no slab activation occurs and only the beam longitudinal reinforcement contributes to the nominal moment.

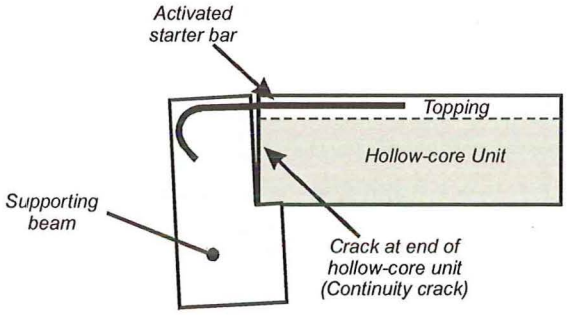

Figure 5-22 Continuity crack that formed between the end of the hollow-core unit and the perimeter beam

For interior plastic hinges, the amount the slab contributes to the negative moment capacity should be based on the same mechanism as for the exterior hinge. Refer to Figure 5-14 to determine the width of activated floor slab for varying levels of interstorey drift. Care needs to be taken to account for any prestressing strands, if a prestressed floor unit spans past a column. The prestressing strands should be multiplied by the strands respective leverarms as shown in Figure 5-10. If the prestressing strands are not included the amount of activation is greatly underestimated as evident from this investigation as well as being reported by Lau et al (2003).

5.12 Concluding Remarks

Although most of the failure modes observed during the experimental program was not expected, some of the failure modes were able to be analytically predicted

whereas others require further investigation in order to ascertain a complete understanding of how the failure occurred.

The analysis found that although the crack at the end of the hollow-core unit (adjacent to the supporting beam, Figure 5-3) was observed at a drift of 0.32%, it actually formed as a hairline crack much earlier (0.16% drift). This value shows that even for a very stiff structure under a moderate earthquake the end of the hollow-core unit is likely to fracture if the hollow-core unit is supported on a mortar/grout seat.

Finally, the evidence showed that the residual load capacity of the floor diaphragm was small once both ends of the hollow-core units had completely fractured and it was only the topping concrete holding the floor in place. By placing the additional concrete mass (to simulate the super imposed dead load and live load) the floor failed. If this load had been applied during the experiment plus the addition of some vertical acceleration (as would occur in a real earthquake) it is felt that the floor would have failed as a complete section at an earlier stage.

Once the tear formed within the floor diaphragm the amount of strength enhancement from the floor slab to the lateral strength of the super-assembly was limited. By plotting the applied base shear versus interstorey drift, it was possible to compare the theoretical prediction for lateral strength, observed test results and the expected diaphragm contribution as recommended by NZS3101:1995 and ACI 318-02. When the specimen was loaded parallel to the hollow-core units (Phase I and III), the frames capacity was underestimated by 45% when NZS3101:1995 and ACI 318-02 were used. The theoretical lateral strength of the super-assembly was able to be accurately predicted using rigid body kinematics (Appendix F) and a graph that predicts the activated slab width for varying interstorey drifts (Figure 5-14). It is

recommended that this mechanism should be used to determine the slab contribution to the beams negative moment capacity.

When loaded in the transverse direction (Phase II), the magnitude of the diaphragm contribution was again limited due to the tear within the floor diaphragm. It was still possible to determine approximate factors that contributed to the lateral strength in the transverse direction. The components that contributed were similar to those adopted in Phase I. Again, NZS3101 and ACI 318-02 underestimate the lateral strength of the super-assembly.

When estimating the amount of slab activation contributing to the negative moment capacity of the beam in the design of a new structure, the amount of slab activation is dependent on the level of drift the structure might experience. The maximum width of floor slab activated in this investigation was 3.1 metres. The slab activation must be incorporated into the negative moment capacity for a plastic hinge.

Velez and French (1989) state that the possibility of full slab width participation should be considered when designing structures that may undergo major earthquakes. This is very much in keeping with the assumption made in the design recommendation proposed herein.

5.13 References

ACI 318-02, *Building Code Requirements for Structural Concrete and Commentary*, American Concrete Institute, Farmington Hills, USA

Cheung P.C., Park R, Paulay T, 1991, *Seismic Design of Reinforced Concrete Beam Column Joints with Floor Slab Support*, Research Report 91-4, Department of Civil Engineering, University of Canterbury, Christchurch, 328 pp.

Fenwick R, Davidson D and Lau D, 1999, *Strength Enhancement of Beams in Ductile Seismic Resistant Frames due to Prestressed Components in Floor Slabs*,

Journal of the New Zealand Structural Engineering Society (SESOC), Vol 12, no. 1, pp 35-40

Lau D, B, N, 2001, *The Influence of Precast-Prestressed Flooring on the Seismic Performance of Reinforced Concrete Perimeter Frame Buildings*, Department of Civil and Resource Engineering, University of Auckland, Report No. 604

Lau D.B.N, Davidson B.J and Fenwick R.C, 2003, *Seismic performance of r/c perimeter frames with slabs containing prestressing units*, Conference Proceedings 2003 Pacific Conference on Earthquake Engineering, February, Christchurch

NZS3101:1995, *Concrete Structures Standard*, Standards New Zealand, Wellington New Zealand

Paulay T and Priestley M.J.N, 1992, *Seismic Design of Reinforced Concrete and Masonry Buildings*, New York, John Wiley and Sons

Velez O and French C.W, 1989, *R/C Beam-Column-Slab Subassemblages Subjected to Lateral Loads*, Journal of Structural Engineering, ASCE, V115, No 6, pp 1289-1308

This Page is Blank

Chapter 6

Diaphragms and Precast Floor Support Details

6.1 Introduction

In the past, research has focussed on the performance of lateral loading resisting systems and floor diaphragms have been overlooked. This is because floor diaphragms have been assumed to act rigidly and hence ease the computational effort required when designing a structure. Is this above statement true? A research programme undertaken at the University of Canterbury has set out to try and answer this question. Within this investigation a full-scale three-dimensional super-assembly was built to investigate the floor performance during an earthquake. By constructing a full-scale three-dimensional super-assembly allowed the boundary conditions to be more accurately modelled than possible in a two-dimensional experiment.

This chapter firstly discusses the investigations undertaken by previous researchers on the performance of the connection detail used for seating hollow-core floor slabs, in particular the shortcomings of their research programme. Next, a comparison of the various connection details used around the world to connect hollow-core units to a supporting beam is made. Chapter 5 discussed the failure modes observed during the experimental programme but herein some possible construction modifications are suggested to increase the performance of a reinforced concrete structure incorporating hollow-core floor units. The definition and role of a floor diaphragm is explained followed by some considerations for when a strut and tie analysis is undertaken. Finally the observed diaphragm performance during this present research will be discussed.

6.2 Findings from previous research.

Previous work undertaken by Mejia-McMaster and Park (1994), Herlihy and Park (2000) and Oliver (1998) focussed on the connection between a precast hollow-core floor unit and its supporting beam. The tests were undertaken to investigate the loss of support of a hollow-core unit during an earthquake due to beam elongation. These tests comprised of pulling a hollow-core unit off its beam support to see whether the cast insitu topping concrete and starter bars were sufficient to stop the unit from collapsing. Several tests were undertaken looking at the affects that various reinforcement arrangements, both in the cast insitu topping and partially filled cores, had on the performance of the connection. The tests comprised of either a monotonic pull-off or cyclic pull-off load applied to the hollow-core unit to simulate the loss of support due to beam elongation. Herlihy and Park (2000) carried out some additional tests in which the hollow-core unit was rotated relative to the supporting beam. This was a monotonic test in which the tip of the hollow-core unit was displaced down to create tension across the topping interface. Both of these set ups used are shown in Figure 6-1.

The mode of failure of the hollow-core unit to supporting beam connection observed in the super-assembly testing was different to those experienced by the above mentioned researchers. The failure of the previous researchers connection was purely due to tension as the hollow-core unit was pulled off its seat (Figure 6-2(a)). The failure of the connection used in the super-assemblies was due to the cyclic rotation of the hollow-core unit relative to the supporting beam, leading to the

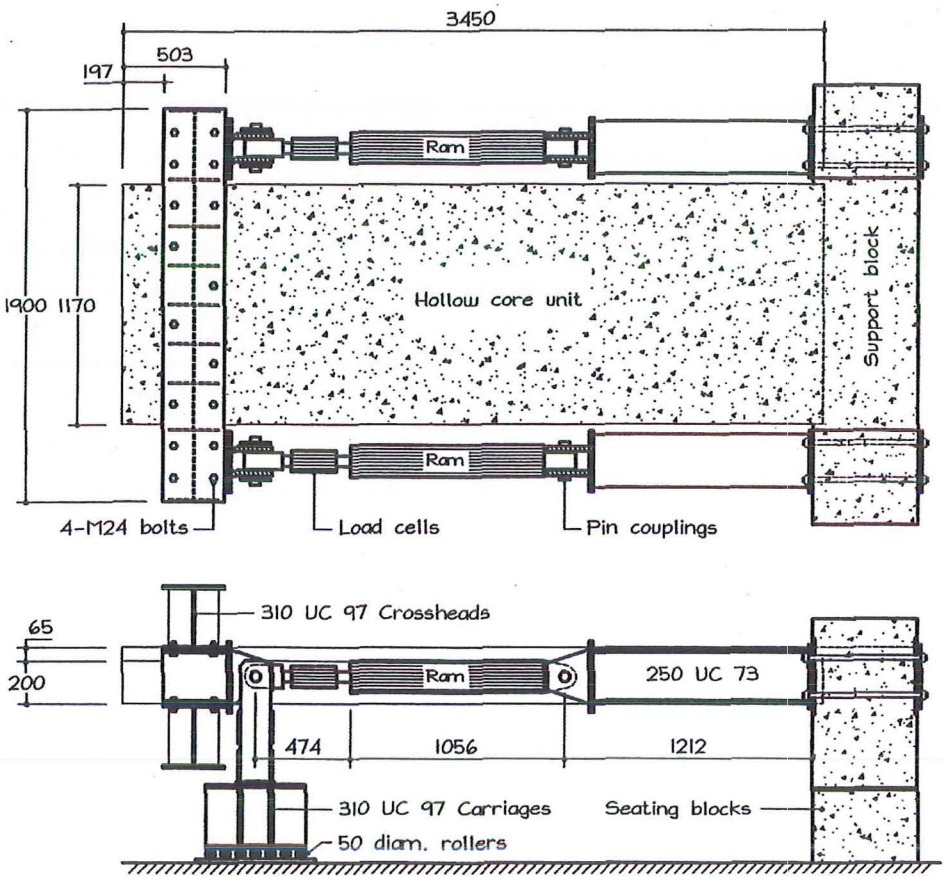

(a) Pull off test set up

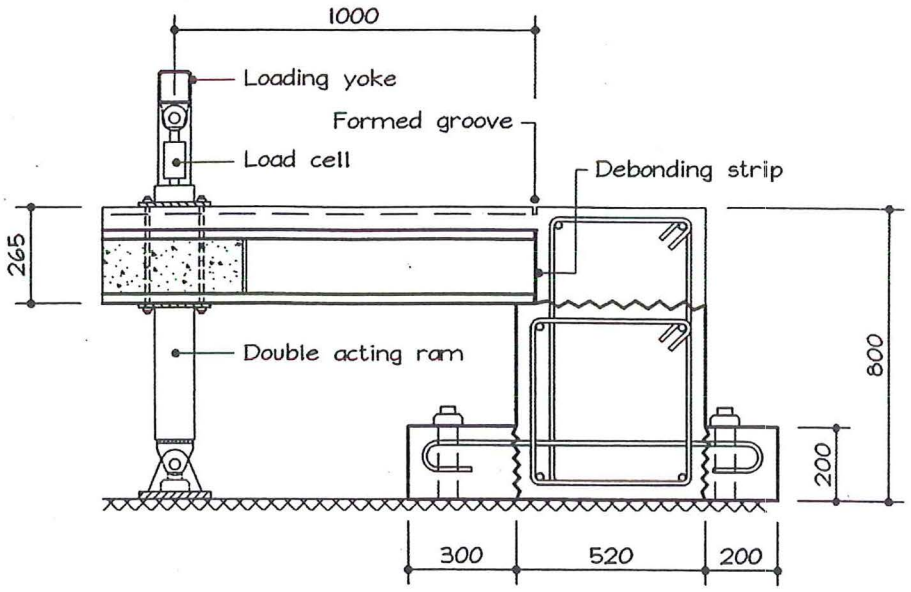

(b) Rotation test set up

Figure 6-1 Previous hollow-core pull off and rotation tests (Herlihy and Park 2000)

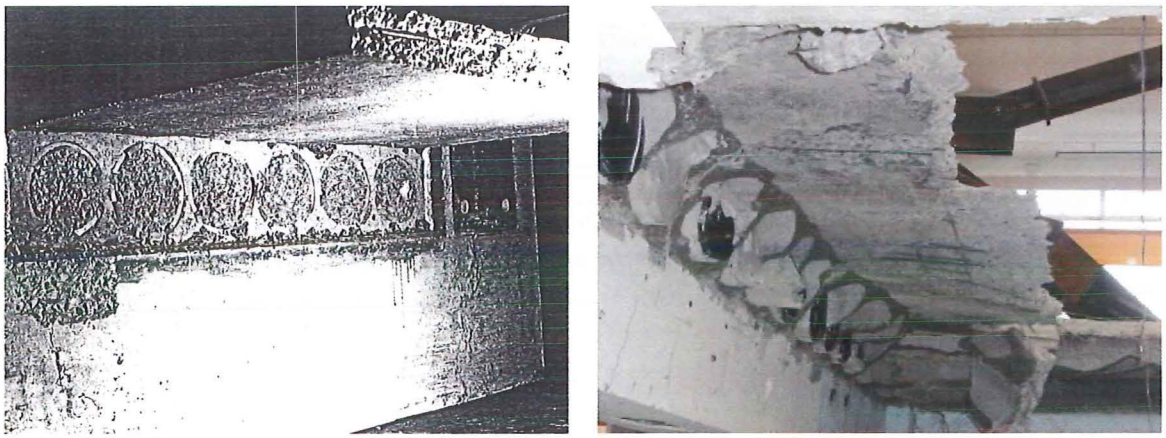

(a) Previous research (Herlihy and Park 2000) **(b) Present research**

Figure 6-2 Comparison between previous test failures and current test failure

fracturing of the edge of the hollow-core unit, rather than the unit being pulled off its seat (Figure 6-2(b)).

The major difference between the expected seating performance (assumed by design) and the observed performance of the test (Chapter 4) was that the floor unit rotated relative to the beam it was seated upon. In design, the conventional wisdom is to assume that hollow-core units would slide relative to the beam; this was not the case in this investigation. There was enough bond/friction to cause the end of the unit to be bind to the beam and then fracture rather than slide (Figure 6-3). It is evident that previous researchers have overlooked the importance of the rotation of the supporting beam relative to the hollow-core unit. The role that beam elongation within the experimental programme was not as significant as originally expected. The reason for this was that this experimental programme was not exposed to the large number of inelastic rotations that other experiments had been exposed too in the past. Therefore the magnitude of beam elongation is less than expected. The floor slab also restrained some of the beam elongation (refer to Chapter 7).

Due to the poor performance of the floor slab and the need to have a point of contact for the construction industry, a Technical Advisory Group on precast floors (TAG) was formed in New Zealand to discuss these experimental results from the

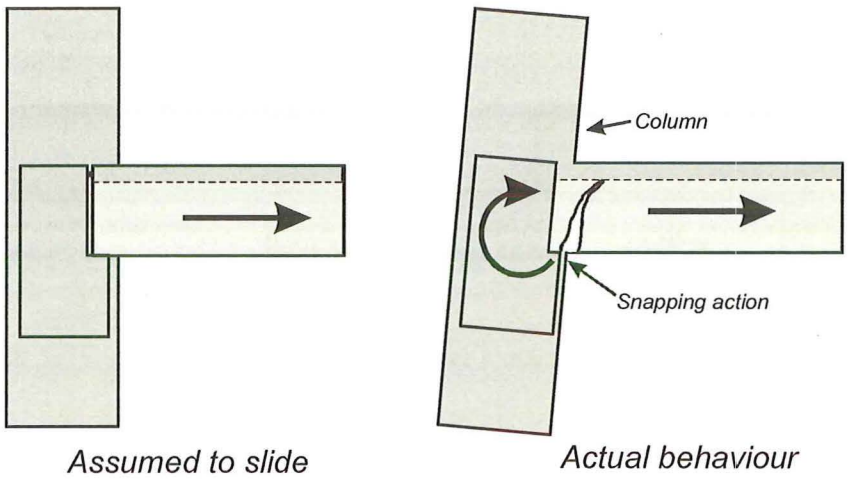

Figure 6-3 Assumed (by design) versus actual hollow-core to beam performance

(Matthews et al, 2003)

testing programme at the University of Canterbury. Also the TAG was to discuss future testing and communication of the results to the construction industry. The main reason for forming the TAG was to establish a group of all relevant parties for discussion on precast floors, in particular to hollow-core floors. TAG consisted of representatives from the Universities of Canterbury and Auckland, the New Zealand Society for Earthquake Engineering, the Society for Structural Engineers of New Zealand, the New Zealand Concrete Society, PrecastNZ Inc., precast floor manufacturers and the Cement and Concrete Association of New Zealand. Upon discussion of the tests results, the TAG recommended a new connection detail that was expected to perform better than the details currently used.

The new detail consists of replacing the dam plug in the end of the hollow-core unit and placing some compressible material across the end of the hollow-core unit. The hollow-core unit will also be placed on a bond breaker, in the form of a low friction (PTFE or equivalent) bearing strip rather than purely on the concrete beam or a mortar/grout pad. A sketch of the proposed detail is shown Figure 6-4 along with the expected improved (damage-free) performance.

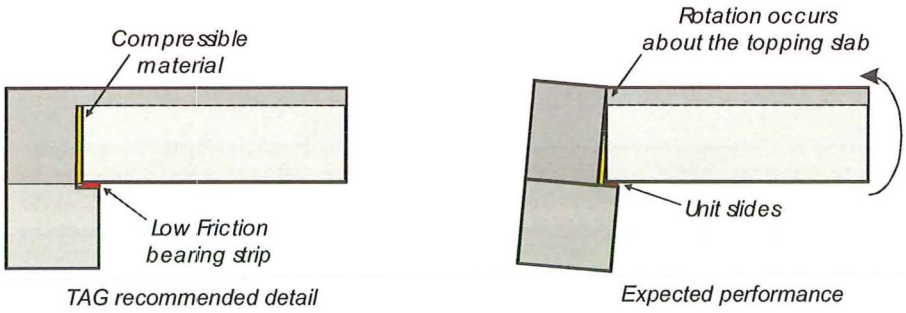

Figure 6-4 Recommended detail and assumed performance (Matthews et al, 2003)

By placing the hollow-core unit on a low friction bearing strip allows the floor unit to slide as previously assumed. Since the unit can slide (on the low friction bearing strip) the tensile stresses formed within the bottom of the hollow-core unit are low and hence the likelihood of the end of the hollow-core unit fracturing is reduced. The compressible material is added to reduce the compression force being applied to the bottom of the hollow-core unit should the unit bear against the beam when a negative moment is applied (Figure 6-5(b)). If the hollow-core unit bears against the beam a large strut (compression field) forms from the bottom of the hollow-core unit up to the topping slab at a relatively flat angle. If this large compression strut forms then principle tensile strains form perpendicular to the strut within the web of the hollow-core unit. It is these tensile strains that cause the initial crack at the base of the hollow-core unit to propagate (Figure 6-5). The combination of the low friction bearing strip and compressible material allows the beam to rotate relative to the floor unit without fracturing the end of the floor unit and hence allowing the connection detail to work as assumed.

The length of seat that the hollow-core unit is placed upon is highly important when a bearing strip is used. The bearing strip must be placed back from the edge of the beam so that the likelihood of the beam spalling is reduced. The bearing strip must also be placed away from the end of the hollow-core unit because as the unit tries to rotate it does not dig into the bearing strip. Figure 6-6 shows the correct positioning of

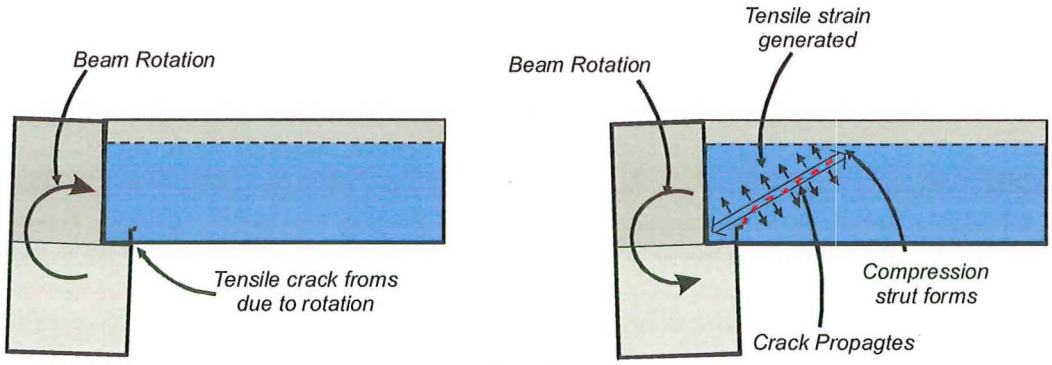

(a) Positive moment **(b) Negative moment**

Figure 6-5 The effect that a positive and negative moment has on the hollow-core units connection to the supporting beam

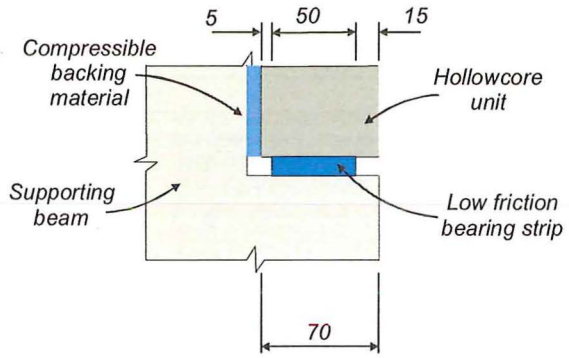

Figure 6-6 Positioning of the low friction bearing strip

the bearing strip. The seat length must be sufficient to account for any beam elongation (that will occur as a result of the beams hinging as the building displaces) and construction tolerances.

The thickness of the compressible material is designed so that, even during the largest expected rotation of the connection, the base of the hollow-core unit does not bear into the beam. The required thickness of compressible material is determined by

$$Backing\ thickness = \frac{D_{HCT} \times \theta_{\max}}{100} \qquad \textbf{(6-1)}$$

in which D_{HCT} = the depth of the hollow-core unit plus the topping slab (mm) and θ_{max} = max expected rotation (% drift) for a maximum credible earthquake.

The initial results from the testing of a sub-assemblage using this modified connection detail appear favourable (Bull and Matthews, 2003). This test consisted of rotating a hollow-core unit relative to the supporting beam in order to replicate the connections performance. Figure 6-7 shows the construction of the connection detail and the level of damage to the connection at the end of the test. Further testing of this connection detail is required in the 3D super-assembly so that second order effects and the influence of beam elongation can be investigated.

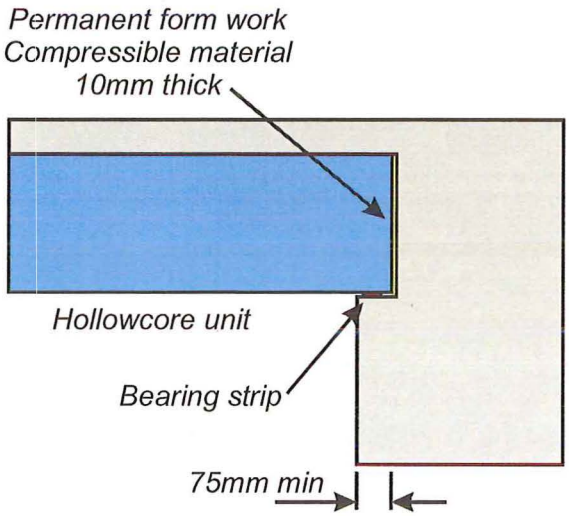

(a) Elevation of the isolation connection detail

(b) During Construction

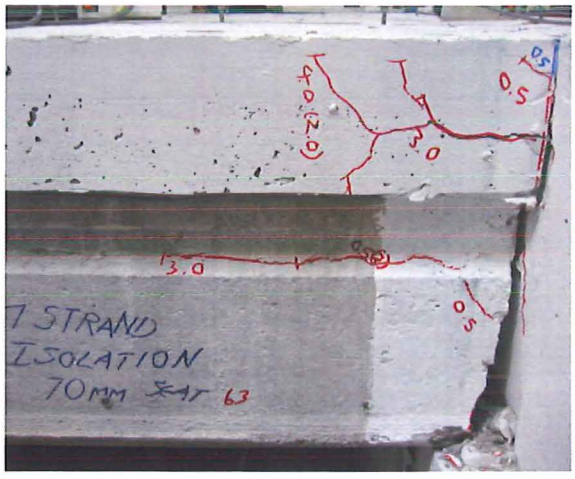

(b) At the completion of ±4.0% load cycle

Figure 6-7 Construction and end of test photos for the performance of the isolation connection detail (Bull and Matthews, 2003)

Another detail (recommended by the TAG) was tested and performed well in a sub-assembly test was one in which two of the cores of the unit had additional reinforcing added in the form of a paperclip (Figure 6-8). The unit was also seated on a low friction bearing strip. This detail should also be tested in the super-assembly. The level of damage to this connection detail was slightly more than that seen when the isolation detail was tested.

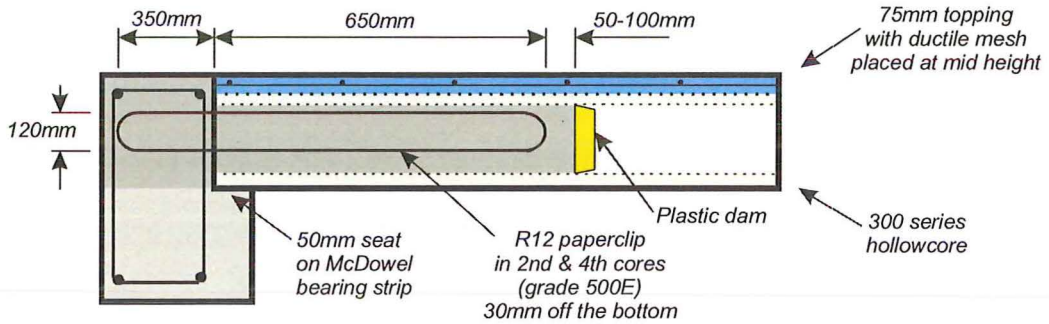

(a) Elevation of the paperclip detail

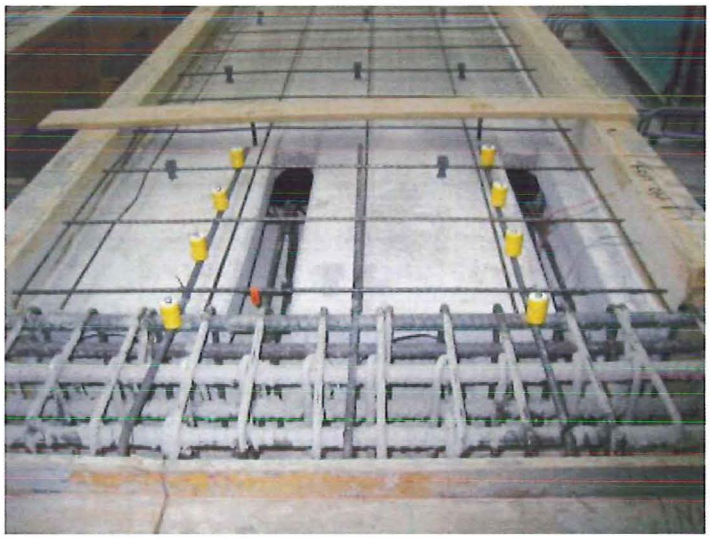

(b) During Construction

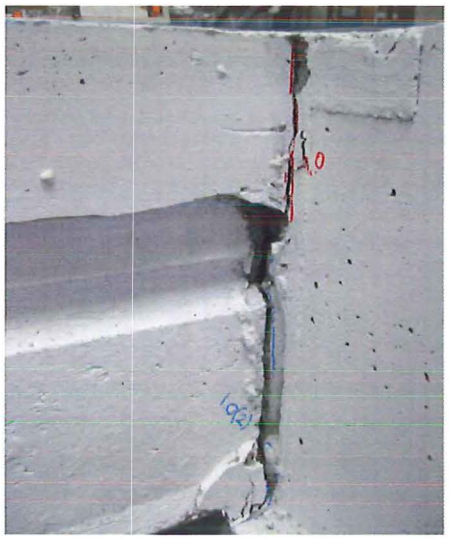

(c) At the completion of ±4.0% cycle

Figure 6-8 Construction and end of test photos for the performance of the paperclip connection detail (Bull and Matthews, 2003)

6.3 The performance of the first hollow-core unit adjacent to the frame.

A hollow-core floor unit is designed to act as a simply supported one-way floor system. The first unit placed adjacent to the perimeter frame (refer to Figure 6-9) does not act in this manner as it was securely tied, not only at its ends, but also along its entire length to the South perimeter beam. This led to the hollow-core unit being displaced in a quasi-two way manner as the hollow-core unit was forced to undergo the displaced shape of the perimeter beam (double curvature, (Figure 6-10)). This displacement incompatibility between the double curvature of the perimeter beam and the simply supported hollow-core unit caused the hollow-core unit to fail. Since the hollow-core unit has no redundancy in its design (due to the lack of any transverse reinforcement), the unit failed through web splitting and the bottom half of the hollow-core unit drops away. The webs became overloaded as the hollow-core unit was displaced in double curvature, a manner for which the unit was not designed.

If the unit was not tied along its length, in other words the hollow-core unit was not forced to undergo the displaced shape of the perimeter beam, it is considered that the unit would perform better. Current design practice does not allow the hollow-core unit to be detached from the perimeter beam because the diaphragm forces generated during an earthquake need to be transferred out of the floor slab and into the perimeter moment resisting frame.

Changing the way in which the first hollow-core unit is connected to the adjacent perimeter beam should allow the unit to perform in the manner in which it was intended by design—that is, a one-way slab. The recommended solution specified by the TAG involves the placing of a 600-750mm timber infill next to the perimeter beam and constructing a reinforced concrete slab between the first hollow-core unit

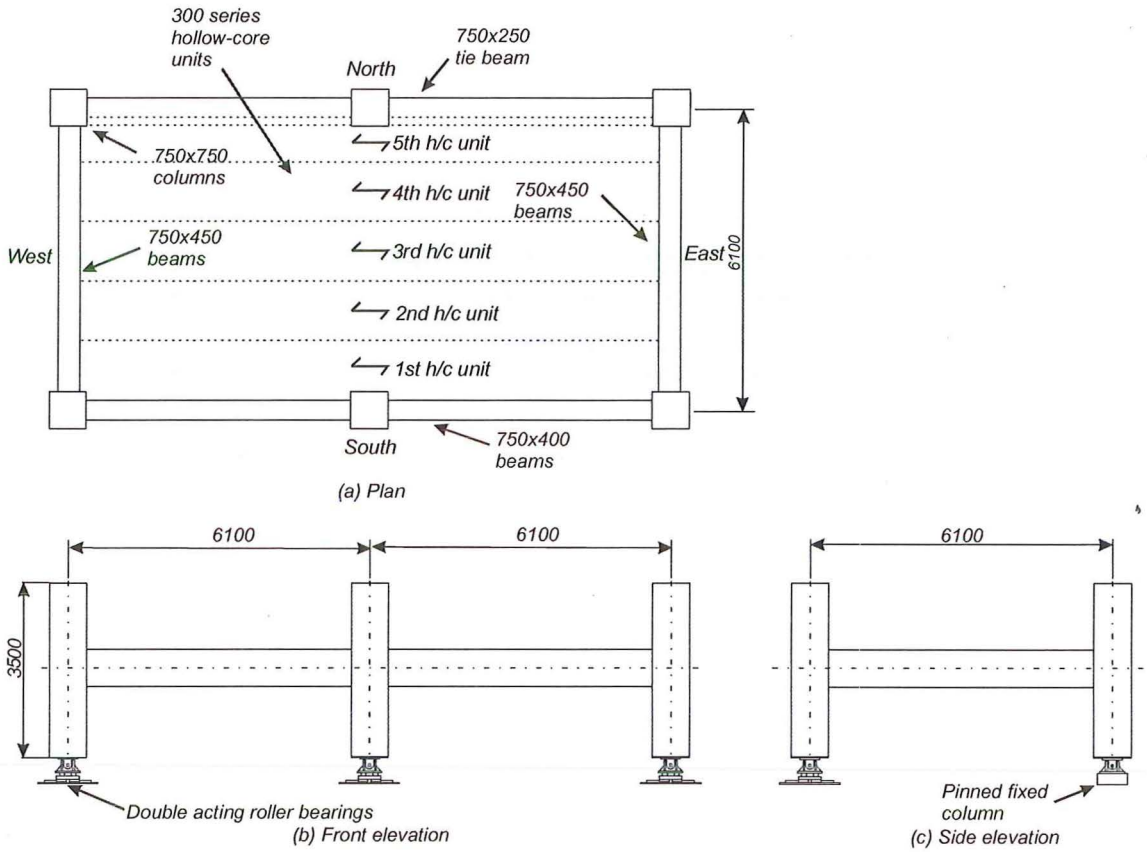

Figure 6-9 A plan and elevation of the super assembly.

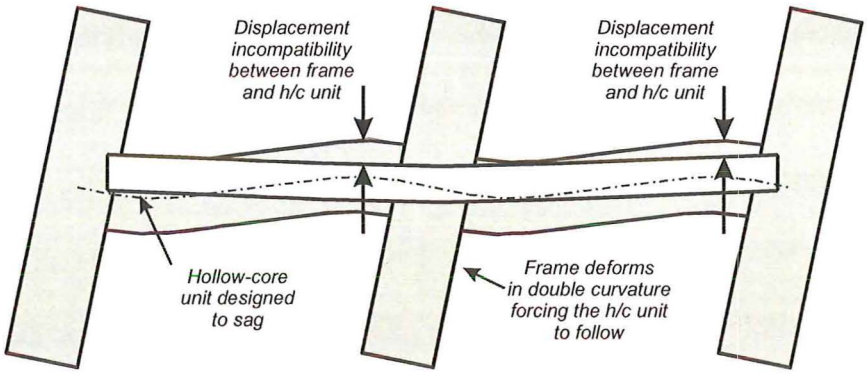

Figure 6-10 Displacement compatibility between the frame and the hollow-core floor units. (Matthews et al, 2003)

and the beam. This results in the hollow-core unit being offset from the perimeter beam as shown in Figure 6-11. The construction of this slab (75mm thick) will allow a more flexible link between the perimeter beam and the first hollow-core unit. Displacement incompatibility is accounted for in the deformation of the link slab. Damage is expected within this link slab (in the form of cracking) due to the

displacement incompatibility. As all the deformation is within the reinforced link slab, the first hollow-core unit should remain undamaged.

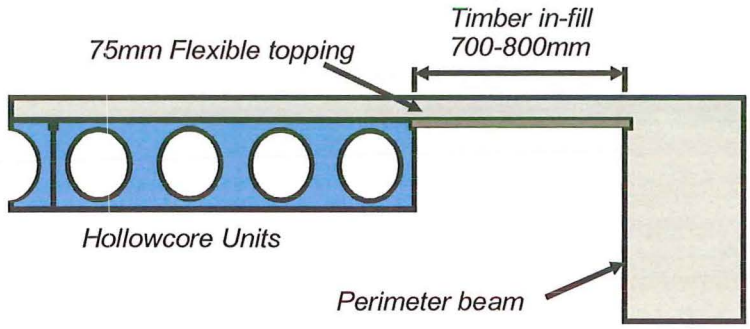

Figure 6-11 Recommended detail allowing the first hollow-core unit to be separated from the perimeter beam.

This detail needs to be tested in the super-assembly to ensure it performs in the desired manner.

6.4 Extra diaphragm tie reinforcement

During the experiment a longitudinal tear formed within the floor diaphragm (refer to Chapter 4) due to the over stressing of the diaphragm reinforcement as the super-assembly displaced. This tear within the floor now affects the effective length of intermediate perimeter columns. If such a tear occurred over several floors in a multi-storey frame then the column may become unstable.

Another scenario that it not usually considered in design is that all the lower level columns within a building need to be adequately tied to the floor diaphragm. These columns need to be tied into the building because as a building displaces in an earthquake all the bottom columns must hinge at ground level. This means the trailing columns are being dragged laterally with the building by floor diaphragm. If the tie force provided to ensure these columns displace with the rest of the building is insufficient then the diaphragm will tear due to this displacement incompatibility and subsequent overloading of the floor diaphragm.

The New Zealand Concrete Standard, (NZS3101:1995), states, "additional tie reinforcement must used to tie the column to the floors at each flooring level. The magnitude of the tie force is equal to the larger of 5% of the maximum total axial compression load on the column or 20% of the column shear force induced by the lateral design forces." The draft joint Australian and New Zealand Structural Design Actions Standard (AS/NZS1170.4:2002) requires that "all parts of the structure shall be interconnected. Connections shall be capable of transmitting 5% of the value of $(G+\Psi_c Q)$ for the connection under consideration". G = design dead (gravity) load, Ψ_c = area reduction factor for determining the live load (Q).

NZS3101:1995 states that the reinforcement should be placed at angles close to 45^0 (Figure 6-12(a)). This does help tie the column in but also contributes to the perimeter beams overstrength actions. The reinforcement would be better placed transverse to the perimeter beam (Figure 6-12(b)) so that the reinforcement does not contribute to the perimeter beams strength. It is the component, of the angled tie reinforcement, parallel to the direction of loading that contributes to the negative moment capacity of the perimeter beam.

If the hollow-core units spanned one-bay (rather than two) then a secondary beam would be located at the central column. If this secondary beam was adequately tied, to the perimeter frame, then the central column would be unable to displace laterally, out of the building, so the need for additional reinforcement would be unnecessary. It is felt that if the secondary beam were sat on a corbel then additional diaphragm tie reinforcement would be required since there is generally no positive connection between the perimeter frame and the secondary beam.

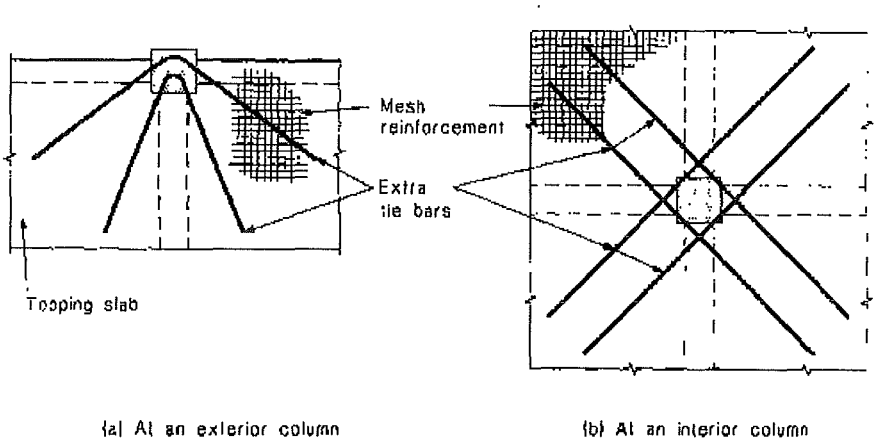

(a) The New Zealand Concrete Design Standard recommendations for the tying of columns into a building (NZS3101:1995)

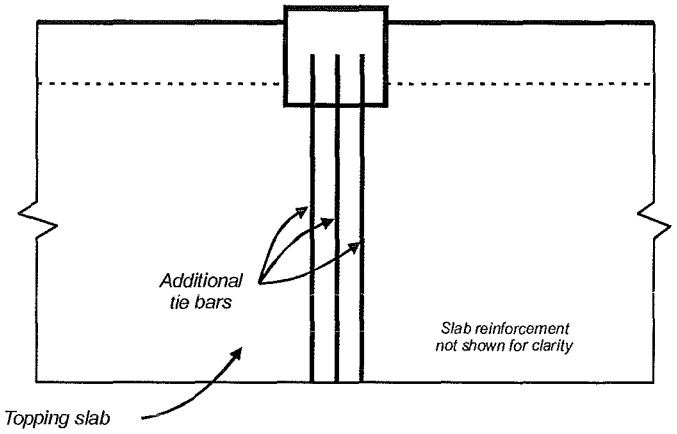

(b) Modified recommended tie detail

Figure 6-12 Tie reinforcement required to tie columns into a building.

6.5 Detailing requirements

New Zealand requirements

A study group consisting of the New Zealand Concrete Society and the New Zealand Society for Earthquake Engineering has produced a set of guidelines titled "Guidelines for the Use of Structural Precast Concrete in Buildings". This document gives guidance on the use of precast concrete; one particular chapter on *floor unit support and continuity* shows the types of connection details that should be used to connect hollow-core floor units to the structural system chosen. The first edition of

this document was published in 1991 (Centre for Advanced Engineering, 1991) and later revised in 1999 (Centre for Advanced Engineering, 1999).

Centre for Advanced Engineering (1999) lists a series of recommended connection details that should be used. The chosen connection depends on the depth of supporting beam prior to the cast insitu concrete topping slab being poured. Additional guidance is given when the hollow-core units are placed in a ductile moment resisting frame or when the unit arrives on site and is too short to be seated on the beam (or its seat length is less than the standard specified minimum). These details are summarised in Figure 6-13(a), (b) and (c). Guidance on the positioning of the unit on the beam is also given (Figure 6-13 (d)) to ensure the edge of the beam is not dislodged or damaged, not only during placement but also during the buildings life.

Cl 4.3.6.4 of the NZS3101:1995 gives guidance on the recommended seat length and placing requirements.

None of the connection details specify that a bearing strip should be used.

American requirements

The Prestressed Concrete Institute (PCI) produced a manual called the "Manual for the design of hollow-core slabs" in 1985 (PCI, 1985). This manual gives a series of connection details for the connection of the hollow-core unit to its supporting beam. Very few of the details require a structural topping slab to be poured once the unit is in place. Since there is no structural topping slab, reinforcing bars are grouted into the keyways between to units while the other end of the reinforcement is usually welded to a steel plate embedded in the concrete beam. Two of the PCI recommended details

are shown in Figure 6-14. All the American connections require the hollow-core unit to be placed on a bearing strip.

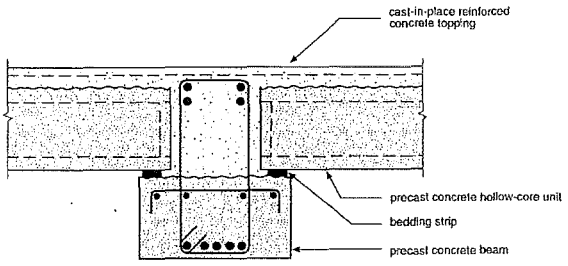

(a) Type 1 precast concrete beam support system

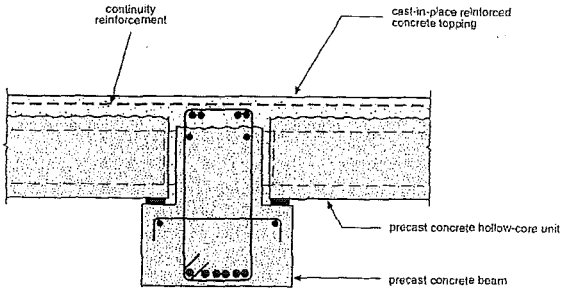

(b) Type 2 precast concrete beam support system

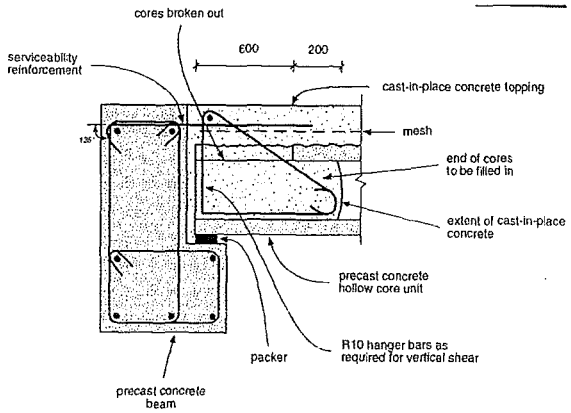

(c) Type 3 precast concrete beam support system

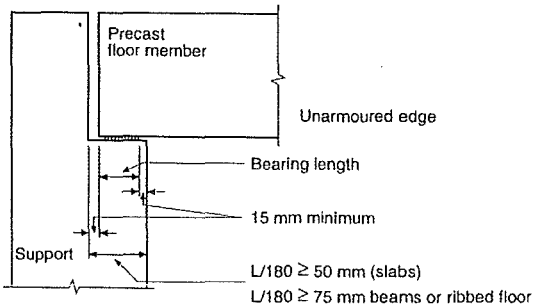

(d) Required bearing length at the support for a precast member

Figure 6-13 NZ recommended details for the support of hollow-core floor units (Centre for Advanced Engineering, 1999)

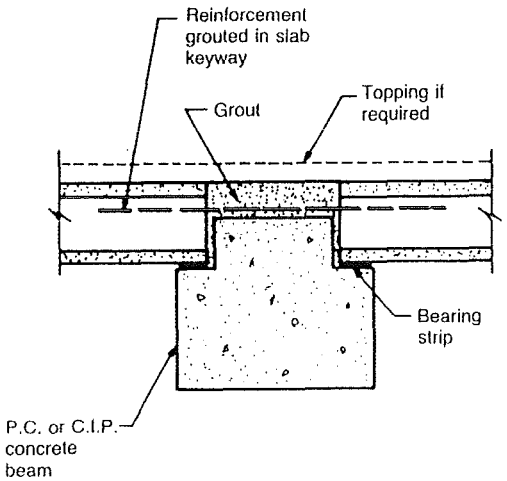

(a) Type A

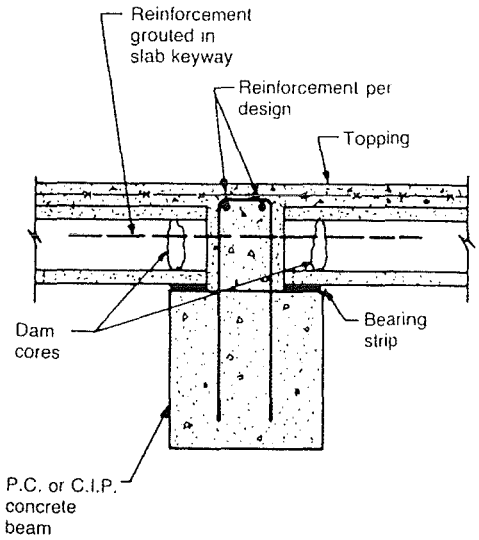

(b) Type B

Figure 6-14 PCI recommended details for the support of hollow-core floor units (PCI, 1985)

European requirements

Fédération Internationale du Béton (FIB) produced a guide to good practice called "Special design considerations for prestressed hollow-core floors" (FIB, 2000). One section within this guide gives information on the detailing of connections and it states that the connection at the support must fulfil the requirements of the structural philosophy of the specific structure. "*In all cases, tie arrangements at support should be able to provide the structural integrity with regard to loads and restrained deformations*". The guide gives recommendations on the number and location of reinforcement to be placed within the hollow-core units to tie them to the lateral load resisting system. Generally the hollow-core units are un-topped so the continuity reinforcement are either grouted between the two units in the keyway or concreted into the cores of the units. An example of a recommended connection detail is shown in Figure 6-15.

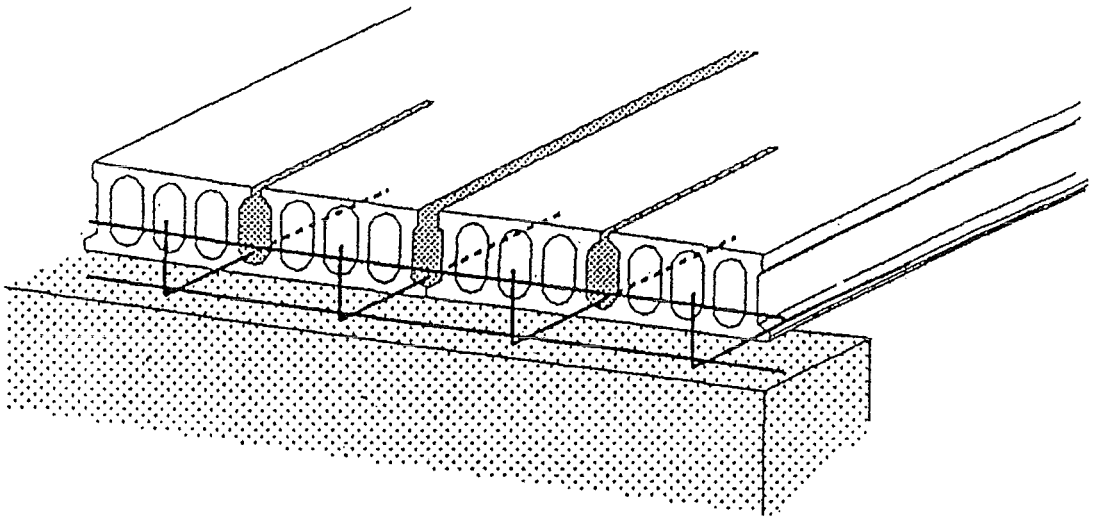

Figure 6-15 FIB recommended details for the support of hollow-core floor units (FIB, 2000)

General comments on the connection of hollow-core units to the supporting beams

There are numerous variations of the recommended connection details from the various countries. There are several key issues that require comments.

The amount of reinforcement used to connect the European style hollow-core units to the supporting beams appears to be much greater than that considered in New Zealand. It is interesting to note that the European connections are generally for non-seismic situations while New Zealand connections are in seismic zones. It should be noted that not all the European floors are topped with a cast insitu topping slab. It is felt that significantly more detailing should be used in a seismic connection (i.e. New Zealand situation in which rotational compatibility with the supporting beam and the hollow-core units must be maintained), as compared with a non-seismic connection (i.e. most of Europe). The Americans connections are very similar to that of the Europeans. The American details use a bearing strip that allows the hollow-core unit to move relative to its seat during seismic movement.

Even though recommendations (in New Zealand, Centre for Advanced Engineering, 1999) are given on how to connect the hollow-core units to the supporting beams in a ductile moment resisting frame these are very rarely followed. There seems to be a large void in the construction process where a detail is recommended but is not followed up. The author feels that there needs to be some educating of the Engineers specifying the product, the manufacturer who manufactures the product and the construction worker who incorporates the product into the structure being built. Both research and earthquakes have shown that the connection of precast floor units to the structural system is a key issue but it does not seem to being addressed. McSaveney (1997) has recommended several types of

connection detail (some including the low friction bearing strip) and these connections have not been greatly used. The answer as to why this is not being addressed is not clear (to the author), perhaps a large level of complacency has grown in New Zealand construction industry since there has not been a major damaging earthquake in New Zealand since the 1931 Napier earthquake.

Another concerning aspect has been the number of variations of connection details used by Engineers across New Zealand (most of which are untested in the laboratory, or have been tested incorrectly). As shown in this experimental programme, a connection detail that was expected to perform reasonably well performed very poorly so it is difficult to see how some of the other connection details being used by other Engineers (within New Zealand) will perform any better. Care also needs to be taken to ensure the testing that is completed is appropriate for purpose of the detail. This has been shown by the variation the applied loading between the work undertaken by Mejia-McMaster and Park (1994), Herlihy and Park (2000) and Oliver (1998) when compared to the actual deformation between the hollow-core floor slab and the supporting beam in this investigation.

6.6 Diaphragms

6.6.1 Diaphragm definition

As well as transferring gravity loads to the main structural system, floor plates are generally required to function as diaphragms, distributing inertia forces to the lateral load resisting system. A floor diaphragm plays an important role in the performance of the whole system and connecting the various lateral load resisting structural systems (frame and walls) across a building. If the diaphragm is able to tie all the

elements of the structure together then alternative load paths can be developed. These load paths will help prevent the structure from collapsing in a major earthquake as well as transferring loads out of the floor slab to the primary lateral load resisting elements.

The role of the diaphragm depends on the geometry of the structure and its location within the structure. Diaphragms are usually defined as one of three types:

(i) Simple (type I) diaphragms resist inertia forces at each floor level and transfer these forces to the primary lateral load resisting system. These are typically provided by standard cast in-situ or precast concrete systems.

(ii) Transfer (type II) diaphragms are required to redistribute seismic forces generated from across a floor, between various lateral load resisting structures. Due to the large shear forces generated, a standard precast hollow-core unit may not be practical. A more robust floor system may be required. Increasing the topping thickness does this, as does using a cast-in-place floor slab (Kolston and Buchanan 1980). Transfer diaphragms are common in buildings that incorporate a set back (in plan) or a basement.

(iii) Hybrid or Dual (type III) diaphragms occur in structures utilising combined frame-wall primary lateral load resisting systems. This type of diaphragm experiences large internal forces due to the deformation compatibility of the two parts of the system (Paulay and Priestley 1992), as shown in Figure 6-16.

6.6.2 Design of diaphragms

Diaphragms are usually modelled as a deep beam (Figure 6-17). The exact design forces are difficult to determine but this is not a concern due to the low flexural and shear stresses when the structure has regular diaphragms of equal length and span, i.e.

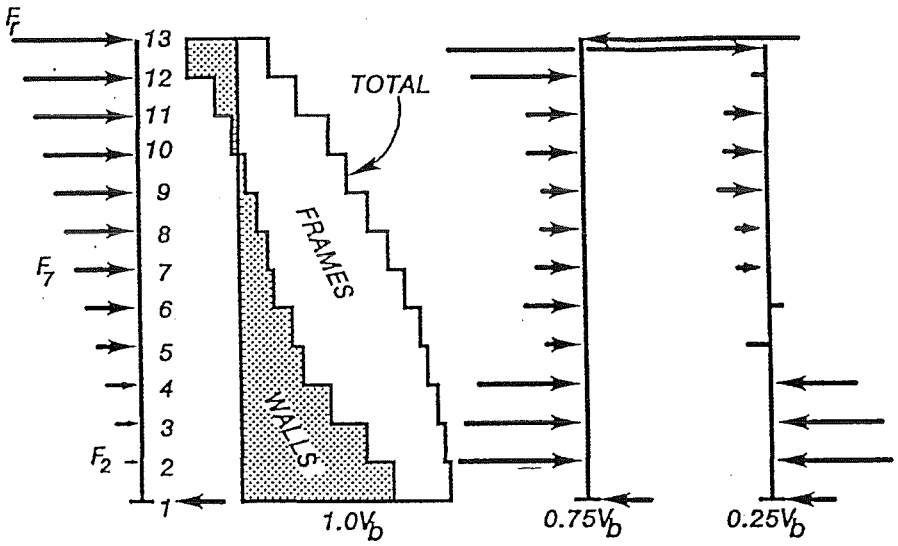

Figure 6-16 Distribution of forces when two structure systems are used within the one building (Paulay and Priestley, 1992)

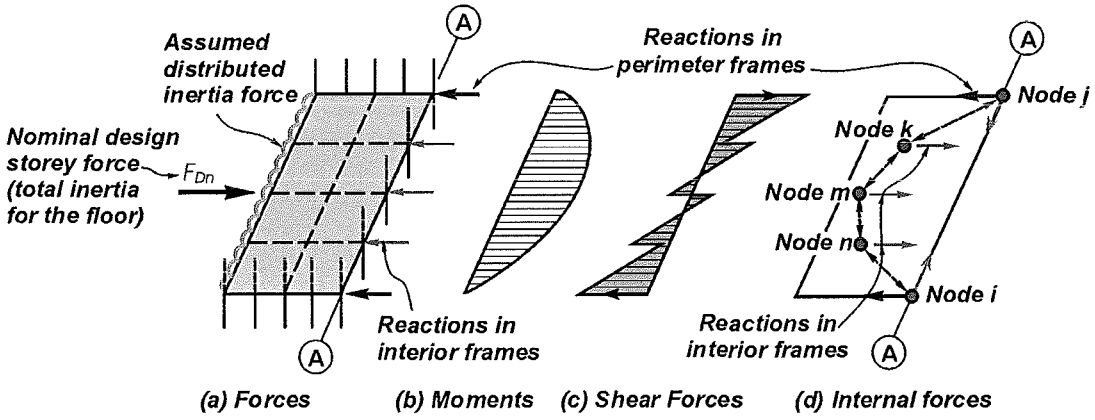

Figure 6-17 Deep beam analogy for the design of diaphragms (NZCS, 1994)

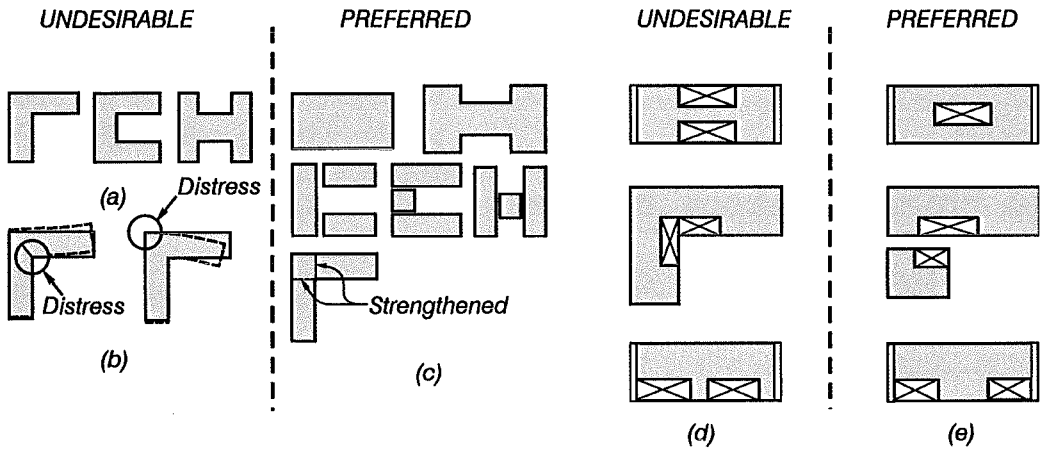

Figure 6-18 Desirable and undesirable configurations for building plans

(Paulay and Priestley, 1992)

squat or compact (Paulay and Priestley, 1992). This is not true, however, for long floors or for floors of irregular plan with a number of changes of directions or "wings" and re-entrant corners such as shown in Figure 6-18.

Diaphragms are assumed to be infinity stiff (i.e. rigid). This is not always true as shown in Chapter 4, when the diaphragm tore. The assumption of an infinity stiff diaphragm is to reduce computational effort. By having an irregular plan structure the computation effort is even greater and more difficult, so Paulay and Priestley (1992) suggested that the irregular planned structures be split into independent structures (Figure 6-18) to improve the diaphragms likely performance and reduce the computation effort. The seismic gaps between these structures must be able to accommodate the possible difference in movement between the two structures. Guidance on the requirements for these separations is given in the New Zealand Loadings Standard (NZS4203:1992).

Since every diaphragm usually has openings or penetrations, care needs to taken to ensure that these penetrations have the smallest effect on flexural and shear capacity of the diaphragm. Incorrectly placed penetrations can greatly affect the loadpaths within the diaphragm. Figure 6-18 shows some preferred locations for penetrations.

6.6.3 Strut and Tie considerations

During an earthquake the beams of a moment resisting frame form plastic hinges and grow in length. This growth is known as beam elongation (refer Chapter 7). This growth could potentially cause the loss of support of gravity loads at several areas within a floor slab. Bull (2003) has shown two modes of deformation (Figure 6-19)

that are possible to occur during a major earthquake. The mode that occurs will determine whether the seat of one or several precast floor slabs is affected.

The common assumption, for a strut and tie model, is for the corner column to act as a node of a truss, tension is taken by the reinforcement within the two beams and the floor transfers a compression strut (Figure 6-20(a)). If either of these deformation modes (shown in Figure 6-19) occurs then this assumption cannot be used, as it is unlikely that the compression struts can be transferred across the damaged corner node. Bull (2003) suggested that the use of the diaphragm reinforcement as tension tie will have a greater possibility of transferring the diaphragm forces (Figure 6-20(b)).

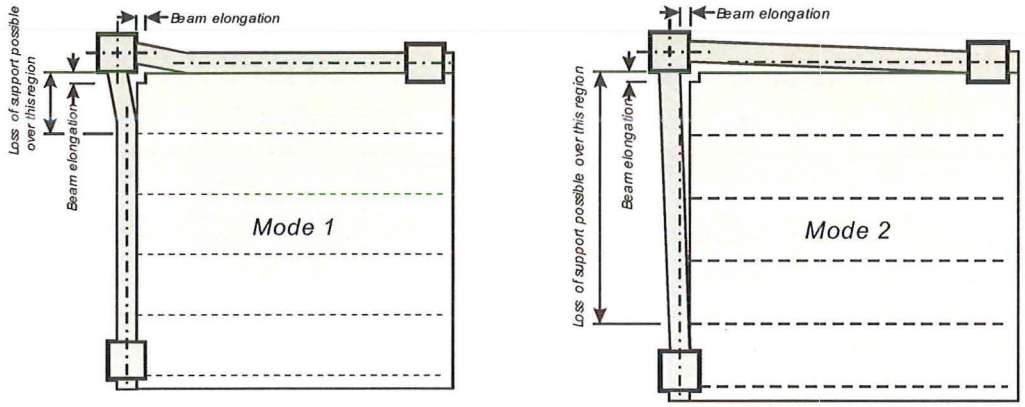

(a) Mode 1-Beam plastic hinge rotates to allow for beam elongation

(b) Mode 2-Entire beam rotates to allow for beam elongation

Figure 6-19 Possible deformation modes caused by beam elongation (Bull, 2003)

Questions have been raised regarding the performance of a tension tie detail, as additional reinforcement has to be placed within the column and extended into the diaphragm far enough to be adequately anchored. Any additional reinforcement placed within the topping slab is likely to provide some additional enhancement of the negative moment capacity of the adjacent beam and needs to be considered if capacity design is being used. The crack that is likely to occur in the corner could be 15-35mm wide, will the placed reinforcement have sufficient ductility?

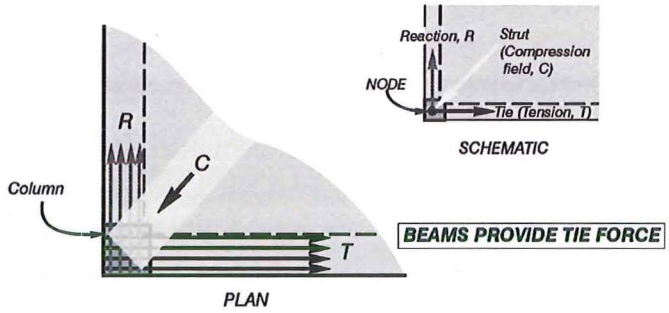

(a) Common assumption for the detailing of a corner node during a strut and tie analysis

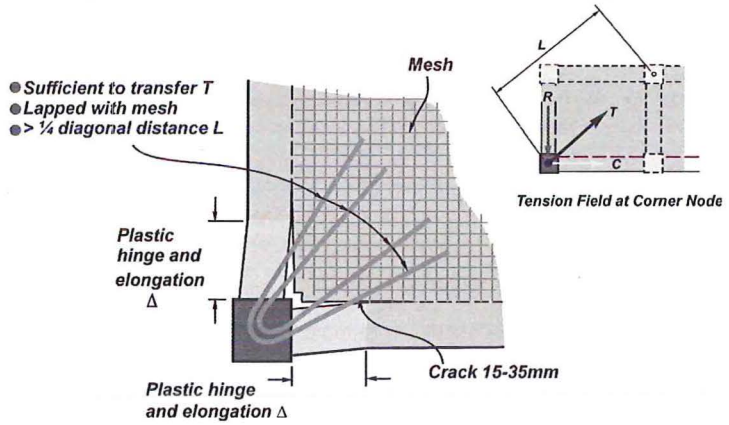

(b) Additional tension reinforcement used at a strut and tie node

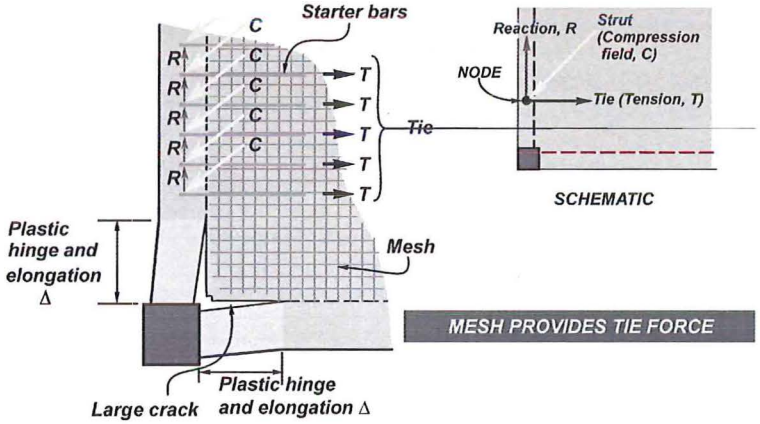

(c) Repositioned node using the existing diaphragm reinforcement to resist the tie force

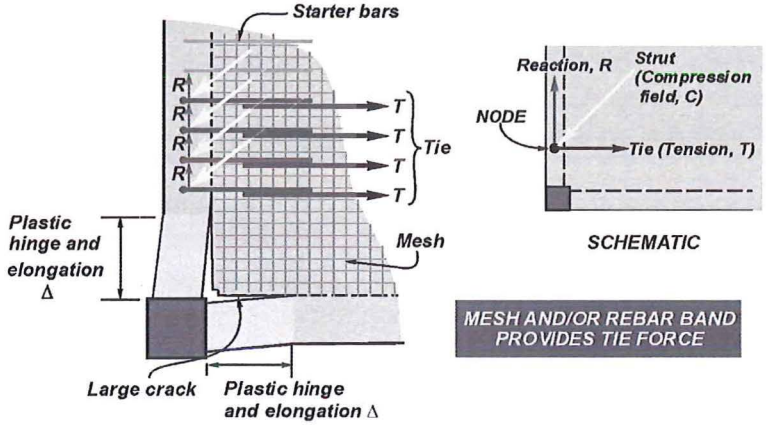

(d) Repositioned node with additional reinforcement within the diaphragm to resist the tie force

Figure 6-20 Detailing of a node in a strut and tie solution dealing with diaphragm forces

(Bull, 2003)

Bull suggested that perhaps the best option would be to shift the node of the strut and tie truss to a location where there is minimal damage (to the beam) away from the plastic hinge zones as shown in Figure 6-20(c) and (d). Additional bands of reinforcement may be placed within the floor slab to carry the tension loads if the current diaphragm reinforcement is insufficient. This additional reinforcement can either be placed within the topping slab or as a series of drag bars in between the precast slabs (refer to Figure 6-21).

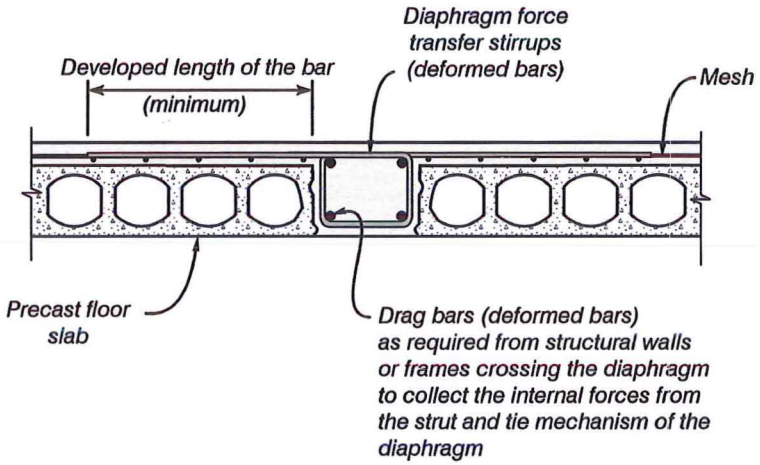

Figure 6-21 "Drag bars" or "Collectors" (McSaveney 1997)

NZS3101:1995 states that the width of slab activated as a flange can be up to half the clear distance to the next parallel beam. This means that any additional reinforcement activated will enhance the negative moment capacity of the beam. In some cases this enhancement may be significant as shown not only by this current investigation but also by others such as Lau (2001).

6.6.4 Diaphragm Forces

Debate arises as to what affect a floor diaphragm has on the seismic response of a building. Should diaphragms be rigid (this eases computation, as mentioned above, but is not necessarily true as explained in Chapter 4) or should they be flexible. If it is chosen to be flexible then what degree of flexibility is required? Researchers such as

Fleischman et al (1996, 2003) and Rodriguez et al (2002) showed that forces experienced within the floor diaphragms can be greatly different to those expected from various design codes. Also, the degree of flexibility of the diaphragm plays a significant role on the demand imposed onto the diaphragm. For example, a structure in which the diaphragm is assumed to be rigid will displace the same as the shear wall within the structure but if the diaphragm was assumed flexible then the diaphragms displacement can be an order of magnitude greater than that of the shear wall (Fleischman et al, 1996).

If the displacement of the two structural systems are different (i.e. a structural wall versus moment resisting frame) then there can be large forces generated within the diaphragm because not only does the diaphragm have to resist the local inertia forces but it must also resist the forces of the two structural systems imposing displacement compatibility (or "fighting") on each other to determine a final displaced shape. Paulay and Priestley (1992) discuss "fighting" within a structure.

6.7 Diaphragm performance in the current research programme

A summary of the demec results is given in Appendix G.

Phase I

Using the data obtained from the arrangement of demec points positioned across the floor diaphragm it was possible to confirm the assumption that the first hollow-core unit was being forced to displace in the same manner as the perimeter beam, i.e. in double curvature (Figure 6-22). As the distance from the perimeter beam increased the

amount of imposed double curvature reduced and the hollow-core units acted more in the manner in which the hollow-core units were designed (i.e. single curvature).

Comparing both the longitudinal and transverse rows of demec points enabled the manner in which the diaphragm deformed during the experiment to be determined. Figure 6-23 shows that the diaphragm deformed in a manner that closely resembles Mode 2 as defined by Bull (2003), both of the transverse beams rotated out over their entire length. Since the floor diaphragm tore, the transverse growth was also plotted to see whether any other deformation patterns occurred. Figure 6-24 shows the affect the diaphragm tear had on the growth within the floor diaphragm. Very little growth occurred during the initial (pre-tear) cycles but once the tear formed the central column displaced significantly in a direction transverse to the direction of loading.

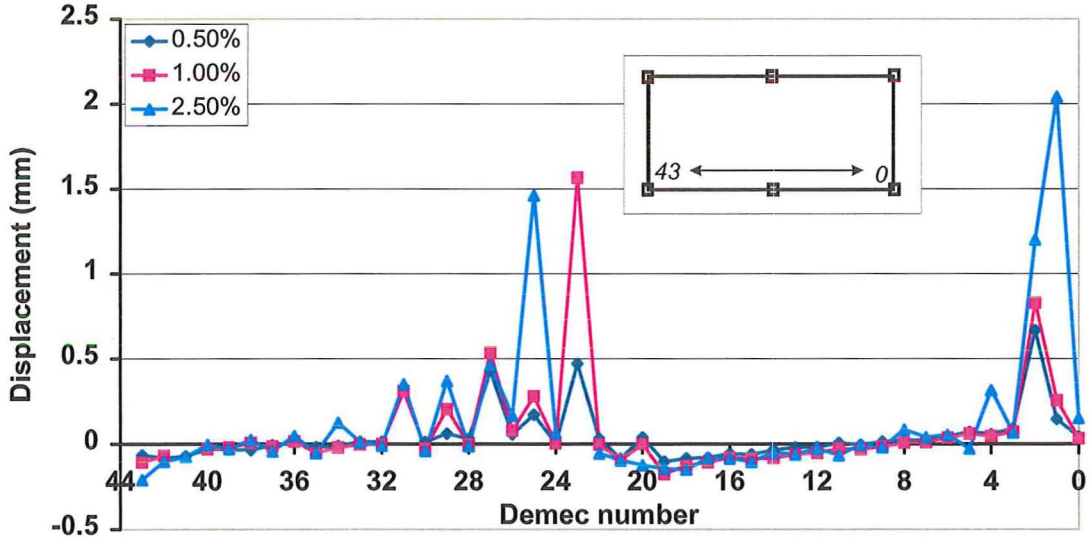

Figure 6-22 Demec points showing the double curvature undertaken by the first hollow-core unit

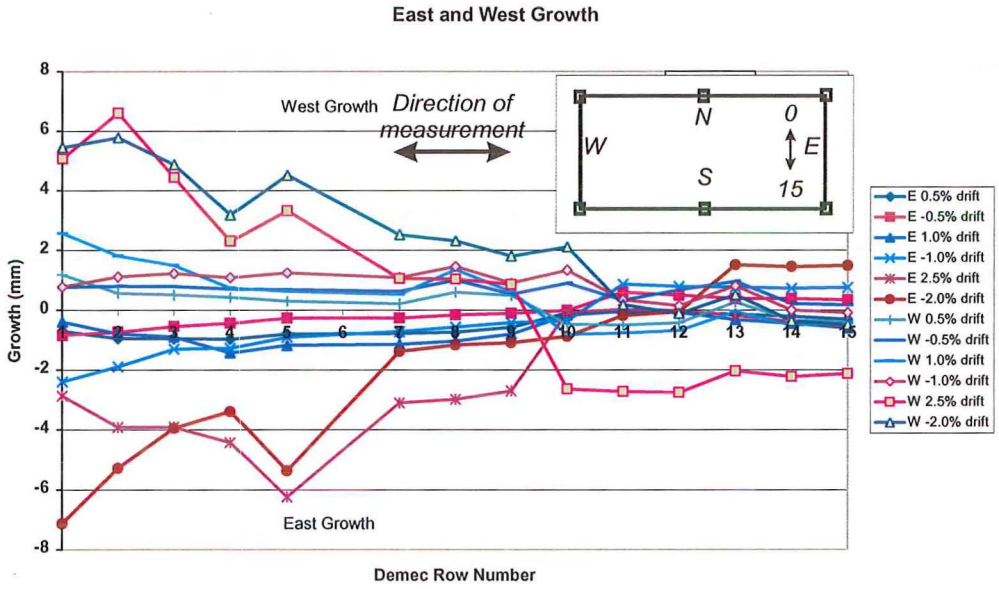

Figure 6-23 Overall diaphragm growth during Phase I

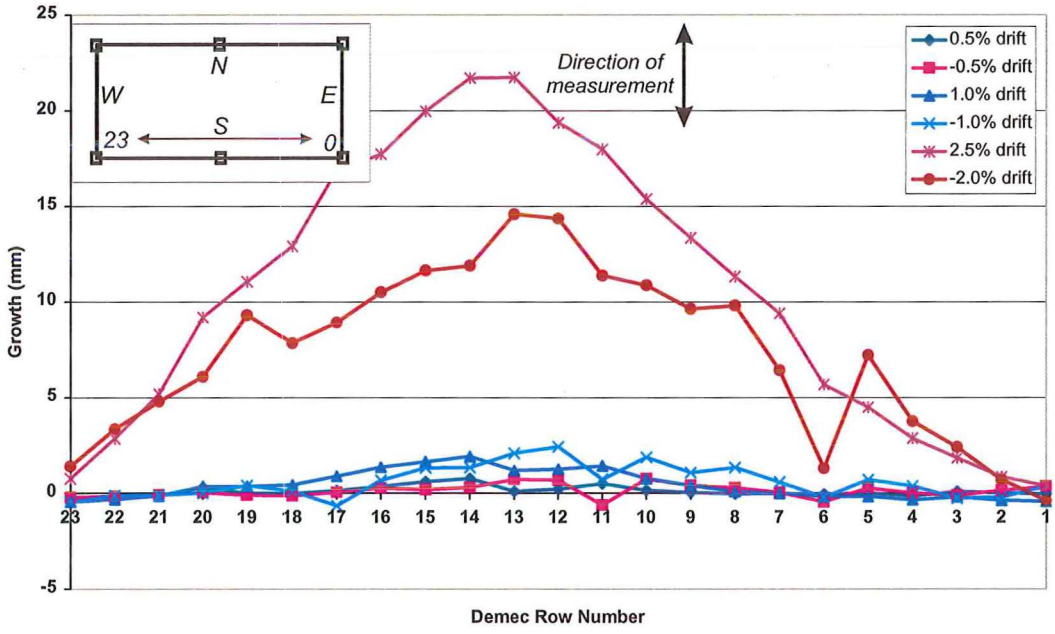

Figure 6-24 Transverse diaphragm growth during Phase II

Rather than just one deformation mode occurring the demec point results showed that a combination of two modes occurred. The first mode was Mode 2 as defined by Bull while the second mode to form was one that will be defined as mode three (refer to Figure 6-25). Mode 3 is a mode in which the central column displaces transversely to the direction of loading. The reasoning as to why the floor tore and displaced laterally was discussed in Chapter 5.

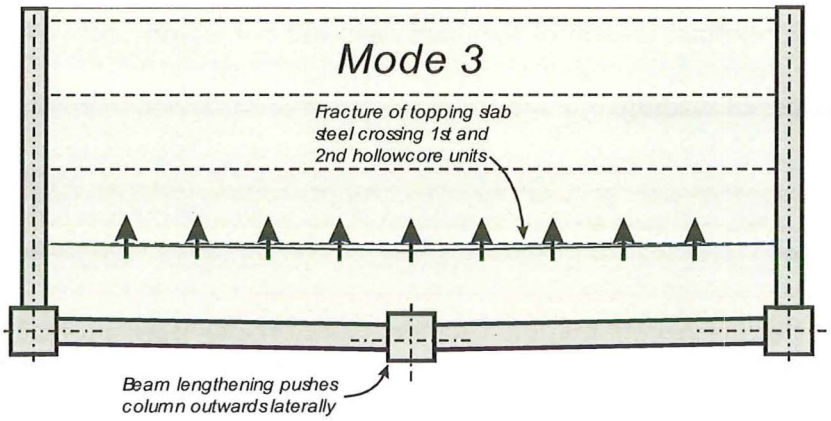

Figure 6-25 Diaphragm deformation Mode 3.

Phase II

The performance of the diaphragm was governed by the major crack that had occurred during Phase I. Very little additional growth occurred during Phase II (Figure 6-26). It was not until the displacement cycle to 3.5% drift that there was a significant increase in growth. It was possible to see the tear propagate towards the East transverse beam (between demec row numbers 1-5). Overall the diaphragm grew by 5-6mm during the 3.5% drift cycle.

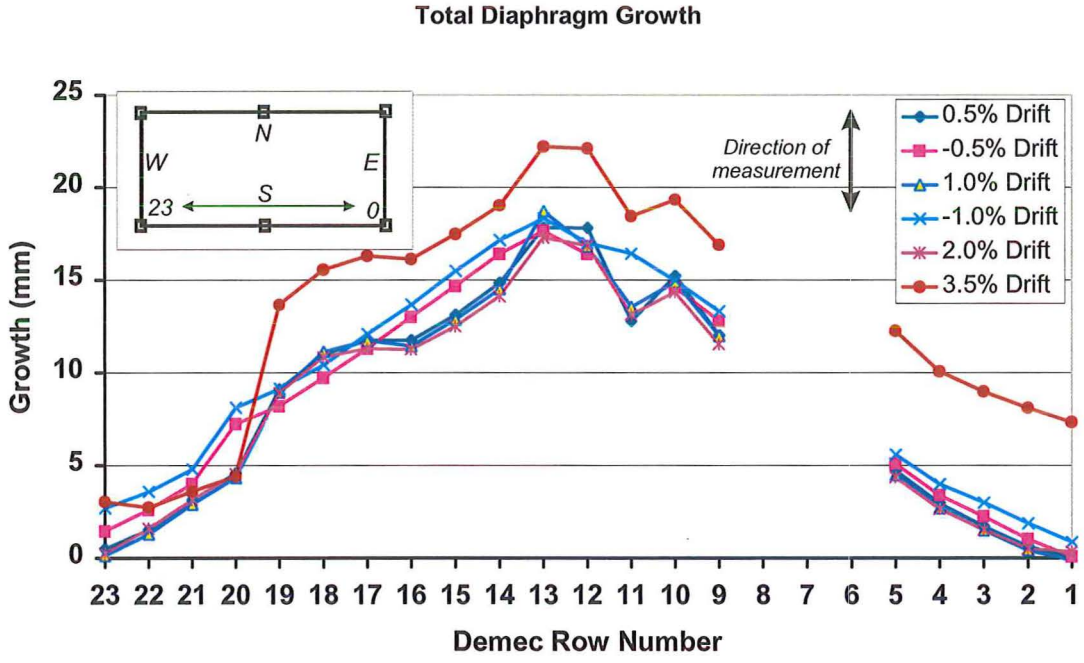

Figure 6-26 Overall transverse diaphragm growth during Phase II.

The longitudinal growth of the diaphragm did not significantly change during the second phase of loading.

Phase III

Due to the major deterioration of the floor the demec points were not read during the third phase of the test.

6.8 Changes to strut and tie modeling

The results from this investigation have shown that a combination of Bulls' Mode 2 deformation mode and a new Mode 3 occurred. This has several implications when detailing the diaphragm for a strut and tie solution. Firstly, since the entire beam has been shown to rotate in the horizontal plane (rather than just the plastic hinge zone) then it is not possible for the strut to be transferred to the central undamaged portion of the beam as explained in Figure 6-20. The reason for this is that there is a zone of damage at this location.

The strut is best shifted so that it lands on the next column in from the corner column (Figure 6-27). The can occur because there has been additional tie reinforcement added to tie that column to the structure. The strut is then transferred into the perimeter beam and the tension force in the tie to the floor via the additional reinforcement. Since the additional tie reinforcement is required to tie the column in place, some additional reinforcement may be required. This depends on the magnitude of the strut that needs to be transferred to the perimeter frame.

The additional reinforcement should not contribute to the negative moment capacity of the perimeter beam.

6.9 Concluding remarks

One major reason for the unexpected failure mode of the hollow-core units connection to the supporting beam was due to the misleading information obtained from previous research. The previous researchers simply undertook pull off tests to investigate the hollow-core units connection detail when in fact the connection should have been exposed to cyclic rotations. It was this rotation that lead to the early damage and eventual failure of these connection details in the super-assembly.

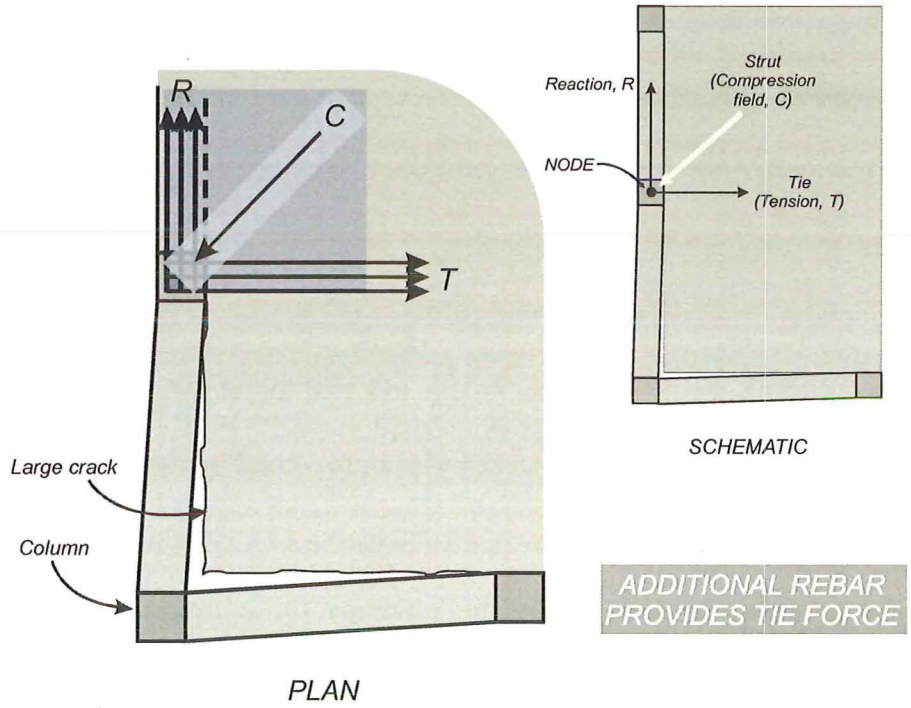

Figure 6-27 New proposed node for a strut and tie solution within a floor diaphragm

A technical advisory group (TAG) on precast floors was formed to discuss the results of this investigation and further research. The new details recommended by the TAG evaluated in two-dimensional sub-assembly tests appear to have a much better performance than the current connection detail used. The new details still need additional testing in the super-assembly, however initial results appear promising.

Diaphragms can be classified into several different types; simple, transfer and hybrid. It is common for several different types of diaphragm to occur within the one structure. Special care and attention needs to be taken to ensure that diaphragms are as

regular as possible and that any penetrations through the floor are positioned in favorable locations. In the event of penetrations or irregularity of the diaphragm, a strut and tie analysis should be undertaken to design the diaphragm. This chapter explained that it is not advisable to use the corner columns as nodes for the transfer of struts within the diaphragm into the perimeter frame. The strut is better directed towards one of the central columns in a zone where its connection to the perimeter frame is undamaged. The additional tie reinforcement used to tie the column into the floor diaphragm can be used to transfer some of the compression strut across the floor slab to the opposite perimeter frame.

By monitoring the demec points positioned over the diaphragm it was possible to determine the mode in which the diaphragm deformed. Bull (2003) had suggested one of two modes could occur. Rotation of the entire beams, in the horizontal plane, (Mode 2) did occur but was influenced by the tear that formed within the diaphragm. The actual deformation mode that occurred was more a combination of Bulls' Mode 2 and a new Mode 3 (intermediate column translating out of the building, rotation of the beam about the corner columns, out of the building). If the central column had been properly anchored to the floor diaphragm, it is highly likely that the tear would not have formed and hence Mode 2 would have been the mode to occur.

6.10 References

AS/NZS1170.4:2002, *Draft Structural Design Actions-Earthquake Loadings,* Standards New Zealand, Wellington

Bull D.K and Matthews J.G, 2003, *Proof of Concept Tests for Hollow core Floor Unit Connections*, Report for Precast NZ Inc, Commercial Report 2003-1, University of Canterbury

Bull D.K, 2003, *Understanding the Complexities of Designing Diaphragms in Buildings for Earthquakes*, Symposium to Celebrate the Lifetime Contributions of Tom Paulay and Bob Park, July, Christchurch, pp 93-113

Centre for Advanced Engineering, 1991, *Guidelines for the Use of Structural Precast Concrete in Buildings*, Centre for Advanced Engineering

Centre for Advanced Engineering, 1999, *Guidelines for the Use of Structural Precast Concrete in Buildings (2nd edition)*, Centre for Advanced Engineering

Fédération Internationale du Béton, 2000, *Guide to good practice, Special design considerations for precast prestressed hollow-core floors*, Bulletin 6, fib Commission 6,

Fleischman R.B and Farrow K.T, 2003, *On the seismic behaviour and design of long span precast concrete diaphragms*, Proceedings, 2003 Pacific Conference on Earthquake Engineering, paper 042, Christchurch: NZSEE.

Fleischman R.B, Sause R, Rhodes A.B and Pessiki S, 1996, *Seismic Behaviour of Precast Parking Structure Diaphragms*, Proceedings, XIV ASCE Structures Congress, Vol 2, Chicago April, pp 1139-1146

Herlihy M.D and Park R, 2000, *Precast Concrete Floor Support and Diaphragm Action*, Research Report 2000-13, Department of Civil Engineering, University of Canterbury, Christchurch, New Zealand.

Kolston D and Buchanan B.W, 1980, *Diaphragms in Seismic Resistant Buildings*, Bulletin of the New Zealand Society for Earthquake Engineering, Vol 13, No.2, June

Lau D, B, N, 2001, *The Influence of Precast-Prestressed Flooring on the Seismic Performance of Reinforced Concrete Perimeter Frame Buildings*, Department of Civil and Resource Engineering, University of Auckland, Report No 604

Matthews J.G, Bull D.K and Mander J.B, 2003, *Preliminary results from the testing of a precast hollow-core floor slab building*, Conference Proceedings 2003 Pacific Conference on Earthquake Engineering, February, Christchurch

McSaveney, L.G. 1997. *Precast Concrete Flooring Systems - Design and Detailing for Seismic Purposes*, New Zealand Concrete Society Conference Technical Papers (TR19), p. 14-26, Wairakei

Mejia-McMaster J.C and Park R., 1994, *Tests on Special Reinforcement for the End Support of Hollow-Core Slabs*, PCI Journal, Vol 39, No. 5, pp. 90-105, September-October

NZCS 1994. *Revisions to the New Zealand Standard for the Design of Concrete Structures: NZS 3101*, Technical Report No. 15 (TR15), May 1994: New Zealand Concrete Society.

NZS3101:1995, *Concrete Structures Standard*, Standards New Zealand, Wellington

NZS4203:1992, *Code of practice for general structural design and design loadings for buildings*, Standards New Zealand, Wellington

Oliver S. J, 1998, *The Performance of Concrete Topped Precast Hollow-core Flooring Systems Reinforced With and Without Dramix Steel Fibres Under Simulated Seismic Loading*, Master of Engineering Thesis, Department of Civil Engineering, University of Canterbury, Christchurch, New Zealand, 176pp.

Paulay T, Priestley M.J.N, 1992, *Seismic Design of Reinforced Concrete and Masonry Buildings*, New York, John Wiley and Sons

Prestressed Concrete Institute, 1985, *Manual for the design of hollow-core slabs*, Chicago

Rodriguez M.E, Restrepo, J.I and Carr A.J, 2002, *Earthquake-induced floor horizontal accelerations in buildings*, Earthquake Engineering and Structural Dynamics, Vol 31, pp 693-718

This Page is Blank

Chapter 7

A Rainflow method for predicting beam elongation history in structural concrete members subjected to cyclic loading

7.1 Introduction

Beam elongation is a phenomenon that occurs as a result of a structural concrete element forming a region of plastic deformation (a plastic hinge) and this region grows in length under reversed cyclic loading. Although the phenomenon of beam elongation has been qualitatively understood for some time, only recently have fundamental theories emerged to predict elongation history as a function of cyclic loading. One recent micro-mechanics based theory has been advanced by Lee and Watanabe (2003). Other investigators, such as Fenwick and Megget (1993) and Restrepo et al (1993) have proposed empirical formulations adjusted to fit experimental data to predict total elongation. While the empirical methods are useful for designers in identifying the length of ledges (seats) required to support precast concrete flooring units in multi-storey frames, these lack the rigour and the intellectual appeal of the method in predicting the time history behaviour of beam elongation developed by Lee and Watanabe (2003).

During an earthquake, well designed buildings are expected to behave by ensuring a beam side sway mechanism forms with plastic hinges at the beam ends. Once plastic hinges form in a beam and the beam undergoes large inelastic rotations, the beam grows significantly in length. The plastic hinges within a beam which

generate beam elongation can be defined as one of two types, either fully reversing or uni-directional (Fenwick and Megget, 1993 and Fenwick et al, 1999). A uni-directional hinge is one that forms within a gravity dominated system in which the positive and negative moment plastic hinges develop in different locations. A reversing plastic hinge is one in which the positive and negative moment plastic rotations develop in the same location.

Beam elongation occurs for two reasons: (i) Recoverable elongation is due to the neutral axis being less than half the member depth and the strain at the mid depth of the beam is in tension; (ii) Non-recoverable (permanent) beam elongation occurs because C_s=T-C_c where C_s<T from the previous reversal (where C_s = compression force in the reinforcement in one face of the beam; T = tensile force in the reinforcement in the opposite face; and C_c = concrete compressive force). The plastic strains in tension are not recovered on the compression reversal.

This chapter first discusses the factors that contribute to beam elongation. It then describes findings from previous work undertaken on predicting beam elongation in the literature. From this, an analysis methodology is proposed for predicting the beam elongation history of structural concrete elements under cyclic loading. The approach is based on a "Rainflow" method adapted from high cycle fatigue counting theory. This theory is then verified in two ways. Firstly, by using data of others reported in the literature for individual beam hinge components. Secondly, the theory is validated against the results from the present super-assemblage experiment and includes both individual hinge elongation and gross seat (ledge) width demands based on the elongation of several hinges across the bent. Finally, conclusions are drawn and a recommendation on the seat (ledge) width demand is given for design code development.

7.2 Findings from previous work on beam elongation

For a detailed breakdown of the mechanism behind beam elongation various researchers work can be examined, for example, Fenwick and Megget (1993), Restrepo et al (1993) and Fenwick et al (1999).

Fenwick and Megget (1993), Restrepo et al (1993) and Lee and Watanabe (2003) have derived equations for determining the amount of expected beam elongation. The experimental programmes that formed the basis for determining these equations did not appear to incorporate a floor slab even though it was evident from the previous investigators work that the role of the floor slab is influential in determining the magnitude of the beam elongation.

Fenwick and Megget (1993) stated two equations for beam elongation. The first assumed zero strain within the compression reinforcement (i.e. it has not previously yielded in tension). Their equation considers the total plastic hinge rotation and was based on a uni-directional plastic hinge forming and is given by

$$Extension = \sum \theta (d - d')/2 \qquad \textbf{(7-1)}$$

in which $\Sigma\theta$ = the sum of the plastic hinge rotations in the beam; and $(d\text{-}d')$ = the distance between the centroids of the top and bottom flexural reinforcement (Figure 7-1).

The second equation proposed by Fenwick and Megget assumed cyclic loading in which the tension reinforcement does not yield back fully in compression. The expected extension is given by

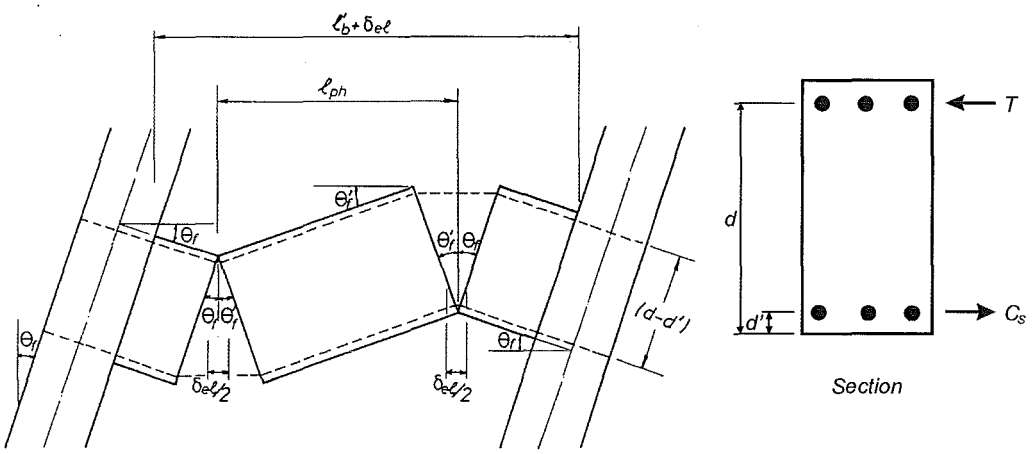

Figure 7-1 Deformed frame assembly showing the beam elongation (altered from Restrepo et al, 1993)

$$Extension = e + \sum \theta (d - d')/2 \qquad \textbf{(7-2)}$$

in which e = the elongation of the reinforcement in the compression zones of the plastic hinges in the beam, from the previous cycles of plastic elongation in tension. According to Fenwick and Megget, Equation (7-2) is approximately three times the value given by Equation (7-1).

Restrepo et al (1993) stated two equations, a lower and upper bound. The lower bound solution was fitted to his experimental data and given by

$$\delta_{el} = \theta_f \frac{l'_b}{l_{ph}} (d - d') \qquad \textbf{(7-3)}$$

in which δ_{el} = total beam elongation for a beam with two hinges; θ_f = the interstorey drift; l'_b = the distance between the column centrelines; l_{ph} = the distance between the positive and negative plastic hinges in the beam; and $(d - d')$ = the distance between the centroids of the flexural reinforcement. Refer to Figure 7-1 for further explanation.

The upper bound solution of Restrepo et al (1993) appeared to be Equation (7-3) multiplied by 2.0. The justification as to why a multiplier of 2.0 was used appears to be an attempt to fit the database studied by Restrepo et al (1993). This upper bound equation is given by

$$\delta_{el} = 2\theta_f \frac{l'_b}{l_{ph}}(d - d') \qquad (7\text{-}4)$$

Both Fenwick and Megget (1993) and Restrepo el al (1993) say that typical values of expected elongation for each plastic hinge are equal to 2-5% of the beam depth.

Fenwick and Davidson (1995) stated that due to extensive cracking in a beam hinge region a truss mechanism is required to transfer the shear mechanism, which leads to beam elongation. This mechanism is shown in Figure 7-2. While the stirrups go into tension, concrete struts resists the diagonal compression force, and equilibrium, at a vertical section, dictates that the tensile force in the longitudinal reinforcing steel must always be greater than the flexural compression force due to the horizontal component of the diagonal compression. As a result the inelastic (plastic) rotation occurs more by the tension reinforcement extending rather than the contraction of the reinforcement in the compression zone.

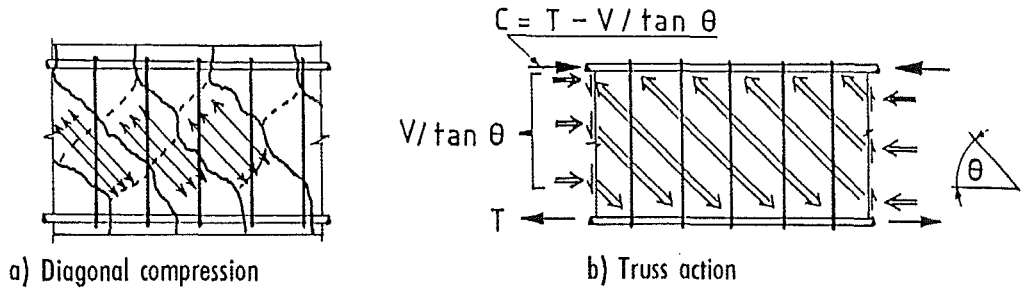

Figure 7-2 Shear action in a plastic hinge zone (Fenwick and Davidson, 1995)

Lee and Watanabe (2003) developed a complex set of equations that can be used to determine the amount of axial strain within a reinforced concrete beam, and hence determine the amount of beam elongation. Within an axial load versus applied rotation plot Lee and Watanabe identified four distinct regions that could be expressed to determine the total beam growth. These four paths were: (1) pre-flexural yielding or unloading region; (2) post-flexural yielding region; (3) slip region; and (4) repeated loading region. These four paths are summarised in Figure 7-3.

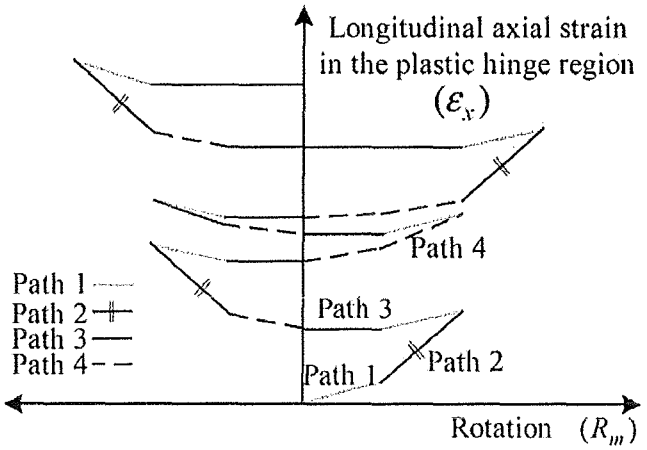

Figure 7-3 Lee and Watanabe (2003) proposed a model for analysing the beam elongation in a plastic hinge region

The complex equations stated by Lee and Watanabe to equate the different paths would be difficult to utilise in a general design practice. Therefore a simplified approximation was made by Lee and Watanabe for the axial strain envelope, for each plastic hinge, given by

$$\varepsilon_x = \frac{(R_{mp} + R_{mn})\, jD}{2l_h} \qquad \textbf{(7-5)}$$

in which R_{mp} = the positive rotation of the beam; R_{mn} = the negative rotation of the beam; jD = the internal leverarm of the beam; and l_h = the length of the plastic hinge region are defined by

$$l_h = 0.5\left(\frac{M}{Vh}\right)d \qquad \text{where } (0.75d \le l_h \le d) \qquad (7\text{-}6)$$

in which M = the applied moment; V = the applied shear force; h = the overall beam depth; and d = the effective beam depth (from extreme compression fibre to the centroid of the tension reinforcement).

Once the strain envelope is determined it can then be transformed into a beam elongation.

7.3 A Rainflow method for predicting beam elongation

Fenwick and Davidson (1995) stated that beam elongation is caused by two factors: (i) when a deformed reinforcing bar yields in tension the region around the bar cracks and (ii) a flexure shear truss is formed within the beam. The former causes the concrete to dilate and aggregate particles get wedged in the cracks so that as the load reverses the cracks do not entirely close as it takes appreciable force to close the cracks. These two reasons are not be the sole explanation for beam elongation.

Herein it will be shown that beam elongation can be explained, relatively simply, in terms of plastic flexure alone via rigid body kinematics. The stress-strain graphs on the right hand side of Figure 7-4 show that for a positive moment the tension reinforcement has yielded and undergone plastic deformation while the compression reinforcement is at a stress below yield. For the negative moment, the top reinforcement recovers the elastic compressive stress and then yields in tension while the bottom reinforcement regains its elastic recovery but has a residual strain at zero stress. Therefore, Figure 7-4 shows that both a positive and negative moment result in a permanent elongation strain at the centre of gravity of concrete section (c.g.c) of the beam (refer to the strain diagrams).

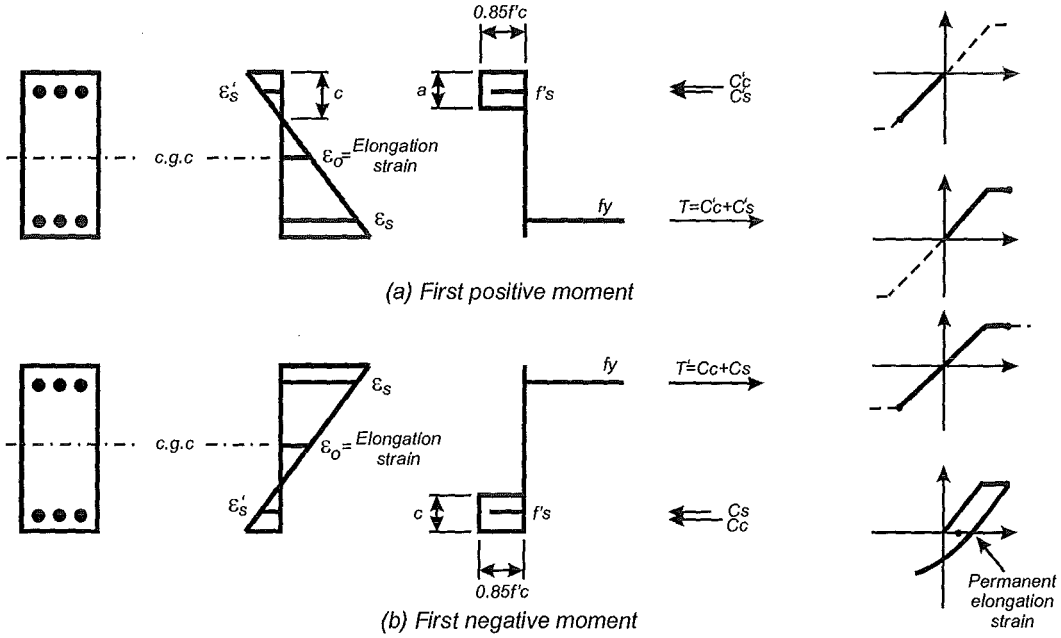

Figure 7-4 Rigid body kinematics used to show that beam elongation can be expressed in terms of plastic flexure

The basis of deriving beam elongation history as a result of reversed cyclic loading is summarised in Figure 7-5. Figure 7-5(a) shows a typical lateral load deflection behaviour of an inelastic frame system. The maximum cyclic amplitudes are numbered (1 to 5) with the odd numbered cycles representing positive displacement peaks, while the even numbered cycles are for the negative displacement peaks. From the hysteresis plot it is possible to determine the yield drift (θ_y) and the amount of plastic rotation (θ_p) that the plastic hinges undergo.

Beam elongation occurs whenever "new" rotation occurs. "New" rotation is defined as the rotation that occurs at a level of interstorey drift that has not been achieved during a previous load cycle. An example of this is from points 3-5 on Figure 7-5(a). Figure 7-5(c) shows that when the load reverses, once it has reached a new maximum, it is assumed that the beam elongation recovers its elastic component but maintains its plastic component. Therefore, at large interstorey drifts, the beam elongation appears to remain essentially constant until some "new" rotation occurs.

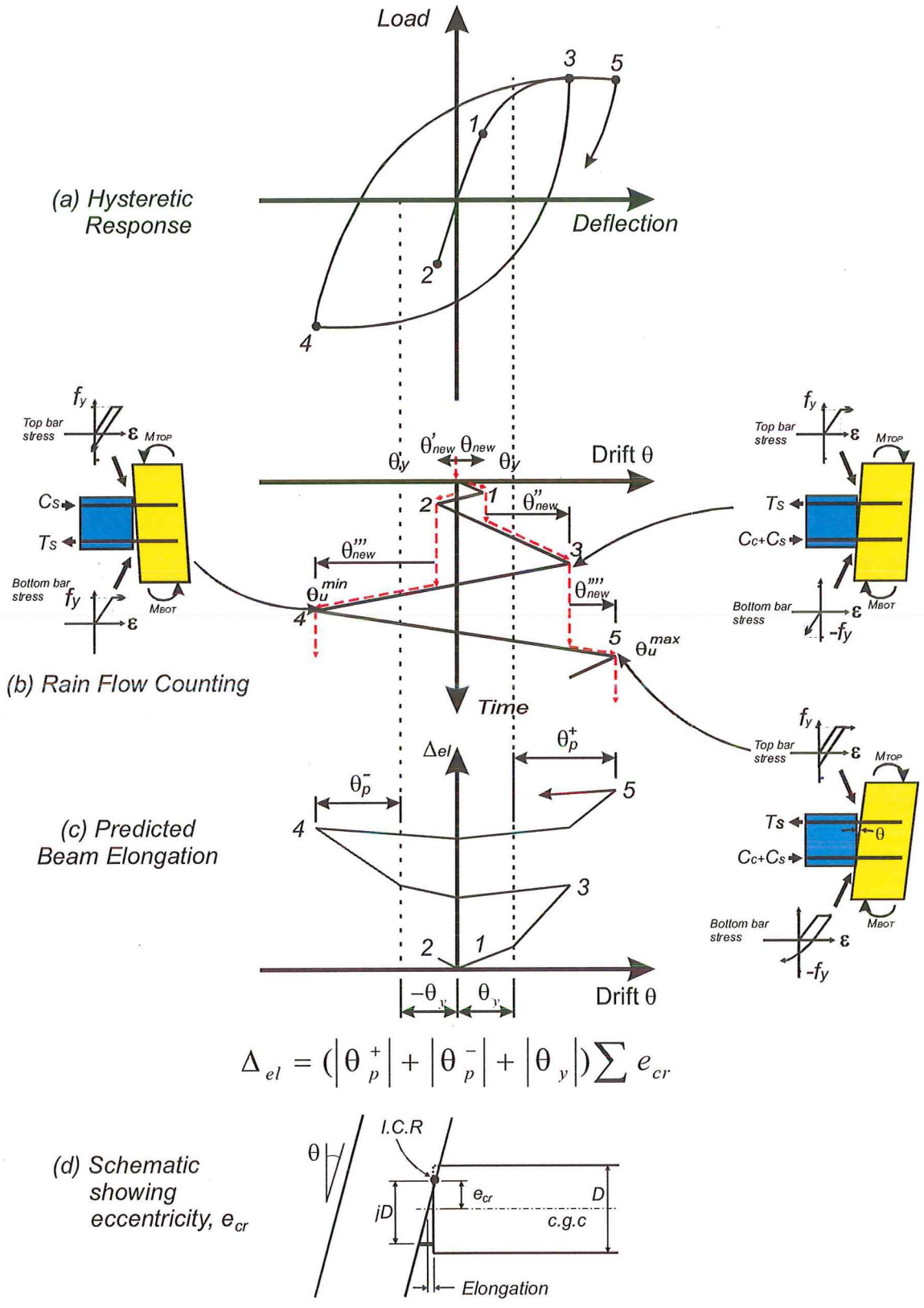

$$\Delta_{el} = \left(\left|\theta_p^{+}\right| + \left|\theta_p^{-}\right| + \left|\theta_y\right|\right)\sum e_{cr}$$

Figure 7-5 General theory for the determination of beam elongation.

The sub-figures shown at points 3-5, Figure 7-5, represent the actual deformation of the particular plastic hinge zone and the strain states within the beam reinforcement. Prior to point 1, in Figure 7-5, whenever the load reverses the reinforcing steel in tension recovers its elastic deformation and the crack at the beam column interface closes. Beam elongation occurs within the elastic range but at zero drift the elastic elongation is recovered. From the yield point (point 1), to point 3, top steel yields in tension and undergoes plastic deformation. The compression force within the concrete and the bottom reinforcement in compression provides the compressive force of the internal force couple. Upon load reversal toward point 4, as there is significantly more top reinforcement (due to the activated floor slab reinforcement), the bottom reinforcing yields in tension before the top reinforcing is able to yield back in compression. This beam elongation is caused because the top crack has not closed fully and the bottom reinforcement has been pulled out of the beam. The compressive force now is resisted by the compression reinforcement alone. Further as the load reverses towards point 5 the bottom crack essentially closes except for the aggregate wedged into the cracks, as there is sufficient force to yield these bars back in compression due to the large area of top reinforcement. Now, the top beam reinforcement undergoes further plastic deformation and the crack width increases. Each of these three points experience new plastic rotation.

Figure 7-5(b) shows a drift versus time graph that is used to determine the amount of rotation that contributes to the beam elongation. Major beam elongation only takes place as the deformation exceeds the previous peak. Therefore, the technique commonly used in high cycle fatigue counting analysis called "Rainflow Counting" (Dowling (1972)) is used to identify new segments of drift that contribute to beam elongation. The solid lines, on the drift versus time graph are imagined as a

series of pagoda roofs. Droplets of rain, starting from zero displacement are then dropped onto the pagoda roofs and allowed to flow down the slope. The drops are tracked (dashed line) until it falls off the edge of the roof and then the amount of rotation is counted. Once the total amount of "new" rotation is determined, (i.e. the portions in Figure 7-5(b) shown by the regions denoted as "θ_{new}"). An expression for the beam elongation can now be determined. If additional cycles to the same rotation occur the elongation may increase slightly due to the additional aggregate being pulled into the cracks.

The amount that a plastic hinge elongates for a given rotation is expressed by

$$\delta_i^{el} = \theta \, e_{cr} \tag{7-7}$$

in which δ_i^{el} = elongation of the i^{th} hinge; θ = rotation the plastic hinge undergoes; and e_{cr} = eccentricity between the c.g.c of the beam and the centroid of the compression force (instantaneous centre of rotation, I.C.R).

A designer is interested in the maximum expected beam elongation for a given frame so that the required seat length for a precast element can be determined. This total elongation can be expressed in terms of an elastic and plastic rotation.

The elastic component of beam elongation can be derived from theory by examining the strain within the beam member at its c.g.c (Figure 7-6). The elastic elongation component (δ_e^{el}) can be found by integrating the neutral axis (c.g.c) strain along the length of the beam as follows:

$$\delta_e^{el} = \frac{1}{2}\varepsilon_o^+ \xi L_b + \frac{1}{2}\varepsilon_o^- L_b (1-\xi) \tag{7-8}$$

in which ε_o^+ = the strain at the onset of first yield at the member end at the c.g.c for a positive bending moment (M^+); ε_o^- = the strain at the onset of first yield at the other

member end at the c.g.c for a negative bending moment (M^-); and ξ = portion of the total beam length (L_b) to where the beam bending moment is zero (Figure 7-6). By substituting in the variables used to determine the yield curvature and simplifying Equation (7-8) the elastic elongation component becomes (refer to Appendix H for full derivation):

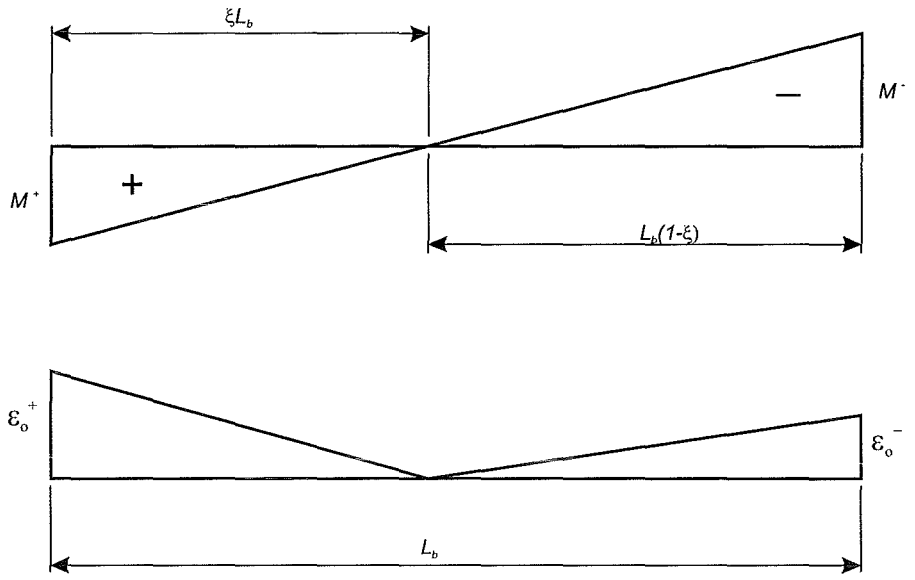

Figure 7-6 Beam bending moment and strain diagrams used to determine the elastic component of beam elongation.

$$\delta_e^{el} = \frac{L_b}{2}\varepsilon_y \left[\frac{\frac{1-2k^+}{2-2k^+}M^+ + \frac{1-2k^-}{2-2k^-}M^-}{M^+ + M^+} \right] \qquad (7\text{-}9)$$

in which ε_y = the yield strain for the main beam reinforcement; k^+ = the proportion of the beam depth (D) to where the neutral axis is located for a positive bending moment; and k^- = the proportion of the beam depth (D) to where the neutral axis is located for a negative bending moment.

This elastic component is considered recoverable when the direction of loading reverses and is best understood by referring to Figure 7-7. Below yield, beam

elongation occurs and is a function of the neutral axis depth as expressed in Equation (7-8). Equation (7-9) is not used to calculate the elastic elongation component due to its complexity. Instead, an equation in keeping with Equation (7-7) is used that expresses the elastic elongation component in terms of e_{cr}. The elastic elongation component (δ_e^{el}) is calculated by

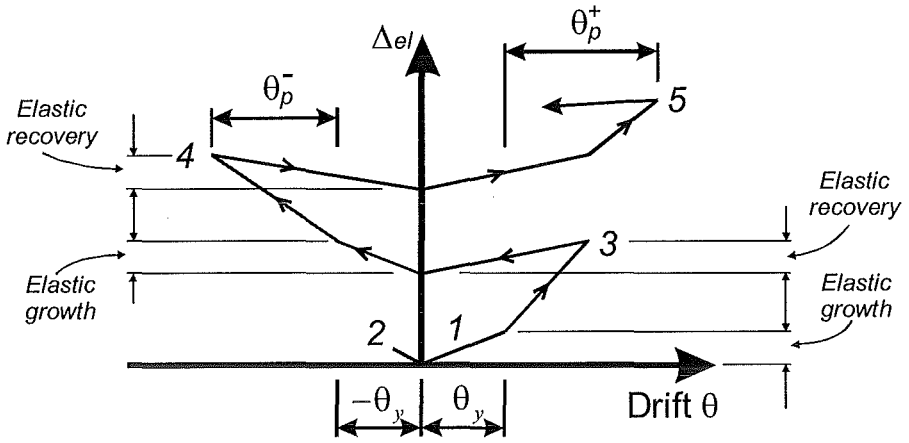

Figure 7-7 Detailed schematic showing the effect elastic elongation has on the total predicted beam elongation

$$\delta_e^{el} = |\theta| \sum_{i=1}^{n} e_{cri} \; but \; |\theta| \le |\theta_y| \qquad \textbf{(7-10)}$$

in which e_{cri} = force eccentricity of the beam depth which is the distance between the beam centreline and the instantaneous centre of rotation (the centroid of the compression force) for the i^{th} hinge; and θ_y = yield rotation of the super-assemblage. The yield rotation is assumed to be the same for each direction of loading. If the total elastic elongation is required then Equation (7-10) becomes

$$\delta_e^{el} = \theta_y \sum_{i=1}^{n} e_{cri} \qquad \textbf{(7-11)}$$

At zero drift this elastic elongation is assumed to be recoverable. The same occurs in the plastic range. The total beam elongation that occurs when the loading direction reverses (i.e. points 1-5 in Figure 7-5(c)) is made up of an elastic and plastic

component whereas at zero drift the elastic component is recovered and the plastic component remains.

The non-recoverable plastic component of beam elongation is determined by

$$\delta_p^{el} = \left(\left|\theta_P^+\right| + \left|\theta_P^-\right|\right)\sum_{i=1}^{n} e_{cri} \qquad \textbf{(7-12)}$$

in which δ_p^{el} = plastic elongation within a frame/bent; and θ_P^+ = maximum positive plastic rotation imposed on the structure; θ_P^- = maximum negative plastic rotation imposed on the structure.

Although Figure 7-5(c) shows a detailed plot of beam elongation versus interstorey drift the equations stated within the chapter are used to calculate the beam elongation at each of the load reversals on the graph and NOT the zero drift amplitudes. The total elongation can also be expressed in terms of interstorey drift by

$$\delta_{\max}^{el} = \delta_e^{el} + \delta_p^{el} = \left(\left|\theta_P^+\right| + \left|\theta_P^-\right| + \left|\theta_y\right|\right)\sum_{i=1}^{n} e_{cri} \qquad \textbf{(7-13)}$$

When the results from Restrepo et al (1993) are compared with Equation (7-13) it is possible to determine where the amplifying value of 2.0 came from. When a specimen is loaded with equal positive and negative amplitudes, Equation (7-7) can be written as $\delta_{\max}^{el} = 2\theta \sum e_{cr}$. Thus the value of 2.0 arises because the maximum positive and negative drift amplitudes are the same (i.e. $\theta_{max}^{+}=|\theta_{min}^{-}|$). Therefore, it can be seen that for the case of Equation (7-4) the amount of expected beam elongation is independent on the shape of the loading history whereas Equation (7-13) is loading history dependent. Therefore, since Restrepo et al had a symmetric loading pattern the value of 2.0 is adequate. In a real earthquake event the loading history is not usually symmetric so therefore the elongation model used should be dependant on the loading history.

7.4 Validation with previous investigators data

The theory proposed in Section 7.3 will now be validated against the experimental results obtained from previous investigations.

The University of Auckland results from Lau (2001) were used to verify Equation (7-13). Since Lau's raw data was not available, Table 7-1 was produced and used to determine the elongation versus load cycle data. Once the loading history and the specimen dimensions are known it is possible to produce a rain flow chart and hence an expected elongation versus drift plot using Equation (7-13). This experimental total beam elongation shown in Table 7-1 is then plotted in Figure 7-8 along side the expected beam elongation obtained from Equation (7-13). The proposed Rainflow counting theory shows good agreement with the experimental observations of Lau (2001) for positive interstorey drifts as the predicted elongation fits in between the observed elongation for the two cycles to each interstorey drift limit (i.e. the predicted elongation matches the average beam elongation for the two load cycles). For negative drifts the predicted elongation slightly overestimates the observed elongation. This difference is most probably due to an overestimation in the e_{cr} value.

A second comparison is made using the raw data from Fenwick et al (1981) and the proposed theory. The observed positive drift cycle elongations are slightly under estimated by the theory, while for the negative drift amplitudes the beam elongation is slightly overestimated (Figure 7-9). If an average of the positive and negative results were undertaken then the results would match well. The variance between the predicted elongation and observed elongation is due to a slight underestimation in e_{cr}.

Table 7-1 Beam elongation results from Lau (2001)

Ductility	Interstorey Drift	Beam Elongation
0	0	0
0.75	0.51	0
-0.75	-0.51	0
0.75	0.51	0
-0.75	-0.51	0
2	1.36	5
-2	-1.36	6.8
2	1.36	9.3
-2	-1.36	10
4	2.72	18
-4	-2.72	21.4
4	2.72	24
-4	-2.72	25.9
6	4.08	30.5
-6	-4.08	32.5

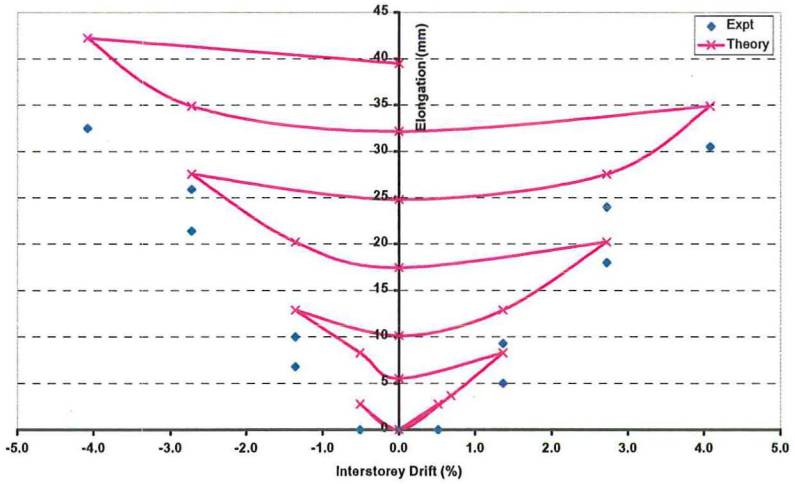

Figure 7-8 The experimental results of Lau (2001) compared with a theoretical prediction of beam elongation

Finally the data from Restrepo et al (1993) was used to verify Equation (7-13). As the raw data was not available Figure 7-10(a) was used to determine the elongation versus load cycle data. The proposed Rainflow counting theory shows good

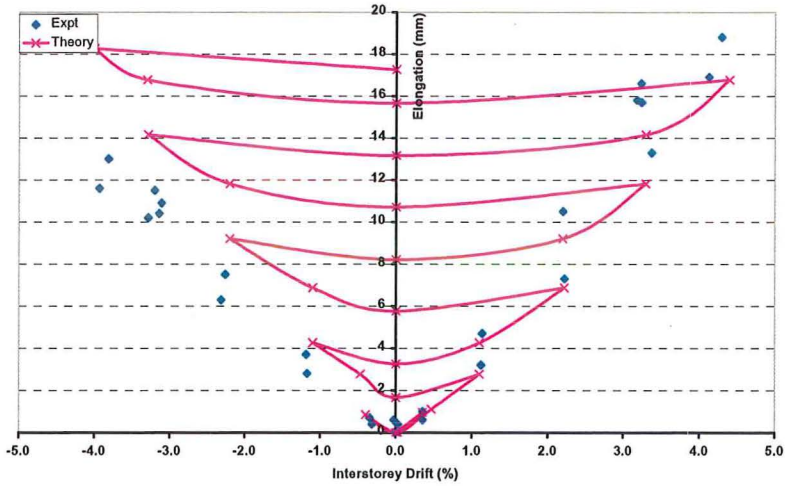

Figure 7-9 Fenwick et al (1981) results versus predicted elongation

agreement with the experimental observations of Restrepo et al (1993) as shown in Figure 7-10. The theoretical elongation prediction is less than the elongation observed for the middle stages of the test but has closer agreement at both the smaller and larger interstorey drifts. The plastic hinge trying to form slightly off the column face (slight relocation) and hence undergoing a larger plastic rotation could cause this discrepancy during the middles stages. At higher drifts the plastic hinge finished at the column face.

In general, all the experimental results compare well with the predicted elongation using Equation (7-13).

7.5 Validation with present study

Beam elongation was monitored during an experimental testing programme in which a two-bay by one-bay moment resisting frame building that incorporated a hollow-core floor slab. The super-assemblage was loaded in three phases: Phase I loading was parallel to the hollow-core floor units; Phase II was loaded transverse to the hollow-core floor units; and Phase III was again parallel to the hollow-core floor units. As there were no new displacements beyond the previous maxima, beam elongation only

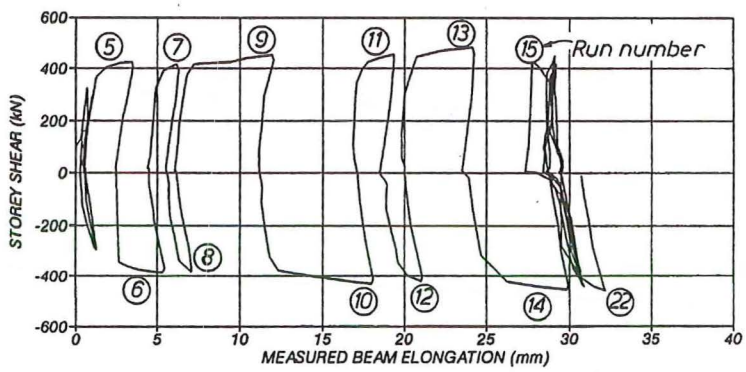

(a) Graph showing the experimental beam elongation obtained from Restrepo et al (1993)

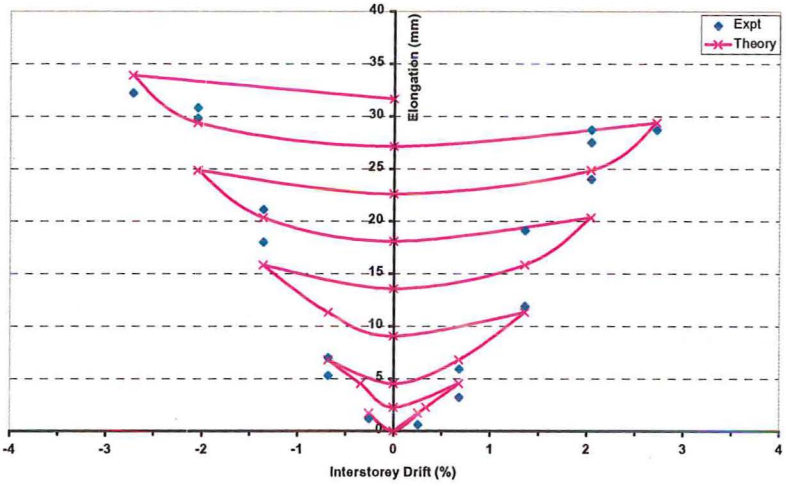

(b) Application of the rainflow theory to the results of Restrepo et al (1993)

Figure 7-10 Restrepo et al (1993) observed elongation versus predicted elongation

occurred in Phase I and II (in the longitudinal and transverse beams, respectively). The experimental results of these two phases are compared with the theoretical prediction in what follows.

7.5.1 Beam Elongation Resulting from Phase I Loading

Due to the composition of the frame, two types of beam-column joints are studied when the super-assemblage was loaded parallel to the hollow-core floor slabs: the first being the exterior joints, and secondly the interior joints.

Figure 7-11(a) shows both the experimentally observed beam elongation and the theoretically predicted beam elongation for the exterior hinges. The direction of the cyclic loading plays a role in the amount of elongation that forms. This is because

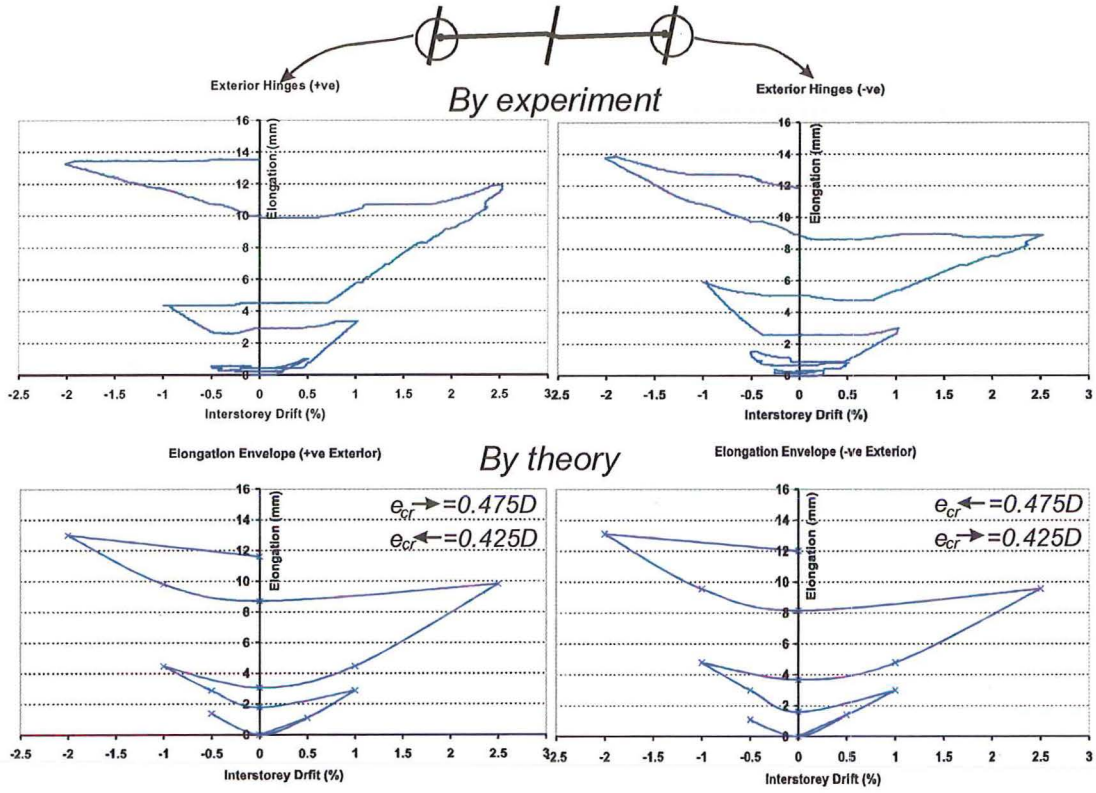

(a) Exterior joint elongation

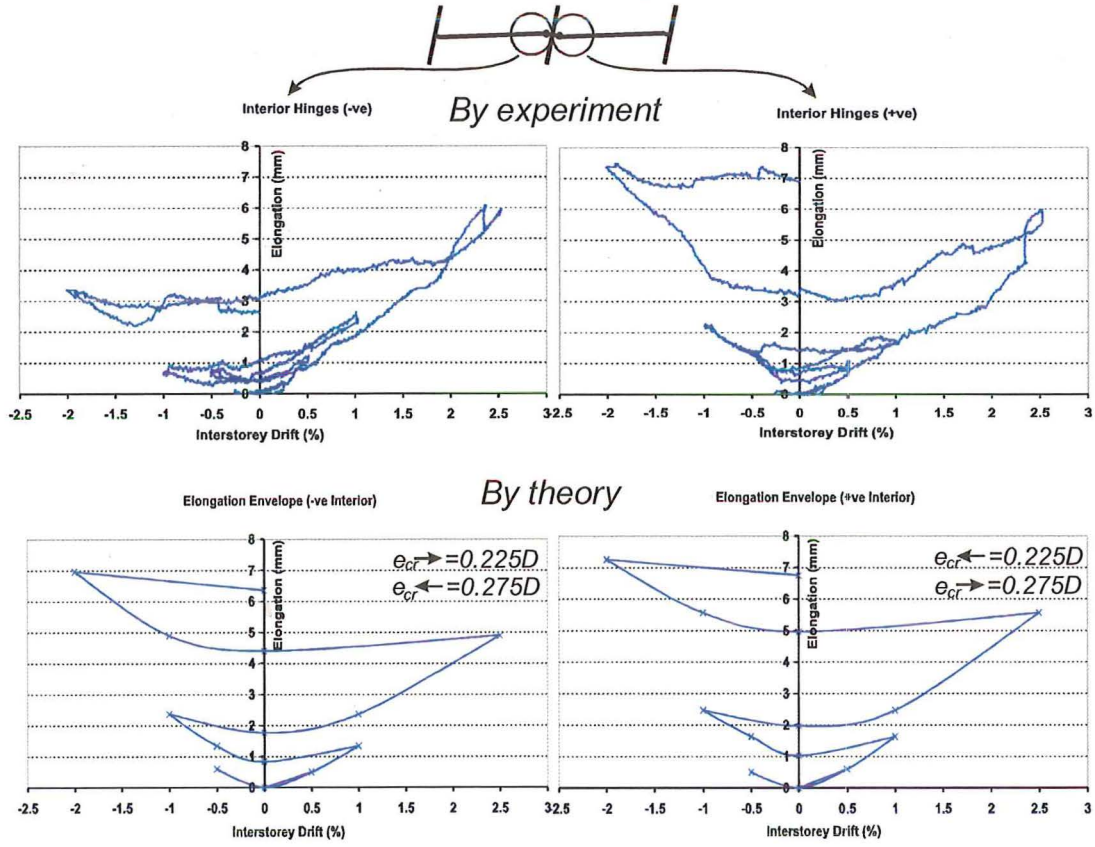

(b) Interior joint elongation

Figure 7-11 Elongation of Super-assemblage beams under longitudinal specimen loading: Phase I

a negative and positive moment for the same plastic hinge has a different internal eccentricity (e_{cr}) due to the different amount of tension reinforcement activated. There was significantly more top reinforcement compared to the bottom reinforcement of the beam (due to the activation of the slab reinforcement), therefore, e_{cr} will also be different (e_{cr} is defined as the fraction of the beam depth from the beam centreline to the instantaneous centre of rotation, I.C.R). Values of e_{cr} were determined by compatibility and equilibrium analysis as $0.425D$ and $0.475D$ for a negative and positive moment respectively (in which D is the overall member depth) (Figure 7-12(a)). A moment-curvature analysis confirmed that the e_{cr} used to determine the plastic elongation were also appropriate in determining the elastic elongation component.

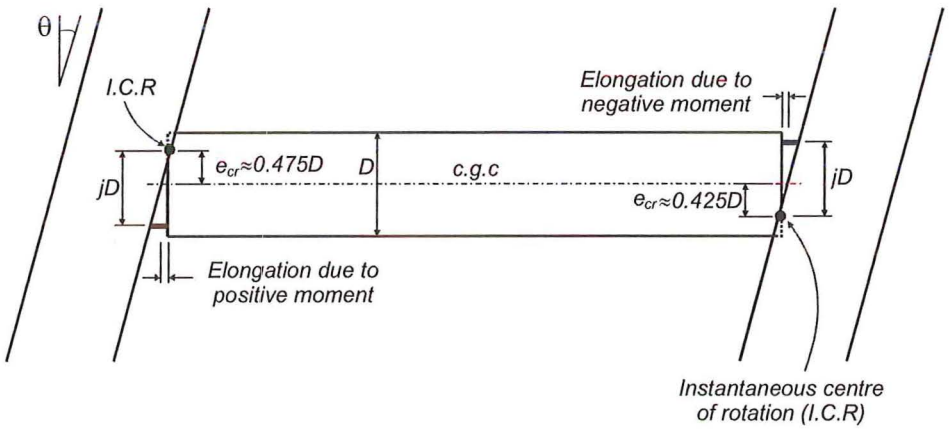

(a) Exterior plastic hinge lever arms for reinforced concrete beam systems

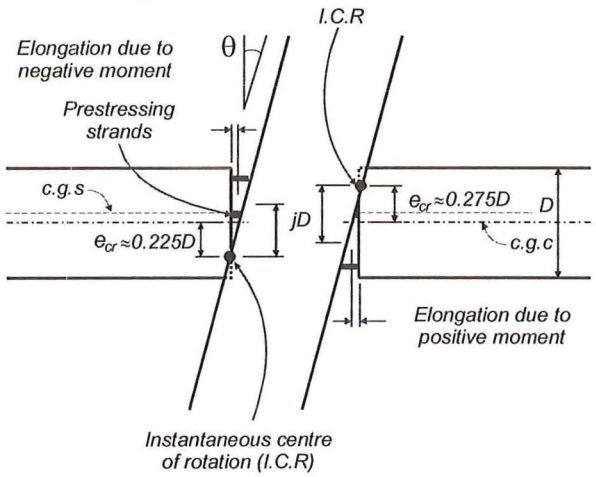

(b) Interior plastic hinge lever arms. Note: Prestress reduces e_{cr}

Figure 7-12 Internal lever arms for an interior and exterior joint

As can be seen from Figure 7-11(b) there is good agreement between the predicted and observed elongations for the two exterior plastic hinge zones. Because the e_{cr} values were different for each of the two loading directions and the imposed loading cycles was not symmetric, the theoretical elongation for each hinge is slightly different.

The interior plastic hinge zones on either side of the central column have different e_{cr} values when compared to the exterior plastic hinges. This is because the hollow-core floor unit spans passed the central column. This hollow-core unit has a large number of prestressing strands in the central region of the reinforced concrete beam. The prestress effectively reduces the internal leverarm factor e_{cr} by moving the centre of rotation closer to the beam centreline as well as causing the centroids of the tension reinforcement to be closer to the beam centreline (Figure 7-12(b)). Based on a compatibility and equilibrium section analysis the calculated values of e_{cr} are $0.225D$ and $0.275D$ for negative and positive moments, respectively. Figure 7-11(b) shows good agreement between the predicted and observed elongations. The left hand interior hinge did not elongate as expected during the cycle to –2% drift. The reason for this is that at this stage during the test the first hollow-core unit had severe web splitting and this affected the hinge performance (in particular the affect the prestressing strands had on the hinge performance).

By adding the elongation from the four plastic hinges, it is possible to determine the total beam elongation. From this outcome and the time history shown in Figure 7-13 there is satisfactory agreement between the theory and observed results. From the experiment, the observed beam elongation equates to a growth of 35mm. Using Equation (7-13) the predicted maximum elongation is $\delta_{\max}^{el}$ =37mm

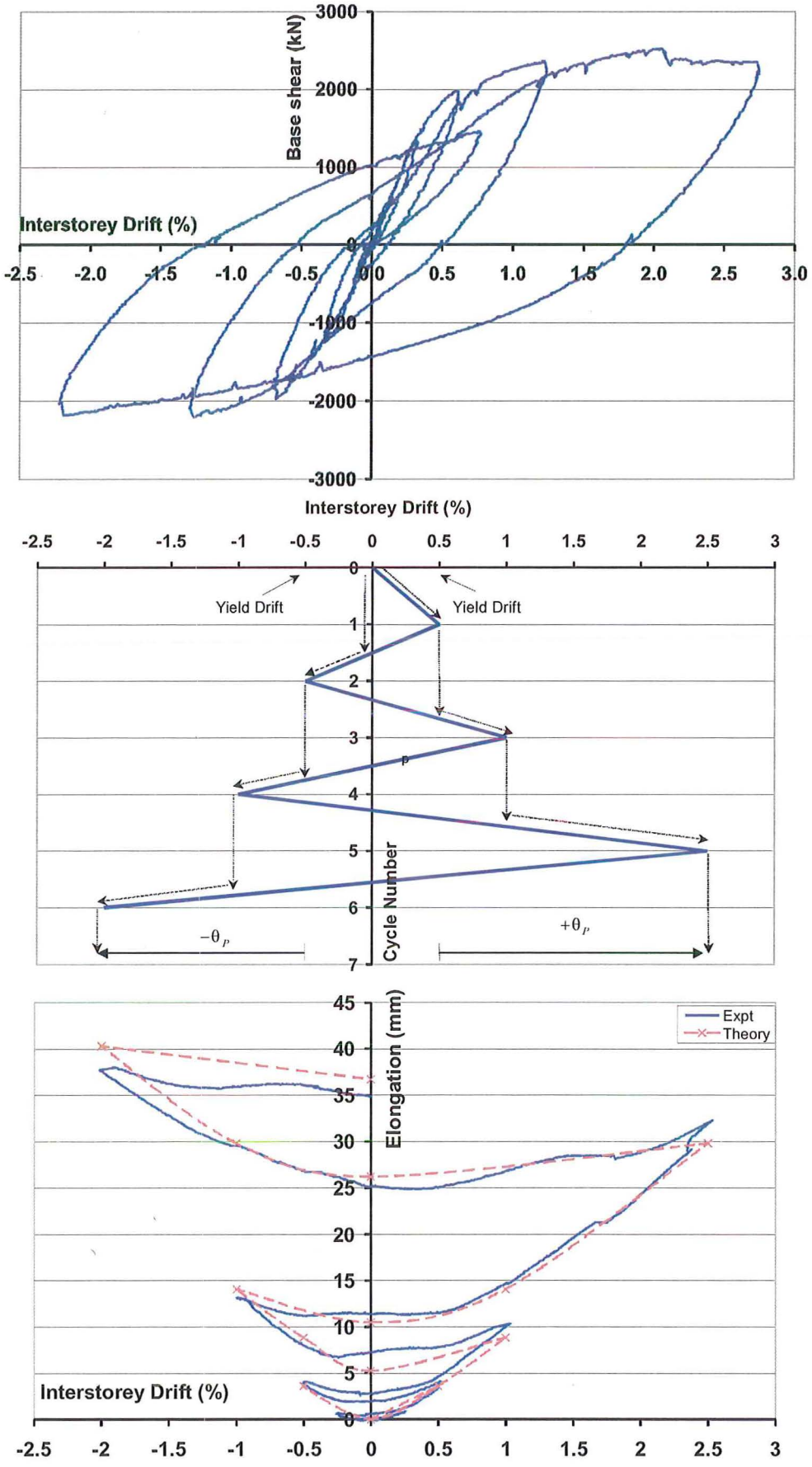

Figure 7-13 Rain flow chart for Phase I

7.5.2 Beam Elongation Resulting from Phase II Loading

This direction of loading (transverse to the hollow-core units) incorporated only one type of plastic hinge: an exterior plastic hinge at each end of each beam. To compare the theoretical versus experimentally observed beam elongation, it is best to compare the two beams in which the plastic hinges form. These beams were the East and West beam of the super-assemblage. For all the plastic hinges the e_{cr} values were either $0.425D$ for a negative moment or $0.475D$ for a positive moment (Figure 7-12(a)).

Figure 7-14 shows good agreement between the theoretical and experimentally observed elongation for the individual hinges. It should be noted that the measured beam elongation, during the low interstorey drift cycles, for the SW plastic hinge was lower than the predicted value, this was because the elongation was suppressed as the initial torsion cracks (that formed during the Phase I loading) meant that the plastic hinge did not develop properly until later into the loading history. Once the hinge developed the magnitude of the additional beam elongation matched the theoretical prediction. Figure 7-15 presents the combined beam elongation results for the East beams. Further validation of the assumption that was mentioned in Section 7.3 that only "new" rotation contributes to beam elongation is evident in Figure 7-15. In between the –2.5% cycle and the 3.5% cycle there was a small cycle to ±0.5% undertaken. Note that this cycle did not contribute to the beam elongation, as predicted, because it did not cause any "new" rotation to occur.

By adding the elongation from the two plastic hinges on both the East and West beams it is possible to determine the total beam elongation for each beam. This equates to a growth of 47.5mm (Figure 7-15) and 44.5mm (refer to Appendix H) for the east and west beams respectively; giving an average of 46mm. This observed

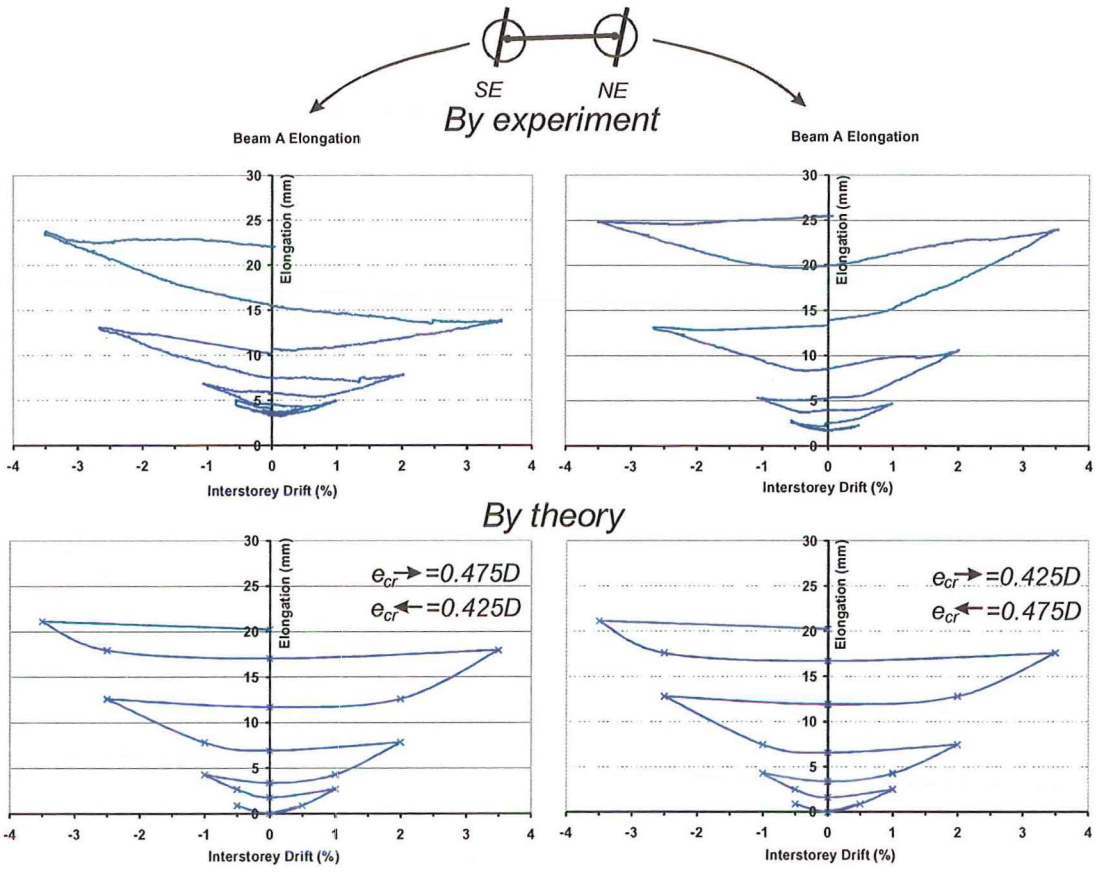

(a) East beam elongation

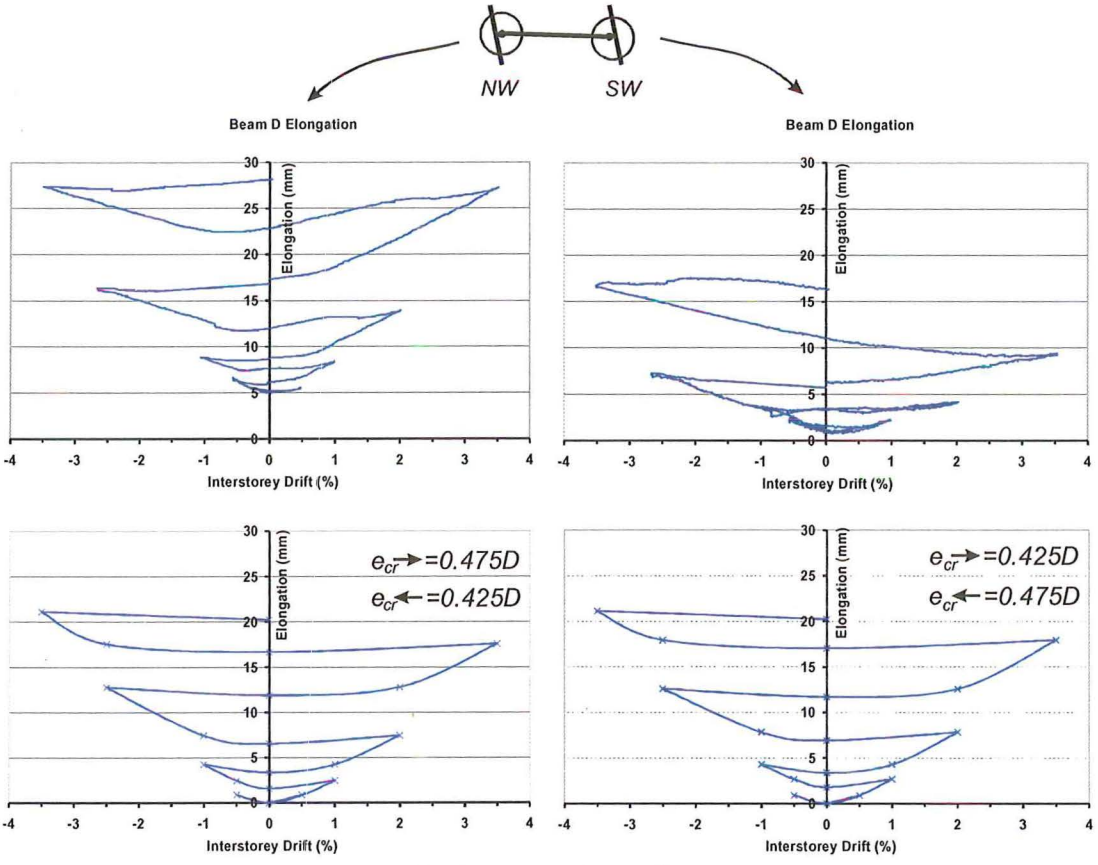

(b) West beam elongation

Figure 7-14 Elongation of super-assemblage beams under transverse specimen loading: Phase II

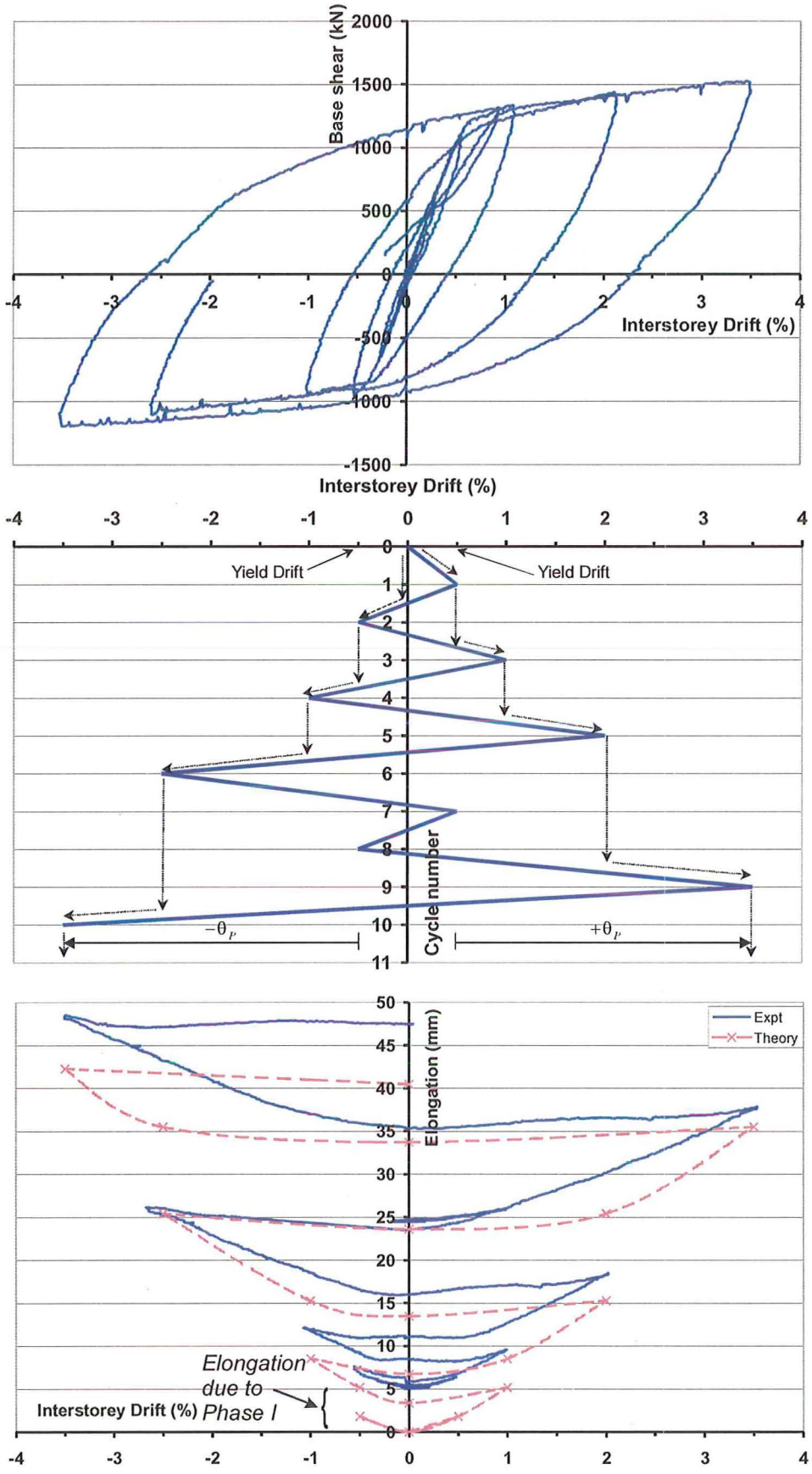

Figure 7-15 Rain flow chart for Phase II (East beam)

average compares well with a predicted result of $\delta_{\max}^{el}$=41mm given by Equation (7-13).

7.6 Design recommendations

The total amount of beam elongation that occurs in a bent during an earthquake is extremely important when precast floor units are seated on the beams of a moment resisting frame. The required seat length must be large enough to account for the total beam growth plus construction tolerances (Centre for Advanced Engineering (1999) and NZS3109 (1997)). Therefore, the seat width demand (for each seat) is given by

$$U_T = U_S + U_D \tag{7-14}$$

in which U_T = seat width requirement; U_D = Dynamic seat width due to beam elongation; and U_S = Static seat width due to construction requirements. U_D is defined as

$$U_D = \frac{1}{2}\delta^{el} = \frac{\omega}{2} n \left\{ \left|\theta_P^+\right| + \left|\theta_P^-\right| + \left|\theta_y\right| \right\} e_{cr} \tag{7-15}$$

in which ω = a magnification factor which may be thought of as a factor of safety (a value of 1.5 is suggested here); n = number of hinges within the span of the floor section under consideration; e_{cr} = average beam depth between the beam centreline and the instantaneous centre of rotation (the centroid of the compression force); θ_P^+ = maximum positive plastic rotation imposed on the beam hinges; θ_P^- = maximum negative plastic rotation imposed on the beam hinges; and θ_y = yield rotation of the structure. The value of e_{cr} can be assumed to be $0.475D$ for an exterior positive hinge, $0.425D$ for an exterior negative hinge and $0.25D$ for an interior hinge (both positive and negative rotations) with prestressing running through the joints (D is the overall beam depth).

Equation (7-15) assumes that the beam plastic hinges form at the column face, this is not always the case especially if the frame is gravity dominated. Therefore, the dynamic seat width due to beam elongation, U_D, can be written as

$$U_D = \frac{\omega}{2} n\, e_{cr} \left(\left|\theta_P^+\right| + \left|\theta_P^-\right| + \left|\theta_y\right|\right) \frac{L}{L_b} \qquad \textbf{(7-16)}$$

in which L = distance between column centrelines; L_b = distance between the assumed centre of rotation of the plastic hinges.

Both the Centre for Advanced Engineering (1999) and NZS3109 (1997) give guidance on allowable construction tolerances. Based on the super-assemblage tested at the University of Canterbury, the following tolerances should be allowed for: linear variance in the length of the hollow-core unit = ±20mm (for units ≥12m in length); and horizontal position of the beam supporting the floor in plan (distance to the nearest reference axis) = ±10mm for each of the two beams. Therefore the total construction tolerances equates to ±30mm for the entire span or ±15mm for each seat.

Given Equation (7-16) and some values for allowable construction tolerances it is possible for Equation (7-14), the seat width demand (for each seat), to be written as

$$U_T = \frac{\omega}{2} n\, e_{cr} \left(\left|\theta_P^+\right| + \left|\theta_P^-\right| + \left|\theta_y\right|\right) \frac{L}{L_b} + 15mm + \mathrm{cover} \qquad \textbf{(7-17)}$$

but $U_T \geq 75$mm as specified by Amendment three (2004) of NZS3101:1995.

7.7 Numerical example

Consider a 10 storey building designed to a design basis earthquake of 2.0% drift. the beams are 750mm deep with 35mm cover to the main bars. Hollow-core units are to be supported spanning two perimeter moment frame bays. Determine the required seat

length given that the yield drift is 0.5%, the columns are 750mm square and the centre-to-centre spacing of the moment frame bays is 6.1m. ω =1.5.

Hinge rotation

$$Elastic \Rightarrow \theta_y = 0.005 \times \frac{6100}{6100 - 750} = 0.0057 rad \quad \textbf{(7-18)}$$

$$Plastic \Rightarrow \theta_p = (0.02 - 0.005) \times \frac{6100}{6100 - 750} = 0.0171 rad \quad \textbf{(7-19)}$$

$$let\ e_{cr} = 0.45D = 0.45 \times 750 = 338mm\ and\ n = 4\ hinges \quad \textbf{(7-20)}$$

Therefore, the required seat length is

$$U_t = \frac{1.5}{2} \times 4 \times 338 \times (0.0171 \times 2 + 0.0057) + 15 + 35 = 90mm \geq 75mm \quad \textbf{(7-21)}$$

Therefore, adopt a seat length of 90mm.

7.8 Concluding Remarks

Previous researchers have predicted the beam elongation by assuming that the elongation varies proportionally with interstorey drift. It is recommended here that a better estimation of beam elongation can be made by using a rainflow counting method while examining the applied loading history. It is possible to more accurately predict the amount of elongation on an individual plastic hinge basis or a frame as a whole. This predictive approach developed herein was successfully validated against the experimental results reported by previous researchers, as well as the results conducted as part of the present research.

Lee and Watanabe (2003) were also able to predict the expected elongation reasonably well. Their method focuses on a micro-mechanics based analysis, whereas the rainflow method proposed herein essentially focuses on rigid body kinematics. The principal advantage for using rigid body kinematics is that it allows for a

simplified set of equations to be used. The approach can be applied either as part of an in-line frame time history analysis or as a post-processing exercise if such models have not been incorporated into an appropriate hysteresis model.

For the design engineer who wants to be able to predict the amount of beam elongation within the building it is now possible using Equation (7-13). All the designer requires is the maximum positive and negative drift amplitudes of the structure, the structures yield drift, and the beam details. Equation (7-17) should be used to determine the required seat length for precast floor units. Care needs to be taken to ensure appropriate values of yield drift (θ_y), plastic rotation (θ_P) and for the construction tolerances are used.

7.9 References

Centre for Advanced Engineering, 1999, *Guidelines for the Use of Structural Precast Concrete in Buildings*, Centre for Advanced Engineering

Dowling N.E, 1972, *Fatigue Failure predictions for complicated stress-strain histories*, Journal of Materials, JMLSA, Vol7, No 1, March, pp 71-87

Fenwick R.C and Davidson B.J, 1995, *Elongation in Ductile Seismic-Resistant Reinforced Concrete Frames*, Recent Developments in Lateral Force Transfer in Buildings, Thomas Paulay Symposium, ACI, pp 143-170

Fenwick R.C, Dely R. and Davidson B.J, 1999, *Ductility Demand for Uni-directional and Reversing Plastic Hinges in Ductile moment Resisting Frames*, Bulletin of the New Zealand Society for Earthquake Engineering, Vol 32, No. 1, March, pp 1-12

Fenwick R.C and Megget L.M, 1993, *Elongation and load deflection characteristics of reinforced concrete members containing plastic hinges*, Bulletin of the New Zealand National Society for Earthquake Engineering, Vol 26, No. 1, March, pp 28-41

Fenwick R.C., Tankut A.T. and Thom C.W., 1981, *The deformation of reinforced concrete beams subjected to inelastic cyclic loading-Experimental results*, University of Auckland Report No 268, University of Auckland

Lau D, B, N, 2001, *The Influence of Precast-Prestressed Flooring on the Seismic Performance of Reinforced Concrete Perimeter Frame Buildings*, Department of Civil and Resource Engineering, University of Auckland, Report No 604

Lee J.Y and Watanabe F, 2003, *Predicting the longitudinal axial strain in the plastic hinge regions of reinforced concrete beams subjected to reversed cyclic loading*, Engineering Structures, Vol 25 No. 7, June, pp 927-939

NZS3107:1997, *Specification for concrete construction*, Standards New Zealand, Wellington

Restrepo J.I, Park R and Buchanan A, 1993, *Seismic Behaviour of Connections Between Precast Concrete Elements*, Research Report 93-3, Department of Civil Engineering, University of Canterbury, Christchurch, New Zealand

Chapter 8

Conclusions, Recommendations and Further Research

8.1 Conclusions and Recommendations

8.1.1 Displacement history development

The displacement history used to load the super-assemblage was developed from a series of time history studies. The history moves away from the traditional Park method (1989) of two reversing cycles of increasing amplitude as it was felt that the Park method imposed too greater demands on the structure. The Park method obtains a conservative dependable result for new construction details (or methods) but is considered excessively harsh when experimentally evaluating the expected performance of existing structures. The new displacement history proposed in this research comprised of one reversing load cycle for each displacement increment. The magnitudes of the displacement cycles were determined so that they included 10% in 50 years (Design Basis Earthquake) displacements as well as 2% in 50 years (Maximum Considered Earthquake) displacements.

8.1.2 Self-equilibrating loading frame

In order to displace the super-assemblage a self-equilibrating loading apparatus was developed. The design of the self-equilibrating frame was governed by several key variables to be accounted for during lateral displacement of the super-assembly. These variables were: to allow beam elongation to occur; to ensure the columns remained

parallel; and finally to ensure the super-assemblage deformed in the correct shape. The self-equilibrating frame was used because the structures laboratory at the University of Canterbury does not have a structural wall to push against.

The loading apparatus was designed so that the super-assemblage can be loaded in two principal directions. Another advantage of the self-equilibrating frame is that it can be used to test other structural forms, provided the new super-assemblage has similar overall dimensions.

The self-equilibrating loading frame is driven by a purpose-built semi-automated controller developed from a series of logic algorithms. The semi-automated controller allows the complicated loading regime to be controlled relatively simply. The valve controller undertakes the simple tasks while the entire decision making was made by the operator.

8.1.3 Experimental performance

Initial damage to the seating connection of the hollow-core occurred much earlier than anticipated during the test and the mode of failure was different to that assumed by design. The rotation of the hollow-core unit relative to the supporting beam, the unit was seated upon, has been something that not only researchers but also engineers have overlooked in the design of such connection details. It was this rotation that lead to the fracturing of the end of the hollow-core unit causing the entire support (seat) at both ends of the units to be lost.

The first hollow-core unit (closest to the South perimeter beam) showed additional signs of distress (in addition to the fractured seat detail) due to the unit being forced to displace in the manner of the perimeter frame (double curvature). This mode of displacement is one for which the hollow-core unit was not designed and

caused the internal splitting of the webs of the hollow-core unit, eventually leading to the collapse of the bottom half of the unit.

This displacement incompatibility between the perimeter beam and the remainder of the floor diaphragm along with the tension forces generated within the floor diaphragm due to beam elongation lead to the fracturing of the cold-drawn wire reinforcing mesh placed within the cast insitu topping slab. The reinforcing mesh fractured at the interface between the first and second hollow-core units at 1.93% drift. If this mesh fractured in a real structure (and the fracture occurred over several floors) and the intermediate column was not adequately tied to the floor diaphragm (as was the case in this experiment) then there is a potential problem for premature buckling of these exterior-intermediate columns leading to the potential collapse of the building.

Once the tear within the diaphragm occurred an upper limit was placed on the contribution of slab acting as a flange to the perimeter beams to the lateral strength of the super-assemblage.

One major point to note from the experimental programme is that even though the floor failed, the perimeter frames beams, columns, and beam column joints remained relatively undamaged. Clearly, significant extra attention is required to be paid to the hollow-core seating details to ensure that this class of precast floor system performs at a level that is not inferior to that of the structural frame.

8.1.4 Broader ramifications from the experiment

By balancing drift demand versus capacity it is possible to determine the implications that the lateral drift damage has on New Zealand reinforced concrete moment resisting frame buildings incorporating hollow-core floors. A probabilistic formulation that used fragility curves indicates the following:

- The number of buildings that would require demolition following a maximum considered earthquake (MCE) for Wellington would be low (<10-15%) if the rating reported was produced for the frame performance and was well in keeping with the expectations of capacity design. The frame performance is also a good guide for the rating for cast insitu reinforced concrete construction.

- If the floor performance was reported (as should be the case for precast hollow-core construction) a 2% in 50 years (MCE) event in Wellington would see almost all of precast buildings either suffering partially or full collapse of the hollow-core floor. Large loss of life could also be expected.

- Under a 10% in 50 year (DBE) event, the situation is not so bleak, but nevertheless some 90% of buildings might be expected to be demolished including 10% of buildings that had likely full collapse of the floors.

8.1.5 Experimental Results

The tear within the diaphragm governed the amount of enhancement that the floor diaphragm, acting as a flange, contributed to the lateral strength of the super-assemblage. It was found that when the specimen was loaded in the longitudinal direction (parallel to the direction in which the hollow-core units spanned) the exterior and interior plastic hinges within the South perimeter beam had different mechanisms that contributed to the lateral strength. By using rigid body kinematics and a proposed theory for determining the width of activated slab as a flange (that contributes to the plastic hinge capacity; increasing participation with increasing interstorey drift), it was possible to predict the components that contributed to the lateral strength of the super-assemblage. The results showed that for an exterior hinge, the nominal beam

moment plus a maximum of 3.05m of slab reinforcement (continuity bars) contribute to the negative moment capacity of the plastic hinge. The amount of activation increases with interstorey drift. At yield, the width of activated slab was the width of the first hollow-core unit (1.2m) whereas the maximum contribution occurred at 2.0% drift and was 3.05m. For a positive moment, the contribution is taken as the nominal beam moment. For an interior plastic hinge, the negative moment capacity is the longitudinal beam reinforcement plus the reinforcing mesh and prestressing strands within the first hollow-core unit. For the positive moment, the capacity incorporates the beams reinforcement plus the prestressing strands within the first hollow-core unit.

For the transverse loading direction (perpendicular to the direction the hollow-core units spanned) it was not possible to determine the maximum contribution from the floor slab when the super-assemblage was displaced to a negative inclination as the diaphragm tear played a significant role in the performance. It was possible to determine the diaphragm contribution for a positive inclination. The lateral strength is developed from the nominal beam longitudinal reinforcement plus a maximum activated slab width of 3.05m for a negative moment. The actual width of activated slab increases with lateral displacement (transversely) and is determined the same way as that proposed when the super-assemblage is displaced parallel to the hollow-core unit. For a positive moment only the nominal beam moment contributes.

Both NZS3101:1995 and ACI318-02 greatly underestimate the contribution that the floor diaphragm makes to the lateral strength of a building. This could lead to a less desirable mechanism (than the weak beam/strong column mechanism) forming within the structure during a major earthquake.

8.1.6 Diaphragm performance

Following this research the level of understanding into how the connection between a hollow-core unit and its supporting beam performs in an earthquake is now better understood. It has become clear that the previous work undertaken in this field was in fact incorrect and over-simplified. The expected performance between a cyclic pull off test and a cyclic rotation test is completely different.

Following the completion of this experimental programme a national study group was formed to study these test results and to discuss new improved details. Initial results, from a two-dimensional sub-assemblage test in which some new connection details were imposed to cyclic rotations appeared promising; further verification in the three-dimensional super-assemblage is required.

Suggestions were made on how to eliminate the failure of the first hollow-core unit placed next to a perimeter beam. This can be achieved by placing a flexible reinforced link slab between the first hollow-core unit and the perimeter frame. This flexible link slab will allow for any deformation incompatibility between the perimeter frame and the hollow-core units to occur within the link slab ensuring the hollow-core unit is not deformed in double curvature (a manner for which it was not designed).

The monitoring of the Demec points placed across the floor showed that as the beams elongated, the displaced shape of the frame formed a shape referred to as Mode 2. This mode is one in which the entire transverse beam rotates, in the horizontal plane, to accommodate the elongation. The mode that occurred in the two-bay beams (South frame) was not entirely a Mode 2 response as the diaphragm tear within the floor played and major role so in fact it was a combination of a Mode 2 & 3 performance. Mode 3 is where the intermediate column translates out of the building

and rotates the perimeter beams about the corner columns (referred to as the bowstring effect), in the horizontal plane.

8.1.7 Predicting Beam elongation

In the past the prediction of beam elongation has not been well understood. A rainflow counting method was adopted to explain in a more accurate way in which elongation history can be predicted for each individual plastic hinge or a complete bent. Accurately predicting beam elongation is important when it comes to determining the seat length required for the placing of precast floor slabs. The devised model predicts elongation using rigid body kinematics allowing for simplified equations to be used. The predictive model proposed was validated against the results from this current research programme as well as the work of previous researchers.

It should be noted that even within an elastically responding structure the beams elongate. This is highly important when determining the type of connection detail to connect a precast concrete unit to a lateral force resisting system.

8.1.8 Recommendations for future construction

Several key issues have risen since the completion of this testing programme. These mainly effect the connection details used to attach the precast floor units to the moment resisting frame of a reinforced concrete frame structure. The following are recommended for future construction:

(i) The hollow-core unit should be placed on a low friction bearing strip rather than on a mortar (or grout) seat.

(ii) The plastic bungs that are placed into the cores of the hollow-core unit should be replaced by a sheet of compressible backing material.

(iii) The recommended seat length for a hollow-core floor unit should be increased to at least 75mm

(iv) A hollow-core unit should not be placed adjacent to a perimeter frame but instead by offset by approximately 600-750 mm. A flexible reinforced link slab should be placed across the gap to allow the cast in place concrete topping to be poured.

(v) If an intermediate column is not adequately tied to the diaphragm than some additional tie reinforcement ("drag" bars) should be placed orthogonal to the perimeter frame.

(vi) Within the concrete topping slab, ductile reinforcing mesh or conventional reinforcing bars should replace non-ductile cold-drawn wire reinforcing mesh.

8.2 Recommendations for further research

This experimental programme has answered several questions regarding the expected performance of precast concrete hollow-core floor slab buildings during a major earthquake. As is usually the case with research, every question answered leads to several more questions to be asked.

This section outlines some of the new (and not so new) questions that still require answers. In particular, comments are made on what needs to be undertaken at a sub-assembly level, super-assemblage level and analytically. Some suggestions on the retrofitting of existing buildings are discussed as is some considerations that need to be examined when using damage avoidance design (DAD) construction.

8.2.1 Connection details

Initially, more two-dimensional (2D) sub-assembly component tests need to be carried out similar to those used to test the technical advisory group on precast floors recommendations (Bull and Matthews, 2003). These component tests should test the most common connection details used in New Zealand to connect hollow-core floor slabs to the supporting beams. The sub-assembly tests are a recommended place to start because of the following advantages: relatively cheap to perform; quick to undertake; do not require a large laboratory space. The results will enable a clearer understanding of how each of the various connections are likely to perform under cyclic rotation. Although the 2D sub-assembly test does not exactly match the boundary conditions it allows a better understanding of how the connection is likely to perform. The results will allow engineers to get a better feeling on how the current New Zealand building stock is likely perform in a major earthquake. The data from these tests can then be used to develop an analytical model for predicting new connection performance or to assess older buildings.

The 2D component experiments should investigate the effect of the following:

(i) What role does the grout that the hollow-core unit was seated on play? Will the same result occur if the unit was placed on a weaker mortar or straight on the concrete beam alone?

(ii) What role does a low friction bearing strip play? During the Northridge earthquake in Los Angeles in 1994 very few hollow-core buildings collapsed. A majority of these buildings had a bearing strip placed under the precast units. Would the initial connection detail tested in this experimental programme perform better if a bearing strip replaced the grout?

(iii) What is the affect of having a negative seating (i.e. precast units are short and therefore do not sit on the beam)? Will the reinforced cores, often used, be enough to prevent the hollow-core unit from splitting and collapsing?

(iv) What affect will placing transverse reinforcement within the ends of the hollow-core unit play on its performance during cyclic rotation?

(v) All the common connection details used in New Zealand should be tested. This will determine to what level of interstorey drift the connection performs adequately. If the connection performance is poor then the structures in which these connections are used may require limits on the buildings allowable level of interstorey drift or may require retrofitting.

(vi) How do the two connection details specified in Amendment 3 of the New Zealand Concrete Structures Standard (NZS3101: 1995) perform? It is crucial that these recommended details be tested in the 3D assemblage.

Once several acceptable connection details have been tested within the 2D sub-assemblage, the connections should then be tested in the more expensive and more realistic 3D super-assemblage. The super-assemblage should be used because it includes most of the second order effects that the 2D sub-assemblage could not. For example: the effect of beam elongation on the seating connection; the effect of the units being loaded transversely to the direction the hollow-core units span; the hollow-core unit being forced to displace in a manner governed by the perimeter frame and the effect of the hollow-core unit seated in a plastic hinge zone.

Currently there does not seem to be any quantifiable engineering analysis used in designing the reinforcement that is used within the connection details used. So much care and attention is spent ensuring a capacity design approach is used in the design of the remainder of the structure (frames, walls and foundations) and these

connections seems to have been overlooked. The key component in the performance of the hollow-core unit is to ensure the yielding and local deformation does not occur within the hollow-core unit but in the connection between the end of the hollow-core unit and the supporting beam.

8.2.2 Analysis Needs

An analytical study needs to be undertaken to develop some analytical techniques to predict the performance of these connections. This will not only aid the Engineer in assessing the likely performance of various connection details during an earthquake but will aid in the modelling of new or existing buildings.

In order to create an analytical model several more sub- and super-assemblage experiments need to be undertaken so that more data is available. These results can be used to validate a range of modelling strategies.

8.2.3 Retrofitting existing structures?

What level of performance is required? Should the retrofit prevent collapse of the floor and allow the occupants to evacuate. However, the building will still need to be demolished following a large earthquake or should the retrofit ensure the building is still occupiable after a major event? The problem with the latter suggestion is that the building could have a large residual drift after the earthquake so therefore the building would need to be demolished anyway. As can be seen from above, there needs to be some thought into what is defined as acceptable performance, particularly in terms of the seismic retrofit. Once the level of acceptable performance is established then three keys issues need to be addressed. These are: the performance of the hollow-core unit to beam connection; the performance of the first hollow-core unit that spanned parallel to the perimeter beam; the effect the hollow-core unit had by spanning past

the intermediate column; the effect of seating a hollow-core unit on a plastic hinge zone of the beam.

How to retrofit the seating detail

There appears to be no simple solution on how to stop the end of the hollow-core unit from fracturing due to the rotation being applied by the supporting beam without greatly reducing the amount of drift that the structure displaces by installing structural walls, dampers or both. Therefore it is proposed that an additional seat is placed under the hollow-core unit to act as a catcher if the unit was to fail and drop. The additional seat could be obtained by bolting a steel angle to the face of the supporting beam (Figure 8-1). The angle should not be placed against the hollow-core unit, as it will just cause the position when the unit fractures to relocate out to the end of the steel angle instead. The steel support angle should be placed 10-15mm below the hollow-core unit. This detail needs to be tested to ensure it performs as expected. The sole purpose of the angle seat is to avoid the collapse of the floor during the earthquake. The angle will not increase the connections performance or stop it from being damaged.

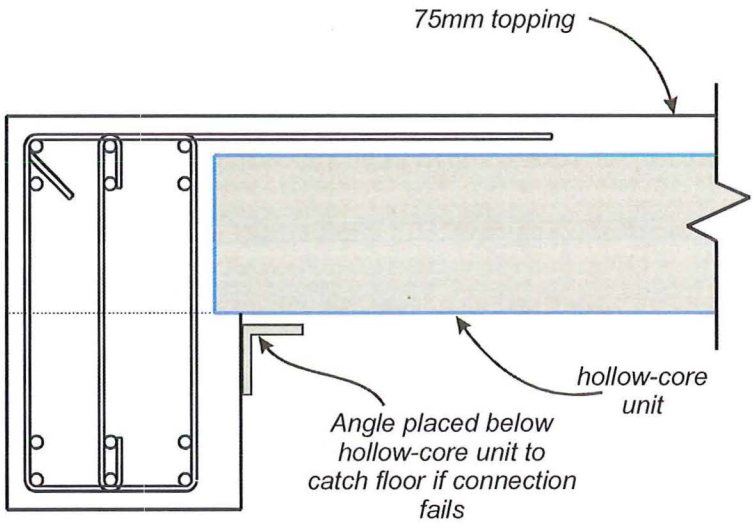

Figure 8-1 Proposed retrofit for seating detail

How to retrofit the hollow-core unit spanning parallel with the perimeter frame

Again, there appears to be no simple solution for stopping the webs of the first hollow-core units from splitting due to the unit being forced to displace in the same manner as the perimeter beam. Therefore, the attention is switched to stopping the bottom of the unit from collapsing. Stopping the bottom half of the unit from collapsing can be achieved in two ways. Firstly, an angle bracket could be bolted onto the side perimeter beam to act as a catcher. A bolt that passes through a hole drilled in the second hollow-core unit will hold the other end of the bracket (Figure 8-2(a)). The second possible option is to use two bolts drilled through the hollow-core unit to hold a bracket that will catch the unit and stop it from collapsing (Figure 8-2(b)). Both of the brackets mentioned would be spaced at 1.5-2m centres along the length of the perimeter frame. One, if not both, of these suggestions need to be tested in the super-assemblage.

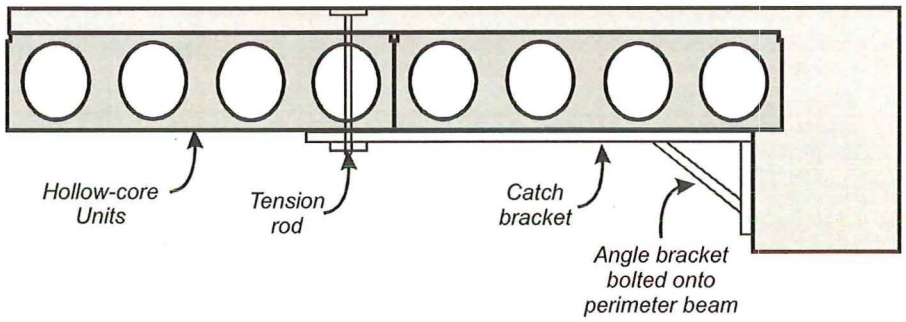

(a) Angle bracket to support the first hollow-core unit

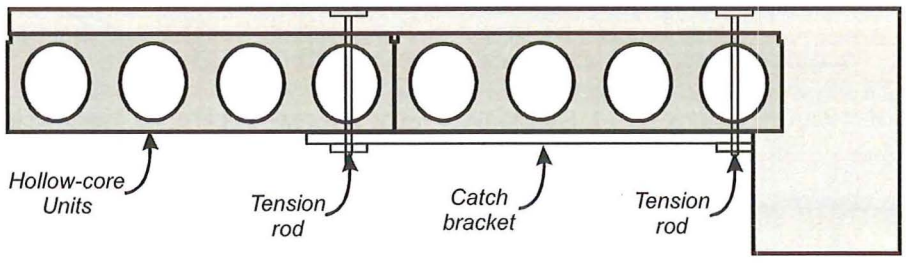

(b) Tie rods to support the first hollow-core unit

Figure 8-2 Possible retrofit details to catch the first hollowcore unit if it was to collapse

How to ensure the central column does not displace laterally

The displacement of the central column laterally (out of the building) only occurs if the column is not adequately tied into the building. For buildings that have a secondary beam at this location then no additional tie reinforcement is required, provided the strength of this beam, acting as a tie is adequate. If the floor units span past this column or the secondary beam is just placed on a corbel then additional reinforcement is required. Both NZS3101:1995 and AS/NZS1170.4:2002 give guidance of the amount of tie force to be provided.

The simplest and least destructive means of applying the additional tie force is to attach some glass fibre or carbon fibre strips to the topping concrete (refer to Figure 8-3). This proposed retrofit also needs to be tested.

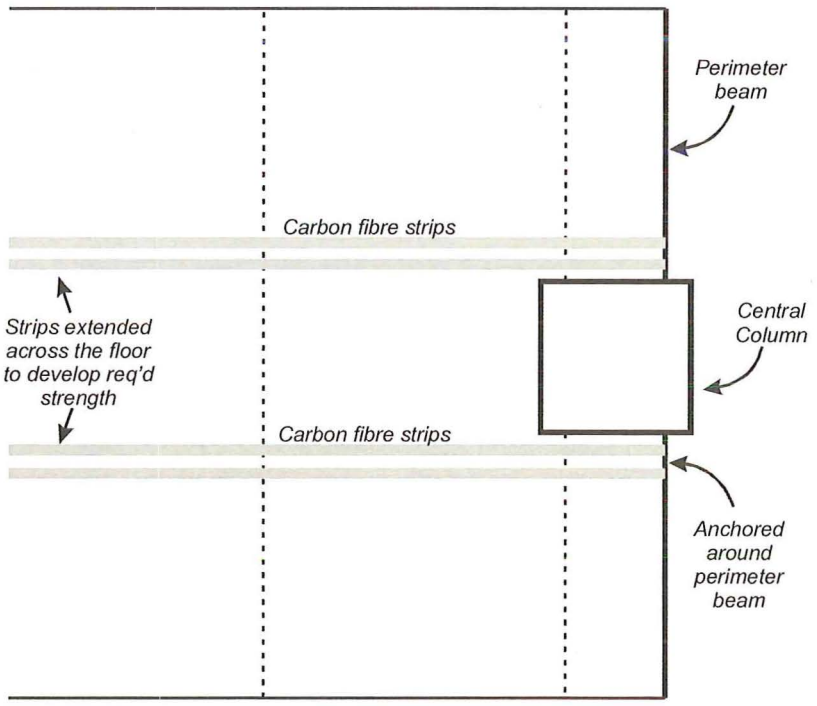

Figure 8-3 Plan view showing the placement of carbon fibre strips around untied columns

8.2.4 Further precast floors to be tested

Although this research programme has focused on hollow-core floor slab buildings some of the issues raised are not only related to this type of structure; other forms of

precast flooring systems are likely to have similar problems. Initial 2D sub-assembly tests should be undertaken to investigate the performance of these other precast floor systems with eventual testing being completed in the 3D super-assemblage.

In the future, new building construction methods will allow structures to remain undamaged during an earthquake. This new category of structure is referred as damage avoidance design (DAD) construction. For this type of structure to be used extensively, new types of connections to connect the precast floors to the lateral load resisting systems are required as all the displacement within the structure is concentrated into discrete zones rather than the dispersed cracking across plastic hinge zones. As this new form of construction is significantly different to what is currently undertaken, the current construction methods will need to be proven inadequate if DAD is going to be accepted widely and used, as this form of construction is currently more expensive than conventional construction. The major advantage of DAD is the costs of repair, and reoccupation post-earthquake, should be significantly reduced.

8.3 References

ACI318-02, 2002, *Building Code Requirements for Structural Concrete*, American Concrete Institute, Farmington Hills, USA

AS/NZS1170.4:2002 , *Draft Structural Design Actions-Earthquake Loadings,* Standards New Zealand , Wellington

Bull D.K and Matthews J.G, 2003, *Proof of Concept Tests for Hollowcore Floor Unit Connections*, Report for Precast NZ Inc, Commercial Report 2003-1, University of Canterbury

NZS3101:1995, *Concrete Structures Standard*, Standards New Zealand, Wellington

Park R., 1989, *Evaluation of ductility of structures and structural assemblages from laboratory testing*, Bulletin of the New Zealand National Society for Earthquake Engineering, Vol. 22, No. 3, Sept, pp155-166.

Appendix A

Estimating Seismic Demands for loading structural components in laboratory experiments

Summarised within this appendix is all the results obtained from the various time history analyses run.

For each earthquake there will be the following summarised:

The earthquake record

General performance of the structure (roof displacement vs time)

Localised storey performance (maximum interstorey drift vs time)

Note that the graphs that have been included for the localised storey performance are only for the floors in which the maximum drift is observed to occur. For example, the results from EL40NSC saw the 3, 6, 9 and 12 storey structures have there maximum interstorey drifts in the 1st, 2nd, 3rd and 5th stories respectively.

A.1 EL40NSC results

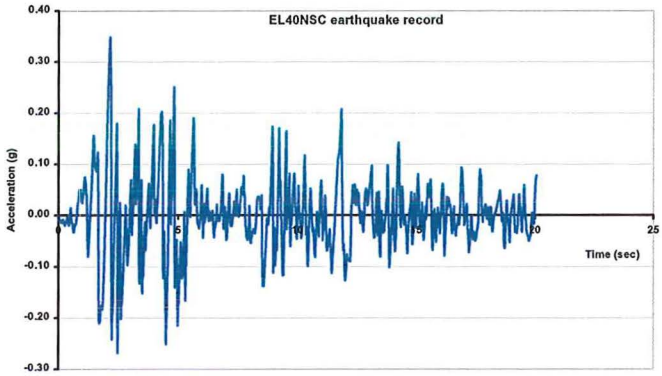

(a) EL40NSC earthquake record

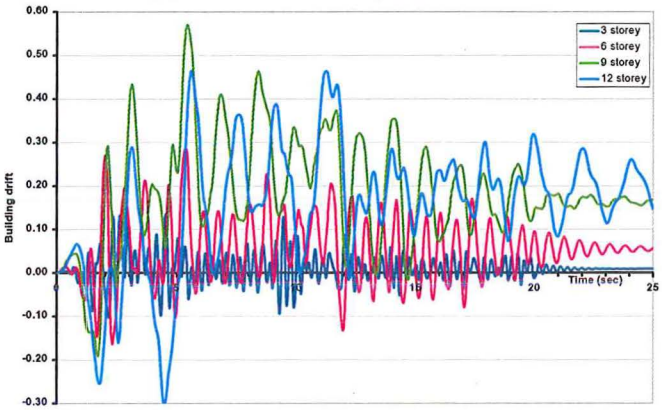

(b) General performance of the structures

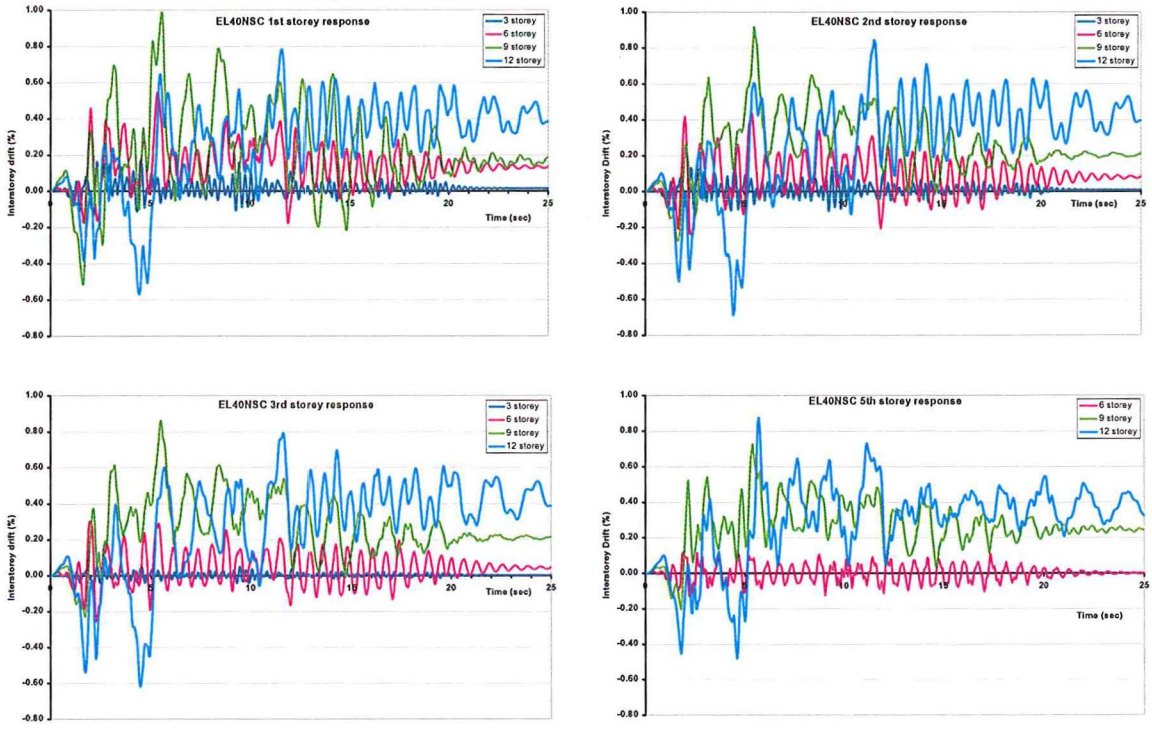

(c) Localised storey performance

A.2 TAFTNW results

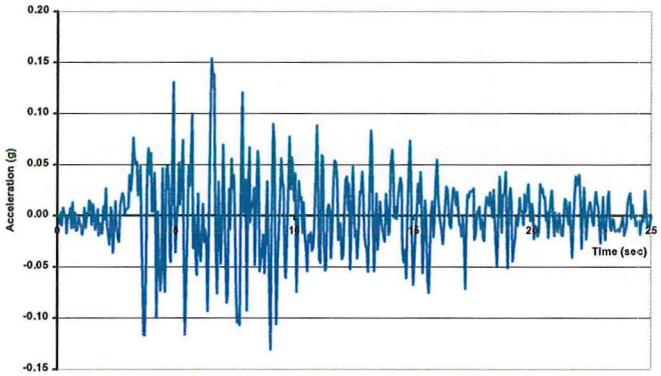

(a) TAFTNW earthquake record

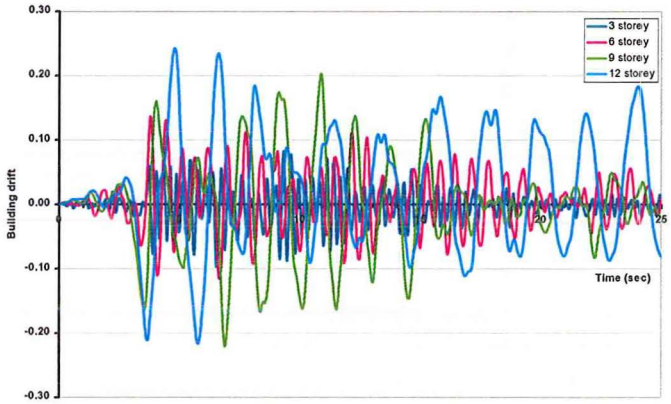

(b) General performance of the structures

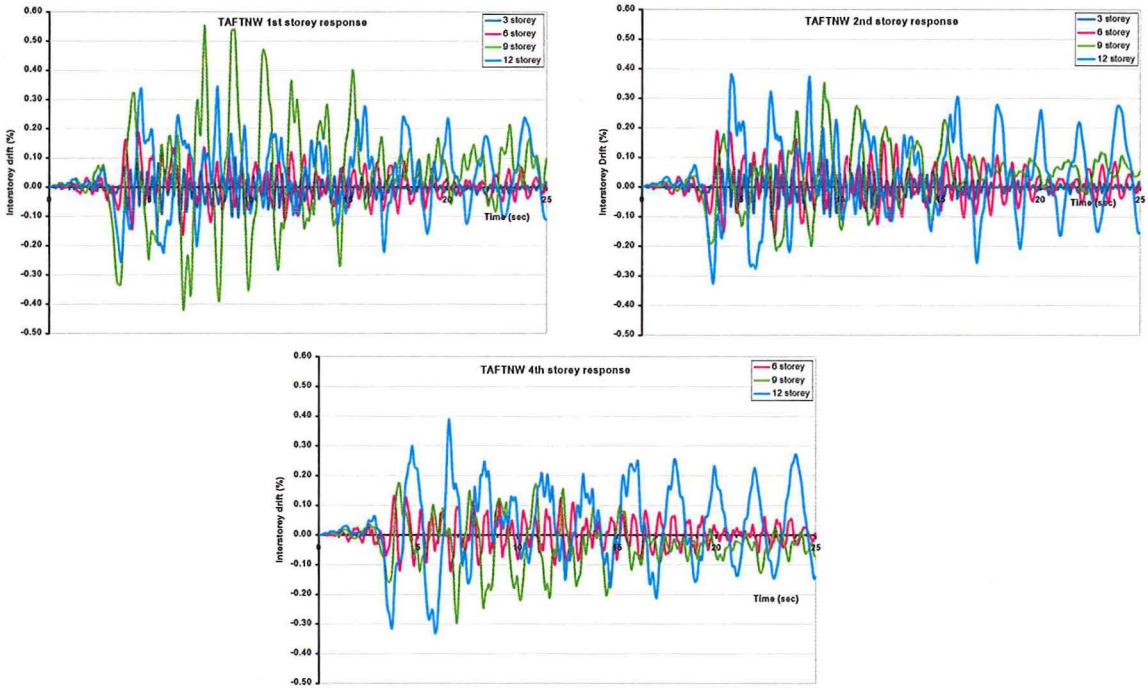

(c) Localised storey performance

A.3 SYFF943 results

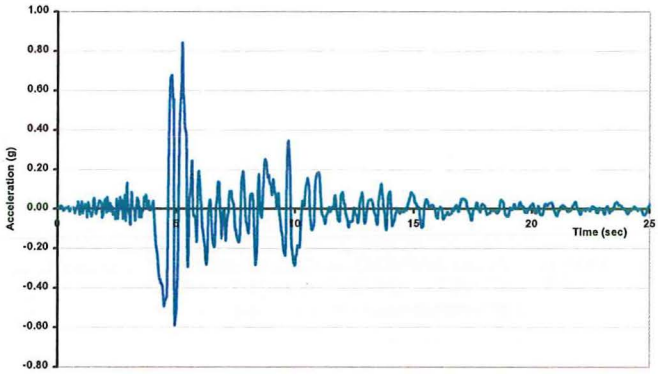

(a) SYFF943 earthquake record

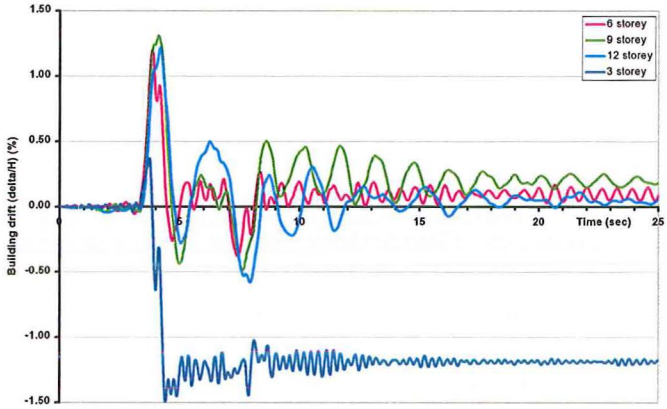

(b) General performance of the structures

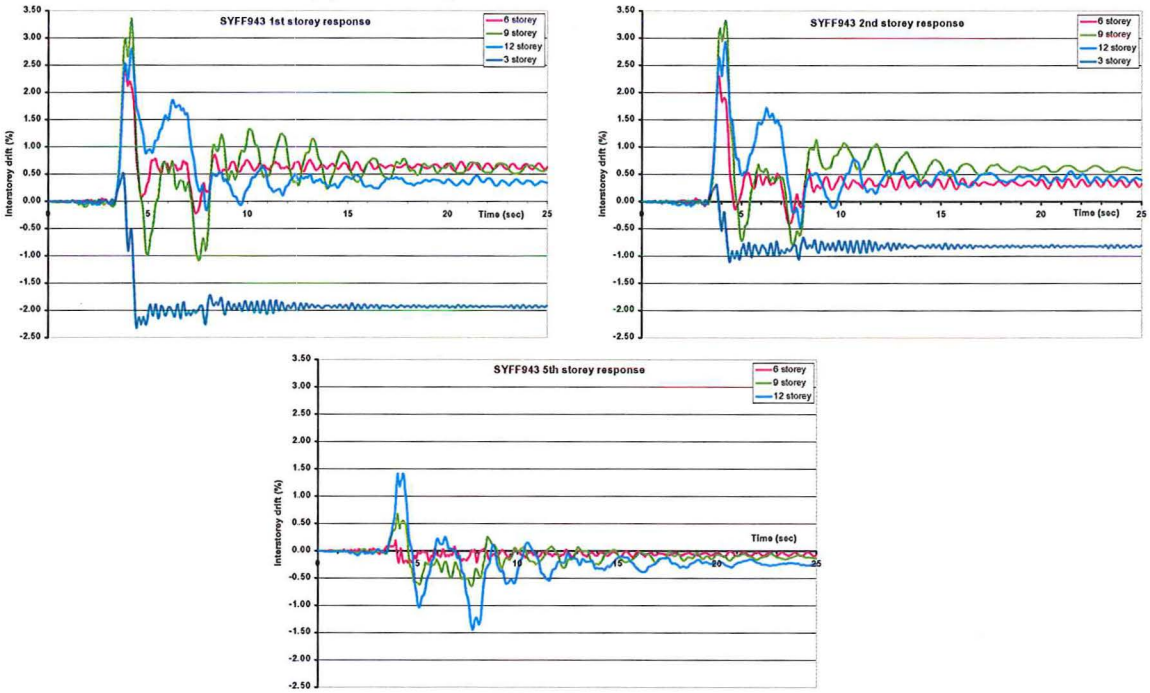

(c) Localised storey performance

A.4 SYLM949 results

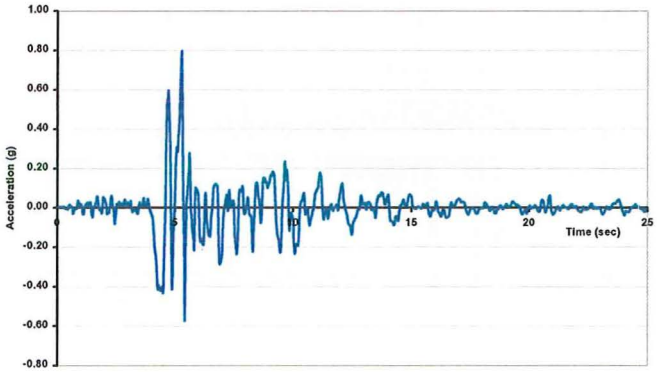

(a) SYLM949 earthquake record

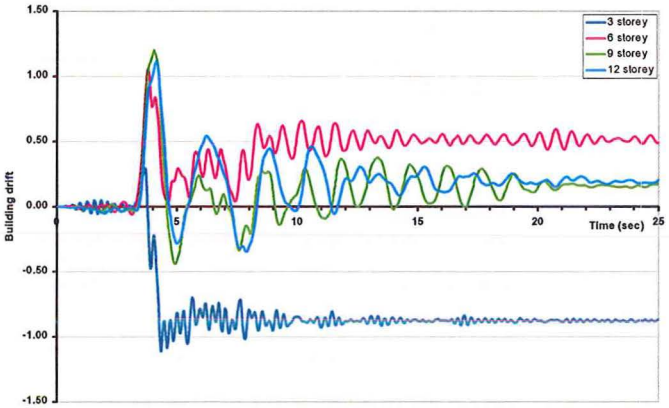

(b) General performance of the structures

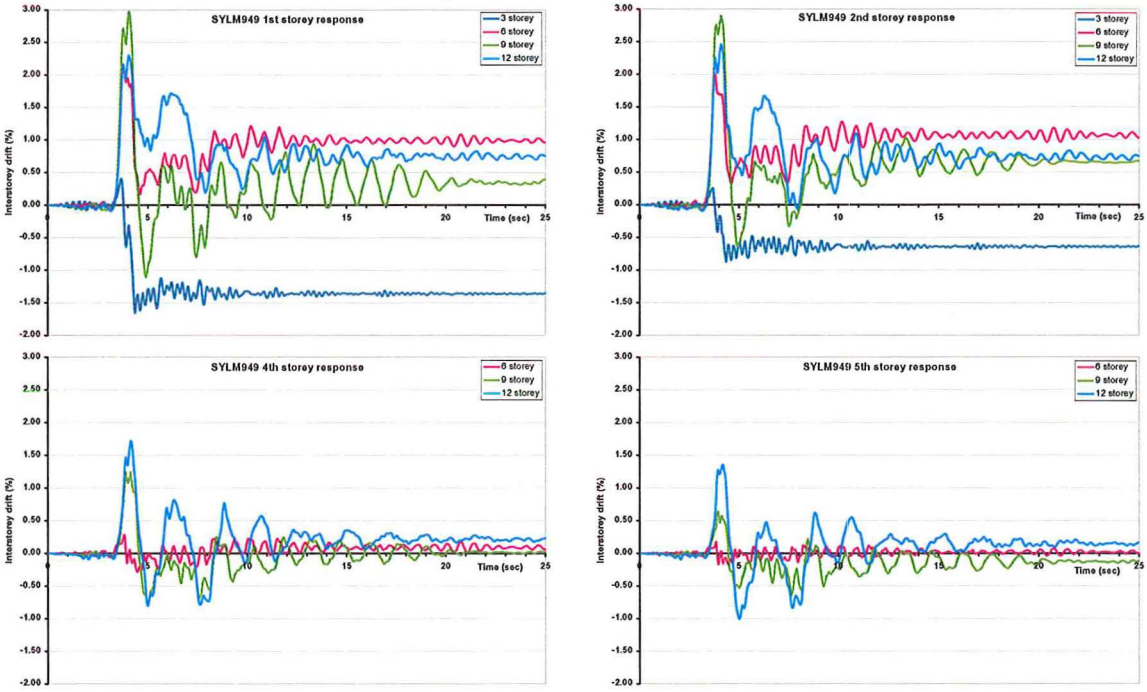

(c) Localised storey performance

A.5 KOBE95NS results

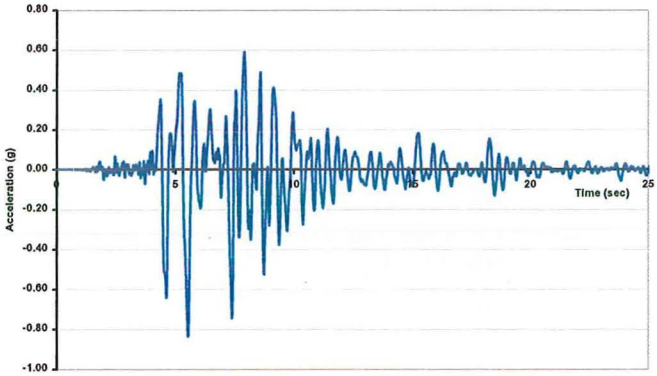

(a) KOBE95NS earthquake record

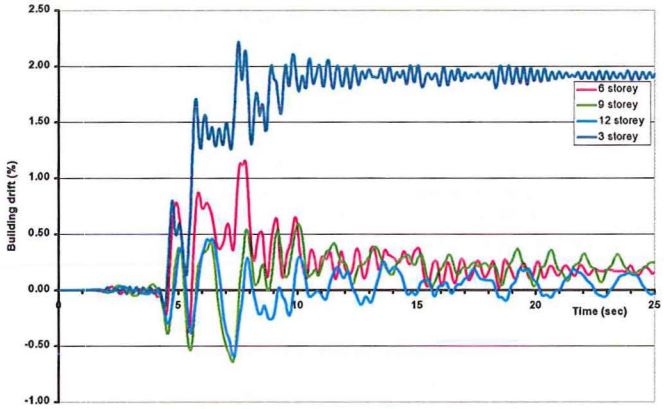

(b) General performance of the structures

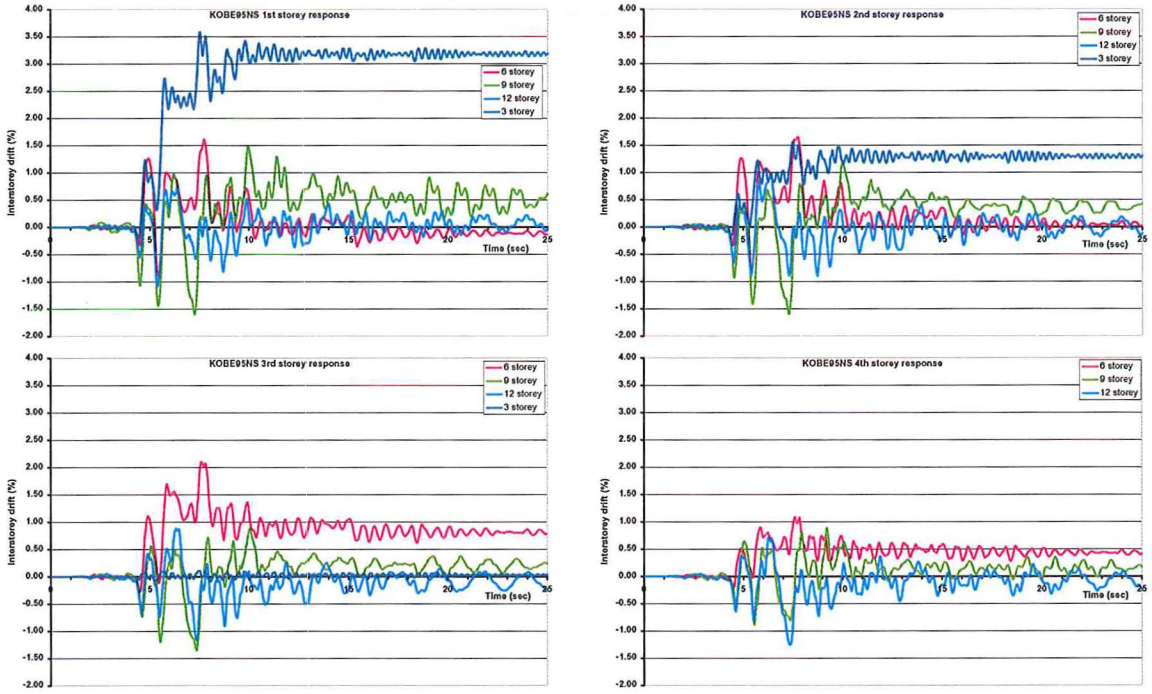

(c) Localised storey performance

A.6 KOBE95EW results

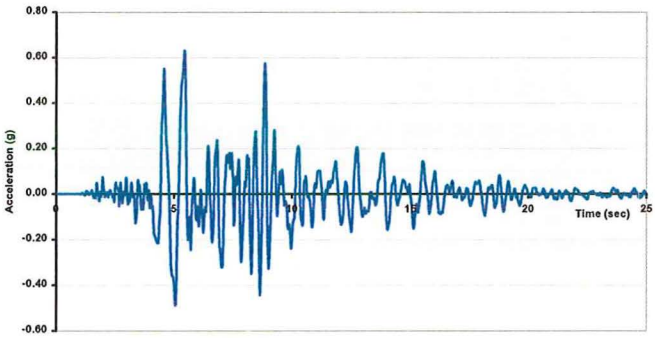

(a) KOBE95EW earthquake record

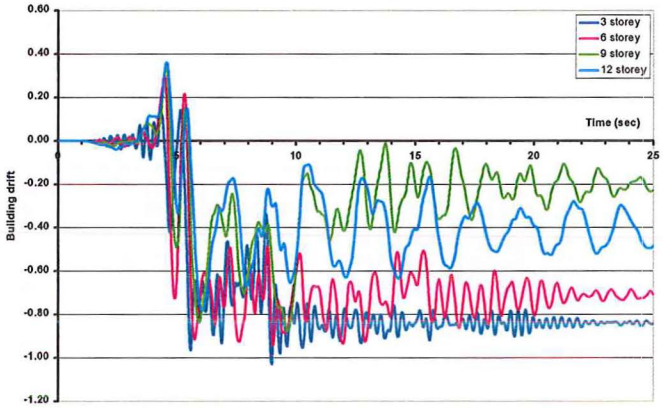

(b) General performance of the structures

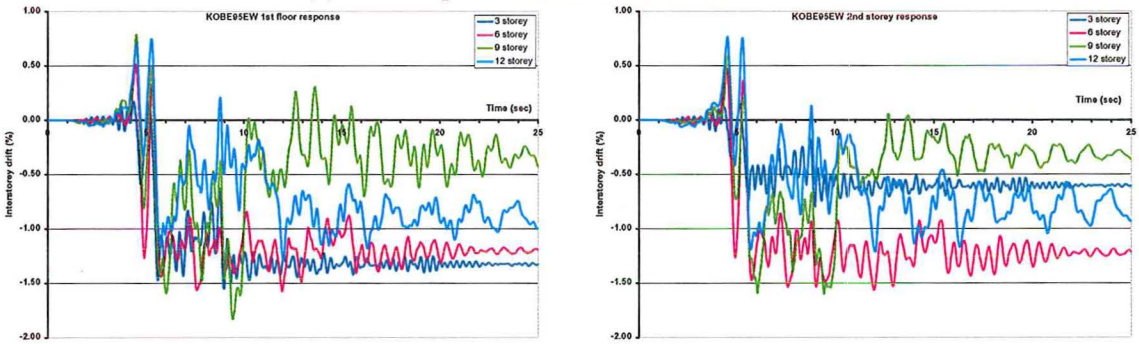

(c) Localised storey performance

A.7 4203ELC1 results

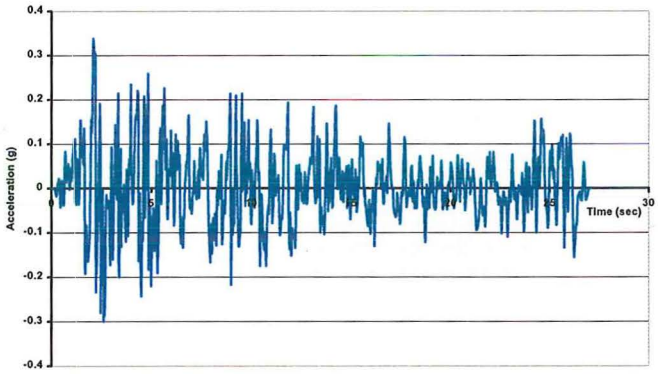

(a) 4203ELC1 earthquake record

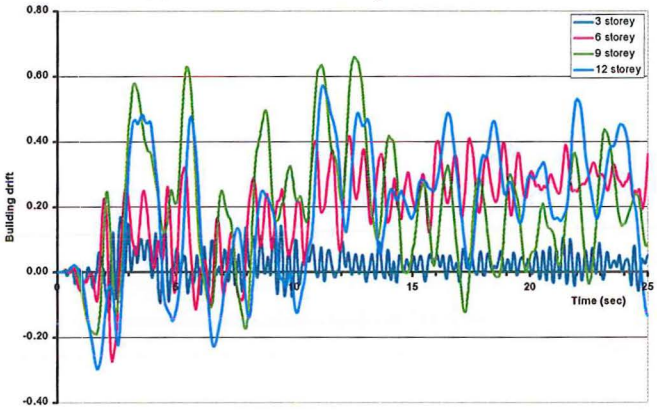

(b) General performance of the structures

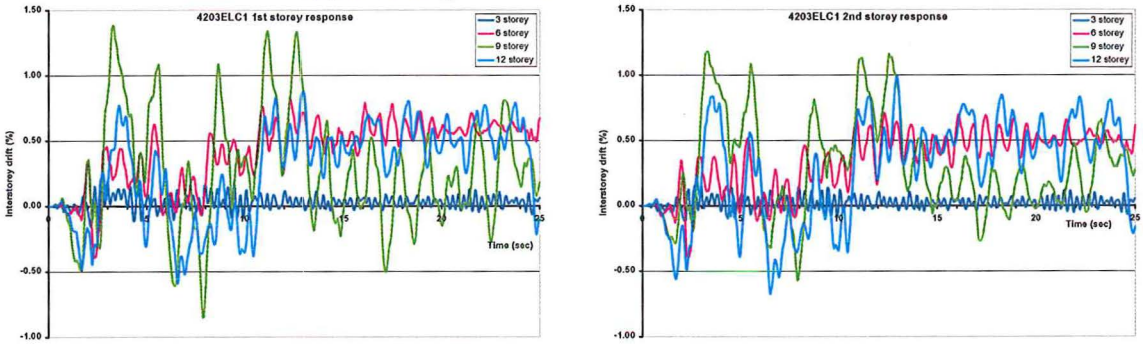

(c) Localised storey performance

A.8 4203ELC2 results

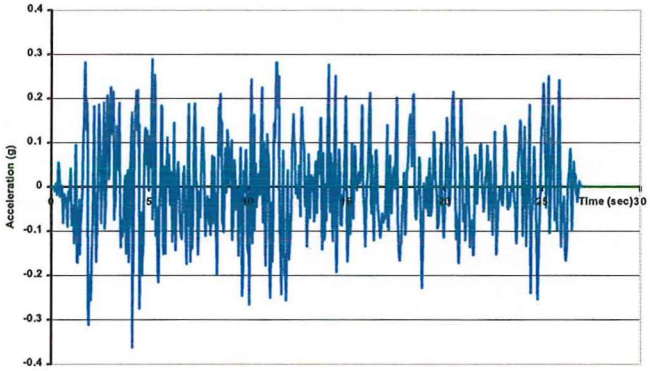

(a) 4203ELC2 earthquake record

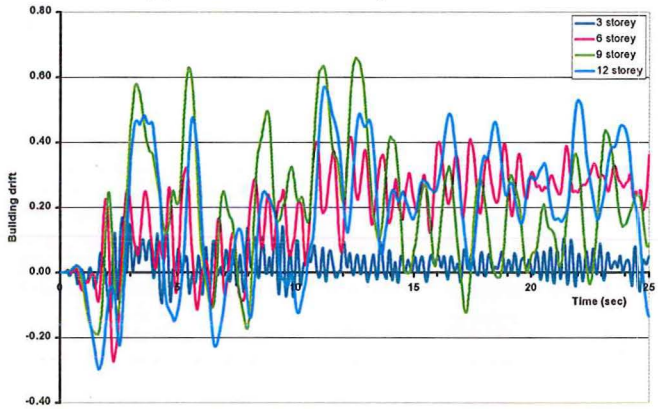

(b) General performance of the structures

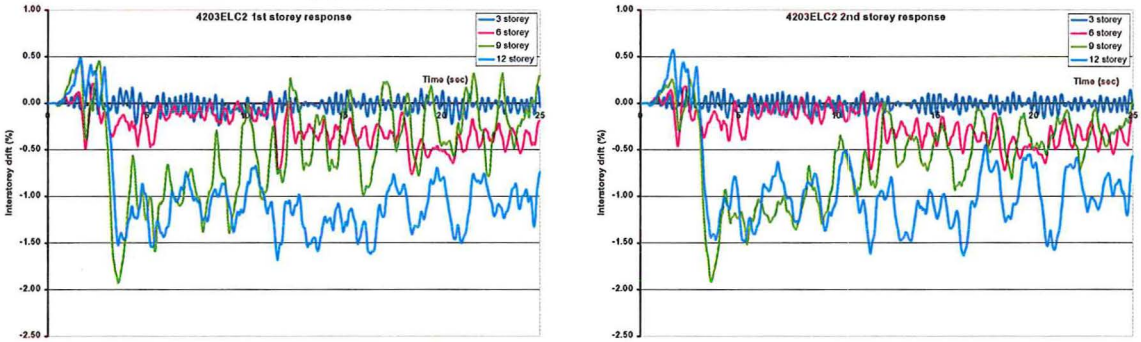

(c) Localised storey performance

A.9 4203OLY1 results

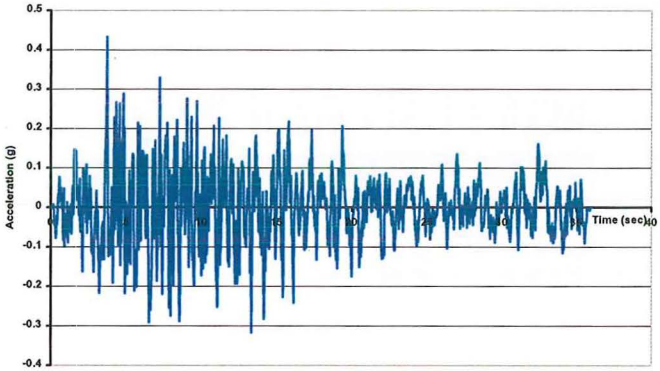

(a) 4203OLY1 earthquake record

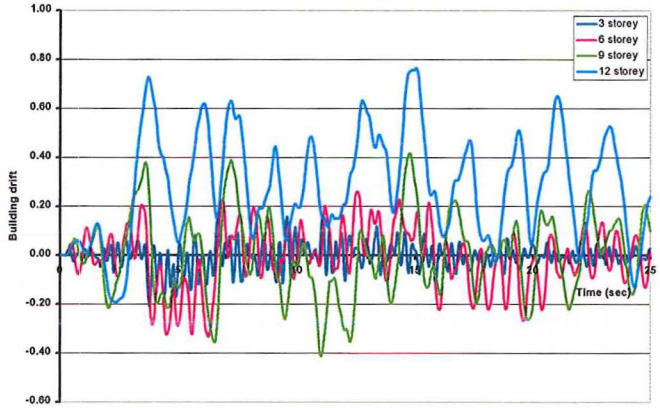

(b) General performance of the structures

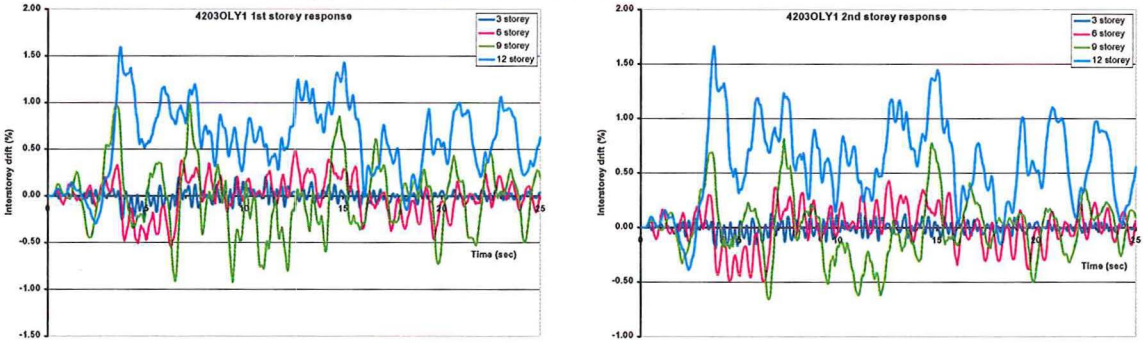

(c) Localised storey performance

A.10 4203OLY2 results

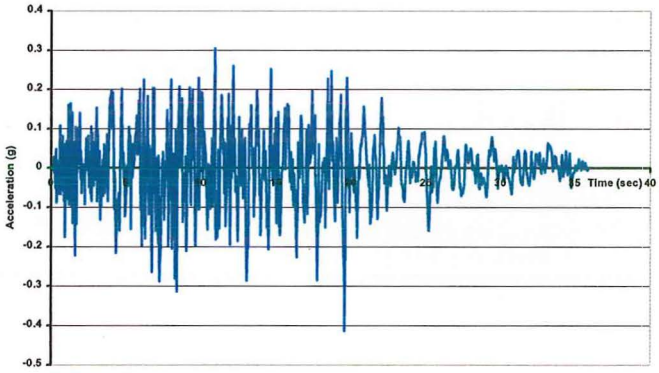

(a) 4203OLY2 earthquake record

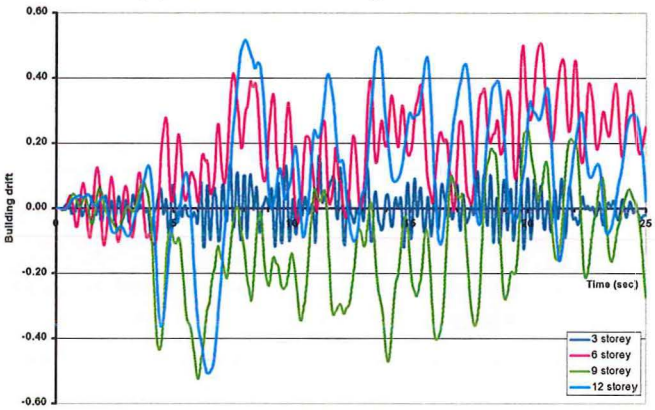

(b) General performance of the structures

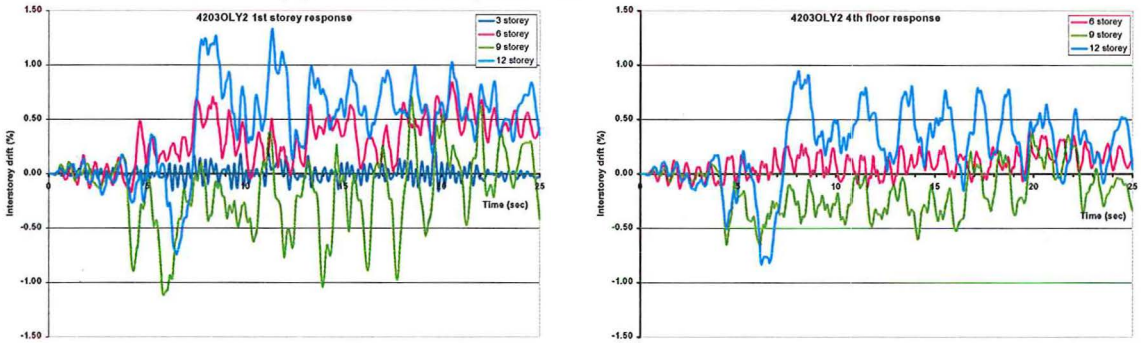

(c) Localised storey performance

A.11 4203TFT1 results

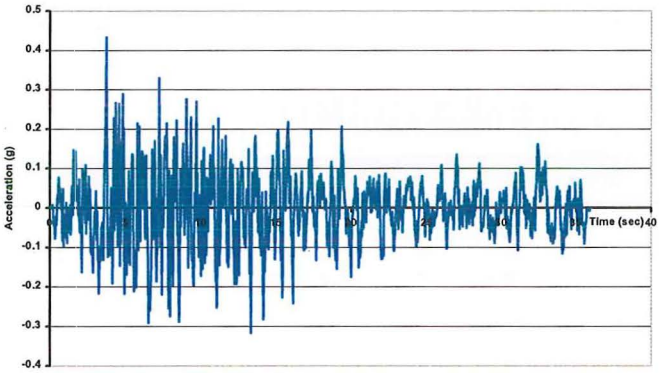

(a) 4203TFT1 earthquake record

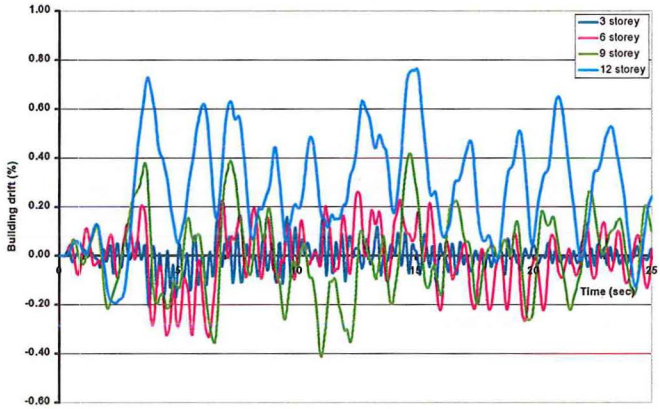

(b) General performance of the structures

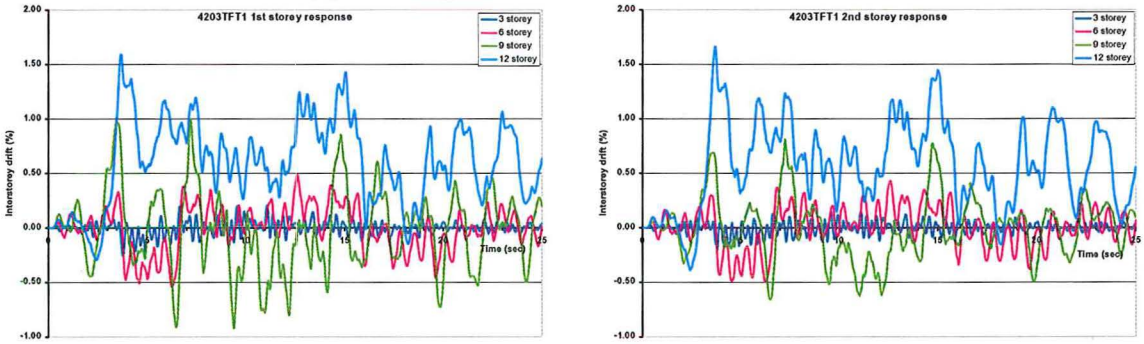

(c) Localised storey performance

A.12 4203TFT2 results

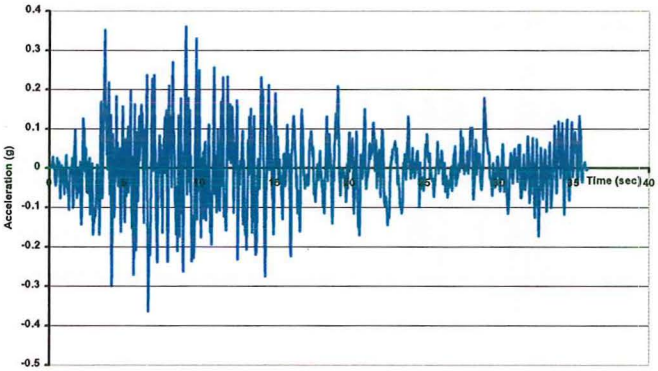

(a) 4203TFT2 earthquake record

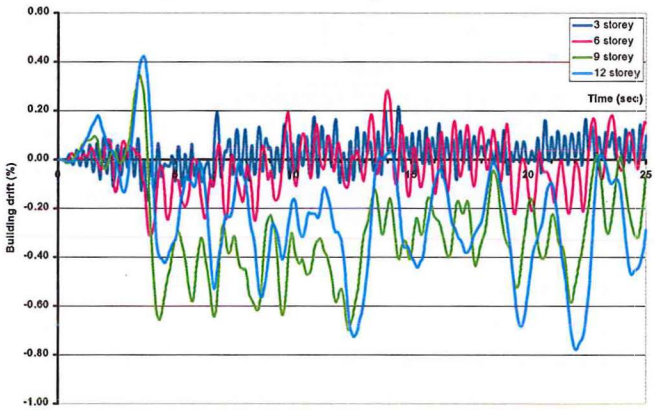

(b) General performance of the structures

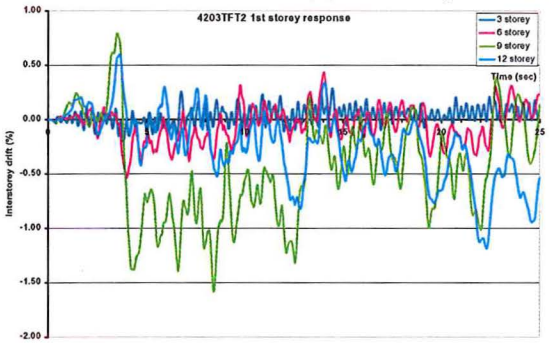

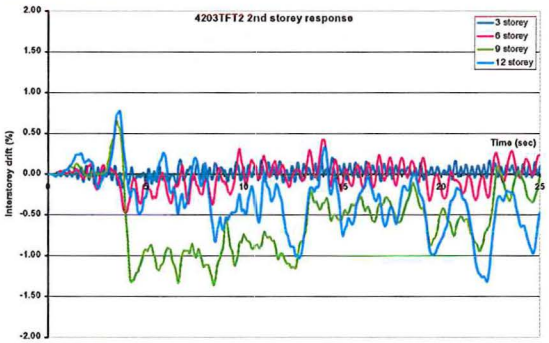

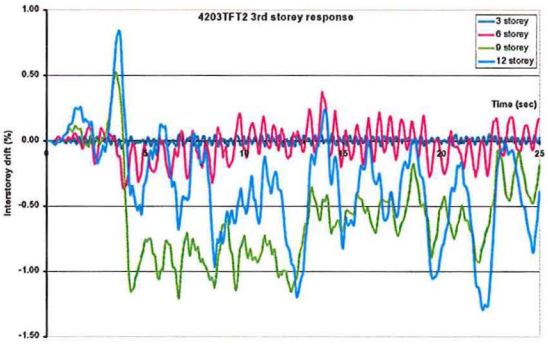

(c) Localised storey performance

A.13 SEC1 results

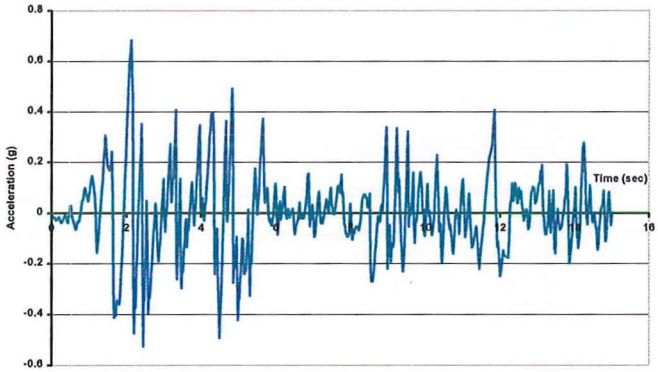

(a) SEC1 earthquake record

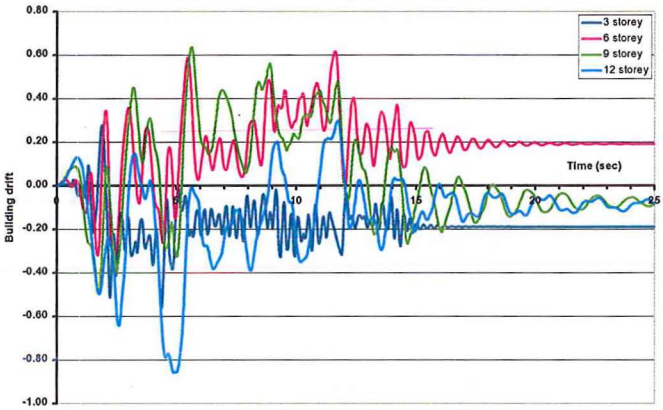

(b) General performance of the structures

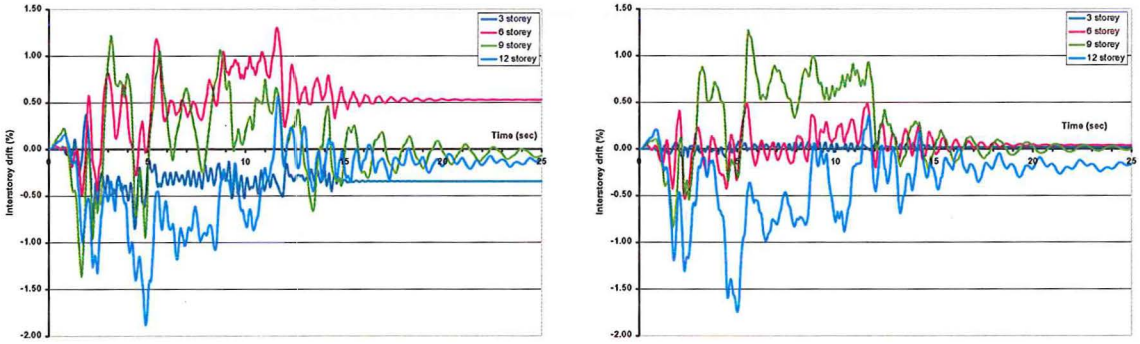

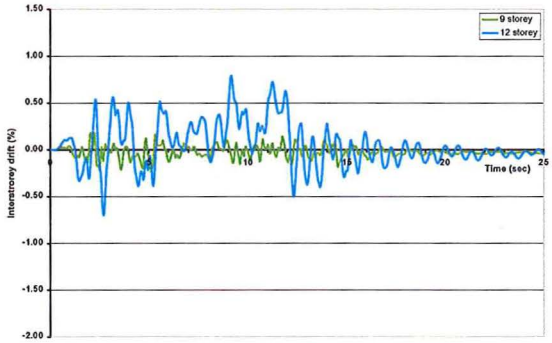

(c) Localised storey performance

A.14 SSF1 results

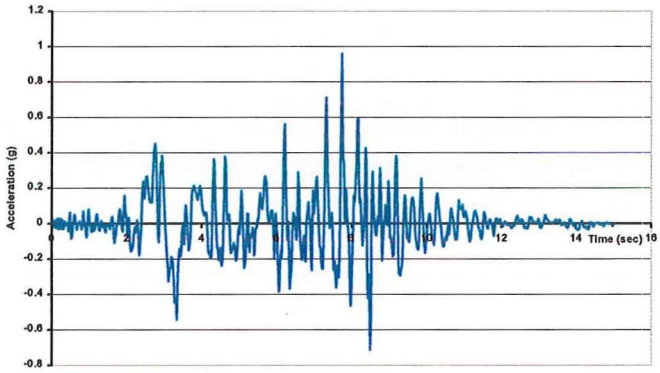

(a) SSF1 earthquake record

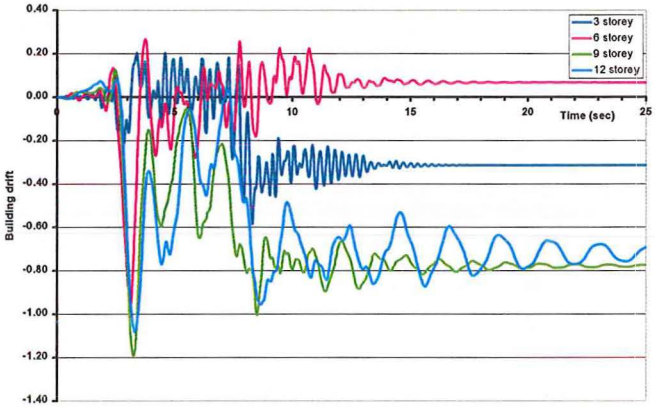

(b) General performance of the structures

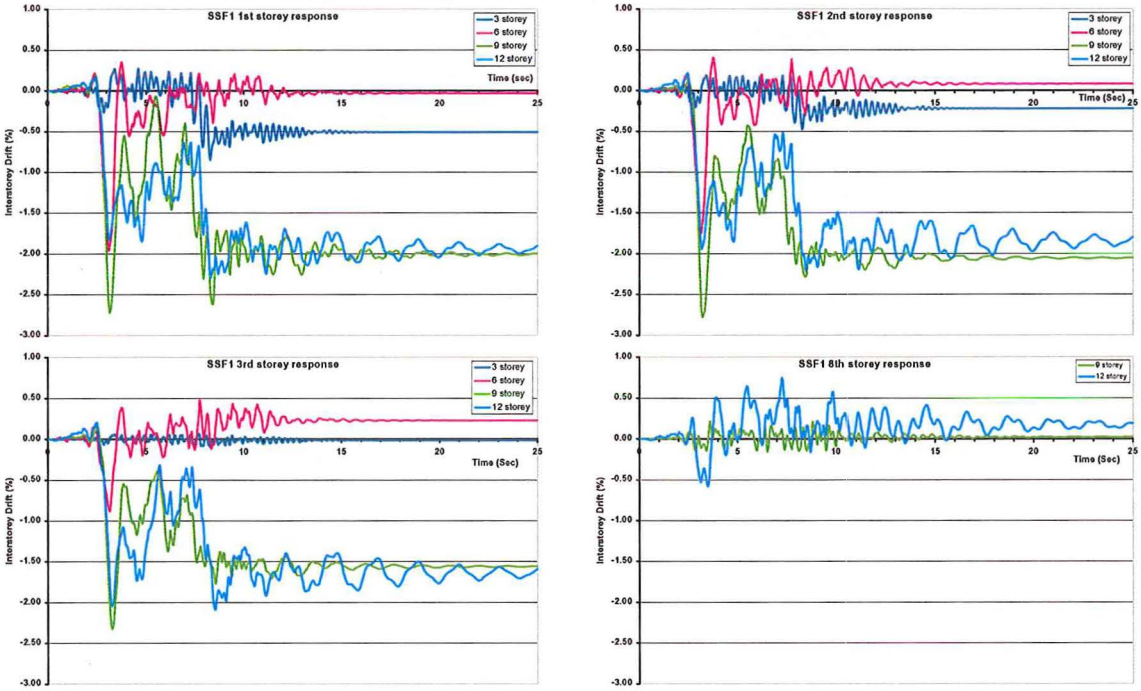

(c) Localised storey performance

A.15 SSF5 results

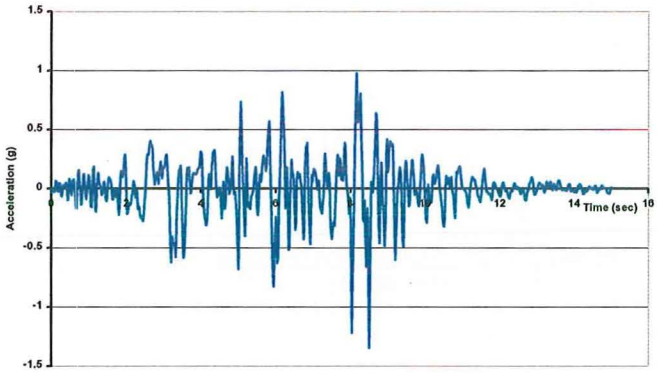

(a) SSF5 earthquake record

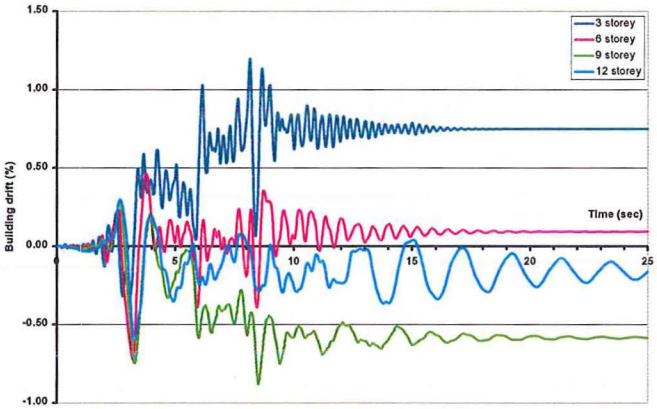

(b) General performance of the structures

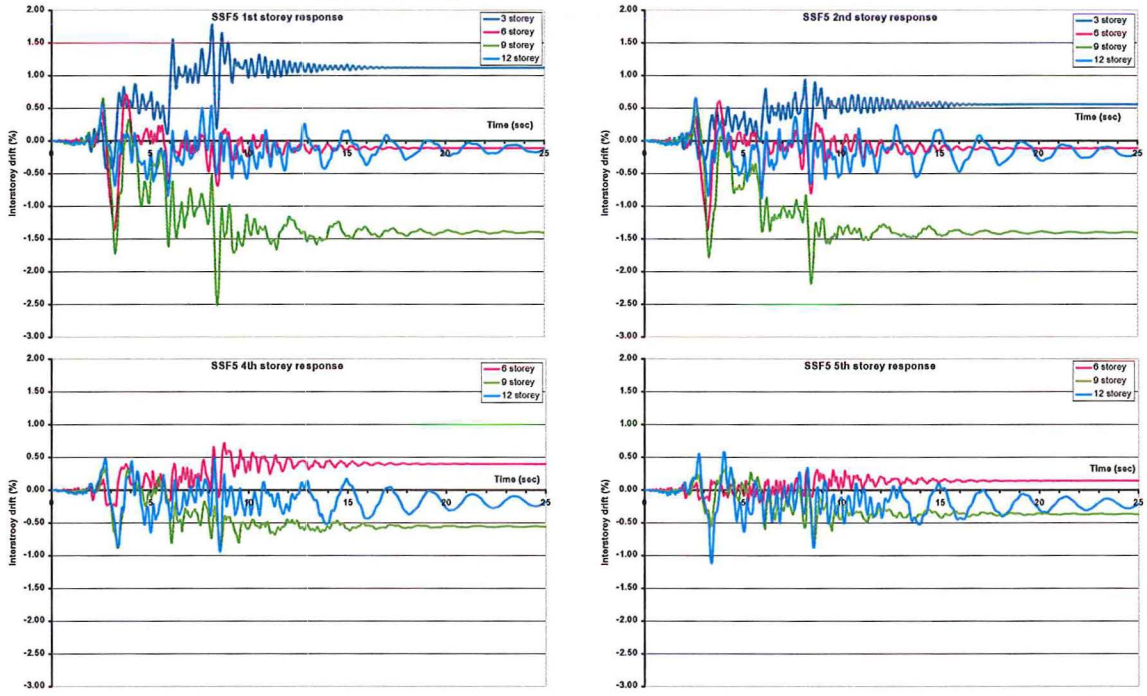

(c) Localised storey performance

A.16 SIV1 results

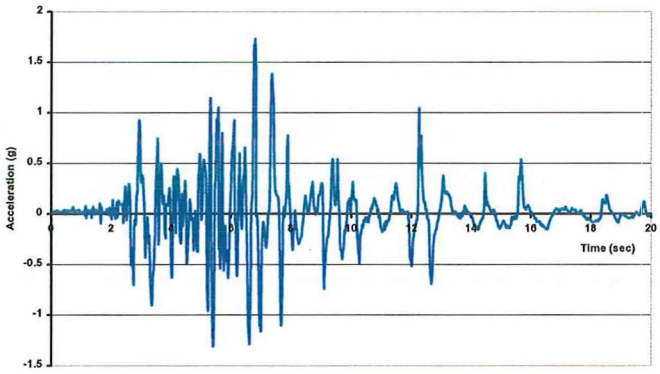

(a) SIV1 earthquake record

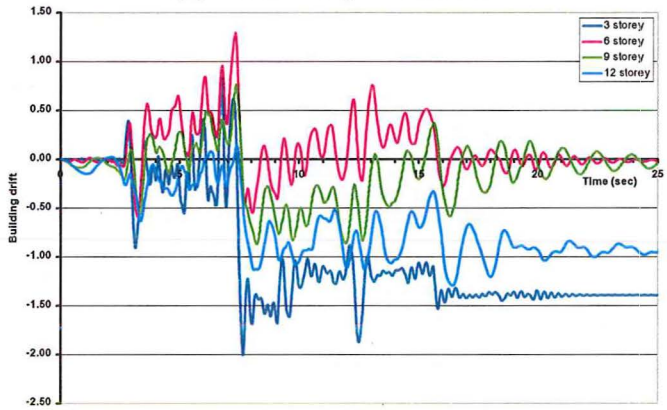

(b) General performance of the structures

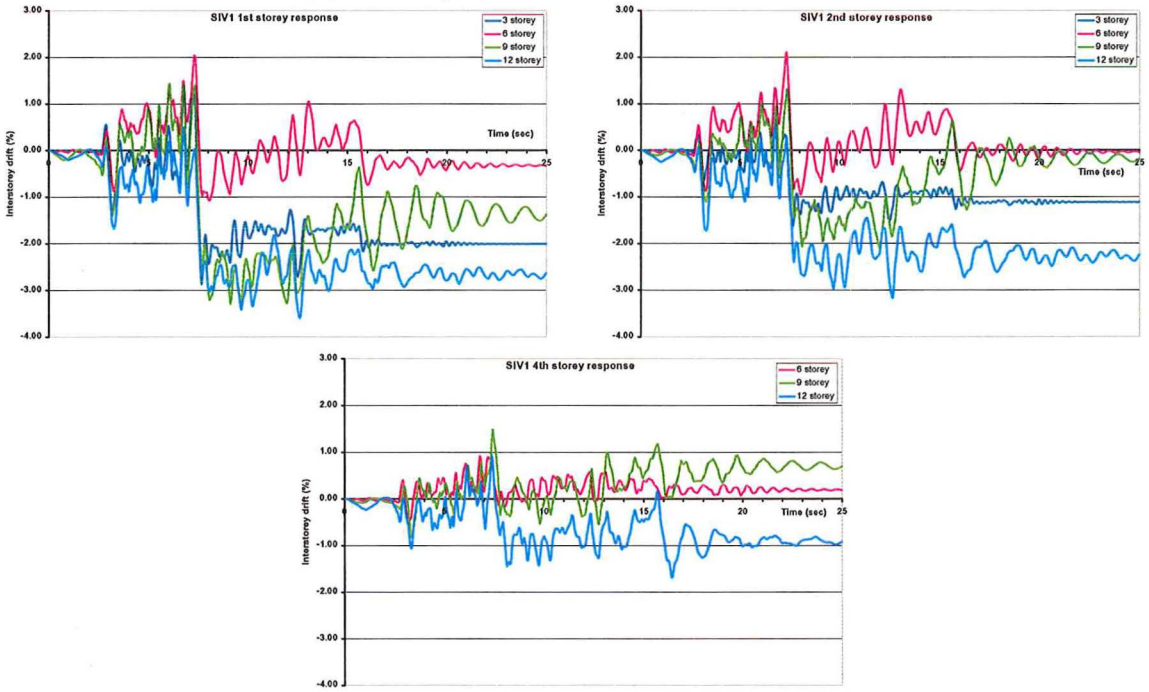

(c) Localised storey performance

A.17 SKB1 results

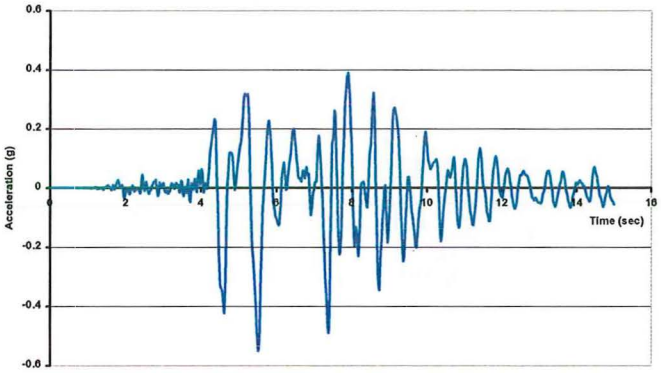

(a) SKB1 earthquake record

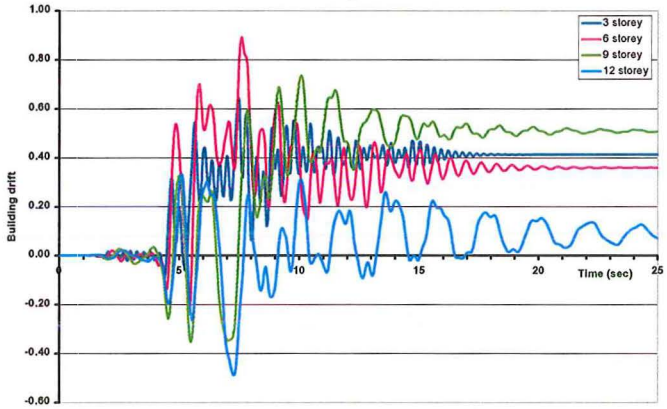

(b) General performance of the structures

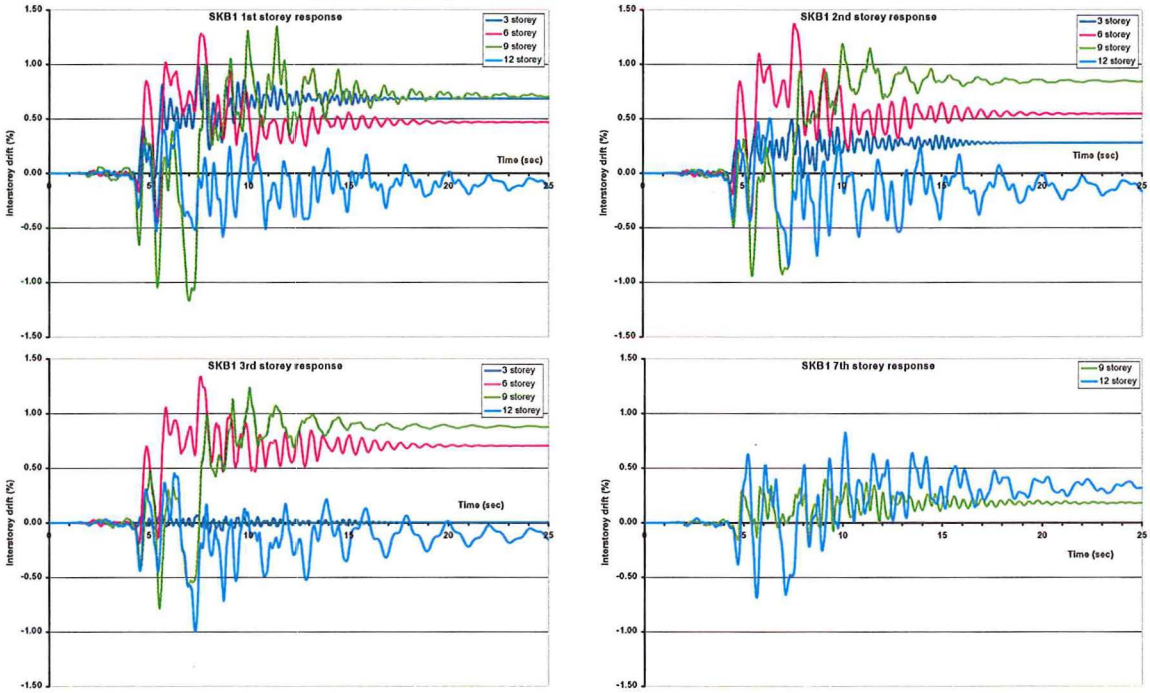

(c) Localised storey performance

A.18 SKB2 results

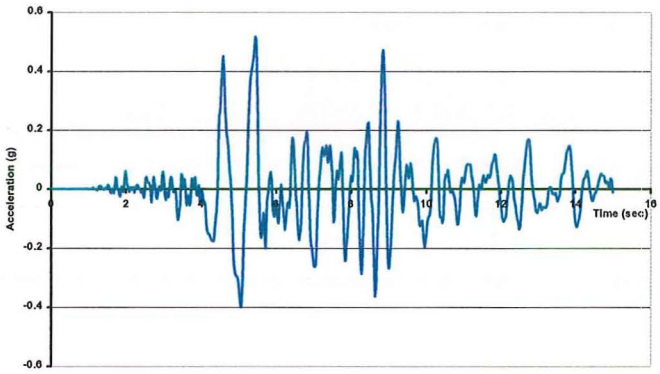

(a) SKB2 earthquake record

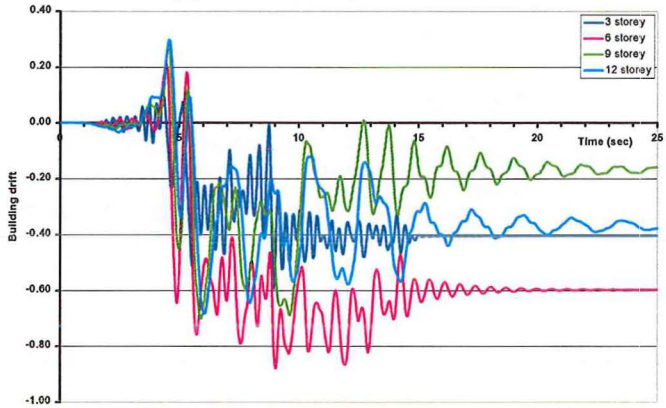

(b) General performance of the structures

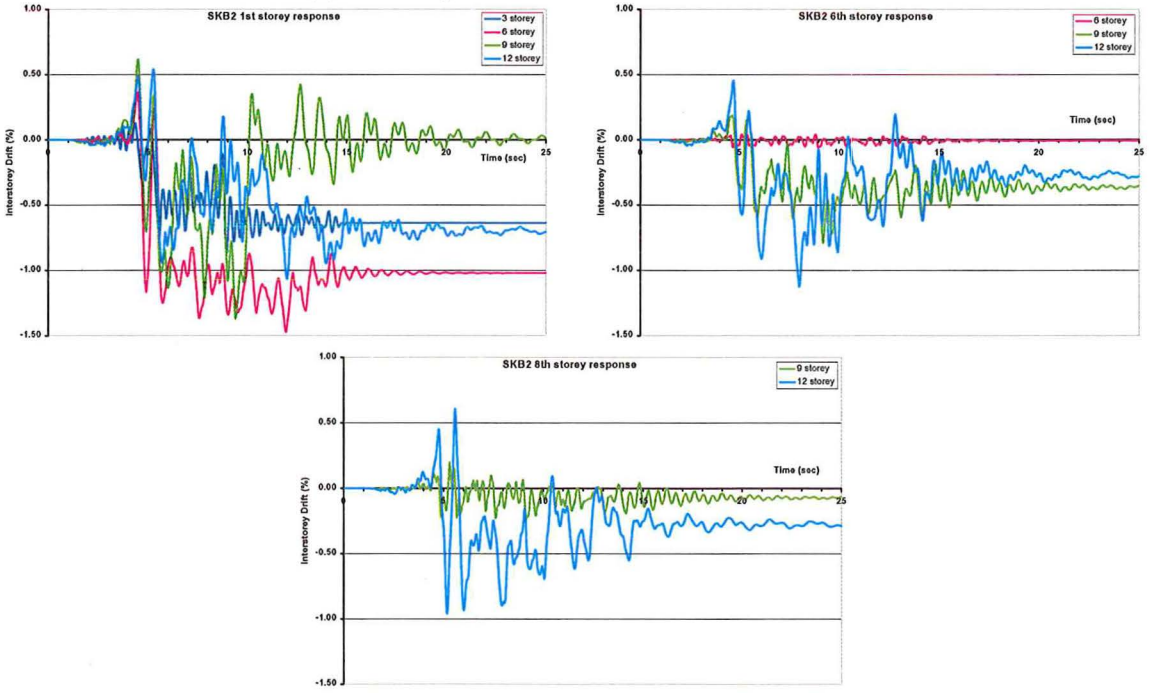

(c) Localised storey performance

A.19 SNOR1 results

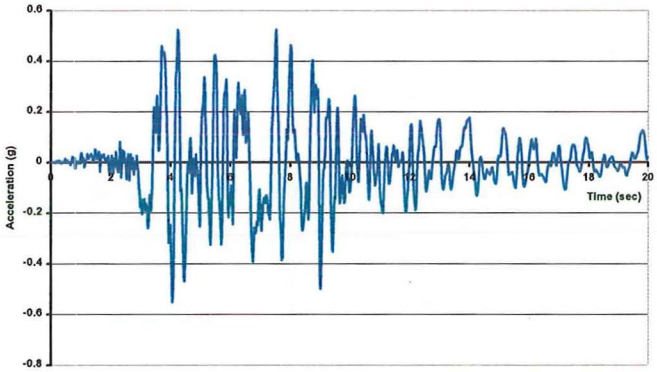

(a) SNOR1 earthquake record

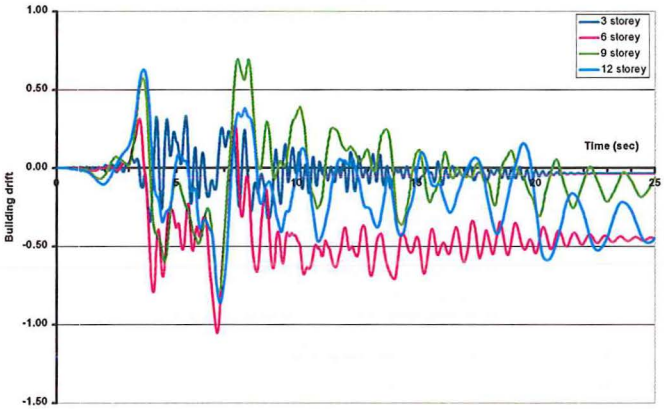

(b) General performance of the structures

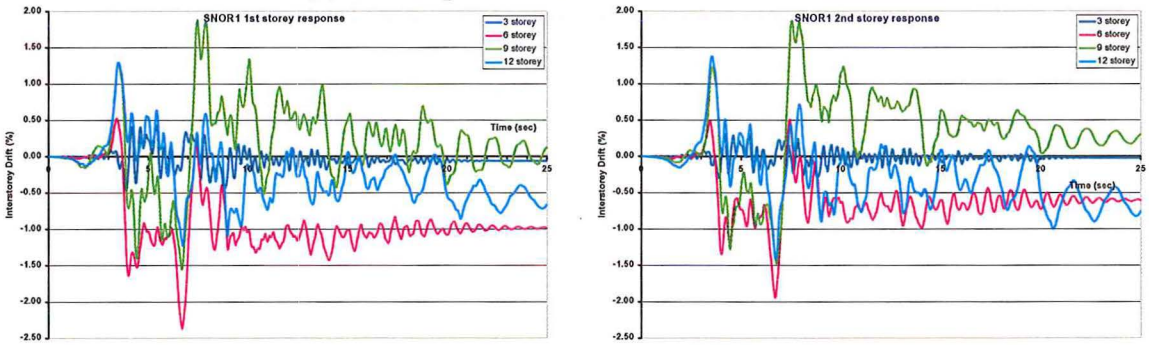

(c) Localised storey performance

A.20 SNOR2 results

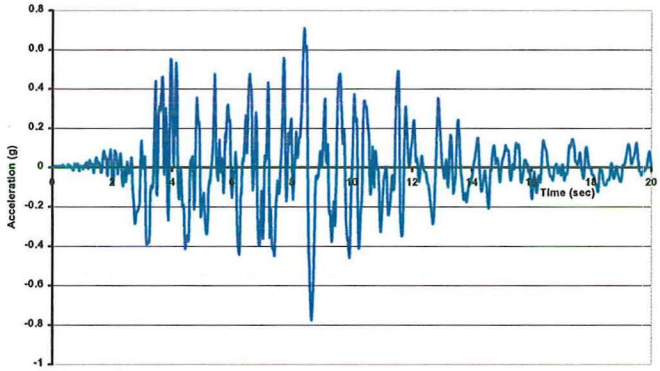

(a) SNOR2 earthquake record

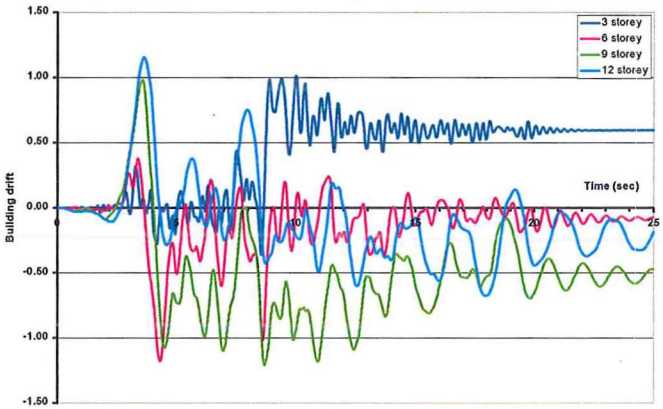

(b) General performance of the structures

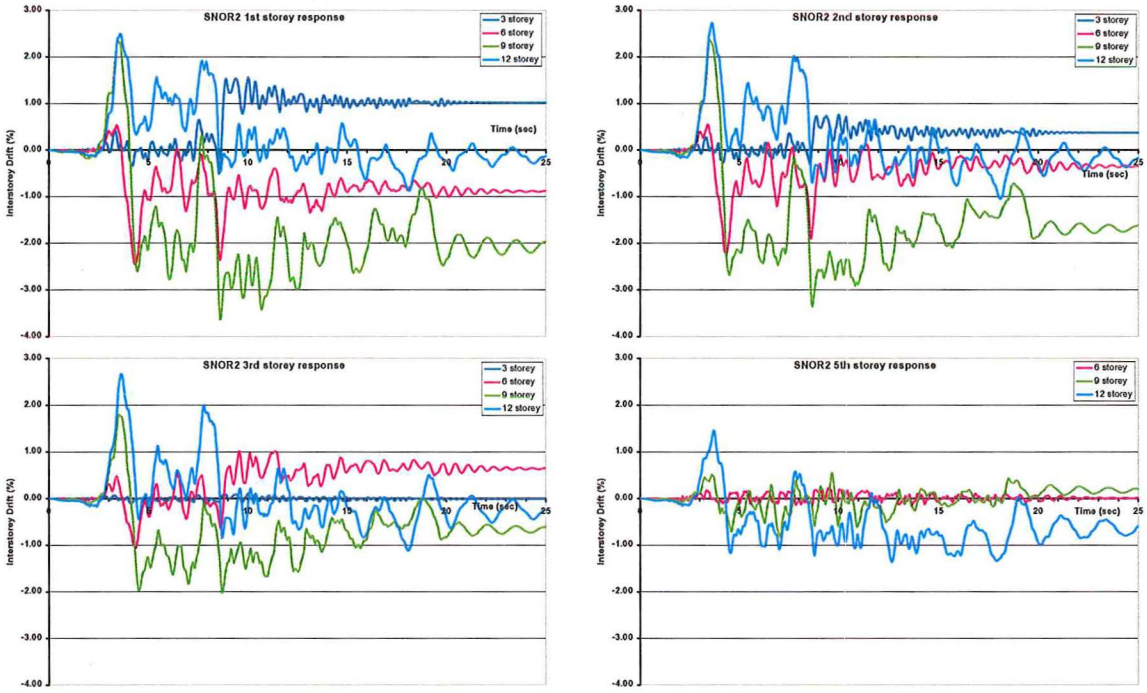

(c) Localised storey performance

This Page is Blank

Appendix B

Design of the Experiment

B.1 Design of the test specimen

B.1.1 Beam design

The beams were designed in accordance with the New Zealand Concrete Standard (NZS3101:1995). A typical longitudinal reinforcement ratio of 0.01 was assumed and then the rest of the design was based around that ratio. In order to ensure a weak beam-strong column mechanism formed several moment curvature analyses were undertaken to determine the possible overstrength actions for the beams. The sensitivity study undertaken analysed the affect that varying effective flange width, varying reinforcement properties and varying concrete strengths has on the beams overstrength actions.

Five different flange widths were investigated. The first being the beam only (i.e. no slab interaction), the second was activating the reinforcing mesh within the cast insitu diaphragm topping, the third was activating the prestressing tendons within the precast prestressed hollow-core units. The fourth was a combination of the second and third scenarios while the fifth scenario was activating the transverse beam starter bars.

Three different concrete strengths were analysed. The first was 30 MPa, as this is the specified 28 day compressive strength for the precast units. Two other concrete strengths (45 and 50 MPa) were also investigated, as the probability of the concrete strength being 30 MPa was quite low.

Combinations of varying reinforcing strengths were investigated to see what effect these had on the overall strength of the beam. The lower fifth percentile values for the reinforcing steel were used as well as the specified maximum allowable values as stated by the NZS3402:1989.

Before the sensitivity study was commenced a preliminary beam design was undertaken to determine the longitudinal and transverse reinforcement ratios. This sensitivity study investigated all the various combinations of overstrength actions that the beams could possibly experience. The maximum overstrength actions obtained from the study were then used to determine the finalised design actions for the remainder of the test specimen and load frame.

According to the NZS3101:1995 and Cheung et al (1991), a portion of the tension flange must be accounted for when determining the negative overstrength bending moment capacity of the beam. The extra tension steel only contributes to the tension reinforcement if it has developed its full capacity at the zone of interest. This increased negative overstrength moment was taken account of when ensuring that the columns did not hinge. Another scenario was also investigated to ensure the columns do not hinge, this case was when a large crack opens at the start of the hollow-core unit. This could quite possibly happen as the discontinuity between the hollow-core unit and the perimeter bream acts as a crack instigator. The length of the crack was taken to be the same as the effective flange width used above.

The discontinuity crack scenario gave a larger negative overstrength bending moment than the NZS3101:1995 recommendation so was used to design the columns and hence protect them against hinging ensuring that the appropriate post-elastic mechanism formed.

B.1.2 Column Design

A capacity design approach was used to design the columns. The overstrength moments and shears acting in the beam plastic hinge zones were used to determine the design actions for the columns. As explained in the beam design the amount of enhancement from the floor diaphragm to the beams flexural strength was unknown. To ensure a strong column weak beam mechanism formed it was crucial to give the central column extra protection to ensure the column did not hinge during testing. To achieve this, the central column had a relatively high percentage of longitudinal reinforcing consisting of 24-HD24 bars (ρ_l=0.022). Since the columns have 12 drossbach ducts per column, this particular column needed two bars per duct. Though this is not common practice it was considered acceptable for this test unit, as the columns performance was not a focal point. The only column performance criterion that this research required was for the columns not to form plastic hinges.

The longitudinal reinforcement at both the top and bottom of the columns was welded onto the column end plates. This ensured the endplates were not pulled off during testing due to the load being transferred from the load frame connection brackets to the columns.

B.2 Loading Frame Design

B.2.1 Primary Loading Frame

Upon completion of the test specimen design it was possible to design the load frame. Since all the overstrength actions were known, as well as the way in which the specimen was loaded, it was possible to size the load frame.

The design of the loading frame was carried out in accordance with the Steel Structures Standard (NZS 3404:1997). A key component to the design of the load frame was to keep all the components as similar as possible for ease of construction. The load frame was designed to withstand a force of 1000 kN being applied from each of the hydraulic actuators. The load frame consists to two sets of scissor arms.

Figure B-1 shows one of the scissor load frames. Each individual loadarm consists of a W12-202 section. A spherical bearing was used to attach the loadarm to the column connection bracket so that all the rotations that occur during testing can be accommodated.

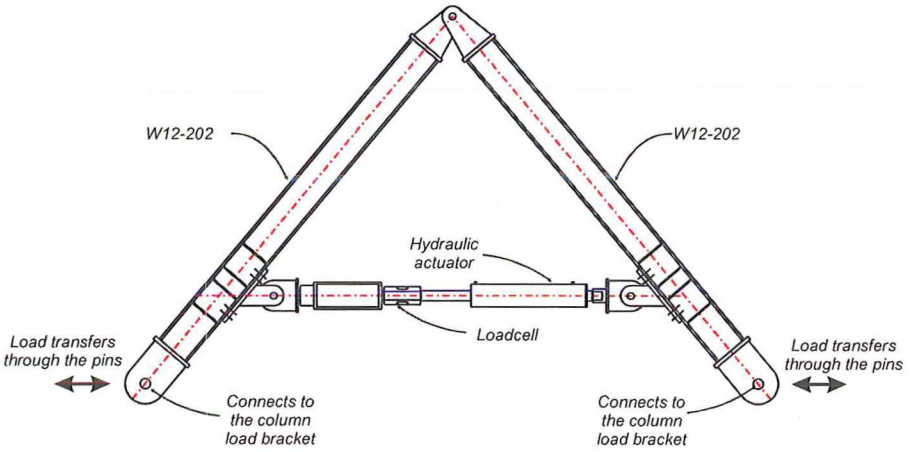

Figure B-1 A typical scissor load frame

Since both ends of the scissor load frame are attached to the columns by spherical bearings a prop (Figure B-2) is required, to be attached to the load frame, to stop the frame from dropping and resting against the opposite load frame. If the load frame was to rest against the opposite load frame there is a possibility that the system could bind. The prop is placed on a load skate so that the inward and outward movement of the frame is accommodated. The load transferred through this prop is only the self-weight of the load frame, hydraulic actuator and loadcell.

Figure B-2 Location of the load frame props

The load frame has been designed so that it can be unbolted from the longitudinal frame and placed onto the transverse frame.

B.3 Secondary loading frame

As the test specimen is taken into the inelastic range, the flexural strength in the positive and negative plastic hinges will not be equal. This could be due to either the slab reinforcement contributing to the beams flexural strength or one of the plastic hinges degrading in strength. When the beam flexural strengths become unbalanced, the diagonal loading frame is unable to maintain equilibrium. To ensure equilibrium is maintained, a secondary loading frame is required.

Due to the large number of components intersecting at the columns point of inflections, it would be extremely difficult to construct the specimen with all the centrelines meeting at the same point. A study was undertaken to see how the loads in the specimen would change if a different connection was used for both the primary and secondary loading frames. The study showed that the variance in loads was little and that at full displacement the centrelines were out of alignment by less than 3% of

the column height. This difference was insignificant allowing the specimen to be designed using separate pins for all the connections. Using separate pins allowed smaller components to be used and many of the components could be duplicated for other parts of the specimen.

B.3.1 Design considerations

A suite of analyses was carried out to determine the maximum expected load in each leg of the secondary loading frame (SLF). The analyses looked at the effect that a varying number of degraded hinges within the bent had on the applied loading. The number of hinges that degraded varied between zero and four. All the analyses were carried out using an elastic structural analysis programme. Since the test specimen will not remain elastic, a pushover type analysis was undertaken to represent this.

The pushover analysis was undertaken in the following way. The test specimens coordinates, end supports, properties and members were all inputted into the programme. An analysis was run and the applied loads were altered until one of the beams reached its yield moment. Once this value was obtained all the applied loads and member forces were recorded and a pin (release) was placed at the location of the expected yielding. Again, the loads were increased until the next member yielded. This process was continued until a mechanism formed. Summation of all the applied loading determined the applied base shear and loads within the SLF.

The initial loadcase consisted of every hinge reaching its full capacity. This determined the maximum load required in the primary load frame and the respective loads in the SLF. The process was then rerun with 50% strength degradation in all the plastic hinge zones. Since the hinges appeared weaker, due to the strength degradation, the load required to form the mechanism was less than if each hinge was

at full capacity. The assumption was then made that the difference in load, in the primary loading frame, between the two mentioned load cases needed to be transferred through the SLF. This is because the load that was initially resisted by the super-assembly would be resisted by the SLF when the plastic hinges degrade in strength. The initial loads in the SLF due to the first loadcase were also added.

Several load scenarios were examined to determine a design envelope of forces for the SLF. The different load scenarios focussed on varying amounts of strength degradation within the plastic hinge zones. This method of determining the SLF loads is conservative, it had the added advantage that the members designed would be relatively stiff ensuring minimal axial lengthening and shortening of the SLF occurred during the experimental programme.

The diagonal arms of the SLF were designed for both compression and tension. Varying effective lengths were used to design these members. Localised buckling of the members was designed for as well as the entire frame buckling.

At the connection where the SLF attaches onto the column face, a spherical bearing was attached to allow for all the displacements expected during the test. The connection is pinned to the column to allow the column to sway during loading. The connection was also required to handle some out of plane rotation to occur when the column is displaced transversely to the main longitudinal frame, hence the reason for using a spherical bearing.

The vertical arm of the SLF was made from two different section profiles, a rigid Universal Channel section and a steel bar. The steel bar is required, as it has to pass through the centre of the perimeter beam. A steel bar was chosen, as this would keep the beams penetration as small as possible (Figure B-3). When designing this vertical member for compression it was too conservative to design it assuming the

entire member was this reduced section. Designing the member in that manner meant that the member was so large it was impossible to make it fit through the beam. Using a more realistic design philosophy made it possible to determine the reduced sections effective length. When the vertical member was split into two portions, a UC and steel bar section, the assumption was made that all the deformation occurred in the steel bar as the ratio of the two sections moment of inertias was greater than five.

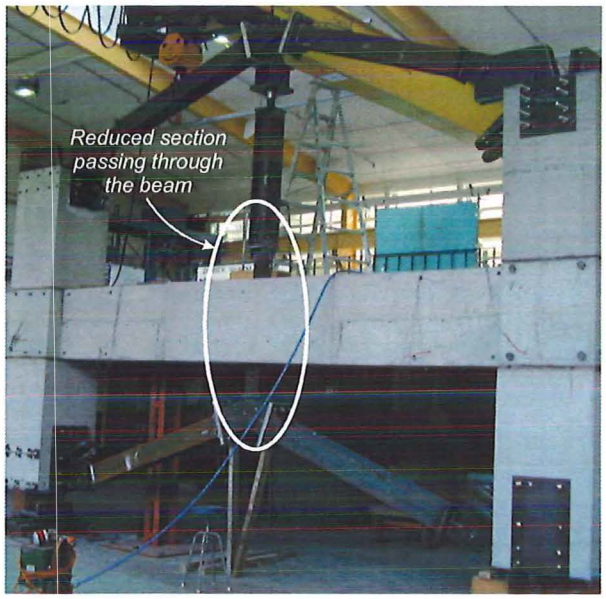

Figure B-3 Photo of the reduced section within the vertical leg of the SLF

Also, within the vertical member of the SLF a pin type arrangement was added to eliminate the vertical member from being subjected to torque. During testing there is a possibility that the columns will not remain parallel with each other in the out of plane context. If this did occur, and the pin was not present, then the vertical member would be subjected to a torque, causing premature yielding of this member. In order for the pin to be able to rotate the bearing stress at the pins connection with the vertical member has been limited to a stress much less than 150 MPa. The threaded pin also allowed some vertical adjustment to the assembly of the SLF.

To allow the reduced vertical member to be passed through the beam the bottom pinned connection will be bolted on after the member has been passed through the beam (Figure B-4).

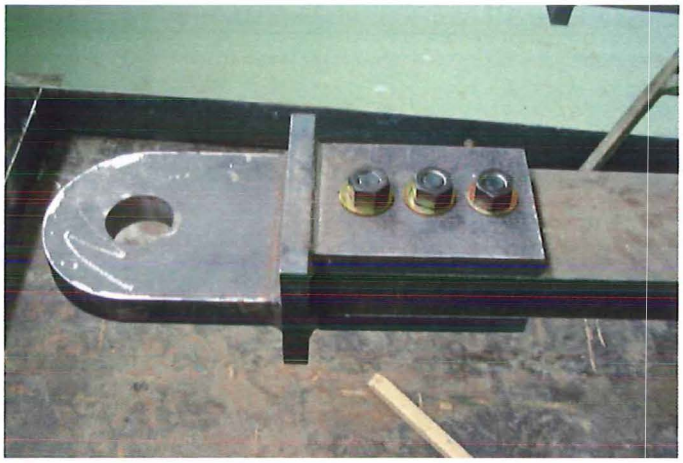

Figure B-4 Bolted connection at the base of the vetical leg of the SLF

B.4 Transverse loading

The primary and secondary loading frames are able to load the super-assemblage in both the longitudinal and the transverse directions. The central column cannot be loaded in the same way in the transverse direction as the floor diaphragm does not allow the scissor load arms to be attached, therefore a new load frame is required. To displace the central column a hydraulic actuator is attached to the top and bottom of the column (Figure B-5). The load frame consists of a Universal Channel and hydraulic actuator placed between two spherical bearings at the top of the column and just the actuator and the spherical bearings at the bottom.

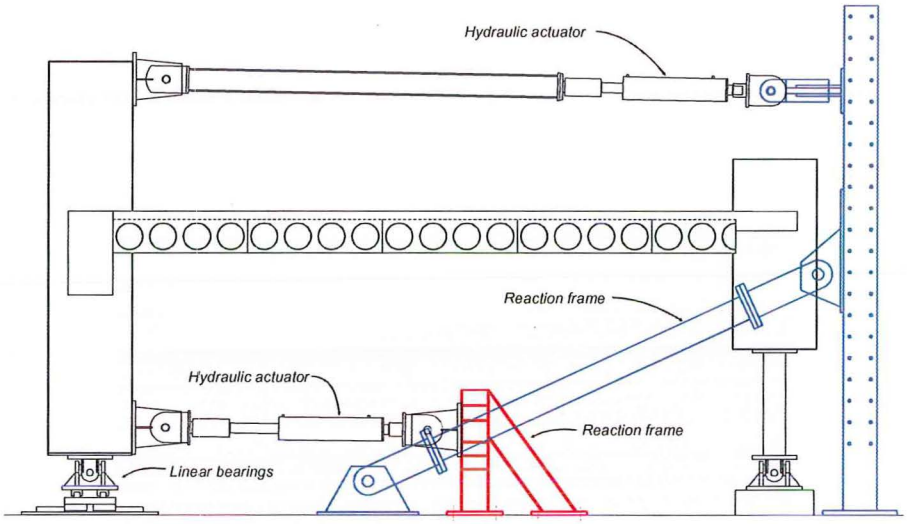

Figure B-5 Loading the central column during phase II

B.5 Special considerations

B.5.1 Catch frames

For safety reasons catch frames were placed under the floor so that if the floor failed and dropped during testing it would not collapse to the ground. These frames were placed each side of the central column as can be seen in Figure B-6(a). At each end of the super-assembly, steel angles were bolted onto the transverse beam face to act as catch brackets (Figure B-6(b)).

(a) Large catch frame either side of the central column to catch the floor if it failed

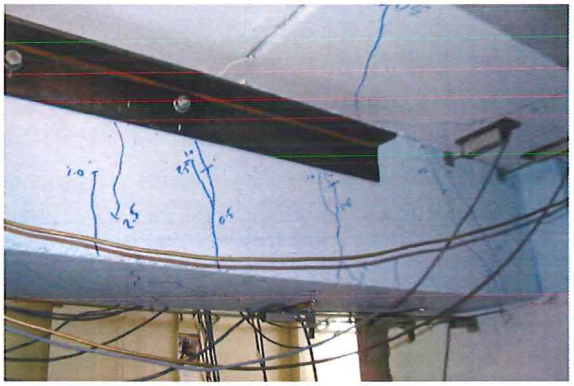

(b) Steel angle bolted to the supporting beam to catch the floor if it loses it seat

Figure B-6 Catch frames placed to catch the floor if it failed during the test.

B.5.2 Universal joint connection

To simulate the columns point of inflection and to allow the column to incline, for either direction of loading, a universal joint was placed at the bottom of each column. The universal joint comprised of a double-pinned connection detail (Figure B-7). The top half of the universal is supported on two legs, which are, seated a 60mm diameter steel pin. This steel pin allows the rotation to occur in one direction. The centre of the 60mm pin is housed within a larger 200mm diameter pin that allows rotation in the other direction. The larger pin is also supported by the bottom half of the universal joint on two legs. These legs allow the pin to rotate when the test specimen is displaced.

The design of the universal joint was governed by bi-axial loading. Although the super-assemblage is not being loaded in that manner, it was designed for those loads as future experiments may include bi-axial loading.

Figure B-7. The universal joint set up

B.5.3 Front bearing design

The bearings required at the base of the three front columns were required to be capable of allowing unrestrained movement in any direction parallel to the floor, while withstanding both compression and tension loading, this was achieved by using linear bearings. A grillage of rails, in both the x and y directions, were set up to allow the direction of movement required. The running blocks that are attached to the ball rails are able to withstand both tension and compression loading. The running block (Figure B-8(a)) units have a series of ball races within its head unit. Each of the ball bearings within the ball races has been designed so that it will have four points of contact that keeps the contact stresses low allowing large loads to be carried. Figure B-8 shows the assembly and completed column base set up.

Design actions and displacement

A design envelope for the axial loads in the bearings was obtained from the analysis undertaken when designing the primary and secondary loading frames. This envelope also included bi-axial loading encase future testing required it.

The expected movement that the linear bearings had to accommodate could be slit up into two components. The first is movement due to the test specimen being displaced. The bearing rails must be long enough to accommodate the movement associated with an interstorey drift displacement of 5%. The second form of movement expected is due to beam elongation. Previous investigations (refer to Chapter 3) found that the magnitude of elongation, per plastic hinge, ranges between 2-5% of the beam depth. This corresponds to a value of 17-38mm of elongation per plastic hinge zone. The value allowed for in the bearing design was 50mm elongation per hinge.

(a) Greasing the running block

(b) Lowering the top section of the double acting rollers into place

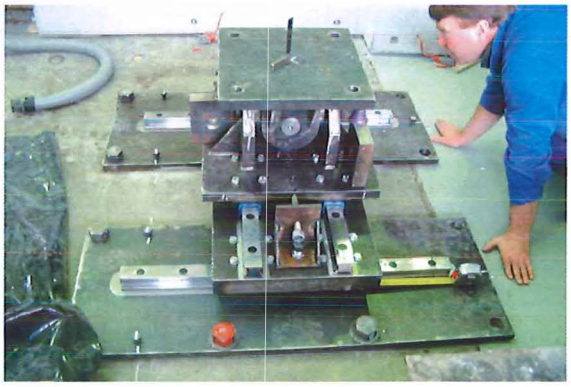

(c) Completed bearing

Figure B-8 Photos showing both the individual components of the base connection as well as the completed unit

B.5.4 Rear bearing design

Since the back frame of the test specimen is supposed to represent the remainder of a building these columns would be fixed against displacement in the y direction but free to displace in the x direction. Rather than using the ball rail bearings, it was possible to use a standard set of steel pins between two plates (Figure B-9), as the back columns would remain in compression throughout the duration of the testing programme.

(a) Base plate and steel rollers in place

(b) Lowering the top section into place

(c) Complete assembly

Figure B-9 Steel pin roller connection

The back columns were also placed on universal joints.

B.5.5 Fixed central back column

The central back column was fixed to the ground to ensure the super-assemblage was tied to the strong floor since the remainder of the columns were on rollers. This was

particularly essential since the back hydraulic actuators were not self-equilibrating, thus this fixity was required to transfer the applied shear from the back two hydraulic actuators to the ground.

B.6 Specimen construction and erection

As far as was possible the test specimen was constructed as if it was on a building site. The only difference was that some of the longitudinal reinforcement had strain gauges or other instrumentation stubs attached. No extra care was taken to ensure the workmanship was of a higher standard than what would normally take place on the construction site.

B.6.1 Concrete test Units

The precast components required to build the test specimen were constructed in three stages. The columns and beams were cast on a casting bed in the laboratory while the hollow-core units were cast at Stresscrete.

Column units.

Both the top and bottom column units were cast with drossbach ducts placed full height of the column. Typically, drossbach ducts are only placed in the tops of columns, not both, but since this research is only focusing on the beam performance the ducts were cast full height to ease construction.

Beam units

The precast beam units were cast as half units. The bottom half of the beams were cast along with the full beam column joint. Figure B-10(a) shows a typical beam unit. The central regions of the beams were not cast to allow a mid-span lap splice to be cast when the beam units were erected. The mid-span splices, the top half of the beams

and the floor diaphragm topping were all cast as one after the specimen had been erected (Figure B-10(b)).

(a) Precast components have been erected

(b) After the topping and lap splices have been poured

Figure B-10 Photographs of the super-assembly

B.6.2 Hollow-core units

Care was taken to ensure the hollow-core units used in project were in a condition similar to what would be expected on a typical building site. The units were not rejected if they have any of the following: incorrect surface roughness; split webs in the units (Figure B-11a); holes in the flanges of the units (Figure B-11b); or significant strand pull in (Figure B-11c).

(a) Edge crack and split web of the hollow-core unit

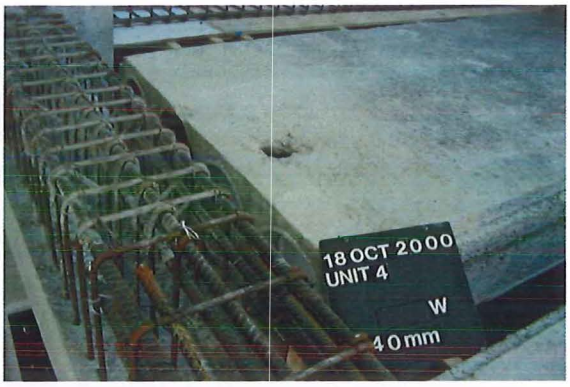

(b) A hole in the top of the hollow-core unit

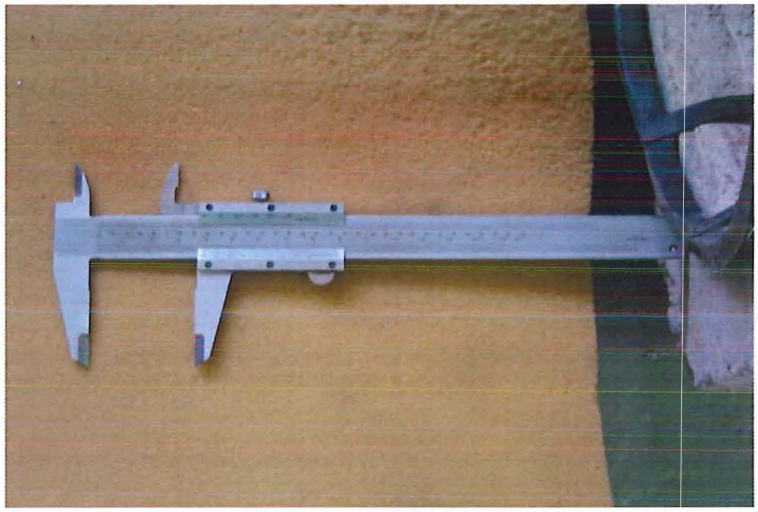

(c) Relaxed prestressing strand, nearly 40 mm

Figure B-11 Photographs showing the defects seem on the hollow-core units used

B.7 Photographs of the construction of the precast components

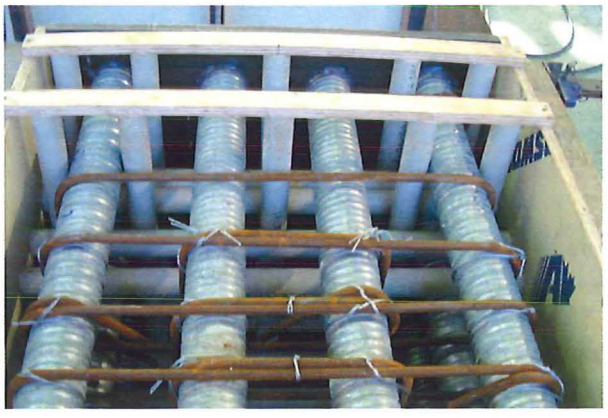

(a) Close up showing ducts within the columns

(b) Column ready to be placed in the formwork

(c) Columns ready to be poured

(d) Corner beam unit being placed in the formwork

(e) Typical corner beam column joint ready for pouring

(f) Pouring one of the corner units

(g) The hollow-core bed before the units is poured. Note: The strands are in place and stressed

(h) Pouring the hollow-core unit

(i) Close up showing the difference between the brushed and un-brushed top of the hollow-core unit

B.8 Photographs assembling the super-assembly

(a) The precast components being set out on the floor

(b) Erected columns ready for the beams to be attached

(c) Lowering a beam into place

(d) Lowering the top of the column into place

(e) All the precast components are in place

(f) A completed lap splice before the formwork is attached

(g) Preparing for grouting of the drossbach ducts

(h) Grouting the ducts

(i) Lifting the hollow-core units into place

(j) Positioning the last hollow-core unit

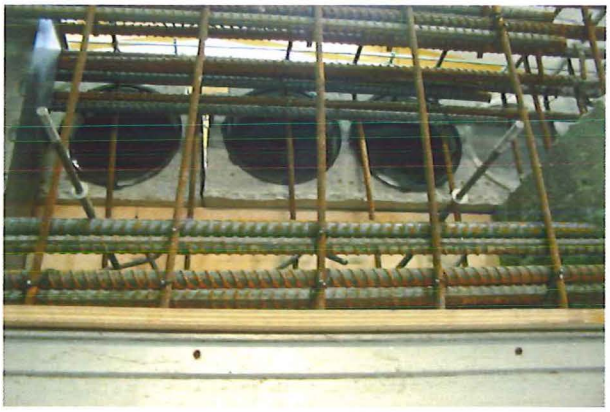

(k) Close up showing the hollow-cores seat length

(l) Formwork in place, ready for pouring

(m) Topping ready to pour

(n) Reinforcing mesh lap splice

(o) Close up showing the starter bars connection detail

(p) Pouring the topping

(q) Finishing off the topping

(r) Complete test specimen just after the formwork has been stripped

B.9 Construction of the Loading and Secondary frames.

The fabrication of the frames was carried out in the Civil Engineering machine shop. This fabrication process was very comprehensive and took several months to complete. All the components that required profile cutting were cut by an outside contractor and then assembled and welded in the Laboratory.

B.10 Photographs showing the erection of the loading frames

(a) Positioning the bottom of the secondary loading frame

(b) Bottom portion of the frame assembled

(c) Most of the secondary loading frame attached

(d) Assembled secondary loading frame

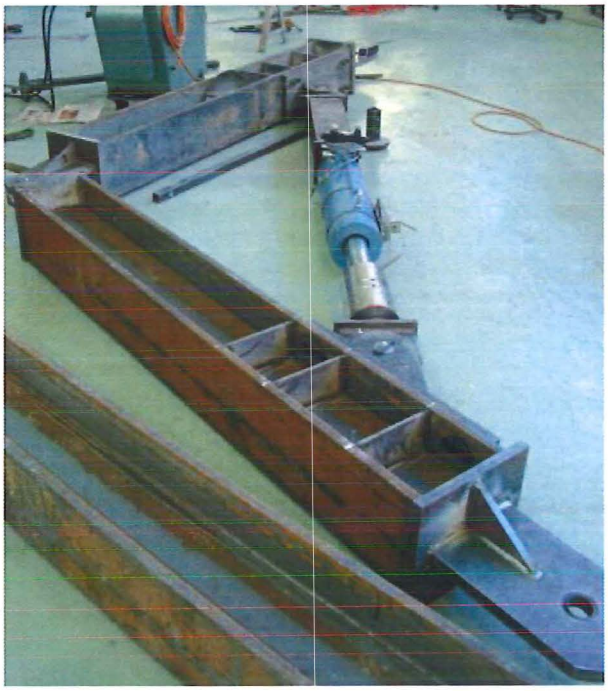

(e) Load frame ready to be attached

(f) Lifting of the load frame into position

(g) Large load frame attached

(h) Large load frames attached, hydraulic actuators are removed to allow the small load frame to be attached

(i) Complete assembly

(j) Positioning the back hydraulic actuator

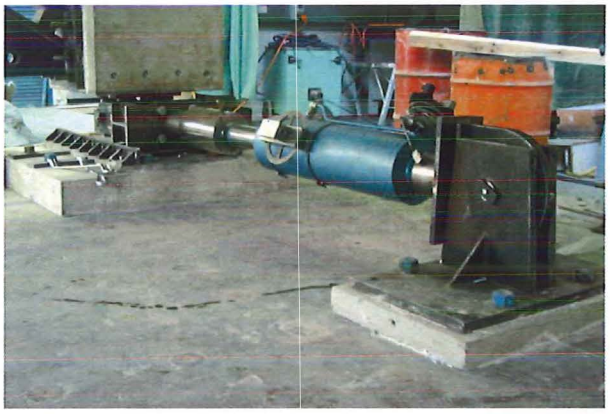

(k) Back hydraulic actuator in position

B.11 Materials

B.11.1 Reinforcing Steel

The tensile properties of the reinforcement used were obtained by monotonic loading in an Avery Universal testing machine. Table B.1 shows the experimental results. Each of the results shown is the average value obtained from the testing of three samples.

Table B.1 Measured properties of the reinforcing tests used in the test specimens.

Type	f_y (MPa)	E_s	E_{sh}	ε_{sh}	ε_{su}	f_u (MPa)	Location
D24	294	238	5.6	0.012	0.11	451	Beam reinforcement
HD24	429	231	4.4	0.015	0.12	582	Column reinforcement
HD28	455	263	8.3	0.008	0.08	620	Column reinforcement
HD12	508	210	4.5	0.011	0.12	680	Starter bars
R12	317	140	2.9	0.009	0.17	438	Stirrups
665 Mesh	-	195	-	-	0.019	654	Diaphragm reinforcement

Figure B-12 shows the individual stress versus strain plots for the various bars tested.

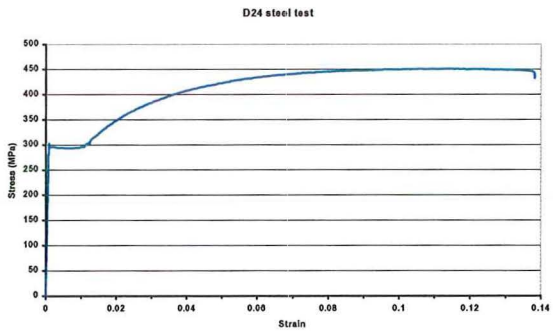

(a) Longitudinal beam reinforcement

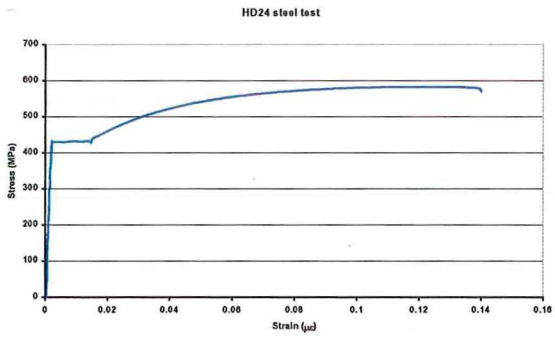

(b) Column reinforcement

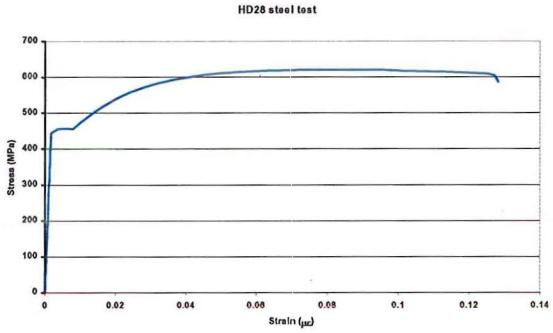

(c) Column reinforcement

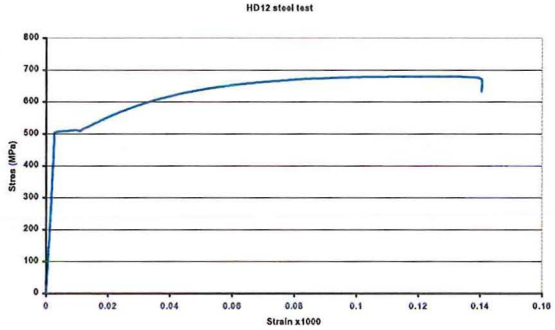

(d) Starter bars

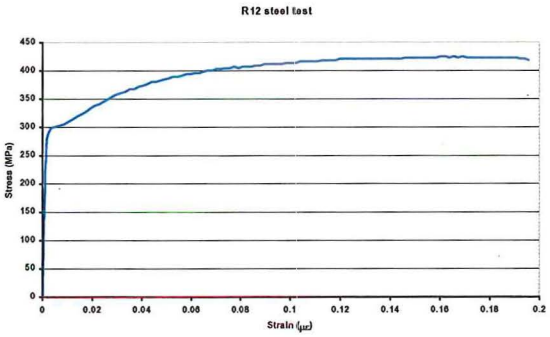

(e) Transverse reinforcement

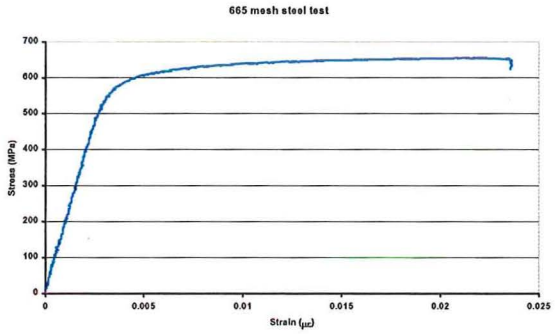

(f) Topping reinforcement

Figure B-12 Individual steel test results

B.11.2 Concrete

The concrete was supplied by Firth Industries Limited. The concretes target 28 day strength was 30 MPa and the maximum aggregate size was 19 mm. Table B.2 shows a summary of the properties for the different portions of the test specimens. Each of the results shown is the average value obtained from the testing of three samples.

Table B.2 Measured concrete properties.

Pour Number	Pour Location	Mix Code	28 day strength	Start of test strength	Age at start of test	End of test strength	Age at end of test
1	Columns	3019AW	40.5	45.7	602	45.6	708
2	Columns	3019AW	38.0	48.5	599	51.9	705
3	Columns	3019AW	27.8	34.7	594	33.6	700
4	Columns	3019AW	31.9	40.8	591	41.8	697
5	Beams	3019AW	36.0	46.7	581	47.1	687
6	Beams	3019AW	31.8	40.6	557	41.0	663
7	Topping	3019AWP	30.2	36.2	437	40.2	543

B.12 Electronic valve controller

The remainder of the flow charts used to are shown below.

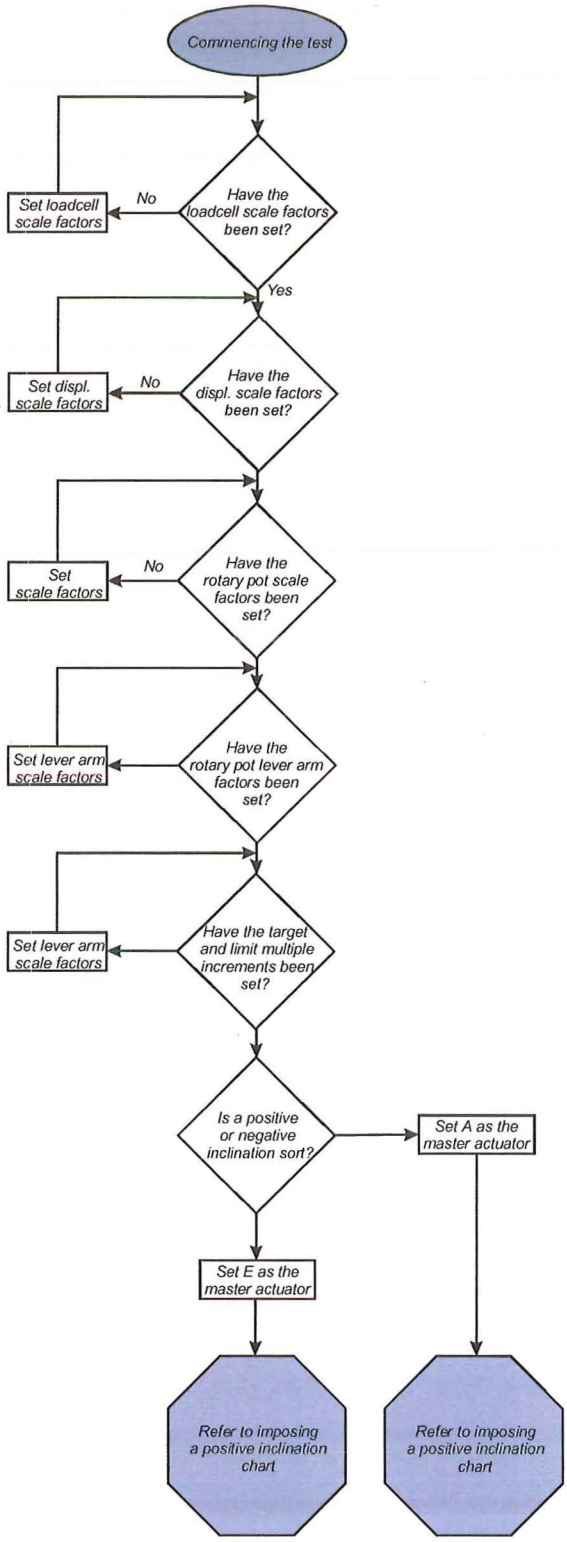

Figure B-13 Initial set up flow chart

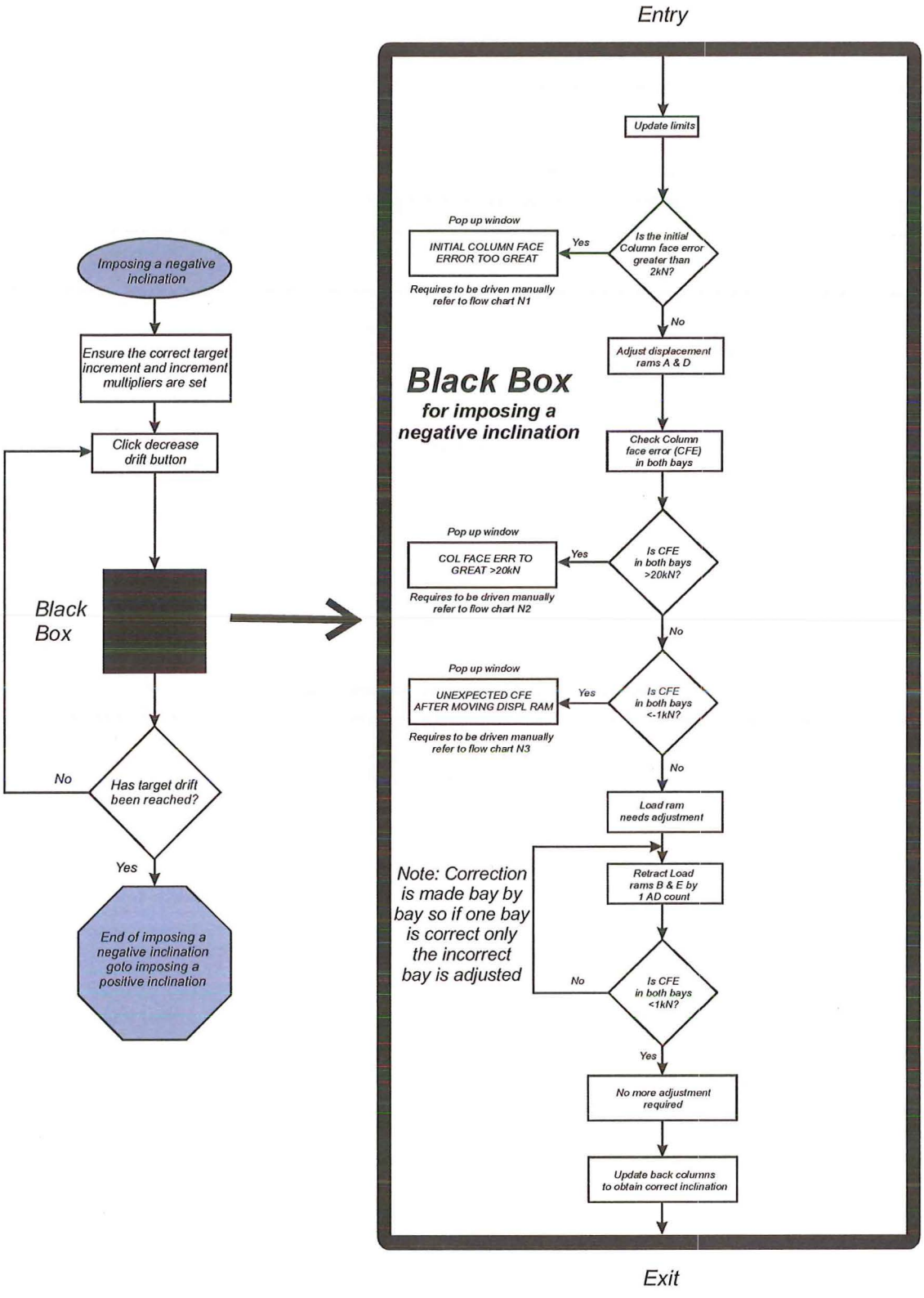

Figure B-14 Flow chart required to impose a negative drift

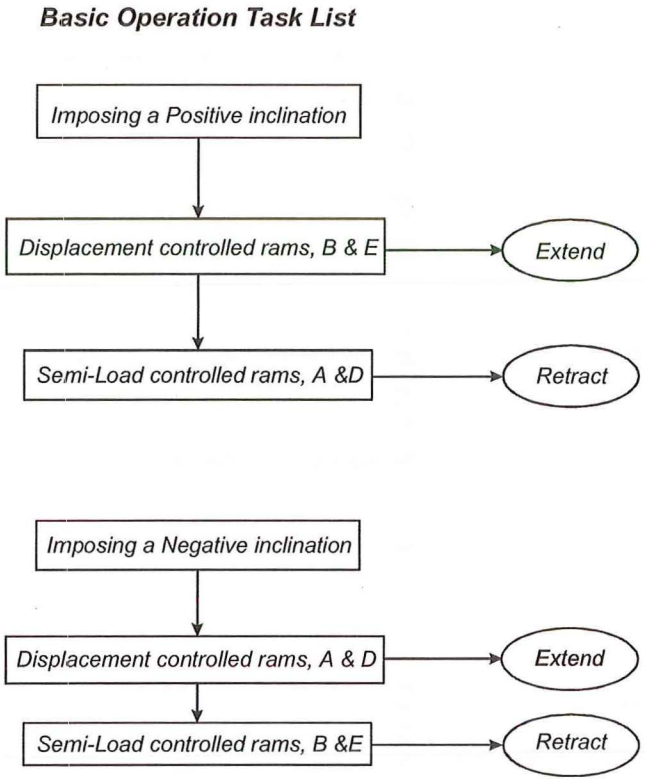

Figure B-15 Basic operation of the controller

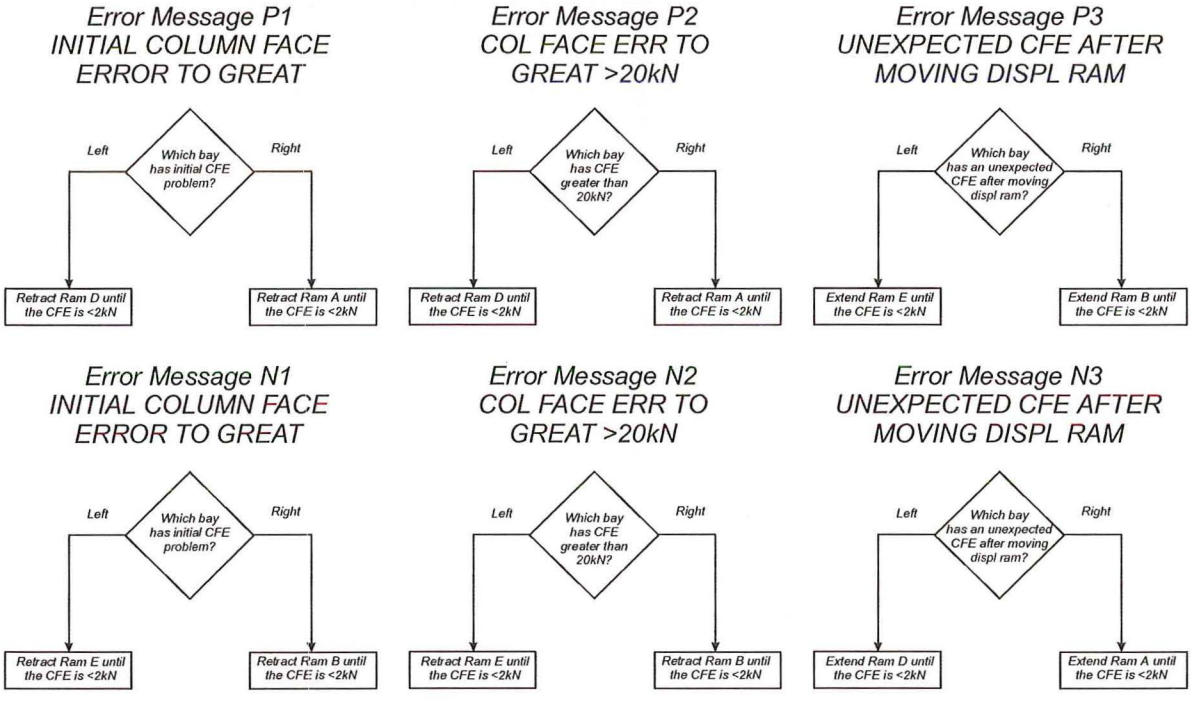

Figure B-16 Additional flowcharts to allow any loading errors to be corrected

B.13 References

Cheung P. C., Park R and Paulay T, 1991, *Seismic Design of Reinforced Concrete Beam Column Joints with Floor Slab Support*, Research Report 91-4, Department of Civil Engineering, University of Canterbury, Christchurch, New Zealand, 328 pp

NZS3101:1995, *Concrete Structures Standard,* Standards New Zealand, Wellington New Zealand

NZS3402:1989, *Steel bars for the reinforcement of concrete*, Standards New Zealand, Wellington New Zealand

NZS3404:1997, *Steel Structures Standard,* Standards New Zealand, Wellington New Zealand

This Page is Blank

Appendix C

Construction Drawings

Note: Drawings are no longer to scale as they have been reduced to fit within this document.

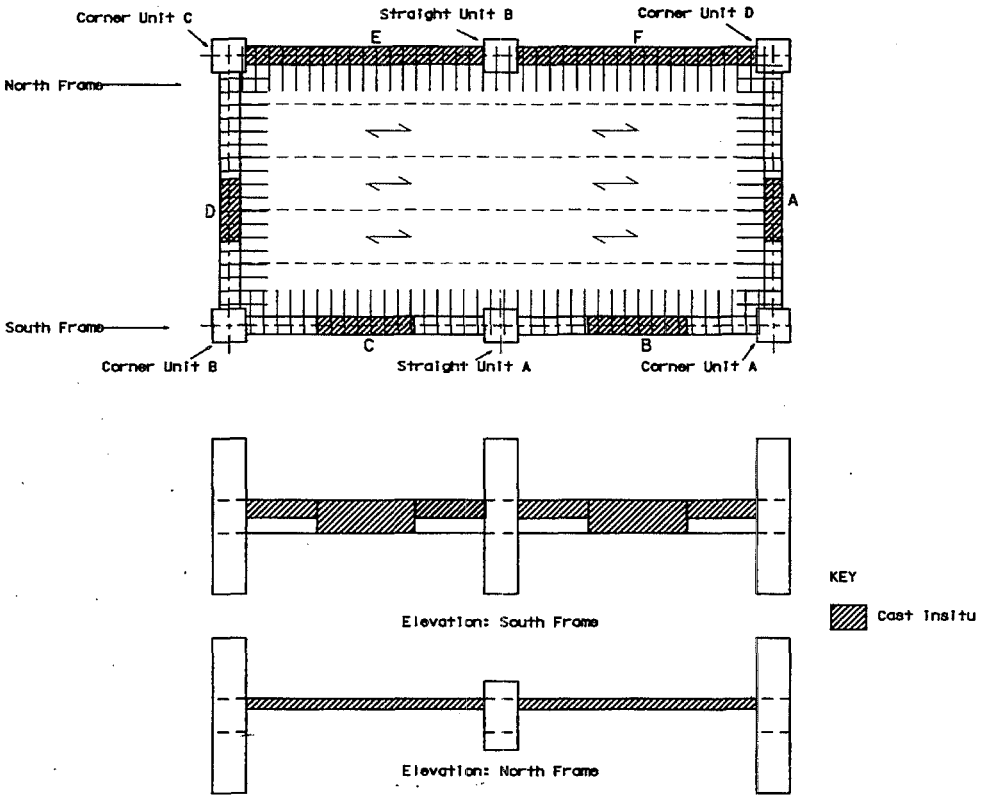

Department of Civil Engineering University of Canterbury Christchurch, New Zealand	Plan and Elevation of the Precast units	Drawn: JGM Date: 27/4/99 Revision: B Scale: 1:100	Drawing No. P0

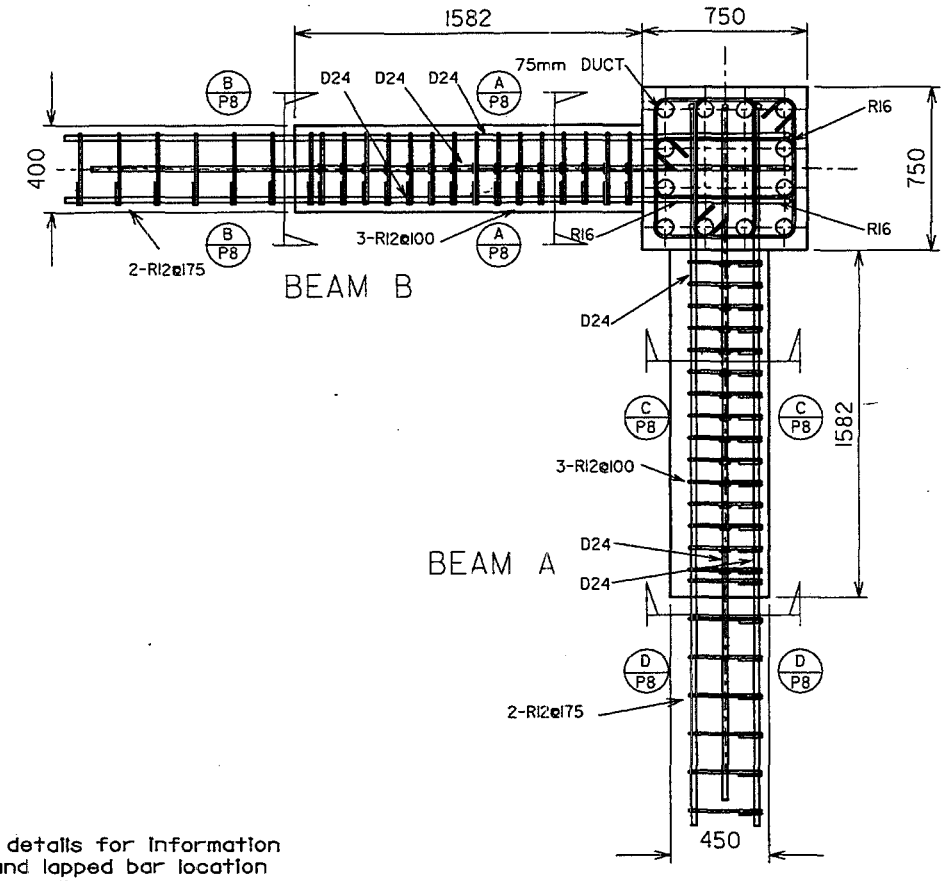

Notes:
Construction tolerance = +/-15mm
fy=300MPa
f'c=30MPa
Min cover=35mm

Note:
Refer to lap splice details for information regarding stirrup and lapped bar location within the in-situ lap splice

Department of Civil Engineering University of Canterbury Christchurch, New Zealand	FABRICATION DRAWINGS Plan of corner unit A	Drawn: JGM Date: 9/3/00 Revision: F Scale: 1:20	Drawing No. P1

Notes:
Construction tolerance
= +/-15mm
fy=300MPa
f'c=30MPa
Min cover=35mm

Beam B
Reinforcement
dimensions

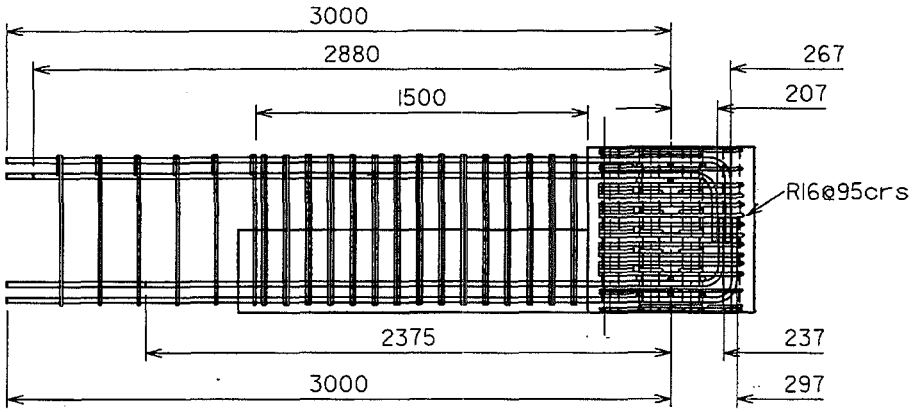

Beam B
Concrete
dimensions

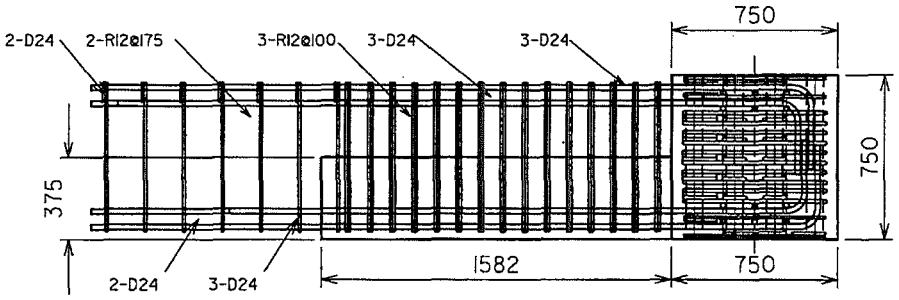

Department of Civil Engineering University of Canterbury Christchurch, New Zealand	FABRICATION DRAWINGS Elevation of precast corner beam B	Drawn: JGM Date: 15/11/99 Revision: E Scale: 1:20	Drawing No. P2

Notes:
Construction tolerances =+/-15mm
All dimensions mm
fy=300MPa
f'c=30MPa
Min cover=35mm
20mm gap between 1st B/C joint stirrup and longitudinal rebar

Beam A
Concrete &
Reinforcement
dimensions

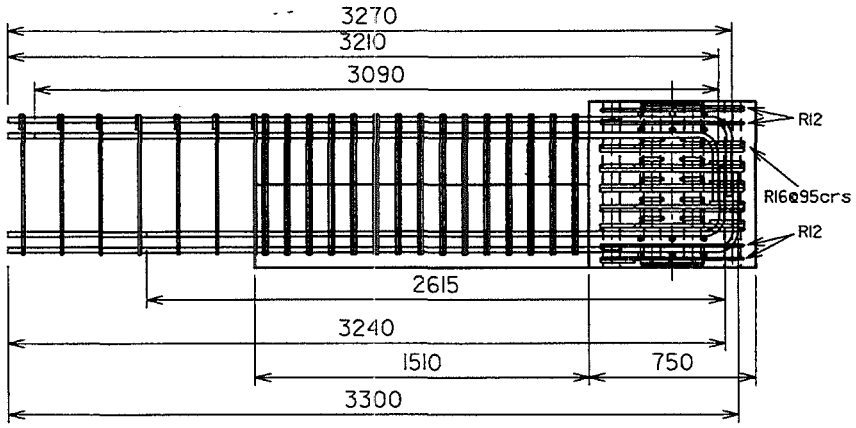

Department of Civil Engineering University of Canterbury Christchurch, New Zealand	FABRICATION DRAWINGS Elevation of precast beam A	Drawn: JGM Date: 9/3/00 Revision: E Scale: 1:20	Drawing No. P3

Notes:
Construction tolerance
= +/-15mm
fy=300MPa
f'c=30MPa
Min cover=35mm

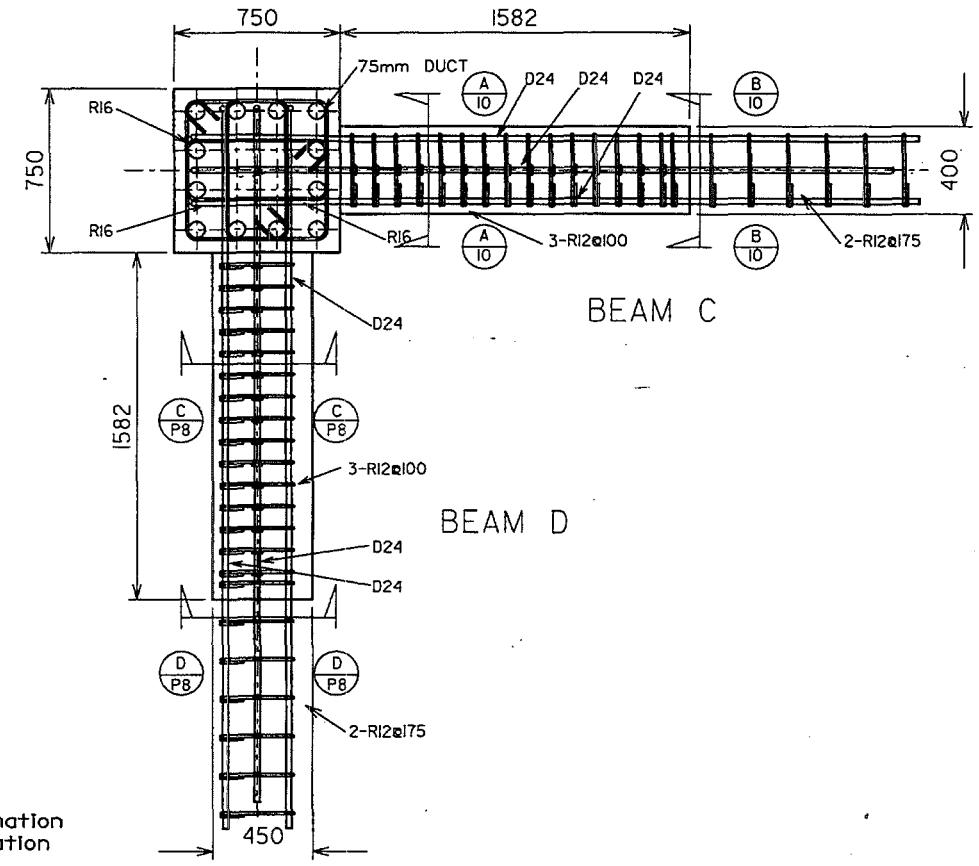

Note:
Refer to lap splice details for information regarding stirrup and lapped bar location within the in-situ lap splice

Department of Civil Engineering University of Canterbury Christchurch, New Zealand	FABRICATION DRAWINGS Plan of corner unit B	Drawn: JGM Date: 9/3/00 Revision: F Scale: 1:20	Drawing No. P4

Beam C
Concrete
dimensions

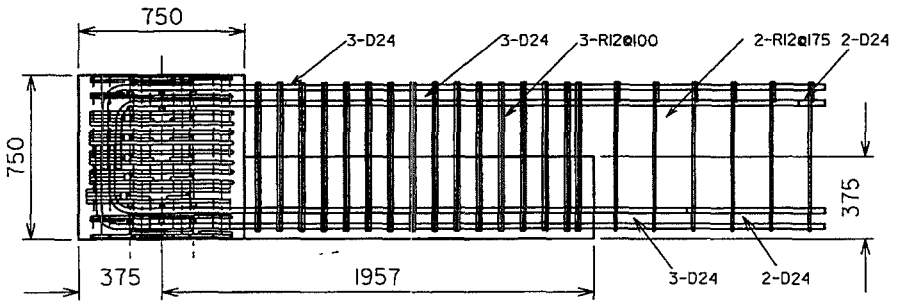

Notes:
Construction tolerance
= +/-15mm
fy=300MPa
f'c=30MPa
Min cover=35mm

Beam C
Reinforcement
dimensions

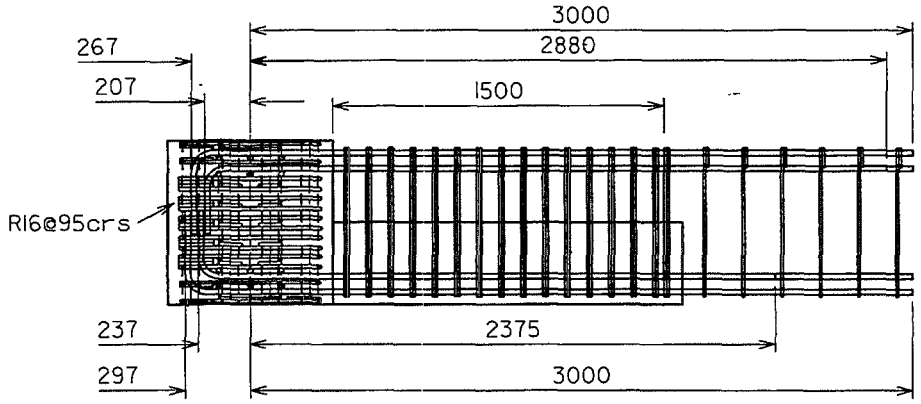

Department of Civil Engineering University of Canterbury Christchurch, New Zealand	FABRICATION DRAWINGS Elevation of precast beam C	Drawn: JGM Date: 9/3/00 Revision: F Scale: 1:20	Drawing No. P5

Notes:
Construction tolerance
= +/-15mm
fy=300MPa
f'c=30MPa
Min cover=35mm

Beam D
Concrete &
Rinforcement
dimensions

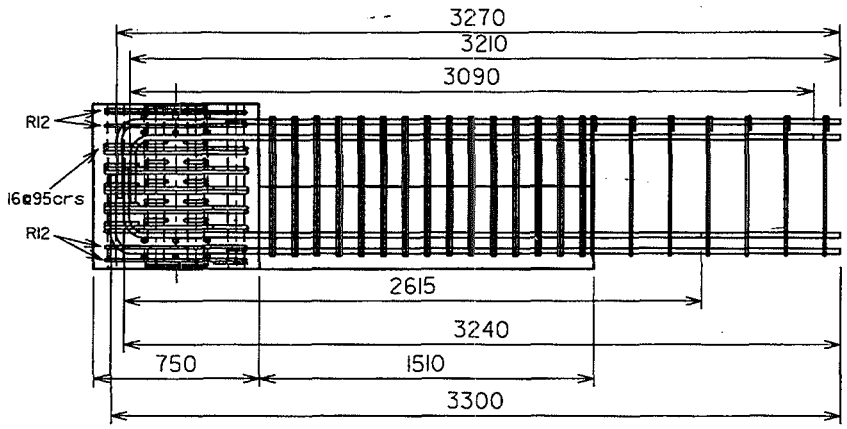

Department of Civil Engineering University of Canterbury Christchurch, New Zealand	FABRICATION DRAWINGS Plan and Elevation of precast unit D	Drawn: JGM Date: 15/11/99 Revision: E Scale: 1:20	Drawing No. P6

Note:
Refer to lap splice details for information regarding stirrup and lapped bar location within the in-situ lap splice

Notes:
Construction tolerance = +/-15mm
fy=300MPa
f'c=30MPa
Min cover=35mm

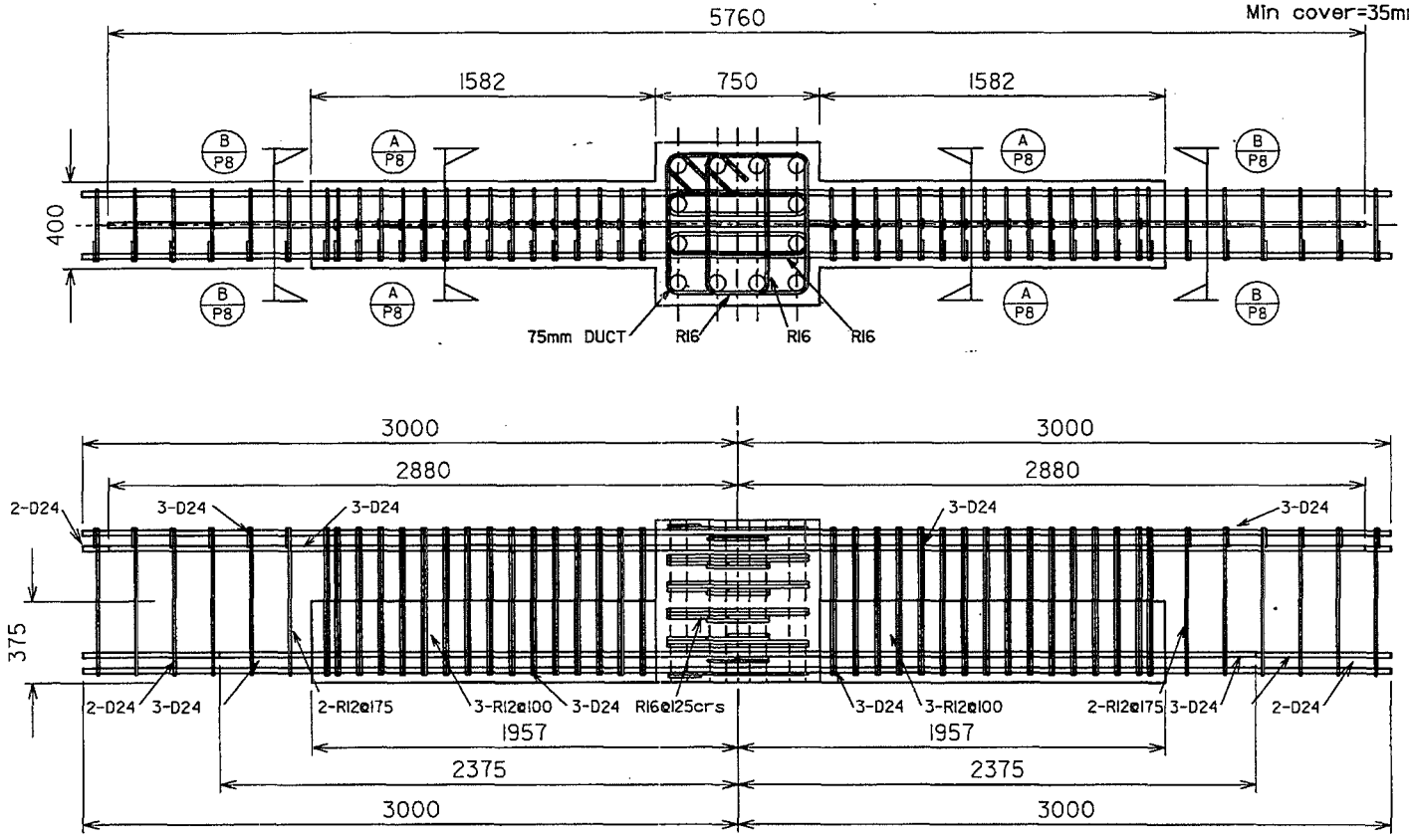

Department of Civil Engineering University of Canterbury Christchurch, New Zealand	FABRICATION DRAWINGS Plan and Elevation of Straight unit B	Drawn: JGM Date: 9/3/00 Revision: F Scale: 1:20	Drawing No. P7

Note:
Refer to lap splice details for information regarding stirrup and lapped bar location within the in-situ lap splice

Notes:
Construction tolerance = +/-15mm
fy=300MPa
f'c=30MPa
Min cover=35mm

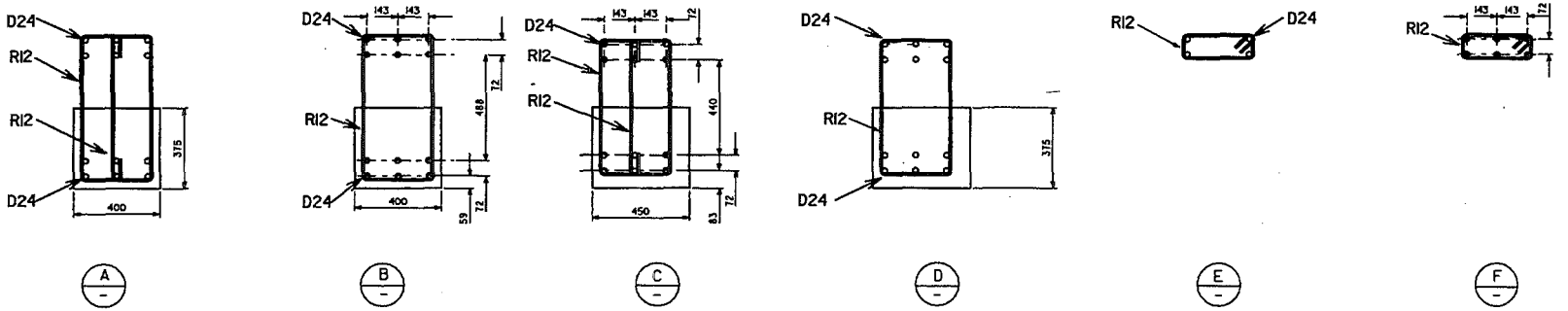

Department of Civil Engineering University of Canterbury Christchurch, New Zealand	FABRICATION DRAWINGS Beam cross section details	Drawn: JGM Date: 9/3/00 Revision: F Scale: 1:20	Drawing No. P8

Notes:
Construction tolerance
= +/-15mm
fy=300MPa
f'c=30MPa
Min cover=35mm

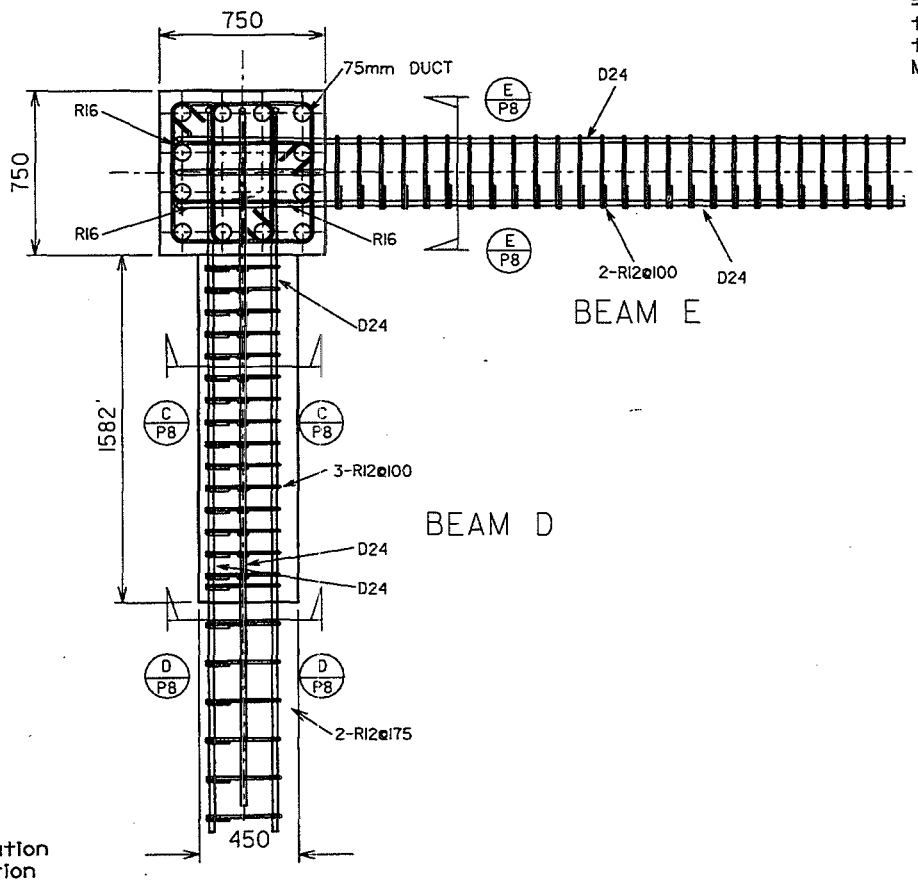

Note:
Refer to lap splice details for information regarding stirrup and lapped bar location within the in-situ lap splice

Department of Civil Engineering University of Canterbury Christchurch, New Zealand	FABRICATION DRAWINGS Plan of corner unit C	Drawn: JGM Date: 9/3/00 Revision: F Scale: 1:20	Drawing No. P9

Notes:
Construction tolerance
= +/-15mm
fy=300MPa
f'c=30MPa
Min cover=35mm

Beam D
Reinforcement
dimensions

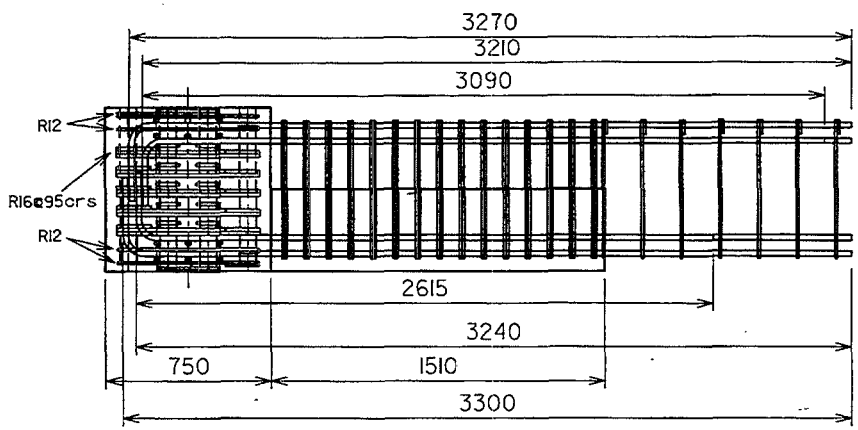

Beam D
Concrete
dimensions

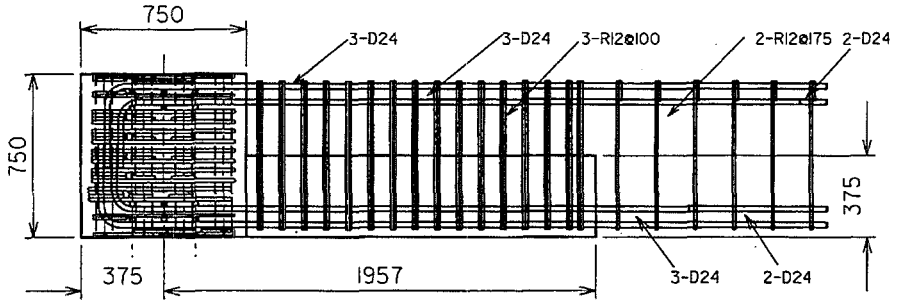

Department of Civil Engineering University of Canterbury Christchurch, New Zealand	FABRICATION DRAWINGS Elevation of precast beam D	Drawn: JGM Date: 15/11/99 Revision: E Scale: 1:20	Drawing No. P10

Notes:
Construction tolerances =+/-15mm
All dimensions mm
fy=300MPa
f'c=30MPa
Min cover=35mm
20mm gap between 1st B/C joint stirrup and longitudinal rebar

Beam E
Concrete & Reinforcement dimensions

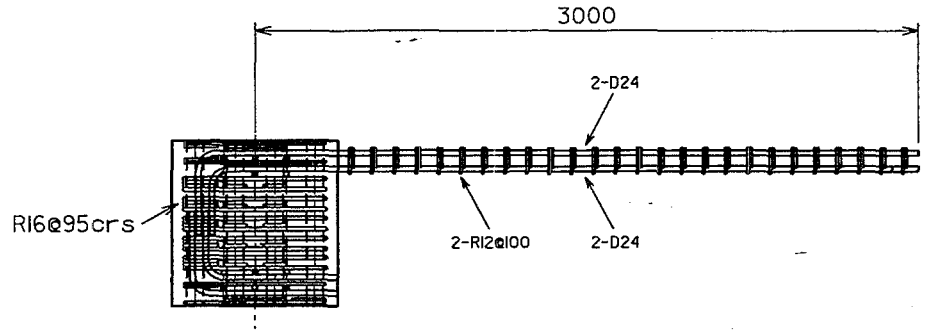

Department of Civil Engineering University of Canterbury Christchurch, New Zealand	FABRICATION DRAWINGS Elevation of precast beam E	Drawn: JGM Date: 9/3/00 Revision: E Scale: 1:20	Drawing No. P11

Notes:
Construction tolerance
= +/-15mm
fy=300MPa
f'c=30MPa
Min cover=35mm

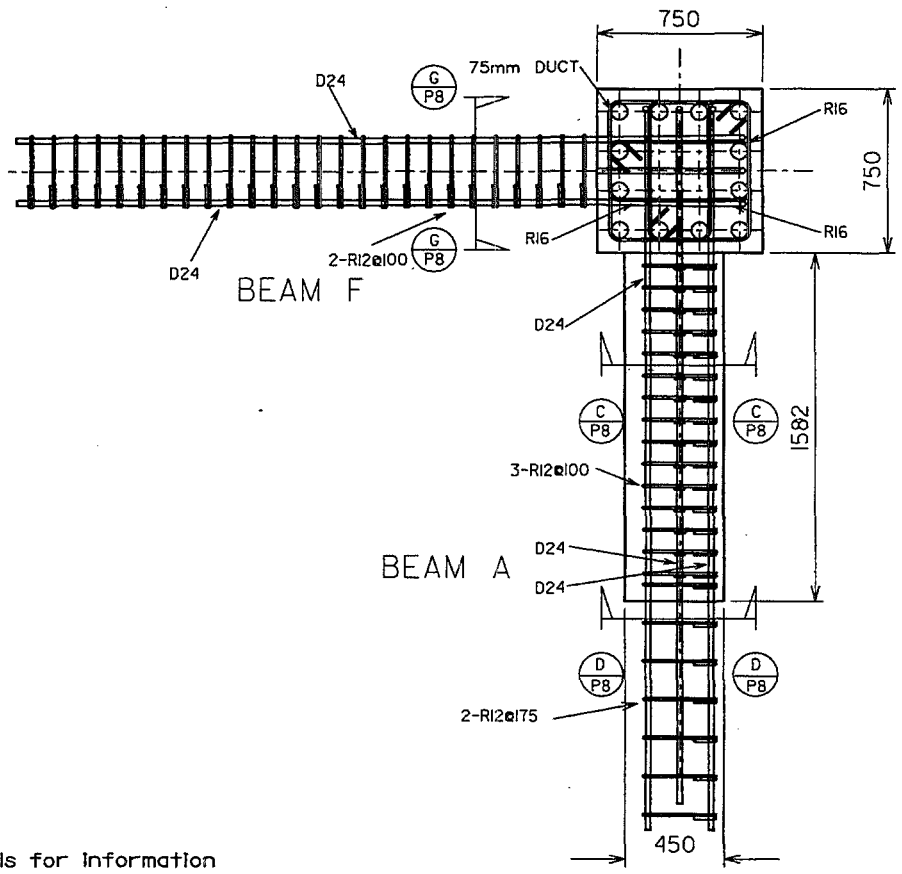

Note:
Refer to lap splice details for information regarding stirrup and lapped bar location within the in-situ lap splice

Department of Civil Engineering University of Canterbury Christchurch, New Zealand	FABRICATION DRAWINGS Plan of corner unit D	Drawn: JGM Date: 9/3/00 Revision: F Scale: 1:20	Drawing No. P12

Notes:
Construction tolerances =+/-15mm
All dimensions mm
fy=300MPa
f'c=30MPa
Min cover=35mm
20mm gap between 1st B/C joint stirrup and longitudinal rebar

Beam F
Concrete &
Reinforcement
dimensions

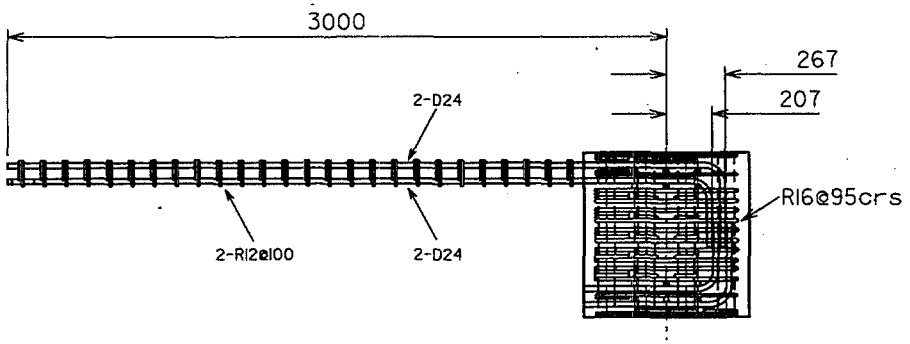

Department of Civil Engineering University of Canterbury Christchurch, New Zealand	FABRICATION DRAWINGS Elevation of precast beam F	Drawn: JGM Date: 9/3/00 Revision: E Scale: 1:20	Drawing No. P13

Notes:
Construction tolerance
= +/-15mm
fy=300MPa
f'c=30MPa
Min cover=35mm

Beam A
Reinforcement
dimensions

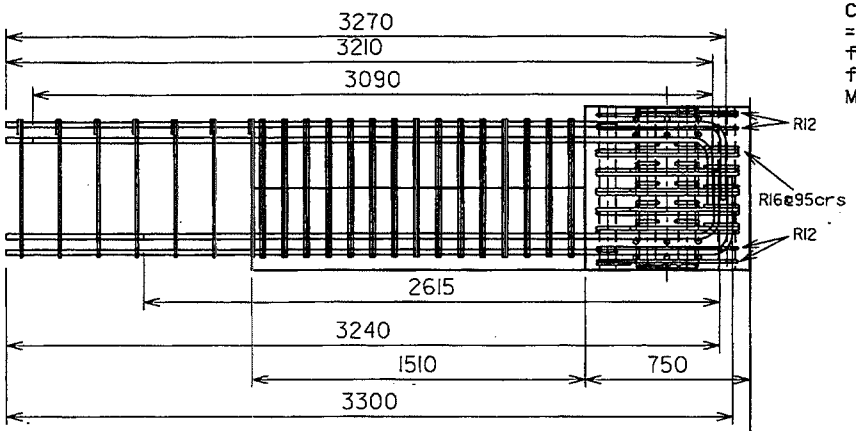

Beam A
Concrete
dimensions

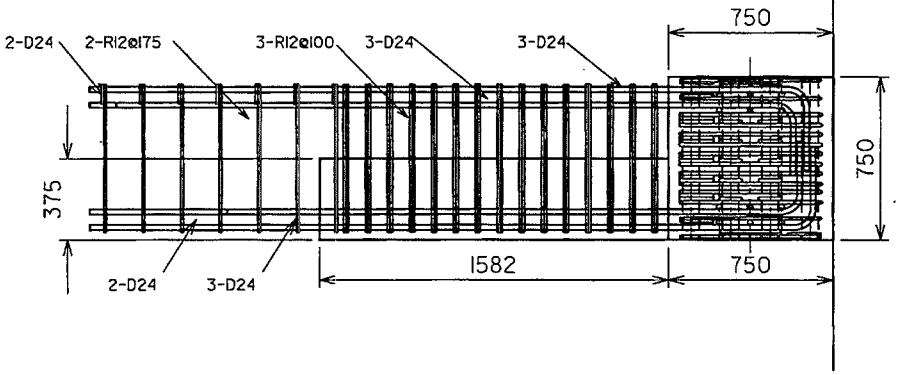

Department of Civil Engineering University of Canterbury Christchurch, New Zealand	FABRICATION DRAWINGS Elevation of precast beam A	Drawn: JGM Date: 15/11/99 Revision: E Scale: 1:20	Drawing No. P14

Note:
Refer to lap splice details for information regarding stirrup and lapped bar location within the in-situ lap splice

Notes:
Construction tolerance = +/-15mm
fy=300MPa
f'c=30MPa
Min cover=35mm

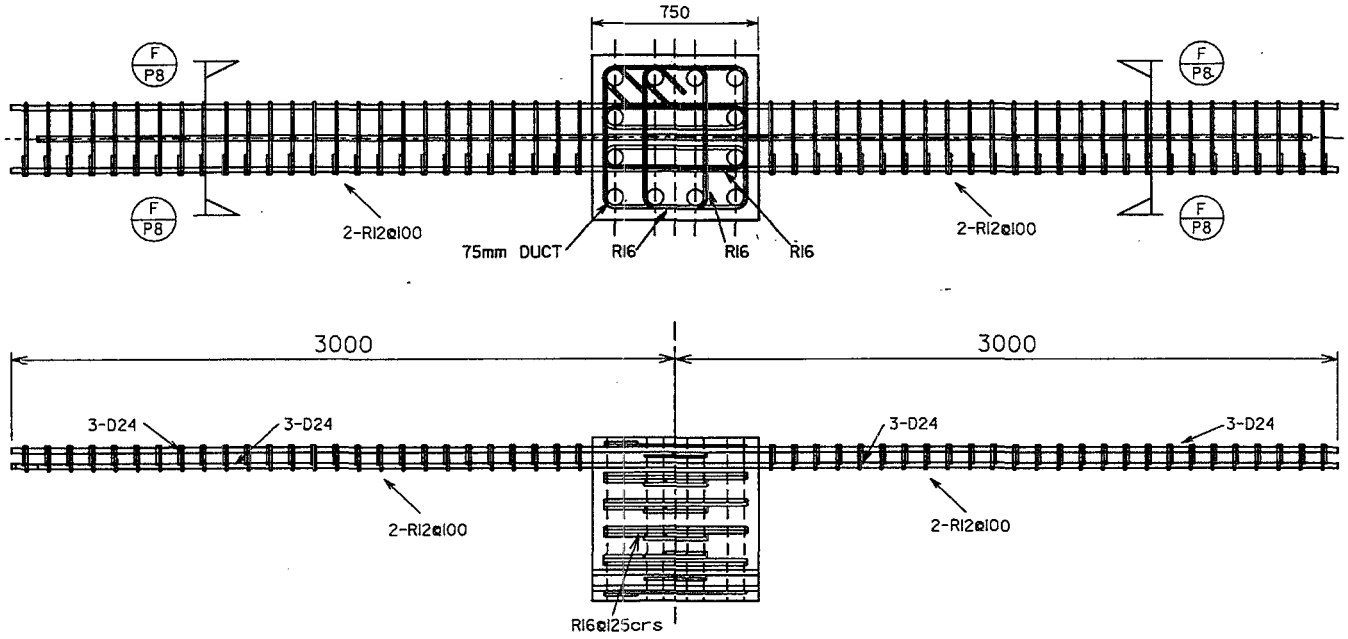

Department of Civil Engineering University of Canterbury Christchurch, New Zealand	FABRICATION DRAWINGS Plan and Elevation of Straight unit B	Drawn: JGM Date: 9/3/00 Revision: F Scale: 1:20	Drawing No. P15

Notes:
Construction tolerances
0 to -3mm
All dimensions mm
fyh=300MPa
fy=430MPa
f'c=30MPa
Min cover= 35mm

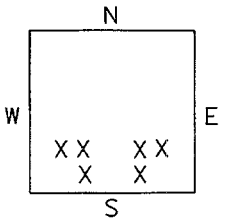

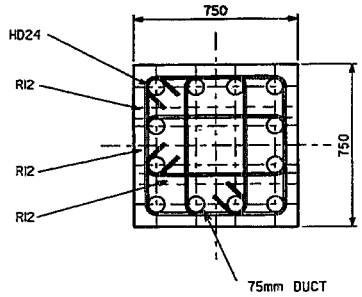

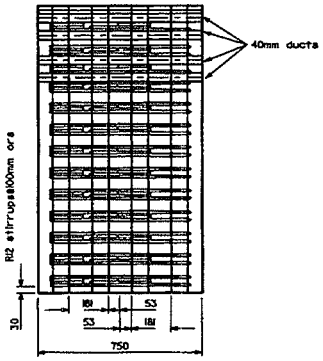

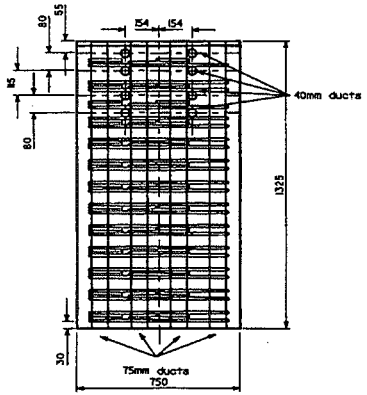

NE and NW columns

East Face

South Face

Department of Civil Engineering University of Canterbury Christchurch, New Zealand	FABRICATION DRAWINGS Plan and Elevation of Column unit 1(top)	Drawn: JGM Date: 9/3/00 Revision: E Scale: 1:20	Drawing No. P16

Notes:
Construction tolerances
0 to -3mm
All dimensions mm
fyh=300MPa
fy=430MPa
f'c=30MPa
Min cover= 35mm

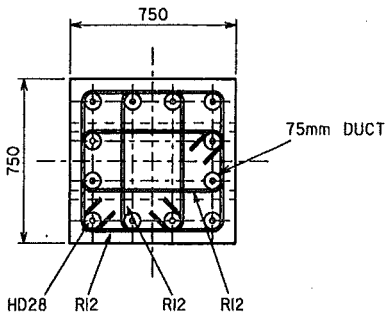

PLAN

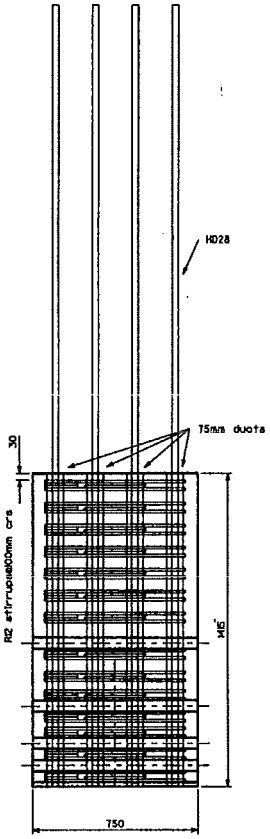

East Face

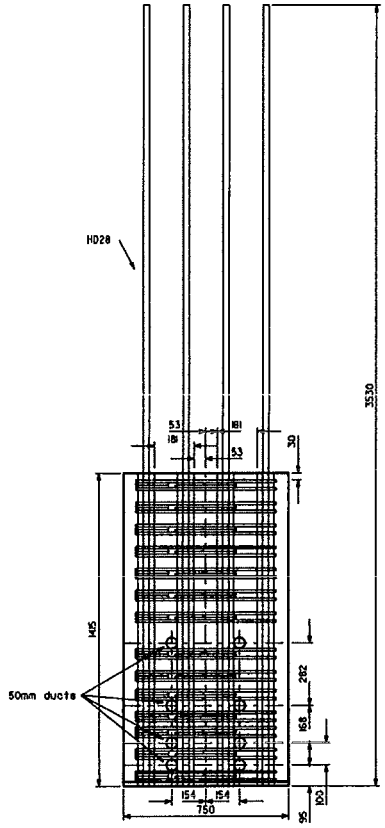

South Face

Number req'd= 2 off

FABRICATION DRAWINGS Plan and elevation of column unit 1(bottom)	NE and NW columns	
Department of Civil Engineering University of Canterbury Christchurch, New Zealand	Drawn: JGM Date: 9/3/00 Revision: F Scale: 1:20	Drawing No. P17

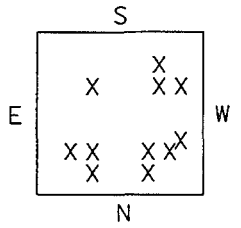

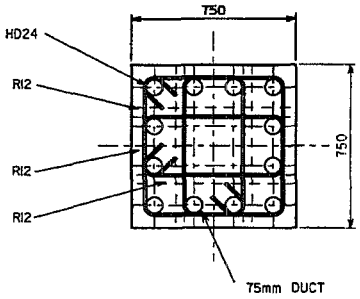

Notes:
Construction tolerances
0 to -3mm
All dimensions mm
fyh=300MPa
fy=430MPa
f'c=30MPa
Min cover= 35mm

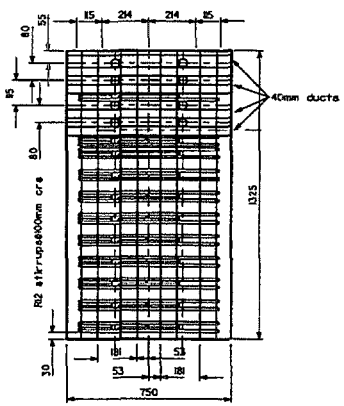

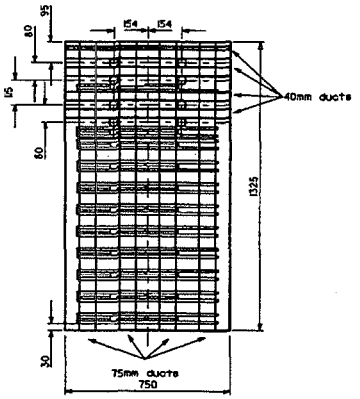

SE and SW columns

South Face

East Face

Department of Civil Engineering University of Canterbury Christchurch, New Zealand	FABRICATION DRAWINGS Plan and elevation for column unit 2 (top)	Drawn: JGM Date: 9/3/00 Revision: F Scale: 1:20	Drawing No. P18

Notes:
Construction tolerances
0 to -3mm
All dimensions mm
fyh=300MPa
fy=430MPa
f'c=30MPa
Min cover= 35mm

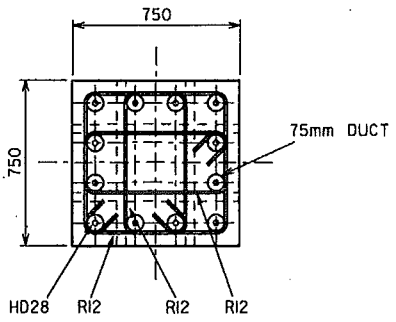

PLAN

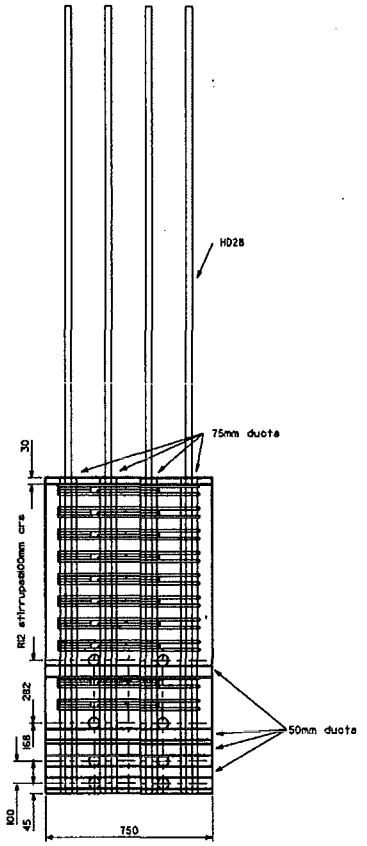

South Face

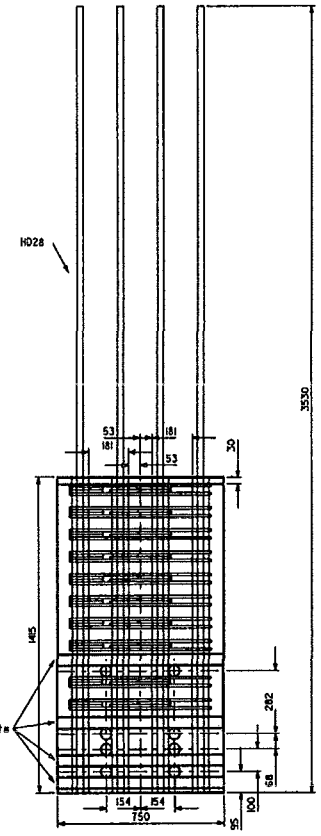

East Face

Number req'd= 2 off

FABRICATION DRAWINGS Plan and Elevation of column unit 2 (bottom)	SE and SW columns
Department of Civil Engineering University of Canterbury Christchurch, New Zealand	Drawn: JGM Date: 9/3/00 Revision: F Scale: 1:20
	Drawing No. P19

Notes:
Construction tolerances
0 to -3mm
All dimensions mm
fyh=300MPa
fy=430MPa
f'c=30MPa
Min cover= 35mm

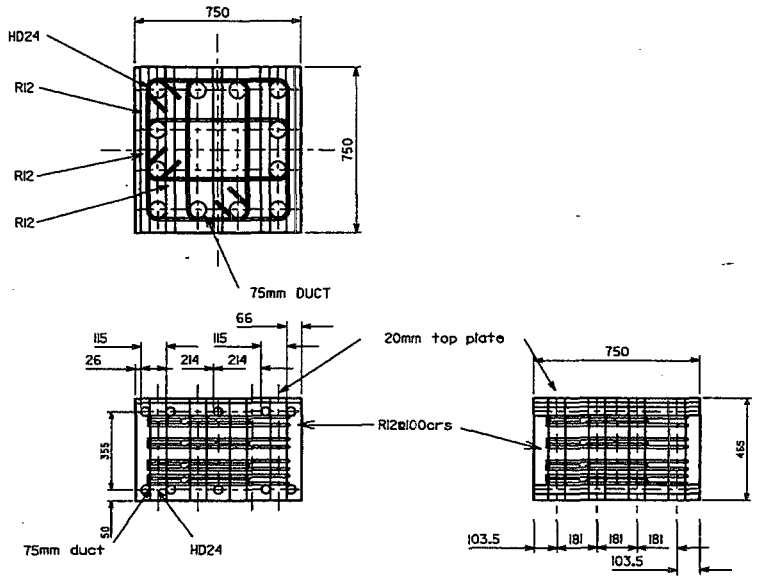

South Face East Face

North Central Column

Department of Civil Engineering University of Canterbury Christchurch, New Zealand	FABRICATION DRAWINGS Plan and Elevation for column unit 3 (top)	Drawn: JGM Date: 9/3/00 Revision: F Scale: 1:20	Drawing No. P20

Notes:
Construction tolerances
0 to -3mm
All dimensions mm unless stated otherwise
fyh=300MPa
fy=430MPa
f'c=30MPa
Min cover= 35mm

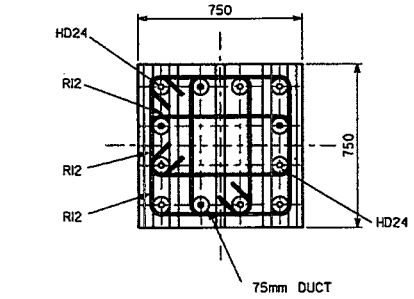

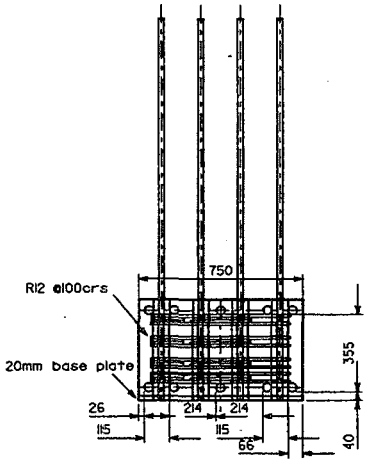

South Face

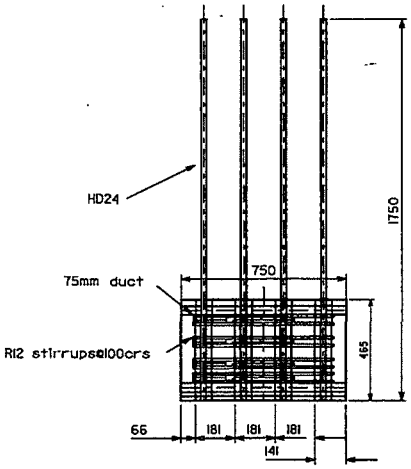

East Face

North Central Column

Department of Civil Engineering University of Canterbury Christchurch, New Zealand	FABRICATION DRAWINGS Plan and Elevation for column unit 3 (bottom)	Drawn: JGM Date: 9/3/00 Revision: F Scale: 1:20	Drawing No. P21

Notes:
Construction tolerances
0 to -3mm
All dimensions mm
fyh=300MPa
fy=430MPa
f'c=30MPa
Min cover= 35mm

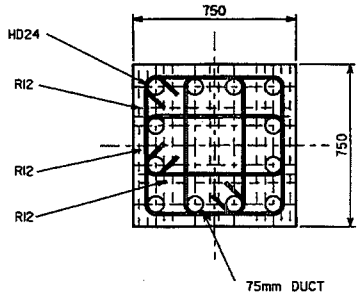

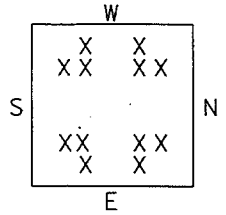

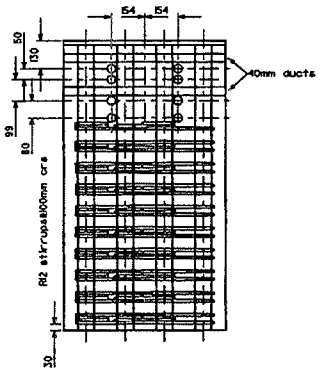

East Face

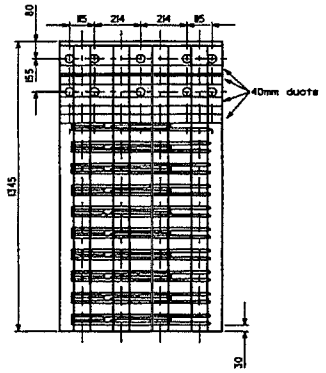

South Face

South Central Column

Department of Civil Engineering University of Canterbury Christchurch, New Zealand	FABRICATION DRAWINGS Plan and Elevation for column unit 4 (top)	Drawn: JGM Date: 9/3/00 Revision: E Scale: 1:20	Drawing No. P22

Notes:
Construction tolerances
0 to -3mm
All dimensions mm
fyh=300MPa
fy=430MPa
f'c=30MPa
Min cover= 35mm

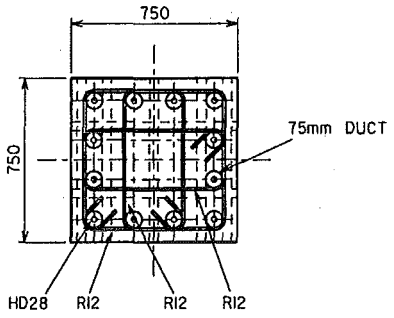

PLAN

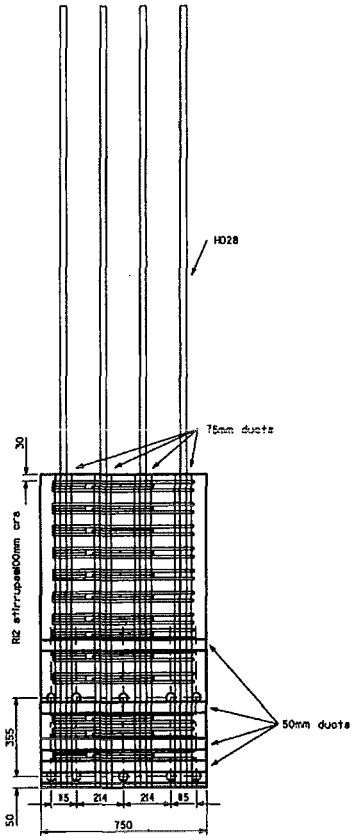

South Face

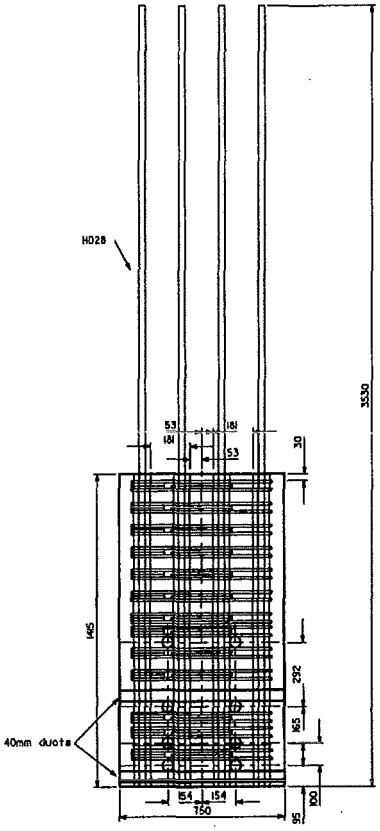

East Face

Number req'd= 1off

FABRICATION DRAWINGS
Plan and Elevation for
column unit 4 (bottom)

South Central Column

Department of Civil Engineering
University of Canterbury
Christchurch, New Zealand

Drawn: JGM
Date: 9/3/00
Revision: F Scale: 1:20

Drawing No.
P23

Notes:
Construction tolerances 0 to -3mm
All dimensions mm unless stated otherwise
fy=300MPa unless stated otherwise
All welds are grade SP
No. required = 2
All bolts are M30 High strength

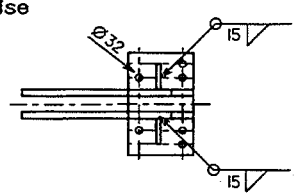

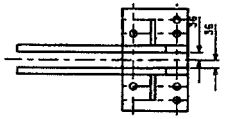

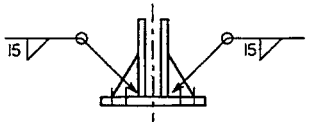

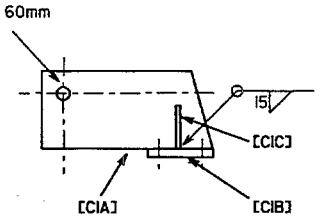

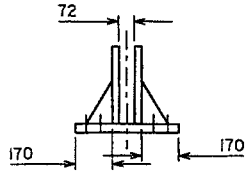

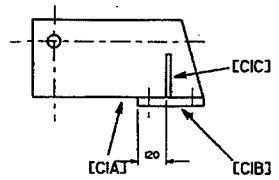

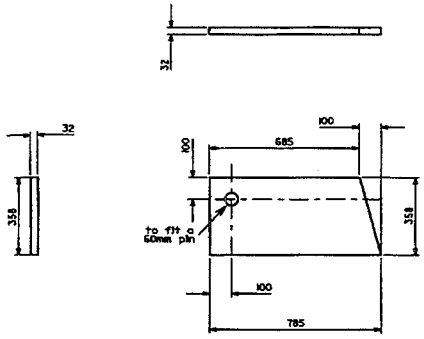

[CIA]

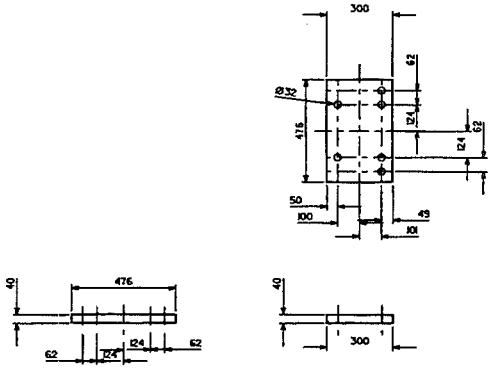

[CIB]

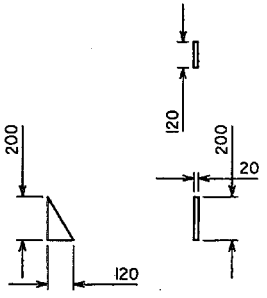

[CIC]

f:/drawings/connections/fabl.dgn
f:/drawings/connections/connections.dgn

Department of Civil Engineering University of Canterbury Christchurch, New Zealand	FABRICATION DRAWINGS Secondary Frame Connection Top detail	Drawn: JGM Date: 16/3/00 Revision: F Scale: 1:20	Drawing No. C1

Notes:
Construction tolerances 0 to -3mm
All dimensions mm unless stated otherwise
fy=300MPa unless stated otherwise
All welds are grade SP
No. required = 2
All bolts are M30 High strength

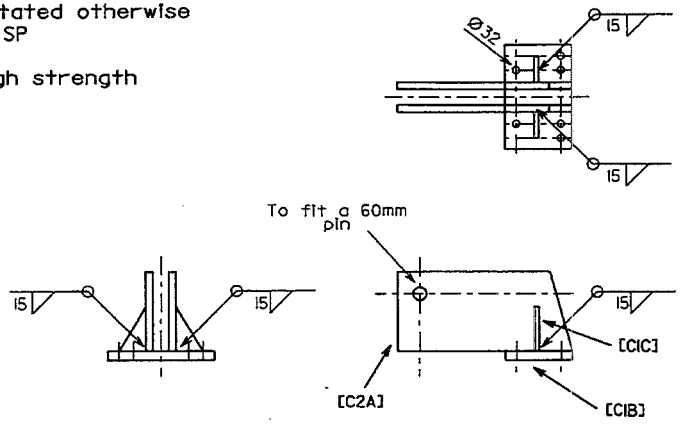

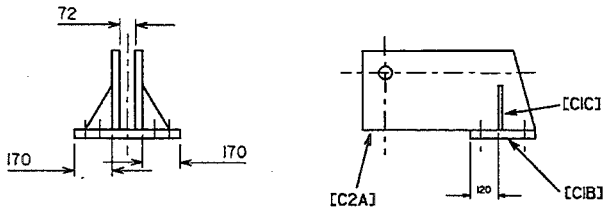

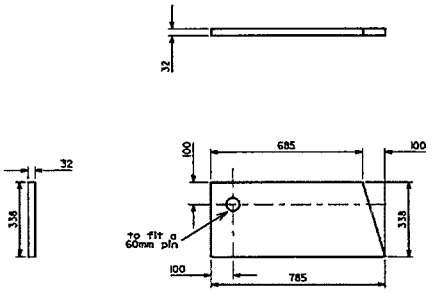

[C2A]

f:/drawings/connections/tab2.dgn
f:/drawings/connections/connections.dgn

Department of Civil Engineering University of Canterbury Christchurch, New Zealand	FABRICATION DRAWINGS Secondary Frame Connection Central detail	Drawn: JGM Date: 3/4/00 Revision: F Scale: 1:20	Drawing No. C2

Notes:
Construction tolerances 0 to -3mm
All dimensions mm unless stated otherwise
fy=300MPa unless stated otherwise
All welds are grade SP
No. required = 2
All bolts are M30

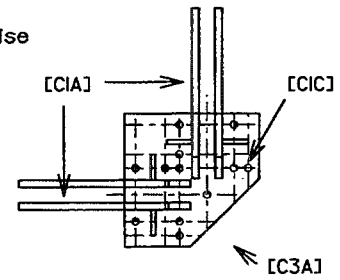

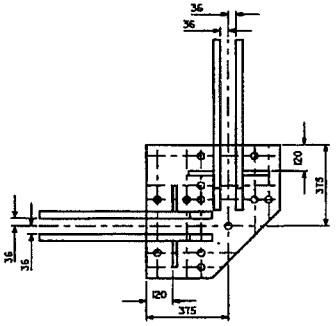

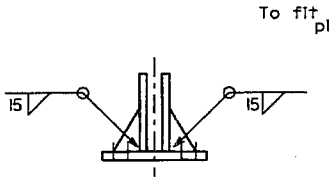

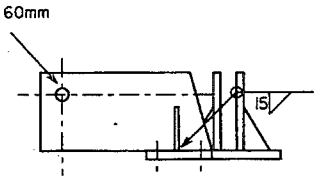

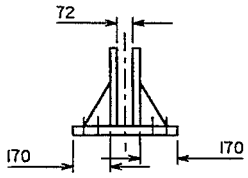

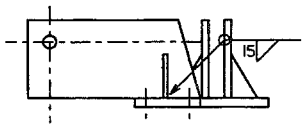

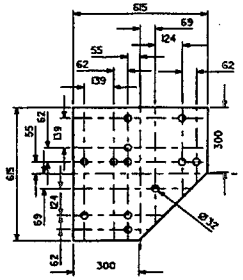

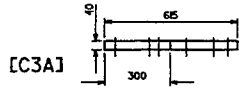

fs/drawings/connections/fab3.dgn
fs/drawings/connections/connections.dgn

Department of Civil Engineering University of Canterbury Christchurch, New Zealand	FABRICATION DRAWINGS Secondary Frame Connection Top corner detail	Drawn: JGM Date: 3/4/00 Revision: E Scale: 1:20	Drawing No. C3

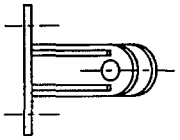

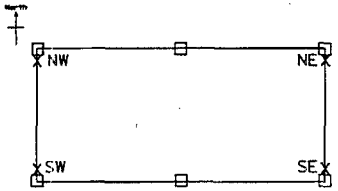

Notes:
Construction tolerances 0 to -3mm
All dimensions mm unless stated otherwise
fy=300MPa unless stated otherwise
All welds are grade SP
No. required = 4
Angle of connection=30deg

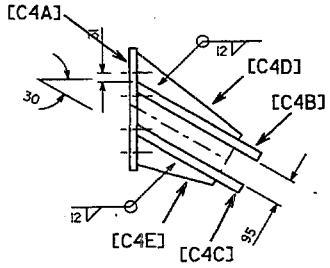

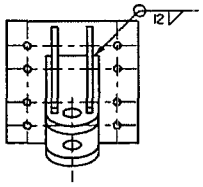

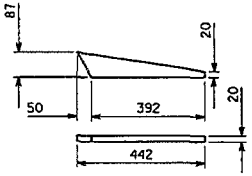

[C4D]

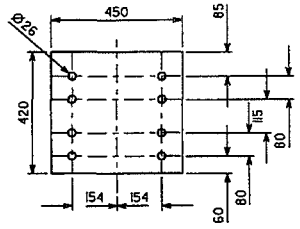

[C4A]

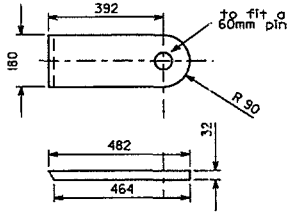

[C4B]

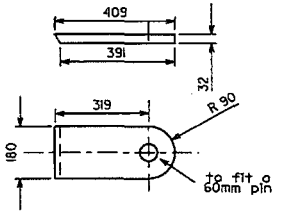

[C4C]

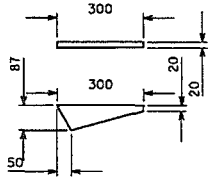

[C4E]

f:\drawings\connections\fabrication
f:\drawings\connections\weldsecn.dgn

Department of Civil Engineering University of Canterbury Christchurch, New Zealand	FABRICATION DRAWINGS Top loadarm connection detail	Drawn: JGM Date: 20/6/00 Revision: F Scale: 1:15	Drawing No. C4

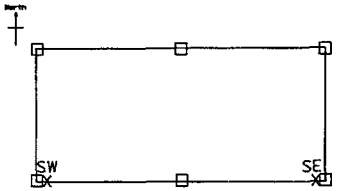

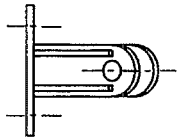

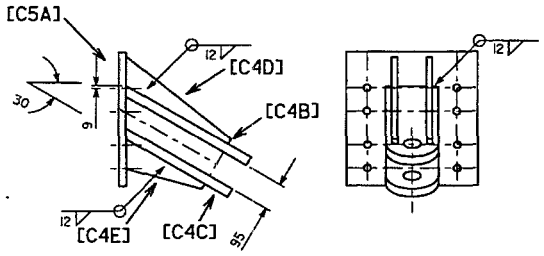

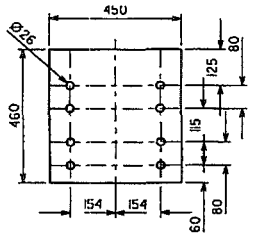

[C5A]

Notes:
Construction tolerances 0 to -3mm
All dimensions mm unless stated otherwise
fy=300MPa unless stated otherwise
All welds are grade SP
No. required = 2
Angle of connection=30deg

Department of Civil Engineering University of Canterbury Christchurch, New Zealand	FABRICATION DRAWINGS Top loadarm connection detail	Drawn: JGM Date: 20/6/00 Revision: B Scale: 1:5	Drawing No. C5

Notes:
Construction tolerances 0 to -3mm
All dimensions mm unless stated otherwise
fy=300MPa unless stated otherwise
All welds are grade SP
No. required = 2
Angle of connection=30deg

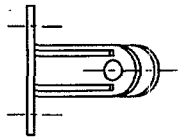

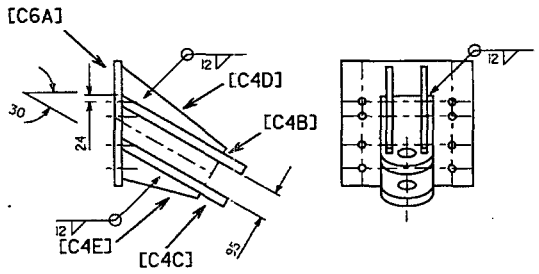

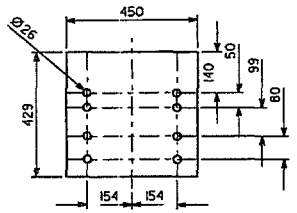

[C6A]

Central Column

Department of Civil Engineering University of Canterbury Christchurch, New Zealand	FABRICATION DRAWINGS Top loadarm connection detail	Drawn: JGM Date: 20/6/00 Revision: B Scale: 1:15	Drawing No. C6

Notes:
Construction tolerances 0 to -3mm
All dimensions mm unless stated otherwise
fy=300MPa unless stated otherwise
All welds are grade SP
No. required = 2
Angle of connection=30 deg

Central Column

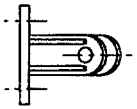

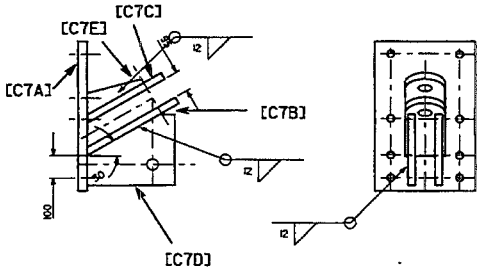

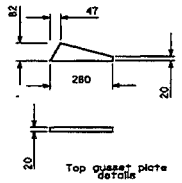

[C7E]

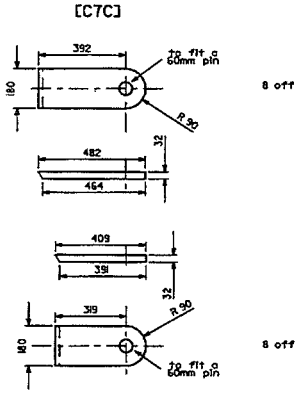

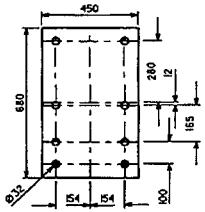

[C7A]

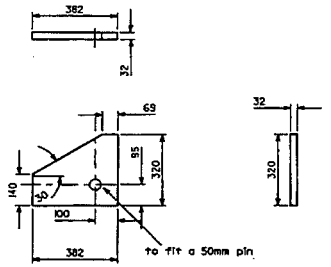

[C7D]

Department of Civil Engineering University of Canterbury Christchurch, New Zealand	FABRICATION DRAWINGS Bottom loadarm connection detail	Drawn: JGM Date: 20/6/00 Revision: B Scale: 1:20	Drawing No. C7

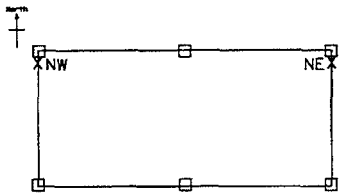

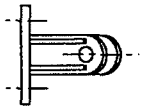

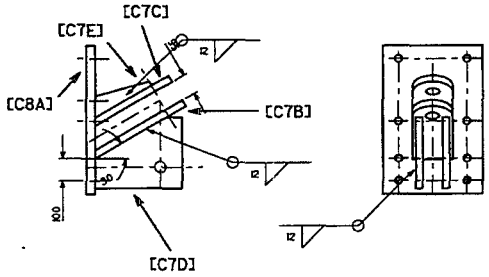

Notes:
Construction tolerances 0 to -3mm
All dimensions mm unless stated otherwise
fy=300MPa unless stated otherwise
All welds are grade SP
No. required = 2
Angle of connection=30 deg

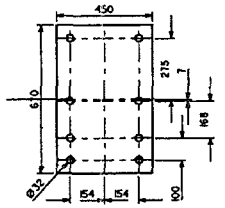

[C8A]

Department of Civil Engineering University of Canterbury Christchurch, New Zealand	FABRICATION DRAWINGS Bottom loadarm connection detail	Drawn: JGM Date: 20/6/00 Revision: B Scale: 1:20	Drawing No. C8

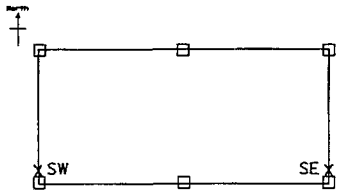

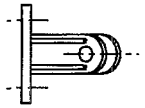

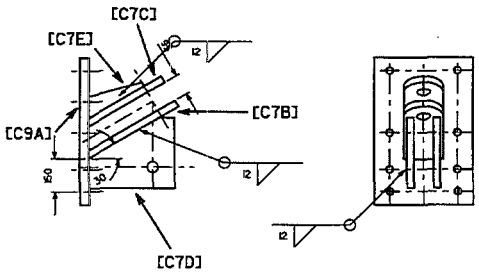

Notes:
Construction tolerances 0 to -3mm
All dimensions mm unless stated otherwise
fy=300MPa unless stated otherwise
All welds are grade SP
No. required = 2
Angle of connection=30 deg

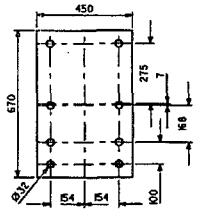

[C9A]

Department of Civil Engineering University of Canterbury Christchurch, New Zealand	FABRICATION DRAWINGS Bottom loadarm connection detail	Drawn: JGM Date: 20/6/00 Revision: B Scale: 1:20	Drawing No. C9

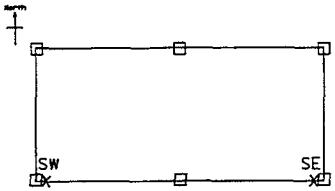

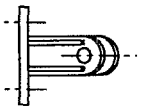

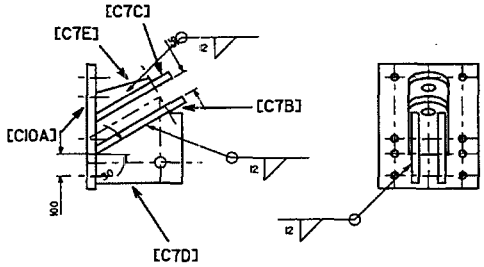

Notes:
Construction tolerances 0 to -3mm
All dimensions mm unless stated otherwise
fy=300MPa unless stated otherwise
All welds are grade SP
No. required = 2
Angle of connection=30 deg

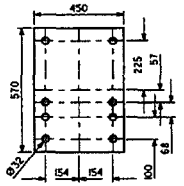

[C10A]

Department of Civil Engineering University of Canterbury Christchurch, New Zealand	FABRICATION DRAWINGS Bottom loadarm connection detail.	Drawn: JGM Date: 20/6/00 Revision: B Scale: 1:20	Drawing No. C10

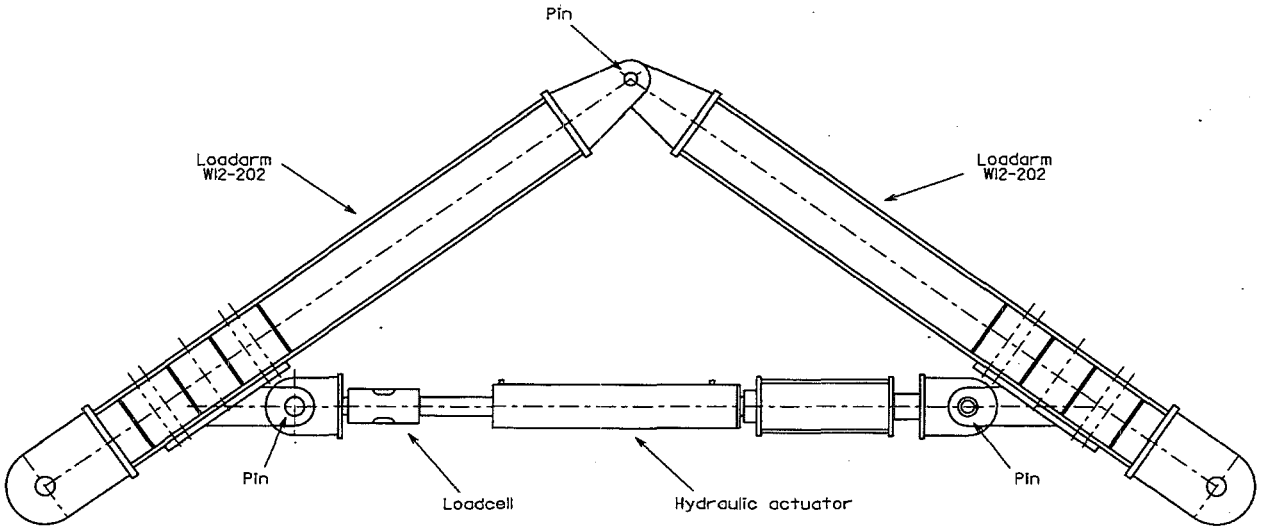

Notes:
Construction tolerances 0 to -3mm
All dimensions mm unless stated otherwise
fy=300MPa unless stated otherwise
All welds are grade SP

f:\drawings\loadrig\fabs0.dgn
f:\drawings\loadrig\scissor.dgn

Department of Civil Engineering University of Canterbury Christchurch, New Zealand	FABRICATION DRAWINGS Complete setup for each loadarm	Drawn: JGM Date: 15/9/99 Revision: C Scale: 1:20	Drawing No. L0

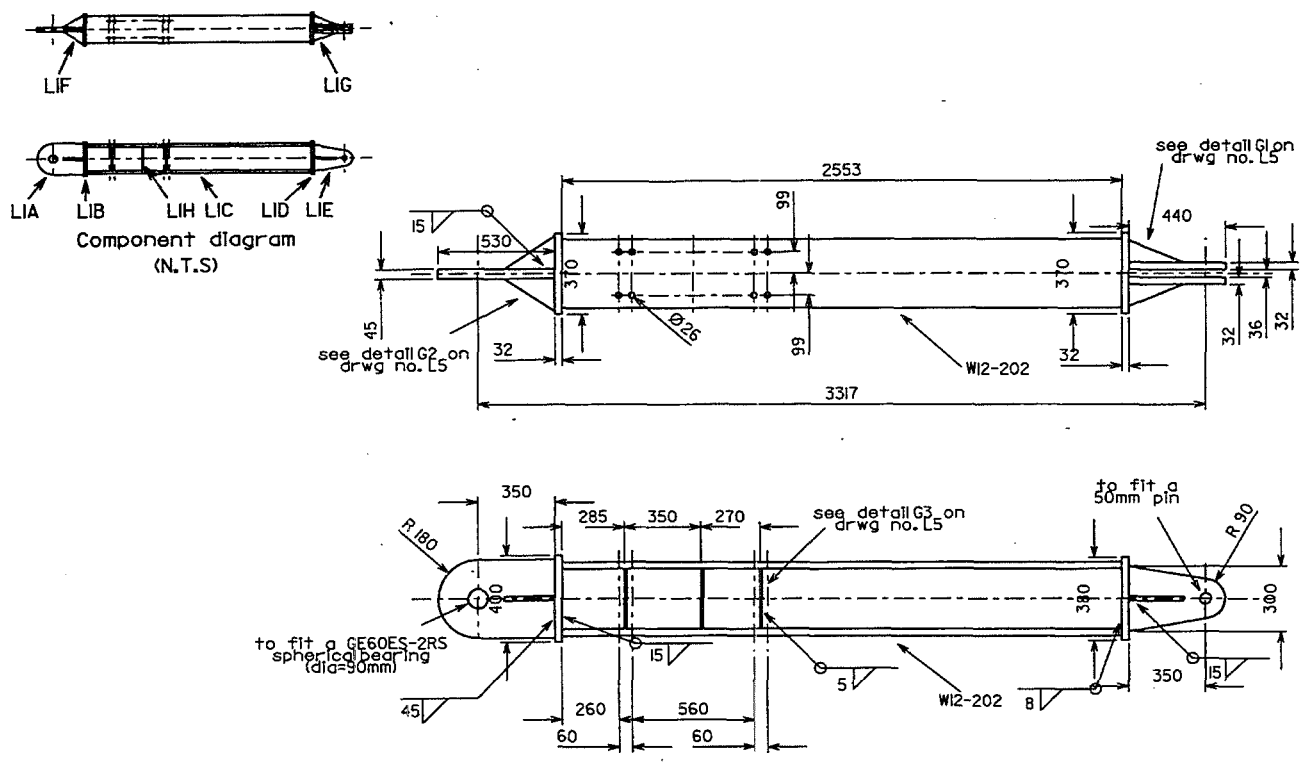

Notes:
Construction tolerances 0 to -3mm
All dimensions mm unless stated otherwise
fy=300MPa unless stated otherwise
All welds are grade SP
No. req'd=2

f:\drawings\loadrig\fabsL.dgn
f:\drawings\loadrig\scissor.dgn

Department of Civil Engineering University of Canterbury Christchurch, New Zealand	FABRICATION DRAWINGS Left component for short load arm	Drawn: JGM Date: 7/11/99 Revision: D Scale: 1:20	Drawing No. L1

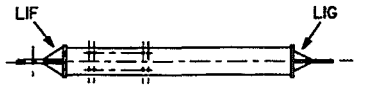

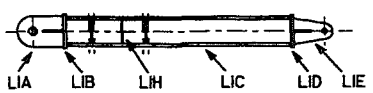

Component diagram
(N.T.S)

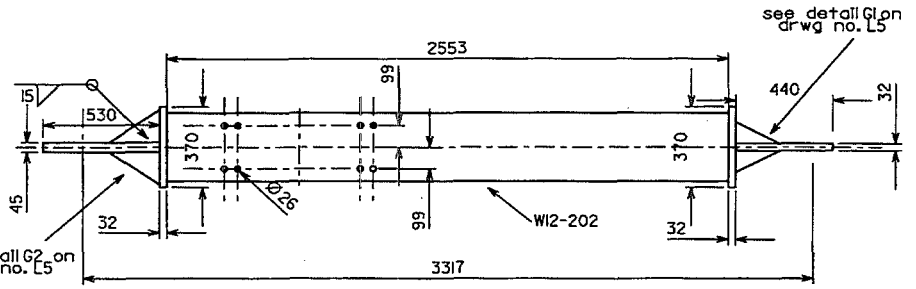

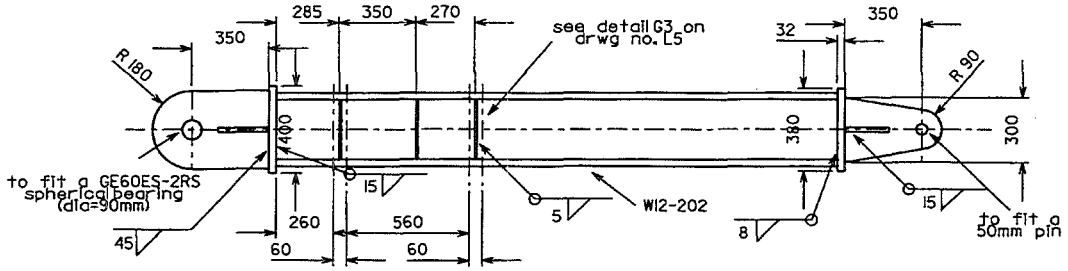

Notes:
Construction tolerances 0 to -3mm
All dimensions mm unless stated otherwise
fy=300MPa unless stated otherwise
All welds are grade SP
No. req'd=2

f:\drawings\loadrig\fabs2.dgn
f:\drawings\loadrig\scissor.dgn

Department of Civil Engineering University of Canterbury Christchurch, New Zealand	FABRICATION DRAWINGS Right component for short load arm	Drawn: JGM Date: 7/11/99 Revision: D Scale: 1:20	Drawing No. L2

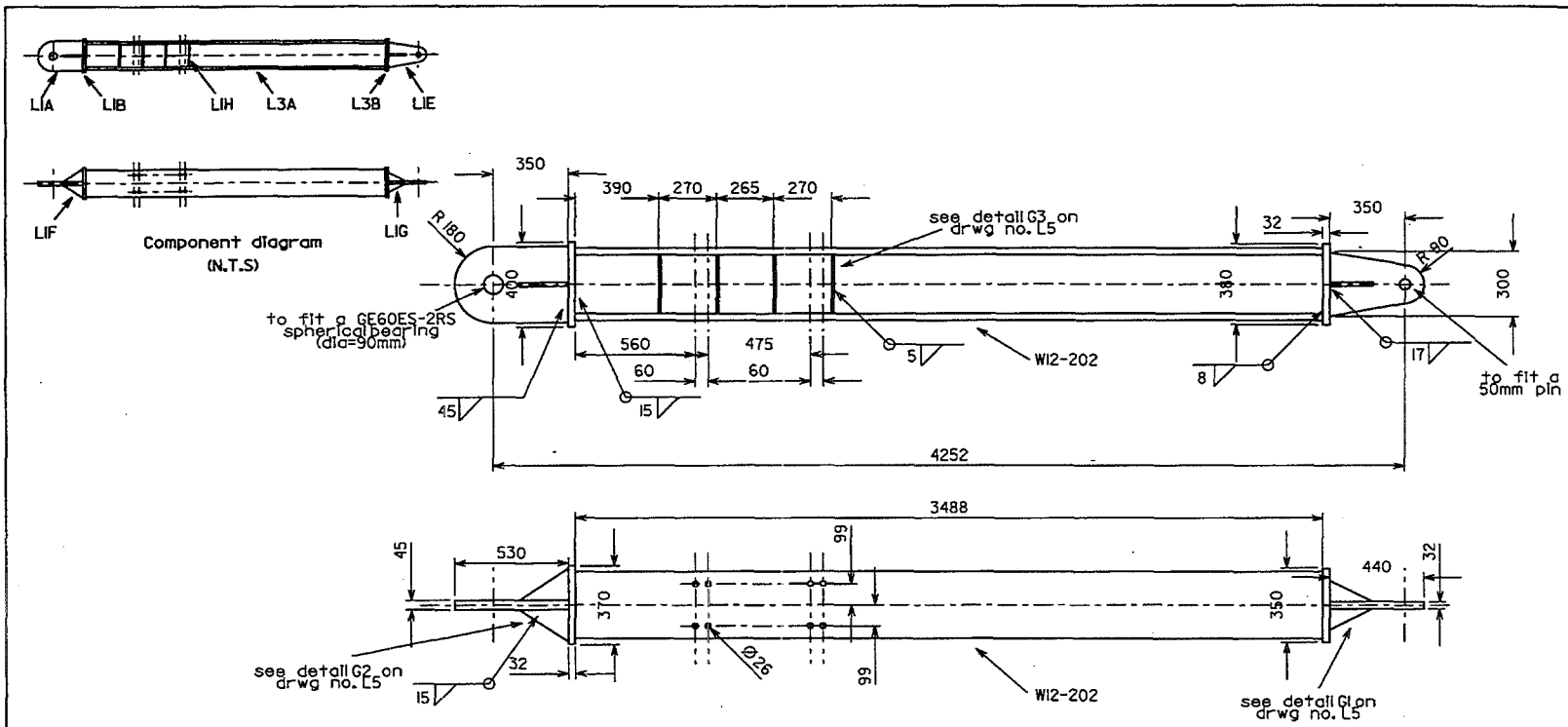

Notes:
Construction tolerances 0 to -3mm
All dimensions mm unless stated otherwise
fy=300MPa unless stated otherwise
All welds are grade SP
No. req'd=2

f:\drawings\loadrig\fabe3.dgn
f:\drawings\loadrig\scissor.dgn

Department of Civil Engineering University of Canterbury Christchurch, New Zealand	FABRICATION DRAWINGS Left component for long load arm	Drawn: JGM Date: 7/11/99 Revision: D Scale: 1:20	Drawing No. L3

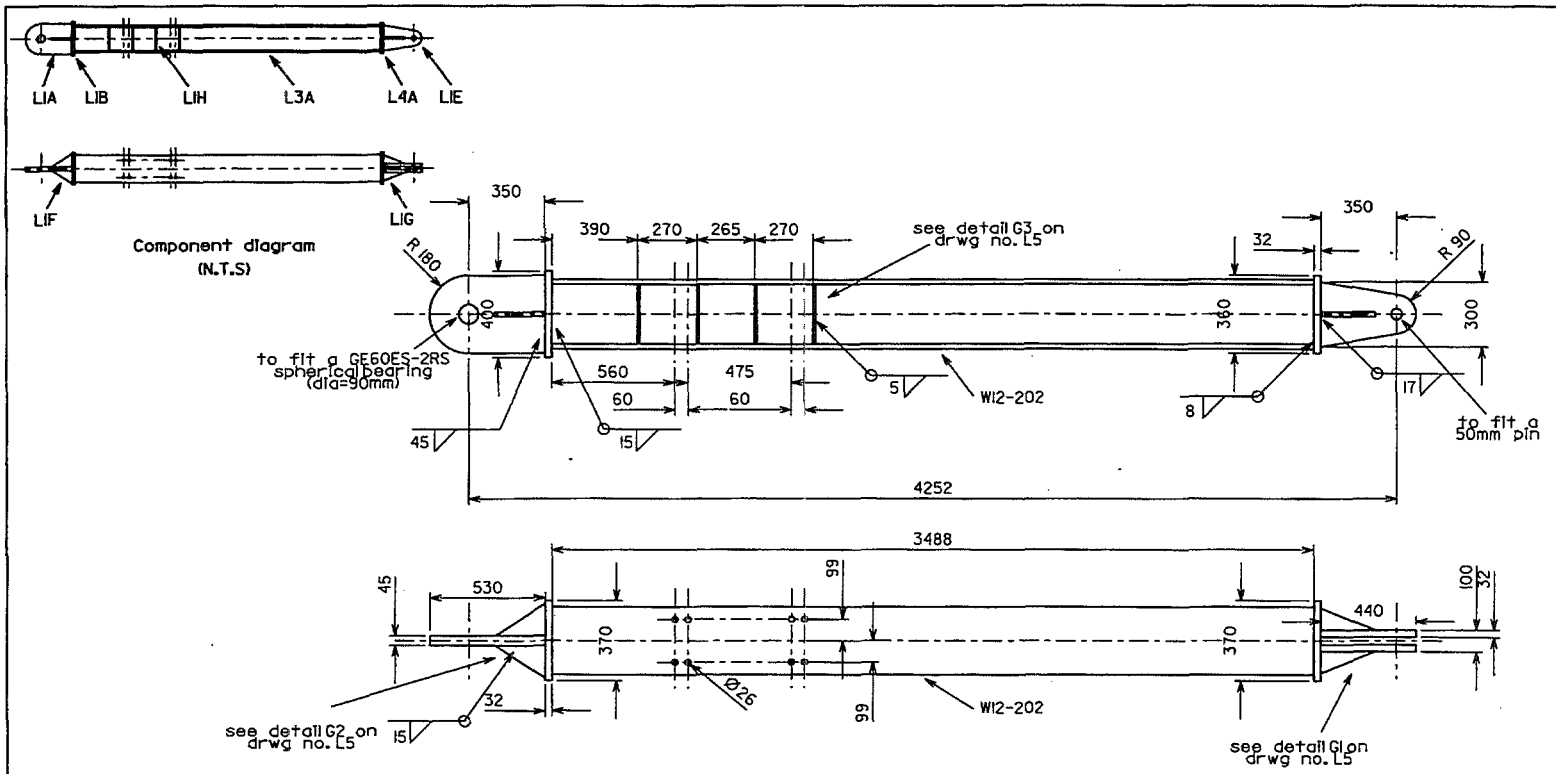

Notes:
Construction tolerances 0 to -3mm
All dimensions mm unless stated otherwise
fy=300MPa unless stated otherwise
All welds are grade SP
No. req'd=2

f:\drawings\loadrig\fabs4.dgn
f:\drawings\loadrig\scissor.dgn

Department of Civil Engineering University of Canterbury Christchurch, New Zealand	FABRICATION DRAWINGS Right component for long load arm	Drawn: JGM Date: 7/11/99 Revision: D Scale: 1:20	Drawing No. L4

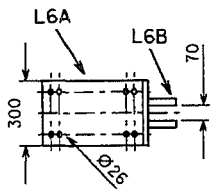

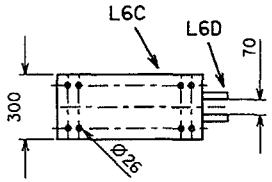

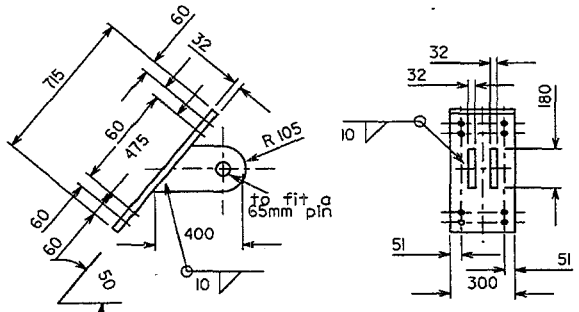

Large load arm bracket

No. req'd=4

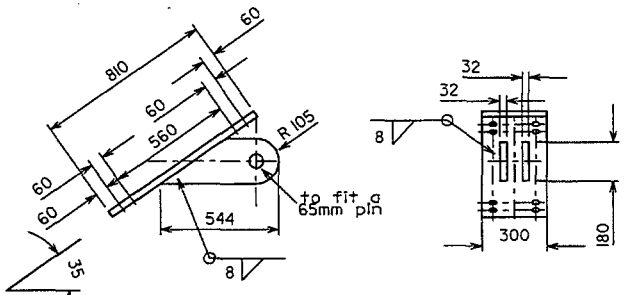

Small load arm bracket

No. req'd=4

Notes:
Construction tolerances 0 to -3mm
All dimensions mm unless stated otherwise
fy=300MPa unless stated otherwise
All welds are grade SP

f:\drawings\loadrig\fabs6.dgn
f:\drawings\loadrig\scissor.dgn

Department of Civil Engineering University of Canterbury Christchurch, New Zealand	FABRICATION DRAWINGS Load arm connection brackets	Drawn: JGM Date: 7/11/99 Revision: C Scale: 1:20	Drawing No. L5

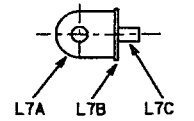

Component diagram
(N.T.S)

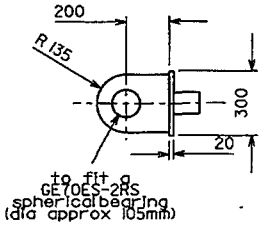

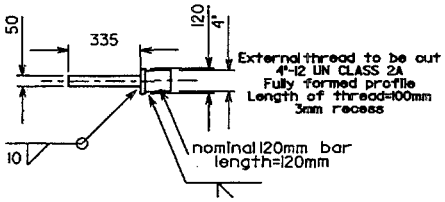

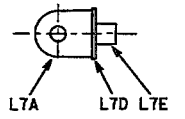

Component diagram
(N.T.S)

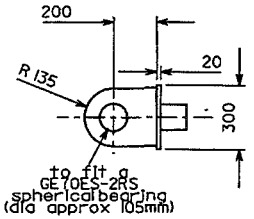

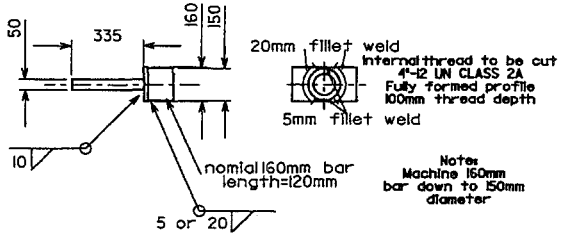

Notes:
Construction tolerances 0 to -3mm
All dimensions mm unless stated otherwise
fy=300MPa unless stated otherwise
All welds are grade SP
No. req'd=4

f:\drawings\loadrig\tube7.dgn
f:\drawings\loadrig\scissor.dgn

Department of Civil Engineering University of Canterbury Christchurch, New Zealand	FABRICATION DRAWINGS Connection details for loadcell & hydraulic actuator	Drawn: JGM Date: 26/11/99 Revision: F Scale: 1:20	Drawing No. L6

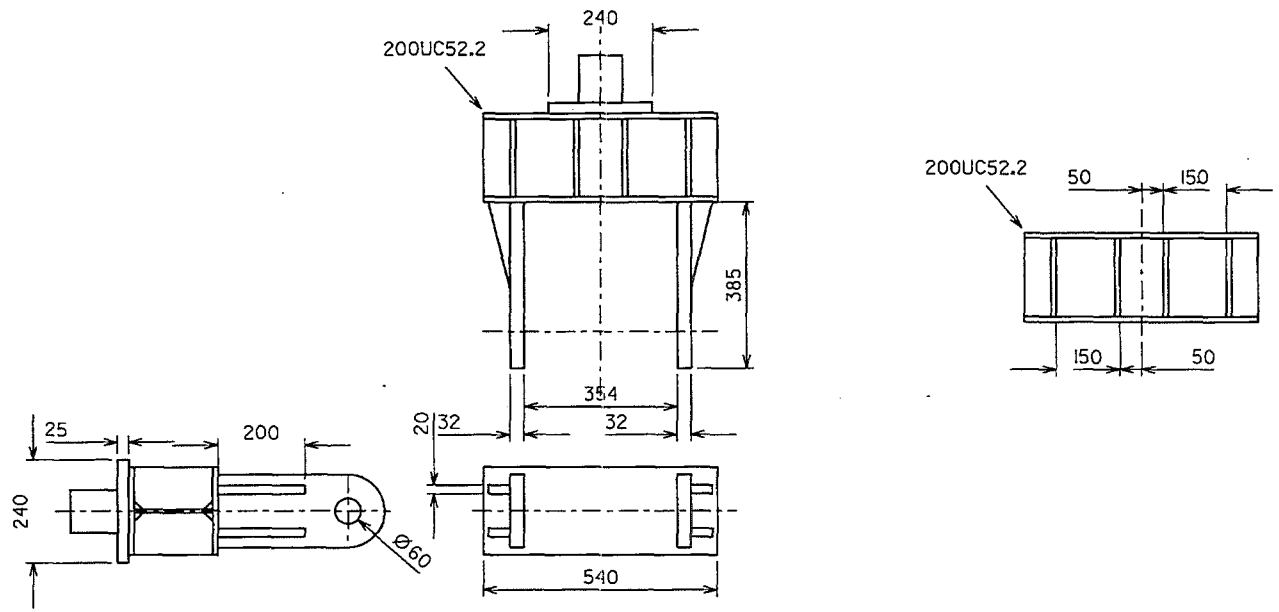

f:\drawings\loadrig\fabs8.dgn
f:\drawings\loadrig\botaalconnection.dgn

Department of Civil Engineering University of Canterbury Christchurch, New Zealand	FABRICATION DRAWINGS Connection details for Bottom hydraulic ram	Drawn: JGM Date: 29/8/00 Revision: A Scale: 1:10	Drawing No. L7

Notes:
Construction tolerances 0 to -3mm
All dimensions mm unless stated otherwise
fy=300MPa unless stated otherwise
All welds are grade SP
No. req'd=4

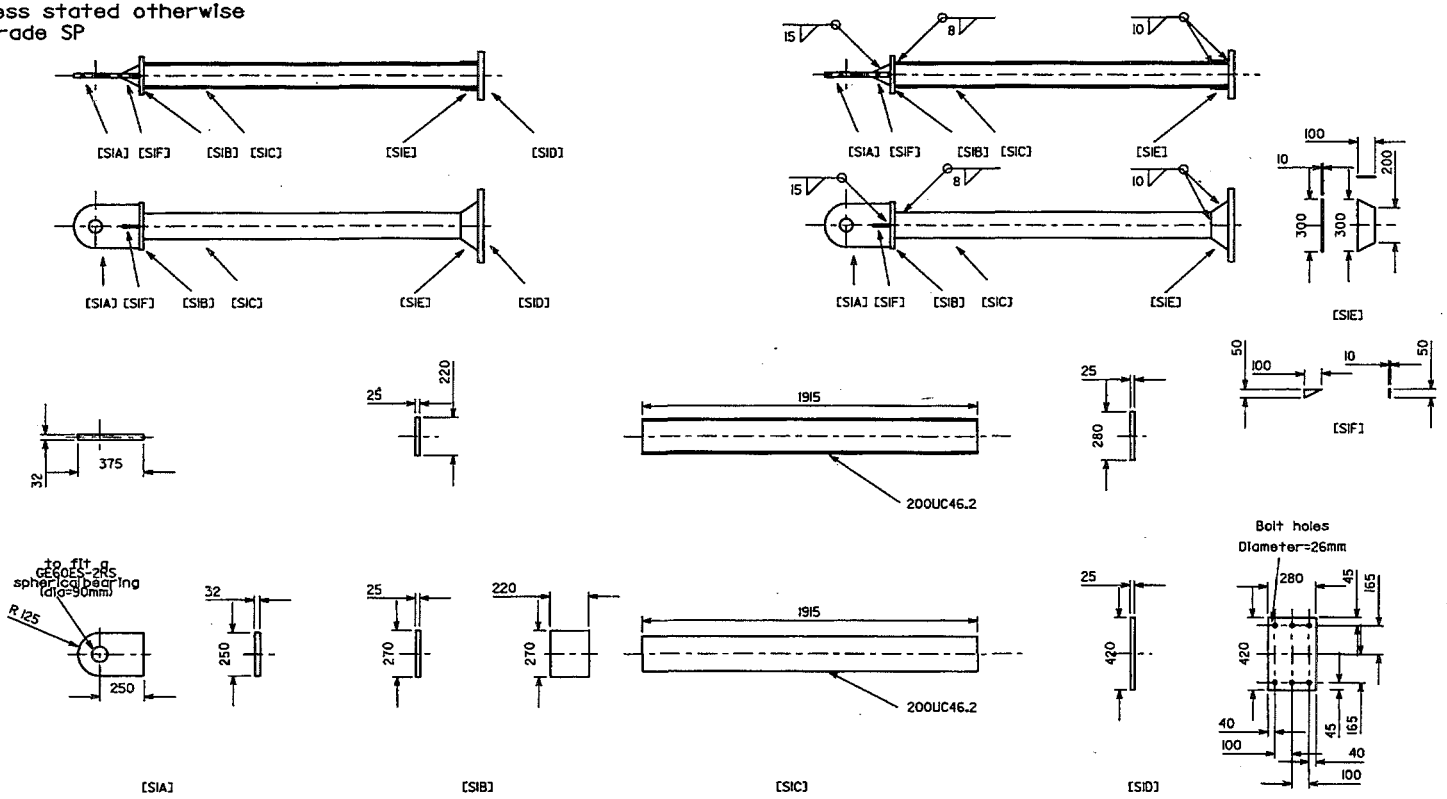

Department of Civil Engineering University of Canterbury Christchurch, New Zealand	FABRICATION DRAWINGS Section A details Secondary frame	Drawn: JGM Date: 16/3/00 Revision: D Scale: 1:25	Drawing No. S1

Notes:
Construction tolerances 0 to -3mm
All dimensions mm unless stated otherwise
fy=300MPa unless stated otherwise
All welds are grade SP
No. req'd=4

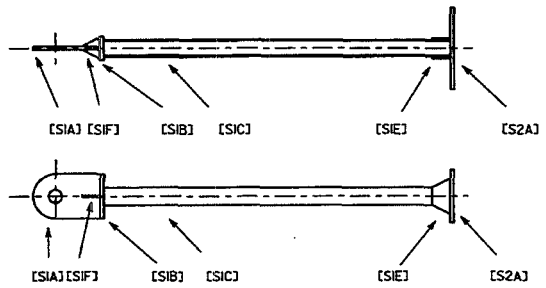

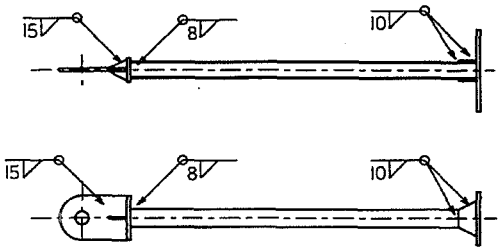

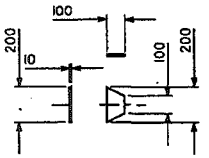

[S1E]

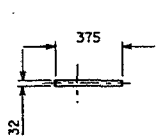

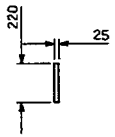

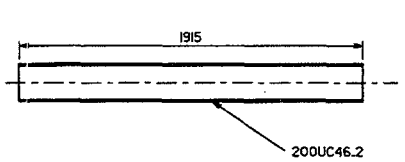

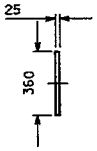

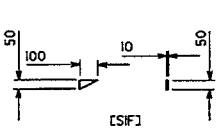

[S1F]

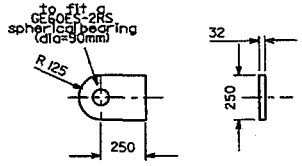

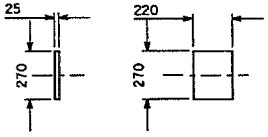

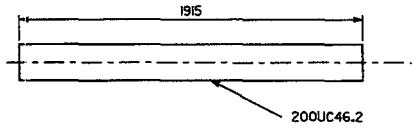

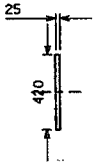

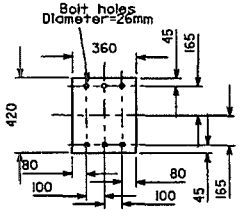

[S1A] [S1B] [S1C] [S2A]

Department of Civil Engineering University of Canterbury Christchurch, New Zealand	FABRICATION DRAWINGS Section B details Secondary frame	Drawn: JGM Date: 16/3/00 Revision: D Scale: 1:25	Drawing No. S2

Notes:
Construction tolerances 0 to -3mm
All dimensions mm unless stated otherwise
fy=300MPa unless stated otherwise
All welds are grade SP
No. req'd=4

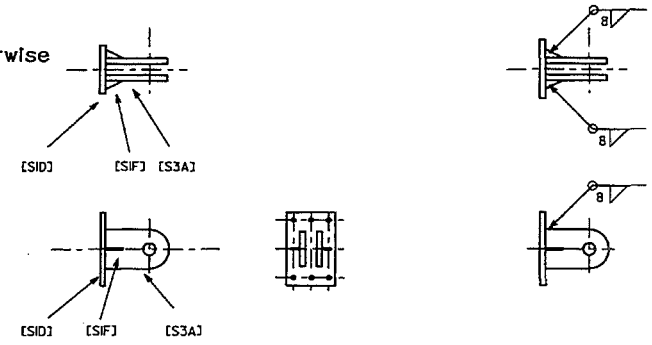

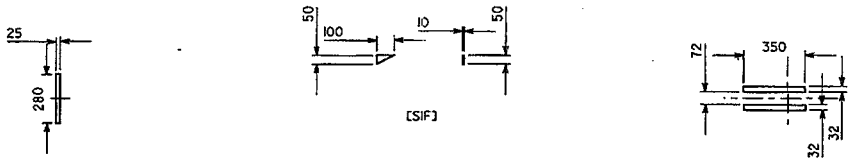

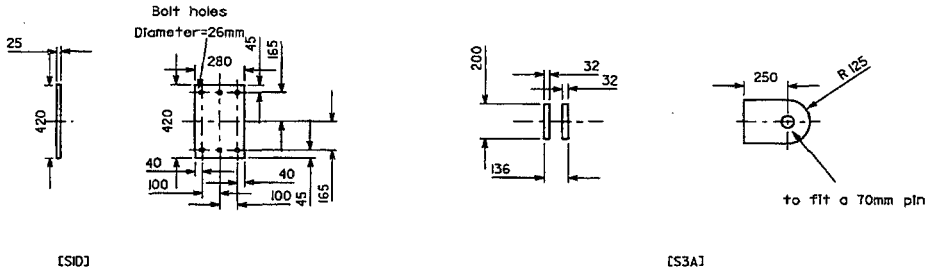

Department of Civil Engineering University of Canterbury Christchurch, New Zealand	FABRICATION DRAWINGS Section C details Secondary frame	Drawn: JGM Date: 16/3/00 Revision: E Scale: 1:25	Drawing No. S3

Notes:
Construction tolerances 0 to -3mm
All dimensions mm unless stated otherwise
fy=300MPa unless stated otherwise
All welds are grade SP
No. req'd=4

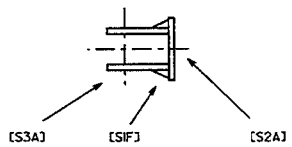

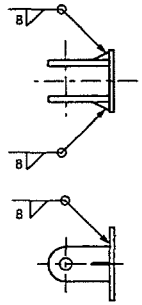

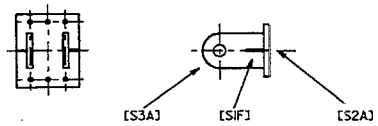

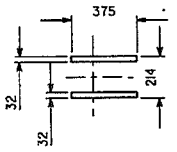

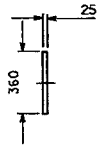

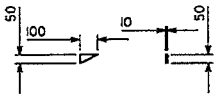

[SIF]

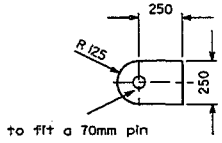

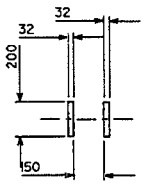

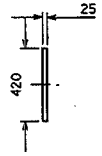

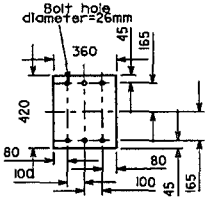

[S3A]

[S2A]

Department of Civil Engineering University of Canterbury Christchurch, New Zealand	FABRICATION DRAWINGS Section D details Secondary frame	Drawn: JGM Date: 12/5/00 Revision: F Scale: 1:25	Drawing No. S4

Notes:
Construction tolerances 0 to -3mm
All dimensions mm unless stated otherwise
fy=300MPa unless stated otherwise
All welds are grade SP
No. req'd=2

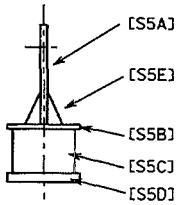

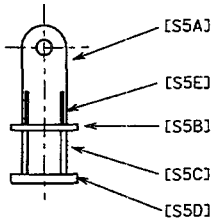

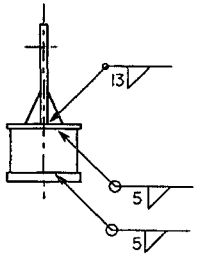

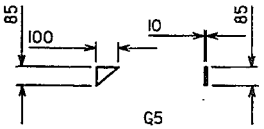

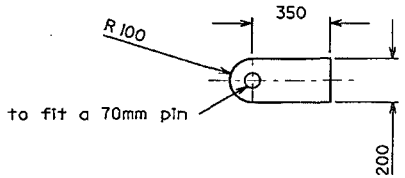

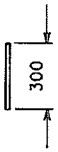

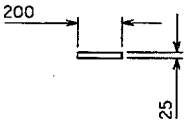

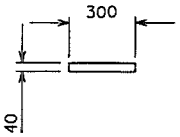

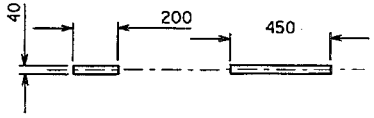

[S5A]

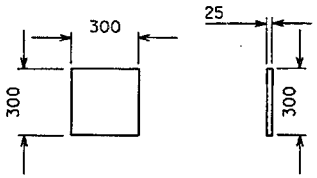

[S5B]

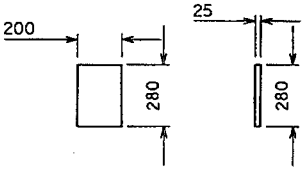

[S5C]

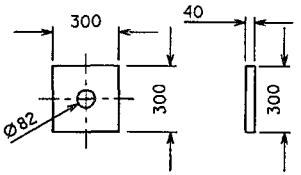

[S5D]

Department of Civil Engineering University of Canterbury Christchurch, New Zealand	FABRICATION DRAWINGS Section E details Secondary frame	Drawn: JGM Date: 13/3/00 Revision: C Scale: 1:20	Drawing No. S5

Notes:
Construction tolerances 0 to -3mm
All dimensions mm unless stated otherwise
fy=300MPa unless stated otherwise
All welds are grade SP
No. req'd=2
Also require 2-M80 locknuts

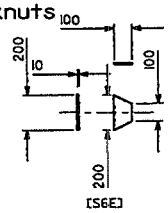

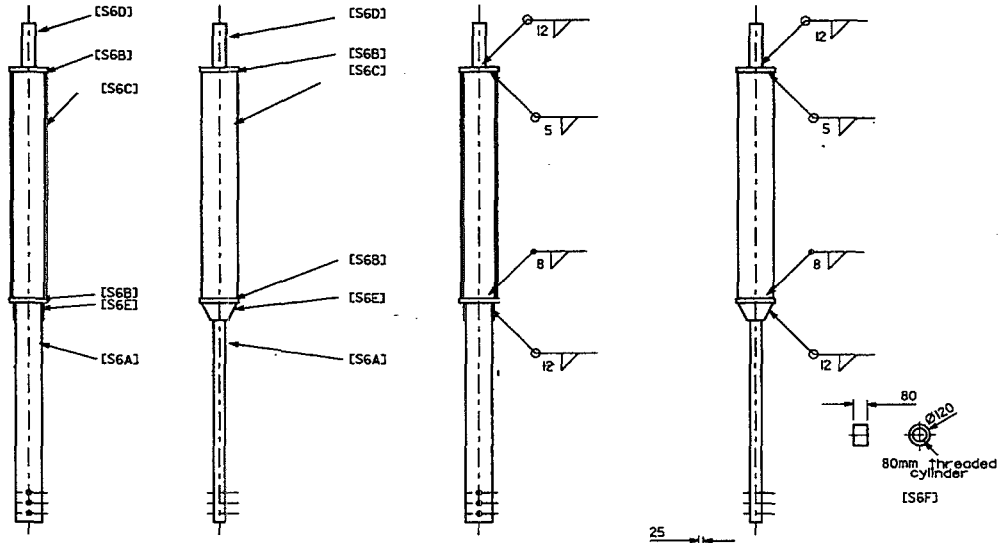

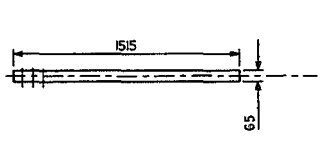

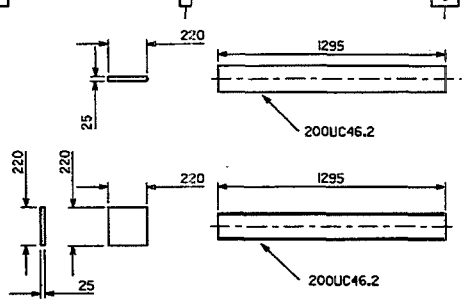

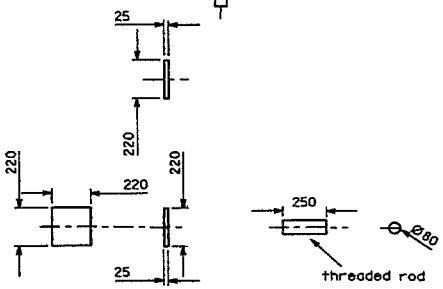

Department of Civil Engineering University of Canterbury Christchurch, New Zealand	FABRICATION DRAWINGS Section F details Secondary frame	Drawn: JGM Date: 16/3/00 Revision: E Scale: 1:20	Drawing No. S6

Notes:
Construction tolerances 0 to -3mm
All dimensions mm unless stated otherwise
fy=300MPa unless stated otherwise
All welds are grade SP
No. req'd=2

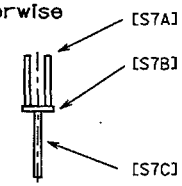

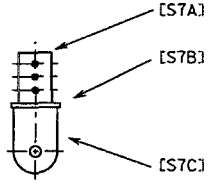

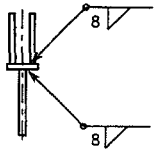

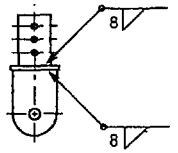

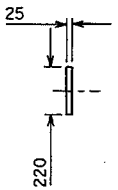

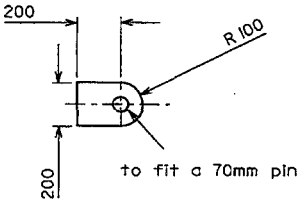

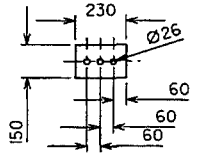

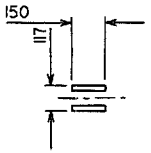

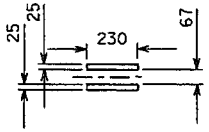

[S7A]

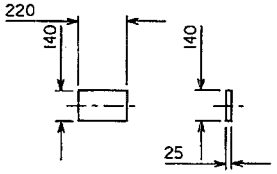

[S7B]

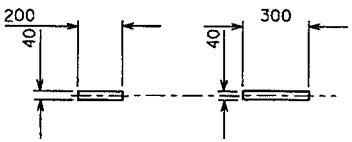

[S7C]

Department of Civil Engineering University of Canterbury Christchurch, New Zealand	FABRICATION DRAWINGS Part G details Secondary frame	Drawn: JGM Date: 16/3/00 Revision: C Scale: 1:20	Drawing No. S7

Appendix D
Extended Experimental Results

D.1 General behaviour and observations during the test

Throughout this chapter reference will be made to particular hollow-core units (1st, 2nd, 3rd, 4th or 5th) within the super-assemblage or to the perimeter beams (North, South, East and West), refer to Figure D-1 for their location.

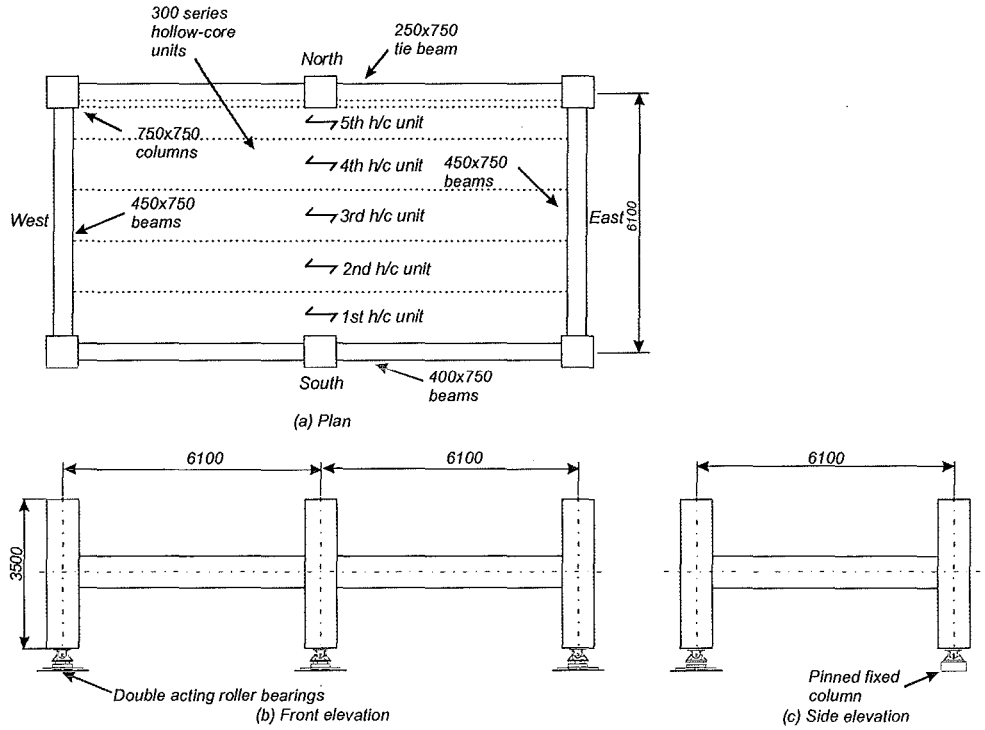

Figure D-1 Plan and elevation of the super-assemblage

The key indicator in determining the performance of the hollow-core unit connection detail is the relative rotation between the hollow-core unit and the supporting beam. Within this document this relative rotation has been defined as interstorey drift as the building investigated was considered to be a generic New Zealand moment resisting concrete frame building in which the interstorey drift closely relates to the relative rotation. In terms of predicting the amount of reinforcement slab activated as flange steel within a structure, the relative rotation between the hollow-core unit and the supporting beam should be used. As torsion of

the beams supporting the hollowcore units reduces this relative rotation, it is considered conservative to assume that the relative rotation and interstorey drift are one and the same. A designer is reminded that if a true assessment of risk or damage to the floor system is required then the designer should focus on the relative rotation between the hollow-core unit and the supporting beam as it is less conservative that using the interstorey drift as the indicator.

D.1.1 Phase I-Longitudinal loading

Initial elastic cycles of ± 0.1% drift were used to ensure all the loading equipment and instrumentation was working correctly.

First cracks appeared in the super-assemblage at a drift of 0.25% drift. These cracks appeared simultaneously in several locations; the main frames plastic hinge zones, beam column joints and in the central column. Further cracks appeared during the –0.25% drift load cycle. The most significant crack was one that formed longitudinally along the soffit of the first hollow-core unit parallel to the direction of loading. The longitudinal crack that formed in the bottom of the hollow-core unit started at the stress concentration created by removing a section of the hollow-core unit around the central column to allow the unit to rest against the main perimeter beam. The crack propagated 850mm towards the east end and 600mm towards the west end and can be seen in Figure D-2. Figure D-3(a) shows the floor slab crack patterns at the end of the ±0.25% load cycle. The blue lines refer to cracks that formed during a positive inclination (the top of the column displaces in an Easterly direction while the base of the column displaces in a Westerly direction) cycle while the red cracks refer to a negative inclination (the top of the column displaces in an Westerly direction while the base of the column displaces in a Easterly direction) cycle.

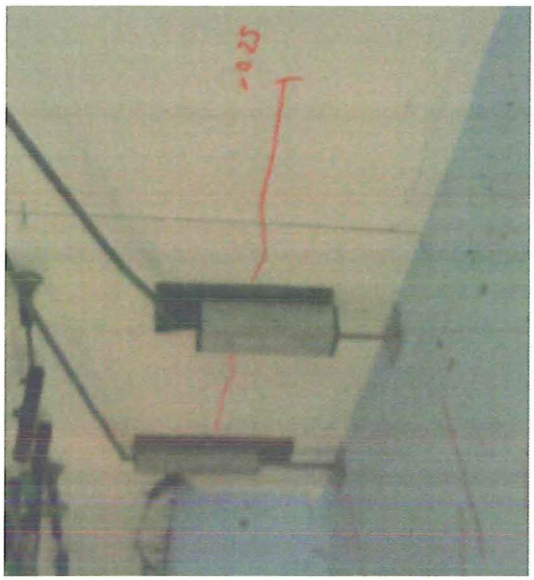

Figure D-2. Initial hollow-core crack that formed in the soffit of the first unit.

The next load cycle was up to 0.5% drift, the approximate first yield as determined by initial calculations. At 0.32% drift the first crack in the end of the hollow-core unit was observed. This crack formed at the west end of the first hollow-core unit, starting at the stress concentration created by the removed section of hollow-core around the corner column and effects the hollow-core units seat connection. See Figure D-4 to see the location and direction of this hollow-core crack. This crack effects the hollow-core units seat connection. This was the onset of potential economic loss as this damage to the hollow-core unit is irreparable.

At 0.5%, drift several cracks formed within the floor diaphragm. A crack 4.5m long formed across the floor diaphragm close to the termination of the floor starter bars. This crack ran perpendicular to the direction of loading (Figure D-5). Several other cracks also formed within the floor slab. Most started at the central column and propagated out towards the centre of the floor slab. A longitudinal crack formed in the topping along the joint between the first and second hollow-core units. Torsion cracks started to form in the east beam (transverse to the loading direction) as it was being exposed to a negative moment (causing tension in the top fibres of the floor topping).

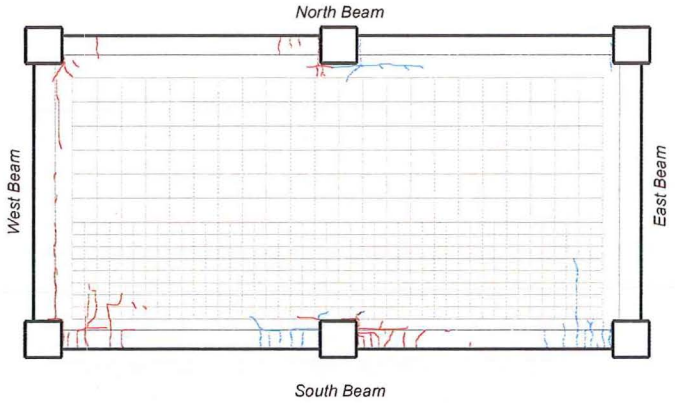

(a) Topping cracks after the ±0.25% drift cycle

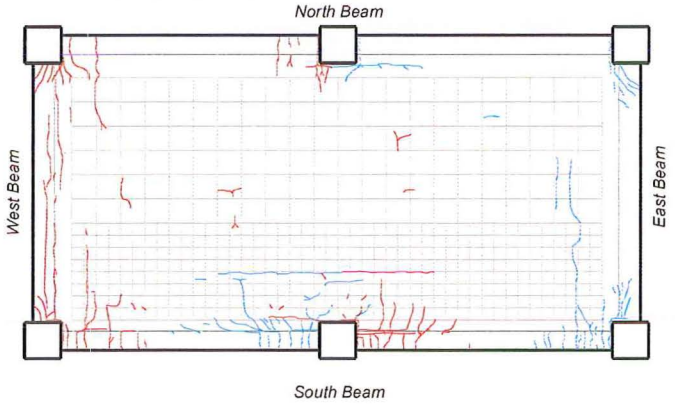

(b) Topping cracks after the ±0.5% drift cycle

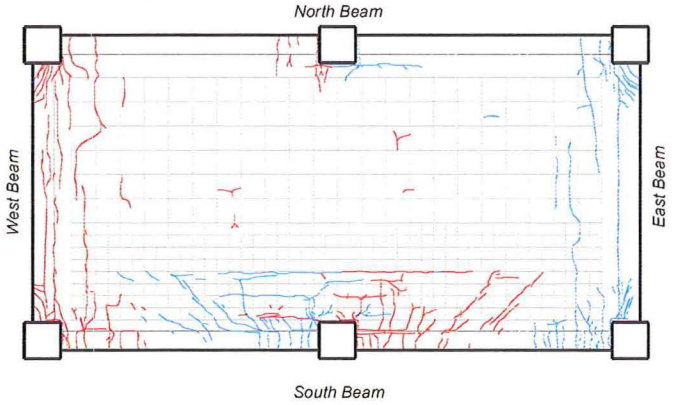

(c) Topping cracks after the ±1.0% drift cycle

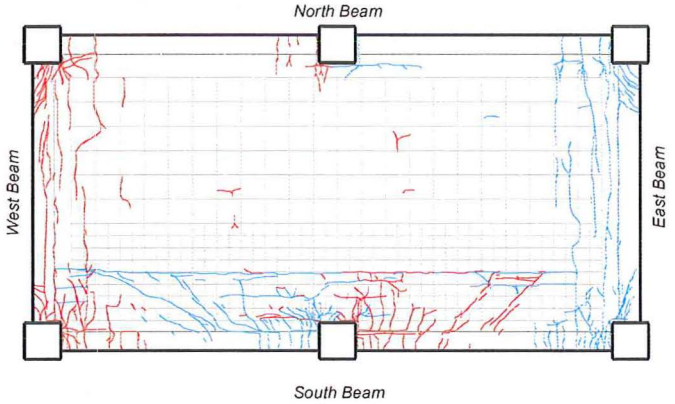

(d) Topping cracks after the +2.5% and –2.0% drift cycles

Figure D-3 Mapping of the topping cracks during the first phase of loading. Blue cracks are due to a positive inclination while the red cracks are due to a negative inclination

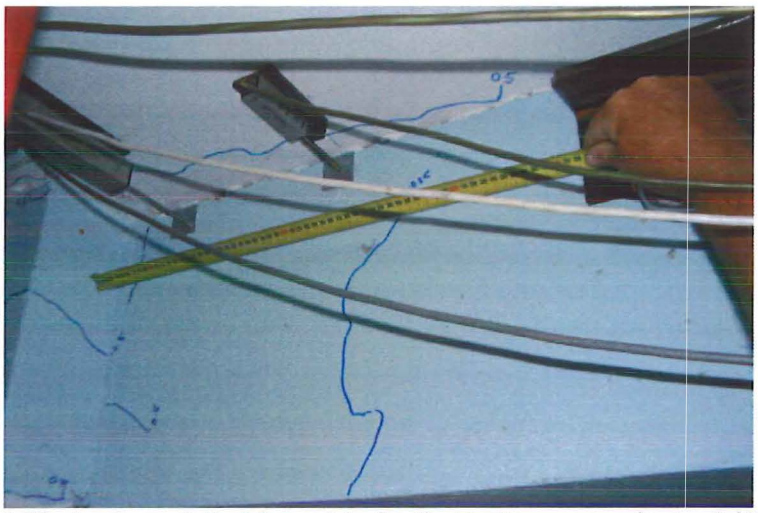

Figure D-4. First end crack that formed in the first hollow-core unit at a drift of 0.32%

These cracks formed due to the restraint being provided by the starter bars in the central region of the beam while the inclined columns tried to rotate the beam ends. This torsion can be seen in Figure D-6.

Torsion cracks started to form in the west beam during the –0.5% drift cycle. The longitudinal crack in the soffit (shown in Figure D-2) had extended nearly the full length of the super-assemblage at the completion of this load cycle. At this drift level a discontinuity crack formed within the floor topping at the west beam. The discontinuity crack is a crack that forms in the topping at the end of the hollow-core unit and is created as the beam rotates relative to the floor slab. This crack only forms in zones of negative moment. This crack formation is depicted in Figure D-7. Figure D-3(b) shows the floor slab crack patterns at the end of the ±0.5% load cycle (the blue lines refer to cracks that formed during a positive inclination cycle while the red cracks refer to a negative).

The 1.0% drift load cycle saw the discontinuity crack form at the east end of the super-assemblage. The crack in the soffit of the first hollow-core unit had now

Figure D-5. The topping crack that formed perpendicular to the direction of loading (SE Corner)

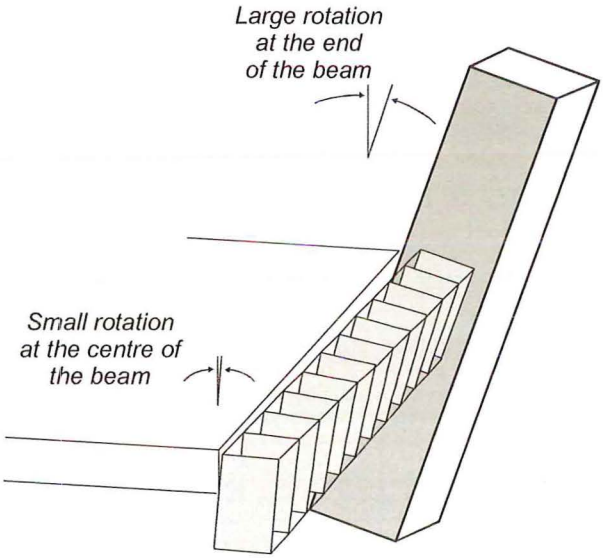

Figure D-6 Torsion generated within the transverse beam due to restraint to from starter bars within the diaphragm

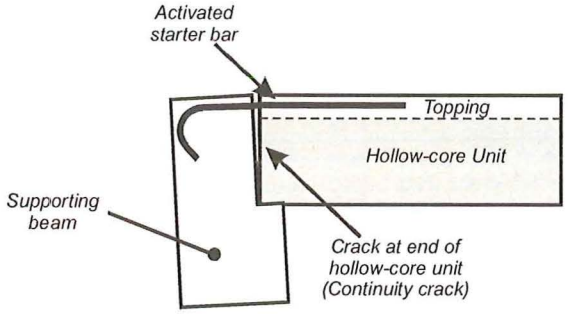

Figure D-7 Continuity crack that formed between the end of the hollow-core unit and the perimeter beam

propagated along the entire length of the hollow-core unit. Both, on the floor topping and on the bottom of the first hollow-core unit, shear lag cracks formed. Shear lag cracks form when the axial tension within a floor slab is transferred to the perimeter beam by means of a compression strut. The angle of the strut was approximately $45^0$and can be seen in Figure D-8.

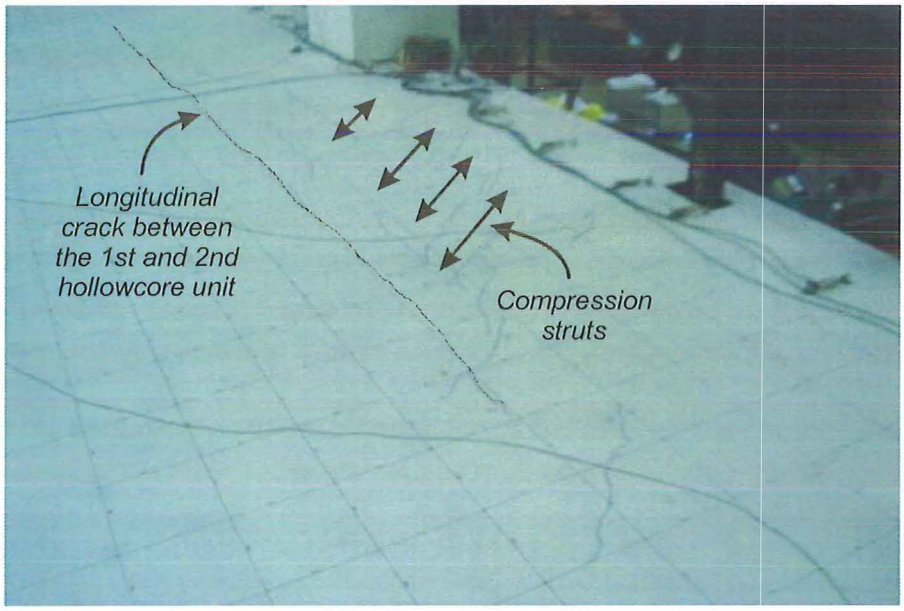

Figure D-8. Shear lag cracks that have formed on the floor diaphragm.

The crack that formed in the bottom of the first hollow-core unit at the west end is now 3-4mm wide. This crack width agrees equates to the interstorey drift multiplied by the thickness of the hollow-core unit and the topping (refer to Figure D-9). Sections along all the hollow-core seats started to show signs of distress. The beam cover concrete spalled in regions where the hollow-core unit had appeared to try and slide off the support. A 6mm crack formed at the column face of the east beam caused by the rotation between the beam and the column. A crack formed in the floor slab from the north edge of the specimen and extended across the floor towards the front perimeter beam. This crack coincided with the termination of the starter bars that were being loaded in tension.

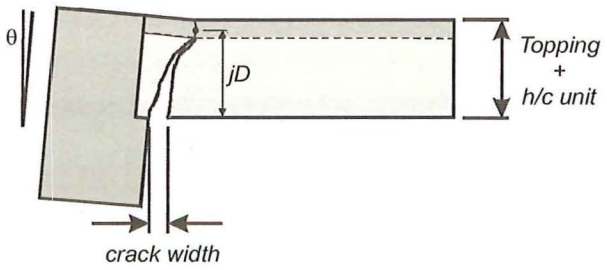

Figure D-9 Determination of the crack width at the end of the hollow-core unit

Delamination was observed around both the central and southeast columns. The delamination map can be seen in Figure D-10(a). Delamination was determined by taping the surface of the topping with the ball from a ball pein hammer and listening for a hollow sound. The zones of delamination made a distinctive hollow sound.

The longitudinal crack (Figure D-8) that formed between the first and second hollow-core unit extended along half the length of the super-assemblage and had an average crack width of 1mm.

The –1.0% drift cycle saw, what appeared to be, the first and second hollow-core unit being pulled off the east beam, thus resulting in the spalling of the cover concrete of the beam. In fact, the edge of the hollow-core unit had fractured, rather than sliding. Shear lag cracks formed in the opposite direction to the previous load cycle on both the top of the floor slab and the bottom of the first hollow-core unit around the central column. The plastic hinge zones of the beams became increasingly cracked with two or three major cracks appearing in each of the plastic hinge zones. The remainder of the plastic hinge zone cracks were hairline in appearance.

At this point it was observed that the inclination of the front three columns (in the plane of the frame) were not exactly the same. The difference between the columns was due to the slop in all the linkages connecting the secondary loading frame. It was decided that the column drift that was being reported would be that of the central column. The level by which the columns were out of parallel was not

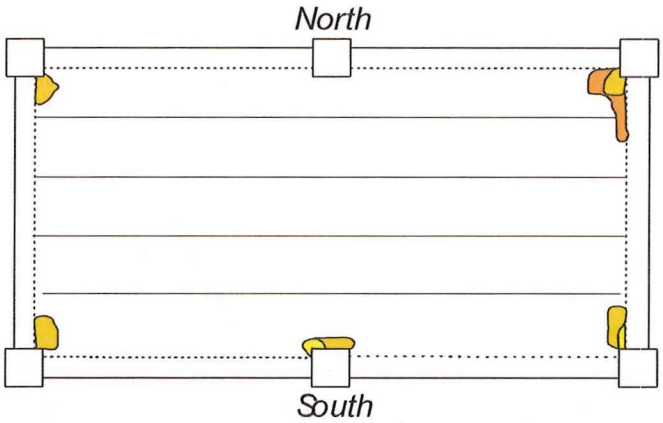

(a) Delamination after the completion of the +/-1.0% loading cycles

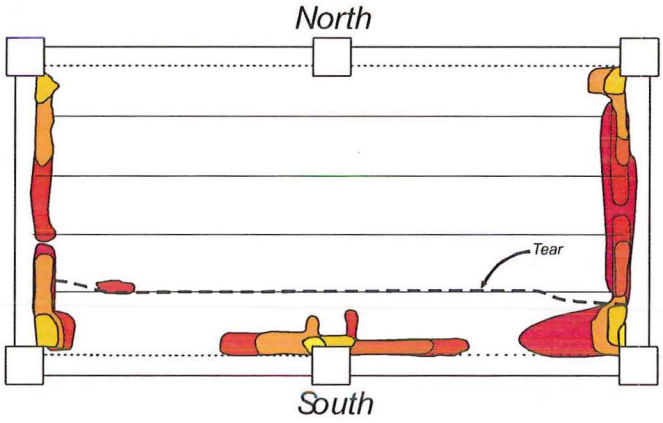

(b) Delamination at the end of Phase I

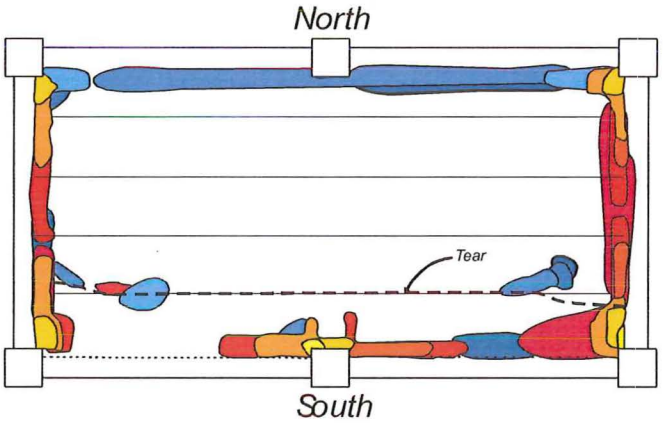

(c) Delamination map after completion of the +2.0% and -2.5% drift cycles

Figure D-10. Mapping of the delamination of the topping from the hollow-core unit during the experimental programme

concerning but did seem to vary linearly with increasing drift. This can be seen in Figure D-11. Since the front columns were not remaining exactly parallel it was decided that the back columns inclination should match the inclination of its partner on the front frame i.e. the inclination of the NE and NW columns match the SE and

SW columns respectively. This would ensure that no loading based torsion was induced into the transverse beams.

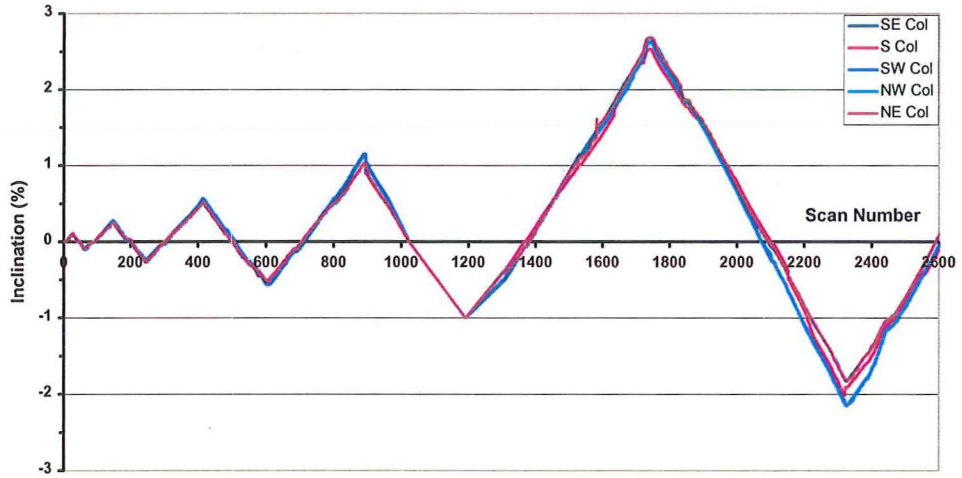

Figure D-11 A plot showing how the columns inclination changed with interstorey drift

All the cracks that had formed in the floor slab were limited to the first hollow-core unit. The only exceptions to these were the cracks that formed at both ends of the units due to the rotation of the beam relative to the floor slab such as the discontinuity cracks. No new torsion cracked formed in the end beams, the existing cracks had continued to open. The 3-4mm continuity crack that had formed in the end of all the west hollow-core units during the previous load cycle did not fully close despite the reversal in inclination. This looked to be a visual sign of beam elongation.

More of the cover concrete of the east beams spalled due to the movement of the hollow-core unit relative to the supporting beam. The crack at the fractured end of the East hollow-core units was 2-3mm wide.

The residual drift at the completion of the load cycle was –0.41%. This recovery equates quite closely to the yield drift of the system (0.5% was the yield drift, refer to Appendix F for determination of the yield drift).

Upon the completion of the –1.0% cycle the delamination of the floor slab was checked and it was found that the zones of delamination were confined to regions

around all the columns (Figure D-10(b)). Figure D-3(c) shows the floor slab crack patterns at the end of the ±1.0% load cycle (the blue lines refer to cracks that formed during a positive inclination cycle while the red cracks refer to a negative). Figure D-12(a) shows the crack patterns on the underside of the floor slab at the end of the ±1.0% load cycle.

At zero drift the front frame was examined to determine whether all the cracks in the plastic hinge zones had closed. It was found that the two end plastic hinge zones cracks had not closed while the plastic hinges on each side of the central column had closed. This shows that the hollow-core unit passing the central column does provide some clamping force that is large enough to close the plastic hinge zone cracks at these relatively low levels of drift.

The next load cycle was to 2.5% drift. At 1.93% drift the reinforcing mesh within the topping started to fracture. The mesh fractured across the crack that had formed between the first and second hollow-core units (Figure D-13), the crack width measured 2mm. At 1.98% drift a continuous sound of fracturing mesh could be heard. Upon inspection it was found that a 9m long crack in the floor slab had opened and measured 3-4mm in width. It was assumed that most of the mesh had fractured over the entire length of the crack (due to the width of crack and the brittleness of the mesh). When the mesh fractured, a drop off in flexural strength of the longitudinal frame was observed. As loading was continued up to a drift of 2.5% more strands of the mesh could be heard to fracture.

At 2.5% drift, two additional strands of mesh fractured after the specimen had been held at that drift for approximately 1.5 hours. At 2.5% drift, the width of crack between the first and second hollow-core units had increased to 20mm in the centre and tapered to zero at the ends of the crack near the supporting beams. The vertical

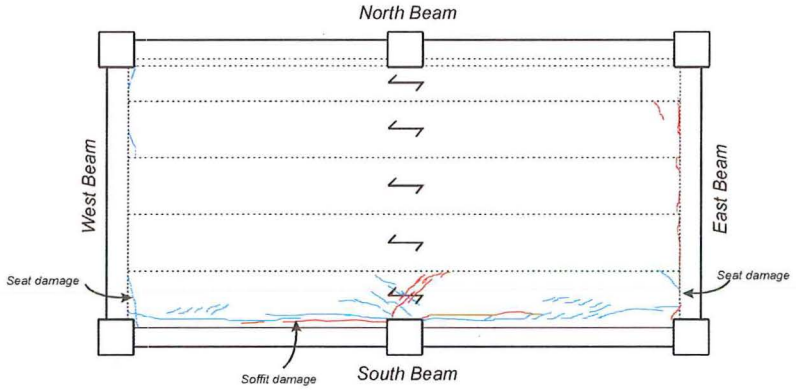

(a) Damage to the hollow-core unit at the end of ±1.0%

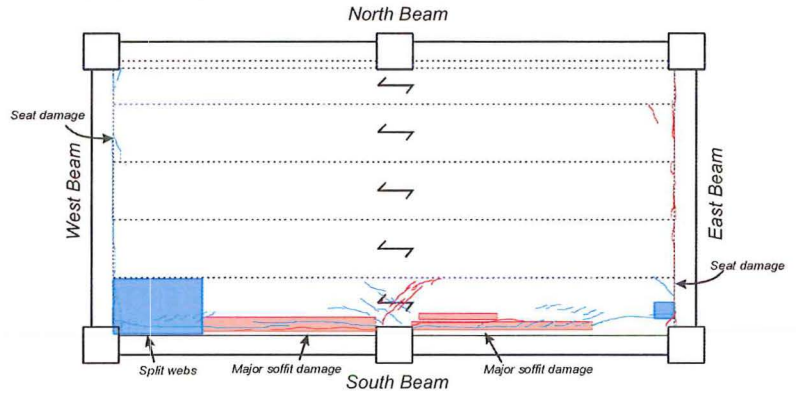

(b) Damage to the hollow-core unit at the end of Phase I

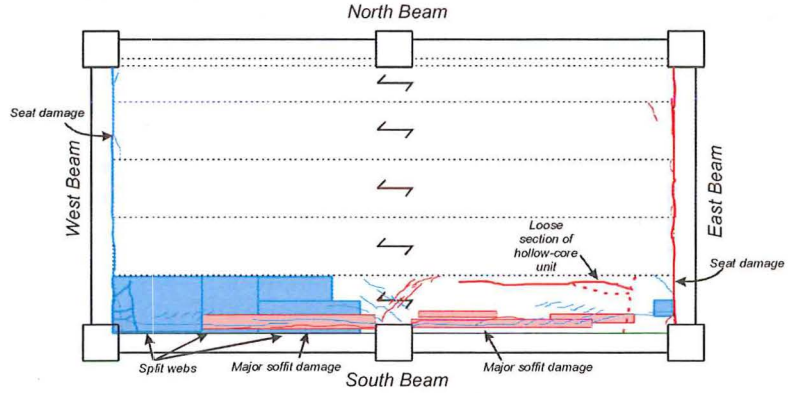

(c) Hollow-core unit damage after the +2.0% and –2.5% displacement cycle during Phase II

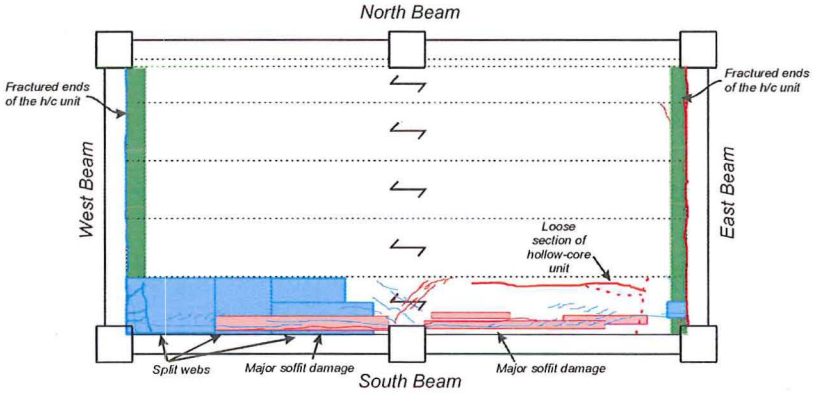

(d) Finalised hollow-core damage at the completion of the test

Figure D-12 Damage to the underside of the hollow-core unit during the experimental programme.

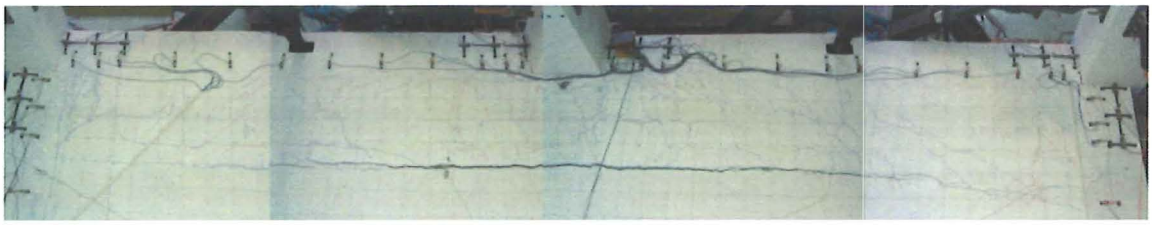

Figure D-13. Longitudinal tear that formed within the floor diaphragm

offset between the two units across the diaphragm tear varied between 6-10mm. Upon inspection of the central columns rotary pots it was found that the column had displaced 25mm in the transverse direction (this movement is orthogonal to the direction of loading and away from the specimen). The drift of the central column in a transverse direction was at 0.5% (with the top of the column tilting in). As the tear in the floor slab was 20mm wide it was no longer possible to read the Demec points using the Demec gauge, a vernier was used in these regions.

The discontinuity crack at the east end now measured 12mm. Minor spalling of the beam cover concrete was observed on both sides of the central column. The regions of delamination on the floor slab had increased. The entire seating on the west beam had been completely lost. The seating had been lost in one of two ways: (a) the edge of the hollow-core unit had been broken off or (b) the cover concrete of the beam had spalled.

At 2.5% drift, the bottom of the hollow-core units were tapped to determine zones of web splitting. Zones where the webs were split made a distinctive hollow sound when tapped with a hammer. It was found that there was web splitting in the first hollow-core unit at the west end and it stretched approximately 3m into the floor slab. There was also a small region around the central column where the webs had split. Portions of the hollow-core unit had now dropped by at least 5mm.

Due to the extensive damage to the hollow-core units and the failure mechanisms observed to be occurring it was decided that additional catch frames

should be placed under the floor for safety concerns as the frames and angles presently being used may not be sufficient to hold the floor if it were to fail.

Upon unloading the super-assemblage had a residual drift of 1.8% at zero load. Several of the potentiometers used to measure the pull off of the hollow-core units from the supporting beam needed to be reattached as the cover concrete had spalled off the beam face affecting the potentiometers target. Figure D-14 shows some of the damage at the completion of this half load cycle.

Since the hollow-core units were performing in a manner different to that initially expected it was decided that some additional manual measurements should be taken. The vertical movement of the hollow-core units relative to their seat height was measured manually at various stages during the remainder of the experimental programme.

The next load cycle was to –2.0% drift. It was at this stage that it was clear that the seat on all the units at both ends of the hollow-core units were damaged. All the ends of the units had at least a 2-3mm wide residual crack when the sub-assemblage was at zero drift. This crack width increased as the inclination was increased. The first hollow-core unit had dropped by at least 5mm and all the others slightly less.

At –1.0% drift (on the way to –2.0%) the first signs of web splitting at the east end of the hollow-core units was noticed. This occurred in the first and second units and measured 500mm into the slab. At several intervals on the way up to –2.0% drift sections of the reinforcing mesh could be heard fracturing. The condition of the seating connections continued to degrade.

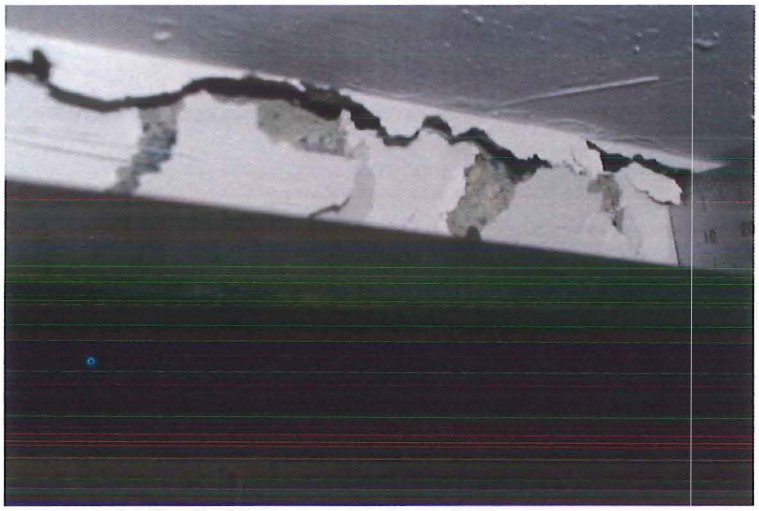

(a) Spalled beam cover on the hollow-core seat.

(b) The entire seat of the hollow-core unit has been lost

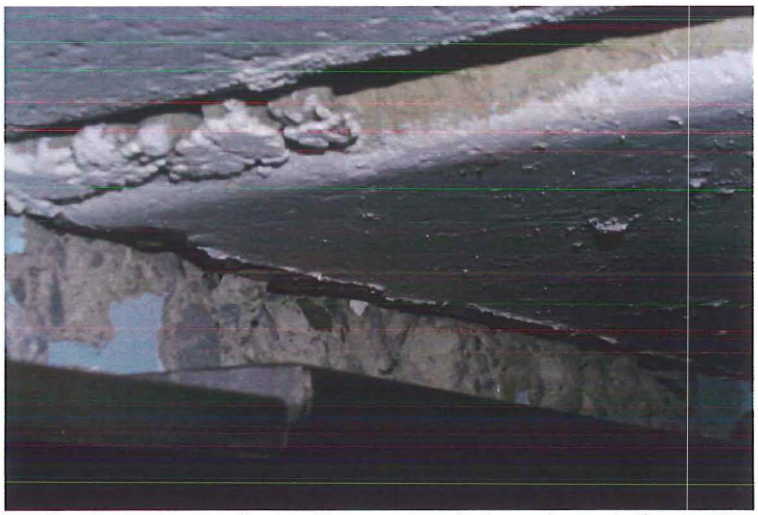

(c) This photo clearly shows the first hollow-core unit dropping relative to the second unit.

Figure D-14. Photos at zero drift after the completion of the 2.5% drift half cycle

Due to the 25mm outward movement of the central column and the softening of the beam slab assembly the central column inclination in the transverse direction had increased to 1.3%.

Figure D-15 shows the diaphragm damage at the end of phase I. At the conclusion of the phase I loading, the first unit had dropped by some 10-12mm. All the others units had dropped by approximately 5mm. The damage seen in the hollow-core units seating detail is irreparable and had been for sometime. Figure D-10(c) shows the extent of delamination at the end of phase I. Figure D-3(d) shows the floor slab crack patterns at the end of the +2.5% and –2.0% load cycle (the blue lines refer to cracks that formed during a positive inclination cycle while the red cracks refer to a negative). Figure D-12(b) shows the crack patterns on the underside of the floor slab at the end of the phase I.

D.1.2 Phase II-transverse loading

Before the transverse loading could begin the loading and secondary frames needed to be connected to the side frames. All the columns were then straightened to ensure that all the columns started vertical.

During the elastic cycles not many new cracks formed, the torsion cracks from the previous load direction opened slightly.

The 0.5% drift cycle started to see a few small cracks forming in the first hollow-core unit around the central column. In both the southeast and southwest corners the topping started to lift. During this load cycle the specimen performed in a manner different to initially predicted. This was due to the influence that the phase I loading cycles had on the system. When a positive inclination (the top of the column displaces in the northern direction while the base of the column displaces in the southern direction, a negative inclination is the opposite) is applied to the super-

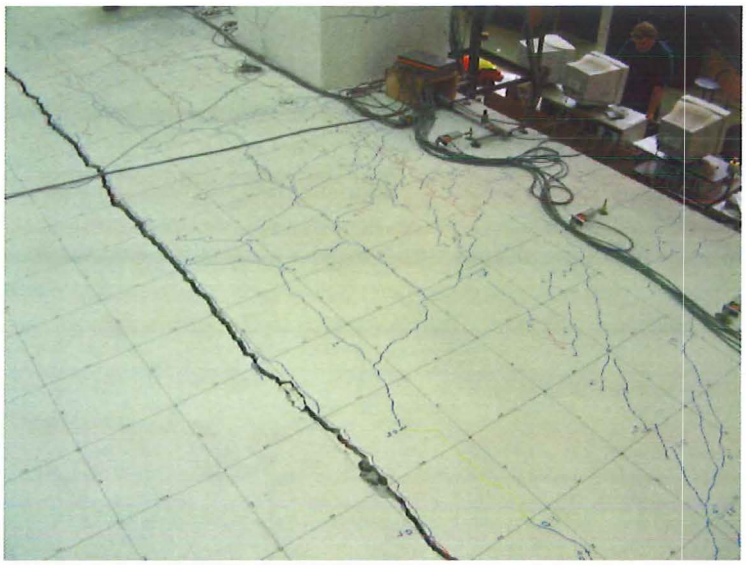

(a) Close up showing the width of tear within the floor diaphragm

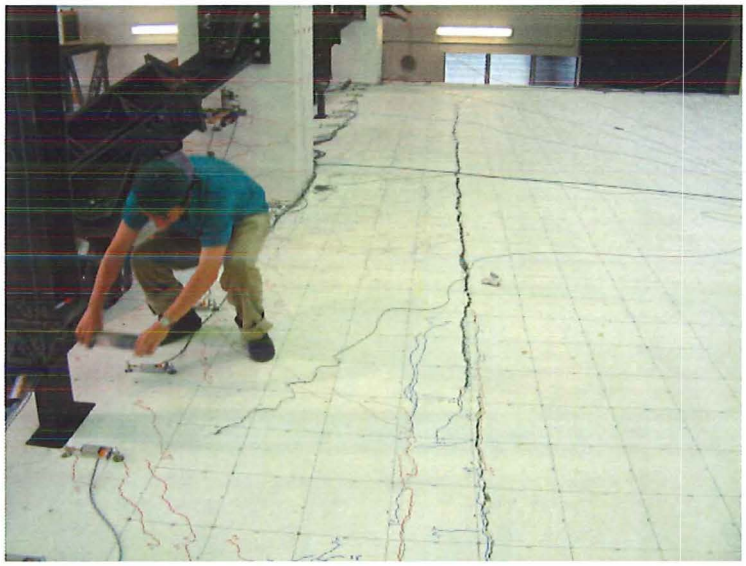

(b) Extent of cracking within the floor

(c) The offset between the two hollow-core units

Figure D-15. Photos of the diaphragm at the end of Phase I

assemblage a crack was expected to open between the perimeter beam and the bottom of the first hollow-core unit. This was not the case since the soffit in the first hollow-core unit had been extensively damaged and had been cracked along its entire length creating a zone of weakness. This is where all the rotation occurred around. Figure D-16 shows the difference between the predicted and actual rotation.

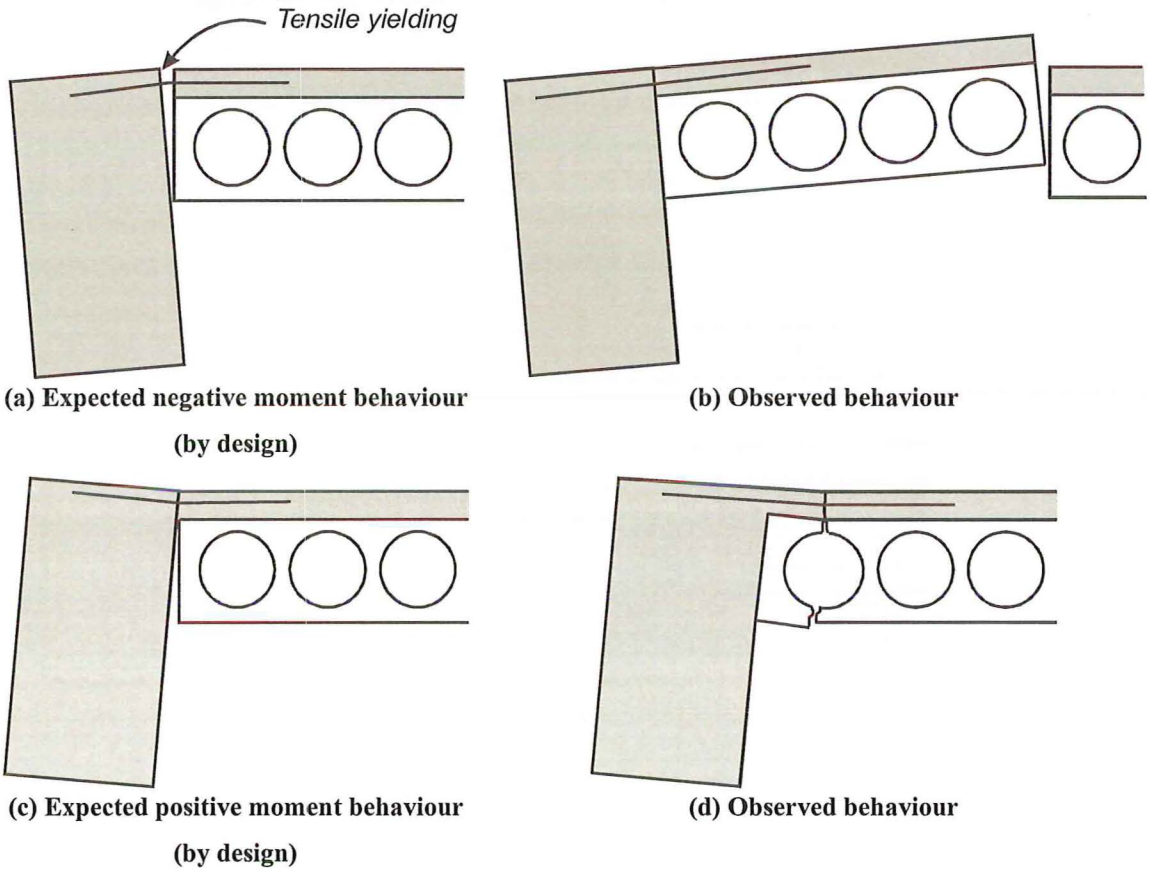

(a) Expected negative moment behaviour (by design)

(b) Observed behaviour

(c) Expected positive moment behaviour (by design)

(d) Observed behaviour

Figure D-16. Expected and actual rotation of the first unit and perimeter during the transverse loading.

The next load cycle was to –0.5% drift. Again the damage from the previous loading direction played a major role in the performance of this load cycle. Initially it was assumed that a discontinuity crack would form at the interface between the first hollow-core unit and the perimeter beam. This did not occur as the longitudinal crack that formed between the first and second unit caused the entire first hollow-core unit to lift. Figure D-16 shows the difference between the predicted and observed results.

The 1.0% drift load cycle saw small pieces of concrete falling out of the crack in the first hollow-core unit soffit. The topping around the central column started to lift. Until this point, all the delamination that had occurred was not visible but now a vertical lifting of the topping can be seen around the central column and the southwest corner. The northwest end of the fifth hollow-core unit is now starting to drop. It had dropped approximately 2-3mm.

The east beams seat became even more extensively damaged during the –1.0% drift cycle. The cracks within the two transverse beams are now forming as flexure cracks rather than being dominated by the torsion cracks that formed during the initial longitudinal loading. More reinforcing mesh started to fracture as the first hollow-core unit was lifted, leading to the extension of the crack between the first and second hollow-core units. At this stage it was clear that the west end of the first hollow-core unit is being held up (and had been for sometime) by a relatively small piece of concrete that has not failed, seen in Figure D-17. This portion of concrete could not be relied upon to hold up the unit, as it is not guaranteed to form every time. The unit has dropped by an additional 8-10mm at 2.0% drift. Just before the target drift of 2.0% was reached a portion of the soffit of the first hollow-core unit fell out. This enabled a camera to be placed in the core to verify the web splitting. The exact length of web splitting was difficult to measure but was at least 4m from the west beam. The width of web crack varied between 15-25mm. This explained why the front edge of the first unit had dropped by that amount relative to the section still attached to the beam. Figure D-18 shows the internal hollow-core damage looking in both the east and west directions.

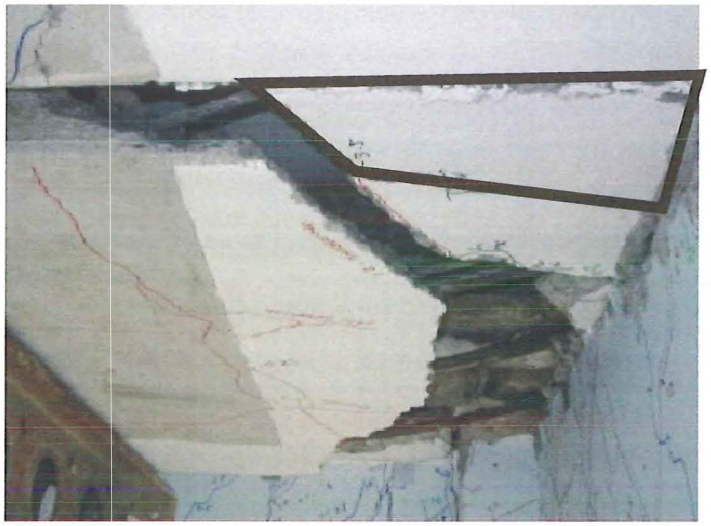

Figure D-17. Section of concrete holding up the hollow-core unit.

During the –2.5% loading cycle the first hollow-core unit is clearly seen to be lifted. This lead to more reinforcing mesh fracturing and at -2.5% drift the difference in height between the two units varies between 27-33mm along the length of the unit (Figure D-19). At the west end of the floor slab the crack between the first and second units changed direction and started to propagate into the second unit, whereas at the east end the crack started to propagate into the first hollow-core. This is shown in Figure D-20.

Throughout the transverse loading the regions of delamination increased significantly. Most of the delamination was confined to within 500mm to 1000mm of the end of the perimeter beam. This coincides with the termination of the starter bars. shows the crack patterns on the underside of the floor slab at the end of the +2.0 and –2.5% load cycle.

After the completion of the +2.0/ –2.5% load cycle the super-assemblage was bought back to zero drift so that a torsion test could be undertaken. The torsion test consisted of imposing a cycle of +/-0.5% drift to the system with one frame being

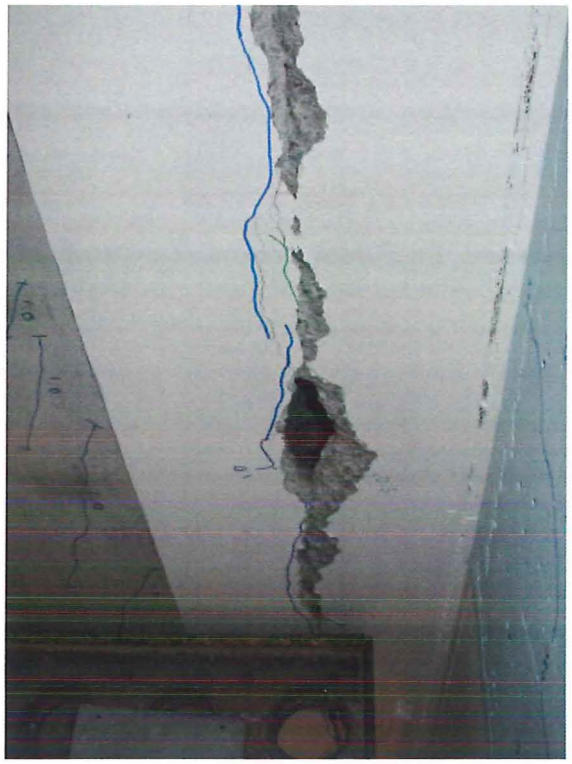

(a) Section of the hollow-core unit that fell out allowing a camera inside

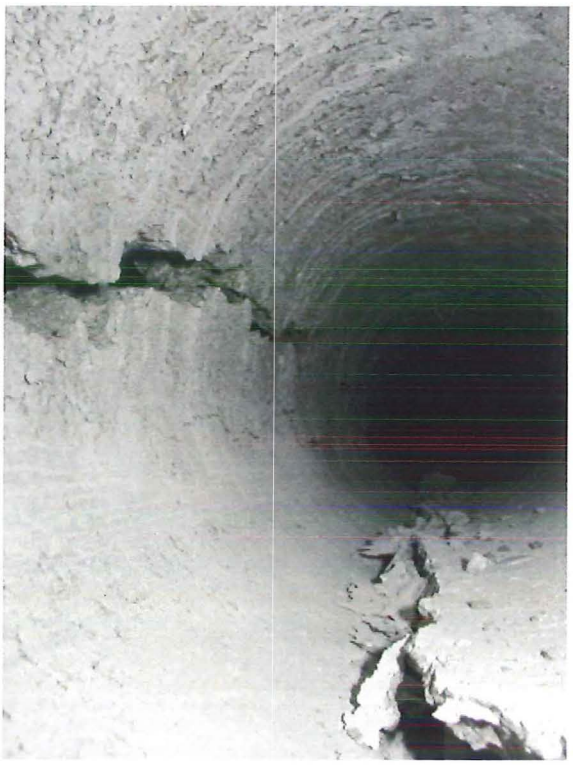

(b) Looking east. Large cracks can be seen in the web and soffit of the unit.

(c) Several cracks can be seen around the dam. Extensive damage to the seat connection as well as the unit

Figure D-18. Web splitting within the first hollow-core unit.

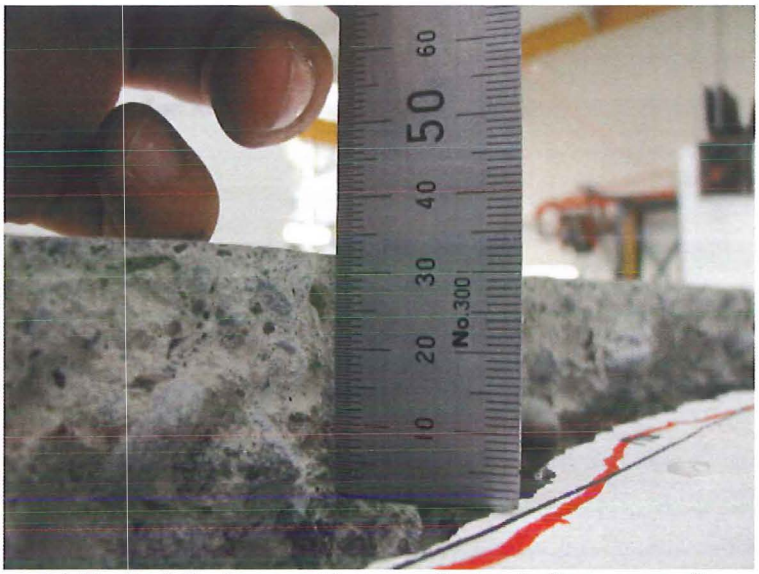

(a) Vertical displacement between the two hollow-core units

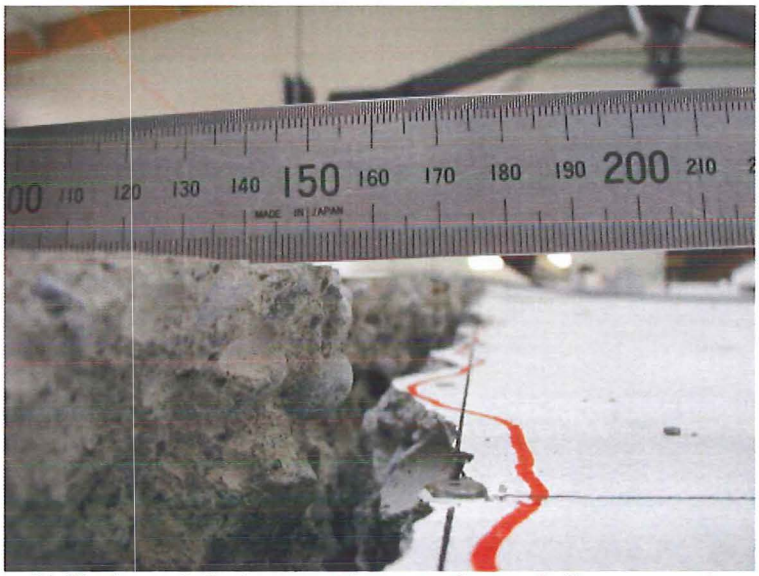

(b) Horizontal displacement between the two hollow-core units

Figure D-19. Vertical lifting of the first hollow-core unit relative to the second unit.

loaded in the positive direction while the other is loaded in the negative direction while the central column remained vertical. This loading cycle was undertaken so that the torsional stiffness of the frame could be assessed. A reading reflecting the state of an undamaged structure could not be obtained as the pre-existing damage in the super assembly greatly affected the buildings strength and performance. Figure D-12(c) shows the crack patterns on the underside of the floor slab at the end of 2.0% and -2.5% cycle.

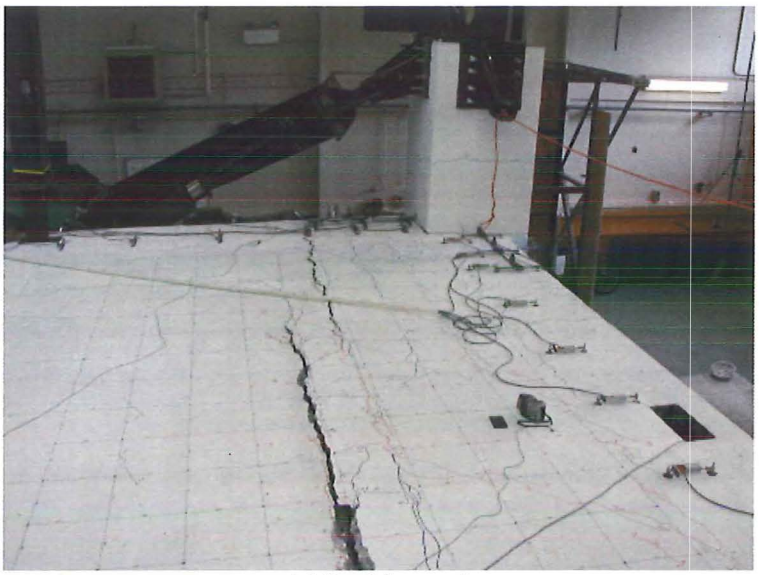

(a) Looking east

(b) Looking west

Figure D-20. Changes in the crack direction at both ends of the first hollow-core unit

Just prior to the start of the torsion test the diaphragms delamination was mapped (Figure D-10(c)). The figure clearly shows that most of the starter bars around the perimeter of the floor had caused the topping to delaminate. One region near the south west corner did not delaminate, this is due to the affect the tear in the floor slab had on the system.

As the drift was increased up to 3.5% drift various noises were heard as the structure slowly deteriorated. These noises varied from the sound of small pieces of

hollow-core units falling out to more reinforcing mesh fracturing. All the hollow-core units were now slowly dropping down the beam face. At 3.0% drift a large section of the first hollow-core unit fell out (Figure D-21). This exposed some of the prestressing strands at the west end. It could be seen that only the one strand was holding the bottom half of the first hollow-core unit from collapsing (as seen in Figure D-17). Once this piece of concrete had fallen it was possible to look up all the cores of the first unit. Shining a torch down the core revelled that all the webs were split to at least the central column (6m from the end). The crack width was at least 25mm.

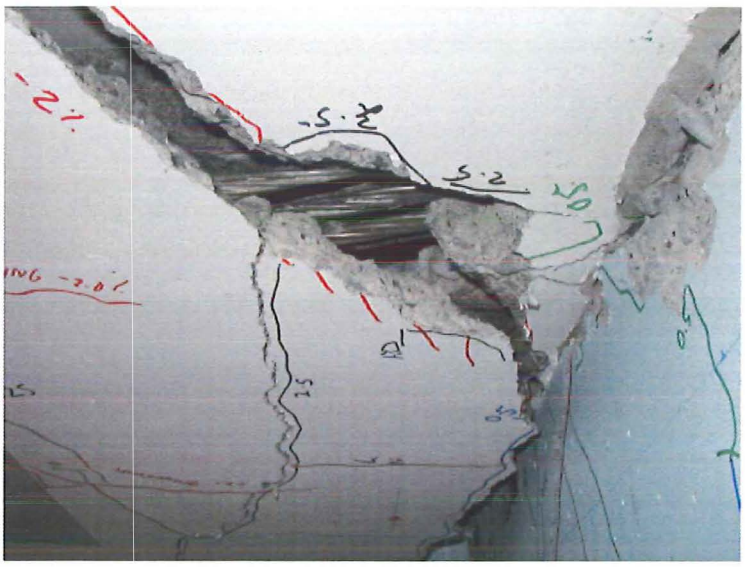

(a) West end damage

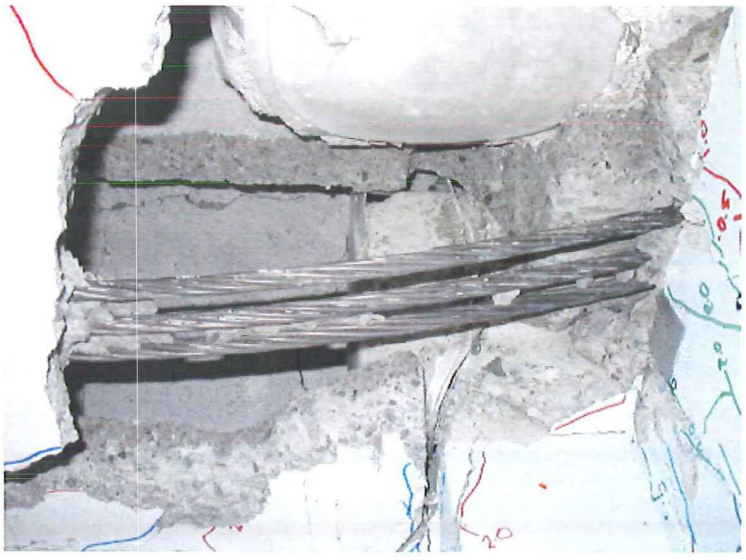

(b) Close up after a large section had fallen out. Note the curved strands no longer supporting the hollow-core unit.

Figure D-21. Damaged section of the first hollow-core unit at the west end.

On the load reversal this hollow-core unit started to drop significantly. At zero drift it had lowered by some 22-26mm, at –1.0% it was down 25-28mm. More mesh across the interface of the first and second hollow-core units fractured at –1.77% drift. The second and third hollow-core units were starting to suffer more damage. At a drift of –2.45% there was a loud thud. Upon investigation it was found that the webs in the northern most hollow-core had split (Figure D-22). The split was over two thirds of the length of the hollow-core unit and occurred around the central column. The webs split due to the horizontal shearing force applied to the hollow-core unit as it bore against the northern central column. The lifting of the first hollow-core unit had lead to the diaphragm crack propagating to the end of the sub-assemblage. Once at the end of the frame the crack then caused the beam cover concrete to be lifted. This is shown in Figure D-23. At –3.5% drift the centre of the first hollow-core unit had lifted 55-60mm relative to the second unit and the width of crack was 15-20mm.

The damage to the west end of the first hollow-core at the end of phase II is shown in Figure D-24.

D.1.3 Phase III- Longitudinal loading

The intention for this final loading direction was to complete the following displacement cycles of ±0.5%, ±2.5% and ±3.5% drift. The initial "yield" cycle was undertaken so that a comparison between the initial phase I longitudinal elastic stiffness and the phase III longitudinal stiffness could be made after the transverse loading has been completed. The ±2.5% cycle was carried out to compare the loss of strength the transverse loading had on the longitudinal strength. Refer to Chapter 5 for details on the strength comparison and initial stiffness for the various displacement phases.

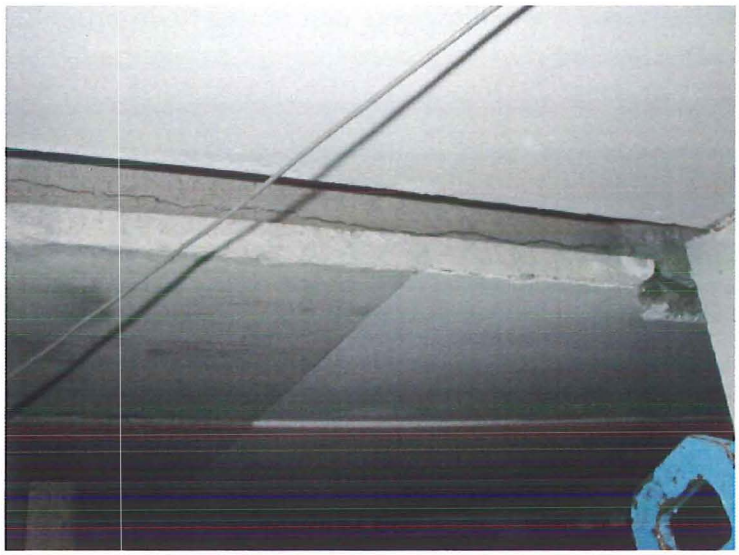

(a) The east side of the back central column

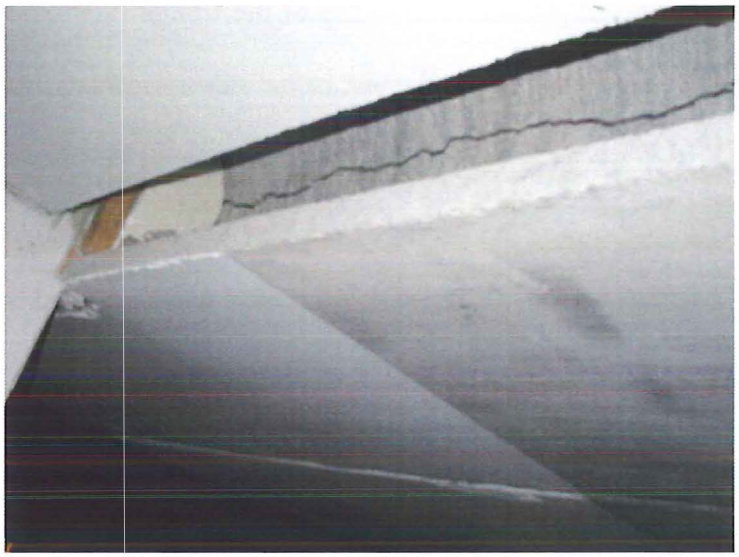

(b) West side of the back central column

Figure D-22. The northern hollow-core units split webs.

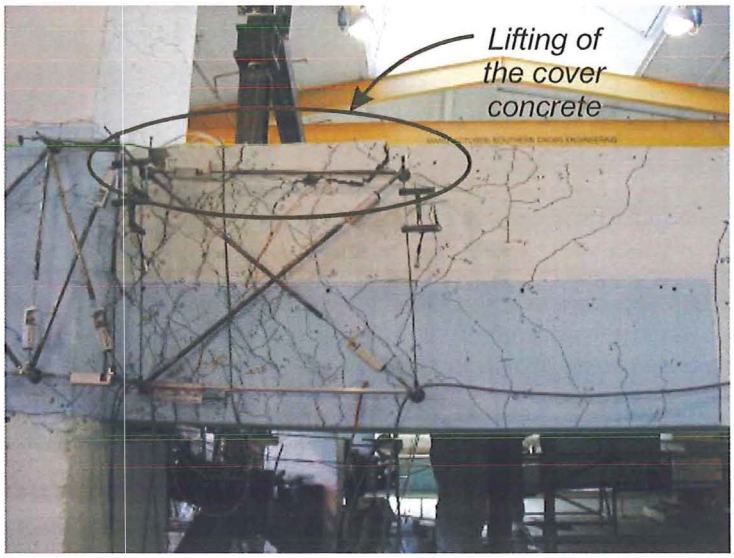

Figure D-23. Lifting of the beam cover concrete due to the imposed displacement to the first hollow-core unit.

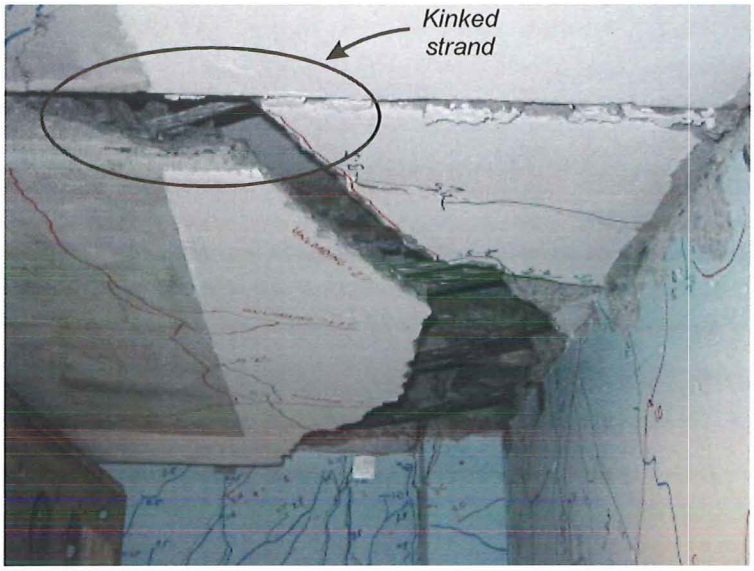

(a) Damage to the first hollow-core unit at the west end. Note the kinked strand holding the unit up

(b) Photo showing the width of web crack in the hollow-core unit

Figure D-24. Damage at the completion of Phase II.

During the first half of the 0.5% cycle there was a 9mm difference in height between the levels of the first and second hollow-core unit at the east end. All the units had dropped further during this load cycle.

At –0.48% drift another piece of hollow-core fell out at the west end. This meant that it was possible to look up all the cores of the first hollow-core unit. At this end of the hollow-core unit it can be seen that all the strands in the first unit except one had been pulled out by 20mm. The concrete around the one strand that is holding this unit is starting to crack. This is shown in Figure D-25.

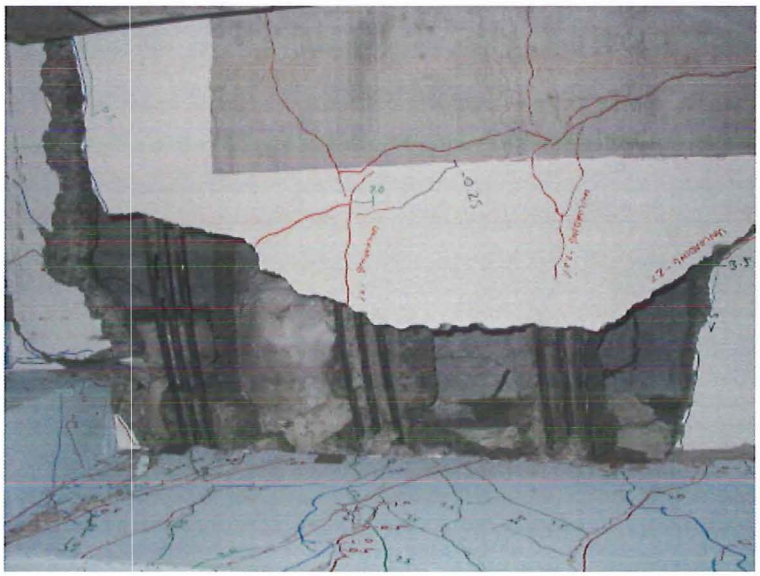

(a) Looking up at the west end of the first hollow-core unit

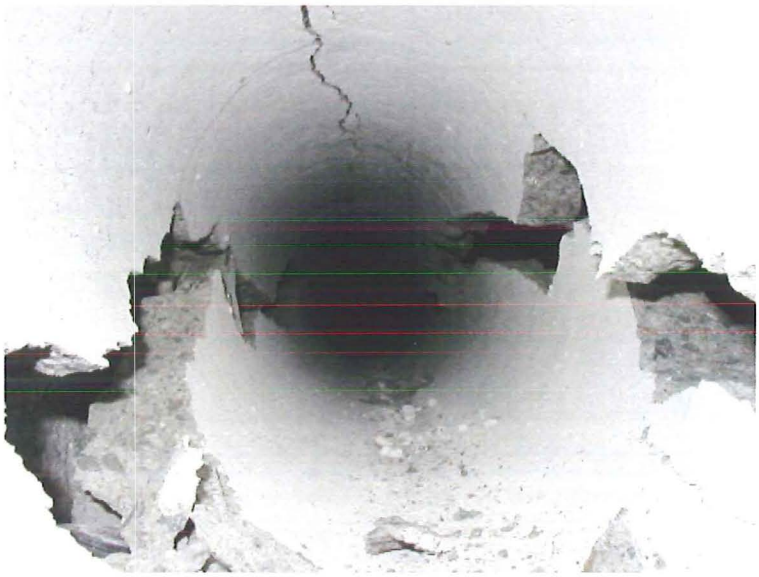

(b) Internal damage to the hollow-core unit

Figure D-25. Damage at -0.5% drift

During the next load cycle there was constantly small pieces of concrete falling out from the underside of the first hollow-core unit. A new longitudinal crack 500mm long formed in the bottom of the third hollow-core unit at the east end. It

looks to have formed due to the hollow-core unit bearing against the beam face since it has dropped relative to its initial seat. This bearing imposes a longitudinal compression strain into the unit. At 1.59% drift more beam cover concrete spalled on the west beam. The southwest corners hollow-core unit continues to break up and drop lower. There is evidence of web splitting at the east end for the first time; units 2 and 4 had split webs for the first 0.5-1m into the slab. The length of split webs in the hollow-core unit is now three quarters of the length of the super-assemblage. At 1.88% drift a region of the topping around the central column has lifted, due to the beam and the hollow-core units having different displacement patterns (Figure D-26). At 2.0% drift the small piece of concrete holding the first hollow-core unit (at the west end) started to be pulled off the beam. There are still continually pieces of concrete falling out of the hollow-core units.

At 2.5% drift the piece of concrete holding the first hollow-core unit failed. The web cracked allowing the bottom of the unit to fall onto the catch frame. The section of floor was then propped so that the catch frames could be removed. The prop was then removed to see whether the remaining uncracked webs had enough strength to hold the bottom of the hollow-core unit up. When the prop was removed the entire bottom of the first unit peeled away. Figure D-27 shows the set up when the unit is propped and then after the prop was removed. Note the similarity with the photos taken following the Northridge earthquake (Chapter 1).

As the remainder of the floor was still present is was decided to complete the load cycle to –2.5% drift. Unloading the specimen from 2.5% down to 0% drift went without incident. The hollow-core units closest to the south beam dropped significantly more than the hollow-core units closest to the north beam. At was at this stage that it was realised that the starter bars used in the tie beam were actually

(a) Plan view showing the topping lifting

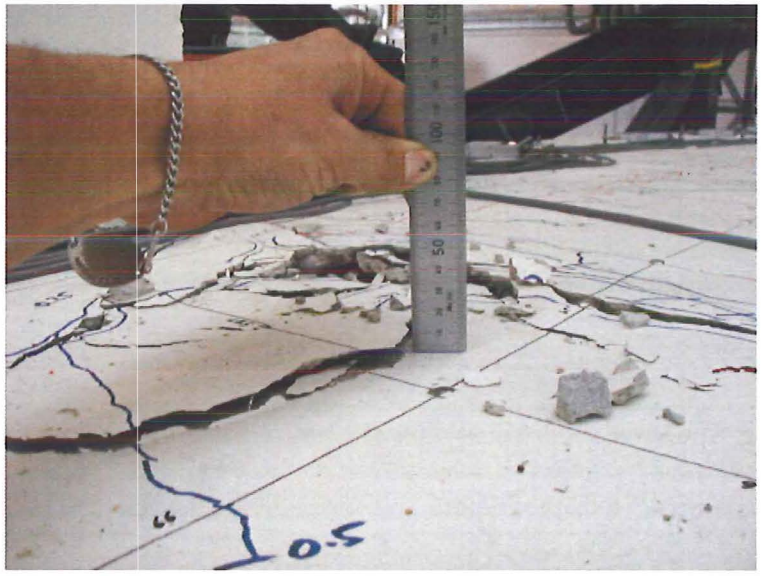

(b) Approximately 10-15mm of lifted has occurred

Figure D-26. Local lifting of the topping around the central column.

holding the remainder of the floor up (in a real structure these starter bars would not be present). At –1.3% drift it could be seen that the reinforced section of the topping slab on the east beam is pushing the floor down. This is due to the rotation being imposed by the edge beam (seen in Figure D-28(a)). Some of the cracks within the bean plastic hinge zones were now 5mm wide. At –1.5% drift the hollow-core units supported by the east beam were checked for split webs. It was found that all the five units now had split webs for at least their first 500mm into the floor slab. The east beams hollow-core units had dropped an additional 15mm. Since

(a) The failed unit resting on the catch frame. Highlighted is the piece of concrete that was holding up the unit

(b) The first hollow-core unit just before the prop (far end) was removed.

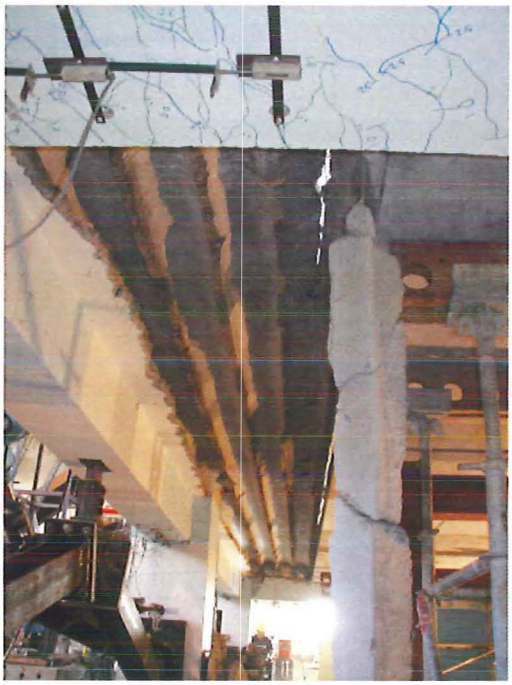

(c) After the prop was removed. The top of the unit remains in place, the soffit of the unit has fallen away.

(d) Looking East. Note the end of the hollow-core units are still attached to the beam

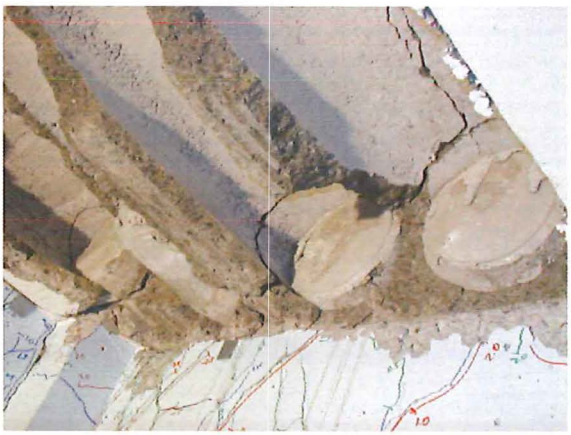

(e) Looking West

Figure D-27. Failure of the first hollow-core unit.

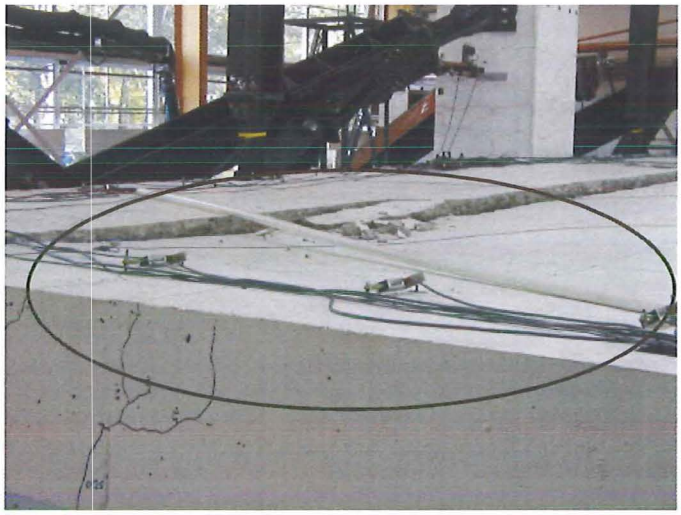

(a) Note the floor has been pushed down by the combination of the end beam rotating and the reinforced topping.

(b) Close up of the second hollow-core unit at the East end (this unit has dropped from 90mm)

(c) The floor prior to the load test

Figure D-28 Photographs of the remaining floor prior to the load test

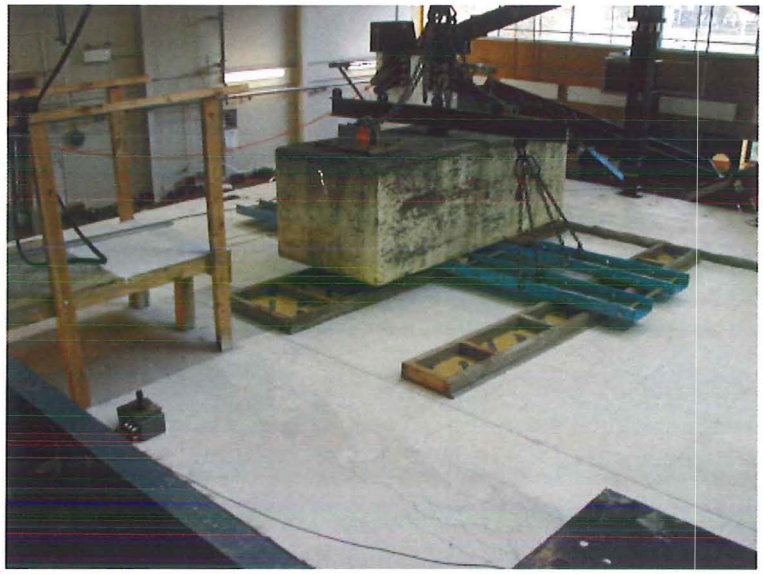

Figure D-29 The concrete mass being used to simulate the live load

the first hollow-core unit no longer had any reinforcement, since the bottom failed, a crack formed across its entire width near the central column. An additional crack formed in the topping at the termination of the starter bars at the west end. The west end hollow-core units did not drop any further during this load cycle. Once the target drift of –2.5% drift was reached if was found that at the east beam the hollow-core units had dropped by the following: 90mm at the unit 2 to 30mm at unit 5 (northern unit i.e. unit 5). This difference in the amount dropped clearly shows the influence the tie beam starters had on the system. As previously mentioned, in a real building these starter bars would not be present as there are usually no intermediate beams spanning in a direction parallel with that of the hollow-core units.

The floor was then load tested to see whether the floor could carry its design load. The key issue with the load test was to ensure the correct shear force was applied to the floor/beam connection. A concrete mass was used to load the floor (Figure D-29) and apply a load equivalent to a load of 1.75kPa (1.0kPa Reduced live load and 0.75kPa Superimposed dead load). When the load was applied, the second, third and fourth hollow-core units failed in one complete unit. This type of failure was

very similar to the failures observed in Northridge (Chapter 1). The photos, before and after load test, are shown in Figure D-28 and Figure D-30, respectively.

Upon inspection of the failed units it was found that what was thought to be split webs in the hollow-core unit near its seat was in fact the fractured end of the hollow-core unit. Refer to Figure D-12(d) for a summary of the damage to the hollow-core units at the completion of the test.

This signified the end of the testing programme.

(a) Failure of the floor after the load test. Units 2, 3 and 4 failed as one.

(b) Looking up at the floor

(c) The starters and the end of the hollow-core units remain attached to the East beam.

Figure D-30. Photos of the floor slab following the load test.

This Page is Blank

Appendix E
Experimental Results 1: Photo Log

E.1 Phase I

E.1.1 ±0.25 Drift photos

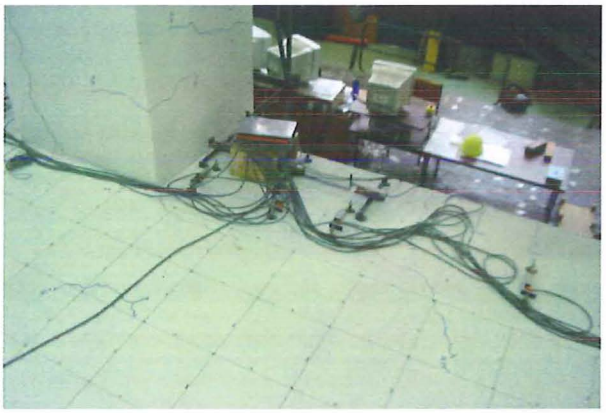

Central Column

- First sign of shear lag cracks

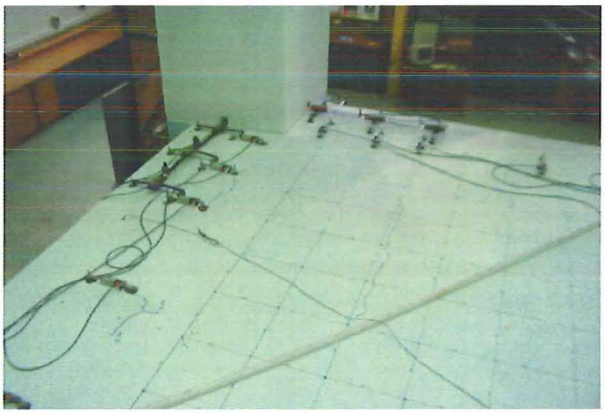

SE column

- Diaphragm crack at the end of the starter bars formed

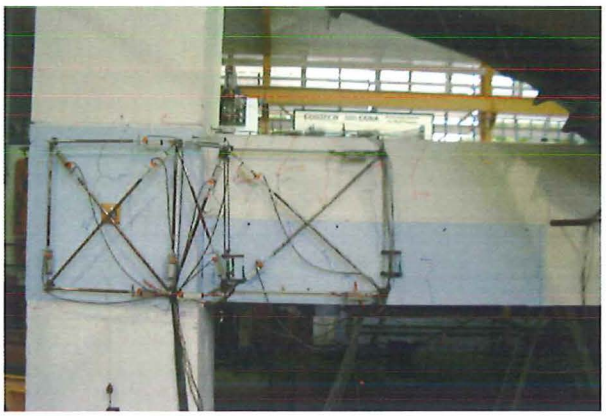

SW column

- Plastic hinge cracks at the completion of the ±0.25% cycle.

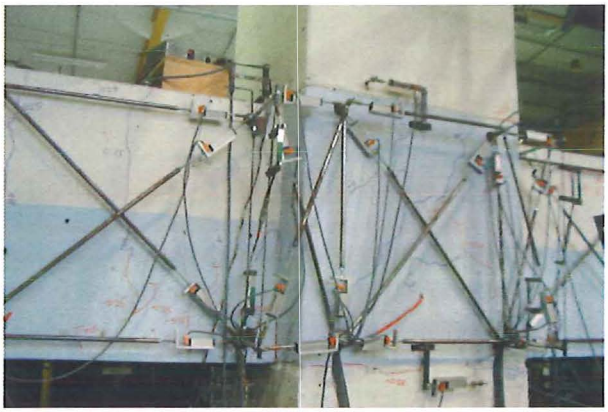

Central Column

- Plastic hinge cracks at the completion of the ±0.25% cycle.

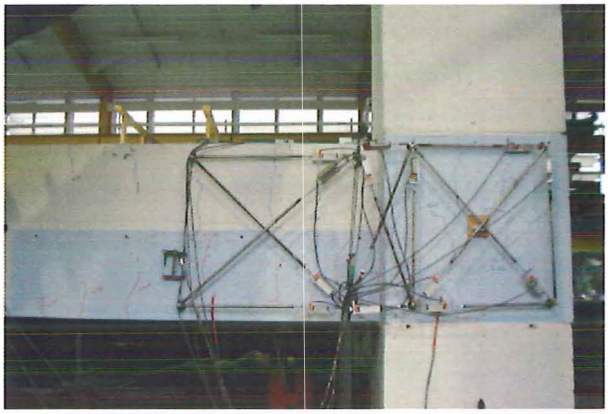

SE Column

- Plastic hinge cracks at the completion of the ±0.25% cycle.

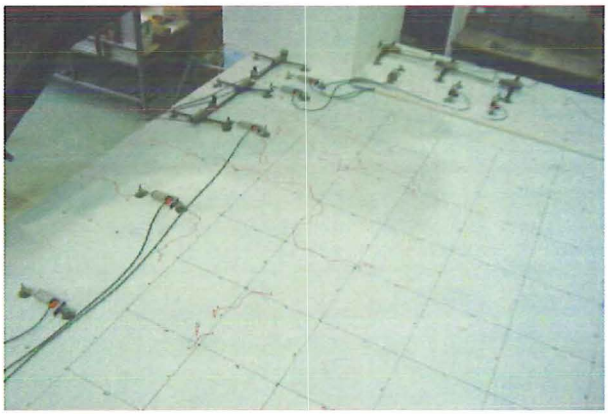

SW Column

- Diaphragm cracks at the end of the cycle

E.1.2 ±0.5% Drift Photos

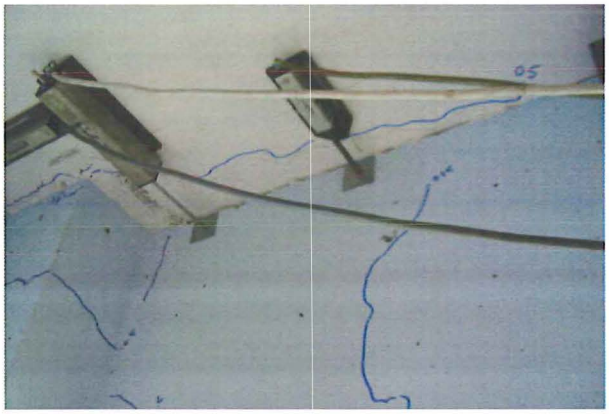

SW Column

- Damage to the hollowcore units connection

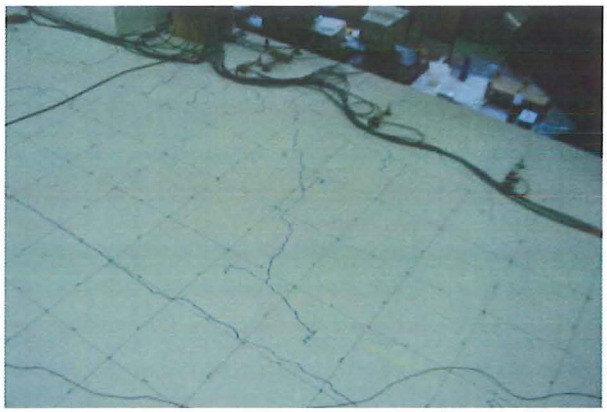

Central Column

- More shear lag cracks formed
- Longitudinal crack between the first and second hollowcore unit formed

NE Column

- Torsion cracks forming in the transverse beam

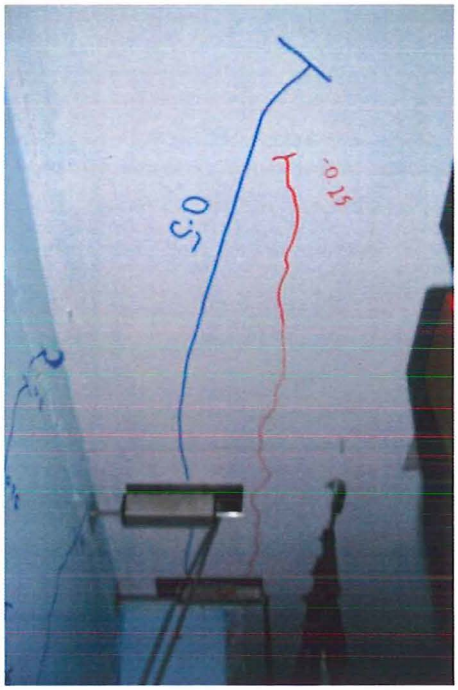

Central Column

- Longitudinal cracks formed in the soffit of the first hollowcore unit

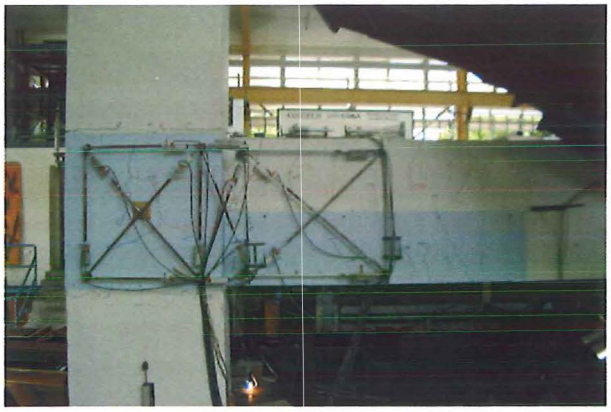

SW column

- Plastic hinge cracks at the completion of the ±0.5% cycle.

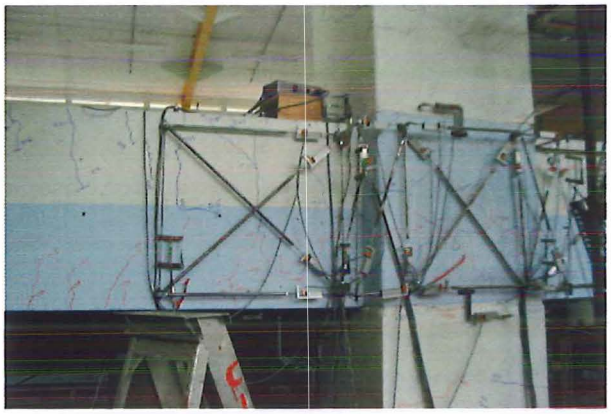

Central Column

- Plastic hinge cracks at the completion of the ±0.5% cycle.

SE column

- Plastic hinge cracks at the completion of the ±0.5% cycle.

West Beam

- Formation of the continuity crack between the end of the hollowcore unit and the beam

E.1.3 ±1.0% Drift Photos

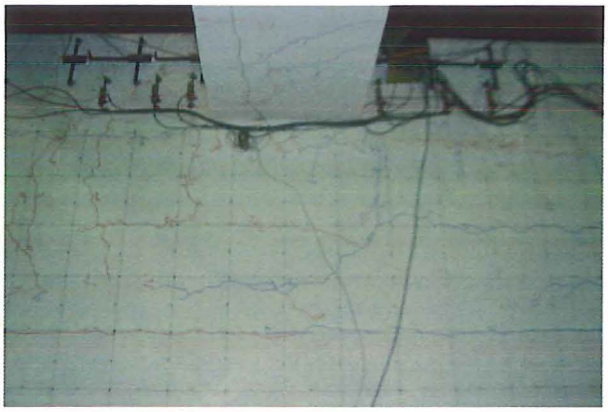

Central Column

- Lots of shear lag cracks present.
- A few small cracks within the column can be seen

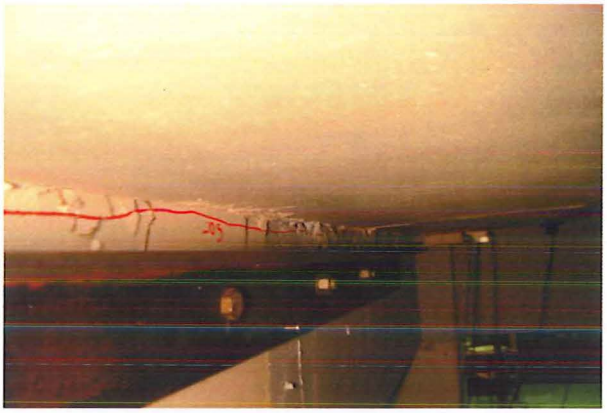

East Beam

- Spalling of the transverse beams cover concrete due to the relative movement between the hollowcore and the beam.

SE column

- The inclination of the column can be seen when compared to the white board.

Central Column

- A lot more cracks formed within the topping around the central column
- The crack between the first and second hollowcore unit increases

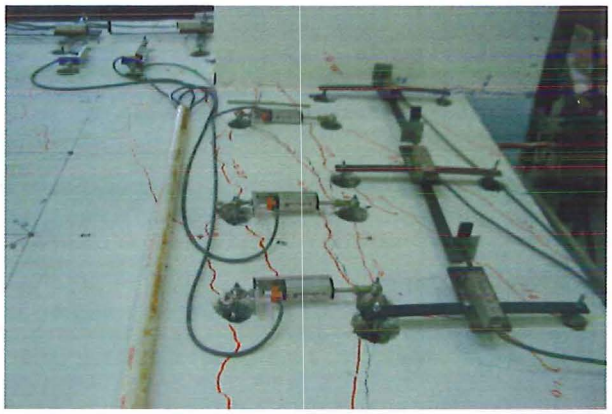

SW Column

- The torsion cracks within the transverse beams met with the continuity cracks on top of the beam

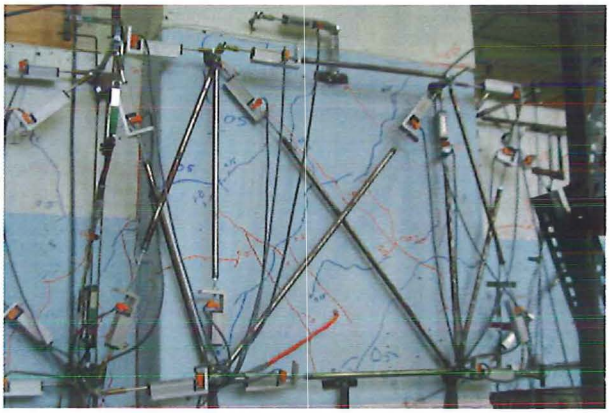

Central Column

- Beam column joint cracks at the end of ±1.0% cycle

E.1.4 +2.5%, -2.0% Drift Photos

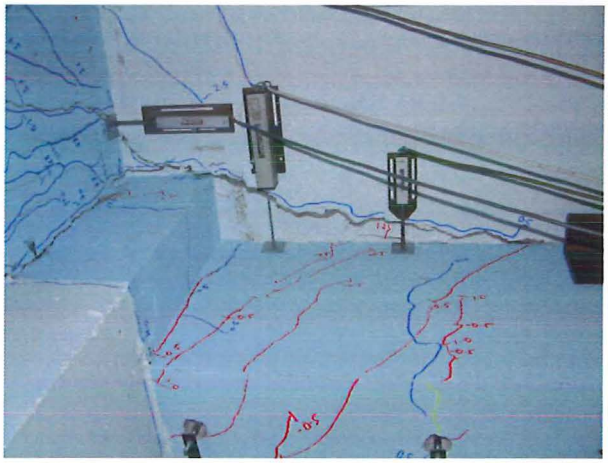

SW Column

- Major damage to the hollowcores seat.
- Crack width is approximately 12mm

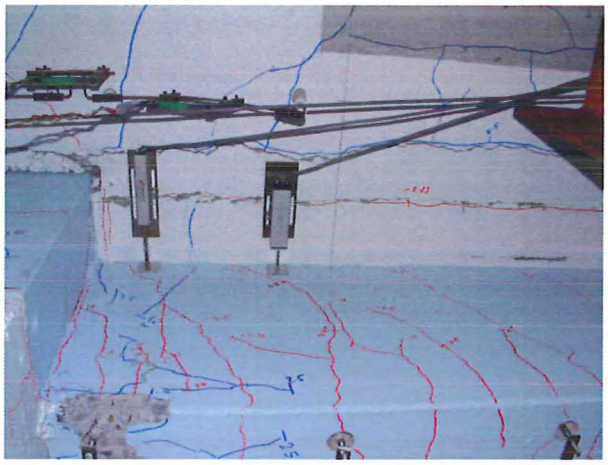

Central Column

- First beam spalling seen
- Longitudinal crack in soffit of hollowcore unit shows a change in height on each side of the crack

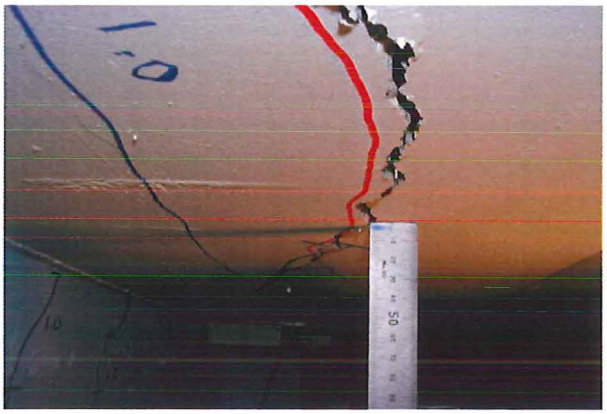

Bottom of first hollowcore unit

- Difference in height each side of the soffit crack

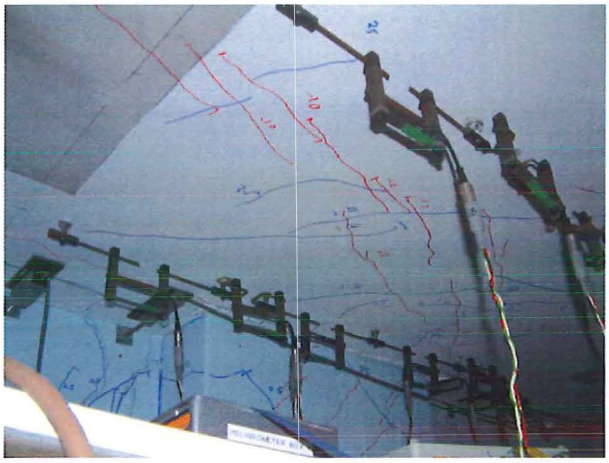

Central Column

- Shear lag cracks on the bottom of the first hollowcore unit

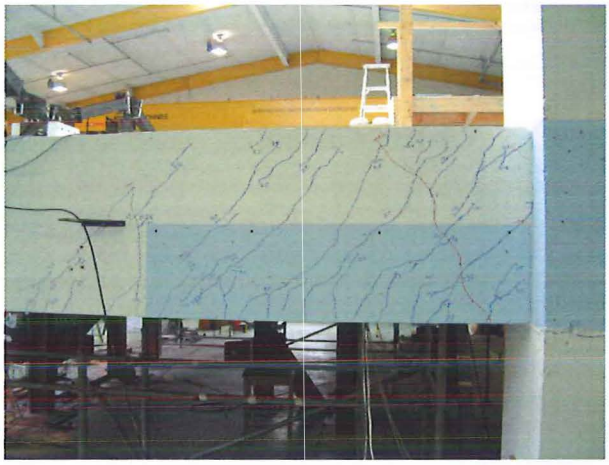

SE Column

- Torsion cracks at the end of Phase I loading

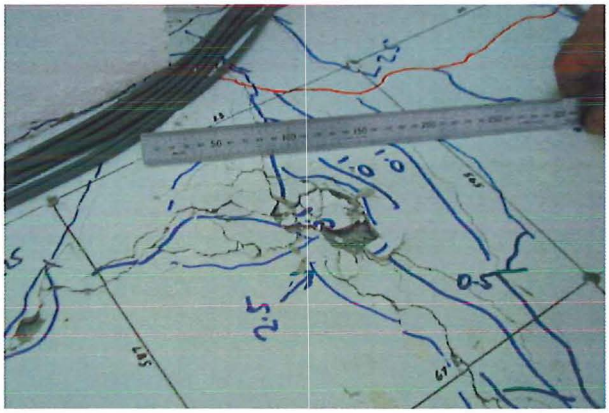

Central Column

- Lifting and deterioration of the topping concrete around the central column
- Full delamination of the topping in this region

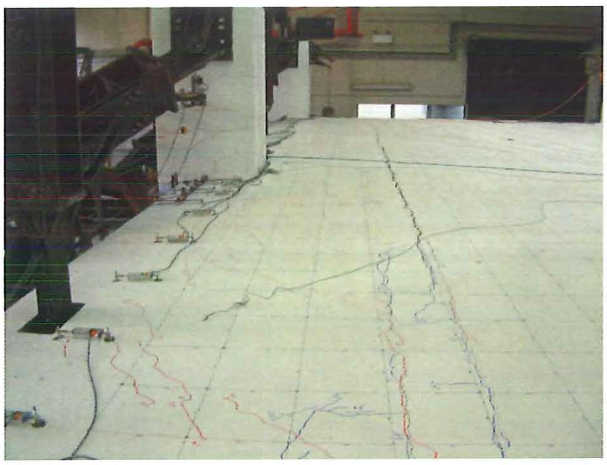

Floor slab

- Diaphragm tear that formed at 1.93% drift

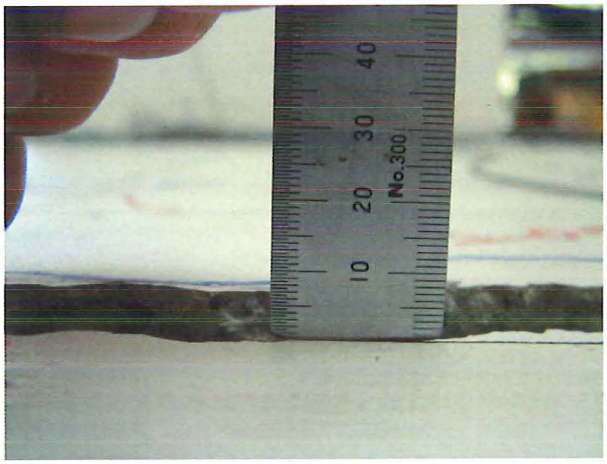

Floor slab

- Difference in height on either side of the diaphragm tear

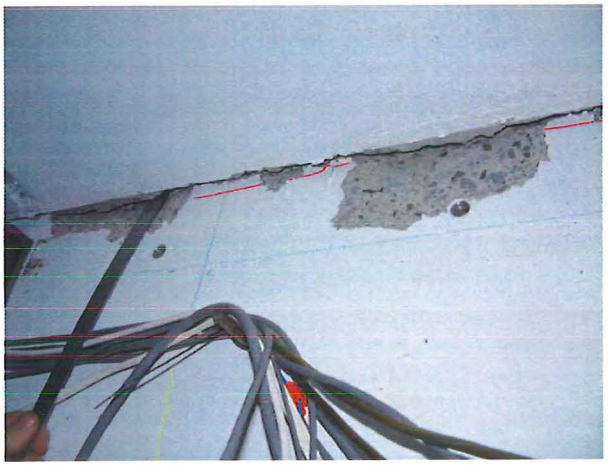

East Beam

- Hollowcore unit seat damage

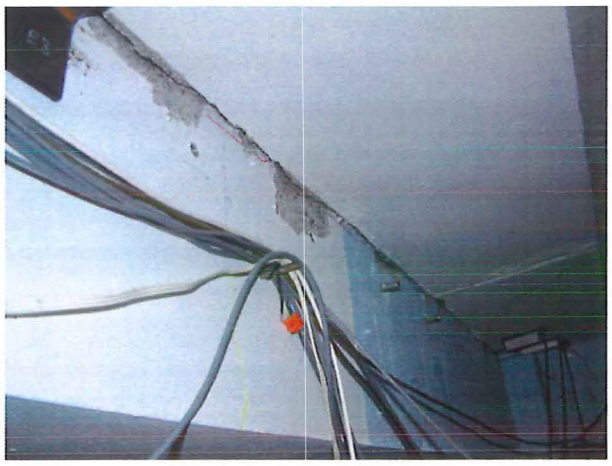

East Beam

- Entire seat lost at the end of Phase I

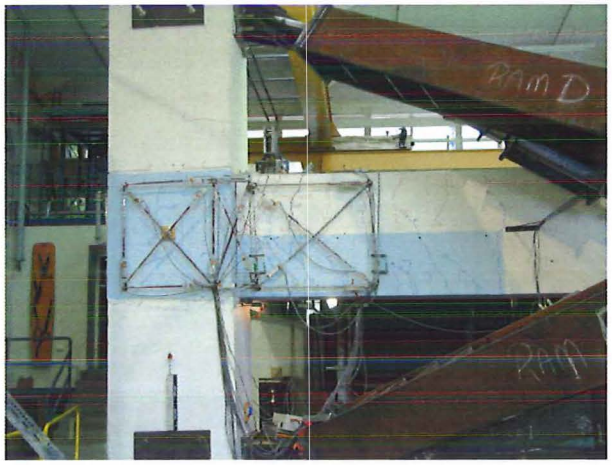

SW Column

- Plastic hinge cracks at the completion of the +2.5% and –2.0% cycle.

Central Column

- Plastic hinge cracks at the completion of the +2.5% and –2.0% cycle.

SE Column

- Plastic hinge cracks at the completion of the +2.5% and –2.0% cycle.

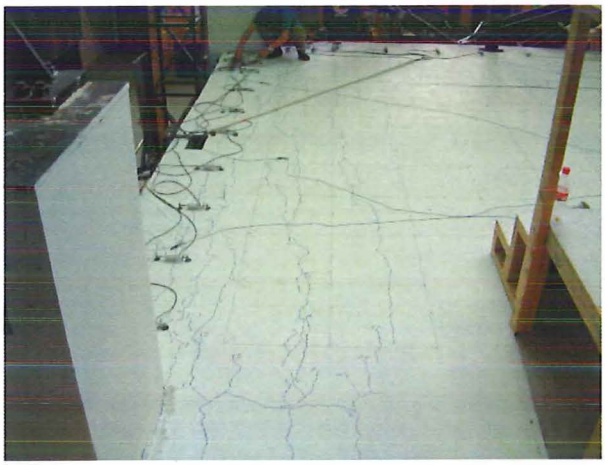

East Beam

- Diaphragm cracks at the end of phase I

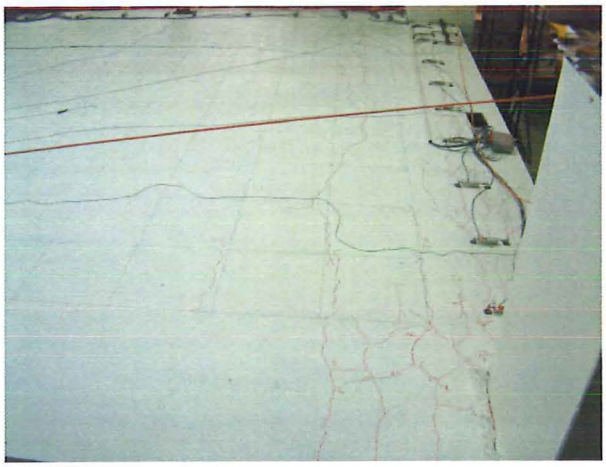

West Beam

- Diaphragm cracks at the end of phase I

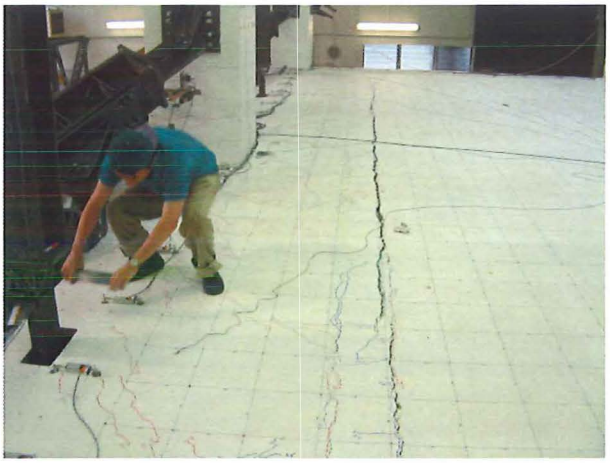

Floor Slab

- The diaphragm tear at the completion of the +2.5% and –2.0% cycle.

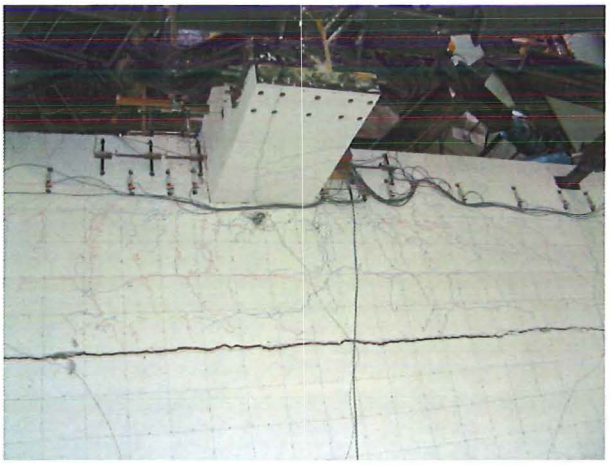

Central Column

- Plan showing the extent of diaphragm cracking at the end of Phase I

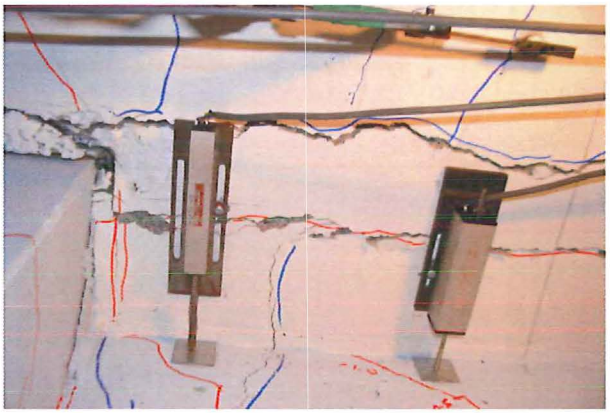

Central Column

- Damage to the underside of the first hollowcore unit at the completion of Phase I

E.2 Phase II

E.2.1 ±0.5% Drift Photos

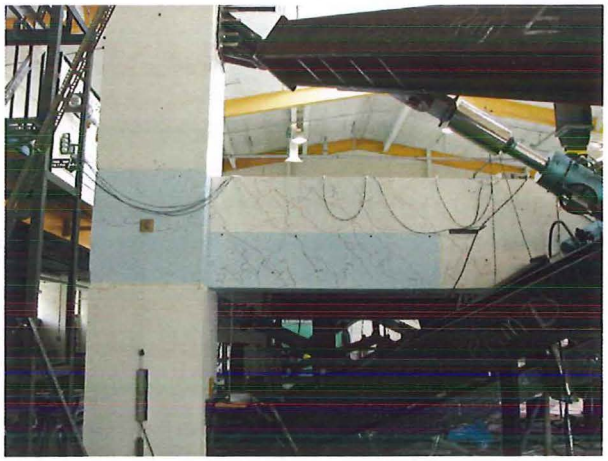

NW Column

- Plastic hinge zone cracks at the completion ±0.5%

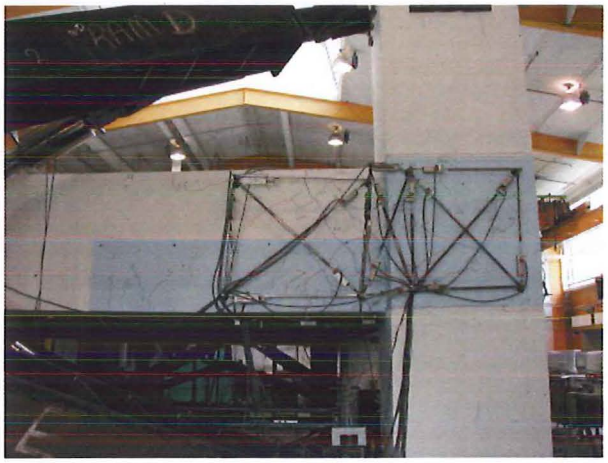

SW Column

- Plastic hinge zone cracks at the completion ±0.5%

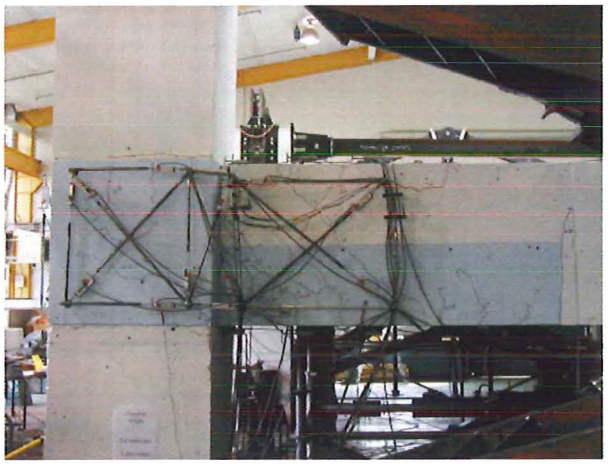

SE Column

- Plastic hinge zone cracks at the completion ±0.5%

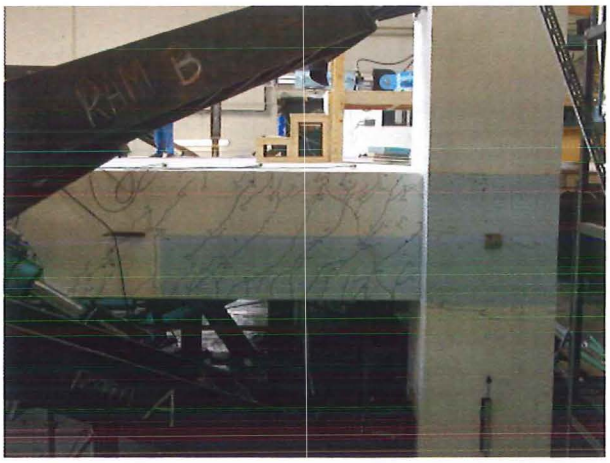

NE Column

- Plastic hinge zone cracks at the completion ±0.5%

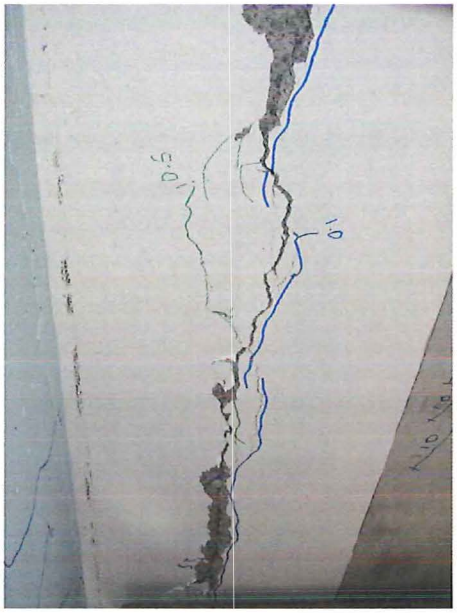

Bottom of first hollowcore unit

- Soffit crack worsening

East Beam

- General set up of the loading frames

E.2.2 ±1.0% Drift Photos

SE Column

- Plastic hinge zone cracks at the completion ±1.0%

NE Column

- End of the Hollowcore unit has fractured

NW Column

- Plastic hinge zone cracks at the completion ±1.0%

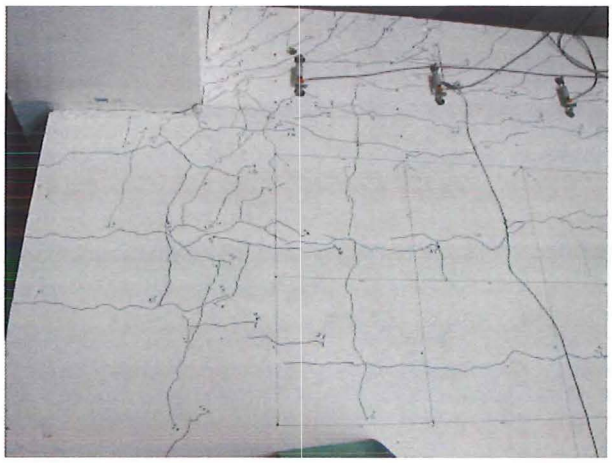

NE Column

- Further cracks form within the floor slab around the corner column
- Cracks form at the termination of the starter bars

E.2.3 +2.0%, -2.5% Drift Photos

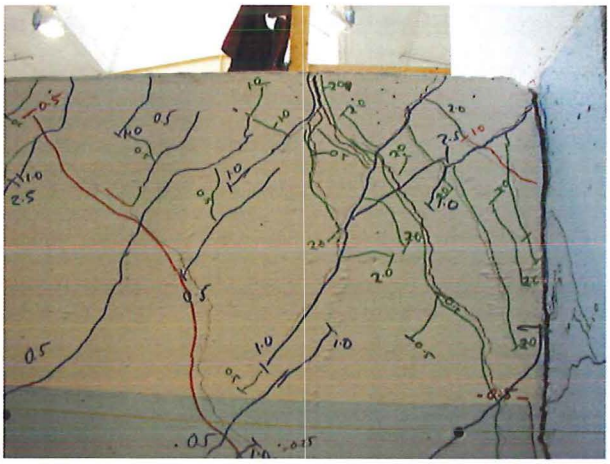

NE Column

- Plastic hinge zone cracks at the completion ±1.0%

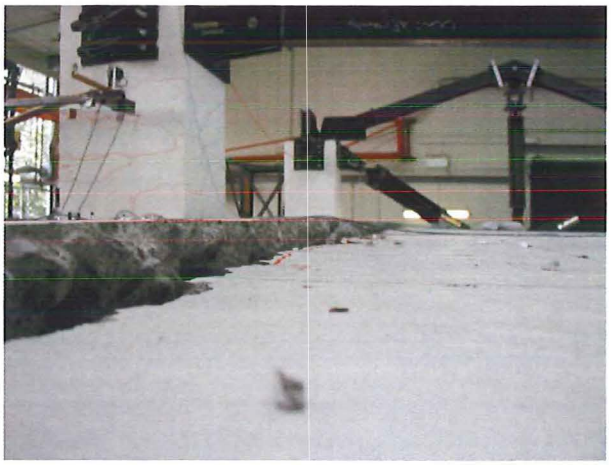

Floor Slab

- Close up showing the difference in height between the first hollowcore slab and the remainder of the floor

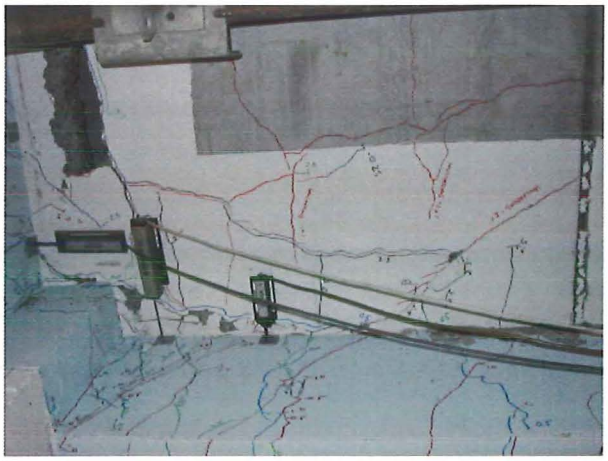

West Beam

- The first section of hollowcore unit falls out of the first unit

Hollowcore Unit Damage

- Looking at the west beam support
- Numerous cracks within the unit are seen

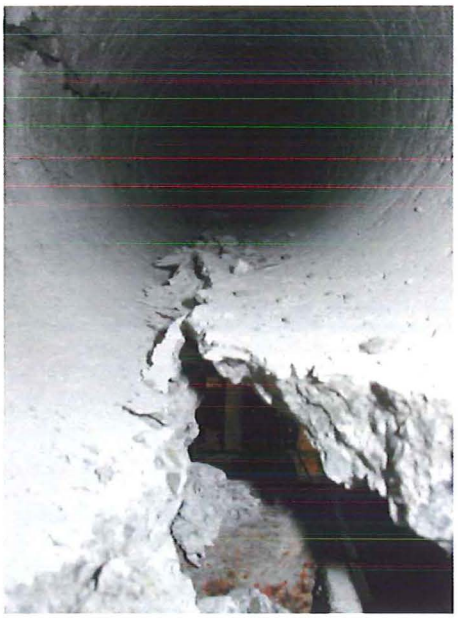

Hollowcore unit damage

- Soffit cracks in the first hollowcore unit
- Spit webs are also be seen

First Hollowcore Unit

- The diaphragm tear shifted from between the first and second hollowcore unit into the first unit near the east beam.

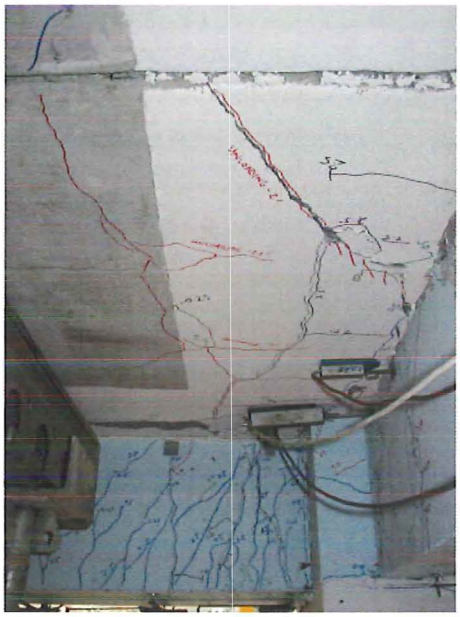

SW Column

- First hollowcore unit has dropped 20mm

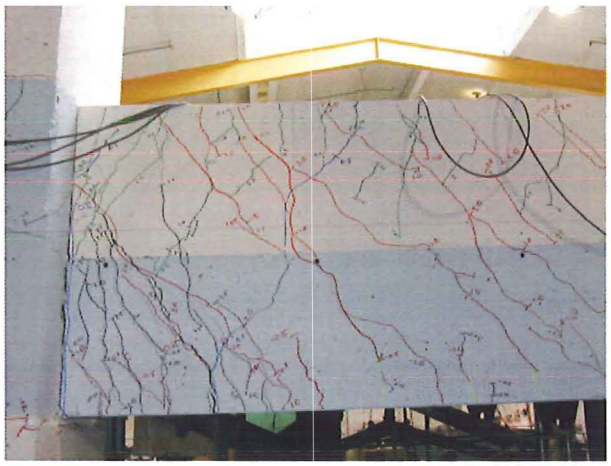

NW Column

- Plastic hinge cracks are now a mixture of torsion cracks from Phase I and new flexure cracks from Phase II.

NE Column

- Plastic hinge cracks are now a mixture of torsion cracks from Phase I and new flexure cracks from Phase II.

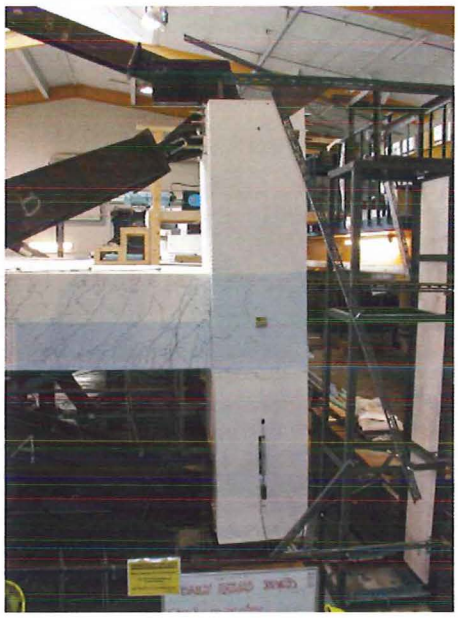

NE Column

- The NE column at 2.5% drift

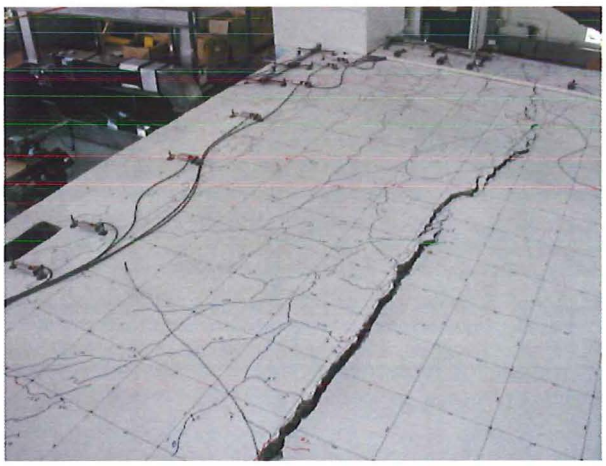

SW Column

- The diaphragm tear propagated into the second hollowcore unit near the west beam.
- Note: Lack of cracks in the second unit, most of the damage is localised to the first hollowcore unit

SE Column

- The diaphragm tear propagated into the first hollowcore unit near the east beam.
- Note: Lack of cracks in the second unit, most of the damage is localised to the first hollowcore unit

E.2.4 ±3.5% Drift Photos

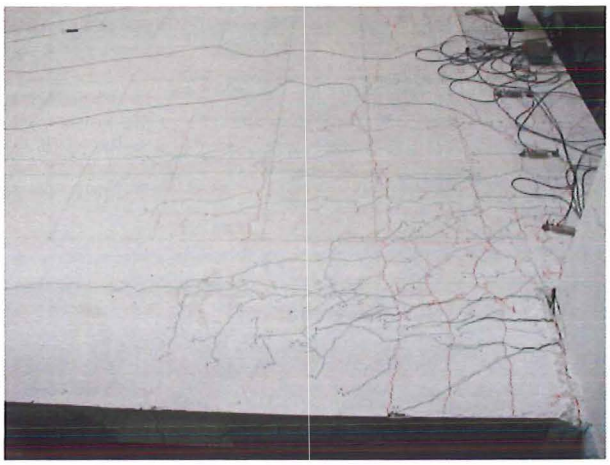

NW Column

- Large flexure cracks form near column

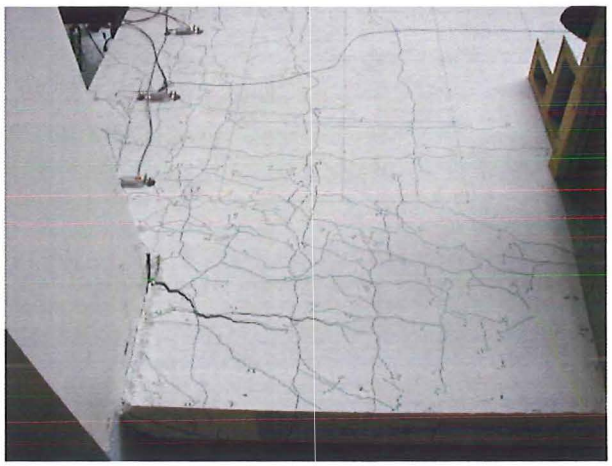

NE Column

- Large flexure cracks form near column

Hollowcore Unit Damage

- The 25mm web cracks relates to the 25mm drop of the unit

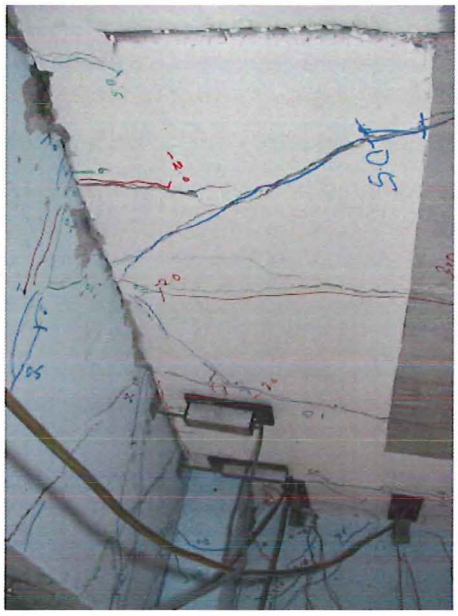

SE Column

- Deterioration of the East end of the hollowcore unit

Hollowcore Unit Damage

- Dropping of the first unit

SE Column

- The diaphragm tear propagated to the end of the super assembly and started to peel off the beam cover concrete

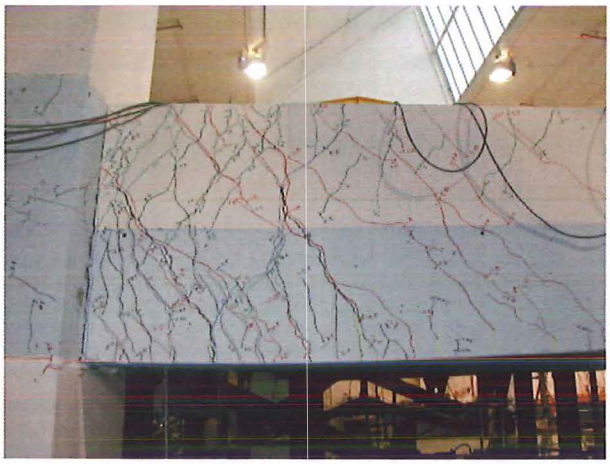

NW Column

- Plastic hinge zone damage at the end of Phase II

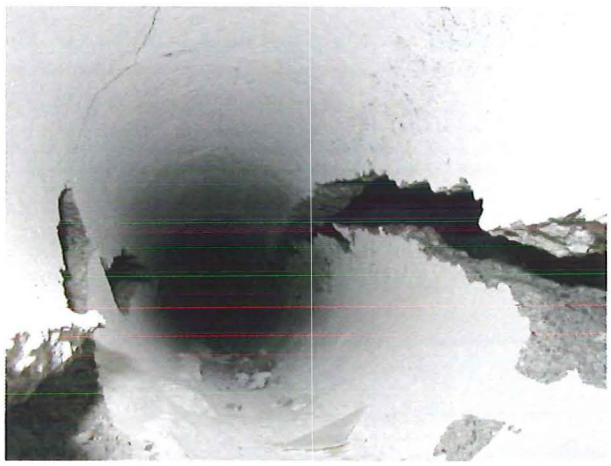

Hollowcore Unit Damage

- West end of the first unit

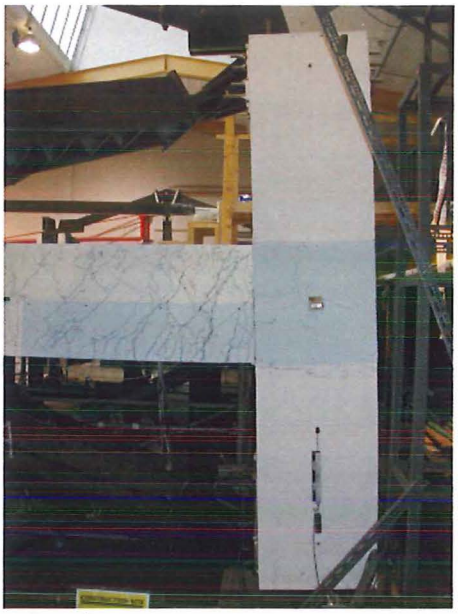

NE Column

- Plastic hinge zone damage at the end of Phase II

North Beam

- The fifth hollowcore units web split around the central column
- Crack propagated for approximately 4m

SE Column

- Lifting of the first unit relative to the floor slab

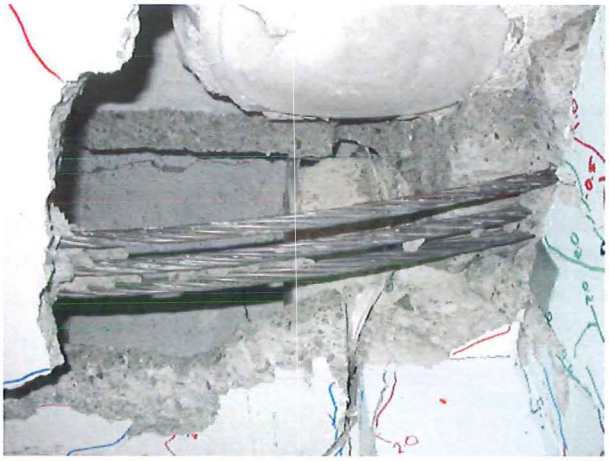

Hollowcore Unit Damage

- A section of the west end of the first hollowcore unit fell out.
- The sagging prestressing strands are not anchored into the beam

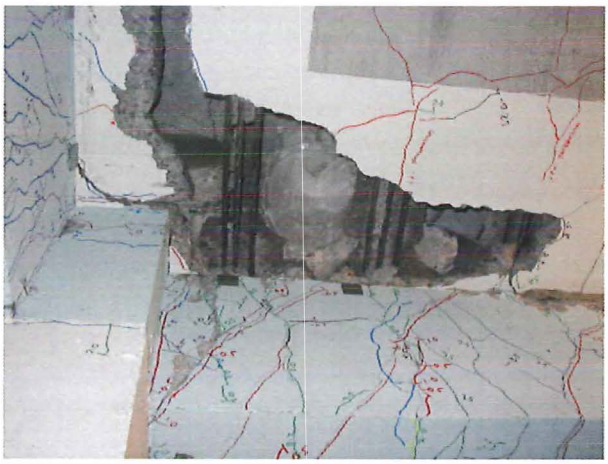

Hollowcore Unit Damage

- Large section of hollowcore unit has failed

Floor Slab

- Lifting of the first hollowcore unit relative to the floor slab

E.2.5 End of phase II

Hollowcore Unit Damage

- West end of hollowcore unit is held up by kinked strand at top of the picture

Floor Slab

- Final difference in height between the first unit and the floor slab at the end of Phase II

E.3 Phase III

E.3.1 ±0.5% Drift Photos

Hollowcore Unit damage

- Strand pull out at the west end of the unit

E.3.2 +2.5% Drift Photos

Hollowcore Unit Damage

- West end after failure
- Hollowcore unit is resting on catch frame
- Section at the top of the photo that was holding up the hollowcore unit has now failed

Hollowcore Unit Damage

- Prestressing strands are sliding down beam face
- Not supporting the unit due to no anchorage

Hollowcore Unit Damage

- Fractured section of hollowcore unit that had been holding up the west end

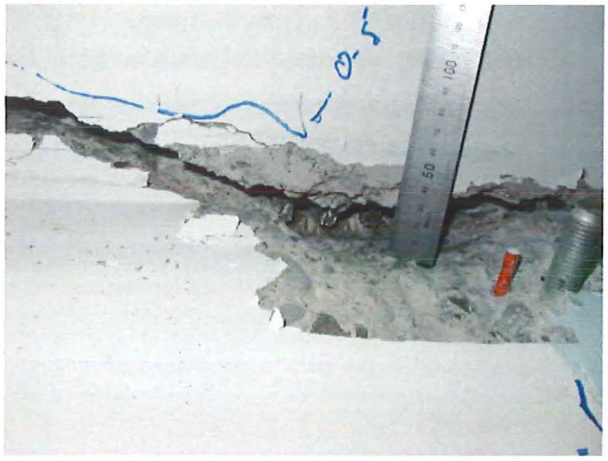

Hollowcore Unit Damage

- East beam damage
- End of prestressing strands can be seen

Central Column

- Lifting of the topping around the central column

Hollowcore Unit Damage

- Damage to the end of the unit at the NW column

Hollowcore Unit Damage

- Propped hollowcore unit after the west end failed
- Extensive damage at east end as well

Hollowcore Unit Damage

- Failed first unit when the prop supporting the unit was removed

Hollowcore Unit Damage

- The ends of the unit is still attached to the beam
- The end of the unit fractured rather than sliding (design assumption)

Hollowcore Unit Damage

- Failed bottom section of hollowcore

E.3.3 -2.5% Drift Photos

Floor slab

- As the east beam rotates the reinforced topping slab push the floor slab down

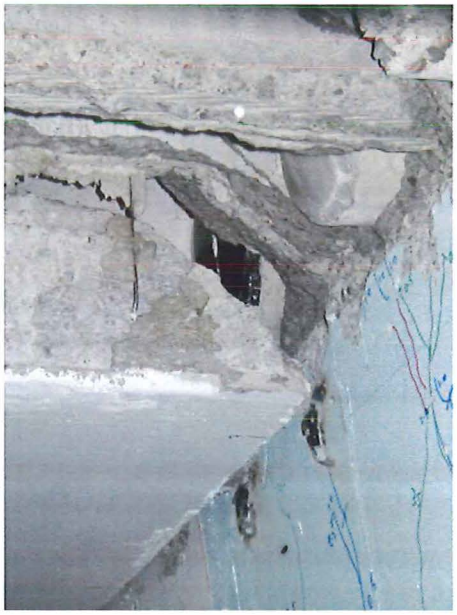

Hollowcore Unit Damage-East beam

- The second unit had dropped by 90mm prior to the load test been carried out

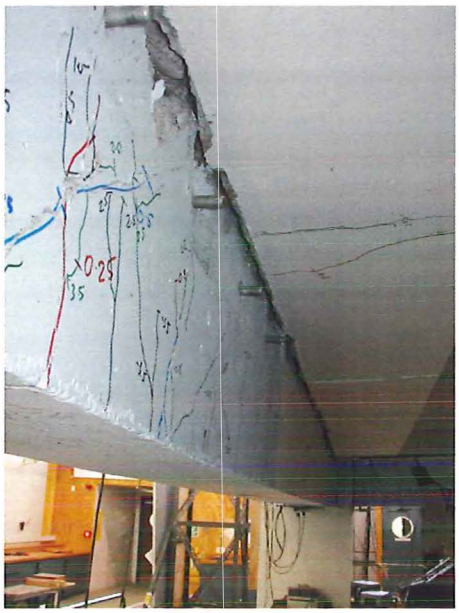

Seat Connection

- Completed damaged floor slab connection just prior to the load test

Hollowcore Unit Damage

- Once the bottom of the unit failed a large crack opened near the central column as the floor slab did not restrain any beam elongation

Floor Slab

- The floor slab just prior to the load test being undertaken

Load Test

- Applying a load to represent the design live load on the floor

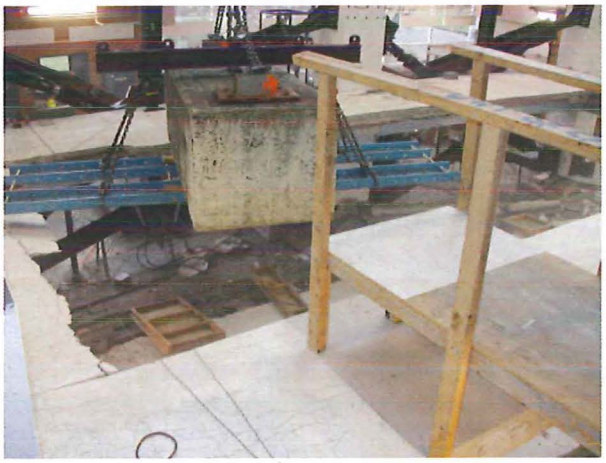

Load Test

- Failure of the floor during the load test

Floor slab failure

- Complete floor slab failure when the floor was loaded tested

East Beam

- Failed floor when the starters and topping still attached to the beam

Floor Failure

- Failed floor with the frame still standing

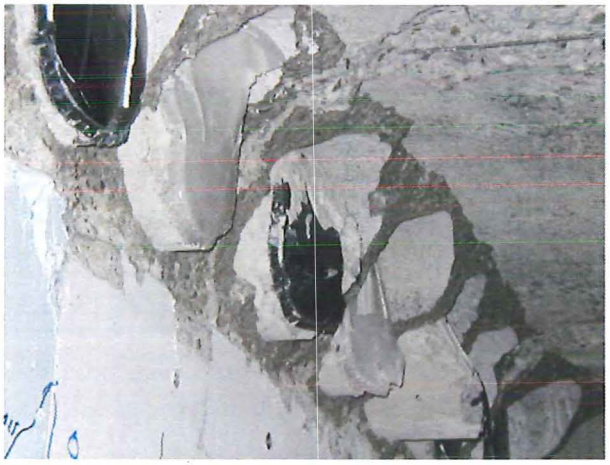

Hollowcore Unit Damage

- End of the hollowcore unit still attached to the east beam

Hollowcore Unit Damage

- Hollowcore ends and topping still attached to the east beam

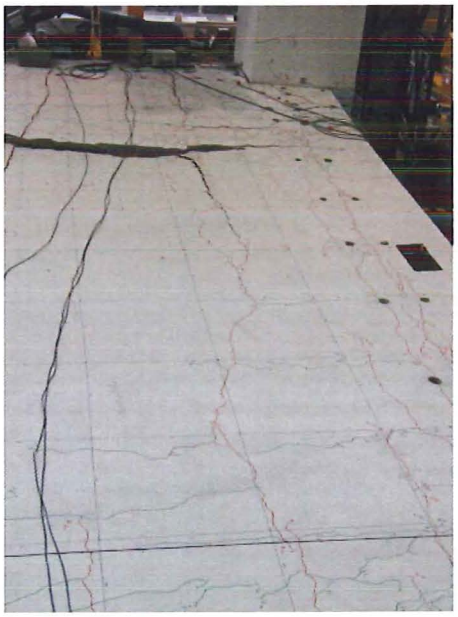

West Beam

- Large crack forming at the termination of the starter bars

West Beam

- Failed floor with the starter bars and topping still attached to the beam

E.4 End of test

End of Test

- Super assembly stripped down to be a basic frame

East Beam

- End of the hollowcore unit still attached to the beam

Failed Floor

- Plan of the floor failure

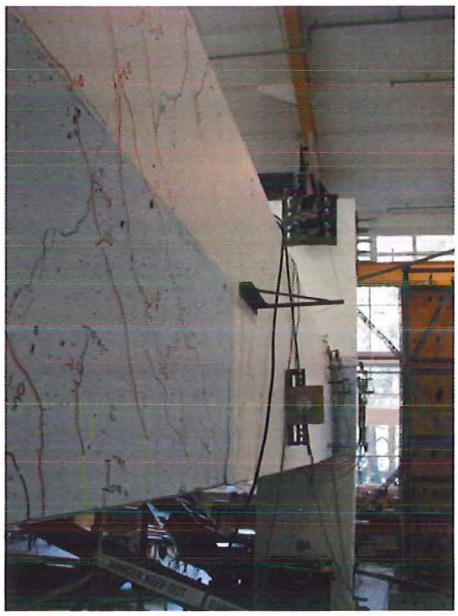

West Beam

- Distorted beam due to the torsion induced by the floor slab and the inclination of the columns

West Beam

- By using a straight edge it is possible to possible to see the final distorted shape of the beam.

Hollowcore Unit Damage

- Failed unit sitting on the laboratory floor

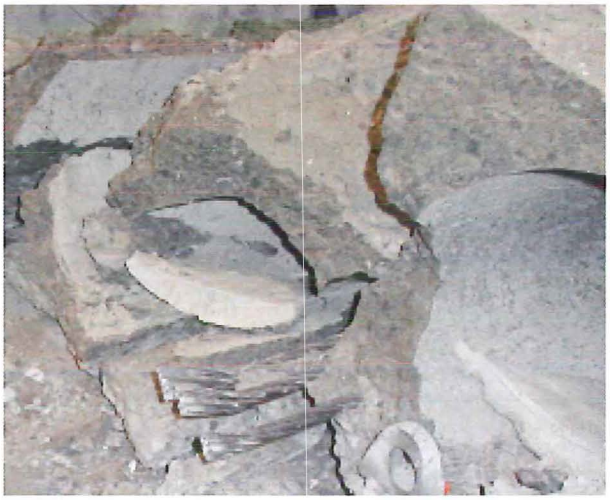

Hollowcore Unit Damage

- Kinked prestressing strands from when they were supporting the unit once its seat was lost

E.4.1 Plastic hinges

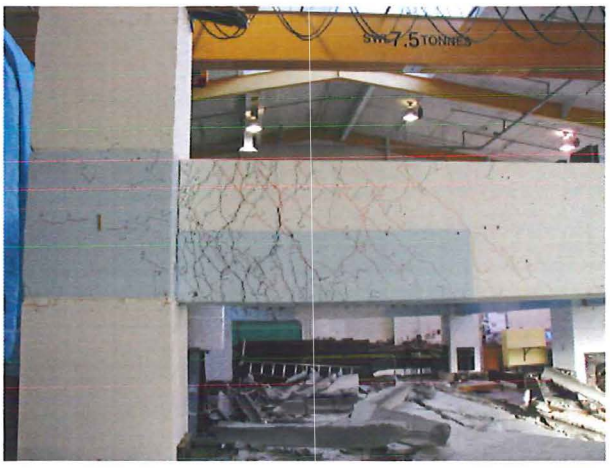

NW Column

- Final plastic hinge zone damage

SW Column

- Final plastic hinge zone damage

SW Column

- Final plastic hinge zone damage

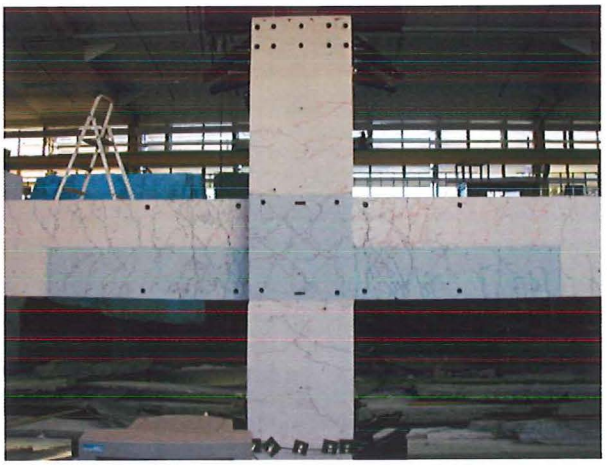

Central Column

- Final plastic hinge zone damage

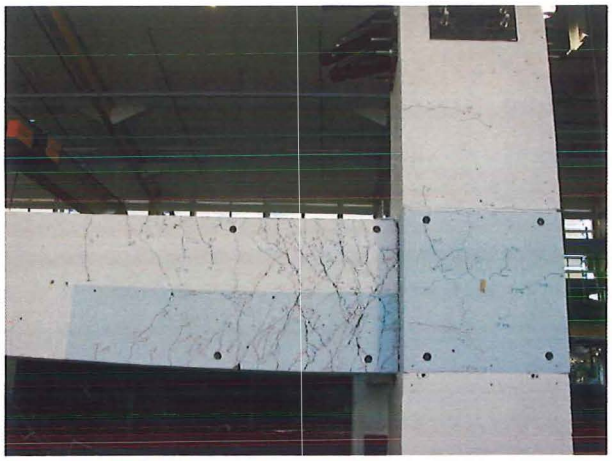

SE Column

- Final plastic hinge zone damage

SE Column

- Final plastic hinge zone damage

NE Column

- Final plastic hinge zone damage

SW Column
Final plastic hinge zone damage

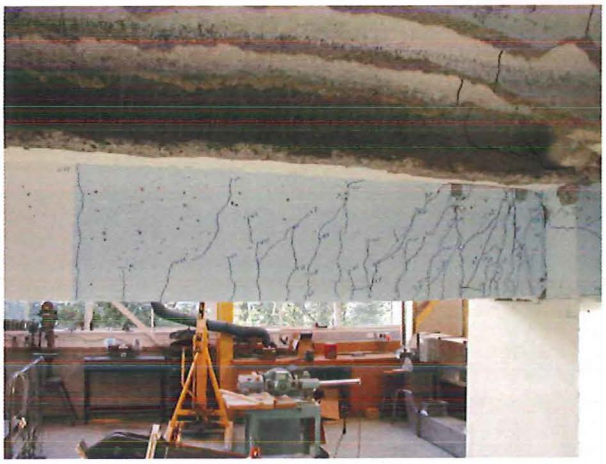

SW Column

- Final plastic hinge zone damage

Central Column

- Final plastic hinge zone damage

Central Column

- Final plastic hinge zone damage

SE Column

- Final plastic hinge zone damage

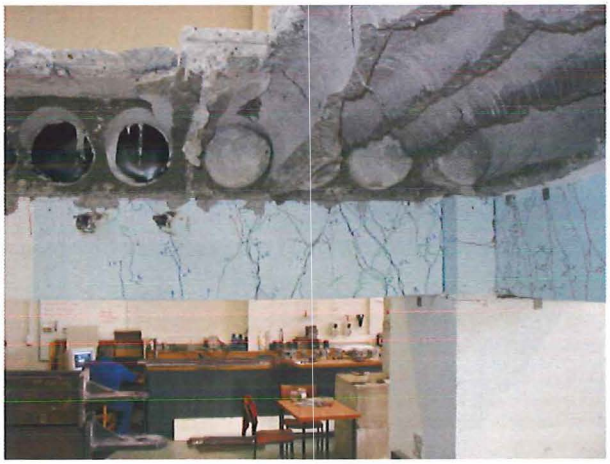

SE Column

- Final plastic hinge zone damage

NE Column

- Final plastic hinge zone damage

This Page is Blank

Appendix F

Hysteretic response

F.1 Determination of the yield displacement and effective stiffness

To determine the yield displacement of the super-assemblage the system was broken up into its individual components.

Beam Contribution

Using a moment-curvature programme the beams yield moment (M_{yb}=522 kNm) and yield curvature (ϕ_{yb}=4.6×10^{-6}/mm) were determined. Knowing the yield moment and curvature it was possible to determine the effective stiffness (EI_{eff}) for the beams.

$$\phi_{yb} = \frac{M_{yb}}{EI_{eff}} \Rightarrow EI_{eff} = \frac{M_{yb}}{\phi_{yb}} \qquad \textbf{(F-1)}$$

or in terms of the effective stiffness over the gross stiffness (EI_g)

$$\frac{EI_{eff}}{EI_g} = \frac{M_{yb}}{\phi_y EI_g} = \frac{522\times10^6}{4.6\times10^{-6}\times30000\times400\times\frac{750^3}{12}} = 0.27 \qquad \textbf{(F-2)}$$

in which E = Modulus of elasticity of the concrete (At the time of the test, the compressive strengths (f'_c) of the topping slab and beam concrete was 45 MPa whereas the actual hollow-core units concrete compressive strength was unknown. The hollow-core manufacturers brochure stated that the minimum compressive strength was 42 MPa. Therefore, for the purposes of the calculations the hollow-core units concrete compressive strength was assumed to be 45 MPa); and I_g = gross beam moment of inertia (based on the beams rectangular dimensions).

Now determine the beam deflection in terms of a column deflection using moment area.

$$\delta_b = \frac{M_y L_b^2}{12EI_{eff}} = \frac{522\times10^6\times5350^2}{12\times30000\times0.26\times400\times750^3/12}10.9mm \qquad \textbf{(F-3)}$$

in which δ_b = displacement of the beam at its point of inflection; L_b = the distance between the beam plastic hinges (5350mm).

To convert a beam displacement to a column displacement the following is used

$$\delta_c^b = \delta_b \frac{L_c}{L_b/2} = 10.9\times\frac{3500}{6100/2} = 12.5mm \qquad \textbf{(F-4)}$$

in which δ_c^b = the column displacement due to the beam deflecting; and L_c = The height of the column between inflection points.

Beam Column joint contribution

To determine the contribution that the beam column joint makes to the lateral displacement of the super-assemblage an expression must be written for the horizontal beam column joint shear (V_{jh}).

Using Figure F-1 and solving for equilibrium

$$2R\frac{L_b}{2} = H_{col}H \Rightarrow H_{col} = R\frac{L}{H} = \frac{2M_b}{H}\frac{L}{L_b} \qquad \textbf{(F-5)}$$

in which R = shear force within the beam; H_{col} = column shear force; M_b = beam moment at the column face; L_b =distance between plastic hinges; L = the centreline distance between beam inflection points; and H = column height.

Therefore, V_{jh} (Figure F-1) can be written as

$$V_{jh} = T + C - H_{col} = 2\left(\frac{M_b}{d-d'}\right) - 2\frac{M_b}{H}\frac{L}{L_b} \qquad \textbf{(F-6)}$$

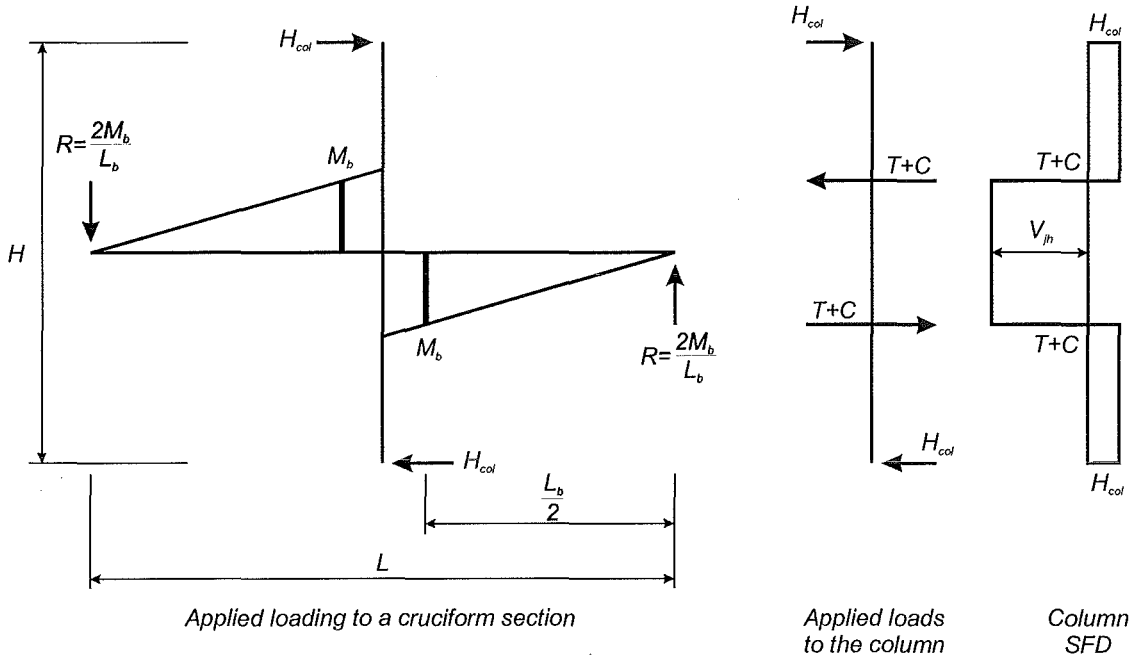

(a) A diagram showing the determination of V_{jh}

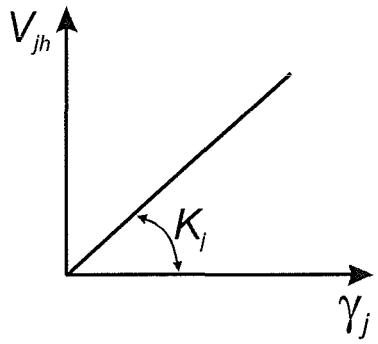

(b) The relationship between the horizontal beam-column joint shear (V_{jh}), joint stiffness (K_j) and joint distortion (γ_j)

Figure F-1 Determination of the beam column joint (γ_j) distortion

in which *(d-d')* = beams internal leverarm. Equation (F-6) can be simplified to

$$V_{jh} = \frac{2M_b}{(d-d')}\left(1 - \frac{d-d'}{H}\frac{L}{L_b}\right) \qquad \textbf{(F-7)}$$

Also an expression for cracked stiffness (K_{scr}) of the joint is required (Kim and Mander, 1999) can be written as a ration f the uncracked stiffness (K_{sun}).

$$\frac{K_{scr}}{K_{sun}} = \frac{\rho_v n E_c A_j}{(1+7.33\rho_v n)0.4E_c A_j} \qquad \textbf{(F-8)}$$

in which ρ_v = beam column joint steel ratio; $n = E_s/E_c$; A_j = cross sectional area of the joint; E_s = Modulus of elasticity of the reinforcement; and E_c = Modulus of elasticity of the concrete.

Equation (F-8)) was simplified by Kim and Mander (1999) to

$$K_{scr} = \frac{0.129 E_c A_j}{1 + 0.02/\rho_v} \qquad \textbf{(F-9)}$$

Knowing both V_{jh} = the horizontal joint shear force and K_j (=K_{scr}) it is now possible to determine the joint distortion (γ_j) (Figure F-1).

$$\gamma_j = \frac{V_{jh}}{K_j} = \frac{\frac{2M_b}{(d-d')}\left(1 - \frac{d-d'}{H}\frac{L}{L_b}\right)}{0.052 E_c B H} \qquad \textbf{(F-10)}$$

in which B= breadth of the column; and H = width of the column

$$\gamma_j = \frac{V_{jh}}{K_j} = \frac{\frac{2A_s f_y (d-d')}{(d-d')}\left(1 - \frac{d-d'}{H}\frac{L}{L_b}\right)}{0.052 E_c B H} \qquad \textbf{(F-11)}$$

in which A_s = area of column reinforcement; and f_y = yield stress of the column reinforcement.

By rearranging Equation (F-11) and substituting in actual values, γ_j is determined.

$$\gamma_j = 38.5 \frac{A_s}{BH}\frac{f_y}{E_c}\left(1 - \frac{d-d'}{H}\frac{L}{L_b}\right) \qquad \textbf{(F-12)}$$

$$\gamma_j = 38.5 \frac{2714}{750^2}\frac{300}{31500}\left(1 - \frac{564}{3500}\frac{6100}{5350}\right) = 0.0014 = 0.14\% \qquad \textbf{(F-13)}$$

When γ_j is converted to an interstorey drift, the column displacement (δ_c^j) due to the beam column joint distortion was 4.9mm.

Column contribution

From statics and knowing the beam yield moment it is possible to determine the column moment. More important in determining the yield displacement is knowing the EI_{eff} for the column. Priestley et al (1996) have shown that it is acceptable to use the yield secant stiffness based on the column yield moment rather than using the exact secant stiffness at the applied moment, as the variance is minimal. This can be seen in Figure F-2.

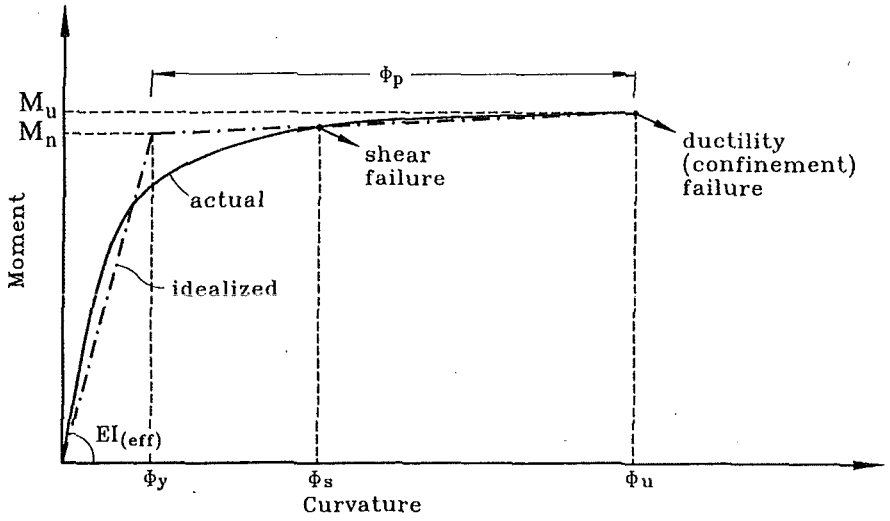

Figure F-2 Comparison between the yield effective stiffness and the exact secant stiffness at a point less than yield (Priestley et al, 1996)

To calculate the EI_{eff} and hence the displacement, the columns yield moment (M_{yc}=790 kNm) and curvature (ϕ_{yc} = 4.44×10^{-6}/mm) were determined using moment-curvature.

To determine EI_{eff} the following was used

$$\frac{EI_{eff}}{EI_g} = \frac{M_{yc}}{\phi_{yc} EI_g} = \frac{790\times10^6}{4.44\times10^{-6}\times30000\times750\times\frac{750^3}{12}} = 0.22 \qquad \textbf{(F-14)}$$

To determine the deflection of the column due to the beam yielding the actual column moment was required. From equilibrium the column moment (M_c) was determined as 234 kNm.

Therefore the column deflection is

$$\delta_c = \frac{2M_c h_c^2}{3EI_{eff}} = \frac{2\times 234\times 10^6 \times 3500^2}{3\times 30000\times \frac{750^3}{12}\times 750\times 0.22} = 1.6mm \qquad \text{(F-15)}$$

Therefore the total displacement due to the three components is summed to give the yield displacement (and hence yield drift).

$$\delta_t = \delta_c^b + \delta_c^j + \delta_c = 10.9+4.9+1.6=17.4\text{mm} \qquad \text{(F-16)}$$

If this lateral displacement is converted into an interstorey drift the yield drift (θ_y) is 0.49%.

F.2 Torsion test

Part way during the second phase of loading a torsion test to ±0.5% was undertaken to examine the torsional stiffness of the super-assemblage. The torsion test was undertaken between the –2.5% cycle and the +3.5% cycle as shown in Figure F-3(a). A torsion test is one in which the East and West frames are displaced in opposite directions (i.e. the East frame was displaced in a positive direction while the West frame displaced in a negative direction and vice-versa as shown in Figure F-3(b)).

Figure F-3(c) shows the hysteretic response for both the East and West bays. When comparing the stiffness of the two bays it is evident that the longitudinal tear that had formed within the floor slab during Phase I affected the torsional stiffness. The East bay had a stiffness of 10MN/m whereas the West bay had a stiffness of 6.2MN/m. This difference can be explained by examining the loading directions for each bay. When the East bay was displaced in a positive direction (the top of the column displaces in a northern direction while the bottom displaces in a southern direction) the starter bars in the northern beam were activated as additional tension

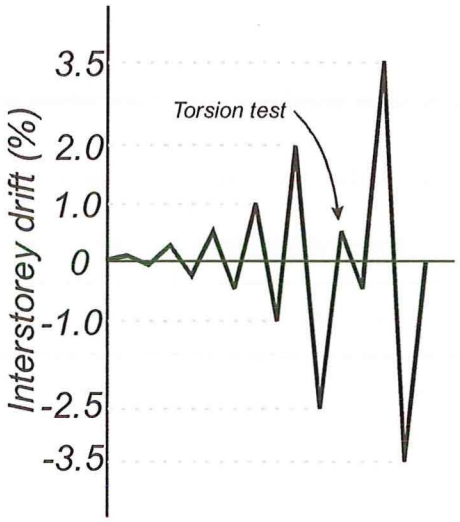

(a) Phase II displacement history

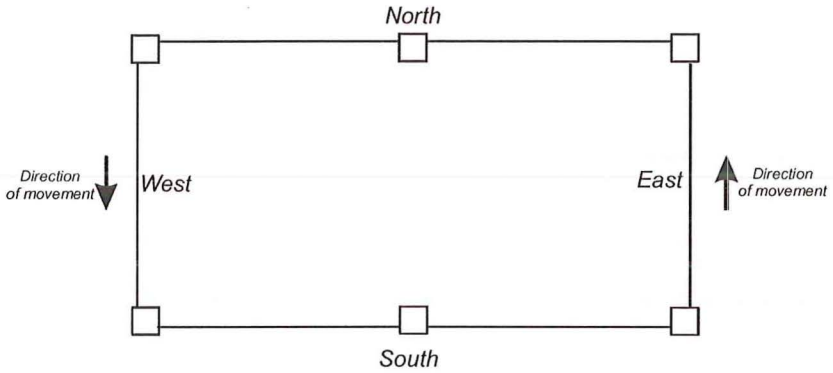

(b) A schematic showing the torsion test

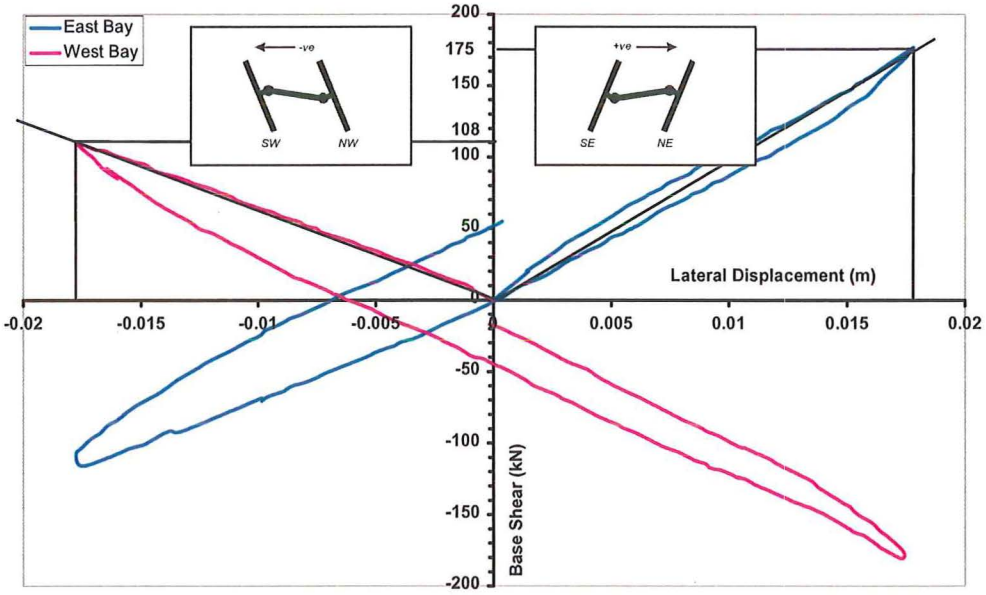

(c) Hysteresis loop for the torsion test

Figure F-3 Details of the torsion test

reinforcement. Whereas when the West bay was displaced by a negative direction (the top of the column displaces in a southern direction while the bottom displaces in a northern direction) that causes the first hollow-core unit to be lifted rather than activating the starter bars in the southern beam. It was this lifting of the hollow-core unit that caused the stiffness to be reduced for a negative inclination.

Due to the damage caused by the diaphragm tear very little information was obtained from the torsion test.

F.3 General super-assemblage performance

Longitudinal bar slip

Phase I

During the experimental programme, the reinforcing bars passing through the central beam column joint were monitored for longitudinal bar slip. As can be seen in Figure F-4(a), minimal bar slip occurred. The top bar moved a maximum of 0.8mm while the bottom bar moved a maximum of 0.1mm. The difference between the two bars is due to the formation of air bubbles on the underside of the top reinforcement when the beams were cast. These air bubbles reduce the bond of the top reinforcement to the concrete making it more prone to sliding through the joint earlier than the bottom reinforcement.

The amount of bond slip was low as the ratio of the beam depth to column depth (d_b/h_c) is a lot less than the maximum allowable by New Zealand Concrete Code (NZS3101:1995). NZS3101:1995 states a maximum allowable bar size to pass through the beam column joint. This maximum bar size is limited by the bond requirements of the bar. For a ductile frame Cl 7.5.2 of NZS3101:1995 governs.

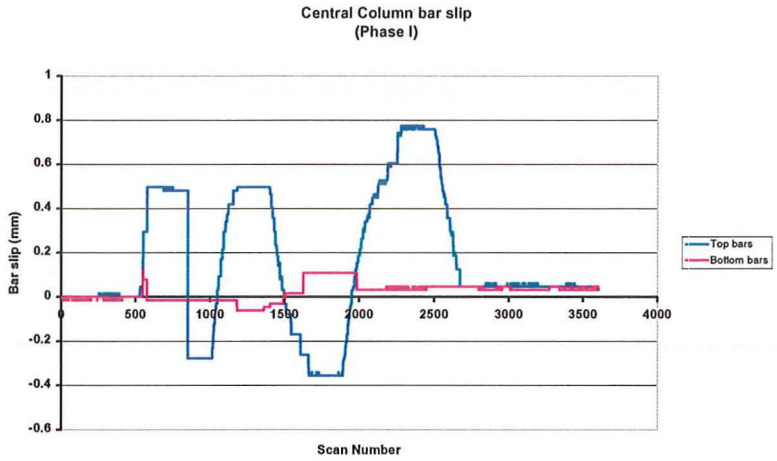

(a) Longitudinal bar slip for Phase I

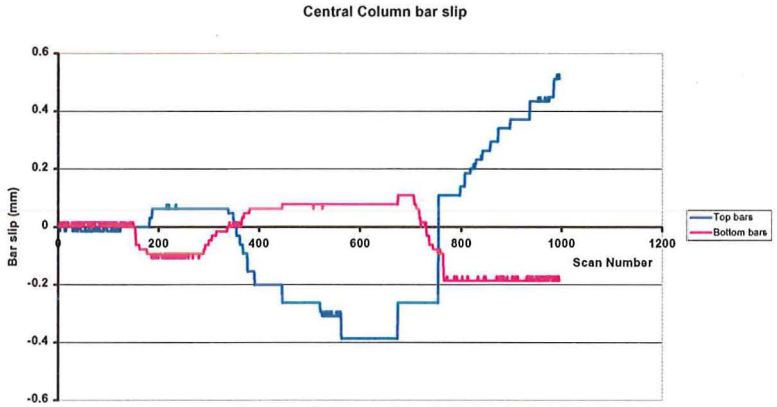

(b) Longitudinal bar slip for Phase III

Figure F-4 Bar slip of the longitudinal reinforcement through the central beam column joint

$$\frac{d_b}{h_c} = 3.3\alpha_f \frac{\sqrt{f'_c}}{\alpha_0 f_y} \qquad \textbf{(F-17)}$$

in which d_b = longitudinal bar diameter; h_c = the depth of column; α_f = 1.0 for one way frames; f'_c = the specified concrete strength (MPa); α_0 = 1.25 when the plastic hinge forms on the column face; and f_y = the nominal yield strength of the longitudinal reinforcement.

From the Equation (F-17) the maximum allowable bar size to pass through the joint is

$$d_b = 3.3 \times 1.0 \times \frac{\sqrt{45}}{1.25 \times 300} \times 750 = 44mm \qquad \textbf{(F-18)}$$

The actual longitudinal bar size used was 24mm, 55% of the allowable maximum bar size. This difference between the maximum allowable bar to be used and the actual bar used explains why there was minimal bar slip as the stresses within the beam column joint would have been low.

Phase III

The degree of bar slip through the central beam column joint for Phase III was similar to that observed during Phase I. This can be seen in Figure F-4(b).

F.3.1 Beam Dilation

Dilation is the increase in the depth of the beam across a vertical section due to the beam forming a plastic hinge.

Phase I

All the plastic hinge with the South frame showed very little dilation except for the left hand side of the central column which grew by 21mm as shown in Figure F-5(a). This growth was large because the hollow-core unit spanned past the central column and restricted some of the beam elongation (Chapter 7). This restraint caused the beam to dilate more than the other plastic hinge zones where the beam elongation was not restrained. This plastic hinge was also the hinge that showed the greatest amount of damage during the first phase of loading.

Phase II

During Phase II very little beam dilation was seen. The West beam grew by approximately 4mm while the East beam grew by 2mm. This growth can be seen in Figure F-5(b).

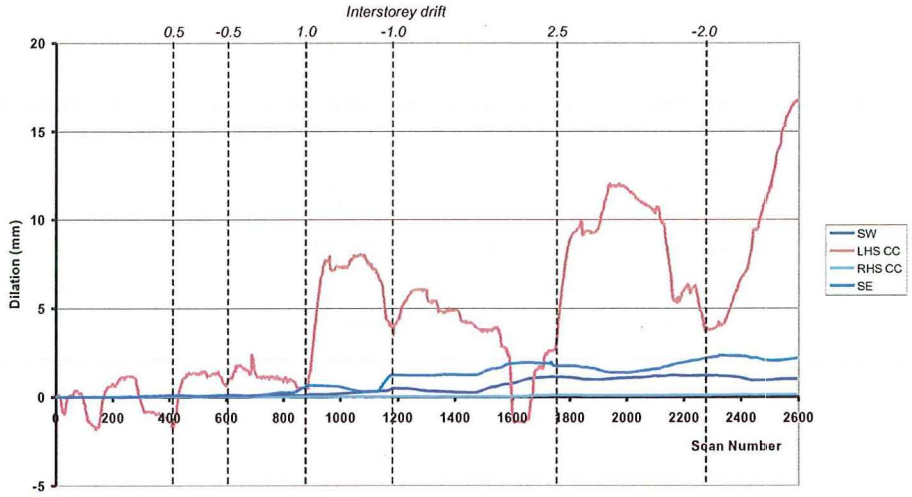

(a) South beam dilation during Phase I

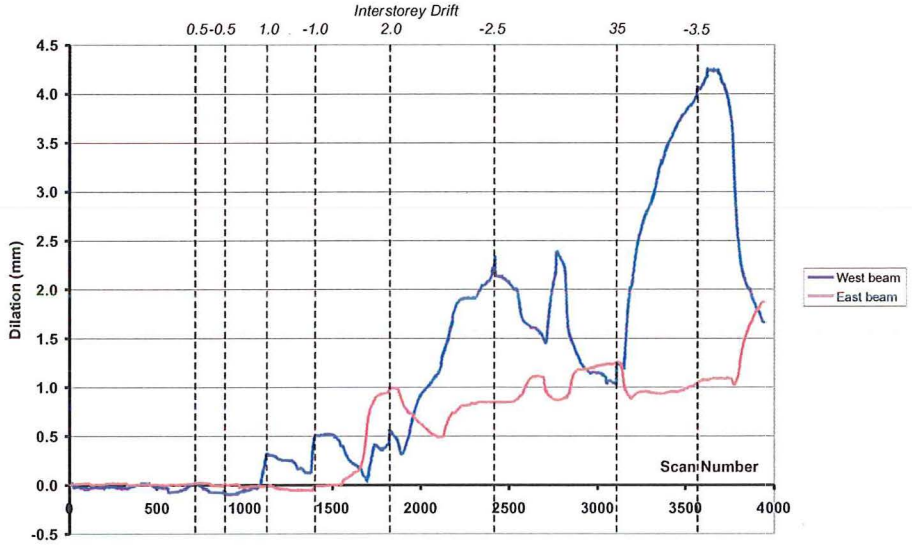

(b) Transverse beams dilation during Phase II

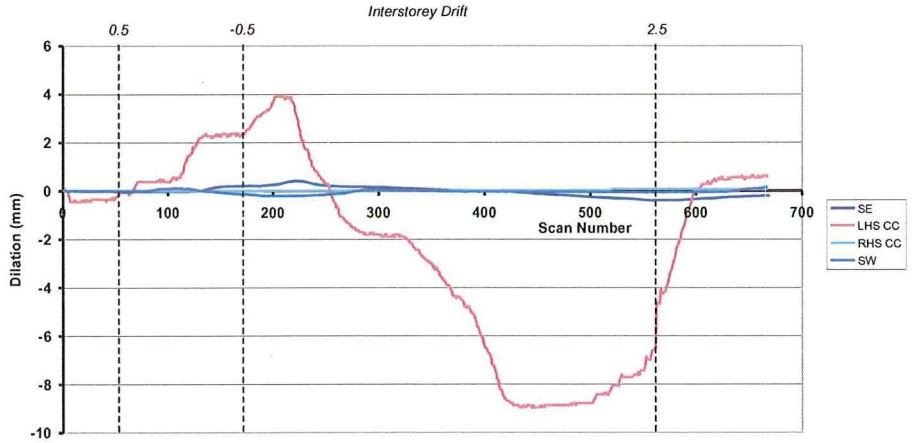

(c) South beam dilation during Phase III

Figure F-5 Perimeter frame beam dilation

Phase III

Figure F-5(c) shows no major dilation occurred. The plastic hinge that formed on the left hand side of the central column actually recovered some of the dilation gained during Phase I. The reason for this recovery was that the bottom section of the first hollow-core unit failed during Phase III allowing the plastic hinge to grow unrestrained and hence relieve some of the restraint forces with the plastic hinge.

F.3.2 Hollow-core pull off

Refer to Figure F-6 for the layout of the potentiometers used to measure the hollow-core pull off.

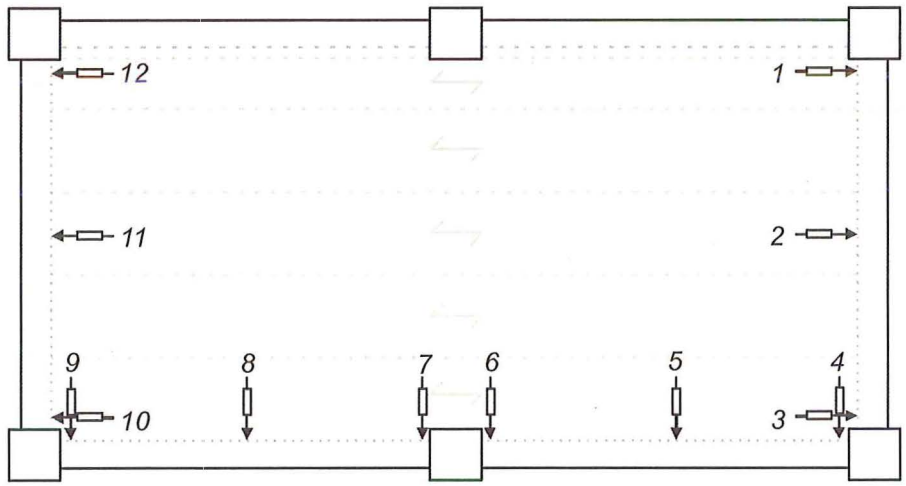

Figure F-6 Plan showing the location of the potentiometers measuring hollow-core pull off

Phase I

Figure F-7 shows the amount that the hollow-core units moved relative to the perimeter frame. Since the hollow-core units did not slide, but fractured (Chapter 4), the measurement recorded at the East and West beams was the hollow-core units crack width at the end of the hollow-core unit rather than the amount the units slid. A maximum crack width of 12mm was located at the SE corner on the East beam during the-2.0% load cycle. It should be noted that five (out of six) potentiometers positioned

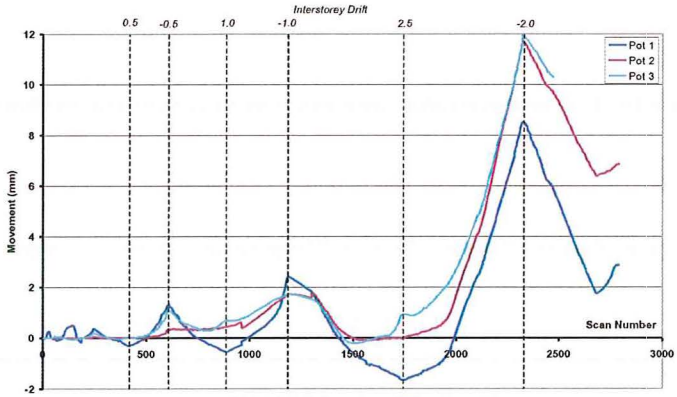

(a) East beam (Beam A)

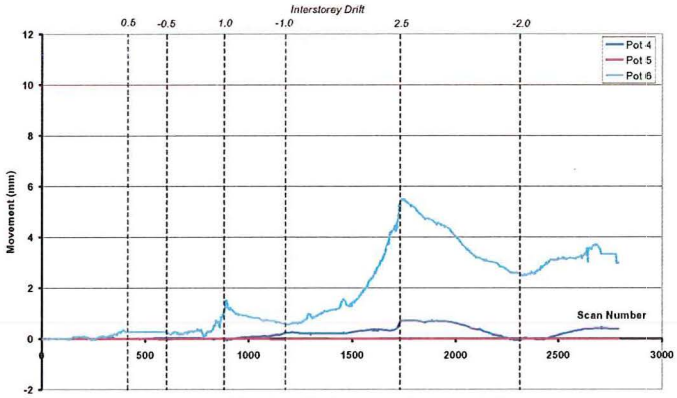

(b) South beam (Beam B)

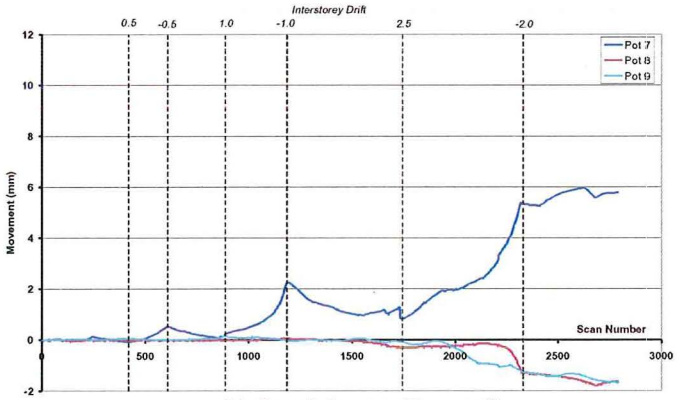

(c) South beam (Beam C)

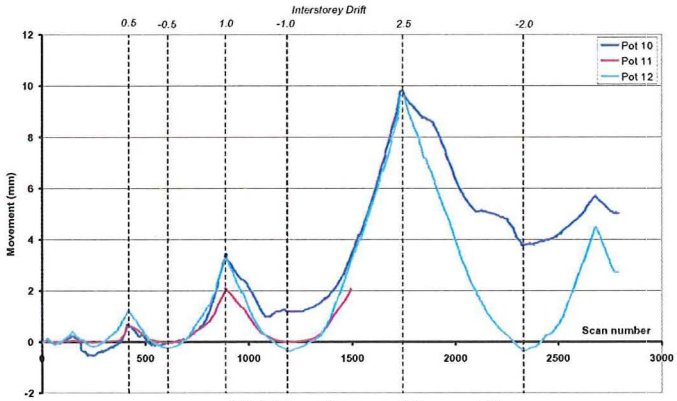

(d) West beam (Beam D)

Figure F-7 Hollow-core unit pull off during Phase I

on the two transverse beams never went negative (in displacement) during Phase I. This meant that for both a positive and negative inclination the bottom of the hollow-core unit was being pulled of its seat.

The two South beams (Beam B and C) potentiometers measured the width of crack that formed in the soffit of the hollow-core unit next to the perimeter frame (Figure F-7(b) and (c)). Most of the movement occurred in sixth and seventh potentiometers located either side of the central column (Figure F-6).

Phase II

Phase II saw an increase in the crack widths for the East and West beams (Figure F-8(a) and (d)). This increase was due to the two transverse beams rotating due to the eccentric load being applied to the beam from the hollow-core units as shown in Figure F-9. This rotation increased as the plastic hinge zones torsional stiffness reduced during the Phase II loading.

Within the southern beams (Figure F-8(b) and (c) only potentiometer number four recorded some significant growth (potentiometer six and seven was removed as it was positioned within a zone of localised damage). The damage that had occurred during Phase I had caused a crack to form in the bottom of the soffit of the hollow-core unit rather than having a crack forming between the hollow-core unit and the perimeter beam (refer to Figure 4-14, Chapter 4). This explains the low readings for most of the potentiometers as the crack occurred outside the instrumented region.

Phase III

No readings were taken during Phase III as the potentiometers were removed to ensure the instrumentation would not be damaged if the floor failed.

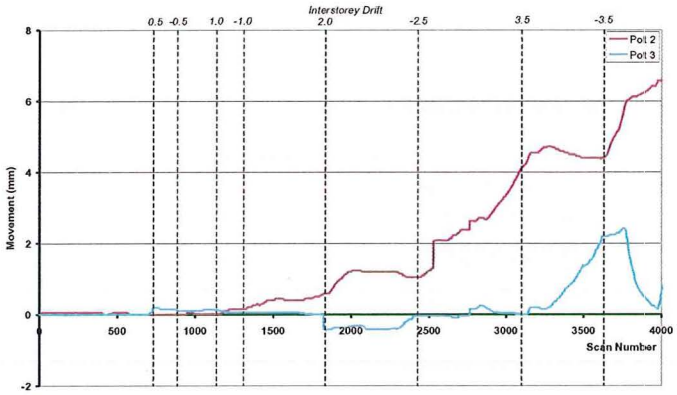

(a) East beam (Beam A)

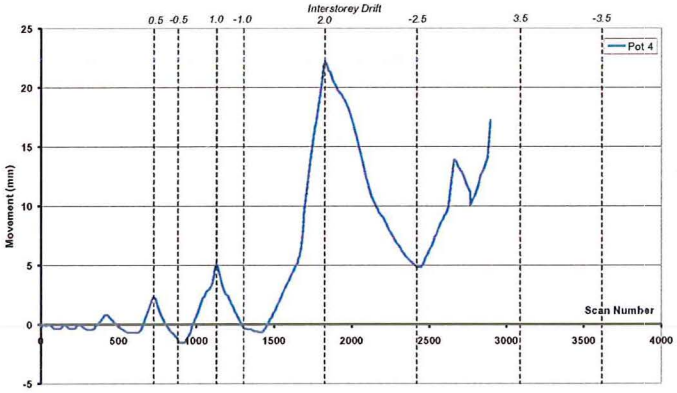

(b) South beam (Beam B)

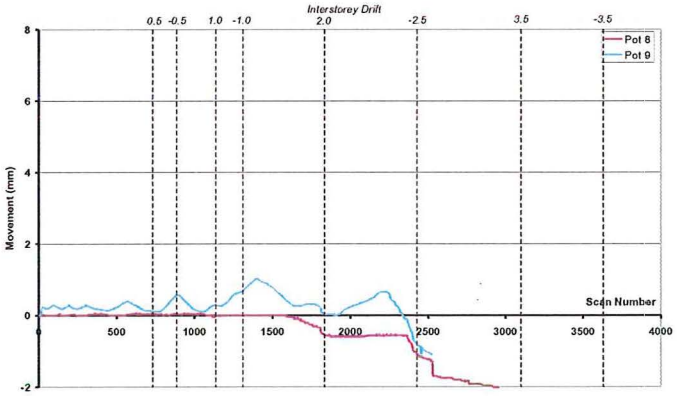

(c) South beam (Beam C)

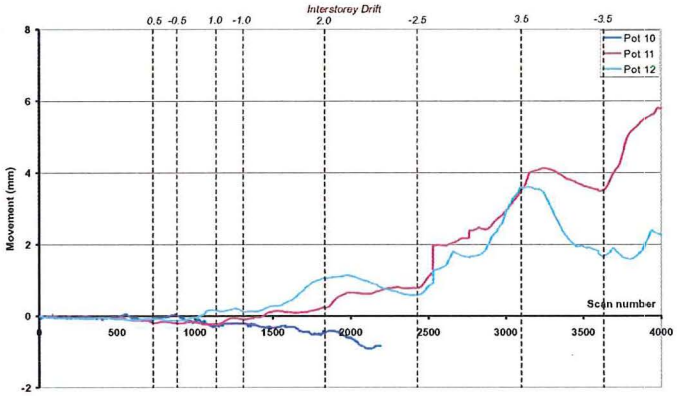

(d) West beam (Beam D)

Figure F-8 Hollow-core unit pull off during Phase II

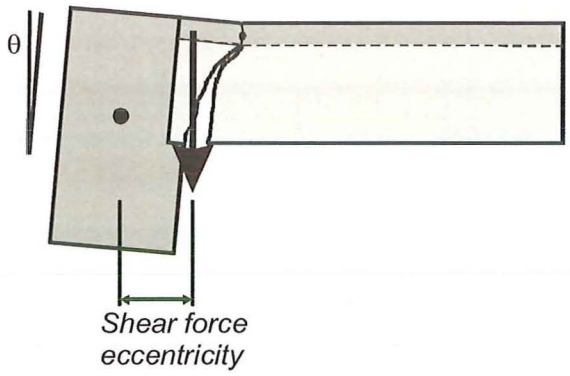

Figure F-9 Rotation of the supporting beam due to eccentric loading

F.4 Initial cracking of the precast units under positive moments.

The failure mechanism that caused the initial cracks in the end of the hollow-core unit to form is shown in Figure F-10. The point at which the unit cracked can be analytically predicted. Firstly the section properties of the topping and hollow-core unit are required as a composite section. These properties are summarised in Table F-1.

Table F-1 Section properties for the hollow-core unit and topping section about the x-axis (refer to Figure F-11 for a diagram showing the composite section)

Part	b (mm)	d (mm)	A (mm^2)	y (mm)	Ay	y-ỹ	$A(y-\tilde{y})^2$	I_{local}
Topping	1200	75	90000	337.5	30.4×10^6	118.5	1.26×10^9	42.2×10^6
H/C unit	1200	300	160600	153	24.6×10^6	66	0.7×10^9	2.04×10^9
		Σ	250600		55×10^6		1.96×10^9	2.08×10^9

$$\bar{y} = \frac{\sum Ay}{\sum A} = \frac{55\times10^6}{250600} = 219mm \qquad \textbf{(F-19)}$$

in which $\bar{y}$ = centroid of the transformed section.

$$I_{xx} = A\left(y - \bar{y}\right)^2 + I_{local} = 1.96 \times 10^9 + 2.08 \times 10^9 = 4.05 \times 10^9 \, mm^4 \qquad \textbf{(F-20)}$$

in which I_{xx} = second moment of inertia about the x-axis of the transformed section; A = cross sectional area of the transformed section; y = distance to the centroid of the localised section; and I_{local} = localised moment of inertia.

Now determine the cracking moment (M_{cr}) of the hollow-core unit. Since the crack formed within 50mm of the edge of the hollow-core unit the presence of prestressing stands in the bottom of the unit is ignored as the strand needs approximately 500mm to develop its full capacity.

$$\frac{M_{cr}}{I_{xx}} = \frac{f_{cr}}{\bar{y}} \Rightarrow M_{cr} = f_{cr} \frac{I_{xx}}{\bar{y}} = f_{cr} S_x \qquad \textbf{(F-21)}$$

in which f_{cr} = tensile strength of the concrete (determined from NZS3101:1995); and S_x = section modulus of the composite section.

$$f_{cr} = 0.5\sqrt{f_c^{'}} = 0.5\sqrt{45} = 3.4MPa \text{ and } S_x = \frac{4.05 \times 10^9}{219} = 18.5 \times 10^6 \qquad \textbf{(F-22)}$$

in which $f_c^{'}$ = concrete compressive strength of the hollow-core unit (=45MPa, as explained earlier).

By substituting in the values for f_{cr} and S_x, Equation (F-21) becomes

$$M_{cr} = 3.4 \times 18.5 \times 10^6 = 62.1 \times 10^6 \; Nmm \text{ or } 62.1kNm \qquad \textbf{(F-23)}$$

Now determine the rotation (θ_{cr}) required to generate this cracking moment by assuming the hollow-core unit and supporting beam can be approximated using moment area.

$$\delta_{cr} = \frac{F_{cr} L^3}{3EI} = \frac{M_{cr} L^2}{3EI} \Rightarrow \theta_{cr} = \frac{M_{cr} L}{3EI} \qquad \textbf{(F-24)}$$

$$\theta_{cr} = \frac{62.1 \times 10^6 \times 5900}{3 \times 30000 \times 4050 \times 10^6} = 0.0010 \qquad \textbf{(F-25)}$$

in which δ_{cr} = tip deflection of the cantilever required to cause the hollow-core unit to fracture; F_{cr} = shear force required to be applied to the tip of the cantilever to cause the end of the hollow-core unit to fracture; L = length from the support of the hollow-core unit to where the shear force is applied, E = modulus of elasticity of the concrete; and I = second moment of area of the topping slab and hollow-core unit.

At an interstorey drift of 0.10%, the end of the hollow-core unit cracks. Once the concrete cracked, the induced strain in the concrete either side of the crack is relieved. Now determine the width of crack (w) that would be present at 0.32% interstorey drift (the drift at which the crack was noticed)

$$w = \Delta\theta \; jD = (0.0032 - 0.0010) \times 335 = 0.74mm \qquad \textbf{(F-26)}$$

in which $\Delta\theta$ = change in rotation between the rotation at first crack and when the crack was first observed; jD = the internal leverarm between the centre of rotation and the extreme tension fibre as shown in Figure F-10.

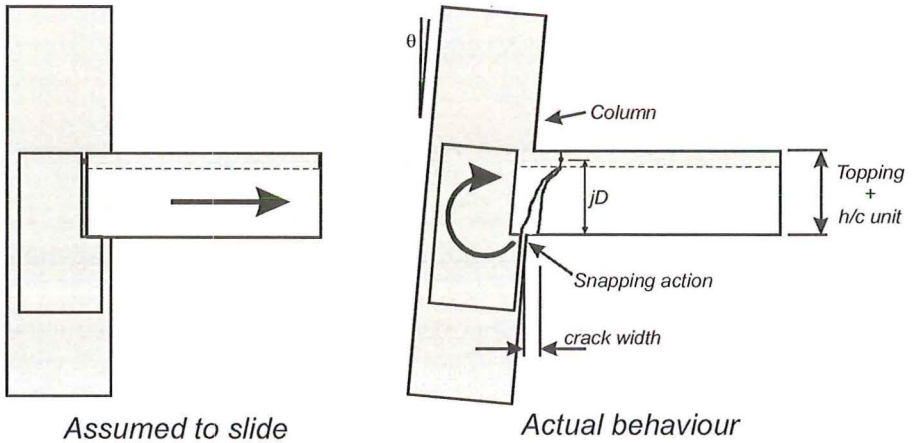

Figure F-10 Assumed versus actual hollow-core to beam performance.

F.5 Bowstring effect

When a reinforced concrete frame elongates due to plastic hinges forming within the beams, the floor slab provides restraint to the beam growth, leading to an increase in the capacity of the frame. This restraint causes the floor slab to act in tension while the beam goes into compression. This phenomena is referred to as the "bowstring effect" and has been explained by Fenwick et al (1999). It is called the "bowstring effect" because the beam in compression acts like a bow and the floor slab in tension acts like the string within a bow.

During the current testing programme a slightly different event occurred. When the floor diaphragm tore the width of floor slab that was in tension reduced to the width of one hollow-core unit (the unit that was still attached to the perimeter beam). The tear then enabled the central column to freely translate in a direction transversely to the direction of loading (out of the building), as the column was not tied into the remainder of the floor slab. The amount that the column translated can be calculated based on a force couple and a calculated moment of inertia.

Firstly, the section properties for the combined beam and floor slab section about the y-axis need to be determined as seen in Figure F-11 and calculated inTable F-2.

$$\bar{y} = \frac{\sum Ay}{\sum A} = \frac{301.6 \times 10^6}{541160} = 557mm \qquad \textbf{(F-27)}$$

in which $\bar{y}$ = centroid of the transformed section.

$$I_{yy} = A(y - \bar{y})^2 + I_{Local} = 96.5 \times 10^9 + 24.5 \times 10^9 = 120.9 \times 10^9 mm^4 \qquad \textbf{(F-28)}$$

in which I_{yy} = second moment of inertia about the y-axis of the transformed section; A = cross sectional area of the transformed section; y = distance to the centroid of the localised section; and I_{local} = localised moment of inertia.

To determine the amount that the column translates due to a horizontally applied moment, caused by the offset between the centroid of the compression and tension forces, moment area was used. Using symmetry (about the central column of the super-assemblage) an expression for the translation (δ) can be written as

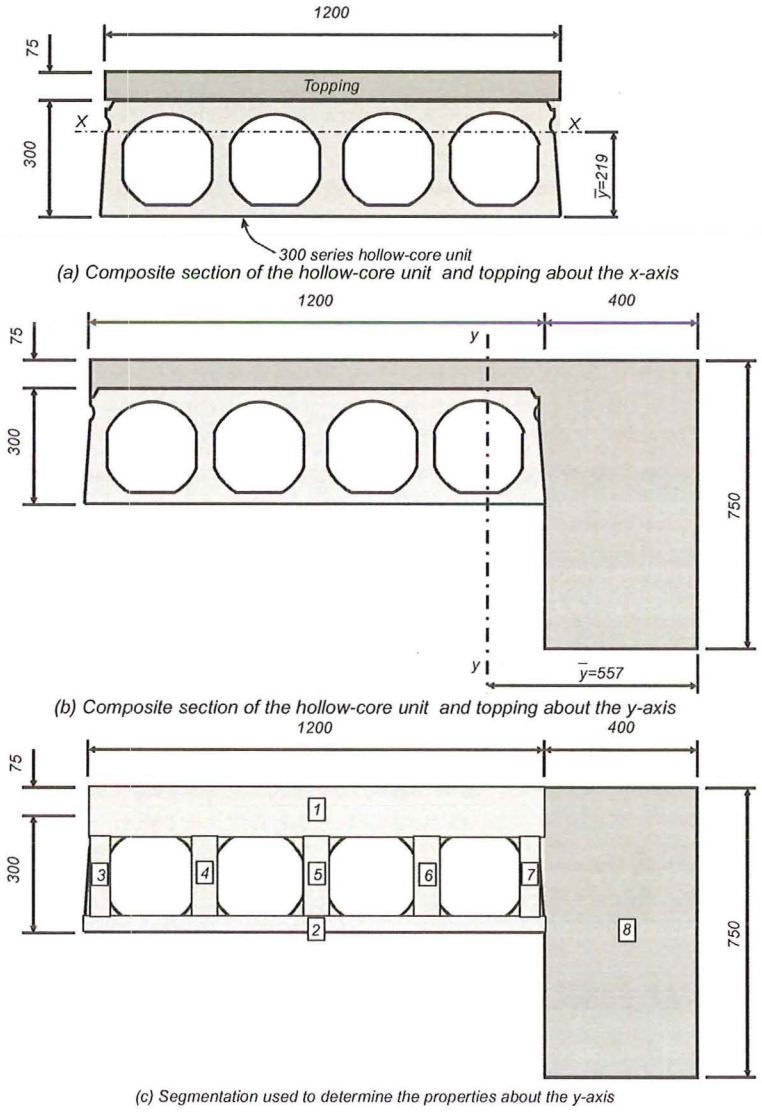

Figure F-11 Section properties for the composite hollow-core and topping sections

$$\delta = \frac{ML^2}{3EI} \qquad \text{(F-29)}$$

in which M = horizontal bending moment induced by the tension field within the floor slab; L = length of the beam; E = modulus of elasticity of the concrete; and I = second moment of inertia of the member.

Table F-2 Section properties for the combined beam and floor slab section about the y-y axis (refer to Figure F-11 for the cross section)

Part	b (mm)	d (mm)	A (mm^2)	y (mm)	Ay	$(y-\bar{y})$	$A(y-\bar{y})^2$	I_{Local} (mm^4)
1	108	1200	129600	1000	129.6×10^6	443	25.4×10^9	15.6×10^9
2	40	1200	48000	1000	48×10^6	443	9.5×10^9	5.8×10^9
3	227	60	13620	1570	21.4×10^6	1013	14×10^9	4.1×10^6
4	227	55	12485	1290	16.1×10^6	733	6.7×10^9	3.1×10^6
5	227	50	11350	1000	11.4×10^6	443	2.2×10^9	2.4×10^6
6	227	55	12485	710	8.9×10^6	153	0.3×10^9	3.1×10^6
7	227	60	13620	430	5.9×10^6	127	0.2×10^9	4.1×10^6
8	750	400	300000	200	60×10^6	357	38.2×10^9	4×10^9
		Σ	541160		301.3×10^6		96.5×10^9	25.4×10^9

Knowing the compression strengths (=45MPa, as explained earlier) it was possible to determine the modulus of elasticity (E) for the composite section.

$$E = 3320\sqrt{f_c'} + 6900 = 3320\sqrt{45} + 6900 \approx 30000MPa \qquad \text{(F-30)}$$

To determine the applied moment due to the centroid of the compression and tension forces being offset (Figure F-12), the magnitude of the tension force (T) and the eccentricity (e) from the centroid of the compression force is required.

The tension force (T) was determined by assuming all the slab reinforcement within the first hollow-core unit was at yield. This assumption agrees with the

effective slab width used to determine the contribution to the super-assemblages lateral strength in Chapter 5.

$$T = mesh + prestress = A_{smesh} f_{ymesh} + A_{shc} f_{yhc} \quad \textbf{(F-31)}$$

$$T = (174 \times 585) + (1000 \times 1030) = 1132kN \quad \textbf{(F-32)}$$

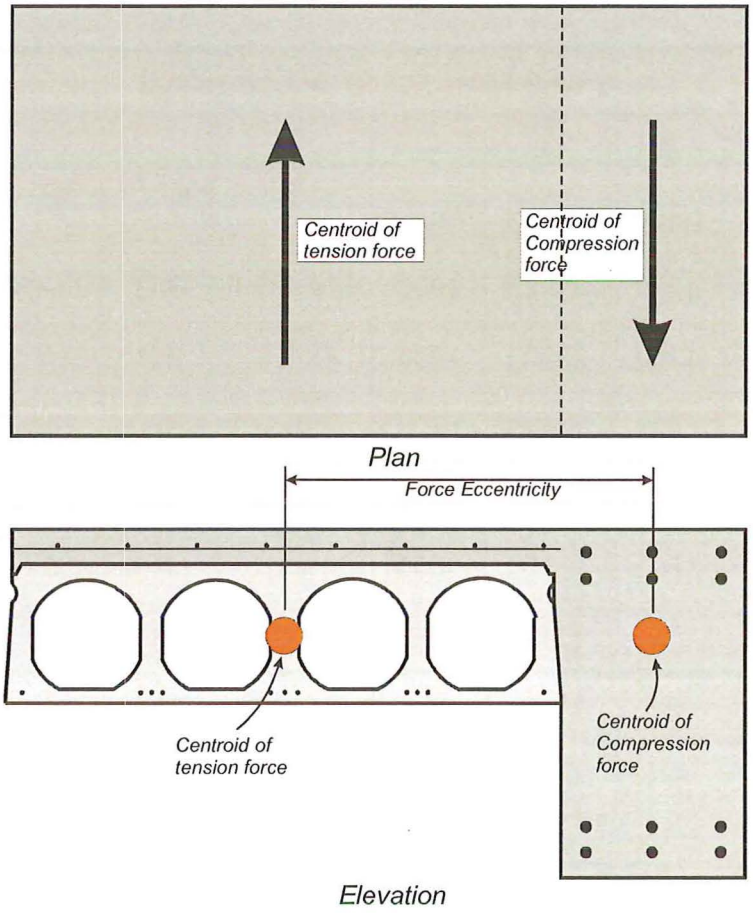

Figure F-12 Plan and elevation showing the offset compression and tension forces that cause the central column to displace laterally.

in which A_{smesh} = area of the reinforcing mesh within one hollow-core unit (=174mm^2); f_{ymesh} = yield stress of the reinforcing mesh (=520MPa, obtained from the steel test results in Appendix B); A_{shc} = area of the prestressing strands in the hollow-core unit within one hollow-core unit (=10 strands of 12.5mm diameter-7wire strand); and f_{yhc} = yield stress of the prestressing strands (taken as 1030MPa)

The eccentricity (e) is assumed to be the distance between the centroid of the section in tension and the centroid of the section in compression (perimeter beam).

$$e = 1000 - 200 = 800mm \quad \textbf{(F-33)}$$

Therefore, the applied moment is determined by

$$M = Te = 1132 \times 0.8 = 906kNm \quad \textbf{(F-34)}$$

In order to determine the deformation of the floor slab in the horizontal plane the stiffness of the beam (EI) and first hollow-core unit needs to be determined. A constant value for EI was assumed based on the gross section properties (denoted as the average EI: for the explanation refer to Figure F-13). Now equate the deflection caused by this applied moment in Equation (F-29).

$$\delta = \frac{906 \times 10^6 \times 6100^2}{3 \times 30000 \times 121 \times 10^9} = 3.1mm \quad \textbf{(F-35)}$$

This deflection of 3.1mm compares well to the observed displacement of approximately 2mm at the initiation of the tear (1.93%).

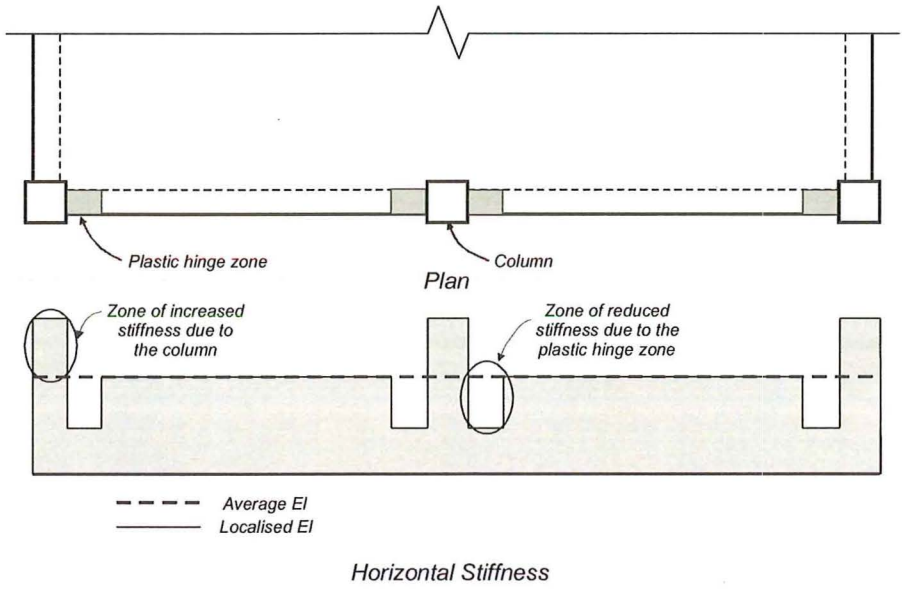

Figure F-13 Determination of EI in the transformed section

F.6 Determining the applied base shear

Using the applied base shear hysteresis loops it is possible to plot different capacity lines on the graph that represent different approximations used to predict the lateral strength of the super-assemblage. Four different mechanisms have been investigated: (i) a proposed theory for predicting the components that contribute to the lateral strength; (ii) the NZS3101:1995 recommendations; (iii) the ACI 318-02 recommendations; and (iv) the progressive activation of the floor slab based on the experimental observations.

To calculate the moment capacities at the various plastic hinge locations, the reinforcement cross sectional areas, yield stress and leverarms for the super-assemblage were required. These values are summarised in Table F-3 and F-4 for the longitudinal (Phase I and III) and transverse (Phase II) loading, respectively. The values in Table F-3 and F-4 for the starter bars, reinforcing mesh and prestressing strands are stated as individual bars/ wires or strands. The yield stresses are measured values, obtained from steel tests on the actual reinforcement used (Appendix B) rather than specified fifth percentile values.

A_s =cross sectional area of reinforcement, f_y = measured yield stress of the reinforcement and jd = internal leverarm between the centre of compression and the centre of the particular reinforcement in tension.

Table F-3 Reinforcement details for the longitudinal loading direction

	Perimeter Beam	Starter Bar	Reinforcing Mesh	P/S Strands (negative moment)	P/S Strands (positive moment)
A_S (mm^2)	2714	113	22	100	100
f_y (MPa)	299	508	520	1030	1030
jd (mm)	560	610	610	360	250
Bending moment (kNm)	455	35	7	37	26

Table F-4 Reinforcement details for the transverse loading direction

	Perimeter Beam	Starter bar	Cold-drawn Wire reinforcing mesh
A_S (mm^2)	2714	113	22
f_y (MPa)	299	508	520
jd (mm)	512	560	560
Bending moment (kNm)	416	32	6

Proposed Theory:

This theory uses rigid body kinematics to determine the moment capacity for the perimeter beam and slab (Figure F-14).

For an exterior plastic hinge, a tripartite curve was proposed to estimate the lateral strength (Chapter 5). A tripartite curve was required because the width of floor slab activated increased with interstorey drift. The amount of activation is dependent on the torsional stiffness of the transverse beam. To define this curve two data points are required: (i) the moment capacity at first yield (the activated slab width =1.2m)

and (ii) at full plasticity (the activated slab width = 3.05m) as shown in Figure F-15. It should be noted that for the proposed theory the prestressing strands within the hollow-core unit contributes to the lateral strength for both a positive and negative moment on either side of the central column.

For an interior plastic hinge, a bi-linear approximation was proposed to estimate the lateral strength. To define this curve only the capacity at first yield is required (the activated slab width =1.2m) as shown in Figure F-15.

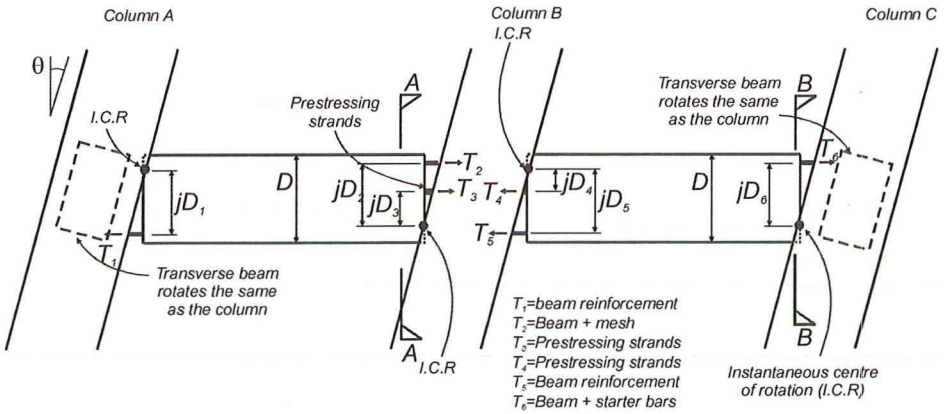

(a) A sketch showing how rigid body kinematics determine the displaced shape and in turn are used to generate the moment capacities for the various plastic hinges.

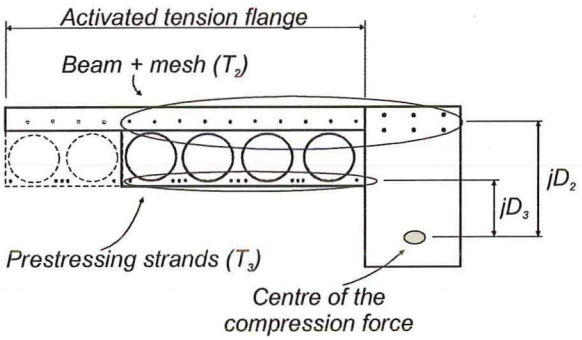

(b) Section A-A at all stages of plastification

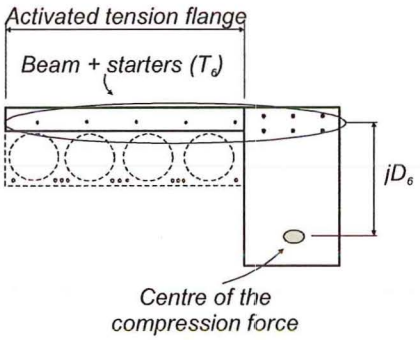

(c) Section B-B at the onset of plastification (yield)

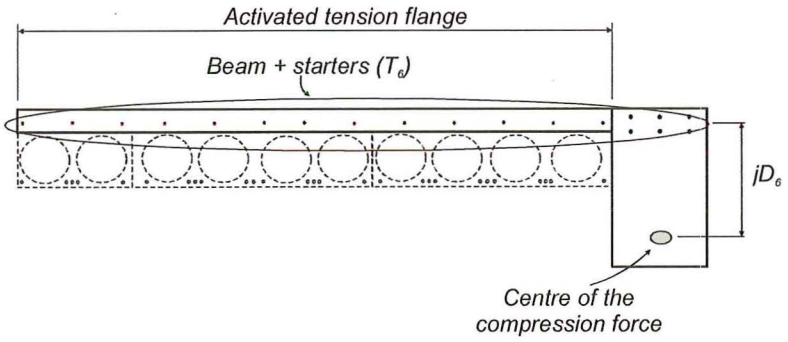

(d) Section B-B at full plastification

Figure F-14 The use of rigid body kinematics to explain how the additional tension reinforcememnt contributes to the lateral strength of the super-assembly at different stages of progressive plastification

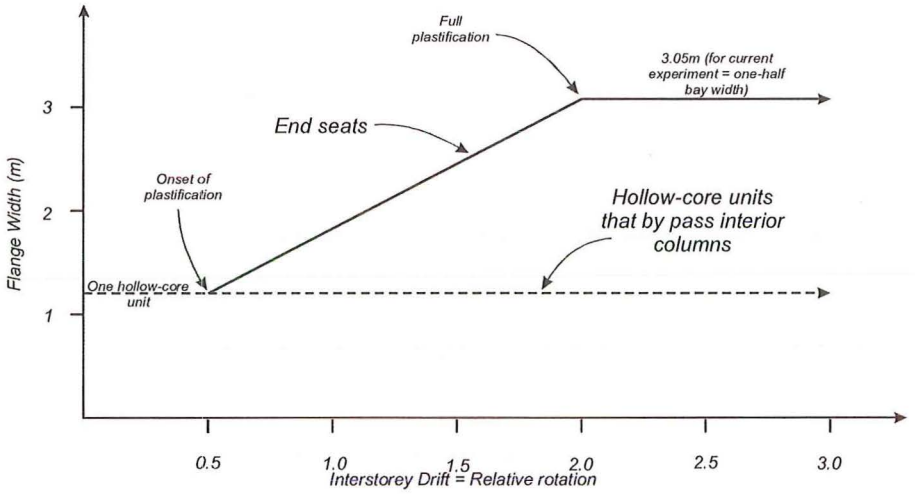

Figure F-15 Proposed floor slab activation with increasing interstorey drift.

Phase I: at the onset of plastification

Table F-5 Nominal moment capacities for the South Frame

	SW	CC-LHS	CC-RHS	SE
Beam	455	455	455	455
Starter bars	-	-	-	4×35
Reinforcing mesh	-	47	-	-
P/S strands	-	11×37	11×26	-
Total	455	909	741	595

Sum of nominal moments = 455+909+741+595

(Column face) = 2700kNm

(Convert to column centreline) = 2700 × 1.14=3078kNm

$$\sum V_{col} = \frac{\sum M_n}{h_s} = \frac{3078}{3.5} = 757kN$$

in which V_{col} = lateral force applied to the column; M_n = nominal beam moment; and h_s = interstorey height of the columns. Refer to Figure F-16 shows the location of V_{col}, M_n and h_s.

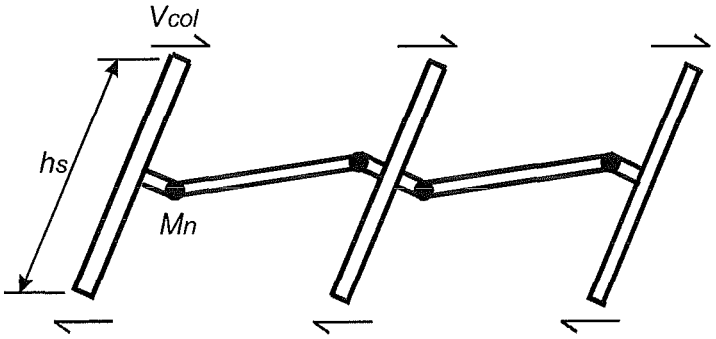

Figure F-16 Notation used to determine the sum of V_{col} (Applied base shear)

Phase II: at the onset of plastification

Table F-6 Nominal moment capacities for the East and West Frames

	SW=SE	NW=NE
Beam	416	416
Starter bars	-	4×32
Reinforcing mesh	-	-
P/S strands	-	-
Total	416	544

Sum of nominal moments = 2(416+544)

(Column face) = 1912kNm

(Convert to column centreline) = 1920 × 1.14=2189kNm

$$\sum V_{col} = \frac{\sum M_n}{h_s} = \frac{2189}{3.5} = 625kN$$

Phase I: at full plasticity

Table F-7 Nominal moment capacities for the South Frame

	SW	CC-LHS	CC-RHS	SE
Beam	455	455	455	455
Starter bars	-	-	-	10×35
Reinforcing mesh	-	47	-	-
P/S strands	-	11×37	11×26	-
Total	455	909	741	805

Sum of nominal moments = 455+909+741+805

(Column face) = 2910kNm

(Convert to column centreline) = 2910 × 1.14=3317kNm

$$\sum V_{col} = \frac{\sum M_n}{h_s} = \frac{3317}{3.5} = 948kN$$

Phase II: at full plasticity

Table F-8 Nominal moment capacities for the East and West Frames

	SW=SE	NW=NE
Beam	416	416
Starter bars	-	10×32
Reinforcing mesh	-	-
P/S strands	-	-
Total	416	736

Sum of nominal moments = 2(416+736)

(Column face) = 2304kNm

(Convert to column centreline) = 2304 × 1.14=2627kNm

$$\sum V_{col} = \frac{\sum M_n}{h_s} = \frac{2627}{3.5} = 750kN$$

NZS3101 prediction (Phase I and II):

The New Zealand Concrete Structures Standard (NZS 3101:1995) gives guidance on determining the amount of strength enhancement from the floor diaphragm. This prediction is based on the work carried out by Cheung et al (1991). This mechanism assumes the beam longitudinal reinforcement plus a contribution from the floor slab are used to calculate the nominal beam moment. Determining the width of slab activated according to NZS3101 can be difficult to follow. Confusion leads as to whether the prestressing strands within the hollow-core units should be included for determining the Phase I mechanism (the direction in which the prestressing strands run parallel to the direction of loading). This mechanism assumes that the prestressing stands do not contribute to the strength enhancement. The width of floor slab assumed to contribute (according to NZS3101:1995) was taken as 1.53m ($L_b/4$) for both the longitudinal and transverse loading directions.

Phase I:

For any slab reinforcement to be considered to contribute to the negative moment capacity of the beam it must be effectively anchored reinforcement within the zone of possible activation.

For an exterior hinge, the number of activated bars equals one HD12 starter bar plus 10 cross wires of cold-drawn wire reinforcing mesh. This is illustrated in Figure F-17.

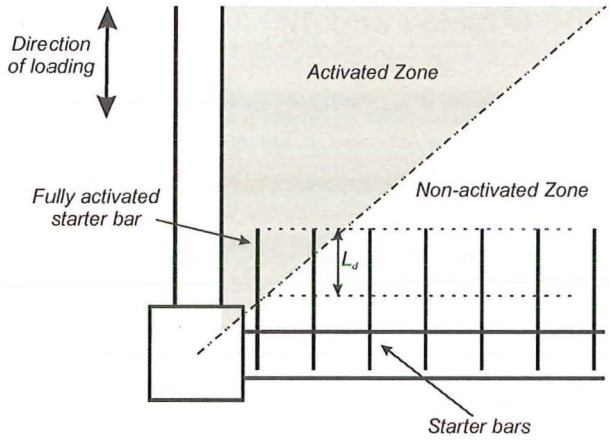

Figure F-17 Determining the number of activated bars in an exterior joint

(reinforcing mesh is not shown for clarity)

For an interior joint, only the reinforcing mesh is assumed to contribute as there are no starter bars present at that location.

Table F-9 Nominal Moment capacities for the South Frame

	SW	CC-LHS	CC-RHS	SE
Beam	455	455	455	455
Starter bars	-	-	-	1×35
Reinforcing mesh	-	10×7	-	10×7
P/S strands	-	-	-	-
Total	455	525	455	560

Sum of nominal moments = 455+525+455+560

(Column face) = 1995kNm

(Convert to column centreline) = 1995 × 1.14=2274kNm

$$\sum V_{col} = \frac{\sum M_n}{h_s} = \frac{2274}{3.5} = 650kN$$

Phase II:

For any slab reinforcement to be considered to contribute to the negative moment capacity of the beam it must be effectively anchored reinforcement within the zone of possible activation.

For an exterior hinge, the number of activated bars equals one HD12 starter bar plus 10 cross wires of cold-drawn wire reinforcing mesh. This is illustrated in Figure F-18.

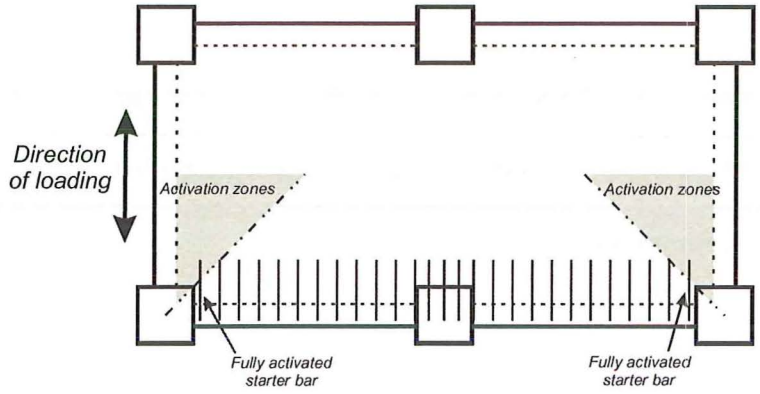

Figure F-18 Determining the number of activated bars in the floor slab (reinforcing mesh is not shown for clarity)

Table F-10 Nominal moment capacities for the East and West Frames

	SW=SE	NW=NE
Beam	416	416
Starter bars	-	1×32
Reinforcing mesh	-	10×7
P/S strands	-	-
Total	416	518

Sum of nominal moments = 2(416+518)

(Column face) = 1868kNm

(Convert to column centreline) = 1868 × 1.14=2130kNm

$$\sum V_{col} = \frac{\sum M_n}{h_s} = \frac{2130}{3.5} = 608kN$$

ACI 318-02 prediction (Phase I and II):

This mechanism assumes the beam longitudinal reinforcement plus a contribution from the floor slab as assumed by ACI 318-02 is used to calculate the nominal beam moment. According to ACI 318-02, the effective flange width was taken as the lesser

of one-twelfth the span of the beam, six times the slab thickness, and one-half the clear distance to the next web. One-twelfth the span of the beam governs in this case and equates to 510mm.

For Phase I, the diaphragm contribution is made up of the starter bars, reinforcing mesh and the prestressing strands within the hollow-core units while for Phase II only the starter bars contribute.

Phase I:

For an exterior hinge, the number of activated starter bars equals two HD12 starter bars. For an interior joint, the amount of activation is three wires of cold-drawn wire reinforcing mesh and four prestressing strands.

Table F-11 Nominal moment capacities for the South Frame

	SW	CC-LHS	CC-RHS	SE
Beam	455	455	455	455
Starter bars	-	-	-	2×35
Reinforcing mesh	-	3×7	-	-
P/S strands	-	4×37	-	-
Total	455	624	455	525

Sum of nominal moments = 455+624+455+525

(Column face) = 2059kNm

(Convert to column centreline) = 2059 × 1.14=2347kNm

$$\sum V_{col} = \frac{\sum M_n}{h_s} = \frac{2347}{3.5} = 671kN$$

Phase II:

For an exterior hinge, the number of activated starter bars equals two HD12 starter bars.

Table F-12 Nominal moment capacities for the East and West Frames

	SW=SE	NW=NE
Beam	416	416
Starter bars	-	2×32
Reinforcing mesh	-	-
P/S strands	-	-
Total	416	480

Sum of nominal moments = 2(416+480)

(Column face) = 1792kNm

(Convert to column centreline) = 1792 × 1.14=2043kNm

$$\sum V_{col} = \frac{\sum M_n}{h_s} = \frac{2043}{3.5} = 584kN$$

F.7 Phase III moment diagrams

Phase III:

For both the SW and SE columns (Figure F-19 (a) and (b)), the positive moment capacity agrees well with the observed moments. The SE observed moment was slightly larger that the prediction because the plastic hinge did not form exactly on the column face. Also, the reinforcement within the plastic hinge had started to strain harden. For a negative moment, the predicted capacity overestimated the capacity. The overestimation was due to the degrading condition of the hollow-core unit and its connection detail to the supporting beam. It was this deterioration that caused the lateral strength to reduce.

For the central column (Figure F-19(c)), the expected capacity was less than that observed as the expected capacity consisted of the negative beam moment plus the contributing slab consisting of the reinforcing mesh and prestressing strands. The

deterioration of the hollow-core unit contributed to the overestimated prediction of the lateral strength.

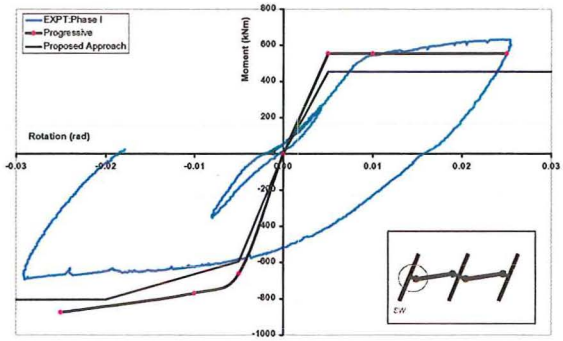

(a) SW columns moment versus rotation

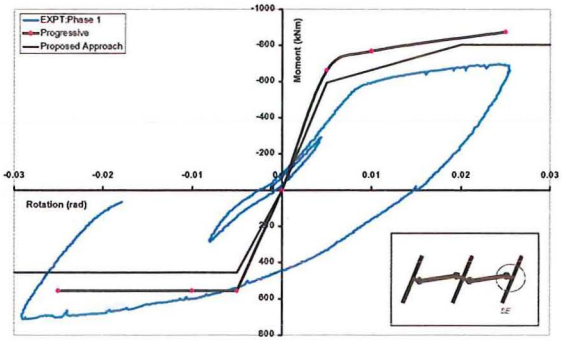

(b) SE columns moment versus rotation

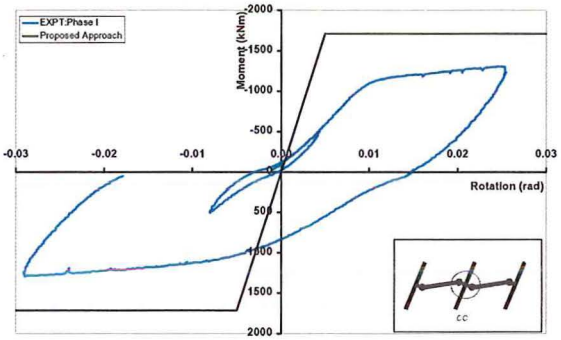

(c) Central Columns moment versus rotation plot for Phase III

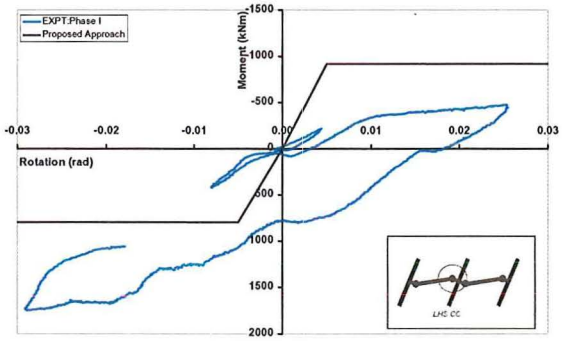

(d) LHS central column beam moments

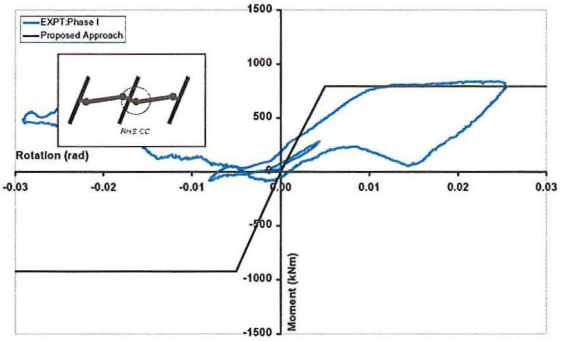

(e) RHS central column beam moment

Figure F-19 Outer column moment versus rotation plots for Phase III

As explained in Chapter 5, the axial load recorded by the instrumented universal joints at the base of the columns was not consistent. This meant that it was not possible to accurately determine the centre column beam moments. The calculation of the beam moments was generally good at low levels of drift, this was because the loading frames were self-equilibrating which meant that all the loads were equalised

within the frame and the column axial load did not change. Once moment redistribution occurred, the column axial loads changed, this caused the incorrect moment to be calculated. Figure F-19(d) and (e) shows the incorrectly calculated beam moment capacities for the interior plastic hinge on either side of the central column. The actual bending moment plots should look similar (in shape) to that of the interior plastic hinge moment diagrams in Phase I (refer to Chapter 5).

F.8 References

ACI 318-02, *Building Code Requirements for Structural Concrete and Commentary*, American Concrete Institute, Farmington Hills, USA

Cheung P.C., Park R, Paulay T, 1991, *Seismic Design of Reinforced Concrete Beam Column Joints with Floor Slab Support*, Research Report 91-4, Department of Civil Engineering, University of Canterbury, Christchurch, 328 pp.

Fenwick R, Davidson D and Lau D, 1999, *Strength Enhancement of Beams in Ductile Seismic Resistant Frames due to Prestressed Components in Floor Slabs*, Journal of the New Zealand Structural Engineering Society (SESOC), Vol 12, no. 1, pp 35-40

Kim and Mander, 1999, *Truss modeling of reinforced concrete shear-flexure behavior*, MCEER Technical Report MCEER-99-0005, March 8

NZS3101:1995, *Concrete Structures Standard NZS3101:1995*, Wellington New Zealand

Priestley M.J.N, Seible F and Calvi G.M, 1996, *Seismic Design and Retrofit of Bridges*, J Wiley and Sons Inc

This Page is Blank

Appendix G

Diaphragm Performance

G.1 Technical Advisory Group (TAG) on precast floors testing

The sub-assemblage used to test the connection details recommended by the TAG is shown in Figure G-1. The shear force pattern experienced during the super-assemblage testing (12m span) is shown in Figure G-2. The 2-D set up used to test the TAG recommended details was based on the expected deformations and shear forces found from the super-assemblage testing programme. Clamping the supporting beam to the structural floor and articulating the hollowcore relative to the beam achieved this. The background to the development of this set up is also shown in Figure G-2.

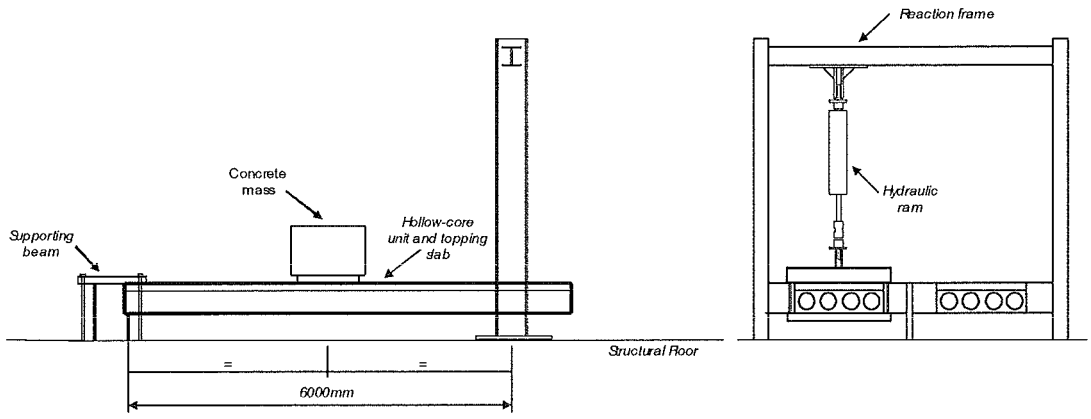

Figure G-1 Sub-assemblage experimental set up (Bull and Matthews, 2003)

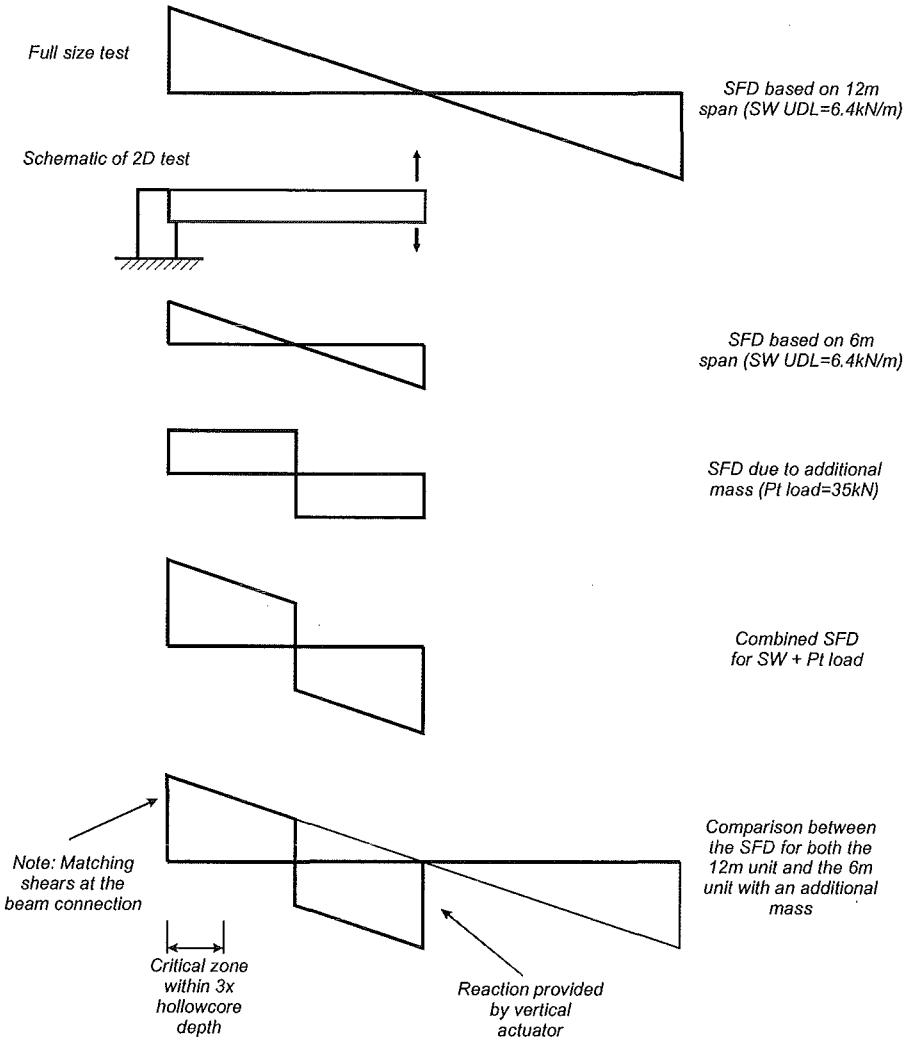

Figure G-2 Schematic showing the determination of the experimental set up

(Bull and Matthews, 2003)

G.2 Diaphragm Performance

Included below are all the various graphs showing the diaphragm growth during the experimental programme. The growth within the floor is obtained from summing the demec points across the floor, refer to Figure G-3 for the location of the demec points.

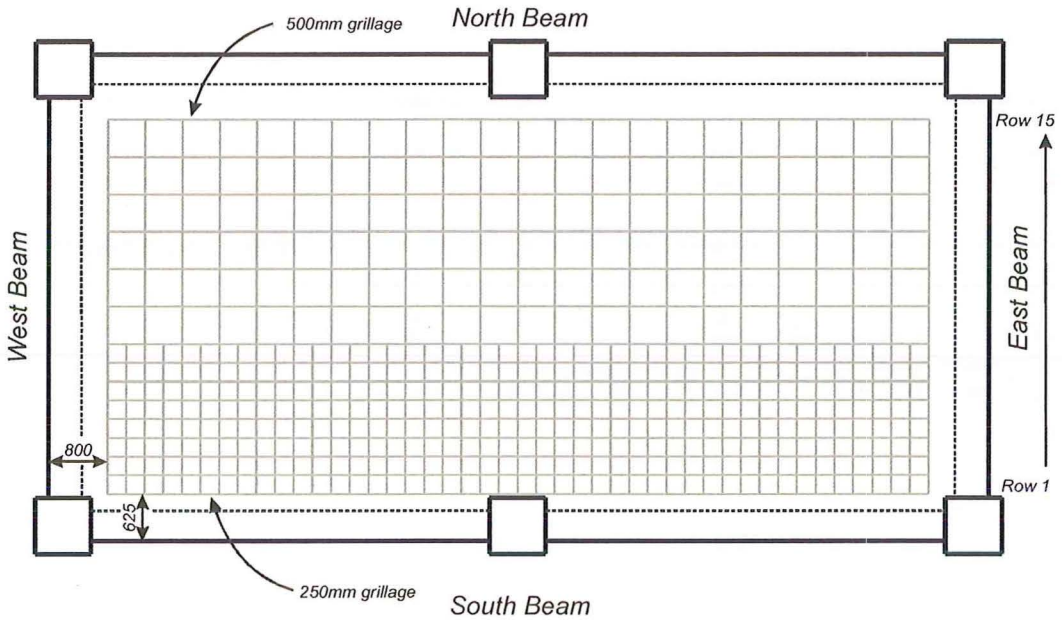

Figure G-3 Demec point location

In the figures below is the longitudinal growth for all the positive drift cycles

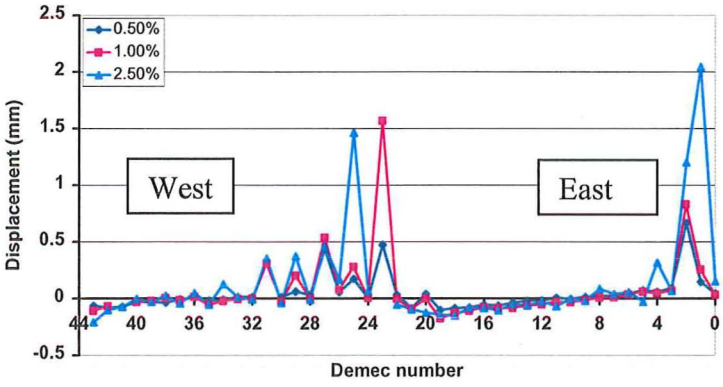

Row 1 for Phase I

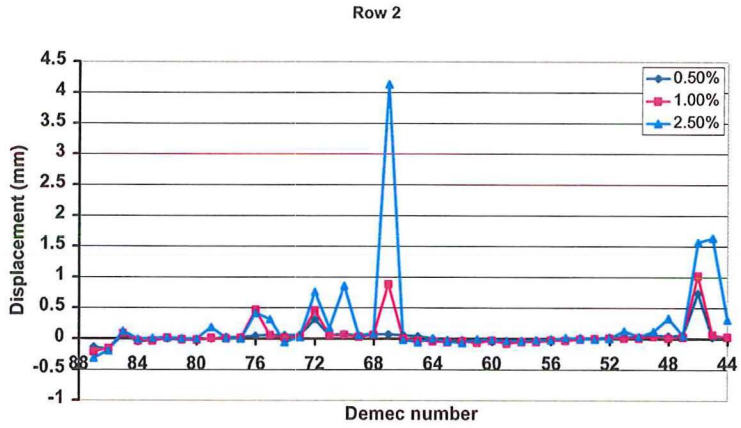

Row 2 for Phase I

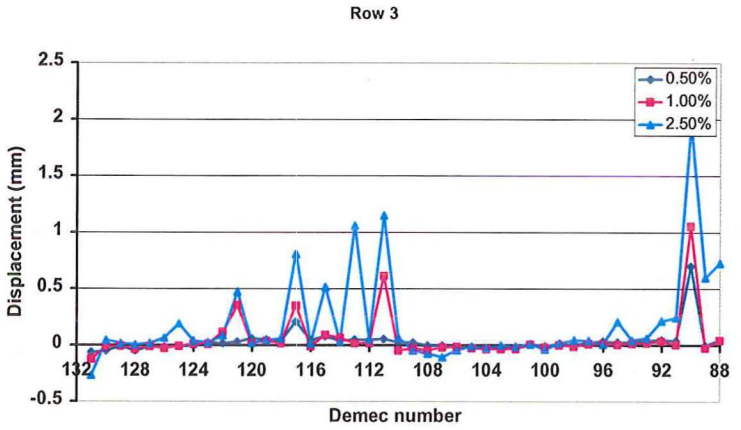

Row 3 for Phase I

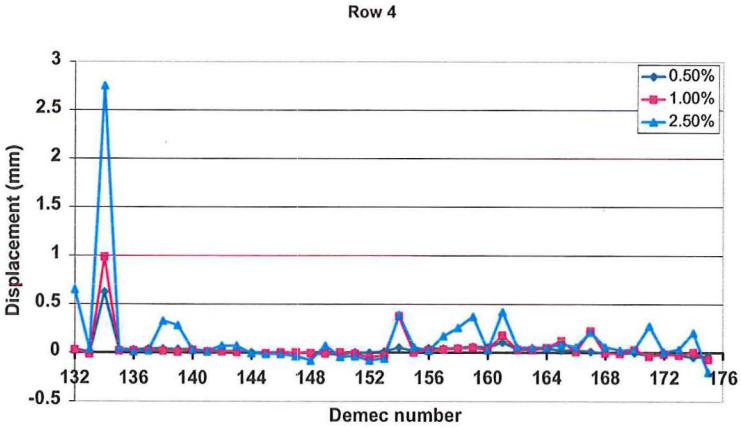

Row 4 for Phase I

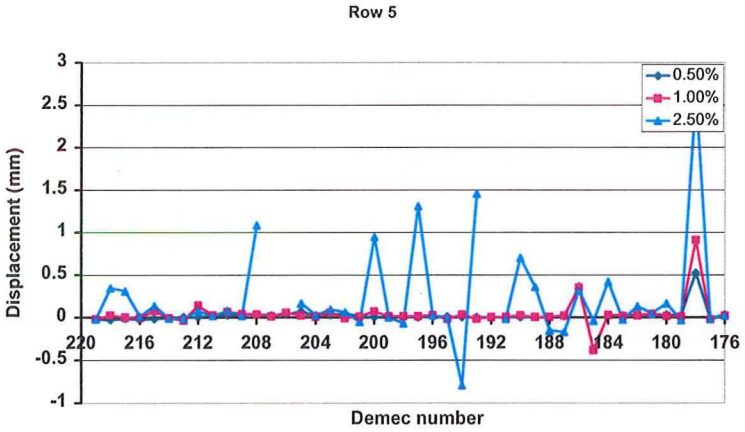

Row 5 for Phase I

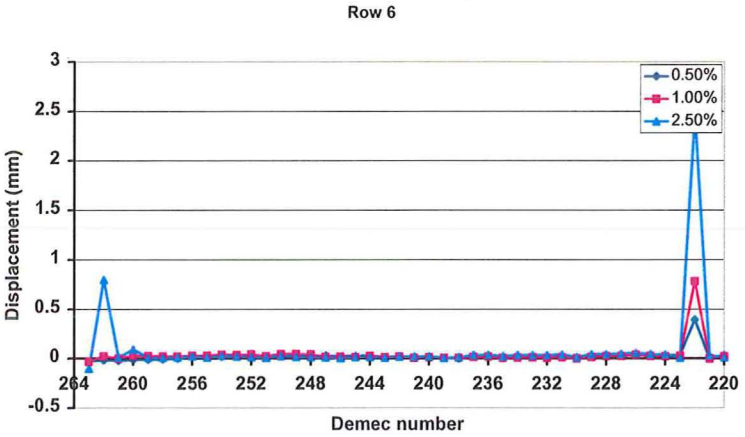

Row 6 for Phase I

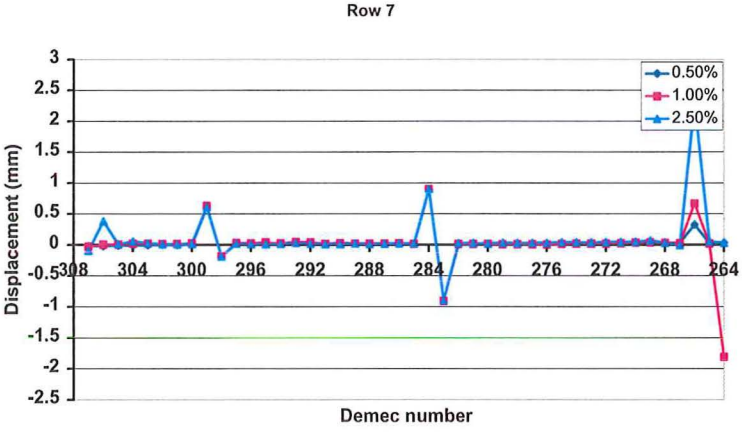

Row 7 for Phase I

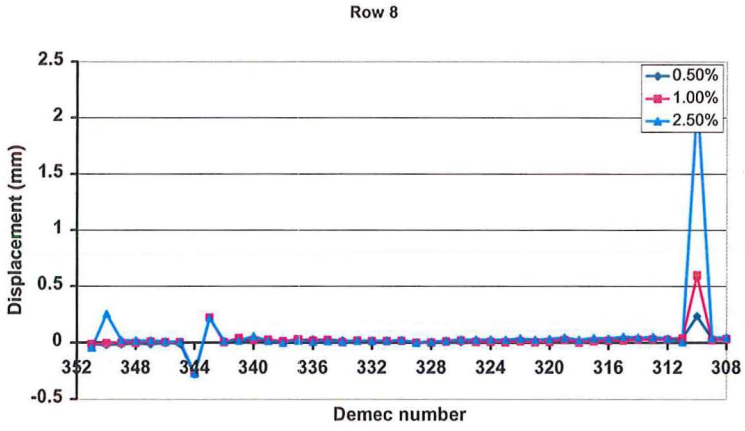

Row 8 for Phase I

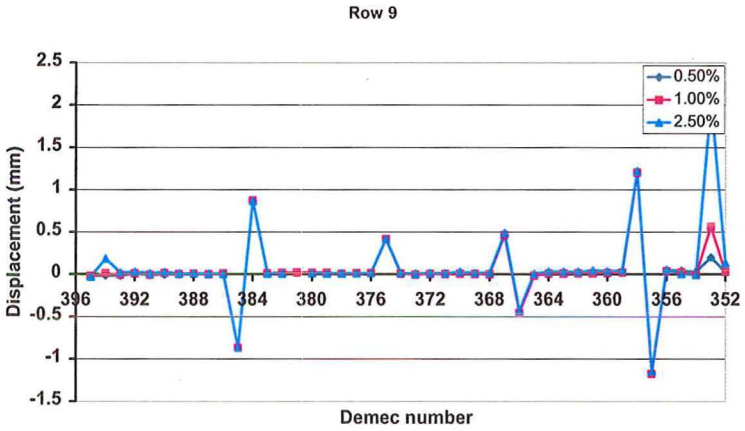

Row 9 for Phase I

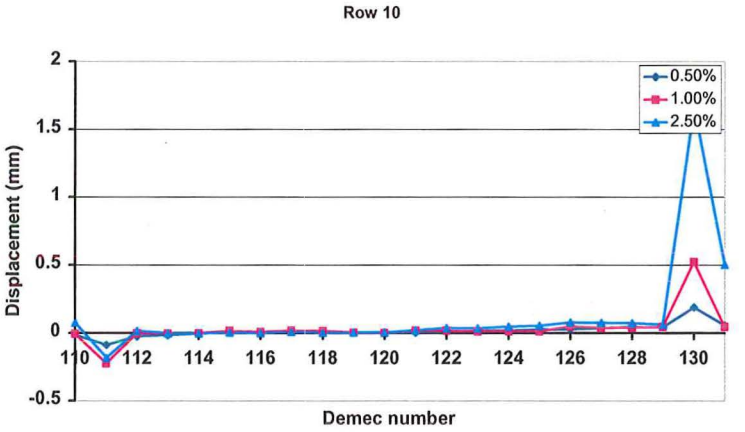

Row 10 for Phase I

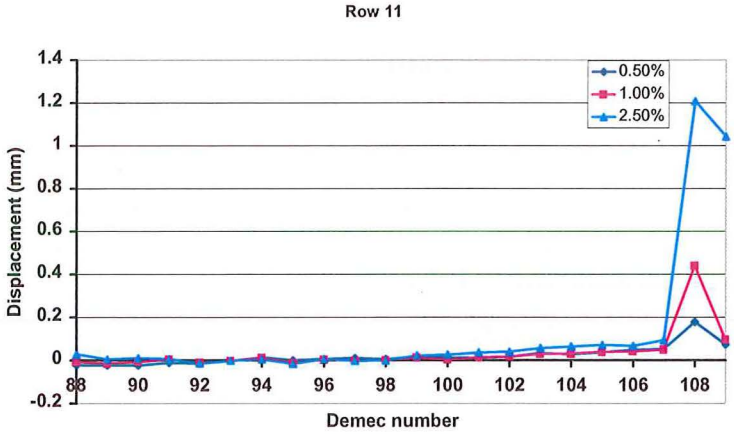

Row 11 for Phase I

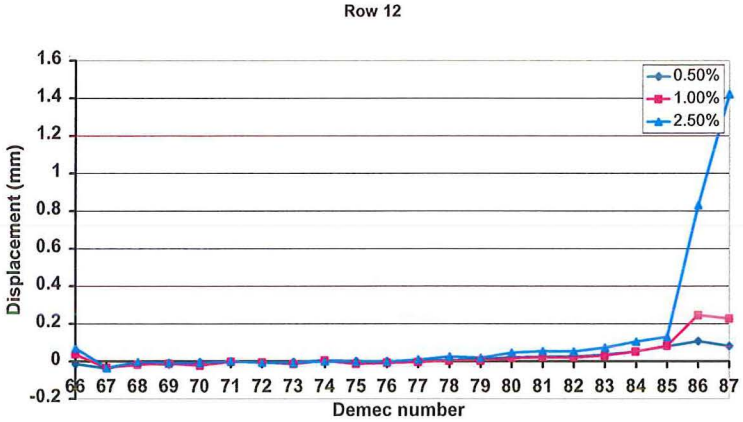

Row 12 for Phase I

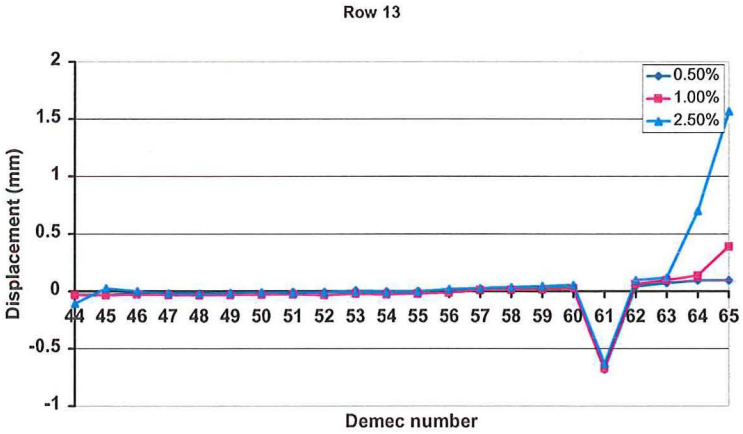

Row 13 for Phase I

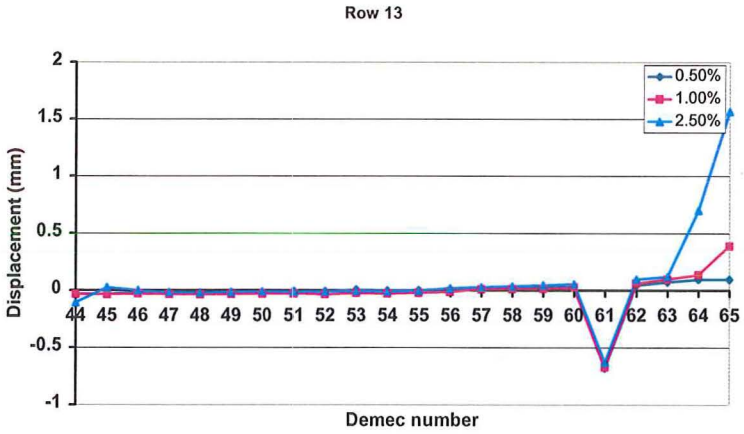

Row 14 for Phase I

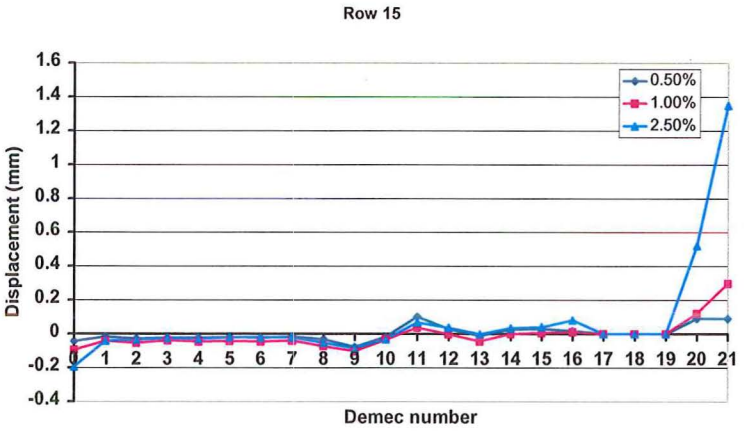

Row 15 for Phase I

In the figures below is the longitudinal growth for all the negative drift cycles

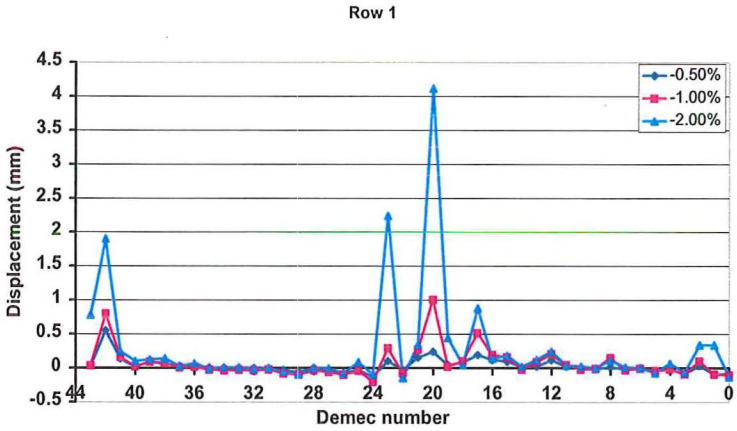

Row 1 for Phase I

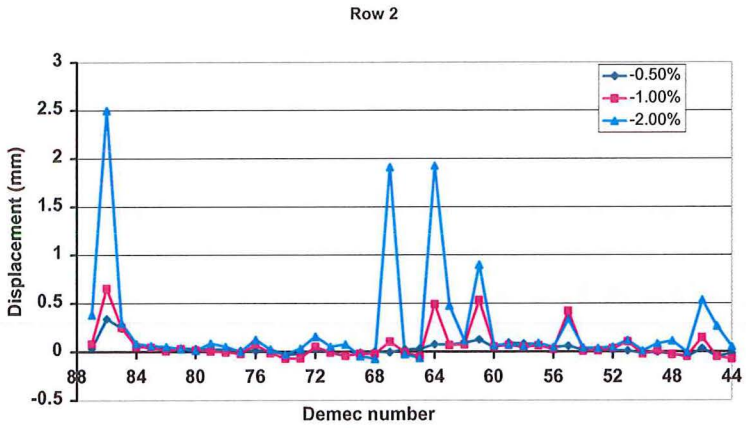

Row 2 for Phase I

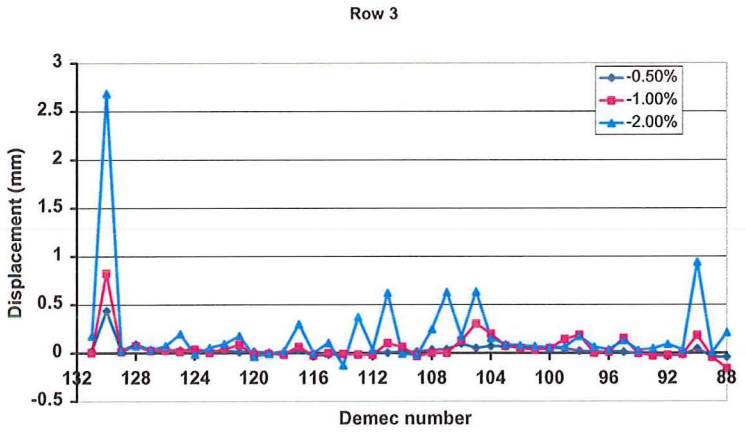

Row 3 for Phase I

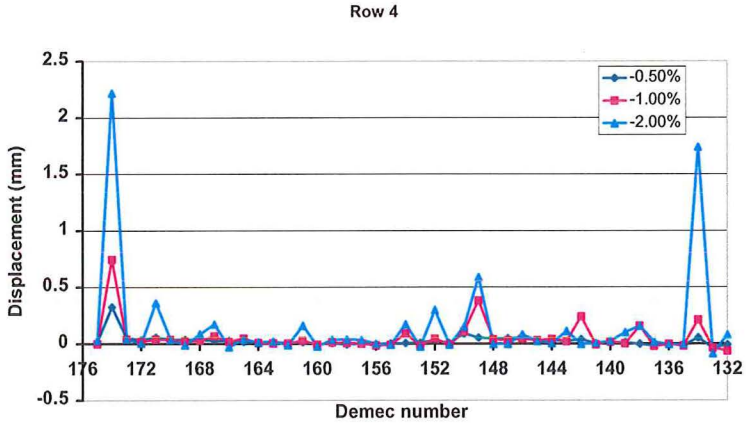

Row 4 for Phase I

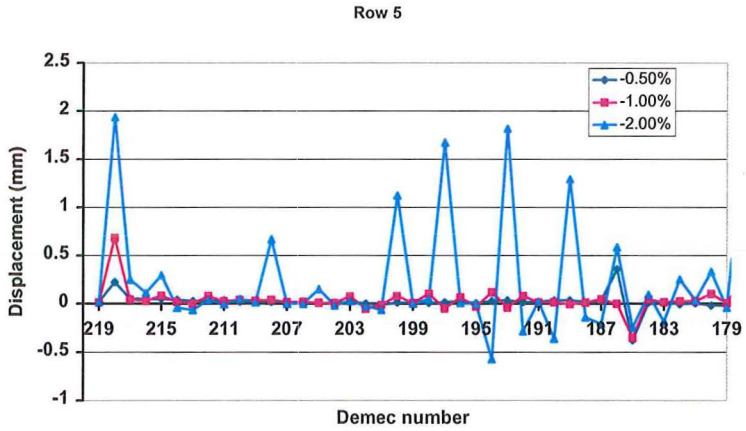

Row 5 for Phase I

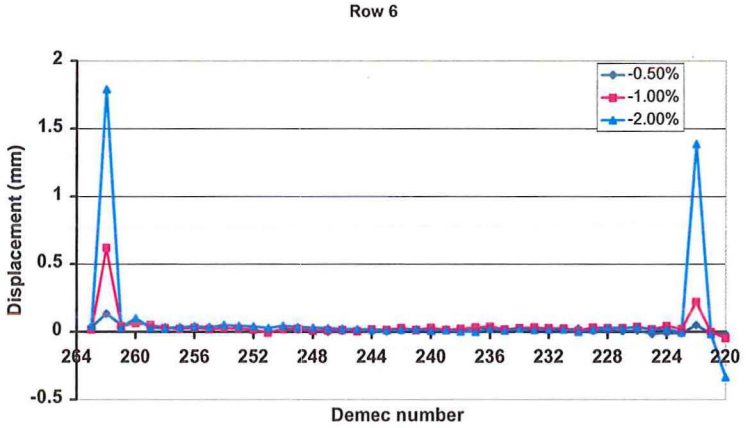

Row 6 for Phase I

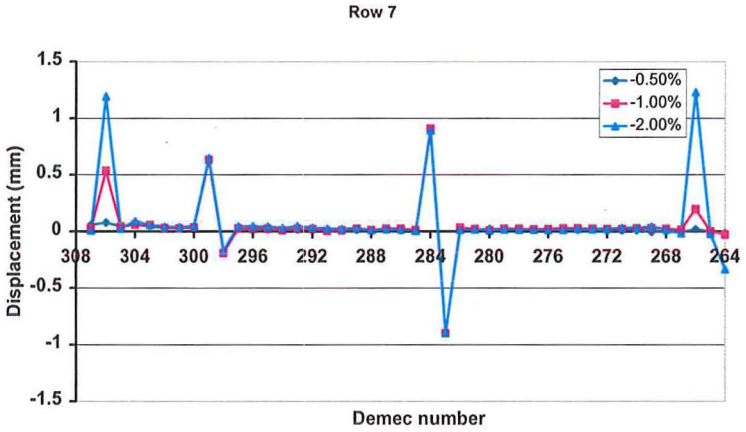

Row 7 for Phase I

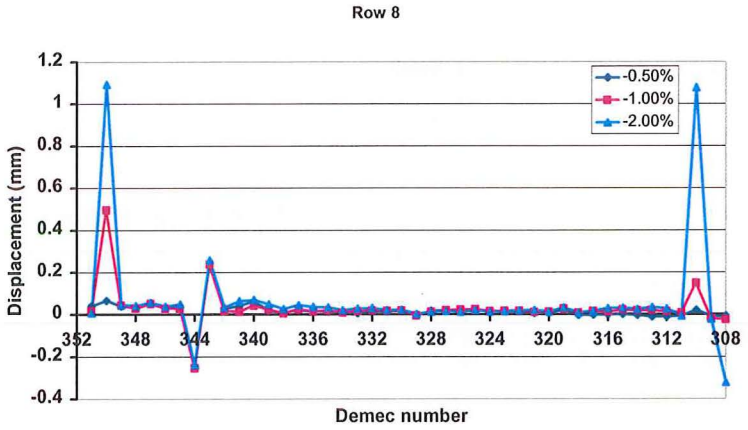

Row 8 for Phase I

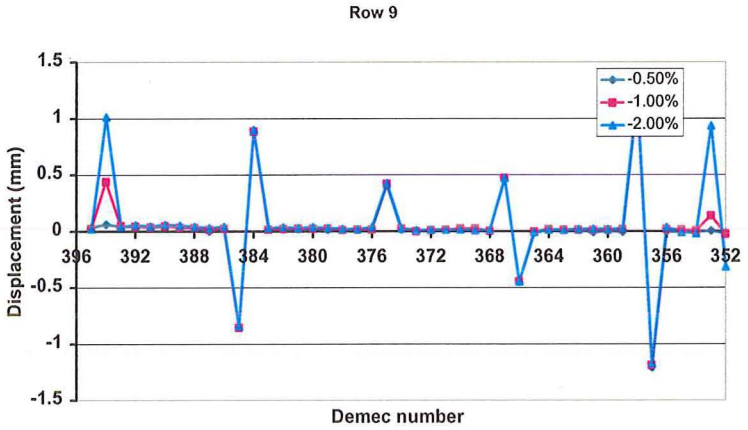

Row 9 for Phase I

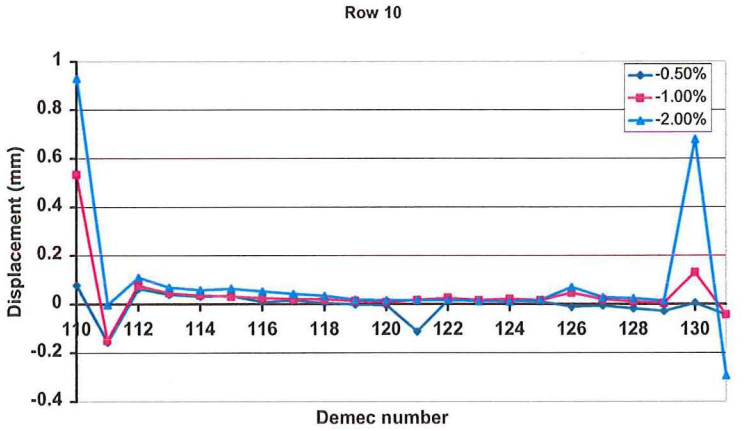

Row 10 for Phase I

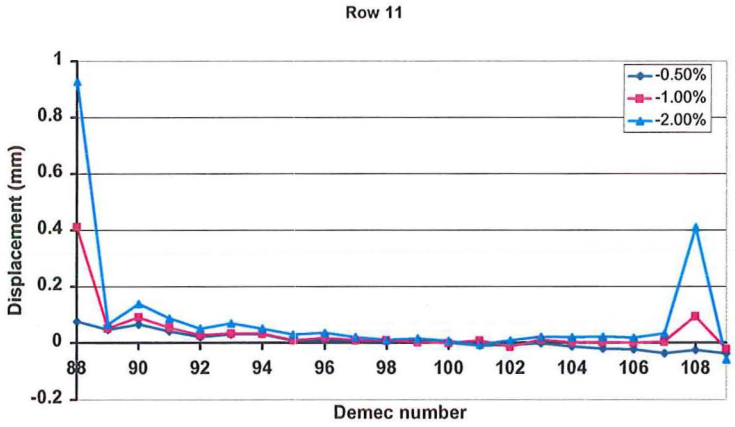

Row 11 for Phase I

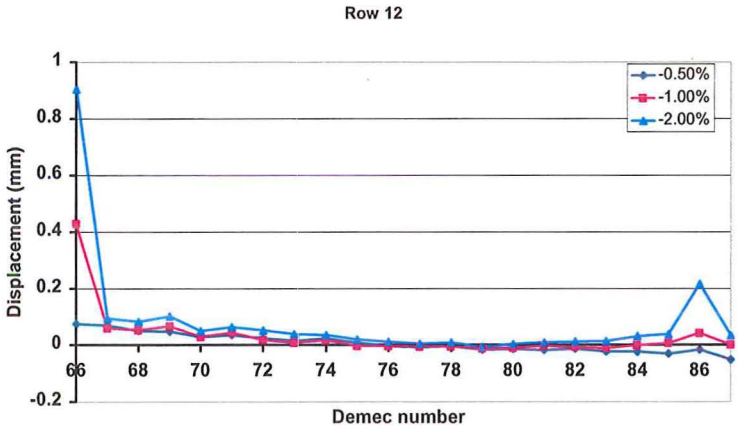

Row 12 for Phase I

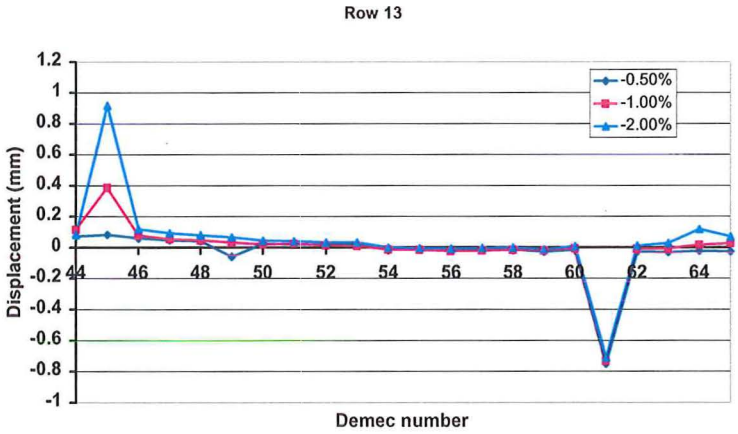

Row 13 for Phase I

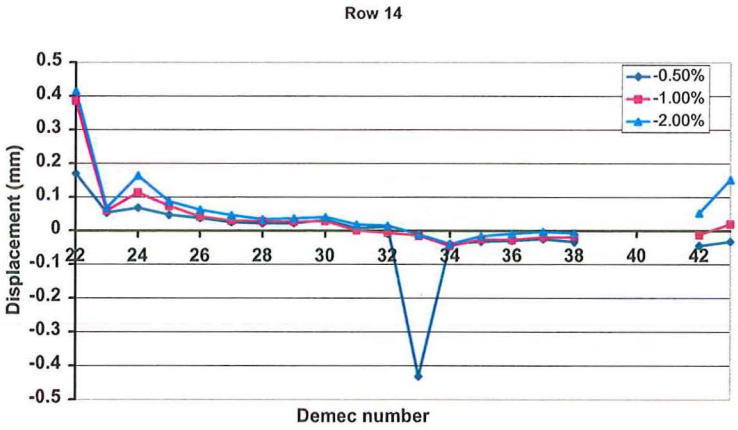

Row 14 for Phase I

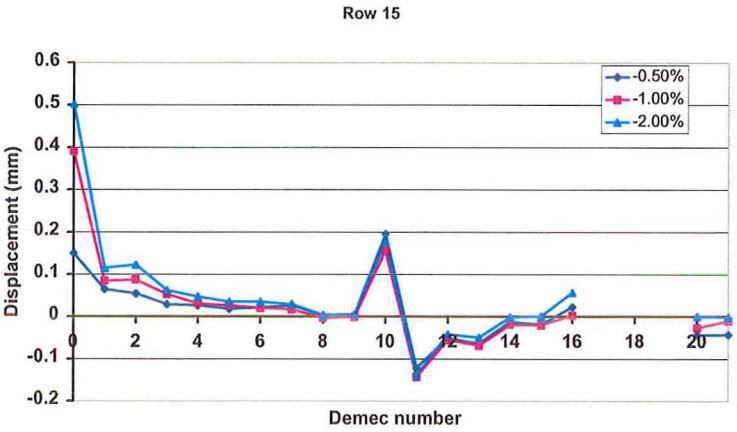

Row 15 for Phase I

Overall longitudinal diaphragm growth for Phase I

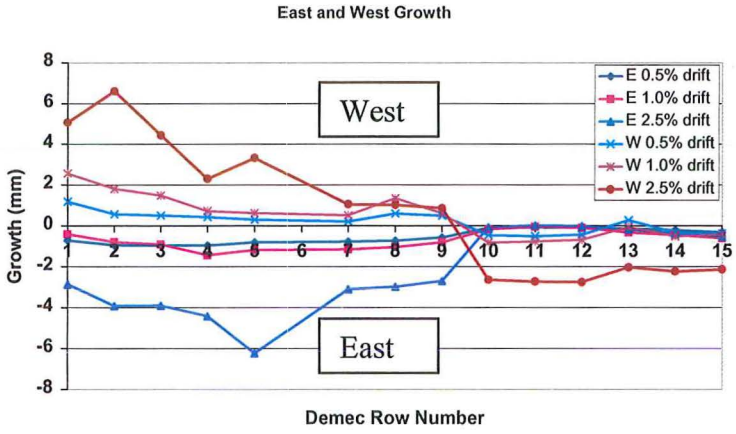

Positive drift growth for Phase I

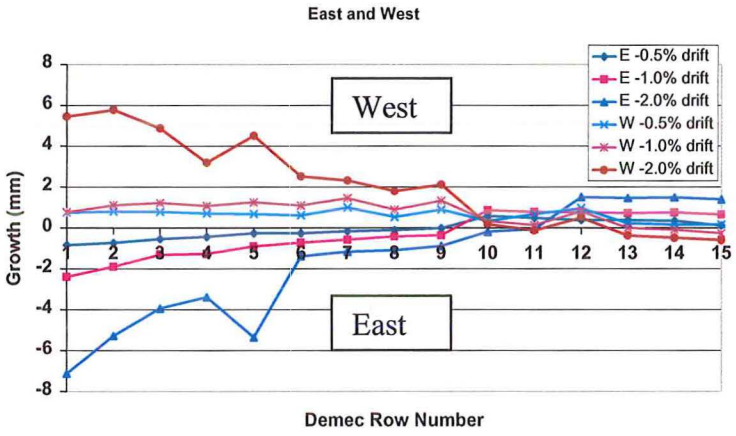

Negative drift growth for Phase II

Transverse diaphragm growth for Phase I

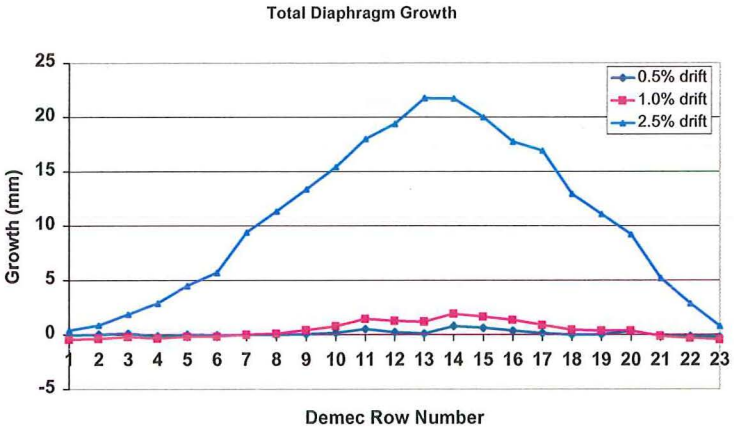

Positive drift transverse growth for Phase I

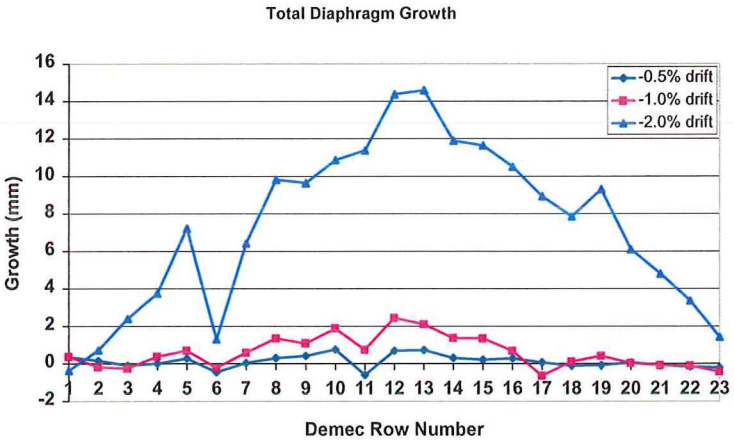

Negative drift transverse for Phase I

Longitudinal growth for Phase II

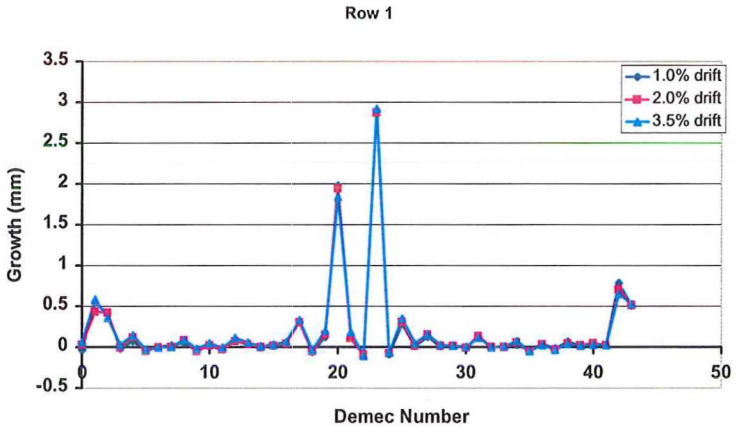

Longitudinal growth

Note: No significant change in the length of the diaphragm occurred during Phase II

Transverse growth for Phase II

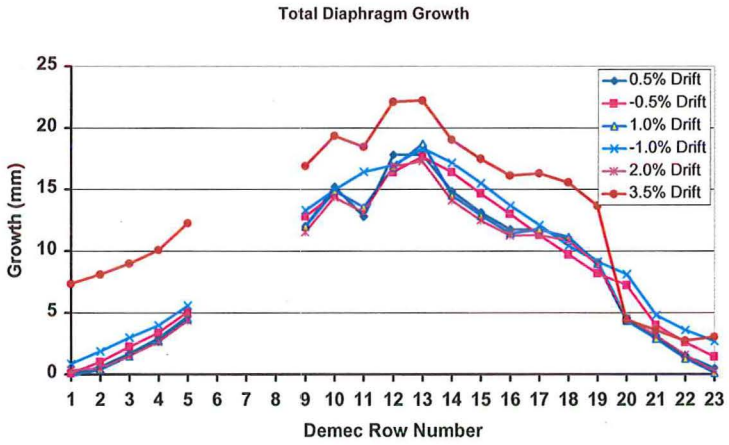

Transverse Growth

Note: The length of the transverse diaphragm only changed during the 3.5% drift load cycle. All the pervious growth occurred during Phase I.

G.3 *References*

Bull D.K and Matthews J.G, 2003, *Proof of Concept Tests for Hollowcore Floor Unit Connections*, Report for Precast NZ Inc, Commerical Report 2003-1, University of Canterbury

Appendix H

Beam Elongation

H.1 Observed beam elongation

All the plots herein show beam elongation starting from "zero elongation". "Zero elongation" is defined as the initial length of the beam at the start of that particular phase of loading. The total beam elongation for each beam is given at the end of this appendix.

H.1.1 Phase I

During loading in Phase I (in the longitudinal direction), beam elongation was seen to occur in all the four beams instrumented. The major elongation occurred in the beams parallel to the direction of loading (Beams B and C), a smaller amount of elongation was also seen in the two transverse beams (Beams A and D). The elongation in all the beams is shown in Figure H-1.

The elongation that formed in beams B and C was similar as the two beams had symmetric reinforcement. A more detailed breakdown of the elongation within beams B and C is shown in Figure H-2. The response from the two plastic hinges within each beam is quite different. The reason for this difference is due to the support connections at each end of the beam and the reinforcement ratios. The exterior plastic hinges in both beams represents a simple support, for the connection of the hollow-core unit to beam, while the central connection acts as a continuous support because the hollow-core unit spans past the central column restraining some of the elongation that tries to form whereas the simple support does not restrain the growth, it is simply

pulled off its support. The reinforcement ratio affects e_{cr}, the force eccentricity of the beam depth that is the distance between the beam centreline and the instantaneous centre of rotation (centroid of the compression force), which in turn affects the amount of elongation.

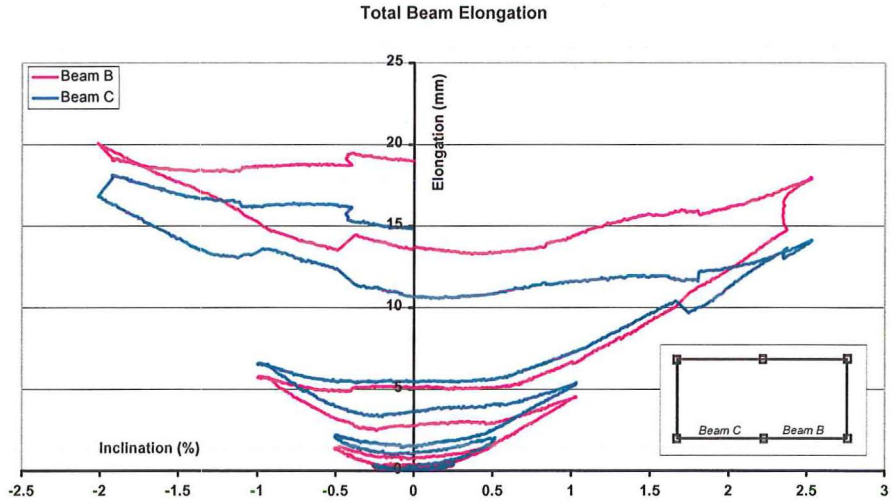

(a) Beam elongation in beams B and C (longitudinal beams)

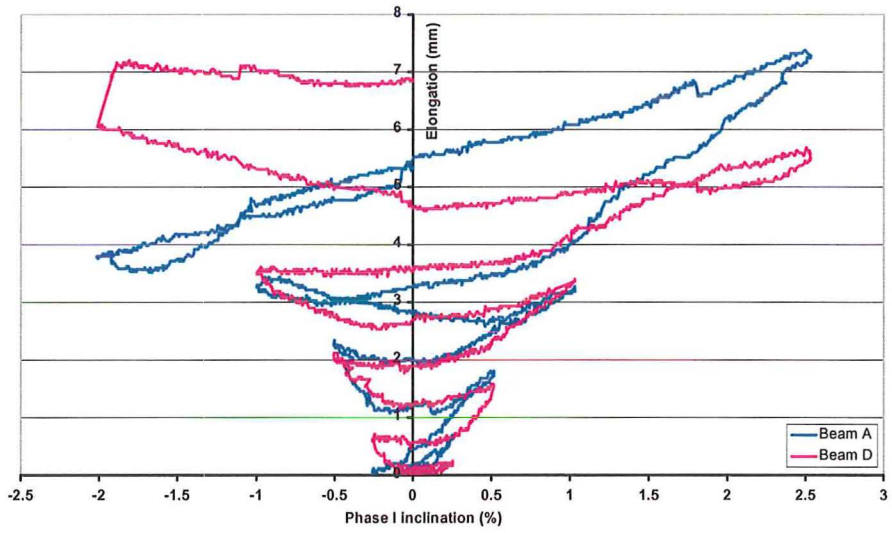

(b) Beam elongation in beams A and D (transverse beams)

Figure H-1 Observed Phase I beam elongation

Figure H-2 shows that the exterior joints (simple support) beam elongation was larger than the amount of elongation at the interior joint (continuous support). When a plastic hinge forms next to the central column and the beam tries to grow, the

floor slab goes into tension and restrains the growth. For a simple support, the floor unit is not sufficiently anchored to the supporting beam to restrain the beam elongation. In the case of this experimental programme the end of the hollow-core unit had fractured before the beam started to gain any substantial beam elongation so there was no appreciable restraint.

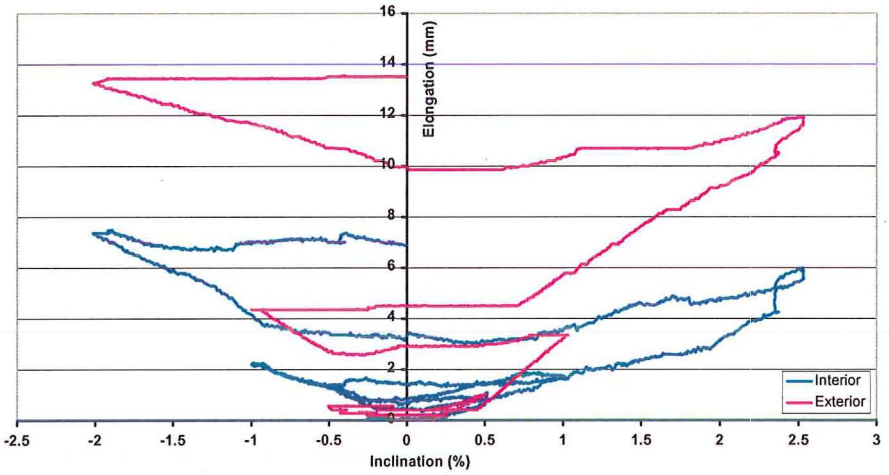

(a) The plastic hinge contribution to beam B's elongation

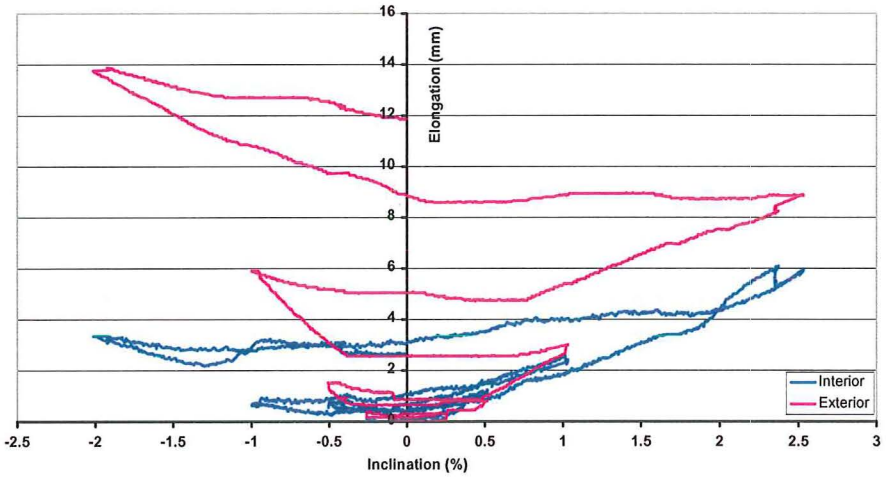

(b) The plastic hinge contribution to beam C's elongation

Figure H-2 The individual components of beam B and C contributing to the total beam elongation

Beams A and D grew in length because of the torsion cracks that formed within these transverse beams (Figure H-1).

H.1.2 Phase II

Phase II loading saw the transverse beams grow in length while the longitudinal beams remained essentially unchanged (Figure H-3). The torsion-induced beam elongation in the beams perpendicular to the direction of loading is seen in Figure H-3(b). Beams B and C grew in length during the displacement cycles but recovered the growth when unloaded. Beam C had a net gain in elongation of 4.7mm at the completion of Phase II while beam B grew under 1mm.

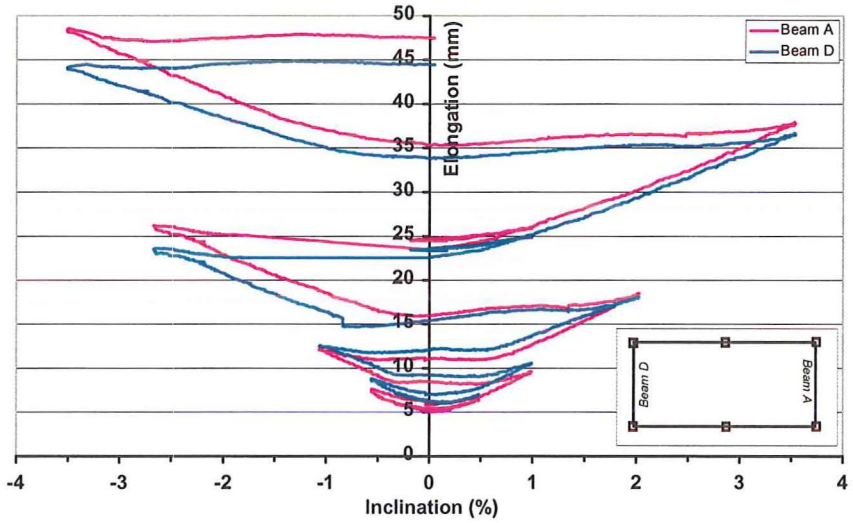

(a) Observed beam elongation in beam A and D

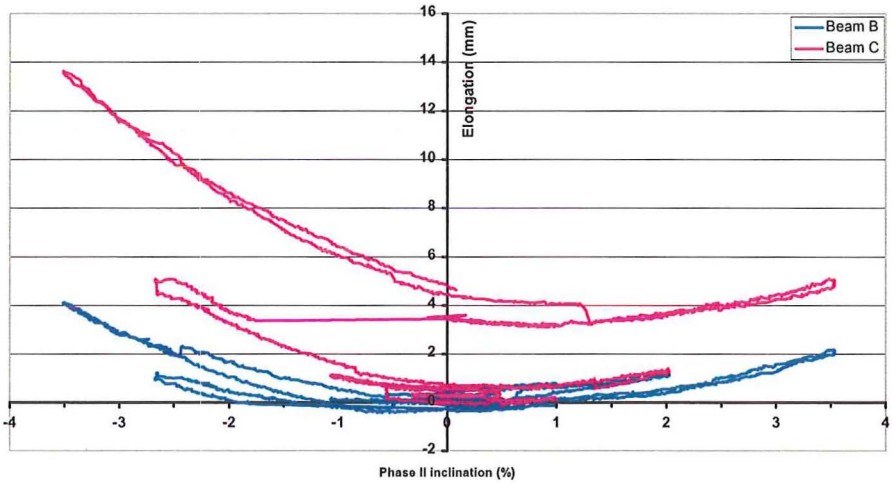

(b) Observed beam elongation in beam B and C

Figure H-3 Observed Phase II elongation plot.

The transverse beams grew approximately 20mm per plastic hinge, as shown in Figure H-4. The reason why the plastic hinges grew the same amount was because all the plastic hinges had similar reinforcement ratios and support details (a simple support).

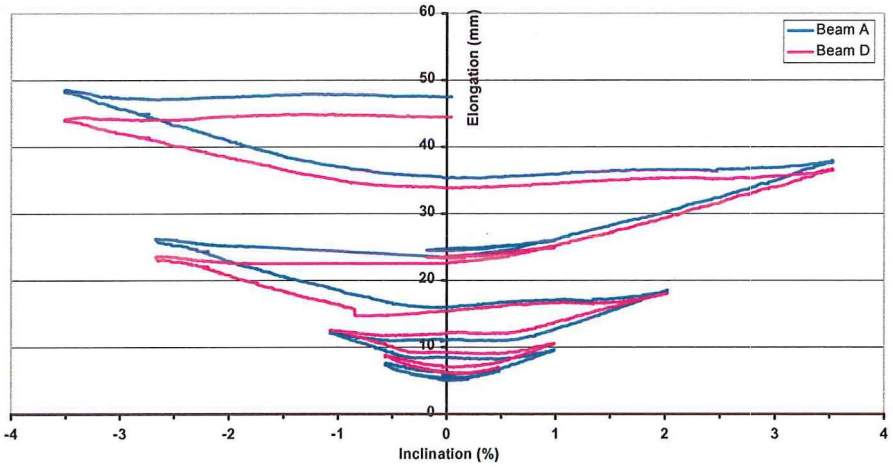

(a) Phase II beam A's elongation plot.

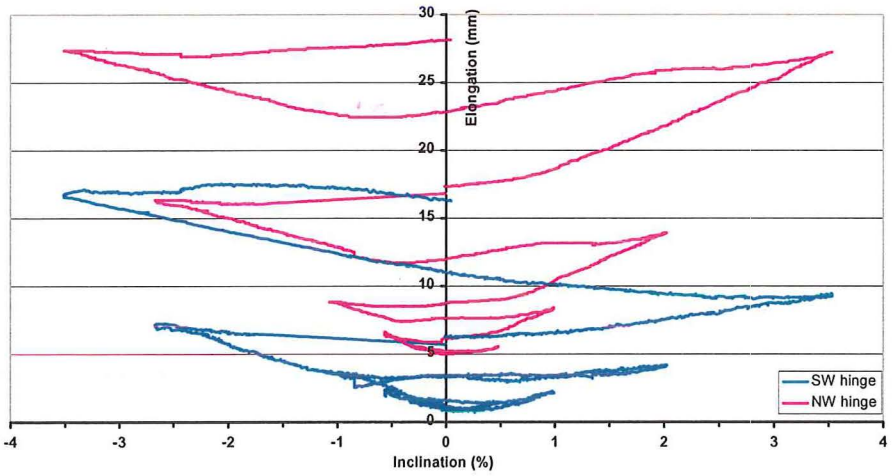

(b) Phase II beam D's elongation plot

Figure H-4. Individual components of beams A and D contributing to the total beam elongation during Phase II

Figure H-5 shows the rainflow plot for the predicted beam elongation for the West beam versus the observed elongation. Again there was good agreement between the theory and the observations.

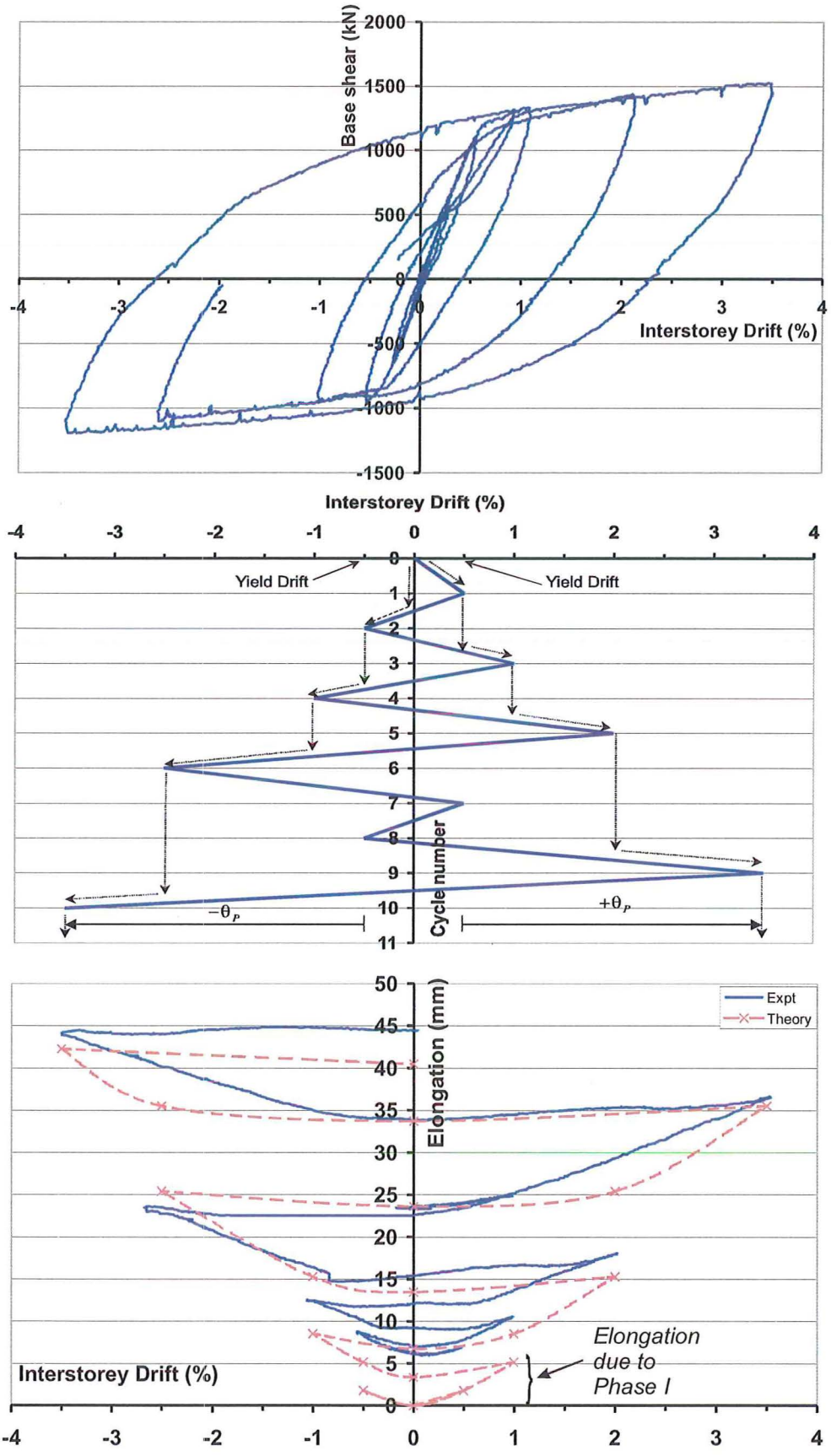

Figure H-5 Rain flow chart for Phase II (West beam)

H.1.3 Phase III

During Phase III, the total growth within the longitudinal beams (beam B and C) was smaller than during Phase I. This is because no new significant plastic rotation was imposed when compared to Phase I. As stated in Chapter 5, a large increase in beam elongation occurs due to an increase in new rotation from a previous maximum. The amount of beam elongation in both the longitudinal beams is shown in Figure H-6.

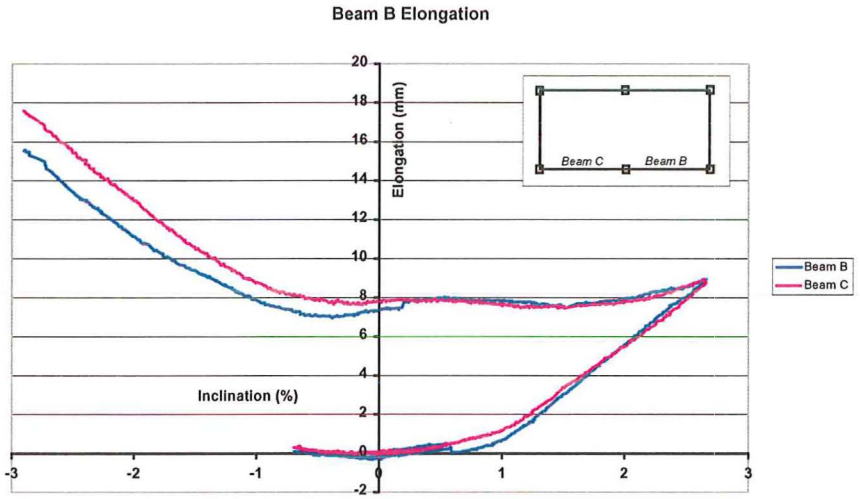

Figure H-6 Observed Phase III elongation plot

Figure H-7 shows the individual hinge elongation within each beam for the third phase of loading. The first section of floor failed at 2.5% drift and from that point onwards the interior plastic hinges grew more than the outer hinge. This is due to the change in e_{cr}, from approximately 0.5 to 0.85 since the central column connection no longer acts as a continuous support. Figure H-7 showed the interior hinge elongated the same amount as the exterior hinge once the floor failed, this is not the case in Figure H-2 where the interior hinge elongation was approximately 40% of the exterior hinge.

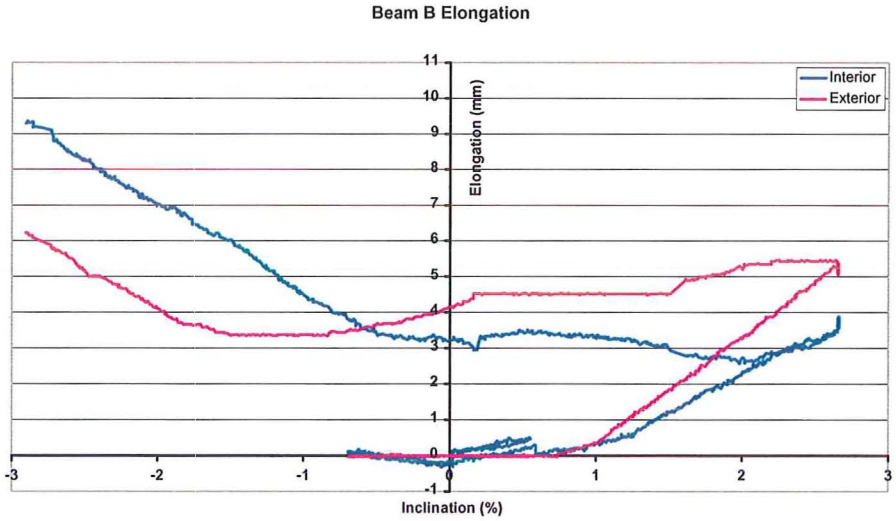

(a) Phase III beam B's elongation plot

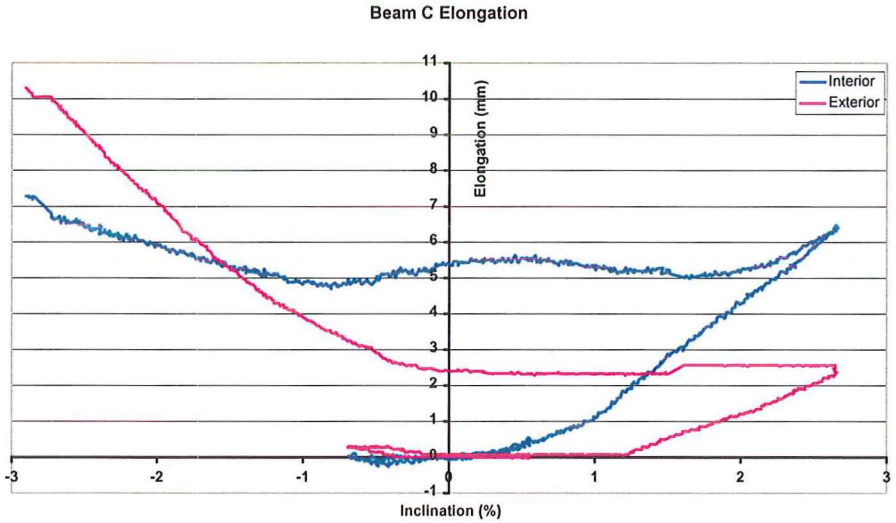

(b) Phase III beam C's elongation plot

Figure H-7 Longitudinal beam elongation during Phase III

H.2 Derivation of the elastic beam elongation

The elastic component of beam elongation can be derived from theory by examining on the strain within the beam member at its centre of gravity for the concrete section (c.g.c) (Figure H-8(a)). The elastic elongation component (δ_e^{el}) can be found by integrating the neutral axis (c.g.c) strain along the length of the beam as follows:

$$\delta_e^{el} = \frac{1}{2}\varepsilon_o^+ \xi L_b + \frac{1}{2}\varepsilon_o^- L_b (1-\xi) \qquad \textbf{(H-1)}$$

in which ε_o^+ = the strain at the onset of first yield at the member end at the c.g.c for a positive bending moment (M^+); ε_o^- = the strain at the onset of first yield at the other member end at the c.g.c for a negative bending moment (M^-); and ξ = portion of the total beam length (L_b) to where the beam bending moment is zero (Figure H-8)

$$\delta_e^{el} = \frac{1}{2}\varepsilon_o^+ \xi L_b - \frac{1}{2}\varepsilon_o^- L_b \xi + \frac{1}{2}\varepsilon_o^- L_b \xi \tag{H-2}$$

$$\delta_e^{el} = \frac{L_b}{2}\left[\left(\varepsilon_o^+ - \varepsilon_o^-\right)\xi + \varepsilon_o^-\right] \tag{H-3}$$

$$\xi = \frac{M^+}{M^+ + M^-} \Rightarrow \delta_e^{el} = \frac{L_b}{2}\left[\varepsilon_o^- + \frac{\varepsilon_o^+ - \varepsilon_o^-}{1 + \left|\frac{M^-}{M^+}\right|}\right] \tag{H-4}$$

$$\delta_e^{el} = \frac{L_b}{2}\left[\frac{\varepsilon_o^- + \varepsilon_o^-\left|\frac{M^-}{M^+}\right| + \varepsilon_o^+ - \varepsilon_0^-}{1 + \left|\frac{M^-}{M^+}\right|}\right] \tag{H-5}$$

$$\delta_e^{el} = \frac{L_b}{2}\left[\frac{\varepsilon_o^+ + \varepsilon_o^-\left|\frac{M^-}{M^+}\right|}{1 + \left|\frac{M^-}{M^+}\right|}\right] \tag{H-6}$$

$$\delta_e^{el} = \frac{L_b}{2}\left[\frac{\varepsilon_o^+ M^+ + \varepsilon_o^- M^-}{M^+ + M^-}\right] \tag{H-7}$$

From a strain diagram (Figure H-8(b)) it is possible to write expressions for the strain at the c.g.c (ε_o) and curvature (ϕ).

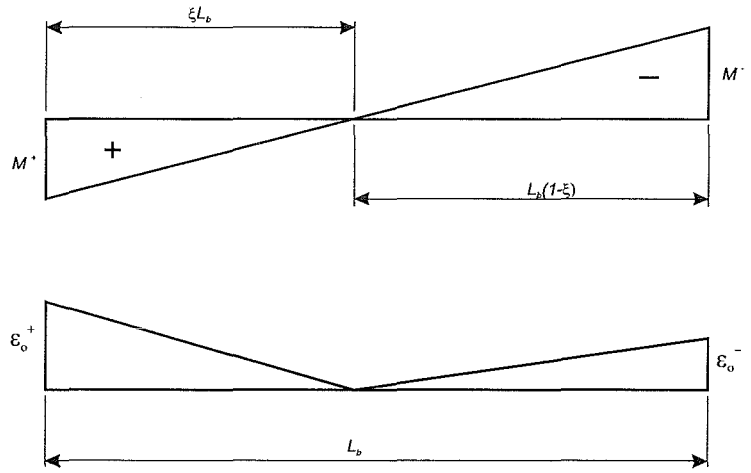

(a) Beam bending moment and strain diagrams used to determine the elastic component of beam elongation.

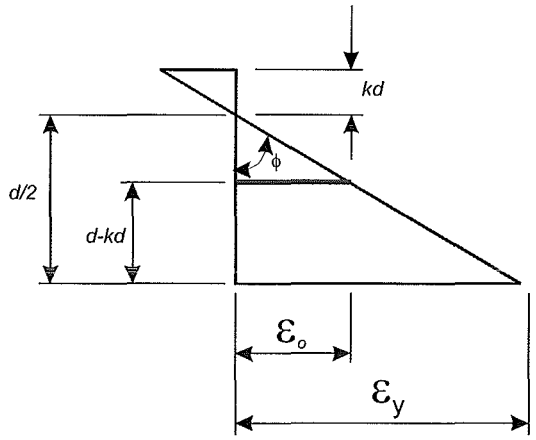

(b) Strain diagram used to determine the yield curvature for a beam

Figure H-8 Figures used to determine the elastic beam elongation

$$\varepsilon_o = \varepsilon_y - \frac{d}{2}\phi \qquad \textbf{(H-8)}$$

in which ε_y = yield strain of the beam reinforcement; and d = effective depth of the beam.

$$\phi = \frac{\varepsilon_y}{d - kd} = \frac{\varepsilon_y}{d(1-k)} \qquad \textbf{(H-9)}$$

in which k = fraction of the beam depth from the extreme compression fibre to the neutral axis depth.

$$\varepsilon_o = \varepsilon_y - \frac{d}{2}\frac{\varepsilon_y}{d(1-k)} = \varepsilon_y - \frac{\varepsilon_y}{2(1-k)} \qquad \textbf{(H-10)}$$

$$\varepsilon_o = \varepsilon_y\left(1-\frac{1}{2(1-k)}\right) \quad \textbf{(H-11)}$$

$$\varepsilon_o = \varepsilon_y\left(\frac{2-2k-1}{2-2k}\right)=\frac{1-2k}{2-2k} \quad \textbf{(H-12)}$$

Substituting Equation (H-12) into Equation (H-7) becomes

$$\delta_e^{el} = \frac{L_b}{2}\varepsilon_y\left[\frac{\frac{1-2k^+}{2-2k^+}M^+ + \frac{1-2k^-}{2-2k^-}M^-}{M^+ + M^-}\right] \quad \textbf{(H-13)}$$

To simply Equation (H-13) assume that the positive yield moment equals the negative yield moment ($M^+=M^-$) and hence the fraction of member depth (k) at yield will also be equal ($k=k^+=k^-$).

$$\delta_e^{el} = \frac{L_b}{4}\varepsilon_y\left[\frac{1-2k}{1-k}\right] \approx \varepsilon_y\frac{L_b}{4}[1-k] \quad \textbf{(H-14)}$$

This Page is Blank